SEDHYD 2019

Proceedings of SEDHYD 2019: Conferences on Sedimentation and Hydrologic Modeling

Volume 4

Sediment Surrogate Measurements, Sediment Yield and Fingerprinting, Stream Restoration, Water Quality, Watershed Management

Proceedings of SEDHYD 2019: Conferences on Sedimentation and Hydrologic Modeling, 24-28 June 2019 in Reno, NV.

These engineering and scientific proceedings provide much of the latest information on sedimentation and hydrologic modeling (applied research and state of-the-practice) from Federal agencies, universities, and consultants. SEDHYD is the successor to the Federal Interagency Conferences on Sedimentation and Hydrologic Modeling. The Subcommittee on Sedimentation convened the first Federal Interagency Sedimentation Conference (FISC) in 1947. Subsequent FISC conferences were convened in 1963, 1976, 1986, 1991, 1996, and 2001. The Subcommittee on Hydrology convened their first Federal Interagency Workshop, "Hydrologic Modeling Demands for the 90s," in 1993. Subsequent to that workshop, the Subcommittee on Hydrology convened the Federal Interagency Hydrologic Modeling Conferences (FIHMC) in 1998 and 2002. Subsequently, the Subcommittees on Sedimentation and Hydrology began convening the Federal interagency conferences together in 2006 and again in 2010, and 2015. Beginning in 2019, the SEDHYD Conference was hosted by SEDHYD, Inc., a non-profit organization.

Since 1947, the Sedimentation and Hydrologic Modeling Conferences have provided over 3,000 technical papers and extended abstracts and provided engineers and scientists with the opportunity to learn and exchange information about the latest developments and research related to sedimentation and hydrologic modeling. As a continuation of these conferences, SEDHYD provides an interdisciplinary mix of scientists and managers from government agencies, universities, and consultants to present recent accomplishments and progress in research and on technical developments related to sedimentation processes, hydrologic modeling, and the impact of sediment on the environment.

The SEDHYD conference provides a mixed set of formats that include formal technical presentations, poster sessions, field trips, workshops, computer model demonstrations, and a student paper competition. The SEDHYD conference also provides excellent networking opportunities.

The SEDHYD 2019 Conference site was at the Peppermill Hotel and Resort in Reno, Nevada. Reno is situated in a high desert just east of the beautiful Sierra Nevada Mountains. The city lies on the western edge of the Great Basin, at an elevation of 4,400 feet (1,300 meters) above sea level. The Reno downtown area (along with Sparks) occupies a valley informally known as Truckee Meadows. The area offers spectacular desert landscapes and ecosystems, as well as numerous indoor and outdoor recreational opportunities.

Suggested Citation:
In Proceedings of SEDHYD 2019: Conferences on Sedimentation and Hydrologic Modeling, 24-28 June 2019 in Reno, Nevada, USA.

SEDHYD 2019 Planning Committee

Planning Committee Position	Volunteer	Organization
SEDHYD Conference Chair	Jerry Webb	West Consultants
SEDHYD Operations Chair	Jennifer Bountry	Reclamation
SEDHYD Technical Program Chair	Chandra Pathak	USACE
SEDHYD Technical Program Chair (YP)	Will Farmer	USGS
SEDHYD Technical Program	Jerry Bernard	NRCS, retired
Sedimentation Conference Chair	Tim Randle	Reclamation
Sedimentation Program Chair	Eddy Langendoen	ARS
Sedimentation Program Chair (YP)	Joel Sholtes	Mesa State
Hydrologic Modeling Conference Chair	Claudia Hoeft	NRCS
Hydrologic Modeling Program Chair	Jim Barton	USACE, retired
Hydrologic Modeling Program Chair (YP)	Jessica Driscoll	USGS
Student Program Coordinator	Amanda Cox	MWRRC
Proceedings Coordinator	Bob Boyd	BLM
Proceedings Coordinator	Peter Doran	BLM
Poster & Computer Model Demonstration Coordinator	Eddie Brauer	USACE
Short Course Coordinator	Jeff Bradley	ASCE, West Consultants
Short Course Coordinator (YP)	Kevin Denn	USACE, St. Paul Dist.
Field Trip Coordinator	Steve Berris	USGS
Field Trip Coordinator (YP)	Jena Huntington	USGS
Web site Coordinator	Darren Nezamfar	USACE
Registration Coordinator	Penni Baker	USACE
Registration Volunteer	Kathy Randle	
Young Professionals Coordinator	Caroline Ubing	Reclamation
Young Professionals Coordinator	Sara Horgen	Reclamation
Exhibit Coordinator	Molly Wood	USGS
Exhibit Coordinator	Tim Straub	USGS
AV Equipment Coordinator	Jeff Harris	West Consultants
Planning Committee	Jo Johnson	NRCS
Planning Committee	Jon Fripp	NRCS
Planning Committee	Paul Boyd	USACE
Planning Committee	Meg Jonas	USACOE, retired
Planning Committee	Robert R Mason	USGS
Planning Committee	Victor Hom	NOAA

SEDHYD, Inc.

SEDHYD, Inc. Position	Volunteer
SEDHYD President & Board Chair	Jerry Webb
SEDHYD Vice President & Board Member	Jerry Bernard
SEDHYD Treasurer & Board Member	Don Frevert
SEDHYD Secretary & Board Member	Matt Romkens
SEDHYD Board Member	Doug Glysson

Table of Contents

Table of Contents

Table of Contents

Stream Restoration

Table of Contents

Table of Contents

Sediment Surrogate Measurements

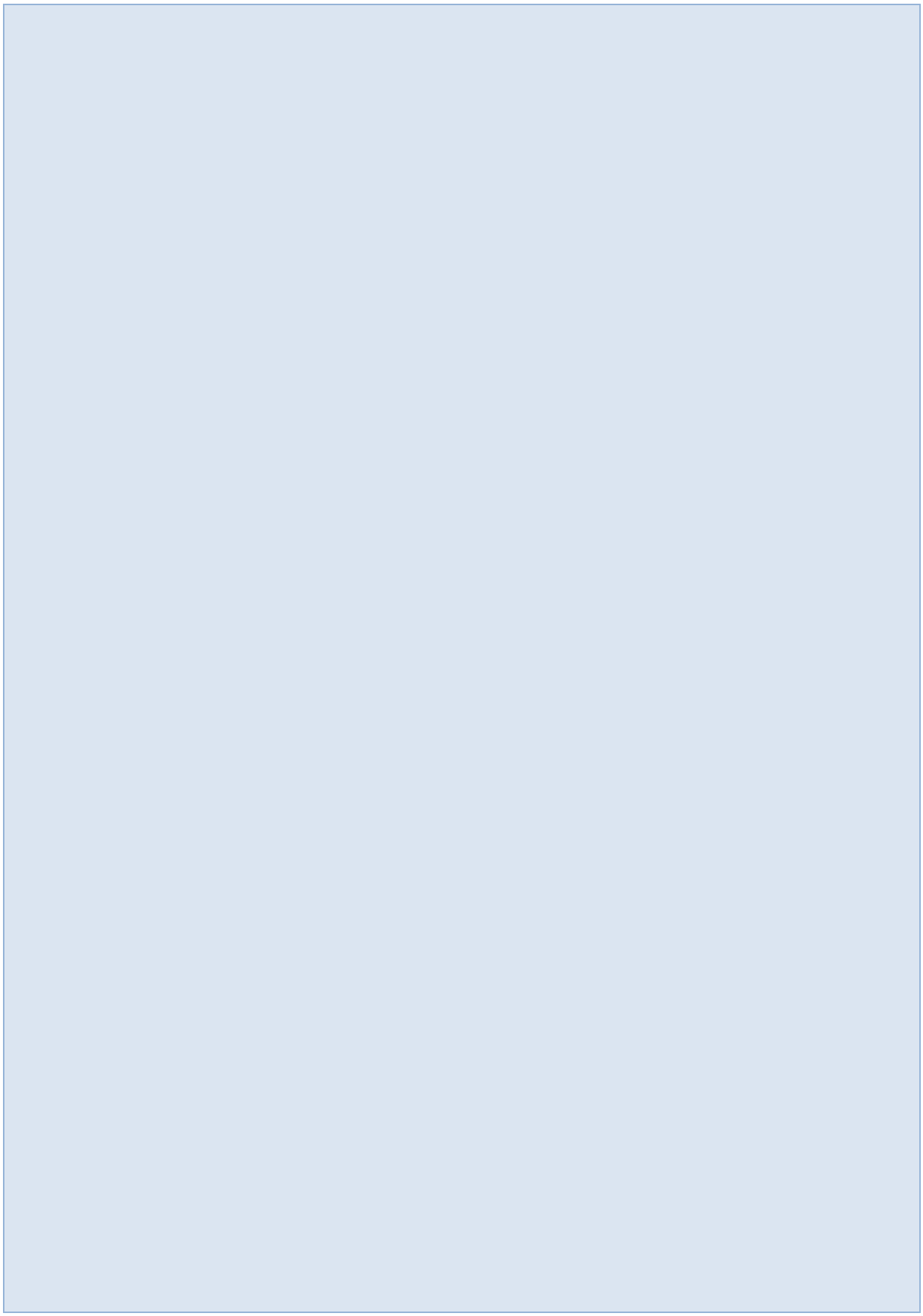

Acoustic Sediment Surrogate Measurements for High Sediment Flux: Case study at Koshibu Sediment Bypass Tunnel

Takahiro Koshiba, Kyoto University, Kyoto, Japan, koshiba.takahiro.47v@st.kyoto-u.ac.jp
Tetsuya Sumi, Professor, Kyoto University, Kyoto, sumi.tetsuya.2s@kyoto-u.ac.jp

Introduction

Surrogate bedload measurement is a promising technique for continuous sediment monitoring (Rickenmann 2017). Actually, more than 300 sites in Japan have employed a steel-pipe type acoustic sediment monitoring device called Japanese Pipe Microphone (JPM). One severe problem for the JPM, however, is pipe deformation due to the high sediment flux that causes the alternation of their acoustic signal properties. Therefore, recently, more and more sites employ an acoustic monitoring system which uses a rigid steel plate instead of a steel pipe.

In this paper, a case study at Koshibu sediment bypass tunnel in Japan is introduced where five plate-type acoustic bedload monitoring systems are installed. The sediment bypass tunnel (SBT) is a facility to mitigate reservoir sedimentation by routing sediment-laden floods to the downstream reaches during flood events (Kondolf et al. 2014).

Bedload monitoring with impact plates at Koshibu SBT

Koshibu sediment bypass tunnel

The Koshibu dam is located at the Koshibu river catchment in Nagano prefecture, Japan, and is operated by the Ministry of Land, Infrastructure, Transport and Tourism (MLIT). Due to a severe sedimentation problem, MLIT constructed the SBT in 2016. The length of the SBT is 3,982 m with a cross section of circular shape and a plane invert with a slope of 2 %. The width and height are 5.5 m and 7.9 m, respectively. Most of the tunnel is straight but the last 600 m from the outlet is curved on the orographic right direction (Radius = 1000 m).

In the SBT, sediment monitoring is desirable to know the transported sediment information, i.e. grain sizes and transport rates, for unveiling the bypass efficiency and required SBT maintenance works. Because the design discharge at the Koshibu SBT is extreme, with a flow rate of 370 m3/s yielding velocities in excess of 20 m/s, the impact plate system was chosen for this site.

Impact Plates

The impact plate (IP, manufactured by Hydrotech Co., Ltd., Japan, Figure 1), consists of a microphone and an accelerometer mounted underneath a steel plate (49.2 cm × 35.8 cm × 1.5 cm), records acoustic and oscillation impact caused by bedload transport on the plate. Five impact plates are embedded on the outlet invert of the Koshibu SBT (Figure 2). Additionally, two JPMs were also placed at the site to confirm the rigidness of the IPs. During the SBT operations, IPs record raw signal data with a 50 kHz of sampling rate and a summary value

called the number of impulses (I_{ps}). After a raw signal is amplified with ten levels of amplification factors (Amp.) from 2 to 1024 times with 2 times of the interval, the number of spikes in each amplified signal being over a certain threshold voltage, which is sufficiently higher than signals produced by water noise, are counted as I_{ps}. High amplification factors correspond to the high sensitivity thus the sediment with wider range of grain sizes can be detected, and vice versa (Koshiba et al. 2018).

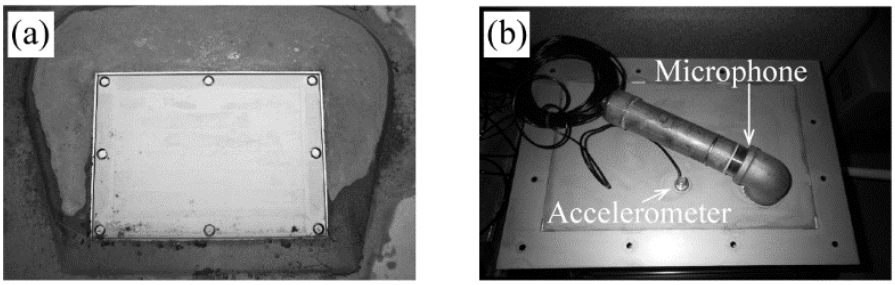

Figure 1. (a) An IP installed in the Koshibu SBT invert, (b) the back side of the IP with a microphone and an accelerometer.

Figure 2. Koshibu SBT outlet part with five IPs for bedload monitoring

Case study: Typhoon in 4th July, 2017

Bedload observation during an SBT operation in 4th July, 2017 is picked up. The hydrograph, bypassed discharge and water level at the SBT inlet gate are shown in Figure 3. SBT was operated from around 21:00 to midnight. In the first half of the operation, the bypassed discharge shows a step-wise increase with following the SBT gate opening, while the latter half of that is in a state of free flow to efficiently bypass sediment.

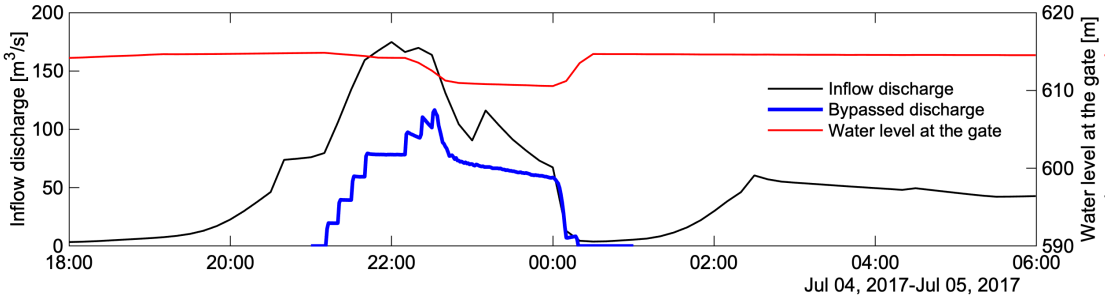

Figure 3. SBT operation and the water level at the gate during a flood event in 4th July, 2017

The timeseries results of bedload observation by the IPs are demonstrated in Figure 4. Figure 4a depicts the I_{ps} with Amp. = 1024 for each plate, and (b) is I_{ps} by five levels of Amplification factors recorded by the plate No. 3 (Figure 2) and the bypassed water discharge. The observation demonstrates that:

1. although the JPMs were completely broken during the first operation of Koshibu SBT, IPs are still working after several SBT operations, thus the IP has the much higher rigidness than JPM.
2. more bedload transported on the plate 1 side which locates tunnel curve inner side. It might be caused by a secondary current (Prandtl's first kind secondary current) and this phenomenon is in line with tunnel invert damage measured in other SBTs (e.g., Nakajima et al. 2017).
3. the result (Figure 4b) depicts the incipient and the termination of sediment flow at the SBT outlet. The time series variation of bedload flow magnitude is also clear.
4. the increase of I_{ps} with Amp. = 256 at 22:30 to 23:00 is larger than that of Amp. = 1024 (Figure 4b). It implicates that the ratio of sediment with the relatively larger grain sizes increased during the period. Monitoring with several Amps gives rough estimation of grain size distribution shift.

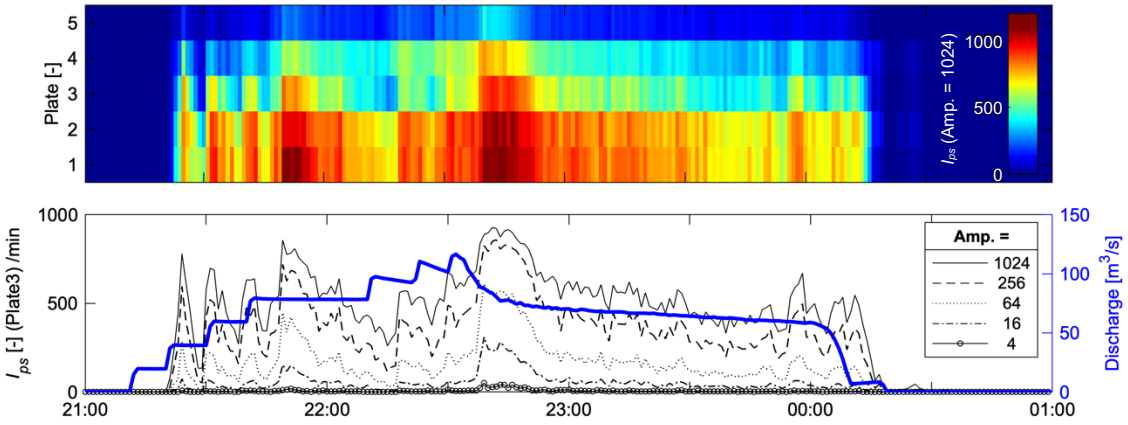

Figure 4. Time series results of bedload observation by IPs. (a) I_{ps} (Amp. = 1024) by five IPs, and (b) Bypassed discharge and the I_{ps} in five Amps by Plate No. 3.

References

Koshiba, T., Auel, C., Tsutsumi, D., Kantoush, S. A., & Sumi, T. 2018. "Application of an impact plate–Bedload transport measuring system for high-speed flows", International journal of sediment research, 33(1):35-46.

Kondolf, M., Gao, Y., Annandale, G., Morris, G., Jiang, E., Zhang, J., Carling, P., Fu, K., Guo, Q., Hotchkiss, R., Peteuil, C., Sumi, T., Wang, HW., Wang, Z., Wei, Z., Wu, B., and Yang, C.T. 2014. "Sustainable sediment management in reservoirs and regulated rivers: Experiences from five continents", Earth's Future 2(5):256-280.

Nakajima, H., Otsubo, Y., & Omoto, Y. 2015. "Abrasion and corrective measures of a sediment bypass system at Asahi Dam", Proc. Int. Workshop on Sediment Bypass Tunnels, VAW-Mitteilung 232 (Boes, R.M, ed.), ETH Zurich, Switzerland:21-32.

Rickenmann, D. 2017. "Bedload transport measurements with geophones and other passive acoustic methods", Journal of Hydraulic Engineering ASCE, 143, 03117004-1-14, doi: org/10.1061/(ASCE)HY.1943- 7900.0001300.

Acoustically Derived Sediment Fluxes: An Acoustic-Index to Channel-Average Concentration Approach

Dan Haught, Hydrologist, United State Geological Survey, California Water Science Center, Sacramento, CA, USA, Daniel.haught@gmail.com

Jeremy Venditti, Professor, Simon Fraser University, Burnaby, BC, Canada, jeremy_venditti@sfu.ca

Introduction

Knowledge of sediment flux in rivers is required for the management of navigable waters and reservoir maintenance. It is also critical to the understanding of aquatic habitat quality and morphodynamics of rivers and their deltas. Suspended sediment flux can be divided into material typically found in the bed, composed of sand-sized particles, and washload, composed of finer silt and clay-sized particles. The former is responsible for channel and bed morphology while the latter builds floodplains, deltas, and tidal flats. Washload is also important in the prediction of the transport and fate of pollutants that adhere to the finer suspended particles. Yet the prediction of washload remains difficult because supply generally determines transport rates, not hydraulics, like in the case of suspended bed material. The difficulty in prediction, along with the importance in higher resolution estimates, has led scientists and engineers to investigate acoustic-based suspended sediment monitoring programs.

Theoretically, the acoustic signal should respond to suspended sediments as a function of particle size, shape, mineralogy, and the number of particles in suspension. Therefore, back-calculating the acoustic signal should produce a reliable estimate of suspend sediment concentration, when minerology, shape, and size can be assumed constant. Clearly the latter is less likely, while the former two change over longer periods. Flammer (1962) shows how the backscatter of the signal is related to coarser suspended sediment such as silts and sands, while the attenuation of the signal with respect to distance away from the transducer is related to finer silts and clays. Additionally, many applications of this theory have related total suspended load to that of the backscatter in a more empirical fashion. Below, we examine these methods in order to derive a channel average concentration and flux.

Though a multitude of acoustic applications have been implemented, a recent approach has been to utilize horizontally projected Acoustic Doppler Current Profilers (H-ADCP) mounted to a stationary structure, such as a pier. This type of application works well in cases where the channel width is close to the range of the H-ADCP or the hydraulics maintain a well-mixed system. In large rivers, where H-ADCPs applied range is much smaller than the channel cross-section, correlation between the acoustically derived concentration and channel-average concentration is needed.

Methods

Discharge and Sediment Measurements:

We use a 600 kHz H-ADCPs to estimate suspended sediment concentration (SSC) and discharge, which provides an SSC flux. The H-ADCP was mounted to a dock at Mission, BC

Canada, in the Fraser River at a fixed elevation (-2.2 m amsl), which roughly covers the top 0.3 to 0.6 of depth depending on flow. The ADCP ensonifies a beam perpendicular to the flow and extends to approximately 60 m, while the total channel width at the site is 550 m. Physical sediment samples were collected within the acoustic ensonified volume as well as velocity profiles collected across five channel panels, to allow for the computation of channel-average SSC and flux. Samples were analyzed for SSC and gradation, allowing for calibration and the examination of the influence that changing gain-size has on the calibrations.

The index-velocity relation (Ruhl and Simpson, 2005) was systematically optimized by regressing measured velocity to the index velocity using the sum of squared residuals (SSR). This method utilizes a correlation between the velocity computed from the ADCP (index) to that of measured channel-average velocity. Using the index-velocity from the ADCPs, we varied the window size and location to identify the ideal fraction of ADCP cells to use in the index-velocity relation. We use the minimum SSR to select the optimized range of cells. Because stage data is a point measurement, we did not use a similar optimization for the stage-area analysis. The product of the channel-average velocity and the area is the channel-average discharge. Figure 1 shows the discharge for all three years of observation.

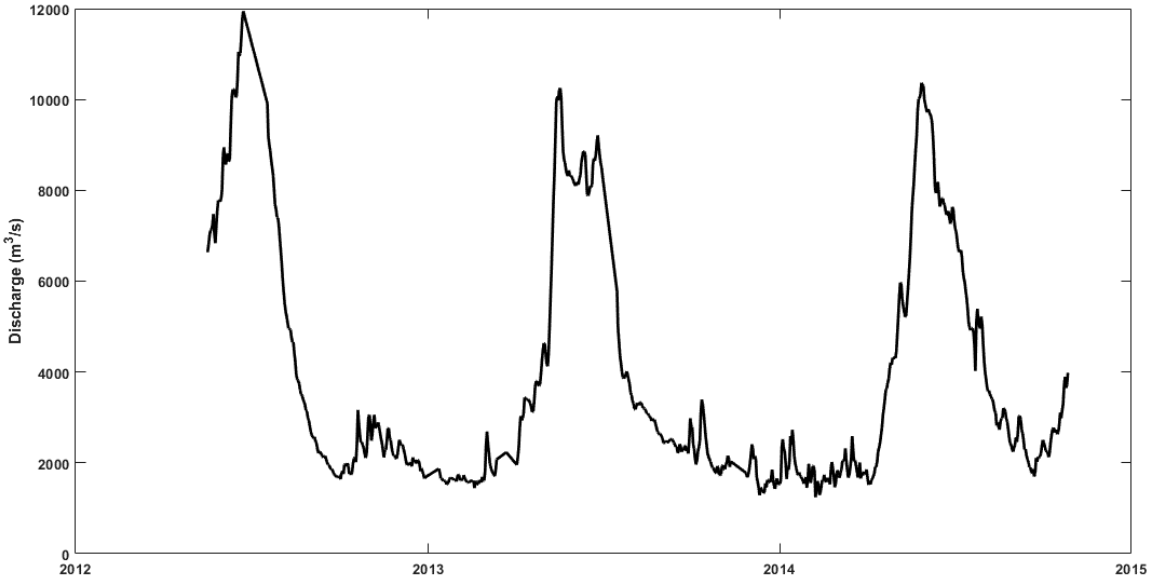

Figure 1. Discharge derived from the index-velocity method.

Acoustic Inversion:

We use a single-frequency acoustic inversion to correct the acoustic signal to account for sediment and fluid attenuation (Haught et al., 2017; Wright et al., 2010). The corrected acoustic signal is related semi-empirically to suspended sediment measurements within the ensonified volume. We calibrate total suspend sediment concentration (TSS) to fluid corrected backscatter (FCB), that is, the backscatter from the H-ADCP corrected to account for the attenuation due to fluid properties (primarily temperature). Sand concentrations are related to sediment corrected backscatter (SCB), which accounts for both fluid attenuation and sediment attenuation. Sediment attenuation is estimated from the slope of the regression between FCB and range (see Haught et al., 2017 and references therein). Because attenuation is derived from a regression with respect to space, it provides a single point in time and does not have a spatial context as does backscatter (Wright et al., 2010). The formal calibrations provide an estimate of TSS, sand

SSC, suspended bed material (SBM), and silt/clay SSC within the ensonified volume, but do not account for concentration variations across the channel.

To estimate channel-average concentration, similar to the index-velocity approach, we relate the index concentration within the ensonified volume to the channel-average concentration. Unlike the index-velocity method, an acoustic inversion must first be done to obtain H-ADCP derived concentrations. Regression relations are developed between the ensonified volume concentrations estimated by the H-ADCP and the measured channel average concentration for the respective suspended sediment fraction. We collected 4 to 6 sediment profiles per campaign with six discrete samples taken at a relative depth of 0.1, 0.2, 0.4, 0.6, 0.8, and 0.9 to compute channel average concentration. Similar to discharge, we optimized the relations by minimizing SSR, as described above.

Channel-average flux is computed from the channel-average discharge and the acoustically-derived channel-average concentration.

Results

Sediment Sampling:

Twenty-five sampling campaigns were carried-out in the Fraser River between 2012 and 2014. Sample concentrations ranged from 20-350 mg/L and were primarily composed of silt to fine sand (Figure 2).

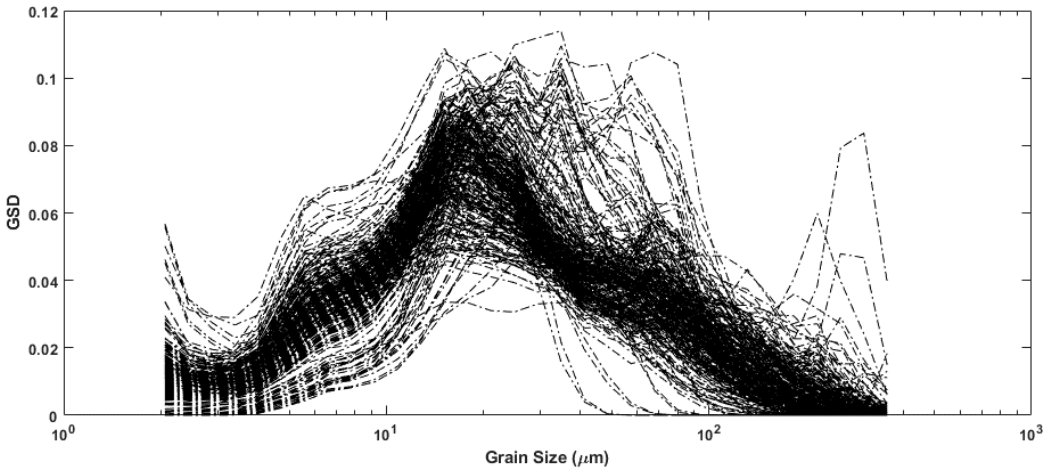

Figure 2. Gradation for samples collected in the ensonified volume and used to calibrate the H-ADCP.

Acoustic Calibration:

Acoustic inversions showed statistically significant calibrations between all SSC constituents. The coefficient of determination (R^2) was strong for Fine SSC, while the other constituents had weaker R^2 values. The TSS SSC calibration showed a large amount of scatter at lower SSC (Figure 3). Sand calibration shows less scatter than the SBM SSC (Figure 3 middle panel), while having stronger correlation (Table 1). Fine SSC provides the tightest grouping but shows some anomalies in the grouping (Figure 3 right panel). Because of the poor relation to SBM, we do not carry it forward in the development of a flux.

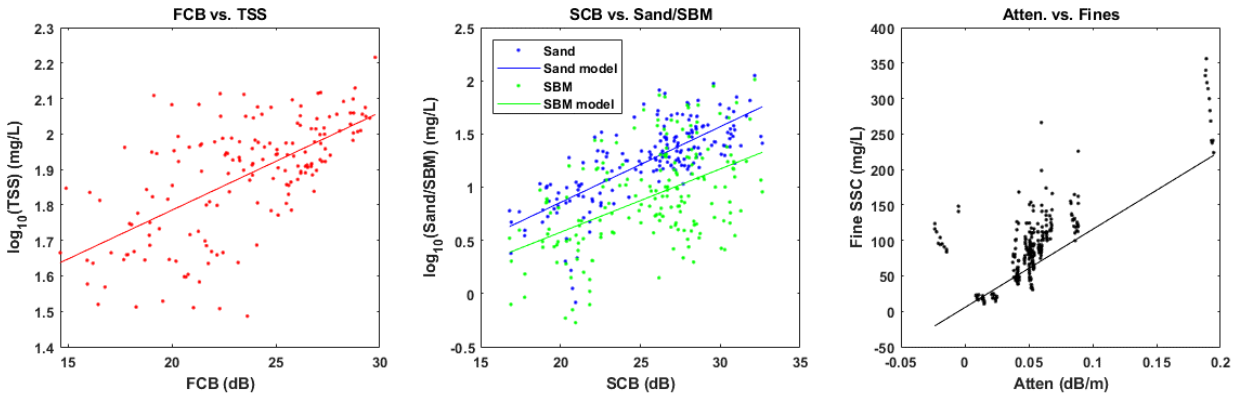

Figure 3. Calibrations between backscatter properties and SSC properties used to estimate ensonifed volume SSC.

Table 1. Statistics for the acoustic inversion calibrations

Calibration	R^2	Mean Square Error	p-value	SE of the slope
TSS	0.4	0.12	0	2.6e-3
Sand	0.57	0.06	0	4.6e-3
SBM	0.24	0.16	9.1e-13	7.7e-3
Fines	0.82	2.1e-4	0	2.2e-5

ADCP to Channel Average Relation:

To account for the limited range of the ADCP (60 m), we make a relation between what the ADCP derived SSC (from the calibrations above) and the measured channel average SSC. Relations between acoustically derived SSC and channel-average SSC had good correlation (Figure 4), allowing for estimates of continuous SSC and flux on a large river. In addition to deriving TSS acoustically, we also sum the acoustically derived sand SSC with fine SSC (Figure 4 right panel). The sum of the sand and fines produces a better result than acoustically derived TSS. Because of the better result from the sum of parts, we do not carry forward the assessment of TSS derived acoustically.

Figure 4 shows the correlations as scatter plots, while Table 2 provides the statistical assessment. The sand SSC relation provides the strongest correlation, while SBM does not capture the high concentrations as well as sand (Figure 4 center panel). Fine SSC shows good correlation, albeit possibly one outlier. We use these relations to develop channel average time series and a channel average flux.

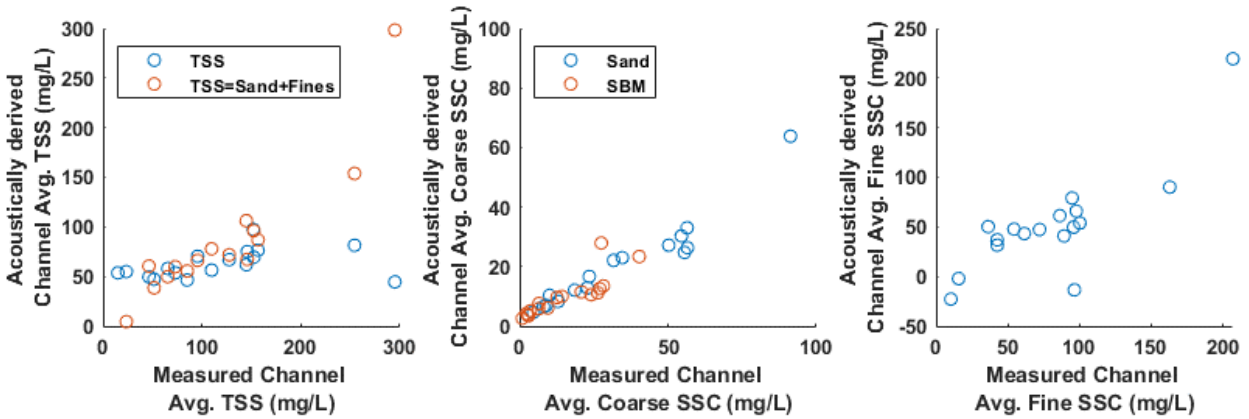

Figure 4. Relation between ensonified volume, acoustically derived, SSC and measured channel average SSC.

Table 2. Statistics for models developed between ensonified volume SSC and channel average SSC. Note SE is the standard error.

Calibration	R^2	Mean Squared Error	p-value	SE of the slope
TSS	0.13	190	0.15	0.05
TSS=Sand+Fines	0.82	858	2.8e-6	0.1
Sand	0.91	36	1.7e-9	0.05
Fines	0.68	946	4.8e-5	0.16

Figure 5 shows the time-series of daily average channel average flux for TSS derived from the sum of sand and fine SSC relation. We also show the discharge and the measured flux. Acoustically derived channel-average TSS tracks discharge well, albeit underestimating measured flux. Measurements from 2012 track the falling limb well but are of greater magnitude. Measurements from 2013 suggest that the acoustically-derived values missed a portion of the freshet possibly due to SSC gradation changes. Measurements from 2014 show that acoustically derived TSS captures the spring flush of fine sediments and the majority of the freshet. The falling limb tends to be underestimated.

Acoustically derived sand flux track measurements well in 2012 and 2014, but less well in 2013. Measurements in 2012 coincide with the falling limb well, but due to a lack of measurements throughout the freshet, it is difficult to predict how well it tracks peak sand fluxes. In 2013, acoustically derived sand fluxes clearly underestimate the freshet, but track the falling limb well, likely contributing to the poor results seen in TSS flux. Measurements in 2014 suggest that acoustically-derived values capture the freshet well but miss the early sand load.

Acoustically-derived fine flux compares well to measurements for all three sampling seasons. Measurements in 2013 are slightly underestimated, while in 2014 measurements track the acoustically-derived values well.

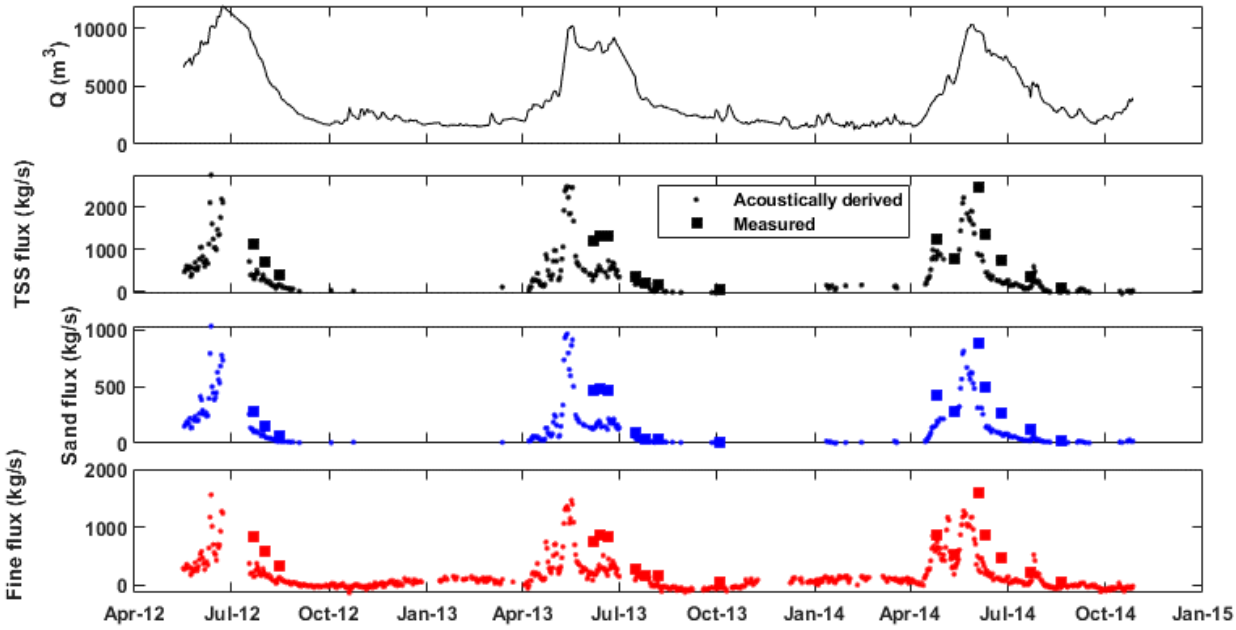

Figure 5. Time-series of flux data with measurements and discharge (top).

Figure 6 shows the relation between discharge and flux. Clearly a hysteretic effect is present. Relations show a clockwise hysteresis, suggesting that flux increases respond before peak discharge. Fine SSC flux shows the greatest hysteretic effect, likely due to an early spring first flush. Sand flux shows a tighter grouping. All three SSC constituents show a non-linear response.

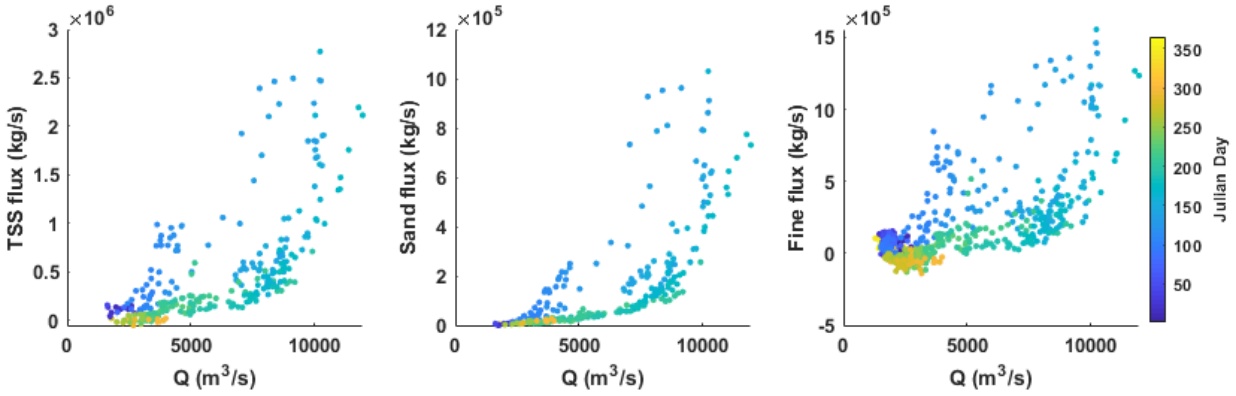

Figure 6. Hysteretic effect from the relation between Q and SSC flux.

Conclusion

Acoustically-derived SSC show that this method can capture the spatial and temporal dynamic that are a contemporary challenge to measure with physical sampling. We show how the direct relation of TSS to fluid corrected backscatter does not produce a strong calibration. This is likely due to the fact that sediment attenuation is not accounted for as it is with sediment corrected backscatter (which is related to sand). The sum of sand and fine sediment flux– both of which

have a better response to acoustics– produces a better result, suggesting that the acoustic inversion is a valid estimate.

When relating the ADCP derived SSC to the channel average SSC, we provide a method for engineers, scientists and river managers to use in large systems where the instrument's range does not span the entire channel or at least a substantial portion of it. The linear relations show strong correlation and fall close to the line of unity. The fluxes from these relations track the flow and measurements well, while occasionally underestimating some measurements. Further measurements at the highest concentrations are needed to further assess these results and methodology.

This application clearly depicts the clockwise hysteretic nature of suspended sediment transport in the Fraser River. The clockwise hysteresis is a function of the spring first flush, where, as the flows rise, finer material stored near the bank is captured by the river and transported prior to the peak flow or sand transport. Once flows reach a threshold flow for sand transport, particularly fine sand, a pulse occurs prior to peak discharge. By the time the peak discharge is reached, there is a depletion of upstream sediment leading to a decline in SSC prior to the falling limb in dishcarge.

These estimates provide engineers and scientists the capability to better manage rivers with respect to dredging for navigable channels, along with the monitoring of sediment adhered pollutants and sediment budgeting.

References

Flammer, G. H., (1962), Ultrasonic measurement of suspended sediment, U.S. Geol. Surv., Bull. 1141-A. Govt. Printing Office, Washington, DC, 48 pp.

Haught, D., J. G. Venditti, and S. A. Wright (2017), Calculation of in situ acoustic sediment attenuation using off-the-shelf horizontal ADCPs in low concentration settings, Water Resour. Res., 53, doi:10.1002/2016WR019695.

Ruhl, C. A., and M. Simpson (2005), Computation of discharge using the index-velocity method in tidally affected areas, U.S. Geol. Surv. Sci.

Invest. Rep., 2005–5004, 41 p., U.S. Geol. Surv., Reston, Va.

Wright, S. A., D. T. Topping, and C. A. Williams (2010), Discriminating silt-and-clay from suspended-sand in rivers using side-looking acoustic

profilers, paper presented at the 2nd Joint Federal Interagency Sedimentation Conference, 27 Jun-1 Jul. Advisory Committee on Water Information, Subcommittee on Hydrology and Sedimentation, June, Las Vegas, Nev. [Available at http://acwi.gov/sos/pubs/2ndJFIC.]

Haught, D., J. G. Venditti, and S. A. Wright (2017), Calculation of in situ acoustic sediment attenuation using off-the-shelf horizontal ADCPs in low concentration settings, Water Resour. Res., 53, doi:10.1002/2016WR019695.

Automated High-Resolution Static Imaging Analysis of Low-Mass Suspended Sand

Daniel J. Gooding, Hydrological Tech., U.S. Geological Survey, Vancouver, WA.
dgooding@usgs.gov
Katherine Norton, Physical Science Tech., U.S. Geological Survey, Vancouver, WA.
knorton@usgs.gov

Abstract

The standard for measuring the physical parameters of discrete sand size particles between 62.5 and 2000 microns has been by sieve analysis. Both dry sieve and wet sieve methods perform exceptionally well when there is sufficient mass to overcome the uncertainties inherent in these methods. Weighing uncertainties, lodged sample particles or dislodging of particles within sieves from prior samples, and sample handling while conducting the sieve analysis are some influences for size distribution precision. These uncertainties can overpower the essential accuracy with low mass samples, giving variable results. As stated by Harold P. Guy, (Laboratory Theory and Methods for Sediment Analysis, 1969) the minimum mass of sand for an accurate sieve analysis is about 0.02 grams. More mass is required if the sample contains particles larger than 1.0 millimeters (mm). Many suspended-sediment samples received by USGS Sediment Laboratories fall below this limit. For the past three years, approximately 8% of suspended sediment samples processed by the 8 USGS Sediment Labs were samples below the recommended weight limit for analysis reliability.
New techniques, either direct or indirect have been long sought out and tested that would be comparable to sieving to produce physical dimensions, with imaging being a promising alternative method.

Introduction

Imaging is a direct method alternative for measuring physical dimensions of discrete particles. When particle size distribution data are approximately between 62.5µm to 2000µm, and the sample mass falls below the limit of 0.02 grams, imaging analysis is a viable particle-size analytical method. When the particles are generally separated, and edges are pronounced, two-dimensional static particle imaging can provide the precision and accuracy comparable to a sieve analysis. Static imaging analysis for sand, dry versus suspended in a liquid, has the benefit of having particles on a single plane, so depth of field (DOF) becomes less of an issue. There is no liquid medium to degrade the particle images, no random particle orientation, and better particle separation.

There are four properties of imaging analysis that are significant for providing accurate results: maximum contrast, particle dispersion/separation, edge gradient that clearly defines discontinuities in the grayscale signal, and sufficient pixels to clearly identify the smallest targeted particles. With the combination of these, the uncertainties will decrease, and results will be reliable.

To discretely measure each particle within a sample and when the field of view is limited to a few millimeters, it can be a tedious task to perform manually and can become susceptible to errors. This paper demonstrates an automated system in which samples can be setup and have the analysis be completed automatically.

Inherently, most particles will orient themselves on the plane surface having their “a” (Maximum) and “b” (intermediate) axes perpendicular to the lens. This allows the image processing to measure the “b” axis which is the axis that determines the finest sieve aperture that will pass or retain the particle. Open-source imaging functions are used to transform the images to produce accurate particle measurement by defining discrete particles and enhancing their edges. Once an image has been simplified by morphological processing, measurements are computed to give a quantitative analysis of the particles that includes size and shape. The data from the individual particles are aggregated to produce a whole sample particle-size distribution. Size distribution by imaging is based on size population within size bins. Each detectable particle is discretely counted.

Materials and method

Equipment

A machine vision camera coupled with an appropriate lens is an essential part of imaging analysis. The lens magnification must provide adequate pixels to identify the smallest particle of interest. The setup for this test uses an Imaging Source monochrome camera, ½ CCD Sony sensor with a 0.5x magnification lens. The field-of-view is 7.68mm x 5.76mm for a 1280 x 960-pixel image, for a minimum target size of 62.5 microns. Approximate working distance equals 18.5 cm. A short-passband wavelength (near the blue side of the visible spectrum) LED backlight is used to create a sharper particle edge and to improve contrast.

A computer numeric control (CNC) table with a carriage using 3 stepper motors, designed to move in a linear path, incrementally pauses equally at each Field of View (FOV) width to capture an image over the entire acrylic imaging plate. The CNC program essentially divides the imaging plate into a matrix of ‘i’ rows and ‘j’ columns. After each move the camera is automatically triggered and image is stored. A single sample may have several hundred images once completed. Once stored, sample images are ready to be processed through the analyzing software.

Particle dispersion across the imaging plate is vital in preventing connecting or overlapping particles that can be interpreted as a single large particle. There are few dispersal methods that are suitable. For this test a micro-splitter was used (Figure 1). Sand size particles are released through the splitter and onto the acrylic imaging plate. The white side panels are to prevent sand grains bouncing off the plate.

Figure 1. Micro-splitter, 2mm vane spacing. Particles pass through the splitter and drop two inches onto the imaging plate. The white panels below the vanes prevent particles from bouncing away from the designated area.

The dispersal of 1.2 grams, 250-500µm sand, is well distributed and ideal for imaging (Figure 2).

Figure 2. Sand size particles after being dispersed. Achieving a comprehensive particle dispersion can prevent misrepresentation of a Particle Size Distribution. Any particles overlapping may be interpreted by the software as a large single particle, biasing the distribution. (note: these particles were dispersed over a white surface and with a standard SLR camera just to show the pattern of particles after dispersion).

Testing

For this test, 20 images were used, and a total of 78 particles were measured. The material used was pre-sieved dry sands between 250-500µm. One of the images displayed (Figure 4), shows five particles, two of which are touching. The software recognized the joining particles as two separate grains. Image processing was conducted using Matrox Inspector 8.0, a commercial image-processing program. The images were binarized using a threshold grayscale value of 128 grayscale units. The software computed the measured properties of the blobs detected in the binarized images.

As a performance check, the software marks the perimeter and the feret diameter for the maximum and intermediate axis (Figure 4 & 5).

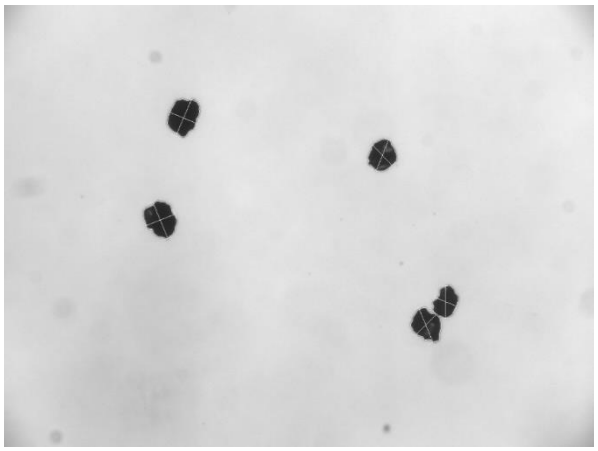

Figure 4. The perimeter and the A and B axis measured by the software are automatically highlighted. Two particles in the lower right were connected. The imaging software did a very good job measuring the particles separately.

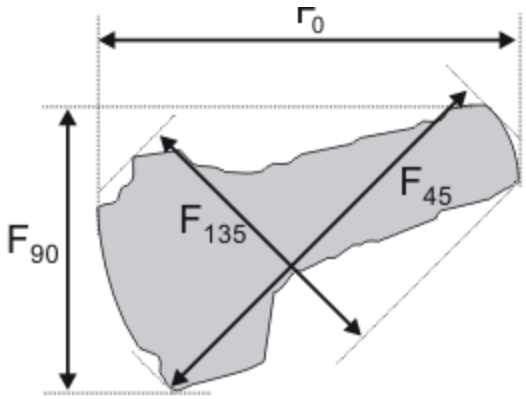

Figure 5. Explanation of the software algorithm for computing feret diameter: "Diameters are determined by checking the Feret diameter of the blob at a specified number of angles. Increasing the number of angles tested increases the accuracy of the results, but also increases the amount of processing time. The maximum Feret diameter is not very sensitive to the number of angles, and 8 angles usually gives an accurate result" (Matrox Electronic Systems Ltd, 2005).

The particle-size distribution for the entire population of 78 particles was computed in a Microsoft Excel spreadsheet. The particles were assigned to a quarter-phi size bin based on the minimum ferret diameter determined by the software. The particle volume of each particle was computed as the volume of a sphere that had a radius equal to the radius of a circle that had the same area as the particle. The volumes of the particles in each size bin were summed to produce the volume in each size class. The volumetric particle-size distribution was then computed based on the estimated volume in each class. As long as there is no systematic difference in the density of the particles with their size, the particle-size distribution produced this way is equivalent to the mass-based particle-size distribution.

Results

The test sample was comprised mainly of particles within 250-500µm. A few particles in the image were found outside of this range, but that was expected from the dry sieve sample used for this test. Generally, the results demonstrate that the imaging analysis did relatively well

(Table 1). Ninety-one percent of the particles in the sample were within the range of 250 - 500µm as shown (Table 1).

Table 1. Imaging data is combined into 1/4phi size bins. Last column shows the cumulative percent finer

Bin Min (retained on)	Bin Max (passing)	Bin Name	Particle count	Est volume in class (um3)	Vol. Percent in bin	Cutoff size (um)	Cumulative percent finer
0	63	<63um	1	0.0002	0.0%	63	0.0%
63	75	63-75um	1	0.0002	0.0%	75	0.0%
75	90	75-90um	1	0.0005	0.0%	90	0.0%
90	106	90-106um	0	0.0000	0.0%	106	0.0%
106	125	106-125um	0	0.0000	0.0%	125	0.0%
125	150	125-150um	0	0.0000	0.0%	150	0.0%
150	180	150-180um	0	0.0000	0.0%	180	0.0%
180	212	180-212um	0	0.0000	0.0%	212	0.0%
212	250	212-250um	2	0.0272	1.0%	250	1.1%
250	300	250-300um	10	0.2070	7.8%	300	8.8%
300	355	300-355um	35	0.8660	32.4%	355	41.2%
355	425	355-425um	18	0.7590	28.4%	425	69.7%
425	500	425-500um	8	0.5906	22.1%	500	91.8%
500	600	500-600um	1	0.0972	3.6%	600	95.4%
600	710	600-710um	1	0.1220	4.6%	710	100.0%
710	850	710-850um	0	0.0000	0.0%	850	100.0%
850	1000	850-1000um	0	0.0000	0.0%	1000	100.0%

Conclusion

The test sample demonstrated in this paper did not incorporate organic particles, though one image did show a single blob that was visually confirmed as organic material. The software excluded this organic particle. Organic material usually has its own visual signature: elongated, unusual angles (contour smoothness), features like narrow or thin (compactness), and semi-transparent. Special imaging processes can filter these out from the images prior to the calculations. In some cases, particles may be connected to organic materials. In those situations, it is very difficult for the imaging algorithm to interpret. This can greatly bias the results. As the imaging software development progresses, it will be able to mark particles having some level of uncertainty and give the analyst the opportunity to visually inspect the point in question and decide whether to eliminate the particle from the results.

Initial results show imaging analysis can be a viable method for producing a particle size distribution for light mass sediment samples. Both dry and wet sieving methods have fundamental uncertainties. This doesn't exclude imaging analysis. What is important is to know what those uncertainties are. Four important factors can skew the results in static imaging: orientation of the particles (both "a" & "b" axis must be viewable); overlapping or connecting particles; clearly defining particle edges; and the presence of organic material, each will contribute to the sample result uncertainties.

One of the main strengths of the imaging analysis for sand is that it can produce high-resolution particle size distributions for the sand fraction, even when there is too little sand for a reliable sieve analysis (<0.0200 grams, Guy, 1969). The recent publication of the multi-frequency acoustic surrogate method (Topping and Wright, 2016) is likely to increase demand for high-resolution PSD analysis of the sand fraction because one of the inputs to the surrogate model is the d50 of the suspended-sand fraction. Suspended-sediment samples frequently have too little mass for sieve analysis of the sand fraction; imaging analysis can possibly fill this emerging need.

References

Matrox Electronic Systems, Inc., 2005, Matrox Inspector 8.0 User's Manual.

Topping, D.J., and Wright, S.A., 2016, Long-term continuous acoustical suspended-sediment measurements in rivers—Theory, application, bias, and error: U.S. Geological Survey Professional Paper 1823, 98 p., http://dx.doi.org/10.3133/pp1823.

Bedload Sampling to Support Surrogate Technology (Impact Plate) Calibration following Elwha River Dams Removal, Olympic Peninsula, WA

Aaron (Smokey) Pittman, Fluvial Geomorphologist, McBain Associates, Placerville, CA, smokey@mcbainassociates.com
Robert Hilldale, Hydraulic Engineer, US Bureau of Reclamation, Denver, CO, rhilldale@usbr.gov

Abstract

Removal of the Elwha River dams (2011-2014) represents the largest dam removal and intentional sediment release in history. Approximately 21 million (+/- 3 million) cubic meters (m^3) (Magirl et.al. 2015, Ritchie et. al. 2018) of stored sediment were exposed to potential fluvial erosion, presenting a unique opportunity to develop emerging bedload-surrogate technologies. Downstream of the dam removal sites, the US Bureau of Reclamation constructed a river-wide impact plate system for the purpose of continually measuring coarse bedload. Bedload samples are required to calibrate the continuous voltage signals and to quantify bedload sediment discharge. A cableway was constructed immediately upstream of the weir and a cataraft was deployed between 2012 and 2016 to collect bedload data using a 12-inch-wide (30.48 cm) Toutle River-2 (TR-2) bedload sampler.

Total bedload discharge across the entire channel width was measured using both the USGS single-equal width increment (SEWI) and unequal width increment (UWI) methods. Due to (1) extraordinarily high transport rates, (2) very high variability at-a-station (i.e. at a plate), and (3) the need to develop at-a-station temporal averages (to calibrate an individual plate), the SEWI method for bedload sampling was modified.

During the first measured events, bedload transport was dominated by very fine sediment and organic matter. Subsequent events signaled the arrival of coarser (>16mm) grain. Delivery of large woody debris, which represents obvious safety concerns, subsided over the study period. Median measured grain sizes varied by event and over time and appeared to be connected to supply properties rather than discharge magnitude. At-a-station bedload discharge ranged from zero to over 900 g/s (per 30.5 cm, the width of the sampler) within an individual 30-minute sampling period. These findings suggest that in extreme sediment loading scenarios, the SEWI method may not be adequate to accurately describe bedload transport. A companion paper by Hilldale et. al. (this volume) provides additional details on the bedload sampling and the impact-plate system.

Introduction

The Elwha River, located in northwest Washington state, primarily within Olympic National Park, endured over 100 years of impoundment following the construction of Elwha Dam in 1912 (Figure 1). Lacking fish passage structures, the dam limited anadromous salmonid access to the lower-most 8.1 km of the river. Construction of Glines Canyon dam in 1927, 12.9 km upstream of Elwha dam, further impacted the river. Beyond simply blocking fish access, the dams impacted the ecosystem in numerous ways, not the least of which was by trapping sediment delivered

from most of the watershed. By the time the dams were slated for removal in 2011, approximately 21 +/- 3 million m^3 (30 Mt) of sediment had accumulated within the reservoirs and their associated deltas (Magirl et.al. 2015, Ritchey et. al. 2018).

Removal of the Elwha River dams (2011-2014) represents the largest dam removal and intentional sediment release in history (Magirl et al. 2015). According to USGS geomorphologist Andrew Ritchie, "(t)he removal of both dams on the Elwha River released a sediment volume 5-fold greater than the next-largest dam removal, creating a fluvial sediment pulse comparable in sediment source area, sediment yield, and watershed area to that of rivers affected by the 1980 Mount Saint Helens volcanic eruption." Intentionally exposing 21 million m^3 of stored sediment to potential fluvial erosion presented a unique opportunity to develop emerging bedload-surrogate technologies. Downstream of the dam removal sites, the US Bureau of Reclamation constructed a river-wide impact plate system located immediately below a concrete weir for continually measuring coarse bedload using an acoustic surrogate (Hilldale et al. 2015). The plate system was keyed into the newly constructed Elwha River Surface Water Intake (ESWI) system, located 2.25 km below the downstream- most dam removal site (Figure 2). The system consists of 72 stainless steel impact plates, 46 of which are instrumented with geophones and 26 are instrumented with accelerometers (Figure 3, 4). A companion paper by Rob Hilldale et. al. (US Bureau of Reclamation, USBR), *Calibration of the Elwha Impact Plate System,* is presented in this conference and further details the specifics of the impact plate system.

Bedload surrogates evolved in response to the need to account for the temporal variability inherent in bedload sediment transport and the difficulty in accurately measuring bedload using conventional sampling techniques (Gray, 2010). A conundrum arises in that surrogate technologies typically require calibration by the conventional methods they are intended to replace (e.g. pressure difference bedload samplers). Thus, the limitations and consequent uncertainty in bedload discharge measurements derived from pressure-difference sampling can propagate in the form of poor calibration data sets.

Bedload data were collected by Graham Matthews and Associates (GMA 2014, 2016) under the direct supervision of USBR during six discrete transport events between 2012 and 2016. Numerous other data types were collected during sampling efforts, including: discharge measurement, ADCP deployment, velocity profiling, water surface slope measurement, continuous turbidity measurement, passive hydroacoustic data collection, and suspended sediment concentration sampling. This paper presents observed bedload transport phenomena from the Elwha impact plate calibration efforts. We describe our approach to mitigating the problems we encountered and discuss the implications for traditional techniques of collecting bedload transport data.

Figure 1. Elwha River location map.

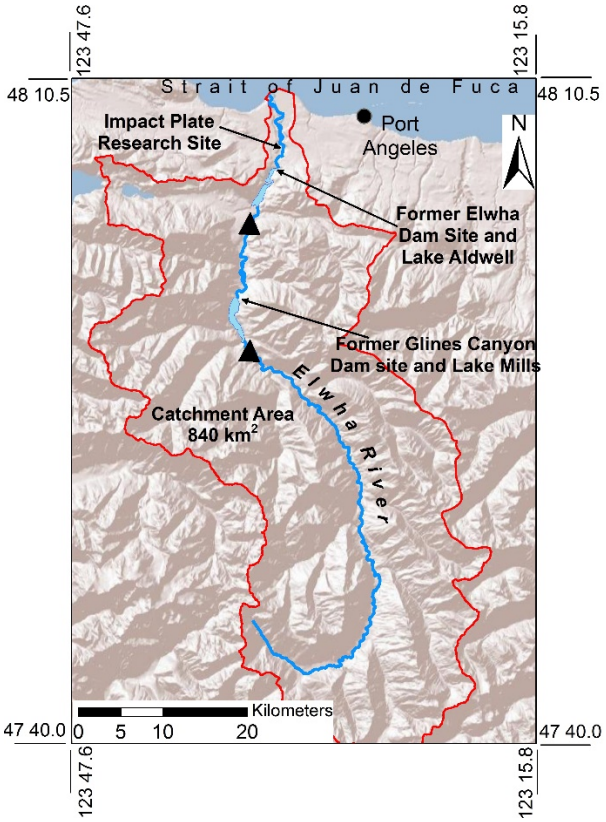

Figure 2. Elwha River bedload sampling (Impact Plate Research Site at ESWI) location map. Triangles represent the location of gaging stations. Northern gage is USGS 12045500 Elwha River at McDonald Br., southern gage is USGS 12044900 Elwha River above Lake Mills.

Figure 3. Aerial view of the weir at ESWI (2008) after installation. Flow is from right to left. Low flow notch is evident along the margin of the concrete structure (photo courtesy Andy Ritchie, USGS).

Figure 4. Pre-dam-removal view from the ESWI structure looking across the weir in July 2010. Flow is left to right, 28.3 cms. The plates can be seen beneath the hydraulic jump at the crest of the riffle.

Methods

Bedload Sampling

The primary goal of the bedload measurement aspect of the project was to calibrate individual impact plates, not obtain a complete bedload discharge across the channel (though we did collect some full cross section bedload measurements). A temporary cableway was constructed immediately upstream of the weir and a cataraft was deployed during six discrete transport events between 2012 and 2016 for collecting bedload sample data (Figure 5). The cataraft sampling system deployed samplers using a crane and an electric winch. This system facilitated precise placement of a 12-inch-wide (30.5 cm) Toutle River-2 (TR2) pressure-difference bedload sampler as close as two meters upstream of individual plates (Figure 6). The cable-deployed TR-2 is 1.52 m long and is widely used for bedload sampling, offering superior performance to the better-known cable-deployed Helley-Smith for river systems exhibiting bi-modal grain size distributions in bedload (large particles and high sand loads -- Childers 1999, Pittman 2005). Mesh sampler bags were constructed of a 2mm mesh. Downtimes (periods when the sampler was resting on the bed) were adjusted to minimize backwatering of the nozzle. Any lateral drift was accounted for in the recorded stationing. Whenever poor touchdowns or liftoffs occurred, the sample was discarded and re-initiated to insure sample quality.

An initial point was established on the concrete wall at river right and was used as a stationing reference for all measurements. Data are presented at-a-station (single vertical) and stationing is expressed as distance from the wall. For full cross section measurements, the single-equal width increment (SEWI) and unequal width increment (UWI) methods, as developed by the USGS and as described in Edwards and Glysson (1999), were used. Beginning and end stations, sample interval, sample duration, start time and end time, beginning and end gage height, and pass number were recorded (if relevant). Samples were assigned a unique identifier (e.g “EM79”), then later assigned a sample number reflecting the number of samples to date (e.g. “2013-125”).

Bedload Sample Analysis

Bedload samples were processed for total mass and a half-phi grain size analysis (down to 2mm) at the GMA coarse sediment laboratory in Placerville, California. Products from the coarse sediment lab analyses included: cumulative frequency distribution of grain sizes, size fraction computations, mass by various size ranges, largest particle in the sample and total mass.

Total bedload discharge across the entire channel width was computed on occasion using the mid-section method applied to either the SEWI and UWI measurements (Edwards and Glysson 1999). However, due to (1) extraordinarily high transport rates, (2) very high variability at-a-station (i.e. at a plate), and (3) the need to develop at-a-station temporal averages (to calibrate an individual plate), the SEWI method for bedload sampling was modified. Samples were collected repeatedly at-a-station for 30+ minute intervals, utilizing downtimes ranging from as little as 5 seconds (at very high transport rates) to over two minutes (at very low transport rates). At-a-station bedload discharge was then computed as mass per unit time over the width of interest (e.g. the width of the sampler nozzle or the width of an individual plate).

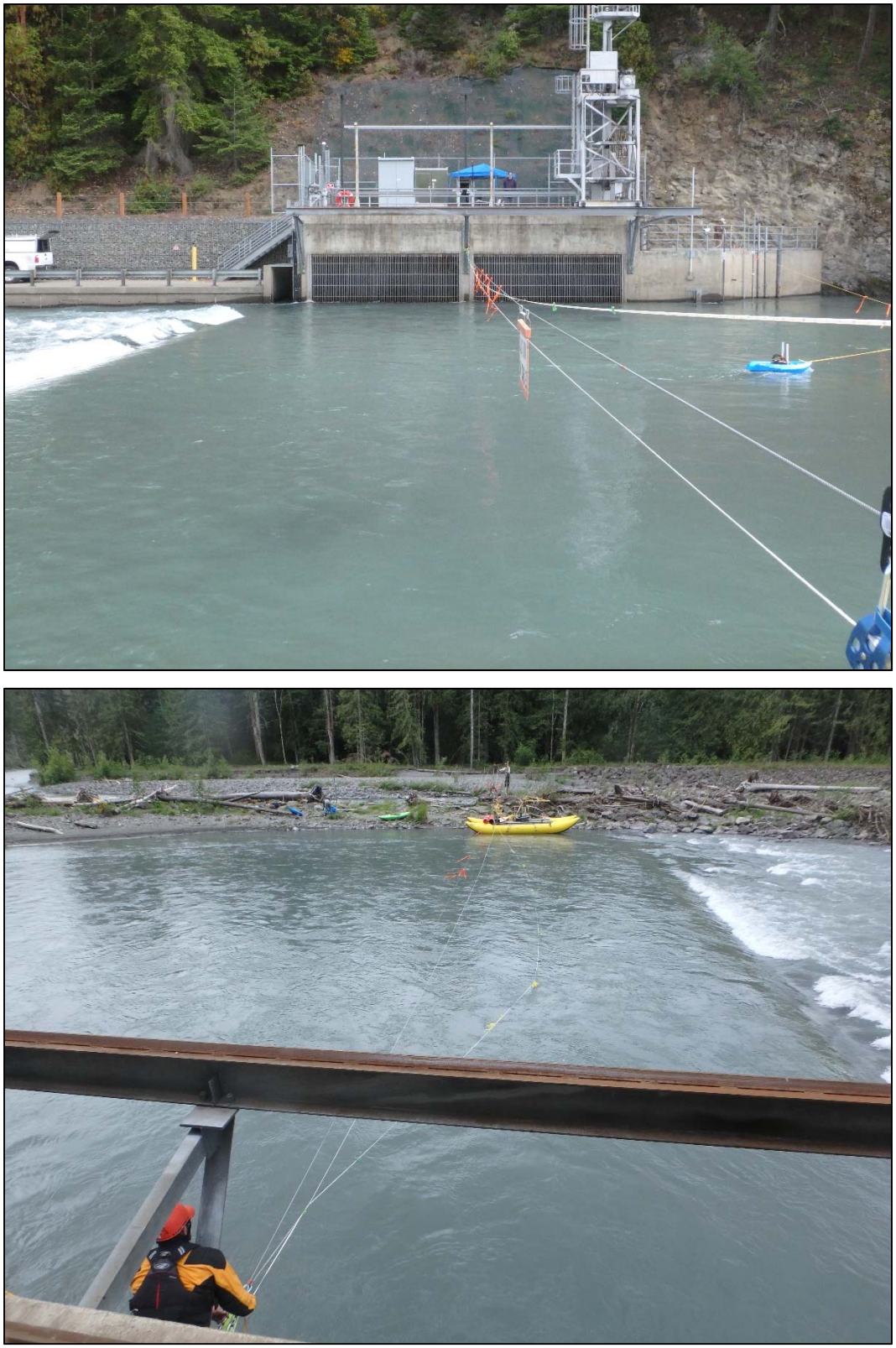

Figure 5. Cross-stream views of the temporary cableway utilized to deploy the cataraft at ESWI. Top photo is from the left bank and bottom photo is from the right bank, May 26, 2016. Discharge is 45.3 cms.

Figure 6. Clockwise from top left: Downstream view of the sampling section as viewed from the ESWI concrete structure (courtesy Chris Magirl, USGS); TR-2 sampling at very low flow with plates in the background; and two views of the TR-2 cable-deployed sampler at work.

Results and Discussion

Bedload Sampling Summary

Some of our results are revisions to the methods discussed earlier. We present those revisions in this section (rather than in "Methods") to promote readability. Between October 2012 and May 2014, bedload samples were collected at discharges ranging from 49.3 to 106 cms (Figure 7). An additional sampling effort was conducted in May 2016 at approximately 45.3 cms. However, no meaningful bedload was measured in May 2016 due to extremely low transport rates. During the first measured events in November 2012, bedload transport was dominated by very fine sediment and organic matter; unusual dunes and abnormal velocity profiles were measured. Dam-notch removals appeared to be correlated with increases of fine sediment delivery. Subsequent high-flow events signaled the arrival of coarser (>16mm) grain sizes and lower dune amplitudes were observed. Delivery of large woody debris (logs), which represent obvious safety concerns, subsided over the study period. Median measured grain sizes varied by event and over

time and appeared to be connected to supply properties rather than discharge magnitude. A summary of sampling events and the range of sampled discharges is provided in Table 1.

Table 1. Elwha River at ESWI: Bedload Sampling Events 2012-2016

DATE RANGE	RANGE OF DISCHARGES SAMPLED (cms)	RANGE OF DISCHARGES SAMPLED (cfs)
November 27-28, 2012	49.3 to 58.9	1,740 to 2,080
March 13-15, 2013	70.8 to 106	2,500 to 3,740
May 13-15, 2013	73.6 to 101	2,600 to 3,560
June 12-13, 2013	54.7 to 60.6	1,930 to 2,140
April 23-24, 2014	56.6 to 70.8	2,000 to 2,500
May 23-26, 2016	45.3 to 46.6	1,600 to 1,640

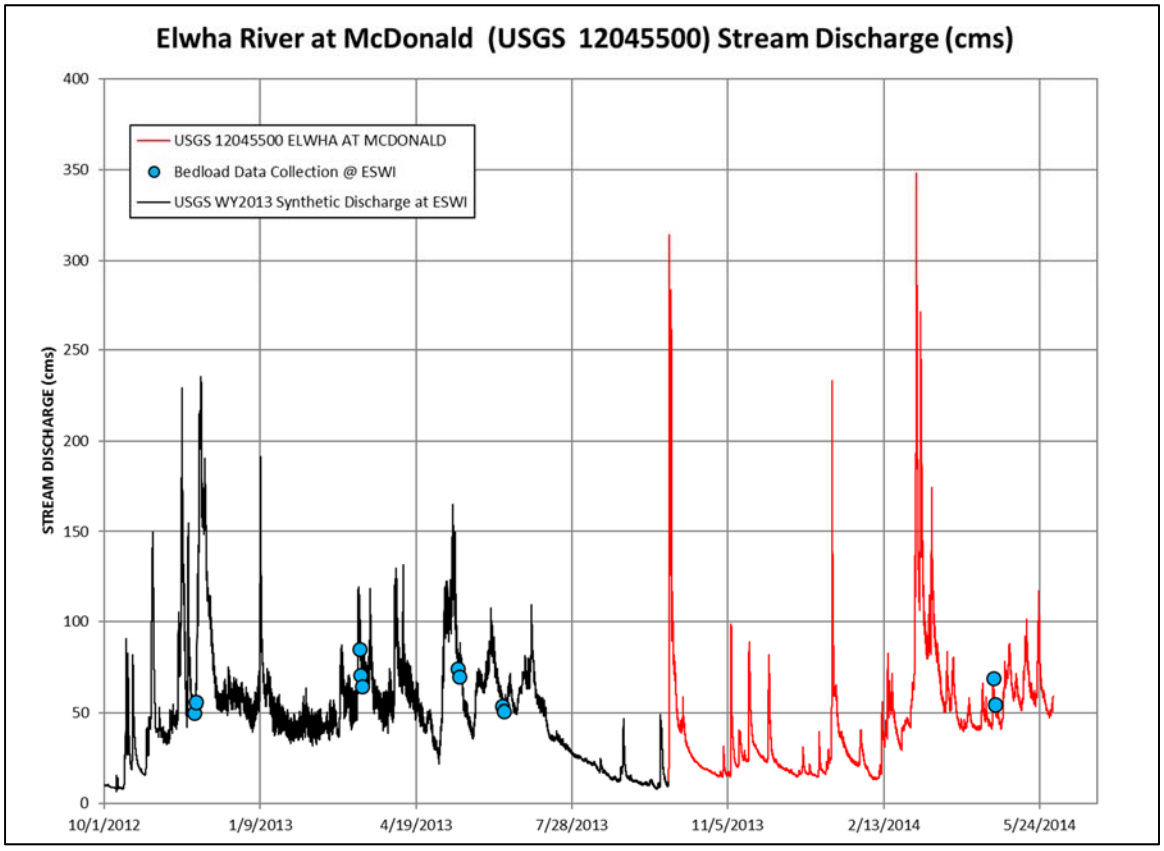

Figure 7. 2012-2014 bedload data collection efforts at ESWI.

We made very few (n=10) full cross section bedload discharge measurements, thus we cannot provide a robust examination of changes in bedload discharge rates over time, though the surrogates may ultimately provide this. Because the sampler mesh was 2mm, we subtracted this fraction from bedload computations. The >2mm bedload discharge for the 10 full cross section measurements from 114 to 10.4 million kg/day (10.9 to 11,500 tons/day) (Figure 8). Bedload

computations used for calibration of the impact plates only included particles >16 mm, the minimum detectable size of the system.

In addition to the full cross section measurements, we collected 378 measurements at-a-station with sample down times ranging from 5 seconds (during very high transport events) to 30 minutes (during near-zero transport events). Of these 378 individual measurements, approximately 320 were utilized in 30-minute sampling periods of repeat sampling at-a-station. The full cross section and at-a-station measurements provided (1) calibration data for the impact plate study, and (2) insight into bedload transport dynamics at ESWI: spatial variability, short-term temporal variability and changes in bedload grain size composition over the study period.

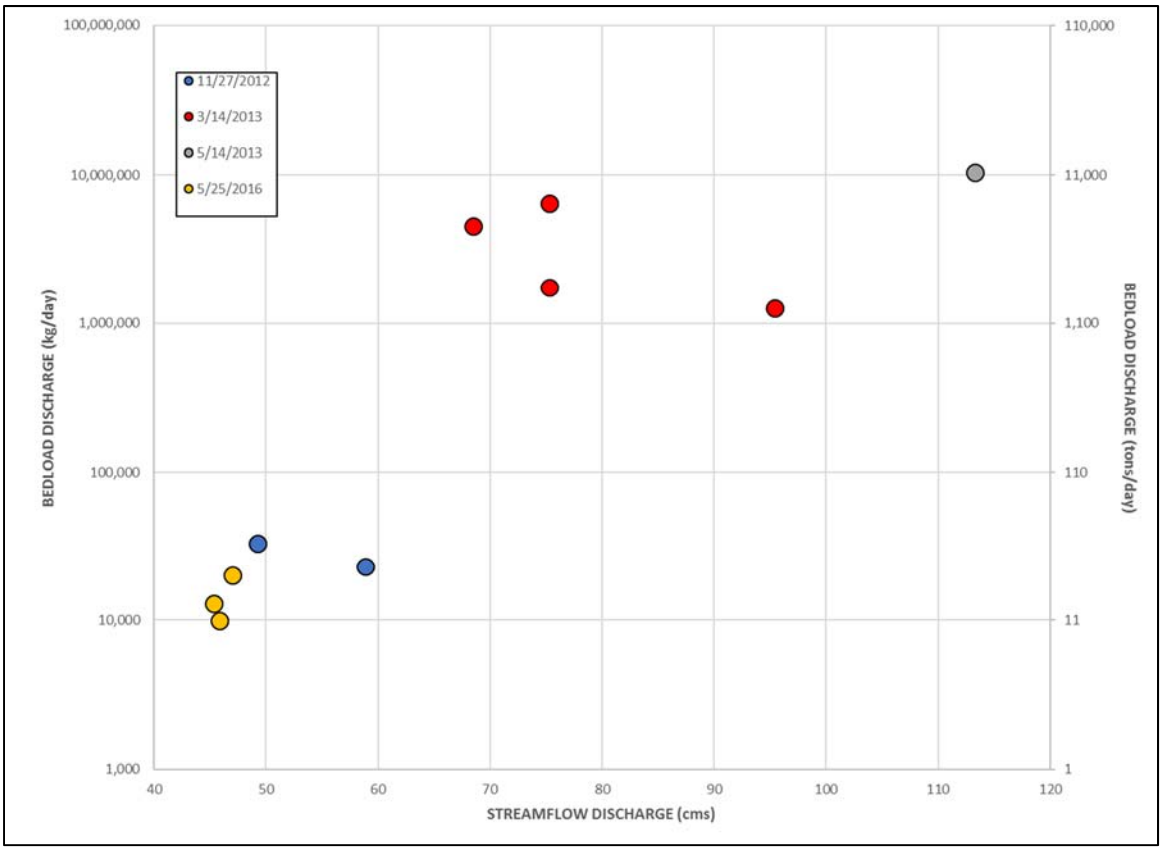

Figure 8. 2012, 2013 and 2016 >2mm (full cross section) bedload discharge at ESWI.

Bedload Discharge: Spatial Variability

For a subset of full cross section measurements, we collected and analyzed each vertical (sampling location along the section, measured in meters from the wall), which facilitated examination of variability across the section. Bedload discharge was typically dominated by a 5.4 m wide strip along the wall (right bank). Figure 9 illustrates an example from May 2014 where 47 percent of the entire measured (>2mm) load was transported in this strip. Twenty six percent of the measured load occurred at the third station from the wall (7.7 m).

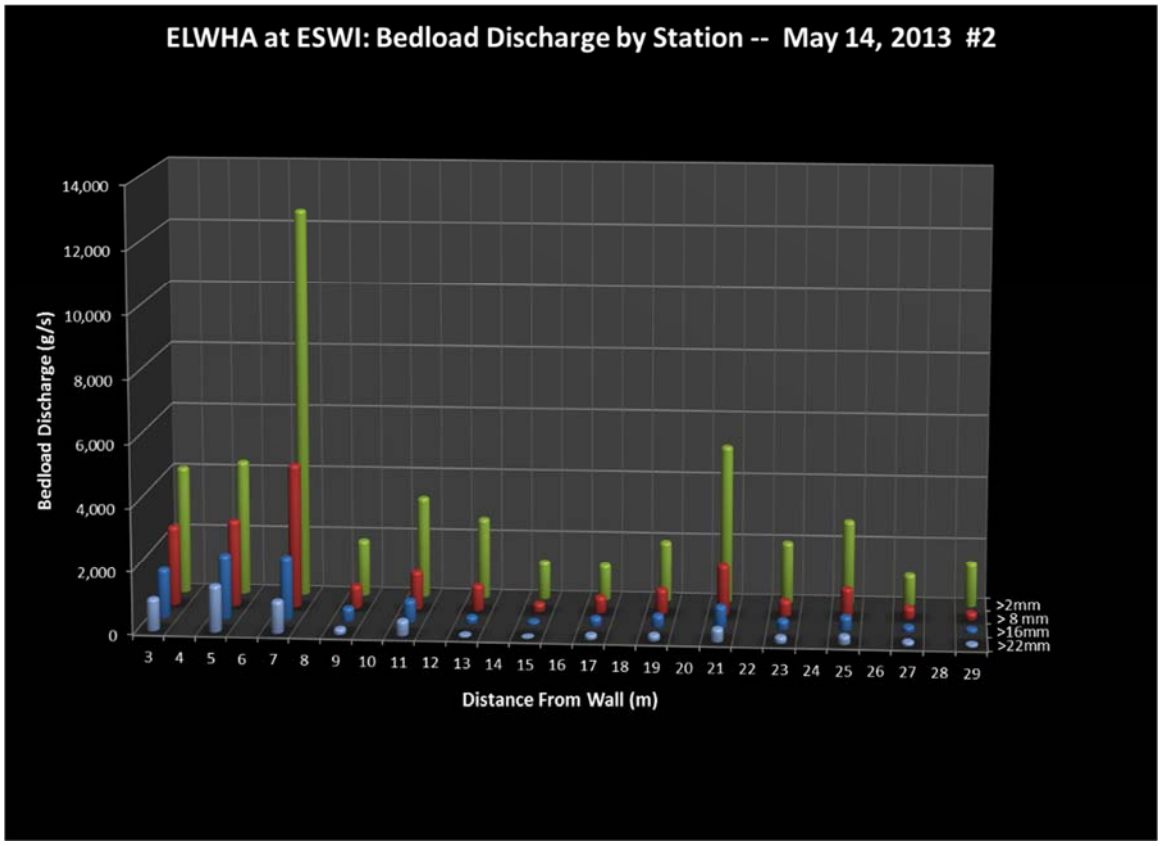

Figure 9. Cross sectional variability in bedload transport for four size classes, measured in May 2013 at 101 cms.

Bedload Discharge: Temporal Variability

For the November 2012 and March 2013 sampling events, we conducted individual plate measurements (single vertical, single sample) and full cross section measurements that were not used for calibration, thus these data are not included in this section. In May 2013, we began at-a-station repeated-bedload discharge measurements. These measurements were typically conducted over the course of 30 to 60 minutes and contained 8 to 18 individual measurements. Sampler down times ranged from 5 to 120 seconds and bedload discharge was computed over the width of the sampler, 30.5 cm. Most of the sample data from June 2013 were not analyzed as the impact plate computer system failed during the sampling event. The May 2016 data are presented separately, as streamflow barely exceeded the bedload threshold of mobility (~45 cms).

For the May 2013 and April 2014 events, collected at flows between 56.6 and 101 cms, at-a-station bedload discharges ranged from zero to over 4,000 g/s (Figure 10). If we ignore the zero transport values, the measured ranges span approximately an order of magnitude, though two sample sets (at Stations 12 and 30) spanned two orders of magnitude (Figure 10). Between the April 2014 sampling event and the April 2016 sampling event, at least nine flow events exceeded 283 cms and two exceeded 566 cms. The largest of these, at 733 cms on December 17, 2015, approximated the 20-year peak flood magnitude (Duda et. al., 2011). It seems likely that these very high flows evacuated a significant proportion of the fine bedload from the system. The May

2016 samples were collected at approximately 45 cms which barely exceeded the mobility threshold for gravel >2mm and measured bedload discharges were considerably smaller than those measured in 2013-2014: they ranged from zero to 5.6 g/s (Figure 11). Again, excluding zero transport values (note the change in scale in Figure 11), sample sets typically spanned approximately an order of magnitude). Stations 16 and 24 however, spanned more than two orders of magnitude.

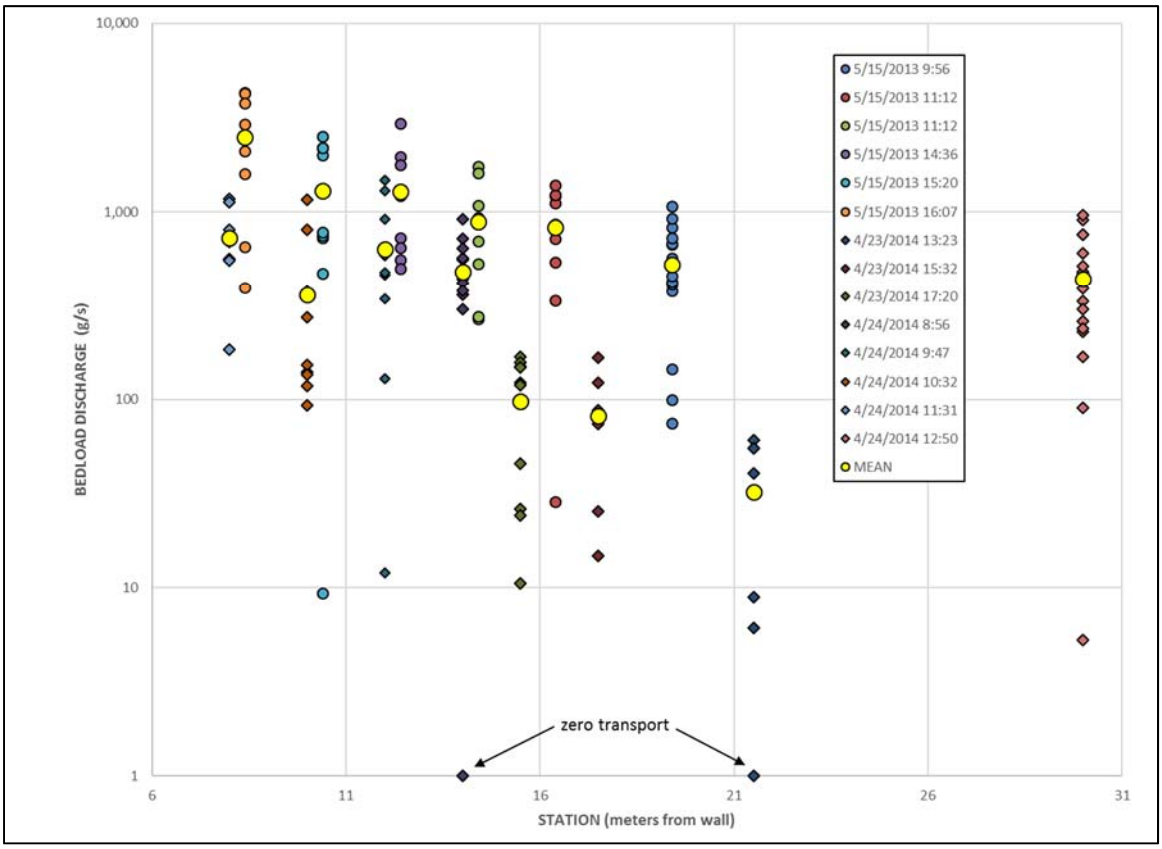

Figure 10. At-a-station >2mm bedload discharge collected May 2013 (73.6 to 101 cms) and April 2014 (56.6 to 70.8 cms). Individual colors represent measurements collected during a 30-minute period. Zero transport values are rounded up to 1.0 for plotting purposes.

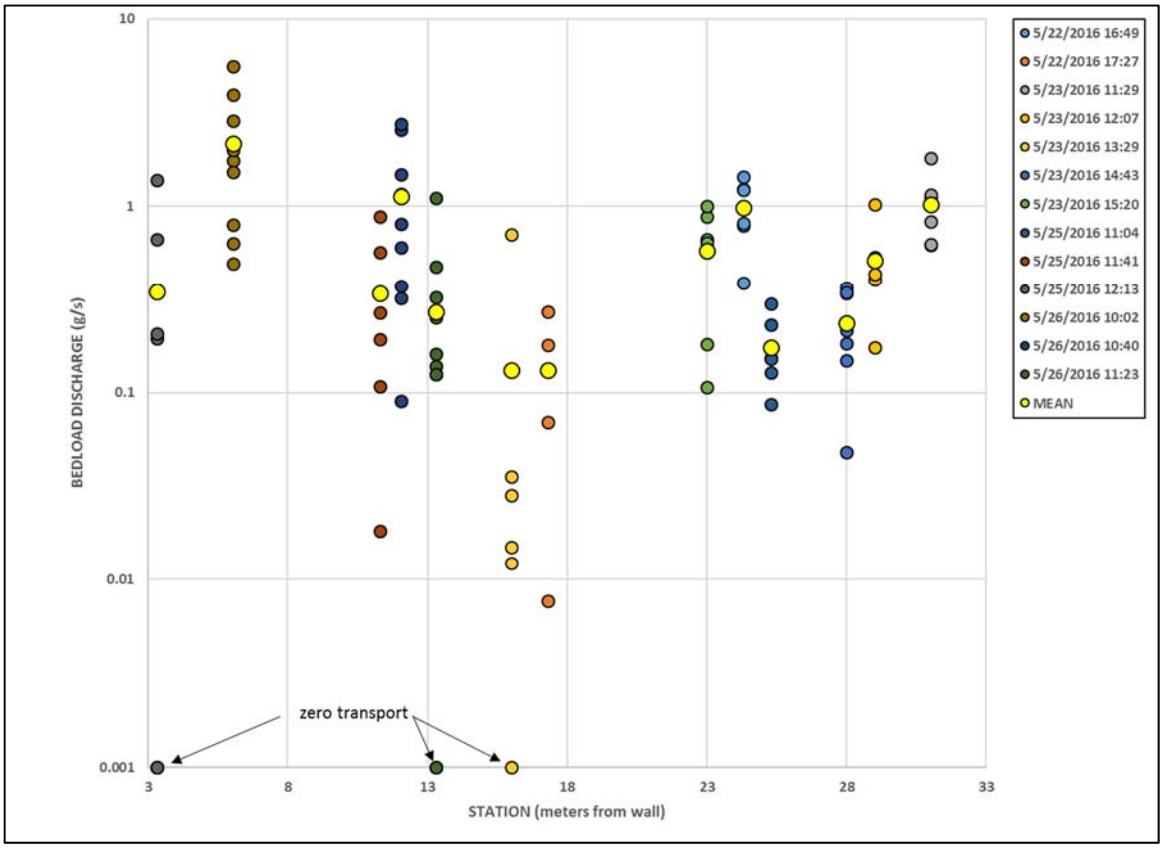

Figure 11. At-a-station >2mm bedload discharge collected May 2016 (~45.3). Individual colors represent measurements collected during a 30-minute period. Zero transport values are rounded up to 0.001 for plotting purposes.

Bedload Discharge: Changes in Composition

During the November 2012 sampling event, bedload discharge was dominated by the preponderance of very fine sediment and organic matter. Despite the mesh sizes of 2mm, up to 96% of the sediment trapped in the sample bag was < 2mm (due to transport rates exceeding the rate at which the sample bag could pass sediment <2mm). This "residual" volume, though not expressly measured, serves as an index for the decrease in fine sediment delivery over the sampling period. In November 2012, on average (n=13), more than 95 percent of the sampled load was comprised of material <2mm. By March 2013 (n=47) the average-sample-percentage <2mm had dropped to 39 percent. By May 2013 (n=87), it was 20 percent, and by June 2013 (n=15) it was 15 percent and by April 2014 (n=85), the percent of samples <2mm had dropped to 8 percent.

Grain size analyses from samples collected between 4 and 8 meters from the wall show a progressive increase in the D50 (Figure 12). The D50 was approximately 0.5mm in November 2012 and by March and May 2013, had increased to over 4mm. The following summer (2014) the D50 had increased to nearly 7mm and by 2016, had increased to 33mm (Figure 12). Even though the samples were collected over a range of discharges, the data in Figure 12 serve to illustrate the decreasing percentage of sand over the study period.

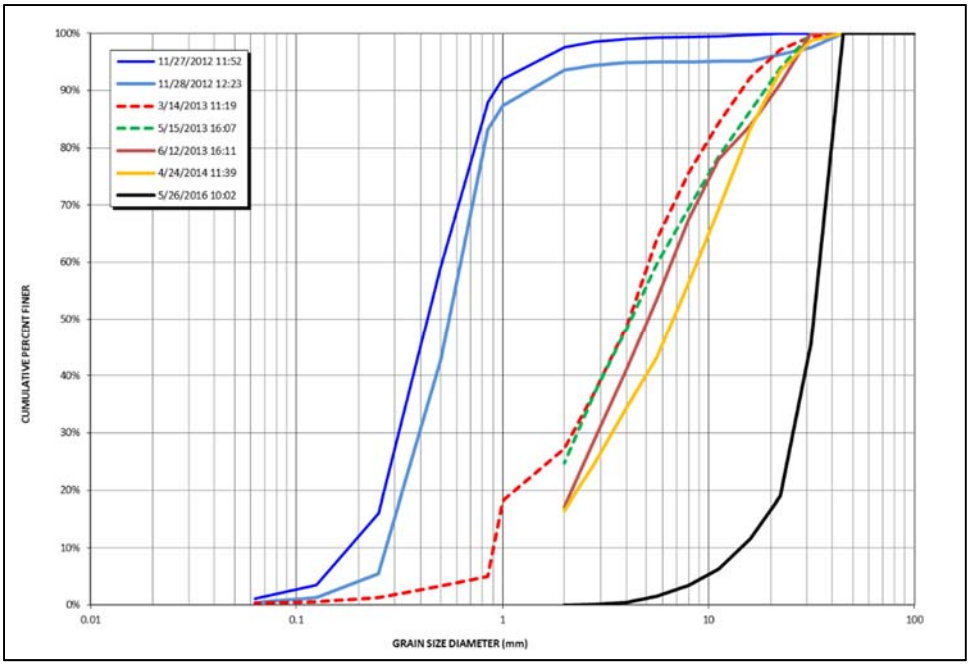

Figure 12. Grain size analyses for samples collected near the wall on the right side of the weir: 2012-2016. Sampled discharges ranged from 45.3 to 106 cms.

Implications

While our objectives were primarily to collect at-a-station measurements, the observations we made have implications for others collecting full cross section bedload measurements using the conventional SEWI technique. We documented that nearly half (47 percent) of the total bedload can be transported in only 20 percent of the channel width and that bedload can vary up to two orders of magnitude and may even drop to zero at times. Repeated sampling at high-transport sections (determined during a full cross section measurement) could reduce potential error estimates for bedload sampling. Longer sampler downtimes can help to reduce uncertainty by capturing more of the temporal variability in each sub-sample. On the Elwha, on some occasions, the extremely high fine sediment component of the bedload prevented increasing downtimes beyond 5 seconds. A longer sampler body which could accommodate a longer sampler bag could mitigate this problem, as might a coarser mesh. In practice it is seldom possible to spend the extra time required to perform repeat measures: debris load, storm peak flashiness and need to collect as many full cross-section samples as possible all tend to preclude efforts to measure variability in bedload discharge. These issues illustrate the importance and the promise of developing surrogate technologies.

References

Childers, D., 1999. “Field Comparisons of Six Pressure-Difference Bedload Samplers in High Energy Flow,” U.S. Geological Survey Water Resources Investigations Report 92-4068, 59 p.

Duda, J.J., Warrick, J.A., Magirl, C.S., (2011). “Coastal and lower Elwha River, Washington, prior to dam removal—History, status, and defining characteristics”. In: Duda, J.J., Warrick, J.A., Magirl, C.S. (Eds.), Coastal Habitats of the Elwha River, Washington—Biological and

Physical Patterns and Processes Prior to Dam Removal: U.S. Geological Survey Scientific Investigations Report 2011-5120, pp. 1–26.

Edwards, T.K., and Glysson, G.D., 1999. Field methods for measurement of fluvial sediment: U.S. Geological Survey Techniques of Water-Resources Investigations, Book 3, Applications of Hydraulics, Chapter C2.

Graham Matthews & Associates, 2014. Elwha River Sediment Transport Monitoring 2012-2014. Final Report to US Bureau of Reclamation, Denver, CO.

Graham Matthews & Associates, 2016. Elwha River Sediment Transport Monitoring 2016. Final Report to US Bureau of Reclamation, Denver, CO.

Gray J.R., Laronne J.B., Marr J.D.G. (eds). 2010. Bedload-surrogate Monitoring Technologies, US Geological Survey Scientific Investigations Report 2010–5091. US Geological Survey: Reston, VA. http://pubs.usgs. gov/sir/2010/5091/

Hilldale, R.C., Carpenter, W.O., Goodwiller, B., Chambers, J.P. and Randle, T.J. (2015). "Installation of impact plates to continuously measure coarse bedload: Elwha River, Washington, USA", J. Hydraulic Eng., Vol. 141, Issue 3, March, DOI: 10.1061/(ASCE)HY.1943-7900.0000975.

Magirl, C.S., Hilldale, R.C., Curran, C.C., Duda, J.J., Straub, T.D., Domanski, M., Foreman, J.R. (2015). "Large scale dam removal on the Elwha River, Washington, USA: Fluvial sediment load", Geomorphology, 246, pp. 669-686, DOI: 10.1016/j.geomorph.2014.12.032

Pittman, S.A. 2005. Water Year 2005 Technical Memo #1, TOUTLE RIVER-2 Bedload Sampler. Report for US Department of the Interior, Bureau of Reclamation, Trinity River Restoration Program, Shasta Lake, CA.

Ritchie, A.C., Warrick, J.A., East, A.E., Magirl, C.S., Stevens, A.W., Bountry, J.A., Randle, T.J., Curran, C.A., Hilldale, R.C., Duda, J.J., Gelfenbaum, G.R., Miller, I.M., Pess, G.R., Foley, M.M., McCoy, R., and Ogston, A.S. (2018). "Morphodynamic evolution following sediment release from the world's largest dam removal", *Scientific Reports*, 8:13279, DOI: 10.1038/s41598-018-30817.

Field Calibration of the Swiss Plate Geophone System at the Albula Stream and Comparison with Controlled Flume Experiments

Tobias Nicollier, Swiss Federal Research Institute WSL, Switzerland, tobias.nicollier@wsl.ch
Dieter Rickenmann, Dr., Swiss Federal Research Institute WSL, Switzerland, dieter.rickenmann@wsl.ch
Arnd Hartlieb, Dr., Obernach Research Institute, Technical University of Munich, Germany, arnd.hartlieb@tum.de

Introduction

The Swiss plate geophone (SPG) system is a bedload surrogate monitoring technique that has been calibrated in several mountain streams to quantify bedload transport (Rickenmann, 2017). The amplitude of the signal recorded by the SPG contains information about the grain-size distribution of the transported bedload. However, determination of bedload transport with the impact plate system ideally requires calibration with direct bedload sampling in the field. At the Albula stream in Switzerland, bedload samples were collected with a large net attached to a steel-frame and operated from a crane. These measurements were compared with the signal of the impact plate geophone system to convert the signal information into bedload transport rates. In addition, a set of controlled real scale experiments was performed at the outdoor flume facility of the Oskar von Miller institute in Germany. The reconstruction of the field conditions met at the Albula stream enabled to investigate various individual aspects influencing the measurement accuracy of the Swiss plate geophone system.

This study is the first step of a project that aims to investigate more in depth various individual aspects influencing the measurement accuracy of the Swiss plate geophone at different field sites, starting with the Albula stream. The objectives of this contribution are: (i) to briefly introduce the Swiss plate geophone system and the amplitude histogram method used to estimate the bedload flux for different grain size classes; (ii) to present the field calibration measurements conducted at the Albula field site; (iii) to describe the controlled flume experiments; and finally (iv) to discuss some results from both sets of calibration measurements and potential errors emerging during their interpretation.

The Swiss Plate Geophone System

Indirect impact measuring systems have been intensively used and developed over the last decade to estimate bedload transport in mountain streams. They have the advantage of providing continuous records of the transport activity both in time and over a cross-section. One of them, the Swiss plate geophone system, has been successfully deployed to quantify bedload transport intensity in several steep streams mainly in Switzerland and Austria (Rickenmann, 2017; Wyss et al., 2016a, b, c). The system consists of geophones fixed under a series of steel plates of standard dimensions embedded along the transect of a stream. While the Japanese pipe microphone (hydrophone) (Mizuayama et al., 2010a, b) and the hydrophone (Geay et al., 2017) both record an acoustic signal generated by an impact on a structure or between the grains, the SPG system records a seismic signal, i.e. vibrations of an elastic medium, generated when bedload particles slide, roll or saltate over a steel plate. The current induced by the geophones is proportional to their vibration velocity (Rickenmann et al., 2014).

Wyss et al. (2016a) developed a method to derive the transport rate as a function of the grain size based on the amplitude of the seismic signal, the amplitude histogram (AH) method. This method relies on the assumption that the amplitude (in Volts) of the seismic signal correlates with the size of the impacting grains. Seven amplitude classes *j* were defined, each corresponding to a defined grain size fraction and amplitude-thresholds. Whenever the signal exceeds one of these thresholds, an impulse is recorded and the summed impulse counts IMP_j are stored for a given time interval and for a given amplitude class *j*.

Assuming that the number of impulses is related to the number of transported particles, a calibration coefficient α was defined for every amplitude class *j* so that:

$$\alpha_{imp\_i,j} = \frac{IMP_{i,j}}{N_{i,j}} \qquad (1)$$

Where $IMP_{i,j}$ is the number of impulses registered for an amplitude class *j* for a bedload sample *i,* and $N_{i,j}$ is the number of particles constituting the different fractions (s. also Wyss et al., 2016a; Rickenmann et al., 2018). The number of particles per grain-size class is determined with a power law relation between the mean weight and the mean diameter for each grain-size class, which was empirically determined for bedload particles sampled at the Albula stream.

Calibration measurements by direct bedload sampling at the Swiss Erlenbach stream were necessary to develop the AH method, i.e. to empirically determine the $\alpha_{imp\_i,j}$ values. This method has recently been slightly improved for the interpretation of the Erlenbach geophone data, based on an extended number of direct bedload measurements (Rickenmann et al., 2018). In addition, it was shown that controlled laboratory flume experiments are important for a better understanding of the factors influencing the calibration of these measuring methods (Wyss et al., 2016 b, c).

Calibration Measurements at the Albula Field Site

In 2015 a new bedload transport monitoring station was put into operation at the Albula stream in Switzerland. The measuring station is located in the village of Tiefencastel in the Eastern part of the Swiss Alps, at 856 m above sea level, and where the catchment area is 529 km². The hydrologic snow melt regime is characterized by low flow in winter and peak flows between late April and early July. At the measuring site, a Swiss plate geophone system is installed, including a total of 30 steel plates embedded into a 15 m wide concrete sill; every second steel plate is equipped with either a geophone or an accelerometer sensor (Rickenmann et al., 2017). A preliminary analysis after one season of measurements showed a fairly good correlation between discharge and impulses recorded by both types of sensors. Also, a rough estimation of the linear calibration coefficient k_b [kg^{-1}] was made, which can be derived from the total number of recorded impulses IMP_G with the geophone sensors and the mass *M* [kg] of bedload transported over the plates (Rickenmann et al., 2017):

$$IMP_G = k_b M \qquad (2)$$

The linear calibration coefficient k_b typically ranges between 2 and 60 kg^{-1} and was found to depend on site-specific parameters, e.g. the mean water flow velocity (Rickenmann et al. 2014).

To further investigate the variability of the SPG signal response between different field sites, and also to calibrate the SPG system at the Albula stream, a field measuring campaign was carried out during the snow melt period in Spring 2018. Direct bedload measurements were made with a net sampler, a development and adaptation of a bedload trap developed by Bunte and Abt (2003). Similar bedload measurements with a net sampler had been previously made in mountain streams in Austria (Kreisler et al., 2017) and in Northern Italy (Vignoli et al., 2016). The sampling device consists of a steel frame, a sampler bag and steel

bar (Figure 1). The 3 m long sampler bag is made of a polyethylene net and has a mesh size of 8 mm × 8 mm, what corresponds to the size of the smallest particle size that can be sampled. The frame on which the net is fixed has an opening size of 500 mm width and 300 mm height in order to cover the whole width of a steel plate. In addition a thin tilted metal plate was welded at the bottom pipe of the intake to ensure a good coupling with the concrete sill. The steel bar mounted centrally on the upper part of the intake frame is connected to a crane over a hydraulic rotator. This system enables to compensate for fluvial forces and place the aperture of the frame perfectly parallel to the steel plate. Three additional elements were necessary to ensure a correct bedload sampling. (i) First, a cable with markers on it was stretched from one bank to the other to indicate the correct position of the sensor plates. (ii) Second, two static ropes attached on each side of the frame and handled from the banks gave support to the hydraulic rotator to correct for fluvial forces at high discharges. (iii) Finally, an aluminum tube was fixed horizontally at the top of the steel bar to facilitate the positioning of the frame parallel to the sensor plates in turbid water. Between bedload measurements the flow velocity was recorded at different depths with an electromagnetic flow meter fixed on the steel frame.

Figure 1. The net sampler used for the calibration measurements at the Albula field site

At all sites equipped with the SPG system, the geophone signal is sampled at a rate of 10 kHz. During normal monitoring conditions (i.e. when no calibration measurements are conducted), a pre-processing of the geophone signal provides summary values (e.g. summed number of impulses recorded within one minute). Due to data storage limitations, the raw signal is not recorded continuously, but only during periods of transport activity. For the relatively short durations of the calibration measurements, the raw seismic signal is recorded.

A calibration measurement starts as soon as the steel frame is placed on the riverbed immediately downstream of a selected sensor plate. The duration of each bedload sampling period had to be carefully controlled for any given discharge and bedload transport activity, to avoid overloading the sampling bag. During the first part of the campaign, at the beginning of May, the estimated discharge ranged between 30 and 40 m^3/s. Measures with an electromagnetic flow meter fixed on the crane showed velocities up to 1.70 m/s around 10 cm over the riverbed. During the second part of the campaign, at the end of May, the discharge

ranged from 45 to 60 m^3/s with flow velocities of up to 2 m/s around 10 cm over the riverbed. In total sixty-two bedload samples with masses *M* ranging from 5 kg to 500 kg were collected over time intervals lasting between 1 and 10 minutes.

This bedload sampling technique proved to be an efficient solution for the calibration measurements conducted at the Albula field site. First, the relatively large capacity of the net allowed to collect bedload samples with a large range of masses. Secondly, having the sampling system fixed on a mobile crane allowed to collect samples at various locations and under different flow conditions within a short time interval; the flow velocity at locations closer to the bank was smaller than in the center of the stream.

Controlled Full Scale Experiments

In addition to the calibration measurements at the field site, controlled real scale experiments were performed at the outdoor flume facility of the Oskar von Miller institute in Germany. The main purpose was to replicate the bed and flow conditions of the Albula field site, i.e. to have a similar channel slope and bed roughness, and to apply similar unit discharges as during the field calibration measurements resulting in similar flow velocities. This set-up then allows investigating changes in the instrument response when variables such as the grain size, discharge and transport rate are being modified.

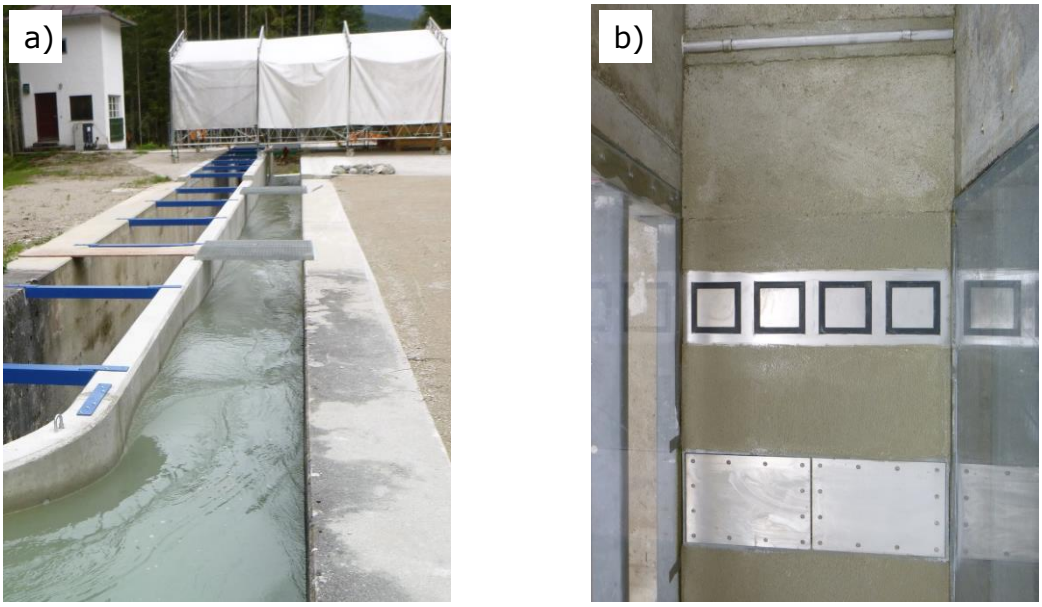

Figure 2. a) Downstream view of the 24 m long flume test section, and b) View of the measuring cross-section with the two steel plates of the SPG system (bottom) and the four smaller steel plates of the so-called Miniplate Accelerometer system (middle) and the Japanese pipe (top) .

The test reach consists of a 24 m long, 1.02 m wide and max. 2.02 m deep concrete flume (Figure 2a). The channel has a slope of 0.7 % and is divided in several subsections. In the first section, the bed of the flume has been paved with pebbles of approximately the D_{67} and the D_{84} sizes of the surface bed material in the Albula stream, reproducing the roughness measured in the field. The relatively large space between the pebbles helps to avoid the retention of bedload particles fed into the flume during the tests. Downstream of that is a short section imitating the concrete sill with large blocks in the field. At the measuring cross-section three different indirect bedload monitoring instruments are embedded: two steel plates with geophones, four smaller steel plates with accelerometers, and a Japanese pipe microphone (Figure 2b). Parts of the concrete wall on each side of the SPG system and the accelerometers were replaced by a Plexiglas window enabling to record the particle transport over the steel plates with a video camera. The most downstream section of the flume is made

of pure concrete ending with an overfall into a large retention basin. The flow conditions at the test site can be adjusted precisely with the help of a series of long intake basins separated from each other by sluice gates. The flume at the test side has a maximum discharge capacity of 2.7 m^3/s what enables to reach a flow velocity of about 2.5 m/s at a vertical distance of 10 cm above the geophone plates.

Two types of experiments were performed. The single grain size experiments were run with a fixed mass or number of grains of each of the seven defined classes mentioned earlier (see previous section titled "Swiss plate geophone system"). This first type of experiment should provide information on the close linkage between the instrument response, the grain size and the flow conditions. In a second stage, grain mixtures reflecting the natural grain size distributions measured at the Albula stream were used. Here the goal was to investigate whether it is possible to reproduce the seismic datasets recorded in the field by imitating the natural flow and transport conditions in the flume. For that purpose sieved bedload material originating from the calibration measurements described in the previous section titled "Calibration measurements at the Albula field site" was used. Each grain, with a b-axis ranging from 10 to 140 cm, was colored depending on the particle-size class to facilitate the later sorting.

In total around 450 runs were performed. Each run consisted of the following main steps. (i) First, depending on their class, grains were fed into the channel either directly on the bed through a vertical plastic pipe, or at the surface using a tiltable basket. Particles were fed into the flow about 8 m upstream from the impact sensors. (ii) Simultaneously, the recording of the raw geophone signal and the video were started. (iii) As soon as all the grains had passed the sensors, which could easily be controlled visually due to the limited turbidity of the water, both recordings were stopped. (iv) Finally, after completion of several test runs, the sluice gates were closed, the grains collected from the retention basin and sorted by size.

Results and Discussion

This section presents a brief comparison between the field and the controlled flume experiment data to address the last but most essential question.

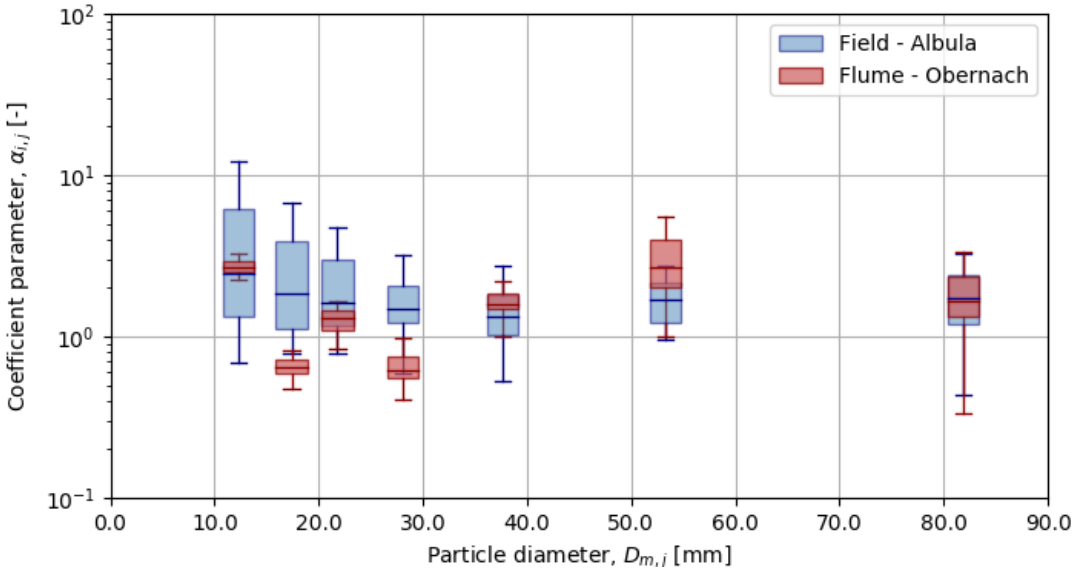

Figure 3. The α coefficient as a function of the geometric mean grain size of each amplitude class j for the calibration measurements at the Albula field site (red) and the outdoor flume facility (blue)

While the single grain class experiments only reproduce individual components of the real bedload transport of the Albula, the second set of experiments, based on particle mixtures, used a similar grain size distribution (GSD) as measured in the field and can therefore be directly compared with the field data. Figure 3 shows the $\alpha_{i,j}$ coefficient of each calibration measurement i conducted at the Albula stream and the outdoor flume facility at water flow velocities of around 2 m/s at a height of 10 cm above the sensor plates. The coefficient $\alpha_{i,j}$ is plotted as a function of the geometric mean particle size $D_{m,j}$ of each amplitude class j (see previous section titled "Swiss plate geophone system").

One can notice the generally reduced scatter of the flume data as compared to the field data (Fig. 3). This is not unexpected since the flow conditions in the flume and the GSD of the particle mixtures were almost the same for each run. On the other hand, the presented field data were collected over two days, and both flow conditions and transport rates and GSD are expected to have been more variable than in the flume. Only the $\alpha_{i,j}$ coefficients of the second and the fourth amplitude classes show clearly lower values on average than in the field. This could be due to a previously uninvestigated aspect of the Swiss plate geophone system, namely the recording of apparent impulses generated by impacts of (larger) particles on a neighboring. In fact, the seismic signal generated by an impact can propagate through the whole metallic structure and can be recorded by other geophones as an additional impulse, mostly in the lower amplitude classes because of signal attenuation. Lateral transmission of the seismic signal would therefore have a smaller impact in the flume experiments, with only two sensor plates, than at the field site where thirty plates are embedded. The high value of the $\alpha_{imp\_i,j}$ coefficient of the smallest amplitude class recorded during the flume experiments was found to be caused by the particles impacting on the concrete bed in the vicinity of the sensor plates. The good correlation between both datasets for this amplitude class therefore needs to be considered with caution. For the larger amplitude classes, a very similar instrument response can be observed for the flume experiments and at the Albula stream field measurements, which is a promising result.

Concluding Remarks

This preliminary analysis showed that the presented flume experiment setup allows a realistic reproduction of the flow and bedload transport behavior as observed at the Albula field site, resulting in a similar signal response of the SPG system for both data sets. The analysis also suggests that controlled experiments may help to refine the interpretation of calibration measurements made in the field. A more detailed analysis of the collected datasets, in particular of the video recordings of each run, is expected to provide further insights into the interpretation of the seismic signal registered by the SPG system.

References

Bunte, K., and Abt, SR. 2003. “Sampler size and sampling time affected bedload transport rates and particle size measured with bedload traps in gravel-bed streams. In Erosion and Sediment Transport Measurement in Rivers: Technological and Methodological Advances ,” (eds Bogen, J., Fergus, T., Walling, D.E.), IAHS Publication no. 283. IAHS: Wallingford; 126 – 133.

Geay, T., Belleudy, P., Gervaise, C., Habersack, H., Aigner, J., Kreisler, A., Seitz H., and Laronne, J.B. 2017. “Passive acoustic monitoring of bedload discharge in a large gravel bed river,” J. Geophys. Res. Earth Surface, 122(2), 528–545.

Kreisler, A., Moser, M., Aigner, J., Rindler, R., Tritthart, M., and Habersack, H. 2017. “Analysis and classification of bedload transport events with variable process characteristics,” Geomorphology, 291, 57–68. https://doi.org/10.1016/j.geomorph.2016.06.033

Mizuyama, T., Oda, A., and Laronne, J.B. 2010a. “Laboratory tests of a Japanese pipe geophone for continuous acoustic monitoring of coarse bedload. In Bedload-Surrogate Monitoring Technologies,” (eds Gray, J.R., Laronne, J.B., and Marr, J.D.G.). Scientific Investigations Report SIR 2010-5091, US Geological Survey; 319–335. http://pubs.usgs.gov/sir/2010/5091/papers

Mizuyama, T., Laronne, J.B., Nonaka, M. 2010b. “Calibration of a passive acoustic bedload monitoring system in Japanese mountain rivers. In Bedload-Surrogate Monitoring Technologies,” (eds Gray, J.R., Laronne, J.B., and Marr, J.D.G.). Scientific Investigations Report SIR 2010-5091, US Geological Survey; 296–318. http://pubs.usgs.gov/sir/2010/5091/papers

Rickenmann, D. 2017. “Bed-load transport measurements with geophones and other passive acoustic methods,” Journal of Hydraulic Engineering, 143(6), 03117004-1-14. https://doi.org/10.1061/(ASCE)HY.1943-7900.0001300

Rickenmann, D., Turowski, J.M., Fritschi, B., Wyss, C.R., Laronne, J., Barzilai, R., Reid, I., Kreisler, A., Aigner, J., Seitz, H., and Habersack, H., 2014. “Bedload transport measurements with impact plate geophones: comparison of sensor calibration in different gravel-bed streams,” Earth Surf. Process. Landf., 39, 928–942. doi: 10.1002/esp.3499.

Rickenmann, D., Antoniazza, G., Wyss, C.R., Fritschi, B., and Boss, S. 2017. “Bedload transport monitoring with acoustic sensors in the Swiss Albula mountain river,” Proc. IAHS, 375, 5-10, doi:10.5194/piahs-375-5-2017.

Rickenmann, D., Steeb, N., Badoux, A. 2018, “Improving bedload transport determination by grain-size fraction using the Swiss plate geophone recordings at the Erlenbach stream,” River Flow 2018, E3S Web of Conferences 40, 02009 (2018), https://doi.org/10.1051/e3sconf/20184002009.

Vignoli, G., Simoni, S., Comiti, F., Dell'Agnese, A., Bertoldi, W., Dinale, R., Nadalet, R., Macconi, P., Staffler, J., and Pollinger, R. 2016. “Monitoring sediment fluxes in alpine rivers: the AQUASED project,” INTERPRAEVENT 2016 – Conference Proceedings, Vol. 1, pp. 426-433.

Wyss, C.R., Rickenmann, D., Fritschi, B., Turowski, J.M., Weitbrecht, V., and Boes, R.M. 2016a. “Measuring bedload transport rates by grainsize fraction using the Swiss plate

geophone at the Erlenbach," Journal of Hydraulic Engineering, 142(5), 1–11. https://doi.org/10.1061/(ASCE)HY.1943-7900.0001090

Wyss, C.R., Rickenmann, D., Fritschi, B., Turowski, J.M., Weitbrecht, V., and Boes, R.M. 2016. "Laboratory flume experiments with the Swiss plate geophone bedload monitoring system: 1. Impulse counts and particle size identification," Water Resources Research, 52, 7744–7759. https://doi.org/10.1002/2015WR018555

Wyss, C.R., Rickenmann, D., Fritschi, B., Turowski, J.M., Weitbrecht, V., Travaglini, E., and Boes, R.M. 2016c. "Laboratory flume experiments with the Swiss plate geophone bedload monitoring system: 2. Application to field sites with direct bedload samples," Water Resources Research, 52, 7760–7778. https://doi.org/10.1002/2016WR019283

Development of a Simple Spreadsheet Approach for ADCP Data Post Processing, Visualization, and Analytics

Bradley Palmer, Hydraulic Engineer, USACE, Rock Island, IL,
bradley.d.palmer@usace.army.mil

Abstract

The Hydrology and Hydraulics (H&H) Branch of the Rock District (MVR) of USACE is tasked with supporting MVR's water management mission in operation and maintenance of 12 Lock and Dams on the Upper Mississippi River, 8 Lock and Dams on the Illinois River, and 3 Flood Control Reservoirs in Iowa. Additionally, the H&H branch plays a key role in the Operation, Planning, and Design for the Upper Mississippi River Restoration (UMRR) Program, which was the first river restoration and monitoring program instituted on a large river system in the United States. Multi-dimensional numerical modeling with ADH and HEC-RAS is vital for the H&H Branch's role in support to these missions and one of the key tools for this modeling is the use of an Acoustic Doppler Current Profiler (ADCP). The ADCP is used to collect velocity and discharge information for rivers and reservoirs in the Rock Island District. This information is used in the construction and calibration of the H&H Branch's Hydraulic numerical models. The ADCP data is collected on transects. Post processing of the data for visualization and use in H&H's numerical models is often a difficult task. The spacing of the data points on the transect is often not conducive for use in the numerical models and requires averaging. Until recently, the post processing of this data for visualization and consumption in numeric models was a difficult task requiring a significant investment of time. In order to simplify this process for employees in the H&H Branch, a spreadsheet was developed to post process the raw ADCP ASCII Out data. The averaging interval can be specified for the entire transect or adjusted during the transect. Also, the discharge calculated for the horizontally averaged velocity vectors is validated against the discharge calculated from the non-averaged vectors. The output from the spreadsheet can be easily imported to a GIS for velocity vector visualization. This spreadsheet, developed for the H&H Branch's usage, will be shared within the USACE Hydraulic, Hydrology, and Coastal User's Group and with other agencies on request.

Introduction

Acoustic Doppler Current Profiler (ADCP) devices are widely used by the water resources community in the measurement of water velocity and discharge. This community includes most District and Division offices of the U.S. Army Corps of Engineers (USACE) including the Rock Island District (MVR) where ADCP devices have been in use for over 20 years. At MVR, ADCPs are used in support of the USACE Water Management, Navigation, and Ecosystem Restoration Missions. One of the largest uses of the ADCP is in support of Hydraulic Modeling for these missions. ADCPs produce considerable data, which can be challenging to process for consumption in Hydraulic Modeling. One of the main processing needs for Hydraulic Modeling is horizontally averaging the depth averaged velocities to a coarser resolution than in the original ADCP transect data. Numerous software programs are available for use in this processing. Many of these programs are robust with a wide array of analytical options, but are sometimes difficult to utilize by inexperienced users. At MVR, a goal was to develop an Excel spreadsheet approach enabling inexperienced users to process ADCP data specifically for creating horizontally averaged velocity vectors for use with Hydraulic Modeling and mapping of this data in ArcGIS.

Other Software Programs

Robust computer applications exist for the detailed analysis and processing of ADCP data. Two of these programs are the VMT (Velocity Mapping Toolbox) and the VMS (ADCP Velocity Mapping Software) program. VMT is a Matlab based toolbox developed by the USGS that allows rapid processing (including averaging), visualization, and analysis (Parsons, et. al., 2012). The software specializes in 3d-analysis by allowing multiple transects to be projected and composited onto a cross section. This allows averaging of multiple transects in 3d and determination of patterns that are otherwise not discernable because of the noise inherent in ADCP data. VMS is a stand-alone program developed by the IIHR (Iowa Institute of Hydraulic Research —Hydroscience & Engineering) and USACE ERDC (Engineering Research & Development Center) with advanced graphical capability and advanced processing and analytical capability for large, reach-scale ADCP data sets. The program allows averaging in 2-d and 3-d and also specializes in the quality control and filtering of data in ADCP data sets (Kim et al., 2009). The MVR spreadsheet approach is not meant as an alternative to VMT, VMS, or other stand along programs, but rather to provide a spreadsheet based alternative for getting data to ADCP data consumers when limited analysis of the ADCP data is required.

MVR Excel Approach

Data Initialization

The Excel spreadsheet works with output from the Teledyne RDI (TRDI) ADCP WinRiver II Program (version 2.18). The “Generic ASCII Output” option (Figure 1) is used with a pre-configured template (Figure 2) to output specific ADCP parameters in a comma delimited ASCII files for each of the transects in a measurement grouping. Also, the discharge summary is exported to a separate Excel sheet (Figure 3).

These text files are then imported to Excel. After this, it is necessary to either enter the starting point coordinates in units of Feet for each transect or convert the GPS coordinates from the transect data to a coordinate system with units of Feet.

In the Excel spreadsheet, lookup formulas determine the transect id, starting bank, and starting position for each transect ensemble. The horizontal averaging distance can be specified for the entire transect or with different averaging intervals along each transect

Calculation Procedures

Numerous procedures are involved in the calculation of horizontally averaged velocity vectors and their verification. These procedures are available to be automated if the user environment allows running macros in Excel. If macros cannot be used, a "cookbook" can be followed to work through the same steps in a non-automated manner. The procedures performed in the Excel spreadsheet for the calculation and verification of horizontally averaged velocity vectors are listed as follows:

1. The incremental distances between ensemble points along each transect are calculated.
2. The total averaged distance along the transect points is calculated.
3. The incremental angle is calculated between each of the transect ensemble points.
4. The "end average" column calculates the ending points for each averaging interval along the transects.
5. The depth averaged velocity is an average of the measured bins for each ensemble. These bins do not measure velocity in portions at the top of the water column and at the bottom surface. Adjusted depth averaged water velocity values are calculated based on the ratio of the WinRiver II middle calculated discharge to the WinRiver II total calculated discharge.
6. The angle between the end points for each averaging interval is calculated.
7. The lines between the ensemble points along each averaging interval are fit to the straight line between the average end points.
8. These adjusted distances are summed for each averaging interval. These distances are also multiplied by the depth to calculate the cross sectional area for each ensemble. These areas are summed for each averaging interval.
9. The product of the velocity and the cross sectional area is calculated at each ensemble for both the x and y velocity components. The sum of these values is calculated over each averaging interval.
10. The sum of the velocity and cross sectional area products are divided by the sum of the cross sectional area for each averaging interval to get the horizontally averaged x and y velocity components.
11. In order to check the accuracy of the horizontally averaged velocity vectors, discharge values are also calculated. The TRDI WinRiver II discharge values are calculated using the cross product of the boat velocity and the water velocity multiplied by the time between ensembles and depth. These values are calculated by equation at each ensemble and totaled for each transect and compared to the TRDI WinRiver II calculated values.
12. The discharge values are also calculated using the horizontally averaged velocity vectors. These values are calculated for each averaging interval using the cross product of the depth averaged velocity vector and the distance between the end points multiplied by the water column depth. The discharge values are totaled for each transect.
13. In order to check whether the discharge calculations using the different cross product equations described above are different, a separate calculation is made. The boat velocity

is multiplied by the time for each ensemble to calculate the boat based distance. This distance is compared to the incremental distance calculated from the total East and North Displacement values obtained through the WinRiver II ASCII Out option. In some cases these distances are different. Discharge cross product calculations using these differences are calculated for comparison purposes.

14. At each ensemble the cross product of the straightened line and the velocity vector is calculated. This value and the cross product described above in paragraph 13 are summed for comparison purposes. The difference between this sum and the cross product described in paragraph 11 is the difference between the discharge calculated from the average velocity vectors and the discharge calculated from the original velocity vectors.
15. After the discharge and velocity vector calculations, the velocity vectors are processed for display in ArcGIS. The distances between ensemble points, x, and y values are calculated at each horizontally averaged point and also at the original ensemble points where velocity vectors were measured. The horizontally averaged depths and the depths at the original transect points are also provided. The distances and points are plotted in Excel to show the difference between the horizontally averaged and original data sets.
16. The table with x, y, velocity, discharge, and depth points is imported from the Excel Spreadsheet into ArcGIS to display the transect tracks and the original and averaged ensemble points.
17. Another step in Excel is used to convert the x, y, and velocity vector points into a format for creating a map showing velocity vector lines. A multiplier is specified for the length of the vector lines. The x and y velocity components are then multiplied by this factor and these values are added to the x and y coordinates to create a vector point. The original points and vector points are combined together and can then be imported into ArcGIS to create a line feature for displaying the velocity vector distribution for the original and horizontally averaged points.
18. Excel spreadsheets with the horizontally averaged and original points are provided to the Hydraulic Modeler. X & Y coordinates, depths, discharges, x & y velocity components, velocity magnitudes, and distances between points and distances between points are provided.

Background and Basis

Background

The equations in the spreadsheet were developed with the main purpose of facilitating velocity vector processing and verification of the horizontally averaged velocity vector calculations. Verification is of interest in determining if the formulas in the spreadsheet are properly calculating the horizontally averaged values and additionally determining how closely the discharge calculated from the averaged velocities matches that calculated from the original values.

Basis

Verification of both the WinRiver II discharge and velocity vector data requires developing an equation for the calculation of discharge values. The WinRiver II User guide describes the moving vessel method for measuring total discharge and utilizes the equation developed by

Simpson and Oltmann, 1990 and Gordon, 1989 for determining total channel discharge (Qt) through an arbitrary surface (s):

$$Q_t = \iint_S V_f \cdot n \, ds \quad (1)$$

where

Qt = total channel discharge through an arbitrary surface
ds = Differential area.
Vf = Mean water velocity vector.
n = Unit vector normal to WinRiver II path at a general point.

The total channel discharge can be expressed using the cross product of the water velocity and boat vessel velocity - for the full derivation, refer to the WinRiver II software user's guide, 2018:

$$Qt = (F_x B_y - F_y B_x) * d * T * RL \quad (2)$$

where

T = Total WinRiver II time
d = Total depth (Dtotal)
Fx = X-component of the mean water velocity vector.
Fy = Y-component of the mean water velocity vector.
Bx = X-component of the mean vessel velocity vector.
By = Y-component of the mean vessel velocity vector.
RL = Right or Left factor.

Because the mean vessel velocity multiplied by the time is equal to the distance travelled for the transect, the total discharge equation in 2 can be written using the x (Lx) and y (Ly) components of the distance travelled:

$$Qt = (F_x Ly - F_y Lx) * d * RL \quad (3)$$

where

Lx = X component of transect distance
Ly = Y component of transect distance

Application in Excel Spreadsheet: Equations 2 and 3 are used in the Excel spreadsheet for the following:

1. Verification of the WinRiver II discharge calculated in the middle of the discharge profile from the depth averaged ensemble velocity. If the discharge calculated by equation 8 in the spreadsheet matches the WinRiver II value, it indicates that the depth averaged velocity is the same as that used by WinRiver II in its calculation of discharge over the middle zone.
2. Determination of the ratio of the depth averaged velocity over the total depth (including the top and bottom unmeasured zones) to the depth averaged velocity in the middle zone. This calculates the ratio of the velocity over the total zone (including the

unmeasured upper and lower zones) to the zone in the middle (where velocity is measured.

3. Comparison of the discharge calculated from the mean boat velocity (Equation 2) to the discharge calculated using the X and Y component of the distance traveled (Equation 3). In ensembles where valid velocities were not measured, WinRiver II uses the boat velocity in the first ensemble with a valid velocity measurement to estimate the distance traveled in areas without valid velocity in Equation 2. The distance calculated from this is different than that calculated using the accumulated distance over each ensemble from Equation 3. This comparison also provides another check that the velocities in the spreadsheet are accounting for the discharges calculated by WinRiver II.
4. Comparison of the discharge calculated from the horizontally averaged velocity vectors to the discharge calculated from the original data. The calculation of discharge from the horizontally averaged velocity vectors and the calculation with the original velocities are both performed with Equation 3.

Application in ADCP Field Deployments: The use of the cross product for discharge calculation means that the discharge is calculated perpendicular to the ship track. This is advantageous in that it creates path independence in the measurement of discharges where there is uniform flow and uniform velocity distribution. The cross product discharge calculation will be the same as long as the endpoints are the same. This is illustrated in Figures 4 and 5, which show an example uniform velocity distribution along a transect with a straight line and a curvilinear transect path. Tables 1 and 2 show that the total channel discharge cross product calculation (Equation 3) is the same for the transects measured along different paths, shown in Figures 4 and 5. The RL factor is -1 since the transect calculations go from left to right. The total discharge calculated for both is 1,680 cfs. Where the velocity vector distribution is non-uniform along the transect paths, path independence does not apply. Figure 6 and Figure 7 show an example velocity distribution that is a non-uniform velocity distribution along a straight and curved transect path. Tables 3 and 4 show that the cross product discharge calculation is different for the same velocity distribution along different paths – Table 3 shows the straight transect cross product discharge calculation of 1,680 cfs and Table 4 shows the curvilinear transect cross product discharge calculation of 2,130 cfs.

These calculations show the importance of location selection when measuring discharge. Locations with uniform flow and velocity distributions ensure the most path independence and likelihood for obtaining the most accurate discharge measurements. These calculations are also relevant in the objective of comparing the discharge obtained from horizontally averaged velocity vectors and the original velocity vectors. The horizontal averaging algorithm described previously computes the product of the distance adjusted to the straight line between end points, the depth, and the velocity vector. The sum of these products is divided by the area fit to the straight line between end points to obtain the average velocity. The cross product determined from the horizontally averaged velocity is equivalent to the discharge obtained from a transect with a straight line between end points. This is shown in Figure 6 and Figure 7. Figure 6 shows a curvilinear transect path and Figure 7 shows the straight line conversion of this path used for horizontal averaging.

Based on this analysis, it is apparent that the transect path and the velocity distribution affect the differences between the discharge calculations from the original and horizontally averaged points. The Excel spreadsheet can be used to determine the magnitude of these differences for each transect and perform a sensitivity analysis on the horizontal averaging interval used.

Application of the Excel Spreadsheet Approach

Project Area, Description, and Objectives

The Excel Spreadsheet was used for post processing of ADCP data collected as part of the Steamboat Island Upper Mississippi River Restoration (UMRR) Program Habitat Restoration and Enhancement Project (HREP). The project is located mid-way between Mississippi River Lock & Dams 13 and 14 along the right descending bank between River Miles 502.5 and 506.5. The Project area contains approximately 4 square miles of backwater complex. Some of the potential project features include diversifying flow within Steamboat Slough, excavating channels in backwater areas, and creating topographic diversity measures. Hydraulic modeling is used as part of the design process for these features. ADCP data was collected to support calibration and verification of the numerical model in July and September of 2017.

ADCP Data Collection and Use of the Excel Spreadsheet

Transects were collected at five locations in July at a higher flow scenario (2-year event) and at eight locations in September at a median flow scenario. The discharge summary was copied and ASCII out files were exported from WinRiver II for each of the transect files from the Steamboat locations. The ASCII out files were imported to Excel. Spatial coordinates and transect file names were established for each of the ensemble points. Horizontal averaging distances were set for each of the transect files. Data was imported into the Excel horizontal averaging and discharge calculation sheet. Discharges were verified for the middle and full water depths for all ensembles. Horizontally averaged velocities were calculated. Discharges calculations from the original and horizontally averaged values were compared from the Excel calculations to the WinRiver II calculated values.

Products

The following products were provided to the Hydraulic Modeling Team:

1. Discharge summary spreadsheets.
2. Excel spreadsheets with x & y coordinates, original velocity vectors, horizontally averaged velocity vectors, distance along transect, and depth.
3. Shapefiles with the transect lines for the Steamboat Deployments.
4. A comprehensive shapefile with all of the original and horizontally averaged velocity vector information and depth for each of the two Steamboat deployments.
5. Individual shapefiles for each of the transect files for the Steamboat deployments for both the original and the horizontally average velocity vectors and depth.
6. Maps showing the original and horizontally averaged velocity vectors for each of the transect measurements in the Steamboat deployments.

Graphics

Figures 8 through 12 show selected velocity vector maps from the Steamboat deployments. The original velocity vectors are displayed in red and the horizontally averaged vectors are displayed in blue. Water depths and velocity magnitudes for the horizontally averaged vectors are displayed at the start of the vector. Tabular information is shown below the velocity vector

mapping. This information lists location information for the transect, horizontal averaging distance, total discharge from the original vectors, and the difference in the discharge calculated with the horizontally average vectors. In most cases the difference between the discharge calculated from the original and the horizontally averaged vectors is negligible, but this difference increases where the transect path is more curvilinear or the velocity distribution is more non-uniform.

Summary

An Excel spreadsheet approach has been utilized successfully in MVR for the post processing of WinRiver II ADCP information to create products for Hydraulic Modelers and for mapping purposes. The spreadsheet approach produces horizontally averaged tabular velocity vector information, mapping input, and the verification of transect discharge values. Several equations and steps are involved in the process of discharge verification and calculation of horizontally averaged velocity vectors. The discharge equations in the process are based on the cross product equation for the calculation of total flow. The discharge calculated from the horizontal average velocity vectors is also compared to the discharge calculated from the original vectors. The averaging distance, transect pathway, and uniformity of the velocity vector distribution affect how closely these values match. This verification provides validation for the horizontal averaged vectors and other information provided to the Hydraulic modeling team. This Excel spreadsheet approach is not an alternative to software dedicated to advanced ADCP analytics and graphics, but instead facilitates the rapid creation of ADCP products necessary for Hydraulic Modeling. This spreadsheet, developed for the H&H Branch's usage, will be shared within the USACE Hydraulic, Hydrology, and Coastal User's Group and with other agencies on request.

Figures

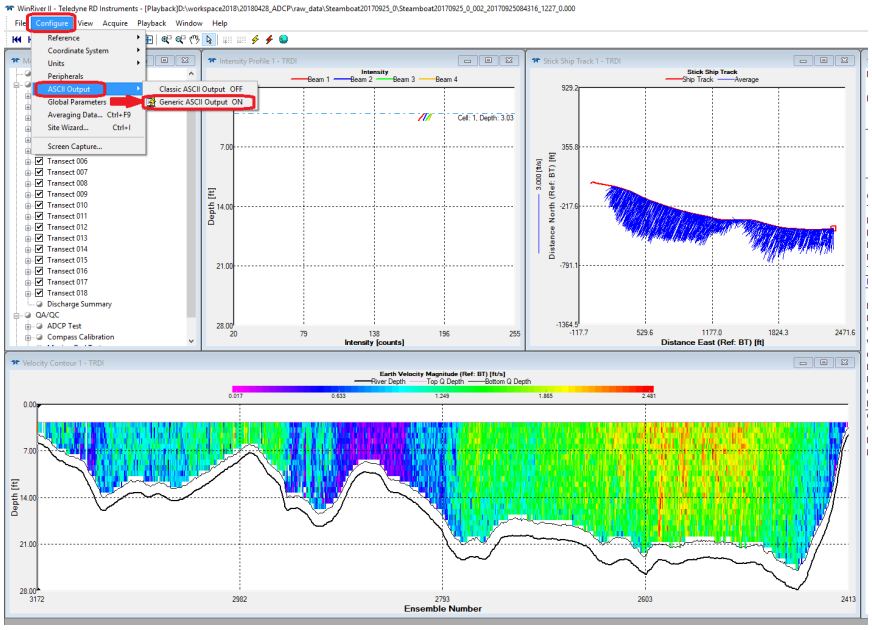

Figure 1. WinRiverII Generic ASCII Ouput with Template

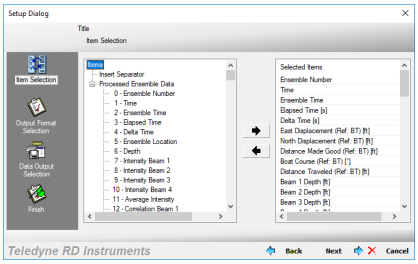

Figure 2. Pre-Configured Template for WinRiverII Generic ASCII Output

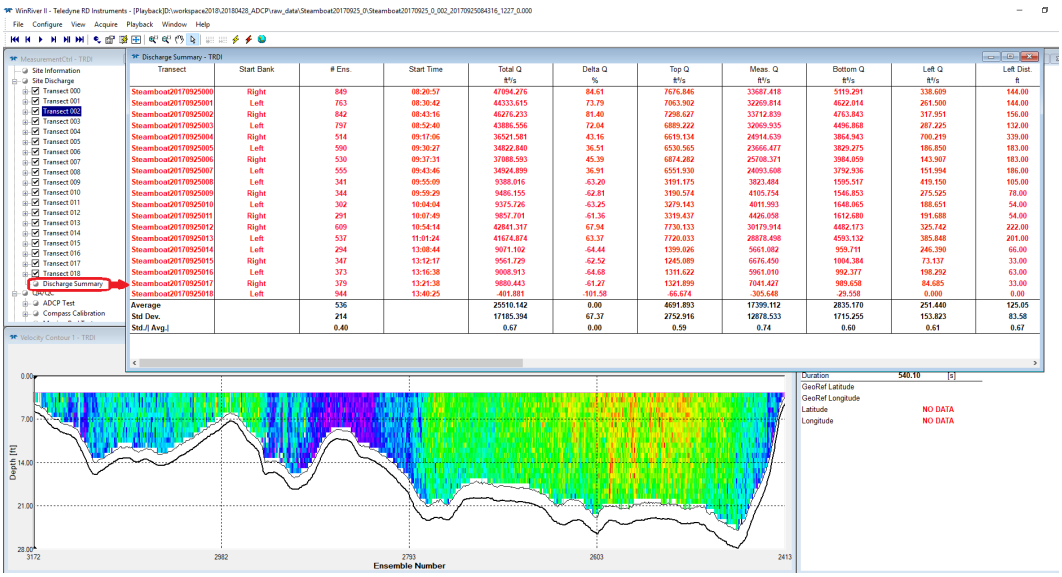

Figure 3. WinRiverII Discharge Summary

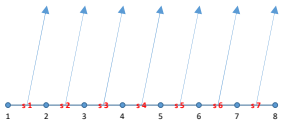

Figure 4. Example Uniform Velocity Vectors along a Straight Transect

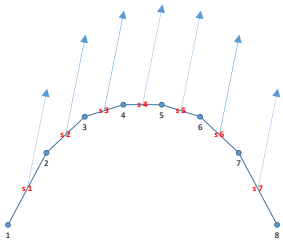

Figure 5. Example Uniform Velocity Vectors along a Curved Transect

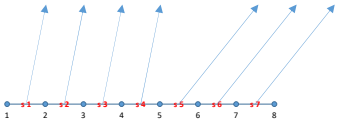

Figure 6. Example non-Uniform, non-Symmetrical, non-Perpendicular Velocity Vectors along a Straight Transect

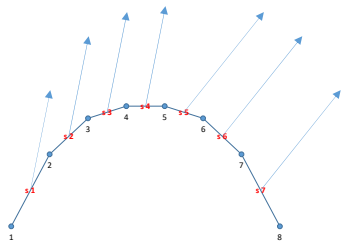

Figure 7. Example non-Uniform, non-Symmetrical, non-Perpendicular Velocity Vectors along a Curved Transect

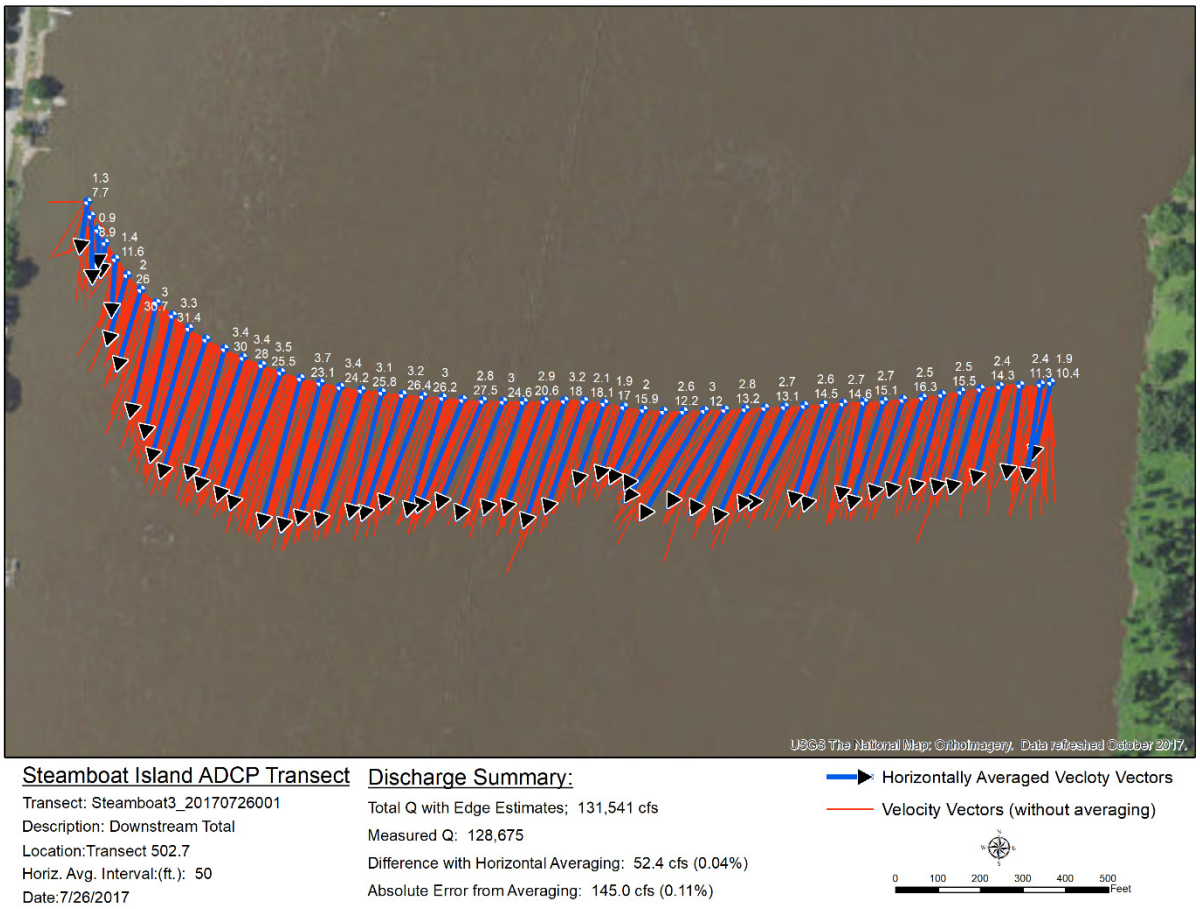

Figure 8. ADCP Horizontally Averaged and Original Velocity Vectors from Transect at RM 502.7 from 7/26/2017

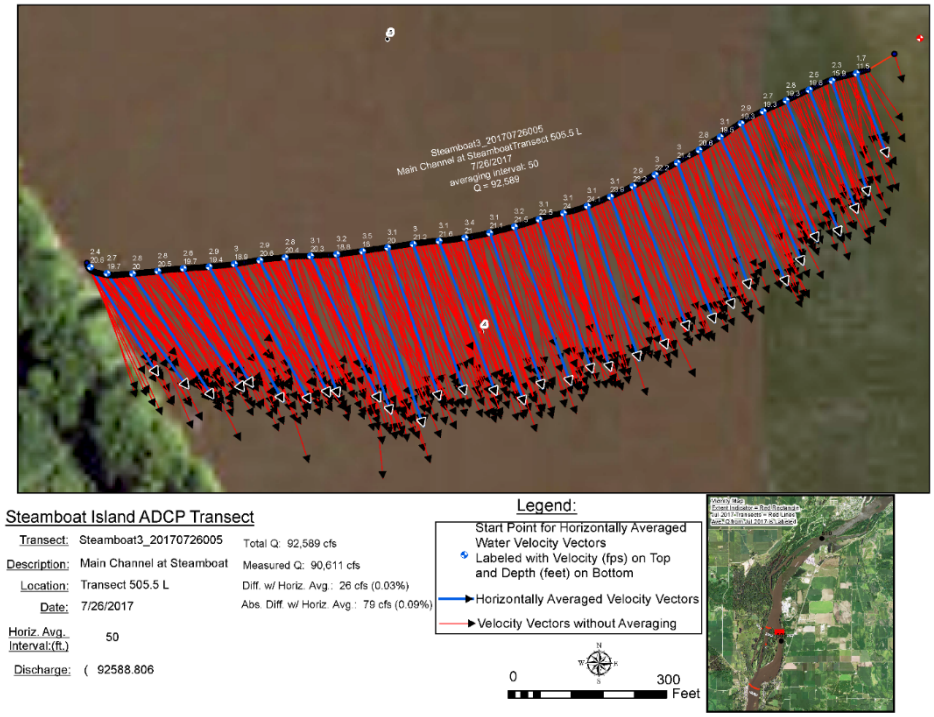

Figure 9. ADCP Horizontally Averaged and Original Velocity Vectors from Transect at RM 505.5L from 7/26/2017

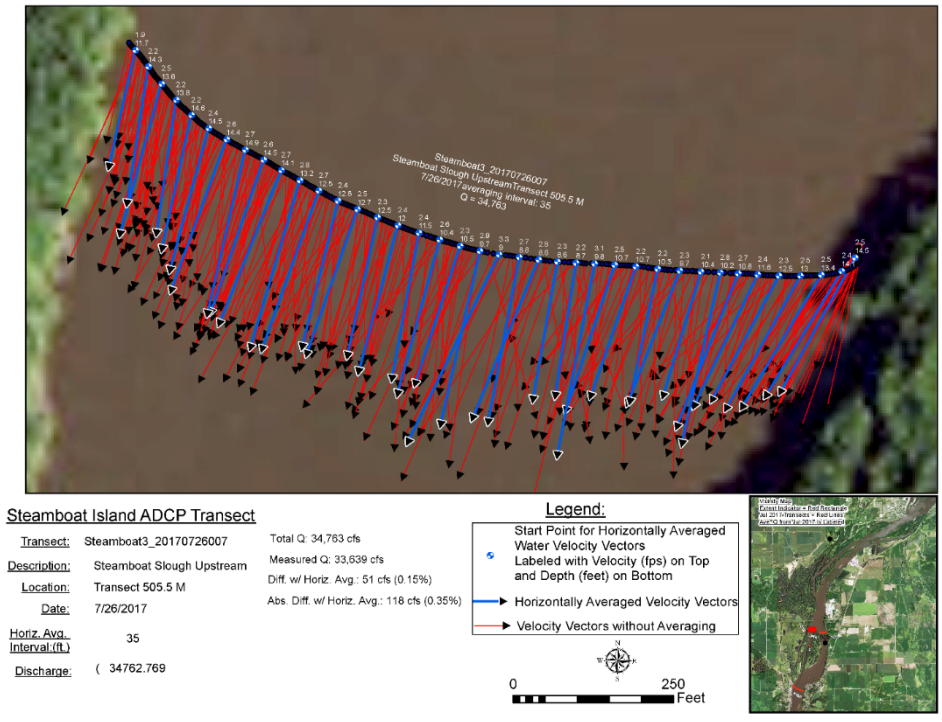

Figure 10. ADCP Horizontally Averaged and Original Velocity Vectors from Transect at RM 505.5M from 7/26/2017

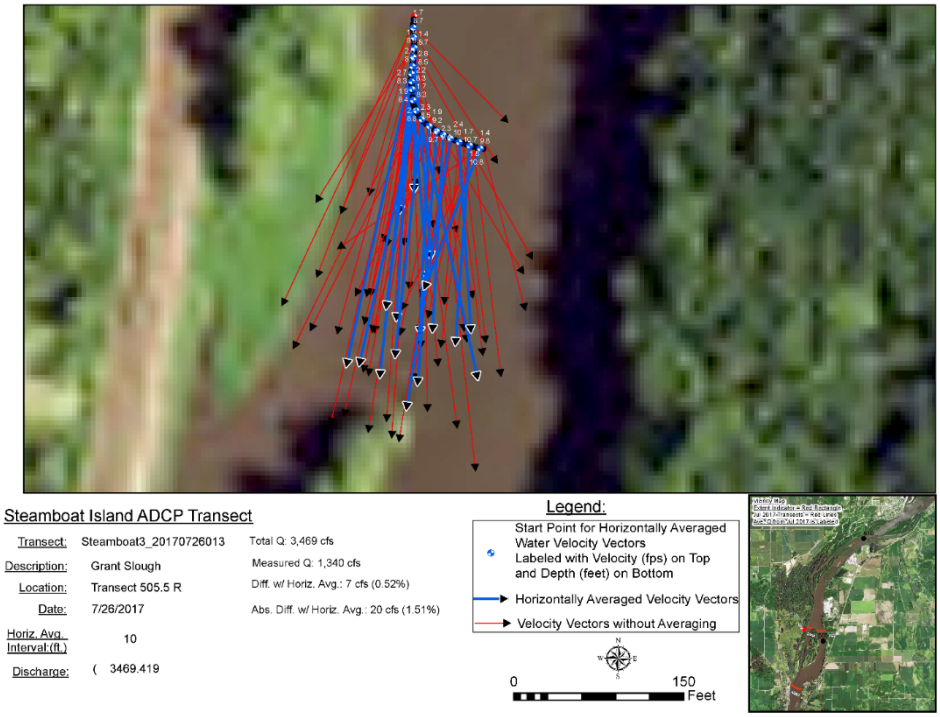

Figure 11. ADCP Horizontally Averaged and Original Velocity Vectors from Transect at RM 505.5R from 7/26/2017

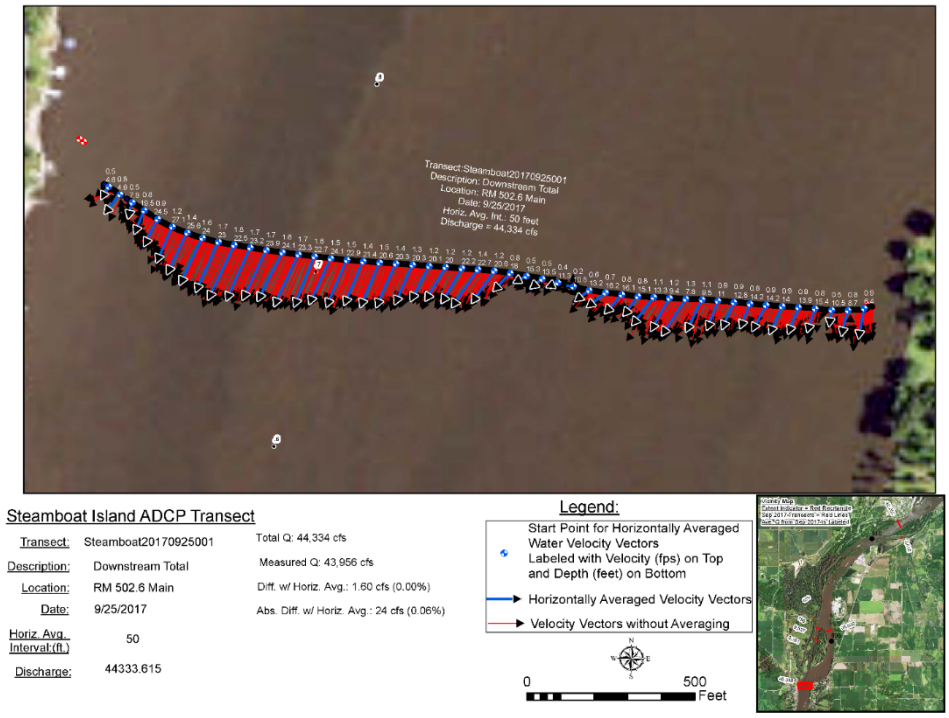

Figure 12. ADCP Horizontally Averaged and Original Velocity Vectors from Transect at RM 502.6 from 9/25/2017

Tables

Table 1. Calculation of Cross Product from Example Uniform Velocity Vectors along a Straight Transect

node	x	y	Segment Length	Segment Angle	x dist segment	y dist segment	x vel fps	y vel fps	Q (cross product)	Total Dist
1	528	555								336
2	576	555	48.0	90.0	48	0	1	5	240	
3	624	555	48.0	90.0	48	0	1	5	240	Assume
4	672	555	48.0	90.0	48	0	1	5	240	1' Deep
5	720	555	48.0	90.0	48	0	1	5	240	Q Tot.
6	768	555	48.0	90.0	48	0	1	5	240	cros prod
7	816	555	48.0	90.0	48	0	1	5	240	**1680**
8	864	555	48.0	90.0	48	0	1	5	240	

Table 2. Calculation of Cross Product from Example Uniform Velocity Vectors along a Curved Transect

node	x	y	Segment Length	Segment Angle	x dist segment	y dist segment	x vel fps	y vel fps	Q (cross product)	Total Dist
1	528	555								484.1686
2	576	465	102.0	28.1	48	90	1	5	150	
3	624	420	65.8	46.8	48	45	1	5	195	Assume
4	672	405	50.3	72.6	48	15	1	5	225	1' Deep
5	720	405	48.0	90.0	48	0	1	5	240	Q Tot.
6	768	420	50.3	107.4	48	-15	1	5	255	cros prod
7	816	465	65.8	133.2	48	-45	1	5	285	**1680**
8	864	555	102.0	151.9	48	-90	1	5	330	

Table 3. Calculation of Cross Product from Example non-Uniform, non-Symmetrical, non-Perpendicular Velocity Vectors along a Straight Transect

node	x	y	Segment Length	Segment Angle	x dist segment	y dist segment	x vel fps	y vel fps	Q (cross product)	Total Dist
1	528	555								336
2	576	555	48.0	90.0	48	0	1	5	240	
3	624	555	48.0	90.0	48	0	1	5	240	Assume
4	672	555	48.0	90.0	48	0	1	5	240	1' Deep
5	720	555	48.0	90.0	48	0	1	5	240	Q Tot.
6	768	555	48.0	90.0	48	0	4	5	240	cros prod
7	816	555	48.0	90.0	48	0	4	5	240	**1680**
8	864	555	48.0	90.0	48	0	4	5	240	

Table 4. Calculation of Cross Product from Example non-Uniform, non-Symmetrical, non-Perpendicular Velocity Vectors along a Curved Transect

node	x	y	Segment Length	Segment Angle	x dist segment	y dist segment	x vel fps	y vel fps	Q (cross product)	Total Dist
1	528	555								484.1686
2	576	465	102.0	28.1	48	90	1	5	150	
3	624	420	65.8	46.8	48	45	1	5	195	Assume
4	672	405	50.3	72.6	48	15	1	5	225	1' Deep
5	720	405	48.0	90.0	48	0	1	5	240	Q Tot.
6	768	420	50.3	107.4	48	-15	4	5	300	cros prod
7	816	465	65.8	133.2	48	-45	4	5	420	**2130**
8	864	555	102.0	151.9	48	-90	4	5	600	

References

Gordon, R. L. (1989). "Acoustic Measurement of River Discharge." Journal of Hydraulic Engineering, Vol. 115, No. 7, July 1989, 925-936.

Kim D., Muste M, Mueller D.S., Winkler M. (2009). A quick tutorial for using VMS. U.S. Army Corps of Engineers.

Mueller, D. S., Wagner, C. R., Rehmel, M. S., Oberg, K. A., and Rainville, F. (2013). "Measuring discharge with acoustic Doppler current profilers from a moving boat: U.S. Geological Survey Techniques and Methods 3A-22." ⟨http://dx.doi.org/10.3133/tm3A22⟩ (Sep. 1, 2015).

Parsons, D.R., Jackson, P.R., Czuba, J.A., Oberg, K.A., Mueller, D.S., Rhoads, B., Best, J.L., Johnson, K.K., Engel, F., and Riley, J. (2013) Velocity Mapping Toolbox (VMT): a processing and visualization suite for moving-vessel ADCP measurements, Earth Surface Processes and Landforms. doi: 10.1002/esp.3367.

Pratt, T. C. and Cook, D. S. (1999) "Hydraulic Processes Analysis System (HyPAS)," Coastal Engineering Technical Note CETN-IV-23, U.S. Army Engineer Research and Development Center, Vicksburg, MS, http://chl.wes.army.mil/library/publications/cetn/

St. Louis District, USACE. (2007). "ArcACDP Toolbar for ArcGIS 9.x." U.S. Army Corps of Engineers.

Simpson, M. R. and Oltmann, R. N. (1990). "An Acoustic Doppler Discharge Measurement System." Proceedings of the 1990 National Conference on Hydraulic Engineering, Vol. 2, 903-908.

Teledyne RD Instruments. (2018). "WinRiver II software user's guide." P/N 957-6231-00, San Diego.

Final Calibration of the Elwha Impact Plate System

Robert C. Hilldale, Hydraulic Engineer, Bureau of Reclamation, Denver, CO rhilldale@usbr.gov
Wayne O. Carpenter, Senior Research and Development Engineer, National Center for Physical Acoustics, University of Mississippi, University, MS, wocarpen@olemiss.edu
Smokey Pittman, Fluvial Geomorphologist, McBain Associates, Arcata, CA, smokey@mcbainassociates.com
Bradley Goodwiller, Senior Research and Development Engineer, National Center for Physical Acoustics, University of Mississippi, University, MS, btgoodwi@olemiss.edu
Daniel Dombroski, Hydraulic Engineer, Bureau of Reclamation, Denver, CO, ddombroski@usbr.gov

Abstract

The Elwha impact plate system was installed on the Elwha River in 2008-2009 for the purpose of continually measuring coarse bed load using an acoustic surrogate. The system consists of 72 stainless steel impact plates, 46 of which are instrumented with geophones and 26 of which are instrumented with accelerometers. Both instruments register an impact on the steel plate and respond with a voltage sent to one of three host computers, where these signals are minimally processed and stored for later retrieval and post-processing. Since installation, there have been several operations to measure bed load for the purpose of calibrating the geophone plates, concurrently gathering acoustic data from the plates and measuring bed load using conventional methods. The calibration of the geophone plates for measuring coarse bed load (mass/time) occurred between November 2011 and May 2016. This paper details the final calibration of the geophone instrumented impact plates and draws comparisons with similar systems in Europe. A companion paper by Pittman and Hilldale (this volume) provides additional details on the bed load sampling.

Introduction

Much discussion has occurred over the past three decades regarding the need for and benefits of continuous bed load measurements (Reid et al. 1980, Reid and Frostick 1986, Habersack et al. 2001), most of which include the use of surrogate methods (Bänziger and Burch 1990, Rickenmann and McArdell 2007, Turowski and Rickenmann 2009, Gray et al. 2010, Barrière et al. 2014, Hilldale et al. 2015, Downs et al. 2015, Mao et al. 2016, Habersack et al. 2017). Among the benefits discussed is a better understanding of bed load transport, including initiation of motion, temporal and spatial variability and the relation of bed load to stage or discharge and hysteretic effects. Indeed, surrogate bed load measurements have the ability to provide the temporal and spatial density needed for a more thorough understanding of these phenomena. In the case of the Elwha River, continuous bed load measurements during and after the removal of two large dams (Magirl et al. 2015, Ritchie et al. 2018) is providing a unique data set that is likely to prove useful as dam decommissioning becomes a viable alternative considering aging infrastructure.

In addition to utilizing continuous bed load data to increase our understanding of bed load transport and evaluate geomorphic change, these data can be used to evaluate and better understand aquatic habitat conditions. A wide variety of vertebrates and invertebrates inhabiting river systems depend on bed material and its condition during some portion of their life cycle (Palmer et al. 2000, Dusterhoff et al. 2017). Understanding the flow conditions under which the bed is disturbed, the temporal extent of its disturbance, and the frequency can provide biologists with critical information as it relates to stream health. A study is currently underway

on the Elwha River to better understand the relationship between sediment discharge and the egg-to-fry survival of salmonids (George Pess, written comm. Jan. 2018). This effort by Pess is making use of continuous surrogate measurements of both suspended and bed load on the Elwha River (Ritchie et al. 2018).

This paper describes the methodology and the calibration of the Elwha impact plate system using only the plates instrumented with geophones. Comparisons are made between the Elwha impact plate system and similar systems deployed elsewhere. Calibration measurements for bed load were collected between fall 2012 and spring 2016. There is a desire to continue physical bed load measurements for calibration, however the untimely removal of the anchor for the cableway assembly has made further measurements difficult.

Elwha Setting

The Elwha River flows north from the Olympic Mountain range in the state of Washington, USA and terminates at the Strait of Juan de Fuca (Figure 1), which connects Puget Sound with the Pacific Ocean. The catchment is largely within the protected lands of Olympic National Park, consisting mostly of forested land, much of it pristine wilderness, and covers an area of 830 km^2. The Elwha River is supplied with varying contributions of snowmelt, rainfall, and groundwater discharge and has a maritime climate with relatively wet, mild winters and dry, cool summers (Curran et al. 2009). Annual precipitation in the basin ranges from 560 cm in the upper basin (elevation 1,350 m) to 140 cm near the mouth (elevation 0 m) (Munn et al., 1998). The 2-year, 10-year, and 100-year recurrence-interval floods are 400 m^3/s, 752 m^3/s, and 1,240 m^3/s, respectively (Duda et al., 2011).

Bed load transport has been monitored on the Elwha River at river kilometer 5 (measured upstream from the mouth) since the removal of Elwha Dam (32 m tall, located at RK 7.9), constructed in 1913, and Glines Canyon Dam (64 m tall, located at RK 21.6), constructed in 1927 (Magirl et al. 2015) (Figure 1). These dams had been operated as run-of-the-river for power generation and provided no flood protection. The two reservoirs behind these dams had trapped 21 million m^3 of sediment (Randle et al. 2015) over their lifetime. Additional information about the dam removal, sediment transport, and geomorphic change, can be found in a series of papers (East et al. 2015, Gelfenbaum et al. 2015, Magirl et al. 2015, Randle et al. 2015, and Warrick et al. 2015).

Measurement Weir Setting

The measurement weir (RK 5), is a vertical concrete wall perpendicular to river flow, spanning the 41 m channel width. The impact plates are mounted flush against the downstream face of the weir (Figure 2). The purpose of the weir is to provide surface water diversion for municipal water supply and fisheries uses. The surface water intake is located at river right with a sizeable platform that provides ample room for the data collection computers. The engineered riffle downstream of the weir is 200 meters long with a bed slope of 0.015 m/m, designed for passage of resident and anadromous salmonids. For a short distance, the channel immediately downstream of the weir is grouted with concrete and contains boulders close to the weir. Depth-averaged velocity approximately 2 meters upstream of the weir exceeds 2.5 m/s at discharges that transport coarse bed load. Flow velocity over and downstream of the weir is significantly higher.

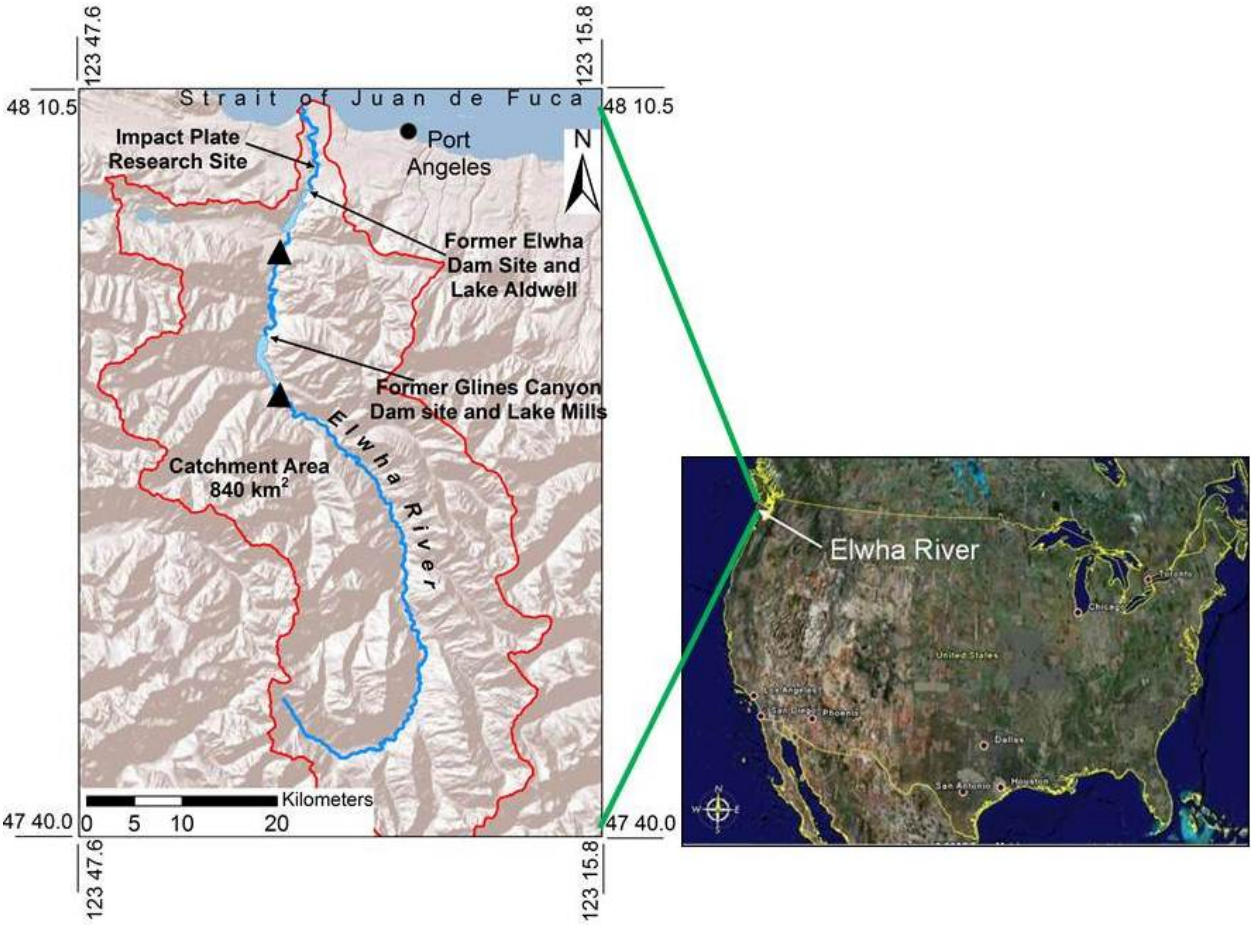

Figure 1. Location map for the Elwha River. Triangles represent the location of gauging stations. Northern gauge is USGS 12045500 Elwha River at McDonald Br., southern gauge is USGS 12044900 Elwha River above Lake Mills.

Figure 2. Photograph of the concrete weir and impact plate system mounted to the downstream side. The intake structure is in the background. Flow (approximately 11.3 m^3/s) is from right to left in the photograph (Sep. 2017).

Impact Plate System

The Elwha impact plate system has been fashioned after the Swiss impact plate system (Bänziger and Burch 1990, Rickenmann and McArdell 2007). The Swiss geophone system has been installed at more than 20 field sites where bed load measurements have been made for calibration (Rickenmann 2017). The decision to pattern the Elwha system after the Swiss system was a pragmatic one. The Swiss plate system had been in operation for over two decades and had proven to be a successful prototype. There are two primary differences between the two systems: 1.) Not all plates in the Elwha system are instrumented with geophones, some are instrumented with accelerometers, and 2.) The instruments in the Elwha system are stud-mounted to the underside of the impact plates, as opposed to being mounted within a box on the underside of the plates.

The Elwha impact plate system includes 72 individual stainless steel plates. The dimensions are L x B x T = 349 mm x 502 mm x 15.9 mm (where L = downstream length, B = transverse width, and T = thickness). Each plate is instrumented with either a geophone (GS-20DX marsh case, Geospace Technologies, Houston, TX) or accelerometer (CMCP-1100, STI Vibration Monitoring, League City, TX). Each impact plate is acoustically isolated with 12.7 mm rubber to minimize cross-plate signal contamination. The acceleration of flow over the weir prevents sediment accumulation on the plates. Figure 3 shows the configuration of the weir, including the location of the surface water intake at river right. The plate numbers and stationing increase from right to left as looking downstream. There are 46 geophone plates and 26 accelerometer plates. For plate numbers 1-12 (within the low flow notch, Figure 3), the geophone and accelerometer plates alternate every other plate. Along the remainder of the weir, the plates are configured such that accelerometers are located every third plate with two geophone plates between. As mobile bed particles move across the plates, their impact causes a deformation (or acceleration) of the steel plate, creating a voltage response from either the geophone or accelerometer. These signals are sent to three host computers for processing.

This paper only describes the calibration of the plates instrumented with a geophone, used for mass/time bed load measurements. Additional details regarding the Elwha impact plate system system can be found in Hilldale et al. (2015).

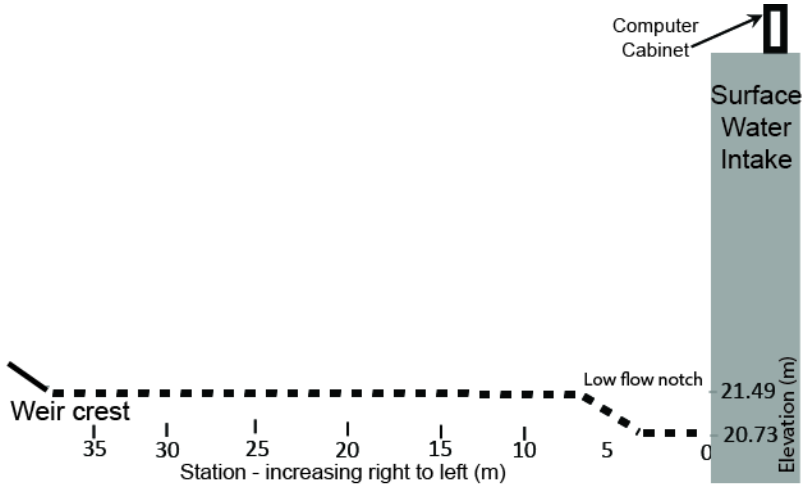

Figure 3. Diagram of the measurement weir showing the surface water intake, location of the computer cabinet, and the low flow notch against the intake

A separate effort is underway to utilize the accelerometer plates to determine the size of particles crossing the plates. One advantage of the accelerometer plates is their ability to detect particles as small as 5.6 mm, determined in the lab using two impact plates identical to those fabricated for the Elwha system. For more information on the effort to utilize accelerometer plates to determine particle size on the Elwha impact plate system, the reader should refer to Kuhnle et al. (2017).

Minimum Size Detection

A minimum voltage threshold of 0.1 volts is used for calibration, although multiple thresholds were evaluated between 0.01 to 0.2 volts. A similar voltage threshold is being used by other Swiss impact plate systems (Rickenmann et al. 2012). The threshold voltage is used to minimize the noise in the geophone signal generated by ambient flow conditions creating small voltage peaks from the sensors. Correlations to measured bed load had the best fit (highest r^2 value) using a threshold voltage of 0.1. When this threshold is used, the smallest reliably detectible particle size is 16 mm. The minimum detectible particle size was determined by releasing particles of known size (sieved to 0.5φ classes) immediately upstream of a given plate and observing the impulses simultaneously recorded on the computer. There was no natural sediment transport occurring in the river at the time of these tests.

Methodology

Physical bed load measurements were collected for the purpose of calibrating the Elwha impact plate system. These measurements were collected concurrent with the recording of impulses on the impact plates. The physical bed load measurements were collected using a Toutle River-2 (TR-2) pressure difference bedload sampler (Hubble et al. 1985; Childers 1999). TR-2 dimensions are as follows: the nozzle opening is 305 × 152 mm; nozzle expansion ratio is 1.4; overall length is 1.52 m; and the weight is 100 kg. The sample bag has a mesh size of 2 mm. The TR-2 is deployed from a 6.4-m long cataraft using a crane and winch (Figure 4). The cataraft is held stationary in the river by attaching the upstream end of the raft frame to a tag line stretched tightly across the channel.

Figure 4. A – TR-2 used for bed load measurements. B – Cataraft used for bed load measurements. The TR-2 is mounted on the downstream side of the raft, operated with a crane and winch.

The measurement weir imposes limitations to the collection of physical bed load measurements due to its construction and the size of the river. The grouted surface immediately downstream of the plates provides an uneven surface, consisting of cobbles and boulders, preventing proper

placement of the bed load sampler. Furthermore, very high flow velocity (> 3 m/s) immediately downstream of the weir adds additional challenges, whereby the sampler drifts well downstream of the weir creating an angle on the cable that is too low for safe and proper retrieval. When the cable angle is too low the sampler will drag forward upon retrieval, causing a potential biasing of the sample due to scooping sediment. Measurements immediately downstream of the weir were attempted one time, and the sampler became caught at the lip of the weir creating a dangerous situation with the tethered raft being pulled downstream against the tag line as the sampler was being retrieved. The only feasible location for physical measurement of bed load is approximately 2 to 3 meters upstream of the weir. This distance allows for variable downstream drift of the sampler, accounting for the length of the sampler (1.52 m) and insuring that the tail was not resting on the plates.

Sediment samples were retained for processing in a lab, where they were dried and sieved at 0.5φ intervals. Sediment smaller than 2 mm was not retained. Only particles sized > 16 mm were used for transport calculations for the purpose of impact plate calibration. The measured fraction of sediment between 2 and 16 mm was used to infer transport rates for the unmeasured portion of gravel (Magirl et al. 2015, Ritchie et al 2018). Further details of the physical collection of bed load samples can be found in Pittman et al. (these proceedings).

Bed load Measurement Protocol for Geophone Impact Plate Calibration

Attempts to measure bed load for calibrating the geophone impact plates were first made in November 2012 and again in March 2013. In October 2012 the bed material from the reservoir deltas arrived at the measurement weir. This material primarily consisted of sand and finer material in very heavy concentrations near the bed (Figure 5). This bed material was too small to be registered on the impact plates, resulting in no bed load collected for the purpose of calibration. Expecting the bed material to coarsen over the period of a few months another series of bed load measurements was made in March 2013. By this time the bed material of the Elwha was coarsening enough to transport particles large enough to be registered on the geophone impact plates (> 16 mm). After analyzing data and attempting to match the measured bed load to the number of impulses on the corresponding plate, it was realized that the bed load measurements had to include a significant temporal component for time averaging to overcome the variability of coarse bed load transport and the calibration method.

A data collection protocol for impact plate calibration was devised beginning with the third set of measurements for calibration in May 15, 2013. The new protocol collects physical bed load measurements at a single station for 30 min, resulting in approximately nine physical samples, depending on how long the sampler rests on the bed, referred to as sampler down time. The time averaged physical measurements create a single measurement of bed load in kg plate^{-1} min^{-1} at a single station. All individual bed load samples were retained and sieved separately and later combined mathematically to obtain an approximate 30 minute measurement. This bed load measurement is used to correlate impulses from the geophone impact plates in units of impulses plate^{-1} min^{-1}. The 30 minute period was chosen based on analyses performed during steady-flow conditions, in which the cumulative mean and standard deviation of bed load flux indicated by the plates arrived at a steady value, indicating a stable average obtained during the sample period. Additional information on temporal bed load variability at this site can be found in Hilldale and Greimann (2018). This bed load measurement and calibration protocol was used for all subsequent calibration efforts.

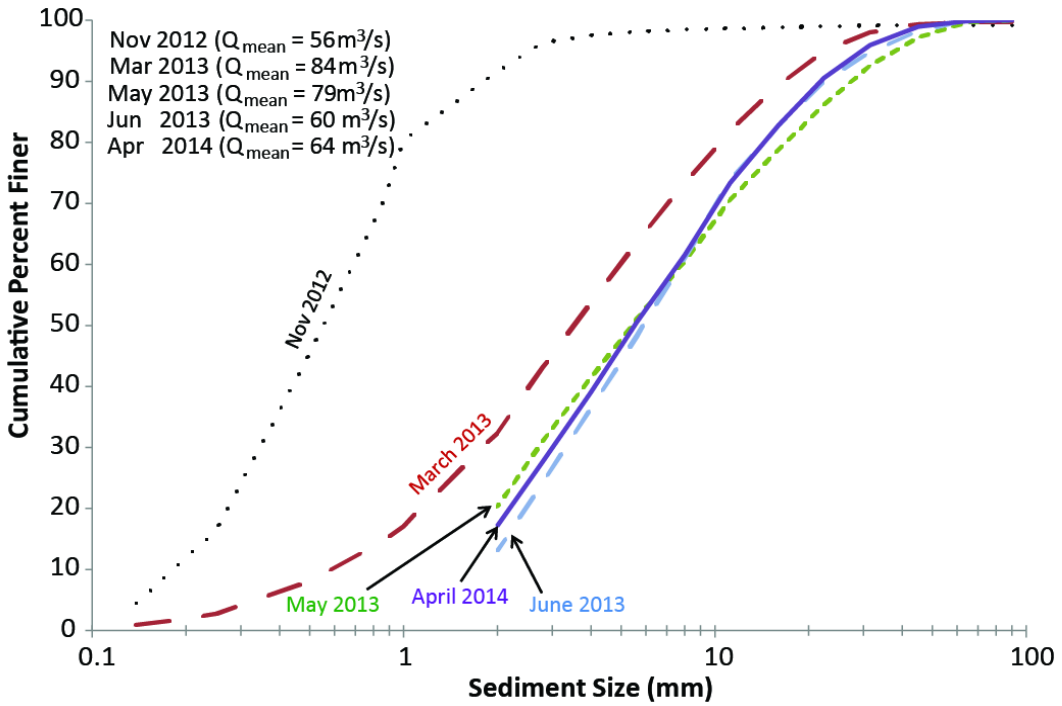

Figure 5. Particle size distribution of captured bed load over 5 separate measurement trips. Discharges were measured at USGS 12045500 Elwha River at McDonald Br.

The measurement protocol described assumes that the interruption of bed load across the plates by the bed load sampler did not create a significant influence on the impact plate measurement. Sampler down times varied from as short as 5 seconds during the May 2013 measurements and 20 – 120 seconds during the April 2014 measurements. Measurements at a single station were used to calibrate plates with a lateral distance of ≤ 1m from the sample station.

Data Processing

The impulse data collection for the geophones is controlled by three host computers and is remotely accessible via internet connection. Each computer is connected via USB 2.0 to a National Instruments cDAQ-9178 Chassis containing multiple National Instruments NI-9215 Modules. Two computers have 8 modules with 4 channels each, providing 64 channels. The third computer has 2 modules with 4 channels providing an additional 8 channels. Impulse data are collected for all 46 geophones for 1 minute, followed by a 20 second rest period, where data are processed and written to the computer in ASCII format. The sampling rate of the data acquisition system is 20 kHz/channel with a dynamic range of ± 5V for the geophones. The format includes the total number of impulses above a given threshold (0.5, 0.75, 0.1, 0.15, and 0.2 volts) with a time and date stamp. Only the impulses exceeding 0.1 volts are used for bed load calculations. These data are then processed with Matlab to provide temporal interpolation for the 20 second down period. The results of this processing are written to csv files to provide impulses for each plate. A second processing step provides spatial interpolation to account for the absence of geophone data where the accelerometer plates are located or where there is a bad geophone sensor.

Calibration Data

Of the six separate trips to measure bed load for calibration, only two produced data useful for calibration. November 2012 and March 2013 trips were discussed above. May 2013 is one data set used for calibration. In June 2013 bed load measurements were taken but a malfunction of the computers recording the impulses prevented proper data collection for calibration. April 2014 was a successful calibration measurement trip and is the second data set used for calibration (Table 1). Another attempt was made to collect a third calibration set in May 2016, but there was no coarse bed load in transport during the measurement period.

The calibration of the Elwha impact plate system relies on 16 total calibration points collected in May 2013 and April 2014 (Figure 6). These data points consist of multiple bed load samples over the 30 minute period and were collected at multiple stations (plates) across the channel under various flow conditions.

Table 1. Information about bed load measurements for calibration

Date	Daily Average Discharge (m^3/s)*	Total Number of Bed Load Samples Collected
May 14, 2013	93.4	26
May 15, 2013	73.9	60
April 23, 2014	42.5	25
April 24, 2014	63.1	58
*As measured at McDonald Gauge, USGS 12045500		

The data are plotted and regressed following the method outlined in Rickenmann et al. (2014) using a linear model. The chosen regression is the one forced through zero. The measured bed load mass, normalized to $kg \cdot plate^{-1} \cdot minute^{-1}$, is plotted on the independent axis and the number of geophone impulses that exceed the 0.1 V threshold are plotted on the dependent axis with units of $impulses \cdot plate^{-1} \cdot minute^{-1}$. Each data point shown in Figure 6 represents multiple discrete bed load measurements with the TR-2 (typically 7-9) over a period of 30 minutes. Mass measurements only include particles > 16 mm, considered the threshold for detection.

The resulting calibration for the Elwha impact plate system is as follows:

$$I_g = 1.843 * M_{bl} \quad (1)$$

where I_g is the number of geophone impulses above the 0.1 volt threshold and M_{bl} is bed load mass.

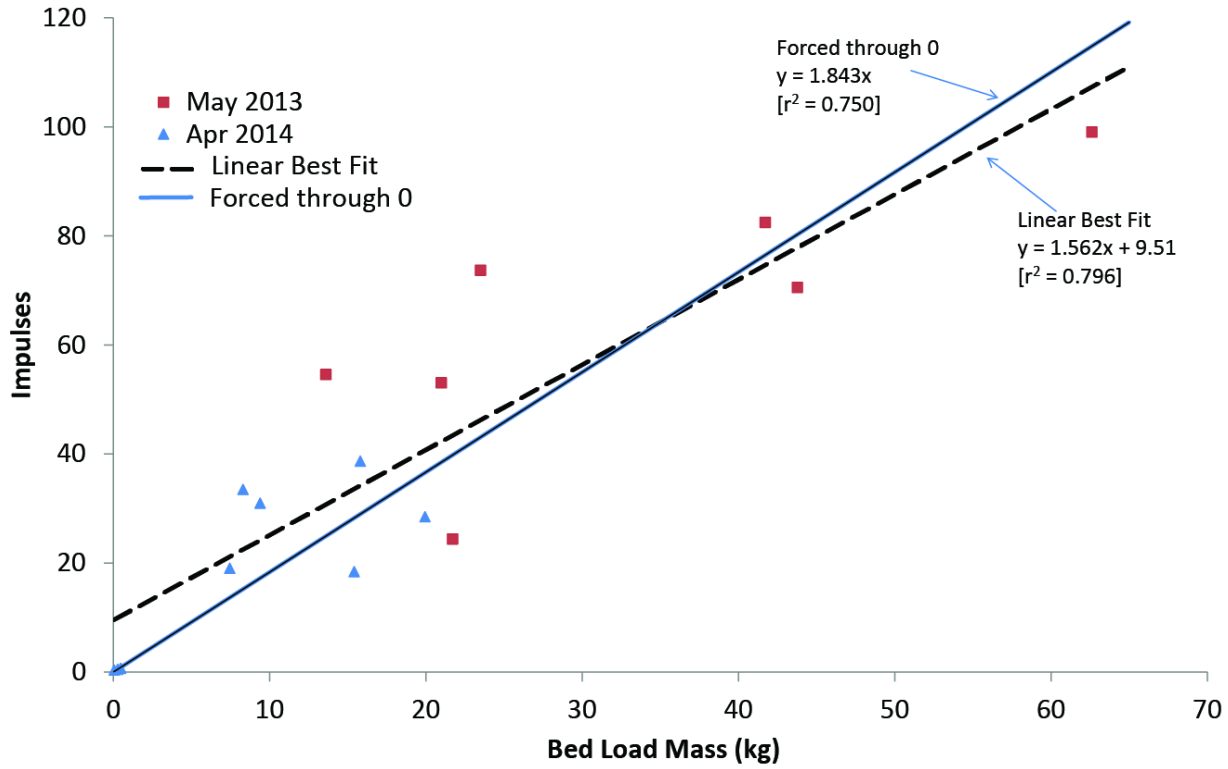

Figure 6. Calibration data for the Elwha impact plate system. The calibration uses the curve that is forced through zero. The units on both axes are normalized to plate-1.minute-1.

Discussion

Calibration Comparison to Other Impact Plate Systems:

The Elwha impact plate system calibration (Y=1.843x) falls between the calibration of the Swiss plate systems installed on the Eshtemoa (y=0.419x) and Rofenache (y=3.87x) (Rickenmann et al. 2014). Habersack et al. (2017) indicate a calibration of their impact plate system on the River Drau ofY=3.54x. The calibration of an impact plate system varies for a number of reasons including; bed load sampling method, threshold voltage, plate dimensions, sensor type, instrument mounting style, bed load velocity over the plates, and particle shape. For most of the Swiss impact plate systems the physical parameters are similar. While most of the parameters of the Elwha system are very similar to that of the Swiss system, the mounting style of the geophone is quite different (stud mount on the Elwha vs. box mount for the Swiss system). Additionally, the calibration of the Elwha impact plate system had to be performed immediately upstream of the plates, where the Swiss systems are typically calibrated with physical measurements immediately downstream of the plates.

Turowski and Rickenmann (2009) demonstrate that particle size, shape, velocity, and transport mode (rolling, sliding, or saltating) influence the impulse signal from a geophone plate. The same authors conclude that the influence of particle shape is not trivial. Three-axis measurements were made on 200 randomly picked Elwha bed particles (Figure 8) to determine the distribution of shapes on the Elwha River using the Zingg shape classification (Zingg 1935 in Pettijohn 1975). As shown in (Table 2), the dominant Elwha particle shape is oblate (discoidal). This shape is most likely to result in a sliding transport mode as opposed to rolling or saltation,

and particle shape and mode of transport have a greater influence on geophone impulses than particle weight (Turowski and Rickenmann 2009). This information would seem to partly explain why the Elwha plate calibration has a lower slope than comparable systems. It is worth noting that the particle shape analysis indicates that approximately 1/3 of particles (prolate and equiaxial) are more likely to roll than slide across the impact plates. Particle velocity also influences geophone response by influencing saltation length and the energy each particle might impart to the plate. Saltation length may influence the number of particles that may skip over a plate, or register more than one impulse.

Figure 7. Photographs of Elwha River bed material. Dimensions of 200 bed particles were measured with calipers on three axes.

Table 2. Results of a particle shape analysis of the Elwha bed material measuring all three axes (A = greatest length, B = intermediate length, and C = least length.

Zingg Shape Classes (after Zingg 1935, cited in Pettijohn 1975)				
Class	**B/A**	**C/B**	**Shape Description**	**Elwha Particles**
I	> 2/3	< 2/3	Oblate (discoidal, tabular)	40.0%
II	> 2/3	> 2/3	Equiaxial (spherical, equant)	15.5%
III	< 2/3	< 2/3	Triaxial (bladed)	26.5%
IV	< 2/3	> 2/3	Prolate (rods)	18%

There are many factors influencing the calibration of an impact plate system, even though the systems may have many things in common. This speaks to the importance of an in-situ calibration under a range of flow conditions. However, Wyss et al. (2016b) have demonstrated that a flume based calibration of an impact plate system is possible although with reduced accuracy.

Conclusions and Outlook

The Elwha impact plate system is expected to continue operation until a critical failure occurs. To date, several geophone and accelerometer instruments no longer work properly, either due to a failed sensor or splice. Their replacement is very challenging due to the perennial nature of the stream and lack of ability to divert flow away from the weir. The inoperable plates are turned off in the host computer and bed load calculations interpolate across the non-functioning plates.

An effort is planned to publish the time series bed load data from the Elwha impact plate system in a publicly accessible database, hosted by the Bureau of Reclamation. This database is currently being created and is expected to be online by the end of 2019. However, time series bed load data is not expected to be available until the middle of 2020. Readers are referred to the ScienceBase catalog referenced in Ritchie et al. (2018) for available sediment data, WY2012 – WY2016 (https://www.sciencebase.gov/catalog/item/5a033d9ee4b0531197b8d58f).

References

Bänziger, R., and Burch, H. (1990). "Acoustic sensors (hydrophones) as indicators for bed load transport in a Mountain Torrent." Hydrology in mountain streams. *I—Hydrological measurements; The water cycle*, H. Lang and A. Musy, eds., International Association of Hydrological Sciences, Wallingford, U.K., 207–214.

Barrière, J., Krein, A., Oth, A., Schenkluhn, R. (2014). "An advanced signal processing technique for deriving grain size information of bedload transport from impact plate vibration measurements", *Earth Surf. Proc. Landf.*, 40, pp. 913-924, DOI: 10.1002/esp.3693.

Childers, D. (1999). "Field comparisons of six pressure difference samplers in high-energy flow." *U.S. Geological Survey Water Resources Investigations Rep. 92–4068*, Vancouver, WA.

Curran, C. A., Konrad, C. P., Higgins, J. L., and Bryant, M. K. (2009). "Estimates of sediment load prior to dam removal in the Elwha River, Clallam County, Washington." *U.S. Geological Survey Scientific Investigations Rep. 2009-5221*, Reston, VA, 1–18.

Downs, P.W., Soar, P.J., Taylor, A. (2015). "The anatomy of effective discharge: the dynamics of coarse sediment transport revealed using continuous bedload monoitoring in a gravel-bed river during a very wet year", *Earth Surf. Proc. Landf.*, DOI: 10.1002/esp.3785.

Dusterhoff, S.R., Sloat, M.R., Ligon, F.K. (2017), "The influence of particle mobility on scour depth in salmonid spawning habitat", River Res. Applic., pp. 1-9, DOI: 10.1002/rra.3178.

Duda, J.J., Warrick, J.A., Magirl, C.S., (2011). "Coastal and lower Elwha River, Washington, prior to dam removal—History, status, and defining characteristics". In: Duda, J.J., Warrick, J.A., Magirl, C.S. (Eds.), *Coastal Habitats of the Elwha River, Washington—Biological and Physical Patterns and Processes Prior to Dam Removal: U.S. Geological Survey Scientific Investigations Report 2011-5120*, pp. 1–26.

Habersack.H.M., Nachtnebel, H.P., Laronne, J.B. (2001). "The continuous measurement of bedload discharge in a large alpine gravel bed river", *J. Hydr. Res.*, 39(2), pp. 125-133.

Habersack, H., Kreisler, A., Rindler, R., Aigner, J., Seitz, H., Liedermann, M., Laronne, J.B. (2017). "Integrated automatic and continuous bedload monitoring in gravel bed rivers", *Geomorphology*, 291, pp. 80-93, DOI: 10.1016/j.geomorph.2016.10.020.

Hilldale, R.C., Carpenter, W.O., Goodwiller, B., Chambers, J.P. and Randle, T.J. (2015). "Installation of impact paltes to continuously measure coarse bed load: Elwha River, Washington, USA", *J. Hydraul. Eng.*, Vol. 141, Issue 3, March, DOI: 10.1061/(ASCE)HY.1943-7900.0000975.

Hilldale, R.C. and Greimann, B.P. (2017). "Variability of coarse bed load: Continuous measurement using a surrogate method", In: Proceedingsof the Hydraulic Measurements and Experimental Methods Conference, Durhan, NH, July 9-12.

Hubble, D. W., Stevens, H. H., Skinner, J. V., and Beverage, J. P. (1985). "New approach to calibrating bed load samplers." *J. Hydraul. Eng.*, DOI: 10.1061/(ASCE)0733-9429(1985)111:4(677), 677–694.

Knighton, D. (1998). Fluvial Forms and Processes: A New Perspective, Arnold, London.

Kuhnle, R.A., Wren, D.G., Hilldale, R.C., and Goodwiller, B.T. (2017). "Laboratory Calibration of Impact Plates for Measuring Gravel Bed Load Size and Mass", *J. Hydraul. Eng.*, Vol. 143, Issue 12, December, DOI: 10.1061/(ASCE)HY.1943-7900.0001391.

Magirl, C.S., Hilldale, R.C., Curran, C.C., Duda, J.J., Straub, T.D., Domanski, M., Foreman, J.R. (2015). "Large scale dam removal on the Elwha River, Washington, USA: Fluvial sediment load", *Geomorphology*, 246, pp. 669-686, DOI: 10.1016/j.geomorph.2014.12.032

Mao, L., Carrillo, R., Escauriaza, C., Iroume, A. (2016). "Flume and field-based calibration of surrogate sensors for monitoring bedload transport", *Geomorphology*, 253, pp10-21, DOI: 10.1016/j.geomorph.2015.10.002

Munn, M. D., Black, R. W., Haggland, A. L., Hummling, M. A., and Huffman, R. L. (1998). "An assessment of stream habitat and nutrients in the Elwha River basin—Implications for restoration." *U.S. Geological Survey Water Investigations Rep. 98-4223*, Tacoma, WA, 38.

Palmer, M.A., Swan, C.M., Nelson, K., Silver, P., Alvestad, R. (2000). "Streambed landscapes: evidence that stream invertebrates respond to the type and spatial arrangement of patches", *Landscape Ecology*, 15, pp. 536-576.

Reid, I., Layman, J.T., Frostick, L.E. (1980). "The continuous measurement of bedload discharge", *J. Hydr. Res.*, 18(3), pp. 243-249.

Reid, I. and Frostick, L.E. (1986). "Dynamics of bedload transport in Turkey Brook, a coarse-grained alluvial channel", *Earth Surf. Proc. Landf.*, 11, pp. 143-155.

Rickenmann, D., and McArdell, B. W. (2007). "Continuous measurement of sediment transport in the Erlenbach stream using piezoelectric bedload impact sensors." *Earth Surf. Proc. Landf.*, 32(9), 1362–1378.

Rickenmann, D., Turowski, J.M., Fritschi, B., Klaiber, A., Ludwig, A. (2012). "Bedload transport measurements at the Erlenbach stream with geophones and automated basket samplers", *Earth Surf. Proc. Landf.*, 37, pp 1000-1011, DOI: 10.1002/esp.3225.

Rickenmann, D., Turowski, J.M., Fritschi, B., Wyss, C., Laronne, J., Barsilai, R., Reid, I., Kreisler, A., Aigner, J., Seitz, H., Habersack, H. (2014). "Bedload transport measurements with impact plate geophones: Comparison of sensor calibration in different gravel-bed streams", *Earth Surf. Proc. Landf.*, 39, DOI: 10.1002/esp.3499.

Rickenmann, D. (2017). "Bed-load transport measurements with geophonesand other passive acoustic methods", *J. Hydraul. Eng.*, 143(6), DOI: 10.1061/(ASCE)HY.1943-7900.0001300.

Ritchie, A.C., Warrick, J.A., East, A.E., Magirl, C.S., Stevens, A.W., Bountry, J.A., Randle, T.J., Curran, C.A., Hilldale, R.C., Duda, J.J., Gelfenbaum, G.R., Miller, I.M., Pess, G.R., Foley, M.M., McCoy, R., and Ogston, A.S. (2018). "Morphodynamic evolution following sediment release from the world's largest dam removal", *Scientific Reports*, 8:13279, DOI: 10.1038/s41598-018-30817.

Turowski, J.M. and Rickenmann, D. (2009). "Tools and cover effects in bedload transport observations in the Pitzbach, Austria", *Earth Surf. Proc. Landf.*, 34, pp. 26-37, DOI: 10.1002/esp.

Wyss, C. R., Rickenmann, D., Fritschi, B., Turowski, J. M., Weitbrecht, V., and Boes, R. M. (2016a). "Laboratory flume experiments with the Swiss plate geophone bed load monitoring system. 1: Impulse counts and particle size identification." *Water Resour. Res.*, 52(10), 7744–7759.

Wyss, C. R., Rickenmann, D., Fritschi, B., Turowski, J. M., Weitbrecht, V., and Boes, R. M. (2016b). "Laboratory flume experiments with the Swiss plate geophone bed load monitoring system. 2: Application to field sites with direct bed load samples." *Water Resour. Res.*, 52(10), 7760–7778.

Hydroacoustic Monitoring of Bedload Transport on the Trinity River, California, USA

Wes Smith, Geomorphologist, Ocean Assoc. Inc. contractor with
NOAA Fisheries, Arcata, CA, floodkayaker@gmail.com

Extended Abstract

In rivers, passive hydroacoustic systems correlated with field based bedload sampling can provide continuous estimates of bedload transport from bedload and channel bed generated sound. A passive acoustic system using hydrophones and digital audio recorders was deployed on the Trinity River near Douglas City, California to examine bedload temporal and spatial transport rates. The hydroacoustic systems recorded continuously during annual spring-dam releases and were located on the left and right banks approximately 30 meters upstream of a bedload sampling cross section and 100 meters downstream of a USGS gaging station. The Trinity River Restoration Program contracted GMA Hydrology Inc. to collect bedload samples during dam releases using a cataraft and Toutle River (TR-2) bedload sampler. Comparisons were made between sediment generated noise (SGN) and total and partial (i.e., grain-size classes) bedload transport rates and right, center, and left channel bedload fractions. Distinct sounds from the cataraft sampling, trees falling into the river, safety kayakers, and other sharp impulse sounds were used to determine the hydrophones' effective distance across a range of acoustic frequencies. Multiple sampling intervals were compared to determine the level of sampling effort necessary to accurately document the temporal variations in acoustic signals.

Introduction

Estimating bedload transport rates and loads from physical bedload measurements is expensive and laborious and generally lacks the number of measurements necessary to accurately characterize the temporal and spatial variations in gravel-bed rivers. Hydroacoustic measurements of bedload self-generated noise (SGN) (Thorne 1985) created by particle to particle and particle to channel bed collisions are used as surrogates for physical bedload measurements to estimate continuous bedload transport rates (e.g., Barton 2006, Rigby et al. 2014, Marineau et al. 2016). Barton (2010) and Marineau et al. (2016) have estimated bedload for dam release hydrographs using near continuous bedload SGN. However, there has been some difficulty estimating bedload particle size distributions from bedload SGN (e.g., Geay 2018b). Multiple researchers have developed a general relationship between particle size and a centroid frequency from lab and controlled experiments (e.g., Jonys 1976, Thorne 1985, and Petrut et al. 2018). Thorne (1985, 1986, 2014) and others work quantified this intuitive relationship that larger particles produce lower frequencies and smaller particles generate higher frequencies. This relationship provided a means for comparisons between measures of integrated acoustic power to different sediment size fractions using frequency. Petrut (2017) and others (e.g., Jonys 1976) have shown that the diversity of fluvial sediments of a particular size class produce a distribution of frequencies depending on particle shape, mass, impact velocity, quantities. Petrut et al. (2018) developed an inversion algorithm based on a theoretical collision model fed by the power spectrum density to estimate the particle size distribution. Geay et al. (2018) evaluated Petrut et al.'s (2018) algorithm and proportional relationships developed by

Thorne (1988) on several other rivers with mixed results. Most investigators have estimated bedload transport rates using a measure of the acoustic power which is then regressed with total and/or partial bedload measurements to develop rating curves similar to discharge to bedload transport rates. Measures of acoustic power were derived by integrating the power spectrum density for select frequency ranges of short (1-2 minute) acoustic recordings (e.g., Barton 2010, Geay 2018a, Rigby et al. 2016, Marineau et al. 2016).

Continuous hydroacoustic data was collected in conjunction with bedload transport samples to provide estimates of bedload transport for use in Trinity River Restoration Program (TRRP) efforts. This work adds to the growing body of bedload SGN work in order to improve our understanding of the relationships between hydroacoustic measurements and bedload transport and determine the level of sampling effort.

Study Site

The Trinity River is the largest tributary to the Klamath River in Northern California (Figure 1) and supported large runs of steelhead and Chinook and coho salmon. In the early 1900's, the river corridor was heavily disturbed by dredger mining for gold (Figure 2) which removed most of the riparian vegetation and completely reworked the river corridor stratigraphy from the North Fork Trinity River to upstream of the Trinity Reservoir. In addition, placer mining eroded many of the hillslopes and tributaries. From 1950 onward, the watershed was heavily logged which introduced large quantities of fine granitic sand into the mainstem. In the early 1960's, the upper third of the watershed was blocked by the Trinity River Diversion Dams which were completely filled during the 1964 flood. Once the dams were built, 90% of the flow was diverted to the Central Valley Project and the downstream release from Lewiston Dam was reduced to a constant 150 cfs year round. After rapid declines in the fisheries populations, the flows were raised to 300 cfs but the low flows, granitic fine sand, and riparian encroachment continued to degrade aquatic habitat. To restore the fisheries, the Secretary of the Interior authorized the Trinity River Flow Evaluation Study (Flow Study, USFWS and HVT 1999) to determine how to restore the fishery resources.

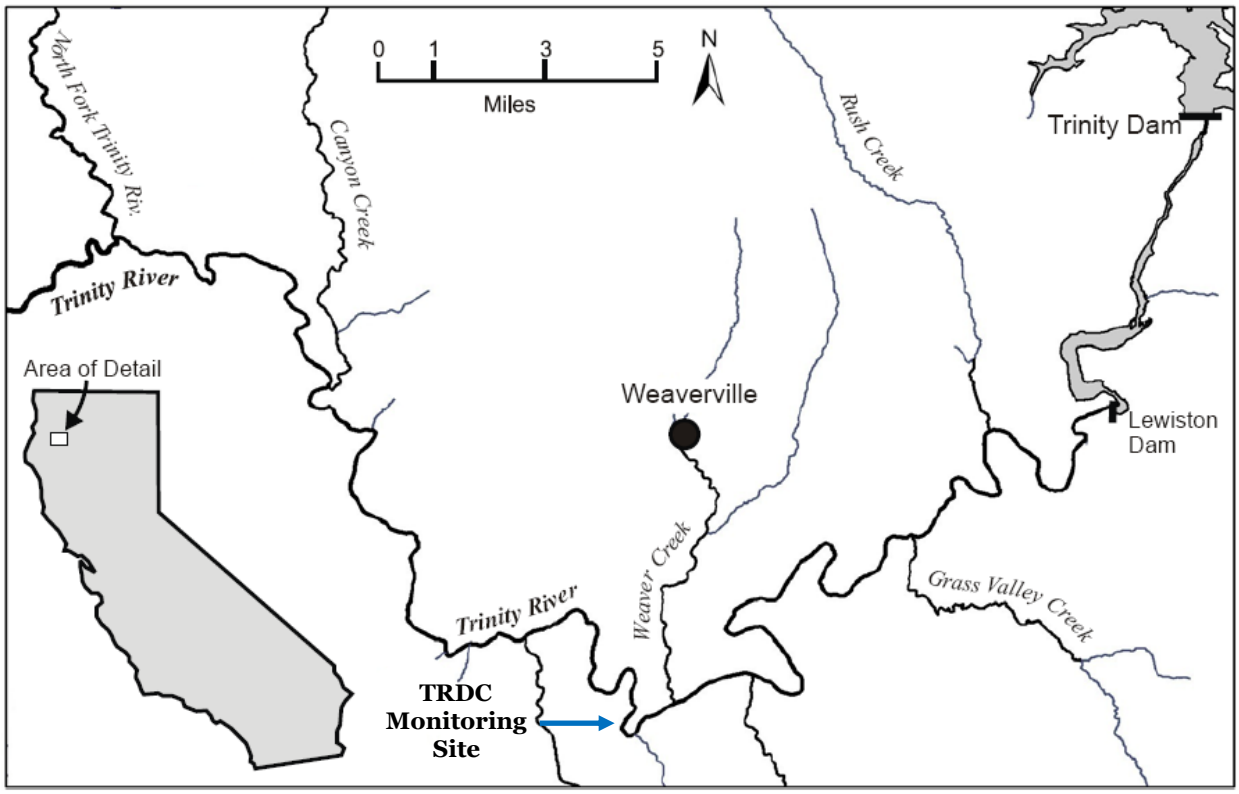

Figure 1. Trinity River restoration reach between Lewiston Dam and the North Fork Trinity River.

Figure 2. Trinity River dredger impacts. Note the removal of the riparian vegetation, the altered stratigraphy, and dredger tailing piles. The heavily placer mined Oregon Gulch flows into the upper center of the photo.

The Flow Study (USFWS and HVT 1999) recommendations for water year based flow and sediment management, mainstem channel rehabilitation, and adaptive management were implemented under the record of decision (ROD, BOR 2000). The Trinity River Restoration Program (TRRP) was established to help implement the ROD and restore the salmonid fisheries in the 40 miles from Lewiston Dam to the North Fork Trinity River. Congress authorized 50% of the reservoir inflow to the river and the 50% to the Central Valley Project. Flows are currently released to the river at a rate of 450 cfs during the summer, 300 cfs during the fall and winter months, and as a spring dam release based on five water year types, with peak flows ranging from 1,500 (critically dry) to 11,000 cfs (extremely wet). The TRRP adaptively develops annual spring flow hydrographs that are intended to achieve specific geomorphic, riparian, and fish habitat related objectives outlined in the Flow Study, other TRRP documents, and as new science adaptively dictates.

Bedload sediment is collected during spring dam releases by Graham Matthews Hydrology Inc. (e.g., GMA, 2017; 2018) for the TRRP at four bedload monitoring stations as part of the sediment management program. The information is principally used to support gravel augmentation efforts tracked using a coarse sediment budget (Figure 3). The downstream monitoring station is located just downstream of the USGS's Trinity River near Douglas City, California (TRDC, Figure 3) streamflow gaging station (#11525854). This station is located just downstream of Indian, Weaver, and Redding creeks where it is generally recognized that the coarse sediment deficit ends below the dams. The channel at the sampling site is approximately 160 feet across (Figure 4).

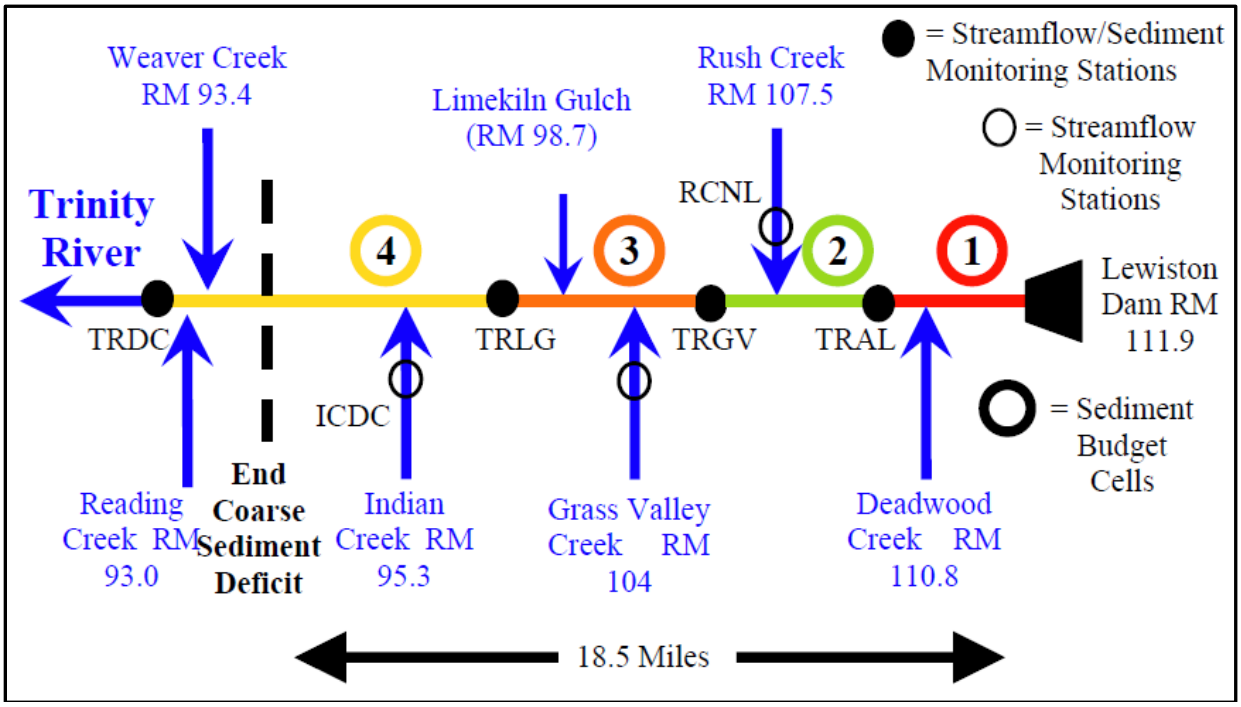

Figure 3. Schematic diagram showing the Trinity River sediment budget cells and tributary inputs (TRRP, trrp.net). This study monitored bedload SGN at the Trinity River near Douglas City (TRDC) bedload monitoring station at the downstream end of the sediment budgeting reach.

Figure 4. Trinity River near Douglas City, CA bedload sampling site. Discharge is approximately 13,000 cfs. The hydrophones were on both banks just upstream of the photo.

While the robust bedload sampling program has provided the TRRP with a wealth of data and information for sediment management, the program is relatively expensive. In an effort to reduce the quantity of physical sample collection and processing - yet improve the temporal resolution - TRRP has encouraged the use of hydrophone systems on the Trinity River (Barton 2006, Smith, unpublished data, Goodwiller 2014; Marineau et.al. 2016) as surrogates for bedload transport.

Methods

Hydrophones and audio recorders were set up on the left and right banks approximately 25 meters upstream of the bedload sampling cross section. Near-continuous hydroacoustic recordings were collected during the 2017 spring dam releases at TRDC in conjunction with physical bedload sampling efforts. The hydrophones were purchased from Cetacean Research Technology which combines pre-amps, coaxial cables and connectors with Sensor Technology Limited SQ26 hydrophones. The hydrophones have a relativity flat frequency response ($\pm$ 3 dB) across the range of 0-30,000 Hz. Tascam DR22-WL recorders were used to record near continuous one hour WAV (96 kHz sampling rate and 24 bit file format) files during the spring dam releases. The hydrophone and recorder systems have a sensitivity of -165.1 dB re 1 V/µPa at a relative, recorder gain setting of 20 (maximum dynamic range).

Bedload samples were collected by GMA Hydrology using a TR-2 bedload sampler operated from a cataraft attached to a cableway. Bedload was collected every 3 meters (10 feet) across the cross section. The number of stations varied from 12-15 depending on flow level and safety concerns (large wood transport). Individual sampling times ranged from 30-60 seconds depending on transport rates. Single pass, cross section samples took approximately 30-45 minutes to collect. Sediment transport rates shifted across the channel throughout the hydrograph. However, the sediment transport rates were typically higher along the right bank or center of the channel. GMA processed all the bedload samples and produced an annual report with detailed technical appendixes that can be found on TRRP webpage's data port (www.trrp.net/library/). WY2017 bedload samples are summarized in Table 1. The annual flow hydrograph for WY2017 is displayed in Figure 5.

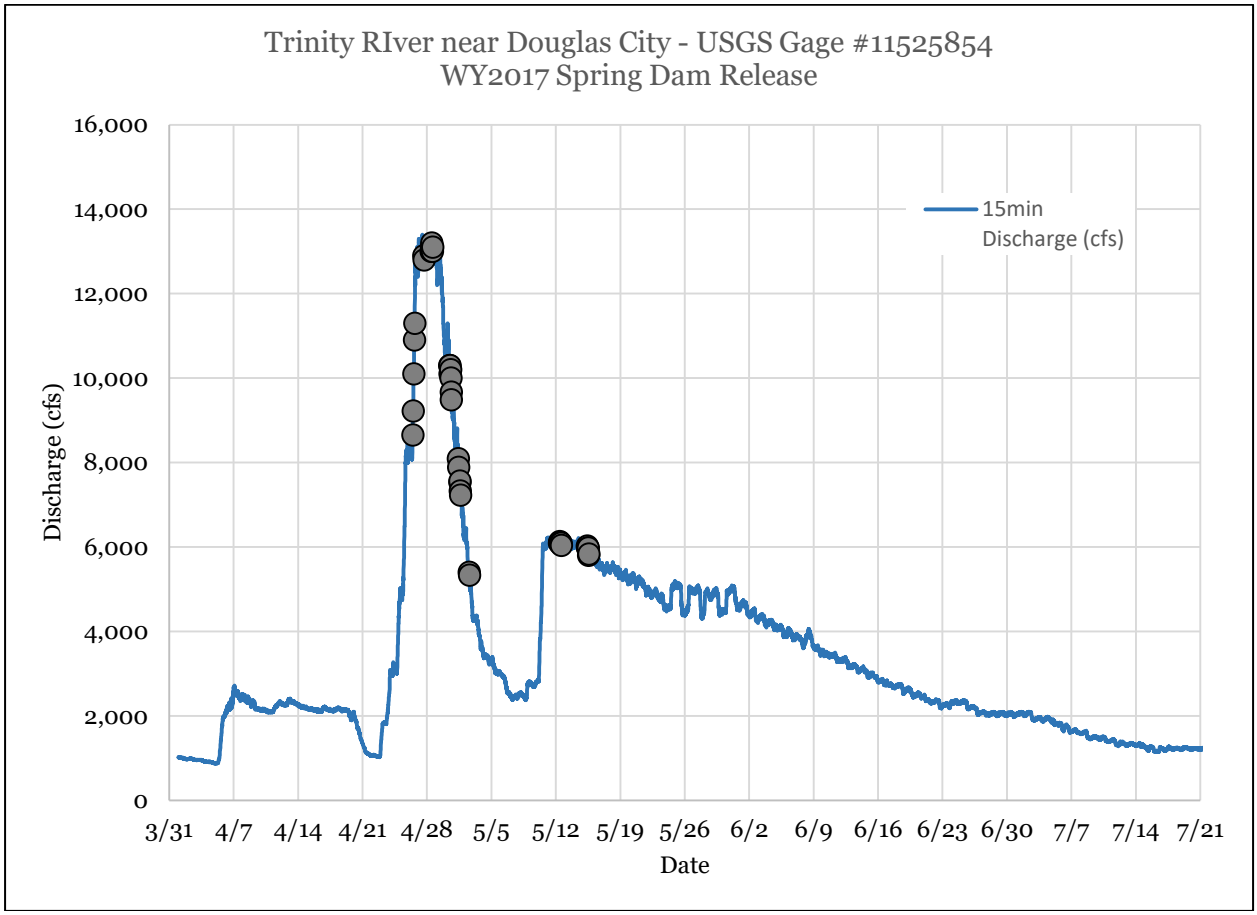

Figure 5. WY2017 spring dam release hydrograph at the USGS's Trinity River near Douglas City, CA (#11525854) displaying when bedload sampling occurred (modified from GMA 2018).

The relationship between underwater sound and bedload sediment transport was evaluated following the logic outlined by Thorne (2014) and others (e.g., Barton 2006, Rigby et al. 2014, Marineau et al. 2016, and Petrut et al. 2018) which integrates hydroacoutic power spectrums across various frequency ranges generated from one-minute recordings of SGN collected during bedload sampling. These values are regressed with total or partial bedload sediment transport rates. Power spectral densities were computed using a Fast Fourier Transform with Hanning window, 2048 window size, and 50% overlap. The frequency resolution was 90,000/2/1024 = 46.9 Hz. Acoustic power was integrated over frequency ranges from particle size to frequency relationships (Jonys 1976, Millard, 1976, Thorne 1985 and 1986, and Belleudy 2016): 7,800-15,000 Hz (8-16 mm), 2,300-7,800 Hz (16-32 mm), 1,700-2,300 Hz (32-64 mm), and 1,400-1,700 (64-90 mm). Estimates were also made for various combinations of the latter frequency ranges and the entire useable frequency range likely producing bedload SGN, 100-21,000 Hz. Based on the work by Jonys (1976), Millard ( ), Thorne (1985, 1986, 2014), Petrut et al. (2018) and others relating particle sizes to different centroid frequencies, it was unlikely that a sampling rate of 96,000 Hz would accurately measure frequencies associated with particles

much <8 mm. Therefore, integrated measures of the PSDs across various frequency bands were compared to fractions of bedload samples including the coarse (>8 mm) partial and total bedload.

Acoustic data files were reduced to 1 minute files and power spectral densities were computed for each file. Following the integrated power approach Rigby et al. (2014) used in equation (1) integrated power was computed across multiple acoustic files that spanned the bedload sampling times. Integrated power should be proportional to cross sectional average bedload transport rates.

$$Integrated\ Power = \sum_{i=1}^{N} \Delta t_i \int_{f}^{f+\Delta f} PSD(f)df \qquad (1)$$

PSD is the power spectral density for a one minute acoustic recording, f is the lower end of the frequency range of interest and Δf is the interval of the power spectral density windows, N is the number of 1 minute acoustic files collected during the bedload sampling period. Acoustic files and bedload sample data were processed using MATLAB and Excel. Various lag times were also examined to account for the hydrophones distance upstream of the bedload sampling cross section.

Results

Most of the linear correlations between bedload SGN derived integrated power and total and partial bedload transport rates were moderate to weak (R^2 <0.7). The best correlations (Figure 6) were from frequency ranges across the peak portion of the PSD (Figure 7) where bedload SGN dominated (approximately 1,000-5,000 Hz). While the regressions bedload with SGN were generally weaker than with discharge, the variability in SGN appears to explain the temporal and to a lessor extent the cross sectional spatial variability better than discharge.

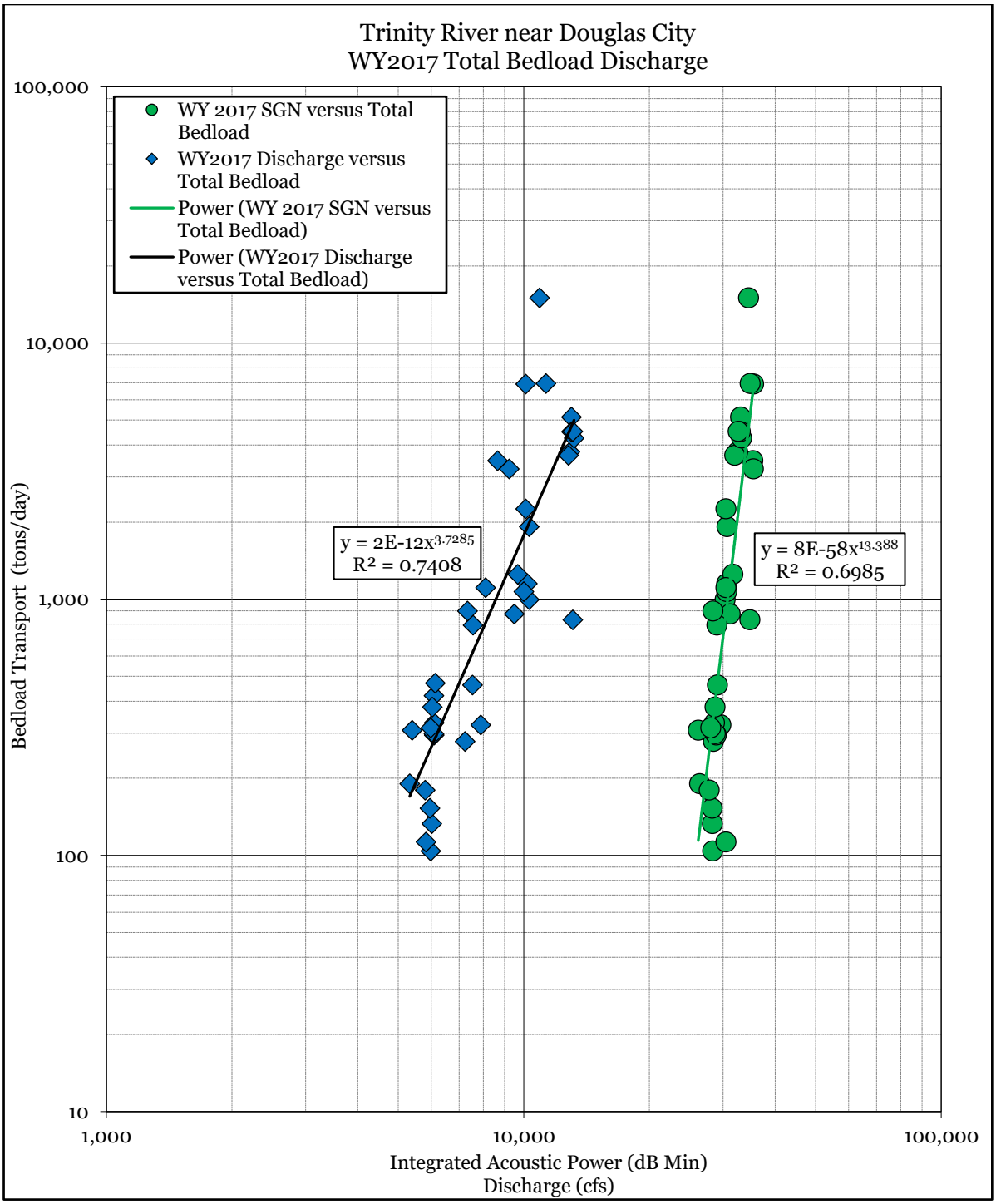

Figure 6. Total bedload transport rating curves derived from discharge (blue diamonds) and SGN across the frequency range 1,700-2,300 Hz (green circles) measured at Trinity River near Douglas City, CA (bedload data from GMA 2018).

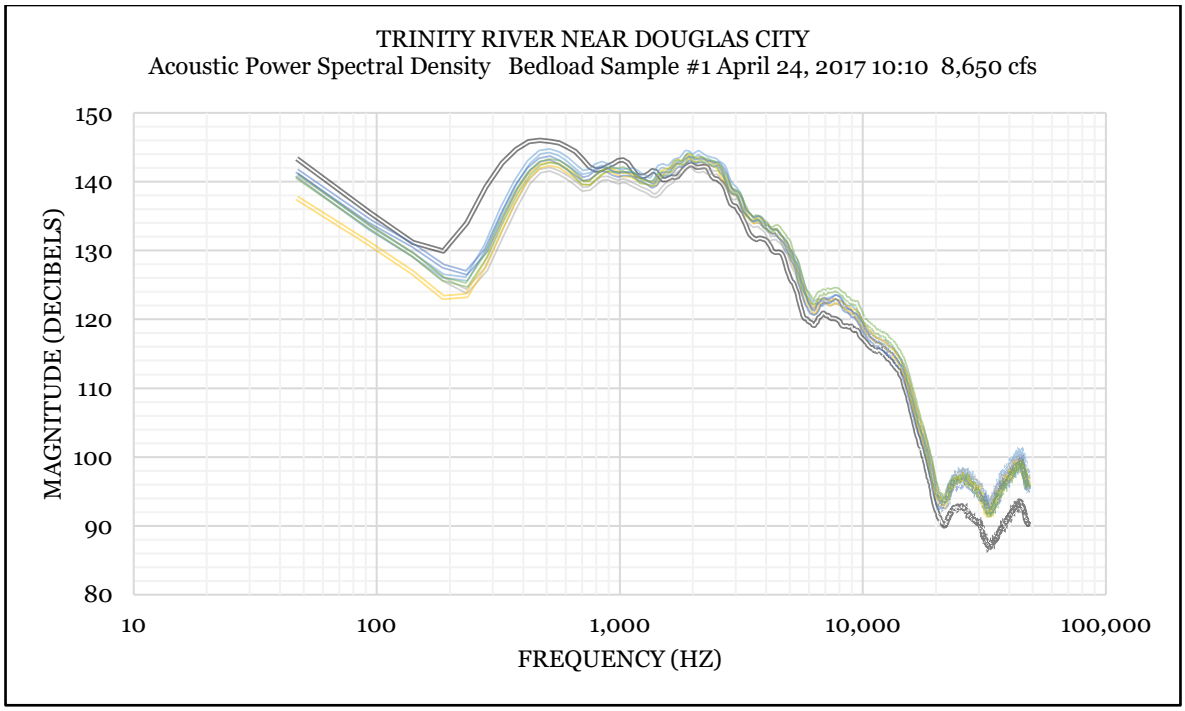

Figure 7. One minute power spectral densities measured at Trinity River near Douglas City. Only four PSDs spread across the entire bedload sampling time are displayed for clarity.

Future work for the presentation include:

1. Comparisons between bedload SGN derived integrated power and the number of particles in each bedload size fraction.
2. Comparison between acoustic frequencies and particle size classes using Petrut et al.'s (2018) algorithm.
3. Evaluation between bedload SGN derived from left and right banks.
4. Sampling interval level of effort. Compare 1, 5, 15, and 1 hour recording time PSDs.
5. Comparisons between visual bedload movements (e.g., turbulent bursts, sand waves, large rock rolling) using underwater video of TR-2 sampling and hydroacoustic recording.

Table 1. WY2017 Bedload samples and corresponding sediment generated acoustic power spectrum densities collected at Trinity River near Douglas City, CA monitoring site (GMA 2018).

Trinity River at Douglas City - 11525854
Bedload Sampling Summary WY2017

Sample Number	Date & Mean Time	Average Discharge (cfs)	Total Bedload Discharge (tons/day)	> 8mm Bedload Discharge (tons/day)	0.5-8 mm Bedload Discharge (tons/day)
TRDC-BLM2017-01	04/26/2017 10:37	8,650	3470	2420	1000
TRDC-BLM2017-02	04/26/2017 11:37	9,220	3220	2450	710
TRDC-BLM2017-03	04/26/2017 13:23	10,100	6910	5450	1340
TRDC-BLM2017-04	04/26/2017 15:09	10,900	15000	13300	1540
TRDC-BLM2017-05	04/26/2017 15:48	11,300	6950	5280	1450
TRDC-BLM2017-06	04/27/2017 15:10	12,900	3760	3330	414
TRDC-BLM2017-07	04/27/2017 15:50	12,800	3640	2960	661
TRDC-BLM2017-08	04/28/2017 10:28	13,000	5140	4090	1020
TRDC-BLM2017-09	04/28/2017 11:29	13,100	830	556	264
TRDC-BLM2017-10	04/28/2017 12:02	13,200	4250	3090	1140
TRDC-BLM2017-11	04/28/2017 13:53	13,000	4510	2560	1910
TRDC-BLM2017-12	04/28/2017 14:32	13,100	4520	4160	338
TRDC-BLM2017-13	04/30/2017 10:42	10,300	1920	1450	451
TRDC-BLM2017-14	04/30/2017 11:30	10,100	2250	1650	580
TRDC-BLM2017-15	04/30/2017 11:58	10,300	996	681	307
TRDC-BLM2017-16	04/30/2017 12:58	10,200	1150	846	295
TRDC-BLM2017-17	04/30/2017 13:53	10,000	1070	885	174
TRDC-BLM2017-18	04/30/2017 14:38	9,670	1250	828	409
TRDC-BLM2017-19	04/30/2017 15:11	9,490	876	481	385
TRDC-BLM2017-20	05/01/2017 09:32	8,090	1110	699	409
TRDC-BLM2017-21	05/01/2017 10:11	7,890	323	229	91
TRDC-BLM2017-22	05/01/2017 13:20	7,530	462	298	155
TRDC-BLM2017-23	05/01/2017 13:52	7,560	792	459	323
TRDC-BLM2017-24	05/01/2017 14:37	7,330	898	538	351
TRDC-BLM2017-25	05/01/2017 15:17	7,230	278	226	50
TRDC-BLM2017-26	05/02/2017 13:55	5,400	308	154	146
TRDC-BLM2017-27	05/02/2017 14:24	5,330	190	112	76
TRDC-BLM2017-28	05/12/2017 08:56	6,090	420	304	112
TRDC-BLM2017-29	05/12/2017 09:48	6,130	470	249	211
TRDC-BLM2017-30	05/12/2017 10:57	6,100	295	123	164
TRDC-BLM2017-31	05/12/2017 11:33	6,100	329	182	140
TRDC-BLM2017-32	05/12/2017 13:36	6,090	299	178	114

TRDC-BLM2017-33	05/12/2017 13:42	6,040	379	148	222
TRDC-BLM2017-34	05/15/2017 09:47	6,020	133	99	33
TRDC-BLM2017-35	05/15/2017 10:30	5,980	104	74	29
TRDC-BLM2017-36	05/15/2017 11:22	5,960	153	98	53
TRDC-BLM2017-37	05/15/2017 12:03	5,980	314	248	65
TRDC-BLM2017-38	05/15/2017 12:46	5,800	180	96	80
TRDC-BLM2017-39	05/15/2017 13:22	5,830	113	91	21

Values Rounded According to Porterfield (1972)

References

Barton, J.S., (2006). Passive acoustic monitoring of bedload in mountain streams: University Park, PA, The Pennsylvania State University, Ph.D., 107 p.

Barton, J.S., Slingerland, R.L., Pittman, S., and Gabrielson, T.B., 2010. Monitoring coarse bedload transport with pas-sive acoustic instrumentation: a field study. in Gray, J. R., Laronne, J. B., and Marr, J. D. G., Bedload-surrogate mon-itoring technologies: U.S. Geological Survey Scientific In-vestigations Report 2010-5091.

Geay, T., S. Zanker, A. Hauet and A. Recking 2018a. An estimate of bedload discharge in rivers with passive acoustic measurements: Towards a generalized calibration curve? Volume 40. River Flow 2018 - Ninth International Conference on Fluvial Hydraulics

Geay, T., S. Zanker, T. Petrut and A. Recking 2018b. Measuring bedload grain-size distributions with passive acoustic measurements. Volume 40. River Flow 2018 - Ninth International Conference on Fluvial Hydraulics

GMA Hydrology, Inc., 2018. WY 2017 Sediment Transport Monitoring Report. Report for Trinity River Restoration Program, US Bureau of Reclamation, Shasta Lake, CA.

Jonys, C. K., 1978. Acoustic Measurement of Sediment Transport. Scientific Series No. 66, Inland Waters Division, Environment Canada.

Marineau, M.D., S.A. Wright, D. Gaeuman. 2016. Calibration of Sediment-generated noise Measured using Hydrophones to Bedload Transport in the Trinity River, California, USA. *In Proc. of River Flow conference* : 1519–1526.

Millard, N. W., 1976. Noise Generated by Moving Sediments, in Recent developments in underwater acoustics: pro-ceedings of the conference held at the Admiralty Under-water Weapons Establishment, Portland, vol. 3.5.

Petrut, Teodor-Ion & Geay, Thomas & Gervaise, Cédric & Belleudy, Philippe & Zanker, Sebastien. (2017). Passive Acoustic Measurement of Bedload Grain Size Distribution using the Self-Generated Noise. Hydrology and Earth System Sciences Discussions. 1-34. 10.5194/hess-2017-171.

Porterfield, G., 1972. Computation of fluvial-sediment dis-charge. Chapter C3, Book 3, Applications of Hydraulics, U.S. Geological Survey.

Rigby, J.R., R. Kuhnle, B. T. Goodwiller, M. H. Nichols, W.G. Wren. 2016. Sediment-Generated Noise (SGN): Comparison with Physical Bed Load Measurements in a Small Semi-Arid Watershed.

Ruggiero, A., M. C. De Simone, D. Russo, and D. Guida, 2016. Sound pressure measurement of orchestral instruments in the concert hall of a public school. International Journal of Curcuits, Systems and signal processing. Volume 10, 2016.

Thorne, P.D., 1986. Laboratory and marine measurements on the acoustic detection of sediment transport. *Journal of the Acoustic Society of America*, 80(3), 899, doi:10.1121/1.393913.

US Fish and Wildlife Service and Hoopa Valley Tribe, 1999. *Trinity River Flow Evaluation Final Report*, Arcata, CA, pp. 400.

Interactions among Gravel and Sand Fractions during Transport as Measured by Impact Plates and Sedflux Monitor in a Laboratory Channel

Roger A. Kuhnle, Research Hydraulic Engineer, USDA-ARS, National Sedimentation Laboratory, Oxford, MS, roger.kuhnle@ars.usda.gov
Daniel G. Wren, Research Hydraulic Engineer, USDA-ARS, National Sedimentation Laboratory, Oxford, MS, daniel.wren@ars.usda.gov
Robert C. Hilldale, Hydraulic Engineer, U. S. Bureau of Reclamation, Denver, CO, rhilldale@usbr.gov

Abstract

Accurate measurements or predictions of bed load transport are difficult to make for alluvial channels especially when the bed material consists of a mixture of sand and gravel. A series of experiments were conducted in a laboratory flume in which gravel and total bed load rates were measured continuously using independent methods. The effect of four different antecedent conditions on the transport of bed load during a standard low flow condition was evaluated in a series of experiments. It was found that different mean rates of bed load transport occurred for the standard low flow following different antecedent flow strengths. This work indicates that a portion of the uncertainty of accurately predicting transport rates for gravel bed streams is likely caused by changes in the surface characteristics of the gravel bed that result from antecedent flows which affect the rate of transport for subsequent other flows.

Introduction

The large temporal and spatial variations that characterize the transport of bed load make it very challenging to measure or estimate accurately. Recent studies have shown that the characteristics of the bed surface layer as well as the grain size information are required to predict rates of bed load transport. The flow history has been shown to be a factor in the type of characteristics that form on the bed of streams with gravel in the bed material (Mao, 2018; Ockelford and Haynes, 2013). Inadequate knowledge of the characteristics of the bed surface layer are among the factors that make it challenging to accurately predict the rate of bed load transport for a given flow strength. In this study the bed load transport was measured using a standardized flow after four antecedent flows had been imposed on a flume channel with a bed consisting of gravel and sand.

Methods

Experiments were conducted in a flume channel 30-m long, 1.2-m wide, and 0.6-m deep with an adjustable longitudinal slope. Seven experiments, in which steady flows were imposed on the channel, were completed in this study. The four standard experiments (1a-1d) had nearly the same flow and the three other experiments (2a-2c) were of greater flows and served along with the initial screeded bed as the antecedent flows in this study (Table 1). The sediment in the flume was a bimodal mixture of sand (modal diameter = 0.5 mm) and gravel (modal diameter =22.6 mm) with a range in sizes from 0.062 to 45 mm. Sediment and water were recirculated

and bed load rate was measured at 1 Hz with two recording drum samplers in a trap which spanned the entire width of the channel.
Four experiments had the same flow but were run after different antecedent flows thus yielding unique recent past flow histories in each case. Experiment 1a was conducted after the bed was mixed and screeded flat. The runs were conducted in the order in which they are listed in Table 1. The bed was not remixed or screeded after the experiments began.

Results

The rates of bed load transport for the four standard flow rates are shown in Figure 1. The mean rates of sediment transport and fluctuations about the mean were different for the four experiments. The magnitude of the first peak in the transport of bed load is also different in the four experiments. The ratios of the standard deviation to the mean bed load rate (coefficients of variation) (Table 1) in the experiments were found to be greatest for the first experiment (1a) and to decrease for the next two standard flow experiments until increasing again for the fourth experiment (1d).

Conclusions

The different mean bed load transport rates and coefficients of variation for the four standard experiments (1a – 1d) resulted from the different previous flows to which the channel was subjected. It is likely that these measured differences in bed load transport for equivalent flows resulted from different characteristics of the bed surface layer which formed during the different antecedent flows to which the channel was subjected. The changes in bed surface characteristics caused by the antecedent flows persisted in the standard experiments for at least 45 hours. These findings are consistent with results from a previous study (Mao, 2018).

Table 1. Flow conditions during the experiments

Experiment	Total run time (hr)	Flow discharge (m^3/s)	Mean flow depth (m)	Froude number	Mean bed load transport rate (kg/hr)	Coefficient of variation of bed load
1a	47.2	0.250	0.253	0.51	28.6	0.94
2a	47.0	0.295	0.256	0.60	189.6	
1b	46.5	0.248	0.260	0.49	39.1	0.92
2b	46.4	0.324	0.268	0.61	359.0	
1c	47.6	0.247	0.262	0.48	35.1	0.71
2c	45.2	0.343	0.264	0.66	666.7	
1d	46.7	0.249	0.263	0.48	33.0	0.79

References

Mao, L., 2018. The effects of flood history on sediment transport in gravel-bed rivers. Geomorphology, 322, 196-205.

Ockelford, A. M., Haynes, H., 2013. The impact of stress history on bed structure. Earth Surface Processes and Landforms, 38, 717-727.

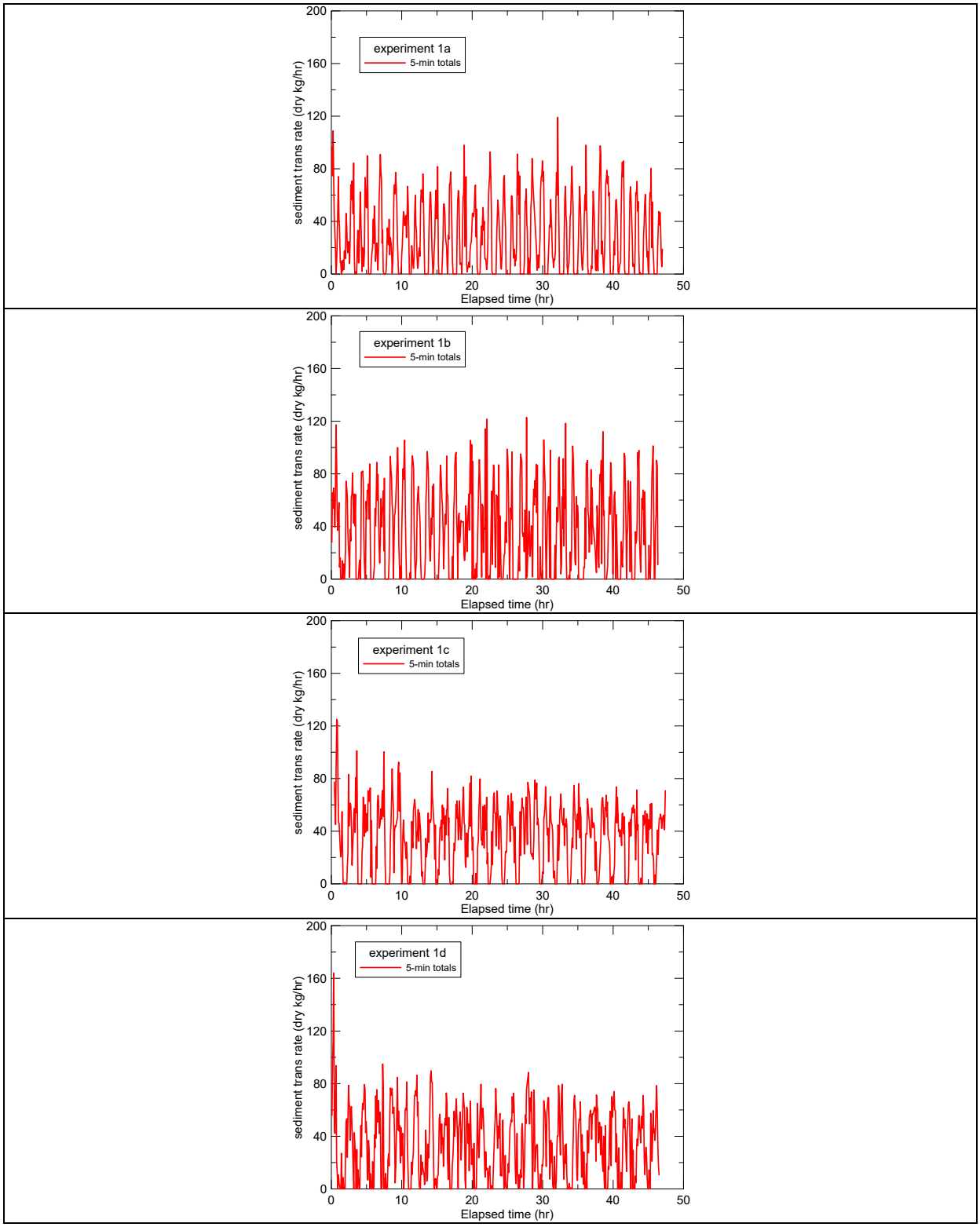

Figure 1. Bed load transport versus time for the four experiments with standard flows in this study.

Initial Calibration of Acoustic Pipe Microphone Sensors to Monitor Bedload During Flash Floods in the Arroyo De Los Piños, NM

Kyle Stark, New Mexico Institute of Mining and Technology, Socorro, NM, kyle.stark@student.nmt.edu
Dr. Daniel Cadol, New Mexico Institute of Mining and Technology, Socorro, NM, daniel.cadol@nmt.edu
Dr. Jonathan B. Laronne, Ben Gurion University of the Negev, Beer Sheva, Israel, john@bgu.ac.il
David Varyu, United States Bureau of Reclamation, Denver, CO, dvaryu@usbr.gov
Eran Halfi, Ben Gurion University of the Negev, Beer Sheva, Israel, eranhalf@post.bgu.ac.il
Madeline Richards, New Mexico Institute of Mining and Technology, Socorro, NM
madeline.richards@student.nmt.edu

Abstract

The Arroyo de los Piños sediment monitoring station includes numerous novel bedload monitoring instruments. Bedload is measured directly using Reid-type slot samplers; these instruments can be used to calibrate a number of different surrogate methods to monitor bedload. Here we present our initial analysis of two pipe microphone impact sensors. Pulses are generated from bedload striking the pipe, causing acoustic noise that is recorded by a microphone sealed within the pipe. A pulse is counted when the acoustic power exceeds a predetermined threshold.

Five flood events, ranging widely in discharge, have been recorded to date at the Piños. The pipe microphone time series differ both laterally and temporally. At times, at a given water depth the pipe microphone positioned near the left bank received nearly twice as many pulses as the right pipe microphone. Counter-clockwise hysteresis takes place in both pipe datasets during the largest event. As much as 50% more pulses were recorded during the recession limb for a given water depth. Some drawbacks of using pipe microphone were also considered. Some dampening of the microphone response was observed, possibly due to partial cover of the pipes by sediment. These sensors have been successfully used in other channels worldwide; once properly calibrated, pipe microphones can be an effective alternative to painstaking manual measurement of bedload transport.

Introduction

Studies of sediment transport in ephemeral channels in arid environments are limited. Few point measurements, let alone continuous datasets, exist in dryland ephemeral channels. These regions are home to more than two billion people; populations in these areas face many obstacles from water scarcity to land degradation (United Nations, 2010). Understanding how ephemeral channels transport sediment is important from a global perspective because of the number of people affected. Comprehension of sediment transport is imperative to understanding the channels, their morphology and dynamics. Flow in these channels can be

rare, but sediment production is high (Langbein & Schumm, 1958), promoting rapid reservoir sedimentation (Laronne & Wilhelm, 2001; Tolouie et al., 1993) and channel instability (Graf, 1981).

The Rio Grande is a perennial river in the center of the largest semi-arid region in the United States. A crucial part of life in the Southwest U.S., the Rio Grande and other mainstem perennial rivers allow for development in this region. Constant maintenance along such rivers is required to ensure that communities have consistent access to water. These rivers are often modeled to predict changes and allow for effective management. The largest source of uncertainty in modeling these rivers is associated with the sediment influx from ephemeral tributaries. The United States Bureau of Reclamation (USBR) is tasked with managing, developing, and protecting water and water-related resources in the western United States. In 2016, the USBR identified the Arroyo de los Piños as a prime candidate to improve Rio Grande sediment dynamics modeling. Once a site was chosen, other federal agencies began to support the project; the U.S. Army Corps of Engineers added financial support as well as technical expertise in experimental design. Work began on a world-class sediment monitoring station on the Piños with construction being completed in early 2018 (Varyu et al., 2019).

As a tributary of the Rio Grande, the Piños is typical of many drainage basins in the southwest. Flash floods carry sediment directly into the Rio Grande causing a localized influx at the confluence. Sediment is easily transported by the Piños due to the lack of armoring and vegetation. Runoff production is highest where intense monsoonal storms cover areas of thin soils and sparse hillslope vegetation in the basin. The geologic setting varies throughout the basin (Cather & Colpitts, 2005). Near the Rio Grande, the channel is anastomosing as it crosses Pliocene and Pleistocene ancestral floodplain and alluvial fan deposits. Further upstream the channels are confined through canyons and valleys eroded into the more cohesive early Paleozoic sandstones, limestones, and shales.

The Piños is located at the northern extent of the Chihuahuan Desert. This desert is semi-arid; it has a mild continental climate characterized by small annual precipitation, year-round sunshine, relatively large annual temperature changes, diurnal temperature changes, and an average annual precipitation of 237 mm (DRI, 2013). July and August are the rainiest months; 35% of annual precipitation falls during these 62 days. Summer monsoonal rains occur during brief, but intense storms. Flash flooding occurs locally in these areas because of the intensity of rainfall, sparse vegetation and thin soils.

Surrogate methods to monitor bedload have been studied for more than 50 years (see references in Rickenmann et al., 2012, 2014). However, field calibrations, especially in arid environments, are relatively rare. Much of the current field calibration relies on few sites (Mizuyama et al., 2010; Rickenmann et al., 2014). One site in particular, the Nahal Eshtemoa, is home to another semi-arid sediment monitoring station. It includes many of the same instrumentation types that are currently deployed at the Arroyo de los Piños (Cohen et al., 2010; Laronne & Reid, 1993). The Nahal Eshtemoa basin is larger and the bed is coarser. Twenty percent of the Eshtemoa bed material is smaller than 2 mm and about 10% is smaller than 62.5 μm (Powell et al., 2001). When considering the 2-fraction theory of bedload transport, this difference suggests that certain fractions of the Piños bed are entrained earlier and at higher fluxes for a given reach shear stress when compared to the Eshtemoa. With a higher sand content, experimental results (e.g. Miwa & Parker, 2017) show that more bedload is transported at lower critical shear stresses. Particular attention should be paid to small flow events (i.e. water depth less than 35 cm); in the Eshtemoa these do not transport much bedload, especially in recent years when the

bed accumulated loess deposits, whereas in the Piños they are likely to move a significant fraction of the bed material. The addition of the Piños-calibrated surrogate methods (see also Dietz et al., 2019; Marineau et al., 2019) will add a much-needed higher sand fraction channel to the list of sites hosting these instruments.

Methods

The heart of the system is three automatic Reid-type slot samplers (Reid et al., 1980, Figure 1). These instruments measure bedload continuously and directly. Bedload falls through a slot in the channel bed into a buried vault containing a steel box. The width of the slot can be adjusted using sliding plates. The box rests on a pillow that records the pressure change associated with the mass of sediment displacing water within the box. A separate transducer located between the outer and inner boxes records the hydrostatic pressure associated with the overlying water column. These pressure gains are converted into a bedload flux per unit width of channel using known masses added sequentially to the pit (Equations 1a-1c):

$$y = 6.8x - 679,\ r^2 = 0.999 \ \text{(left sampler)} \qquad \text{Eq. 1a}$$
$$y = 6.9x - 691,\ r^2 = 0.997 \ \text{(center sampler)} \qquad \text{Eq. 1b}$$
$$y = 6.2x - 602,\ r^2 = 0.997 \ \text{(right sampler)} \qquad \text{Eq. 1c}$$

where y is the response of the pillow and x is the mass on the pillow. The slopes of the lines are different due to the slight differences in the setup of each sampler. These samplers provided a physical basis to evaluate all of the surrogate methods deployed at the Arroyo de los Piños (Cadol et al., 2019).

Indirect methods of monitoring bedload at this site include pipe microphones, a plate microphone, a geophone underneath an impact plate, hydrophones, and a seismometer. Here, we evaluate the results from the pipe microphones during the first set of seasonal monsoonal flows. The pipe microphones are installed directly upstream of the left and the right slot samplers. Bedload strikes the pipe and continues downstream. The acoustic sound is recorded by a microphone installed within the pipe; A pulse is recorded when the acoustic power of the impact exceeds a threshold. These pulses are counted continuously at multiple amplifications, similar to the process described in Mizuyama et al., 2010(a) and Mizuyama et al., 2010(b). At the Piños site, ten amplifications are recorded. Each amplification requires a different threshold of acoustic power to count a pulse.

Results

Five flood events were recorded at the Arroyo de los Piños sediment research station during 2018 (Table 1). Water depth, bedload and acoustic data were collected automatically. Bedload flux measured by the Reid samplers represents a small fraction of each flood; the Reid samplers filled quickly once water depth reached a critical level. The response from the pipe microphones preserves a record of bedload flux during the entire event. Some of the largest amplifications become saturated at higher bedload fluxes (Figure 2). These amplifications are removed so that the response of each microphone can be compared between events (Figure 3). The non-saturated amplifications can be calibrated for the filling time of the Reid samplers. Traditionally, this was accomplished using time-averaging methods. The instruments were calibrated during a given predetermined timeframe. Here, we adopt a mass-threshold technique developed by Halfi et al., 20189 [*in review]*. This technique is more robust; once a mass threshold is reached, the

pulses are counted within that time period, regardless of its length. Our data are collected every one minute, which far exceeds the typical threshold used for the Reid sampler system, but the practice of comparing cumulative mass and cumulative pulses is sustained.

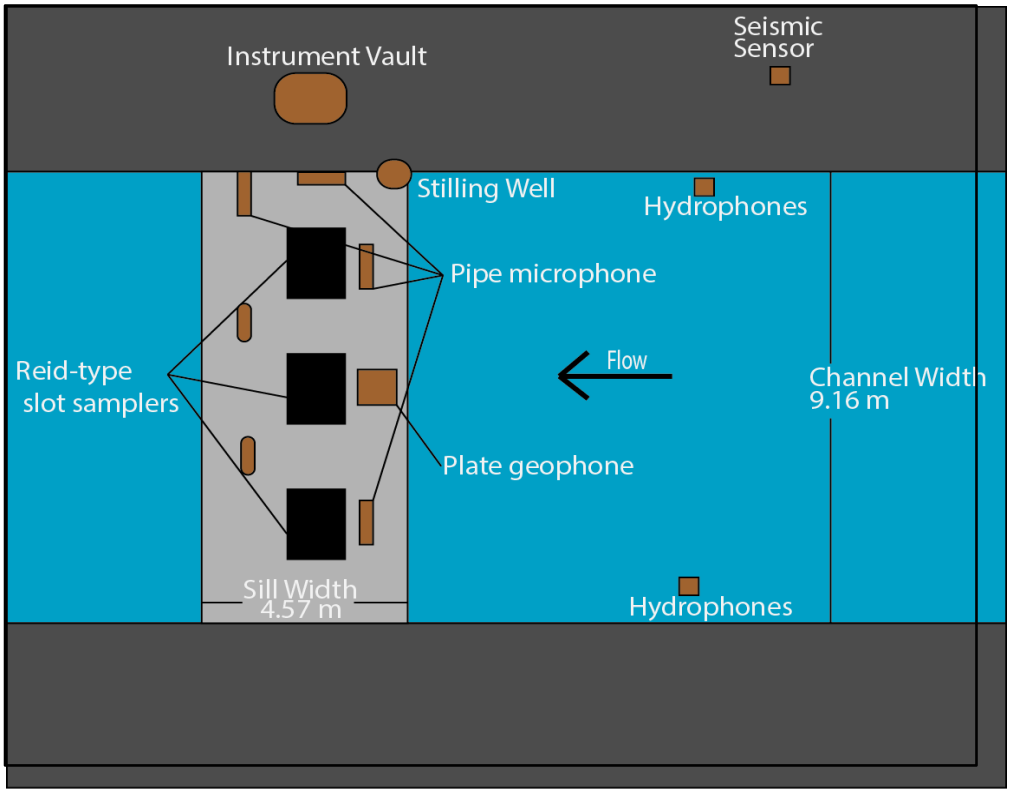

Figure 1. Schematic of the Piños monitoring station and instrument design.

Table 1. Characteristics of the five floods recorded to date at the Piños sediment monitoring facility. They include a wide range of discharges. The bedload fluxes are high by all standards.

Flood	*Duration (hours)*	*Maximum Water Depth (cm)*	*Maximum Bedload Flux (kg/sm)*
July 16th	3.00	60	8.0
July 26th	5.50	161	16.5
August 9th	1.75	17	6.5
August 24th	2.75	32	10.5
September 1st	5.50 (two storms)	15	2.5

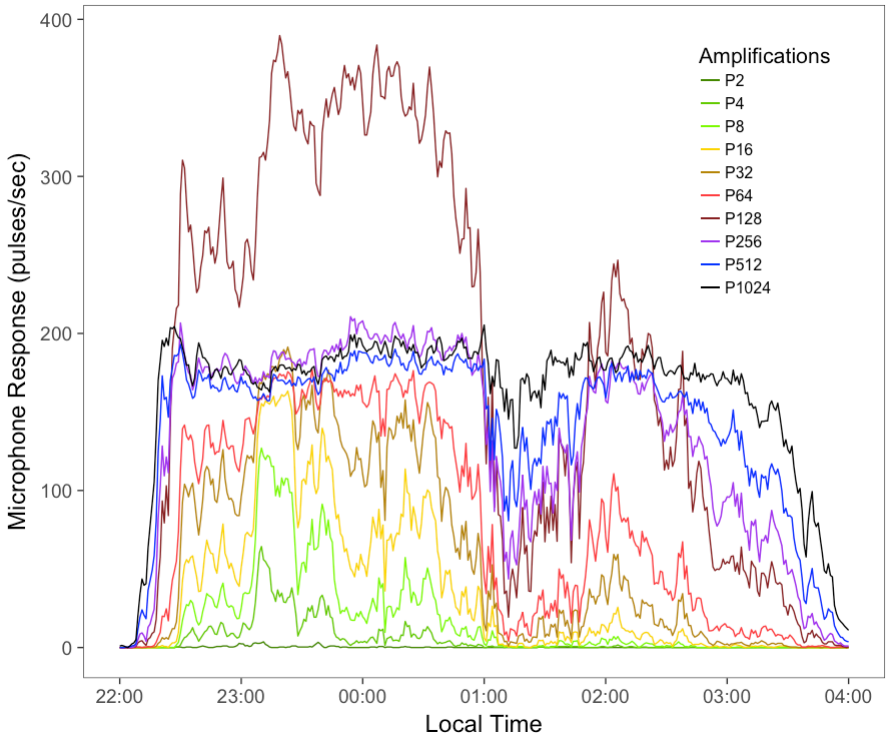

Figure 2. Record of the ten amplification of the left pipe microphone during the July 26th flood. Amplifications P1024, P512, and P256 are saturated and were hereafter removed prior to undertaking further analyses.

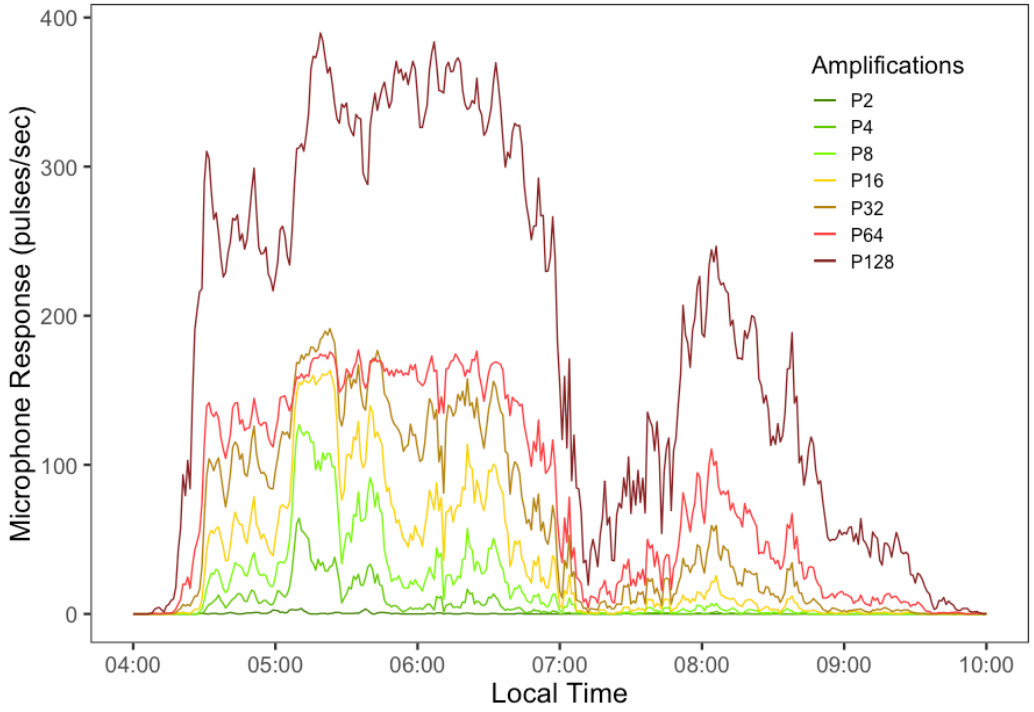

Figure 3. Unsaturated amplifications recorded by the left pipe microphone during the July 26th storm. These amplifications are eligible to be calibrated against Reid slot sampler bedload fluxes.

Discussion

Before attempting to calibrate the pipe microphone responses, the quality of the signals was investigated. How these signals respond to floods is an important context for understanding the best calibration approach. Calibration between a single amplification (P16, P32, P64, etc.) and bedload flux as measured by the corresponding Reid slot sampler is a good first goal. The P32 amplification was chosen here because it is the highest amplification that was not saturated during any of the flood events at either microphone.

Lateral and Temporal Differences in Pipe Response

Bedload is often described by its pulsed nature (Reid et al., 1985; Rickenmann, 2018) and lateral variability (Habersack et al., 2017; Powell et al., 1999). Data collected from the pipe microphones at the Piños show similar trends; they are often pulsed and vary laterally across the channel (Figures 3 and 4). For a given water depth, generally higher pulse rates were monitored by the left pipe. This is particularly true for the August 9th and July 26th events. The most likely cause of the difference is channel morphology. The channel thalweg was located on the left bank while a secondary channel formed on the right bank after the July 26th event. Monitoring bedload during the next monsoon season will include information on the accurate topography of the approach reach. Significant pulse rates were observed when water depth was as shallow as 5 cm depth; pulses were counted during all events when water depth exceeded 10 cm.

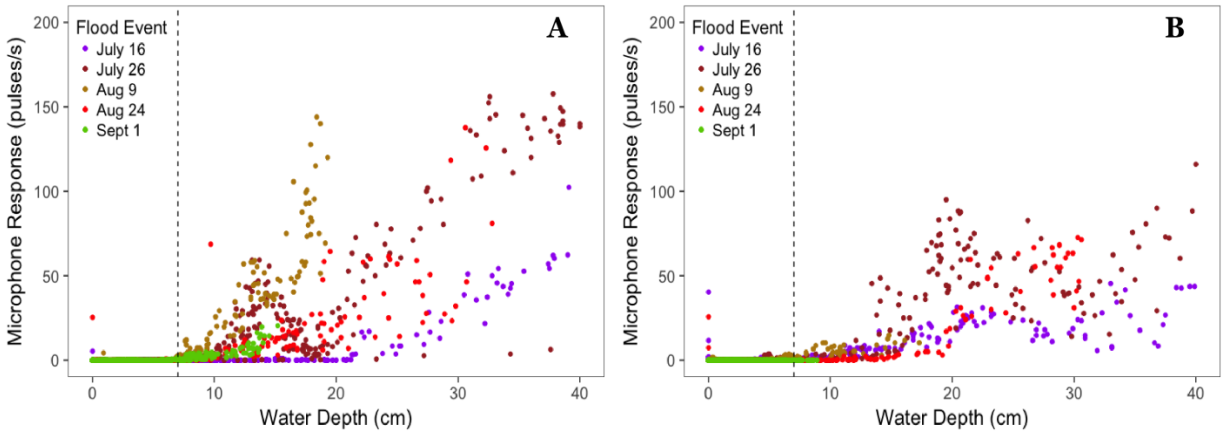

Figure 4. Pipe microphone response (P32) vs water depth for the Left pipe (A) and Right pipe (B). The largest events exceeded the maximum water depth shown here but the majority of the data are collected at these lower stages. The dashed line represents the likely depth for initiation of motion.

Some evidence of counter-clockwise hysteresis is also observed. During the fast and large rise of the July 26th event, more pulses are recorded during the falling limb than on the rising limb (Figure 5). This signal was particularly obvious in the left pipe, where there was often a >50% increase in pulse rate during the falling limb. The same counter-clockwise behavior is observed in the right pipe, although less obvious. Some dampening is also observed which makes the trend harder to visualize. Other floods of significant discharge (July 16th and August 24th) were

bore floods with very limited rising limbs. Hysteresis was not prominent during these events (Figure 6). One possibility for these patterns is the damage to station structures that occurred during this event.

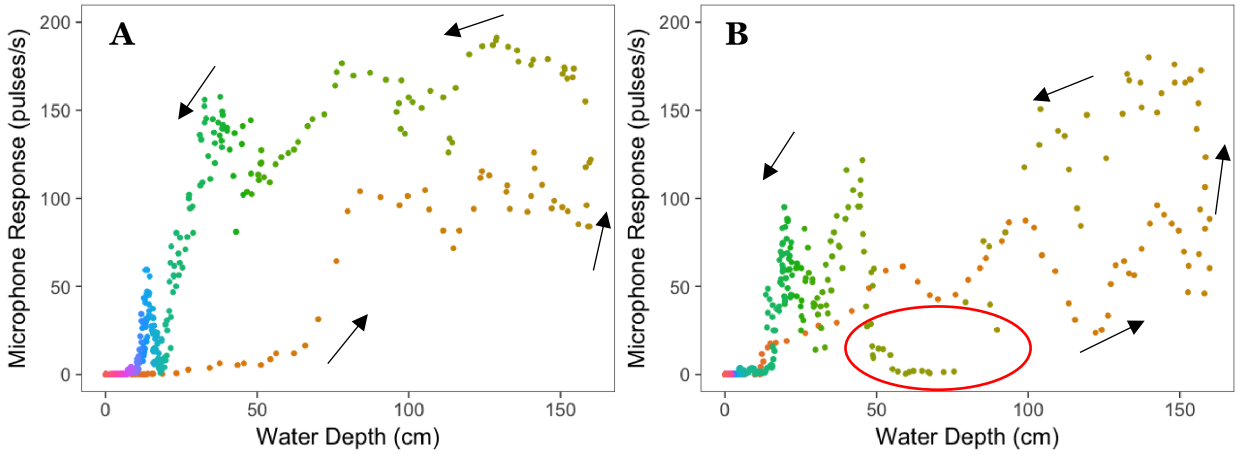

Figure 5. Left (A) and right (B) variation of pipe microphone response with depth during the July 26th flood event. Point color is associated with time during the event; warmer colors indicate early time (rising limb) while cooler colors indicate later time (falling limb). Dampening effects are observed in the falling stage of the right pipe microphone, as indicated by the circle.

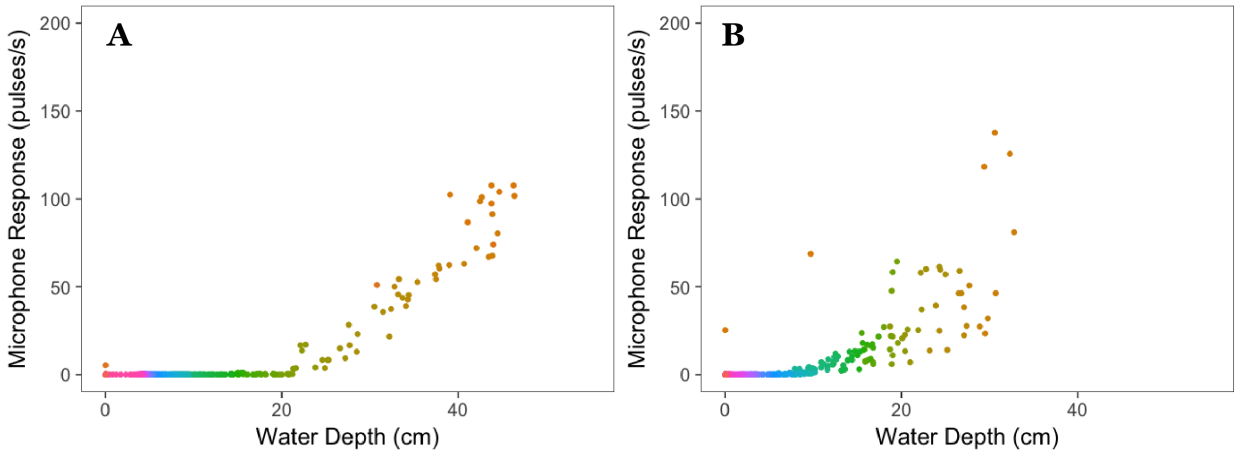

Figure 6. The variation of the left pipe microphone response with water depth for the July 16th (A) and August 24th (B) flood events. These events are characterized by very fast rising limbs; peak discharge was attained within 10 minutes from the onset of flooding. As such, there is no clear evidence of hysteresis. Point color is associated with time during the event; warmer colors indicate early time while cooler colors indicate later time.

Comparing Pipe Response to Bedload Measurements

The strength of the pipe microphones is the continuous monitoring of bedload flux for the duration of each flood event. However, they must be calibrated using the Reid slot samplers. Following the procedure developed by Halfi et al. (2019) we compared the cumulative microphone response to the cumulated mass in the Reid samplers. Bedload flux was as high as 16 kg/sm in some instances, meaning much of the flood is not captured by the Reid slot

samplers and only the beginning of the flood can be used for the calibration, because the Reid samplers fill very quickly in these ephemeral regimes.

Our initial attempt at pipe calibration resulted in large divergence of the calibration (Figure 7). There is a strong relationship during the beginning of each flood until the sampler is ~25% full. From there, a different calibration slope is characteristic for the rest of the sampler duration. There could be many reasons for this divergence; one of the most obvious is grain size. These pipe microphones are only efficient for a certain range of grain sizes. Particles that are too small do not cause sufficient acoustic power at this amplitude (P32) to register a pulse with the system. Studies using pipe microphones and other impact sensors suggest this lower grain size threshold is ≈ 2-8 mm (Mizuyama et al., 2010b; Wyss et al., 2016). The Reid samplers fill in a predictable fashion for given hydraulic conditions (Powell et al, 2001). Samples collected given depth in the sampler represent the grain size distribution for the hydraulic conditions associated with that time period in the flood. Before an accurate evaluation of the effect of grain size on the pipe response is made, additional bedload samples at a wider range of discharges must be collected. Other possible causes for the divergence in slope could be related to the channel morphology; there is noticeably more variance in the slope associated with the left sampler-pipe pairing. As more data are collected at the Piños site, these pipe microphones (as well as the other surrogate bedload devices) will be calibrated so that an estimate of the total bedload flux can be calculated with higher precision.

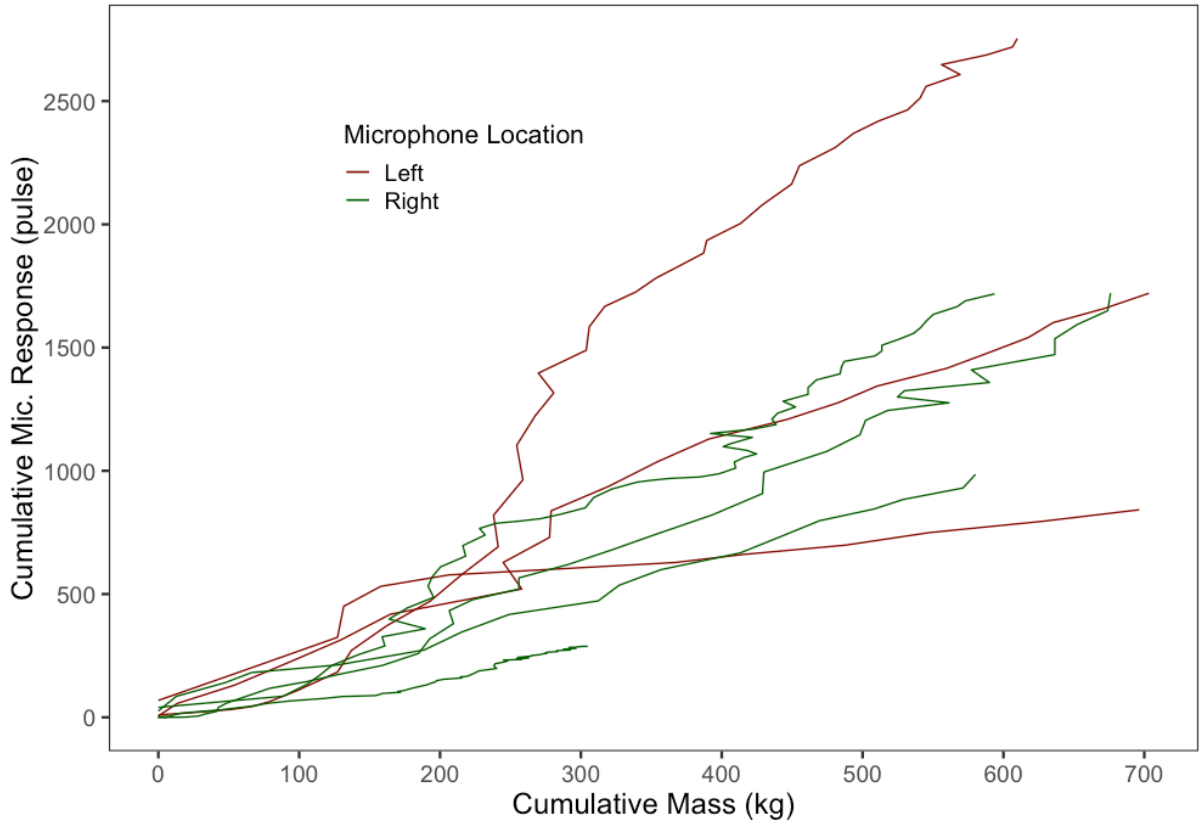

Figure 7. Double mass curve depicting cumulative microphone response vs the cumulative mass measured by the Reid sampler. The different slopes arise from different flood conditions and grain size distributions during each event.

Potential Drawbacks of Using Pipe Microphones

Impact pipe microphones have been successfully implemented in many climate regimes. Some of the drawbacks observed in other deployments are also relevant to the Piños site. In a number of our flood events, we observed clear instances of signal dampening due to covering effects. For example, during the July 26th event the pulse rate of the left pipe dropped to nearly zero after 01:00, although water depth was above 10 cm (Figure 8). Pulse rate measured by the right pipe remained high (40 – 80 pulses/s) during this period and at this water depth. At 01:45 pulse rate began to recover while the response measured by the right pipe was reduced due to the receding flood. This does not invalidate the data collected by the pipe microphones, but merely requires an extra layer of scrutiny, particularly during receding limbs of hydrographs. The additional required data are, amongst others, the cross section and grain size distributions of the immediate approach reach.

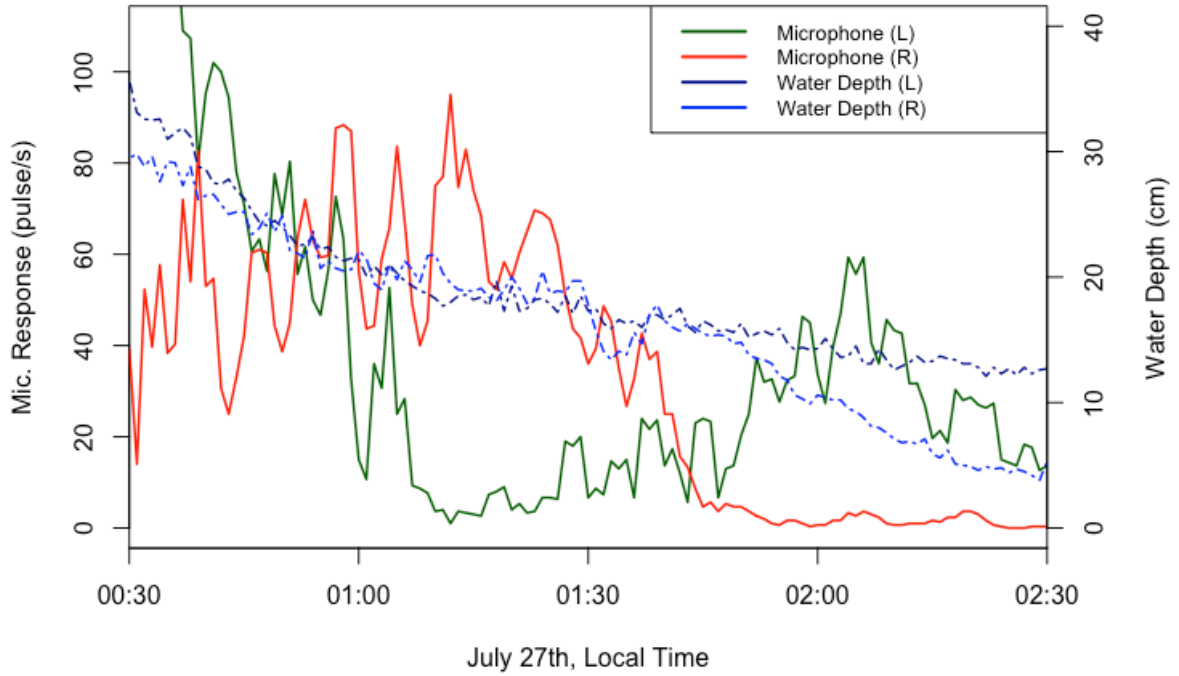

Figure 8. Example of dampened signal recorded during the July 26th flood event. Pulse rate monitored by pipe microphone R remains high while dropping significantly at pipe microhome L.

Conclusion

Data collected from each of the first five flood events at the Arroyo de los Piños monitoring station show the potential of this site. Many different methods are deployed to monitor sediment transport in these arid understudied regimes. The data from the pipe microphones reveal lateral and temporal variability during flashflood events. Evidence of counter-clockwise hysteresis was observed in hydrographs with long rising limbs.

Pipe microphone pulses were compared to the direct measures of bedload flux. The initial attempts at calibrating the pipe microphone data reveal a complicated calibration process. Effects of bedload grain size, approach reach channel morphology and bed material texture could influence these calibrations. Samples collected from the Reid samplers can be used to process the pipe signals after an event but additional data from future flood events are required to fully evaluate the effect of factors on pipe microphone calibration.

References

Cadol, D., Stark, K., Laronne, J.B., Varyu, D. & Richards, M., 2019. Bedload flux and characteristics from flash floods in the Arroyo de los Piños, NM – initial results. SedHyd2019, *Federal Interagency Sedimentation and Hydrologic Modeling Conference. June 2019, Reno NV*.

Cather, S. M., & Colpitts, R. M. (2005). *Geologic Map of the Loma de las Cañas Quadrangle, Socorro County, New Mexico*. Socorro, New Mexico.

Cohen, H., Laronne, J. B., & Reid, I. (2010). Simplicity and complexity of bed load response during flash floods in a gravel bed ephemeral river: a 10 year field study. *Water Resources Research*, *46*(11).

DRI. (2013). Socorro Monthly Climate Summary. Retrieved from https://wrcc.dri.edu/cgi-bin/cliMAIN.pl?nmsoco

Graf, W. L. (1981). Channel instability in a braided, sand bed river. *Water Resources Research*, *17*(4), 1087–1094. https://doi.org/10.1029/WR017i004p01087

Habersack, H., Kreisler, A., Rindler, R., Aigner, J., Seitz, H., Liedermann, M., & Laronne, J. B. (2017). Integrated automatic and continuous bedload monitoring in gravel bed rivers. *Geomorphology*, *291*, 80–93. https://doi.org/10.1016/J.GEOMORPH.2016.10.020

Halfi, E., Paz, D., Stark, K. A., Reid, I., Dorman, M., & Laronne, J. B. (2019). Robust bedload flux estimation for flash floods deploying a mass-aggregation method and its use in calibrating an acoustic sensor. *Journal of Hydraulic Engineering* [in review].

Langbein, W. B., & Schumm, S. A. (1958). Yield of sediment in relation to mean annual precipitation. *Transactions, American Geophysical Union*, *39*(6), 1076. https://doi.org/10.1029/TR039i006p01076

Laronne, J. B., & Reid, I. (1993). Very high rates of bedload sediment transport by ephemeral desert rivers. *Nature*, *366*(6451), 148–150. https://doi.org/10.1038/366148a0

Laronne, J. B., & Wilhelm, R. (2001). Shifting stage-volume curves: predicting event sedimentation rate based on reservoir stratigraphy. In *Applying Geomorphology to Environmental Management* (pp. 33–54). Water Resources Publ.

Marineau, M., Wright, S., Gaeuman, D., Curran, C., Stark, K. & Siemion, J. (2019). Recent acoustic bedload monitoring field experiments using hydrophones. Monitoring the transport of sediment in an ephemeral stream. *SedHyd2019, Federal Interagency Sedimentation and Hydrologic Modeling Conference. June 2019, Reno NV*.

Miwa, H., & Parker, G. (2017). Effects of sand content on initial gravel motion in gravel-bed rivers. *Earth Surface Processes and Landforms*, *42*(9), 1355–1364.

Mizuyama, T., Laronne, J. B., Nonaka, M., Sawada, T., Satofuka, Y., Matsuoka, M., … Watari, M. (2010). Calibration of a passive acoustic bedload monitoring system in Japanese mountain rivers. *US Geological Survey Scientific Investigations Report*, *5091*, 296–318.

Mizuyama, T., Oda, A., Laronne, J. B., Nonaka, M., & Matsuoka, M. (2010). Laboratory tests of a Japanese pipe geophone for continuous acoustic monitoring of coarse bedload. *US Geological Survey Scientific Investigations Report*, *5091*, 319–335.

Powell, D. M., Reid, I., & Laronne, J. B. (1999). Hydraulic interpretation of cross-stream variations in bed-load transport. *Journal of Hydraulic Engineering*, *125*(12), 1243–1252. Retrieved from https://ascelibrary.org/doi/pdf/10.1061/(ASCE)0733-9429(1999)125%3A12(1243)

Powell, D. M., Reid, I., & Laronne, J. B. (2001). Evolution of bed load grain size distribution with increasing flow strength and the effect of flow duration on the caliber of bed load sediment yield in ephemeral gravel bed rivers. *Water Resources Research*, *37*(5), 1463–1474. https://doi.org/10.1029/2000WR900342

Reid, I., Frostick, L. E., & Layman, J. T. (1985). The incidence and nature of bedload transport during flood flows in coarse-grained alluvial channels. *Earth Surface Processes and*

Landforms, *10*(1), 33–44. https://doi.org/10.1002/esp.3290100107

Reid, I., Layman, J. T., & Frostick, L. E. (1980). The continuous measurement of bedload discharge. *Journal of Hydraulic Research*, *18*(3), 243–249.

Rickenmann, D. (2018). Variability of Bed Load Transport During Six Summers of Continuous Measurements in Two Austrian Mountain Streams (Fischbach and Ruetz). *Water Resources Research*, *54*(1), 107–131. https://doi.org/10.1002/2017WR021376

Rickenmann, D., Turowski, J. M., Fritschi, B., Klaiber, A., & Ludwig, A. (2012). Bedload transport measurements at the Erlenbach stream with geophones and automated basket samplers. *Earth Surface Processes and Landforms*, *37*(9), 1000–1011.

Rickenmann, D., Turowski, J. M., Fritschi, B., Wyss, C., Laronne, J., Barzilai, R., … Seitz, H. (2014). Bedload transport measurements with impact plate geophones: comparison of sensor calibration in different gravel-bed streams. *Earth Surface Processes and Landforms*, *39*(7), 928–942.

Tolouie, E., West, J., & Billam, J. (1993). Sedimentation and desiltation in the Sefid-Rud Reservoir, Iran. In *Geomorphology and Sedimentology of Lakes and Reservoirs* (pp. 125–138). Wiley & Sons, England.

United Nations. (2010). 2010–2020: UN Decade for Deserts and the Fight against Desertification. Retrieved July 10, 2018, from http://www.un.org/en/events/desertification_decade/whynow.shtml

Varyu, D., Laronne, J.B., Cadol, D., Padilla, R, Lampert, T., Stark, K., Scissons, S., AuBuchon, J. & Munwes, Y. 2019. Monitoring the transport of sediment in an ephemeral stream. *SedHyd2019, Federal Interagency Sedimentation and Hydrologic Modeling Conference. June 2019, Reno NV*.

Wyss, C. R., Rickenmann, D., Fritschi, B., Turowski, J. M., Weitbrecht, V., & Boes, R. M. (2016). Laboratory flume experiments with the Swiss plate geophone bed load monitoring system: 1. Impulse counts and particle size identification. *Water Resources Research*, *52*(10), 7744–7759.

Time-Series Sediment Acoustics and LISST-ABS Testing

Tim Straub, Acting FISP Chief, USGS, Urbana, IL, tdstraub@usgs.gov
Molly Wood, National Sediment Specialist, USGS, Boise, ID, mswood@usgs.gov
Marian Domanski, Hydrologist, USGS, Urbana, IL, mdomanski@usgs.gov
Adam Manaster, Student Hydrologist, USGS, Urbana, IL, amanaster@contractor.usgs.gov

Abstract

Acoustics and other surrogates can be used to accurately and cost-effectively provide time-series estimates of suspended-sediment concentration and load, which is essential for creating informed solutions to many sediment-related environmental, engineering, and agricultural concerns. Interagency efforts in recent years have advanced the testing, methods development, operational guidelines, and training on sediment acoustics. This extended abstract provides an update on horizontal profiling methodologies and introduces the testing of the LISST-ABS (Acoustic Backscatter Sensor).

Introduction

Fluvial suspended-sediment characteristics relate functionally to acoustic parameters. Some of the earliest U.S. Geological Survey (USGS) research at sediment acoustic sites was done by Wall and others (2006), Topping and others (2006, 2015), Wright and others (2010), Landers and others (2012), and Wood and Teasdale (2013). The USGS has partnered with interagency groups to test instrumentation and develop operational methodologies for using acoustics to estimate suspended-sediment concentration. The primary collaborative groups involved are the Federal Interagency Sedimentation Project (FISP) and the Sediment Acoustic Leadership Team (SALT). The currently active FISP agencies are the Bureau of Reclamation, U.S. Army Corps of Engineers (USACE), U.S. Department of Agriculture-Agricultural Research Service, U.S. Forest Service,

and USGS. The SALT members include Reclamation, USACE, and USGS. The FISP was created in 1939 to research and standardize fluvial sediment science methods and instruments. Information on the current and recent FISP research can be found on the FISP website (FISP, 2019). The multi-agency SALT was established in 2012 and develops technical guidance and training for using acoustic metrics to monitor aquatic sediment (SALT, 2019).

This extended abstract gives an update on horizontal profiling methodologies and point sampling instrumentation. Profiling instrumentation includes Acoustic Doppler Velocity Meters (ADVMs) of various frequency ranges; point instrumentation includes the LIST-ABS (Acoustic Backscatter Sensor) (Sequoia Scientific, 2019).

Horizontal-Profiling Sediment Acoustics

Fluvial suspended-sediment characteristics can be derived from backscatter data collected using fixed-mounted, horizontally-looking acoustic Doppler velocity meters (ADVMs). The goal is to "index" acoustic readings in the volume measured by the ADVM to the overall mean channel sediment concentration. The sediment acoustic index method applied can be used to accurately and cost-effectively provide time-series estimates of suspended-sediment concentration (SSC) and suspended-sediment load (SSL), which allows for informed solutions to sediment-related environmental, engineering, and agricultural concerns.

A web-based course is available to teach hydrographers the fundamentals of the sediment acoustic index method using a single frequency ADVM and how to establish a sediment acoustic index station. The web-based course provides introductory material and is a prerequisite to the full, week-long USGS course H-17-037 Acoustic Index Method for Estimating Fluvial Suspended Sediment. The material presented summarizes and augments information in the USGS

Techniques and Methods 3C-5 report "Sediment Acoustic Index Method for Computing Continuous Suspended-Sediment Concentrations" (Landers and others, 2016). The Surrogate Analysis and Index Developer (SAID) tool is a stand-alone tool to assist in processing the acoustic parameters using data from the single frequency ADVM using methods outlined in the USGS Techniques and Methods 3C-5 report. The tool uses acoustic parameters as predictor variables in the creation of ordinary least squares (OLS) regression models to predict SSC. The regression models can be used to provide time-series estimates of SSC. Sediment acoustic index methodology has been applied to multiple sites across the country; additional information about the sites, methods, and training can be found at the SALT (2019) website. Topping and Wright (2016) describes additional methods to obtain sediment-size and sediment-concentration data using multiple frequencies of ADVMs. These methods and functionality are being incorporated into an updated version of SAID.

LISST-ABS Testing

The LISST-ABS (Acoustic Backscatter Sensor) is considered a point-sediment acoustic instrument (Sequoia Scientific, 2019). The LISST-ABS operates at 8,000 kilohertz (kHz) and measures 5.5 centimeters (cm) in front of the sensor. The point measurement capability makes it suitable for use in similar field installations as a turbidity meter. However, the LISST-ABS can measure changes in concentration of coarse-grained material (Sequoia Scientific, 2019), unlike turbidity meters. The manufacture specified range of suspended-sediment concentration for the LISST-ABS is 1 mg/L to 30,000 mg/L (7-micron dust particle size) or less than 20,000 mg/L (200-micron sand particle size) (Sequoia Scientific, 2019). The LISST-ABS was independently tested in a laboratory setting for concentrations ranging from 100 mg/L to 3000 mg/L and particle sizes ranging from 1 to 149 microns (Snazelle, 2017). Field testing of the LISST-ABS by multiple agencies is being compiled by members of the FISP and SALT. Field and laboratory

testing is planned to include the LISST-AOBS (LISST-Acoustic Optic Backscatter Sensor) by Sequoia Scientific (2019), which combines the LISST-ABS and turbidity, allowing for a more ideal response across a wide range of grain sizes. Multiple reports and papers are planned for the compiled results.

References

Federal Interagency Sedimentation Project [FISP], 2019, Federal Interagency Sedimentation Project Website, https://water.usgs.gov/fisp/, last accessed February 15, 2019.

Landers, M.N., Straub, T.D., Wood, M.S., and Domanski, M.M., 2016, Sediment acoustic index method for computing continuous suspended-sediment concentrations: U.S. Geological Survey Techniques and Methods, book 3, chap. C5, 63 p., http://dx.doi.org/10.3133/tm3C5.

Landers, M.N., Arrigo, J., and Gray, J.R., 2012, Advancing hydroacoustic technologies for sedimentology research and monitoring: American Geophysical Union, Eos Transactions, v. 93, no. 26, p. 244, doi: 10.1029/2012EO260007, accessed March 11, 2016, at http://onlinelibrary.wiley.com/doi/10.1029/2012EO260007/pdf.

Sediment Acoustic Leadership Team [SALT], 2019, Sediment Acoustic Leadership Team website, https://water.usgs.gov/osw/SALT/index.html, last accessed February 15, 2019.

Sequoia Scientific, 2019, LISST-ABS Submersible Acoustic Backscatter Sediment Sensor, https://www.sequoiasci.com/product/lisst-abs/, last accessed April 30, 2019.

Snazelle, T.T., 2017, Laboratory evaluation of the Sequoia Scientific LISST-ABS acoustic backscatter sediment sensor: U.S. Geological Survey Open-File Report 2017–1154, 21 p., https://doi.org/10.3133/ofr20171154.

Topping, D.J., and Wright, S.A., 2016, Long-term continuous acoustical suspended-sediment measurements in rivers—Theory, application, bias, and error: U.S. Geological Survey Professional Paper 1823, 98 p., http://dx.doi.org/10.3133/pp1823.

Topping, D.J., Wright, S.A., Griffiths, R.E., and Dean, D.J., 2015, Physically based method for measuring suspended-sediment concentration and grain size using multi-frequency arrays of single-frequency acoustic-doppler profilers—Proceedings of the Third Joint Federal Interagency Sedimentation Conference on Sedimentation and Hydrologic Modeling, April 19–23, 2015: Reno, Nev., p. 833–846, accessed March 8, 2016, at http://acwi.gov/sos/pubs/3rdJFIC/Proceedings.pdf.

Topping, D.J., Wright, S.A., Melis, T.S., and Rubin, D.M., 2006, High-resolution monitoring of suspended-sediment concentration and grain size in the Colorado River using laser-diffraction instruments and a three-frequency acoustic system—Proceedings of the Eighth Federal Interagency Sedimentation Conference, April 2–6, 2006: Reno, Nev., U.S. Geological Survey, p. 539–546, accessed March 8, 2016, at http://pubs.usgs.gov/misc/FISC_1947-2006/pdf/1st-7thFISCs-CD/8thFISC/Session%206C-3_Topping.pdf

Wall, G.R., Nystrom, E.A., and Litten, S., 2006, Use of an ADCP to compute suspended-sediment discharge in the Tidal Hudson River, New York: U.S. Geological Survey Scientific Investigations Report 2006–5055, accessed March 9, 2016, at http://pubs.usgs.gov/sir/2006/5055/.

Wood, M.S., and Teasdale, G.N., 2013, Use of surrogate technologies to estimate suspended sediment in the Clearwater River, Idaho, and Snake River, Washington, 2008–10: U.S. Geological Survey Scientific Investigations Report 2013–5052, 30 p., accessed March 9, 2016, at http://pubs.usgs.gov/sir/2013/5052/.

Wright, S.A., Topping, D.J., and Williams, C.A., 2010, Discriminating silt-and-clay from suspended-sand in rivers using side-looking acoustic profilers—Proceedings of the Second Joint Federal Interagency Conference: Las Vegas, Nev., 12 p., U.S. Geological Survey [Abstract], accessed March 11, 2016, at http://acwi.gov/sos/pubs/2ndJFIC/Contents/2C_Wright_03_01_10_paper.pdf.

Disclaimer

Any use of trade, firm, or product names is for descriptive purposes only and does not imply endorsement by the U.S. Government.

Measured Bedload (ISSDOTv2) Values as Validation Data for Numerical Sedimentation Modeling

Keaton Jones, Keaton.E.Jones@erdc.dren.mil, **David Abraham,** David.D.Abraham@erdc.dren.mil, and **Tate McAlpin**, Tate.O.McAlpin@erdc.dren.mil, Research Civil Engineers, US Army Corps of Engineers, Coastal and Hydraulics Laboratory, Vicksburg, MS,

Extended Abstract

The ISSDOTv2 (Integrated Section Surface Difference Over Time version 2) method of computing bed-load transport in sand bed rivers has now been in use for nearly 10 years. The computational procedure uses time sequenced three-dimensional bathymetric surfaces of dune fields to compute bed-load transport rates. Automation of the computations and consistency of the method have been an important focus of the ISSDOTv2 team and thus improvements to the code and/or data collection procedures continue to be made as necessary. Usage of the method continues to grow and the database of measurements is expanding as well. Abraham et al, (2018) presented an update on the method and the available data collected up until that point. Figure 1, a figure from Abraham et al, (2018), maps the locations of the available ISSDOTv2 data. A majority of the data (85 measurements) have been collected on the Mississippi and Missouri Rivers at 24 different locations. Since publication of Abraham et al, (2018), additional data have been collected on the Chippewa River in Wisconsin and at four sites in the vicinity of the Old River Control Complex (ORCC). Two on the main stem Mississippi River, one in the ORCC Outflow Channel, and one on the Red River several miles upstream of its confluence with ORCC. Further data collection efforts have been funded for the Rio Grande in Albuquerque, New Mexico for the spring of 2019, and planned for the Mississippi River upstream of Vicksburg, where currently no measurements exist.

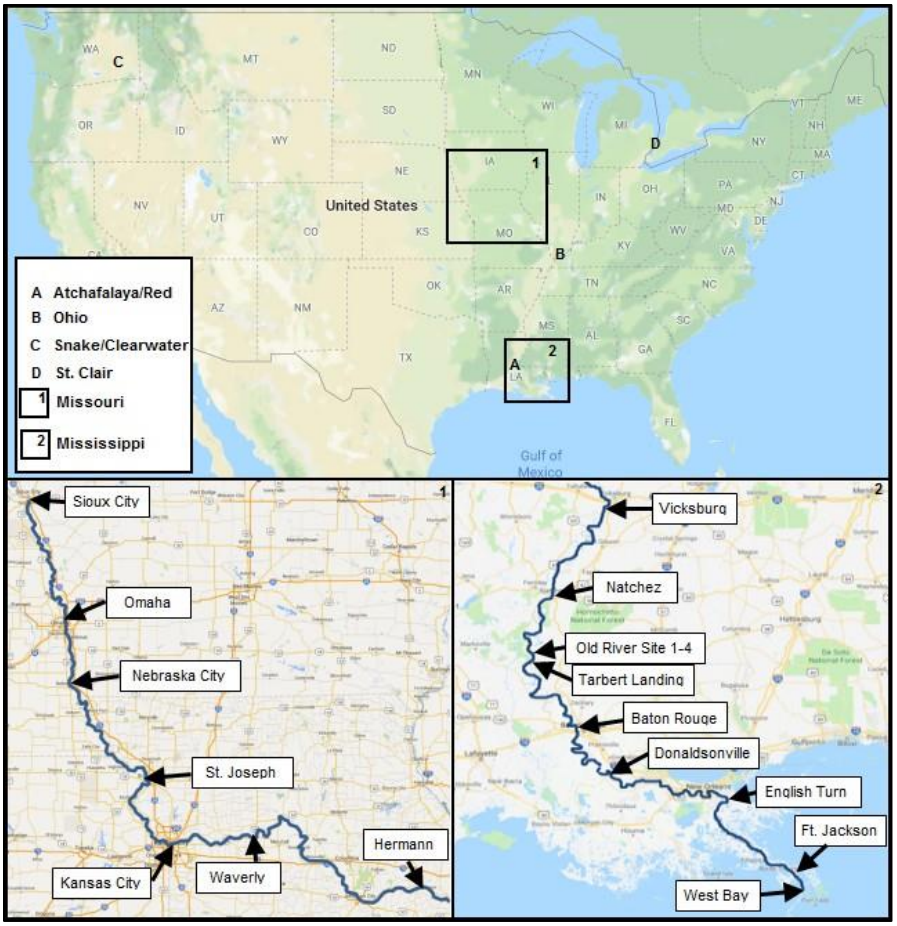

Figure 1: Map of measurement locations (Abraham et al. 2018)

One important benefit of ISSDOTv2 measured bed-load values is utilization as validation data for numerical sediment transport models. As sediment modeling capabilities continue to advance, the usage and application of these models continue to grow as well. With this increased use, comes the increased need for accurate sediment data for both boundary condition inputs and model calibration/validation. Below are two examples where ISSDOTv2 bed-load values were used as validation data for sediment models of large, sand bed rivers. The first example is from Heath et al, (2011) in which data collection, numerical modeling, and geomorphic analyses were used to investigate sediment diversion characteristics through the ORCC which regulates the diversion of flow between the Mississippi River and the Atchafalaya River. A portion of the study included a two-dimensional Adaptive Hydraulics (AdH-2d) sediment transport model of the Mississippi River in the vicinity of the ORCC. Figure 2 is a portion of a graph from Heath et al. where ISSDOTv2 measured values (green dots) are compared with modeled bedload (green line) at a cross section on the Mississippi River near RM 315. In this case, five bed-load measurements were collected during a nine month period, which allowed comparisons with the model throughout a hydrograph.

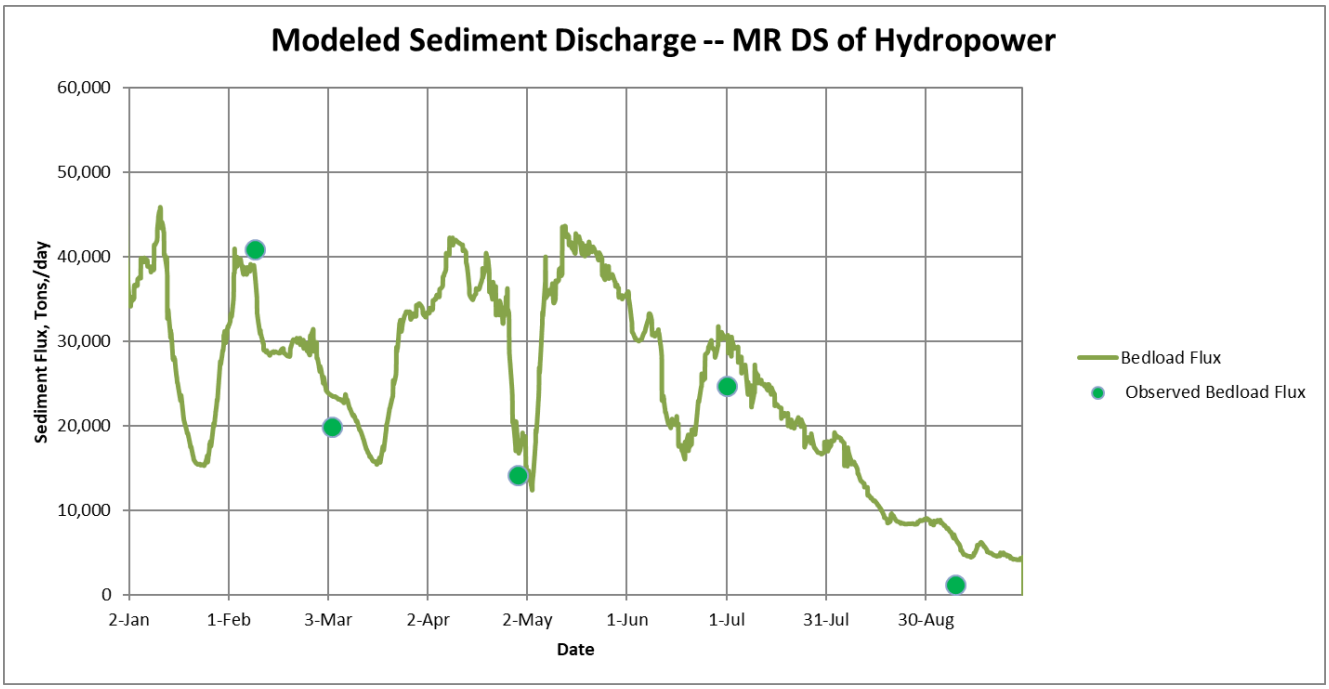

Figure 2: Mississippi River modeled bedload (line) compared with measured ISSDOTv2 bedload (points) (Heath et al. 2011)

A second example is from a sedimentation study investigating dike impacts to shoaling in the Ohio River at Mound City, Illinois. In this study, an AdH-2d sedimentation model was validated with data that included ISSDOTv2 bed-load flux measurements. Unlike the previous example where each data point represented the total bed-load transport flux through the entire cross section, this study compared the measured lateral distribution of the bedload with the modeled distribution across the channel (Figure 3).

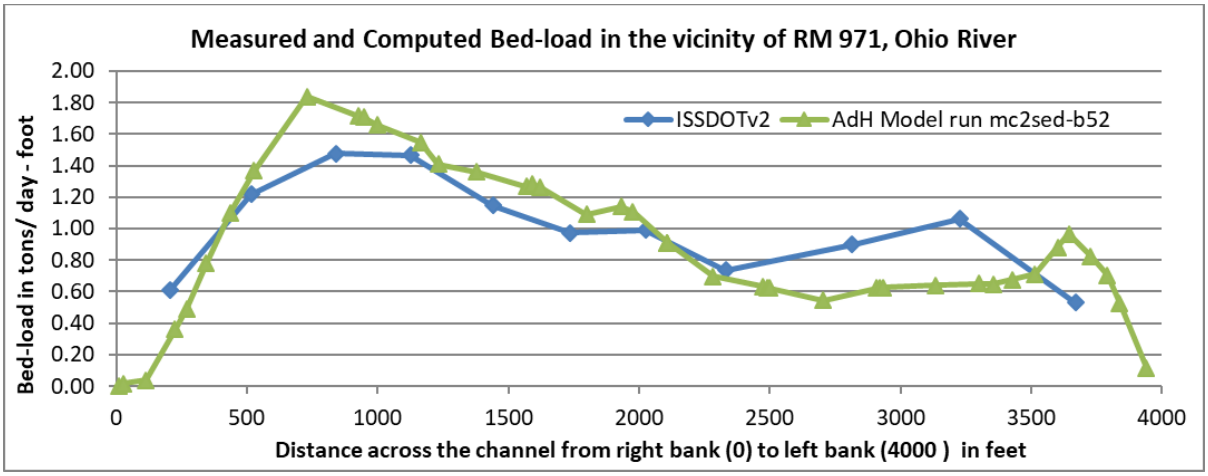

Figure 3: Ohio River modeled bed-load comparison with measured ISSDOTv2 bedload (Abraham et al. 2015)

The ISSDOTv2 values were obtained from each individual swath of multi-beam data and located at the lateral center of each swath while the AdH model results were taken from nodes on a line through the same location as the ISSDOTv2 measurements and at the same flowrate and time

during the hydrograph simulation. The figure shows that both the temporal and spatial variability of computed bedload reported by numerical models can be checked against measured values. The relatively close agreement, for these kind of sediment measurements, indicates that the numerical model and selected transport function are appropriate and capable of yielding reasonable results for the given study. Both of the examples presented above clearly show how the ISSDOTv2 data can be useful in validating multidimensional sediment transport models.

In closing, the method can be used for model validation, but it is also being used as a yardstick for comparison with other bed-load measurement techniques. On the Chippewa River in Wisconsin, it is being used in conjunction with standard physical samplers and some new acoustic techniques. Determining which methods provide the best results in representing the real transport in the field is difficult. To help answer this question, funding was received through the Regional Sediment Management program (RSM) for a series of flume tests and experiments with the National Sedimentation Laboratory (NSL) in Oxford, Mississippi. These tests will be carried out in the second half of 2019 and early 2020. The intent will be to address new changes to the code, non-equilibrium transport, lateral variability of transport, and the uncertainty issues inherent with these conditions. When successfully completed, it is anticipated that ISSDOTv2 measurements can be bounded with verifiable confidence intervals allowing for more confidence in the measured results and more informed comparisons of measurements to numerical model results.

References

Abraham, D.D., McAlpin, T.O., and Jones, K.E. 2018. “Bed-load measurements on large, sand-bed rivers in the United States,” Proc. Of the Ninth International Conference on Fluvial Hydraulics (River Flow 2018). Lyon, France: E3S Web of Conferences 40, 06021. https://doi.org/10.1051/e3sconf/20184006021

Abraham, D.D., Clifton, N.D., and Vessels, B.E. 2015. “Numerical Sedimentation Study of Shoaling on the Ohio River near Mound City, Illinois”. US Army Corps of Engineers, Engineering Research and Development Center, Vicksburg MS, ERDC/CHL TR- 15-12.

Heath, R.E., Brown, G.L., Little, C.D., Pratt, T.C., Ratcliff, J.J., Abraham, D.D., Perkey, D., Ganesh, N.B., Martin, K., and May, D.P., 2015. “Old River Control Complex Sedimentation Investigation”. US Army Corps of Engineers, Engineering Research and Development Center, Vicksburg MS, ERDC/CHL TR- 15-8.

Measuring Suspended Sediment in Sand-Bedded Rivers Using Down-Looking Acoustic Doppler Current Profilers

Molly S. Wood, National Sediment Specialist, U.S. Geological Survey, Boise, Idaho, mswood@usgs.gov
Ricardo Szupiany, Associate Professor, International Center for Large Rivers Research, Universidad Nacional del Litoral, Santa Fe, Argentina, rszupian@fich.unl.edu.ar
Justin Boldt, Hydrologist, U.S. Geological Survey, Louisville, Kentucky, jboldt@usgs.gov
Tim Straub, Federal Interagency Sedimentation Project Chief, U.S. Geological Survey, Urbana, Illinois, tdstraub@usgs.gov
Marian Domanski, Hydrologist, U.S. Geological Survey, Urbana, Illinois, mdomanski@usgs.gov

Abstract

The use of side-looking acoustic Doppler velocity meters (ADVMs) to estimate fluvial suspended-sediment concentrations (SSC) has become more operational by the U.S. Geological Survey in recent years; however, direct transfer of these techniques to down-looking acoustic Doppler current profilers (ADCPs) currently is not widely feasible. Key assumptions in the side-looking ADVM method related to sediment homogeneity within the acoustic measurement volume are almost never met in wide, sand-bedded rivers because SSC and particle size commonly vary with depth and location in the river cross section. The use of ADCPs to estimate SSC has been investigated by researchers, but the requirements and limitations of an operational method that could be successfully applied at many locations are not well defined. If an operational method could be developed, the use of ADCPs, which are routinely used for flow measurements, would revolutionize sediment science by providing rapid measurements of sediment flux and spatial distribution.

We collected detailed datasets in six sand-bedded rivers in the U.S. in 2016-2018, to evaluate the efficacy of using down-looking ADCPs of multiple frequencies to estimate SSC. The datasets included replicate sets of point and depth-integrated suspended-sediment samples and stationary and cross-sectional backscatter profiles using multiple ADCPs with differing frequencies. Reasonable calibrations were developed at all sites measured when calibrating to the coarse fraction (R^2 0.66 to 0.98 with slopes close to 0.1 using 1200kHz ADCPs). Calibrations to the fines fraction were problematic because acoustic backscatter response was dominated by coarse particles when present, and substantial attenuation was contributed by coarse particles at some sites. A sensitivity analysis on minimum datasets showed that good calibrations could be developed using two verticals of data collected over a range of backscatter and sediment conditions, with a minimum of three points sampled for sediment within each vertical. Overall, results to date show great promise in using ADCPs to rapidly estimate and visualize SSC with high spatial resolution, and a new beta software tool called Sediment Transect Acoustics simplifies data processing. Improvements are underway to the beta software used in processing to allow incorporation of more acoustic and sediment characteristics and to estimate SSC in areas of the river cross section unmeasured by the ADCP.

Introduction

Acoustic Doppler meters typically are used in rivers to measure water velocities and flow (Mueller and others, 2014) and are deployed in "side-looking" and "down-looking" orientations. A side-looking meter is typically fixed to the river bank and emits an acoustic pulse horizontally within the river. A down-looking meter is typically attached to a floating, tethered boat platform on the water surface or a mount on a motorized boat. A down-looking meter can be held stationary at one point for a given time or can be moved across the river, and it emits an acoustic pulse vertically into the river's water column. The acoustic pulse bounces off particulate matter in the water and is measured by the meter as acoustic backscatter, which can be related to the amount of suspended sediment in the water after correction of the signal for losses (Wood, 2014). The use of side-looking acoustic Doppler meters to estimate fluvial suspended-sediment concentration (SSC) has become operational in recent years, providing continuous, high temporal resolution data on sediment concentration, load, and size based on a horizontal section of the flow. However, key assumptions in the operational, side-looking meter method (as described in Wood and others, 2015, and Landers and others, 2016) related to sediment homogeneity within the acoustic measurement volume are almost never valid vertically in sand-bedded rivers because SSC and particle size commonly vary with depth and location in the river cross section. As a result, operational side-looking methods are not directly transferable to a down-looking application. The use of down-looking acoustic Doppler current profilers (ADCPs) to estimate SSC has been investigated by other researchers (Gartner, 2004; Wall and others, 2006; Boldt and others, 2012; Guerrero and others, 2013; Moore and others, 2013; Latosinki and others, 2014; Boldt, 2015; Szupiany and others, 2009, 2016, 2018; Guerrero and others, 2017). Yet, an operational method, using commercially available and commonly used instrumentation over changes in sediment characteristics (particle size distribution) and hydrologic conditions is not well defined. If an operational method could be developed, the use of ADCPs would increase access to sediment data by allowing rapid and accurate measurements of suspended-sediment transport and distribution at spatial and temporal scales that are far beyond the capabilities of traditional physical samplers. Such spatial resolution of concurrent sediment, hydraulic, and fluvial geometric data has not been previously possible and can immediately address and improve our understanding, modeling, and prediction of fluvial sediment transport. In the U.S. alone, measurements of flow are made with ADCPs nearly every day at streamgages. If calibrations could be developed at even a fraction of these locations, the amount of sediment information available to the public and science communities would be greatly expanded.

Calibration Method

Implementing the calibration method for relating down-looking ADCP data to SSC requires an understanding of how acoustic pulses passing through a water-sediment mixture will scatter and attenuate as a function of fluid, sediment, and acoustic instrument characteristics (as described in Thorne and others, 1991; Landers and others, 2016). Various researchers (Gartner, 2004; Moore and others, 2013; Latosinski, 2014; Boldt and others, 2015; Szupiany and others, 2016, 2018) have presented an empirical sediment surrogate approach involving the need to adjust acoustic backscatter data obtained from an ADCP to isolate the attenuation (rate of absorption of the signal with distance from the instrument) and backscatter characteristics of sediment. The basic approach in many of these studies involves collecting a series of stationary profiles using an ADCP, collecting concurrent or near-concurrent sediment samples at multiple points in each profile, and developing a calibration between the ADCP data (corrected for losses)

and the sediment sample results. The ADCP data undergo a conversion from raw backscatter to sediment corrected backscatter using the following equation (Gartner, 2004):

$$SCB = K_c * RB + 20 * \log_{10}(\psi R) + 2\,\alpha_w R + 2\alpha_s R \quad (1)$$

where:

SCB is the sediment corrected backscatter (dB),
RB is the raw backscatter data or echo intensity recorded by the instrument (counts),
K_c is the instrument- and beam-specific echo intensity scale factor (dB/count),
ψ is the non-dimensional function describing the non-spherical spreading of the backscattered signal in the near field (Downing and others, 1995),
R is the range or distance along the beam (m),
α_w is the sound absorption coefficient due to water viscosity (dB/m) (Schulkin and Marsh, 1962), and
α_s is the sediment attenuation coefficient (dB/m).

The first three terms on the right side of equation (1) are commonly referred to as the water corrected backscatter (WCB). The sediment attenuation coefficient can be determined through knowledge of sediment characteristics and theoretical assumptions (most notably the hybrid Urick-Sheng-Hay method described in Wright and others, 2010; Landers and others, 2016) or through actual measurements of the slope of the WCB profile. The latter approach for determining sediment attenuation is common in the side-looking acoustic method (Wright and others, 2010; Landers and others, 2016), but may not be appropriate in a down-looking application because of the previously mentioned variations in particle size and concentrations with depth. Latosinki and others (2014) and Szupiany and others (2018) present a method for addressing the attenuation contributed separately by fines (particles < 63 μm) and coarse (particles >= 63 μm) sediment and use of theoretical assumptions appropriate for particle sizes in transport. This method was incorporated into the processing of datasets described in this paper as a modification of equation (1):

$$SCB = K_c * RB + 20 * \log_{10}(\psi R) + 2\,\alpha_w R + 2(\alpha_{sS} + \alpha_{sF})R \quad (2)$$

where:

α_{sS} is the sediment attenuation coefficient from coarse sediment,
α_{sF} is the sediment attenuation coefficient from fine sediment, and
other variables are as previously defined.

Some researchers (Topping and others, 2007; Wright and others, 2010; Landers and others, 2016) have noted that the backscatter response (WCB or SCB) often correlates well with the coarse fraction in transport, and the sediment attenuation coefficient often correlated with the fines fraction in transport. However, both coarse and fines can contribute to attenuation from sediment, hence the desire to separate the attenuation coefficients for coarse and fines in eq. (2) to investigate the effect of each fraction.

In sediment surrogate applications, Moore and others (2013) and Topping and Wright (2016) note the need for describing a sediment particle size distribution as the distribution by number of particles (hereafter called the number distribution), rather than the distribution by volume of particles (hereafter called the volume distribution), which is the typical distribution obtained from a laboratory analysis. Thus, the particle size distribution data collected in this study were converted to number distributions to better represent the true scattering cross section of the particle according to theory (Thorne and Meral, 2008). The median sediment diameters for the fines and coarse fractions were then used to determine sediment attenuation.

Field Data Collection

We collected six datasets in sand-bedded rivers in the U.S. in 2016-2018 (Table 1) to advance our understanding of the factors influencing successful use of down-looking ADCPs to estimate SSC and load. With a few exceptions, the data collection efforts consisted of:

- Stationary acoustic backscatter and velocity profiles using ADCPs of various makes, models, and frequencies, all referenced to differential GPS (Figure 1, level 1). This paper focuses on results obtained from 600kHz and 1200kHz Teledyne RD Instruments Rio Grande ADCPs (any reference to trade names does not imply endorsement by the U.S. Government), which were used at all sites. Acoustic cell size was set to 0.5 m for the 600kHz ADCPs and 0.25 m for the 1200 kHz ADCPs for consistency across sites.
- Point sediment samples from multiple locations in the cross section, typically collected using a P-6 sampler (Figure 1, level 1). Point samples were typically collected within five verticals in the cross section, selected using the Equal Discharge Increment (EDI) method described in Edwards and Glysson (1999), and within five depths within each vertical (0.2-depth (D), 0.4-D, 0.6-D, 0.8-D, and 0.9-D). At many sites, three replicate sets of samples were collected at each point sample location.
- Moving-boat discharge measurements before and after sample collection using ADCPs of various frequencies, typically 600kHz and 1200kHz Teledyne RD Instruments Rio Grande ADCPs, following procedures in Mueller and others (2014) (Figure 1, level 2).
- Cross-sectional- and depth-integrated (EDI method) sediment samples collected to validate estimates produced by acoustic calibrations (Figure 1, level 3). If EDI samples could not be collected, one set of the point sediment samples was used to validate estimates produced by acoustic calibrations.

Sediment samples were analyzed for concentration, coarse/fine break (percent finer than 0.0625 mm), and particle size distribution. Individual point samples were analyzed for particle size distribution in both coarse and fines fractions if sufficient sediment mass was available. In some cases, samples had to be composited to obtain enough mass for analysis.

At several sites, the following additional data were collected:

- Diagnostic tests with ADCPs to measure background noise with and without the other ADCP pinging.
- Point measurements of turbidity and acoustic backscatter (Sequoia Scientific LISST-ABS) at all point sample locations.
- Bed material samples at one or all EDI stations or verticals.

Table 1. Research sites and datasets collected to evaluate use of down-looking ADCPs for estimating suspended sediment [USGS, U.S. Geological Survey; EDI, equal discharge increment method]

River site	Nearest USGS streamgage number	Drainage area at nearest USGS gage (mi^2)	Date of data collection	Discharge (ft^3/s)	Number of point samples collected	Number of sets of cross section EDI samples collected
Missouri River at St. Charles, MO	06935965	524,000	July 20, 2016	95,300	75	0
Sacramento River at Freeport, CA	11447650	Indeterminate	May 3, 2017	69,100	75	2
Illinois River at Florence, IL	05586300	26,870	May 23, 2017	69,300	60	2
Missouri River at Nebraska City, NE	06807000	410,000	May 25, 2017	75,000	55	2
St. Joseph River at Napier Ave. at St. Joseph, MI	04102080	4,260	February 23, 2018	24,600	50	0
Cowlitz River at Castle Rock, WA	14243000	2,238	March 5, 2018	7,920	32	2

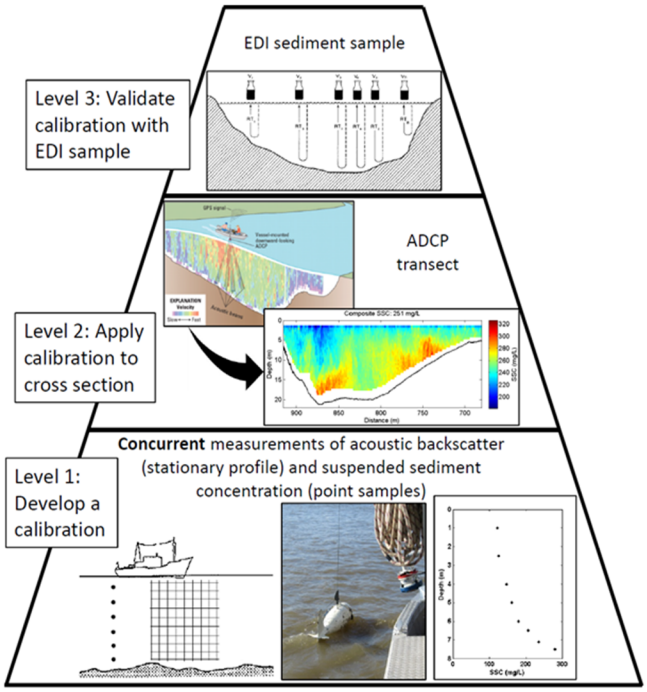

Figure 1. Basic procedure and data collection requirements to estimate suspended sediment using down-looking ADCPs using the Sediment Transect Acoustics software

Software Used for Developing Calibrations

Datasets collected at sites in Table 1 were processed in the Sediment Transect Acoustics (STA) software, beta version 4.0, written in Matlab and described in Boldt and others (2012), Boldt (2015), and at https://water.usgs.gov/osw/SALT/discrete_methods.html. STA is not yet available for public release. STA temporally and spatially matches the nearest SCB value in a vertical ADCP backscatter profile to a point sample SSC. Given the different acoustic response from fine and coarse fractions of particles, STA can perform linear regression between the matched values to develop a calibration for fine (SSC_f), coarse (SSC_c), or total (SSC_t) sediment concentration of the form:

$$\log_{10} SSC_f \textit{ or } \log_{10} SSC_c \textit{ or } \log_{10} SSC_t = a * SCB + b \quad (3)$$

where a is the slope and b is the y-intercept. The theoretical value for the slope, a, is 0.1, but testing to date has shown variability in this slope among sites and acoustic instruments (Wright and others, 2010; Landers and others, 2016).

After the calibration was developed at each site, it was applied to a moving boat ADCP discharge measurement made before or after the stationary profile data collection to obtain an estimate for SSC for each bin of acoustic data comprising the measured cross section using the following transformation of eq (3):

$$SSC_f \textit{ or } SSC_c \textit{ or } SSC_t = 10^{(a*SCB + b)} \quad (4)$$

If the option is selected in STA to calibrate to SSC_f or SSC_c, a cross-sectional estimate of SSC_t is still reported by adding the calibration estimates (SSC_f or SSC_c) to the average sample value of the fraction not included in the calibration (SSC_f or SSC_c). For example, if a calibration is developed to SSC_c, the reported cross-sectional estimate of SSC_t is the summed calibration estimates of SSC_c plus the average SSC_f from the samples used in the calibration.

The method employed within STA for the analysis described in this paper did not report suspended sediment in areas unmeasured by the ADCP, including the ADCP draft and transducer blanking distance near the water surface, sidelobe interference zone near the bed, and shallow areas near banks.

Substantial enhancements have been made to STA as part of this research effort since initial presentation in Boldt and others (2012). The new interface (Figure 2) allows for loading up to five verticals of ADCP and sediment sample data per cross section. The new interface also allows for:

- Entry of different sediment characteristics (sediment density and median sediment diameter, or separate characterization of attenuation) for the coarse and fines fractions.
- Use of individual or combinations of ADCP beams and their accompanying echo intensity scale factors.
- Ability to obtain a calibration or apply an already-developed calibration to another ADCP-measured cross section.
- Ability to separately characterize sediment attenuation from the coarse and fines fractions.
- Visualization of the box coefficient, sediment load, ADCP echo intensity, velocity and SCB distribution in the cross section, in addition to SSC.

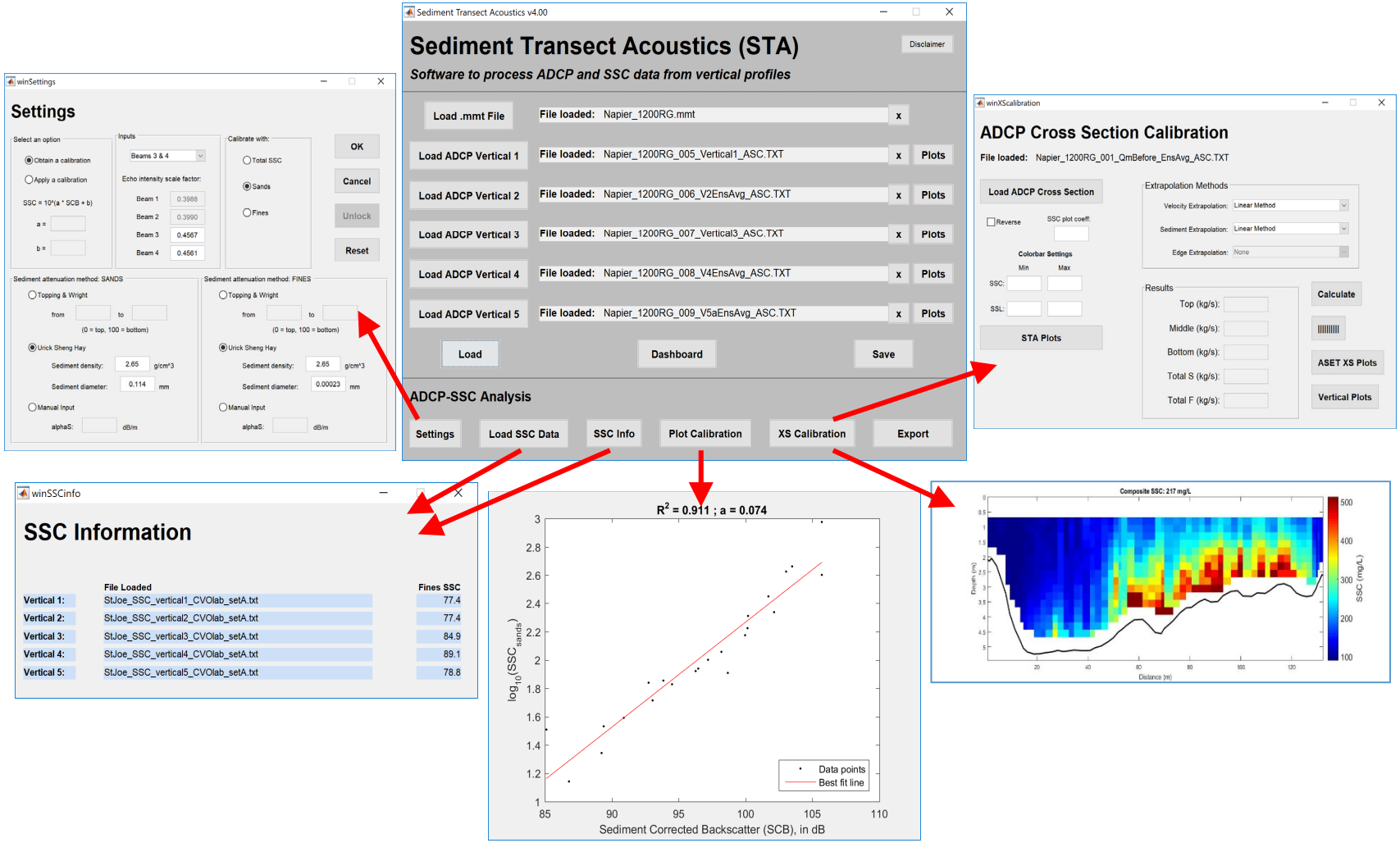

Figure 2. Main software elements of Sediment Transect Acoustics software (beta version 4.0) and calibration results from the St. Joseph River at Napier Ave. at St. Joseph, Michigan

Summary of Calibrations

Reasonable calibrations (R^2 0.66 to 0.98) and rating slopes close to 0.1 (expected from theory (Landers and others, 2016)) were developed for the coarse fraction (SSC_c >= 63 μm) at all sites over a wide range of sediment conditions (i.e. particle size and coarse/fine concentration ratios). The best calibrations were found with the 1200kHz ADCP compared to the 600kHz ADCP (Table 2). The best calibrations also were obtained at sites with relatively high coarse concentrations and stable sediment distributions during the sampling campaign (such as those in the St. Joseph River at Napier Ave. at St. Joseph (Figure 2) and Missouri River at St. Charles (Figure 3)). The comparisons between STA-estimated SSC_t and sampled SSC from the validation EDI samples also were good; the average percent difference among all sites between validation samples and STA estimates was -16.5 and -20.0 percent for the 1200kHz and 600kHz ADCPs, respectively. The negative percent differences were expected because the selected processing methods in STA do not yet report SSC in the unmeasured areas of the cross section and would therefore be less than the validation EDI sample. STA estimates of SSC_t were less than validation sample SSC in all cases except the Missouri River at Nebraska City (Table 2). Flow and sediment transport were especially turbulent at the Missouri River at Nebraska City, as demonstrated by the "banding" and non-uniform appearance in sediment distribution in the cross-sectional estimate of SSC (Figure 4). The range of SSC in sediment samples collected in the Missouri River at Nebraska City was large (451 mg/L to 838 mg/L) at individual EDI validation sample verticals and within replicates, suggesting that sediment transport conditions were highly variable during the research campaign.

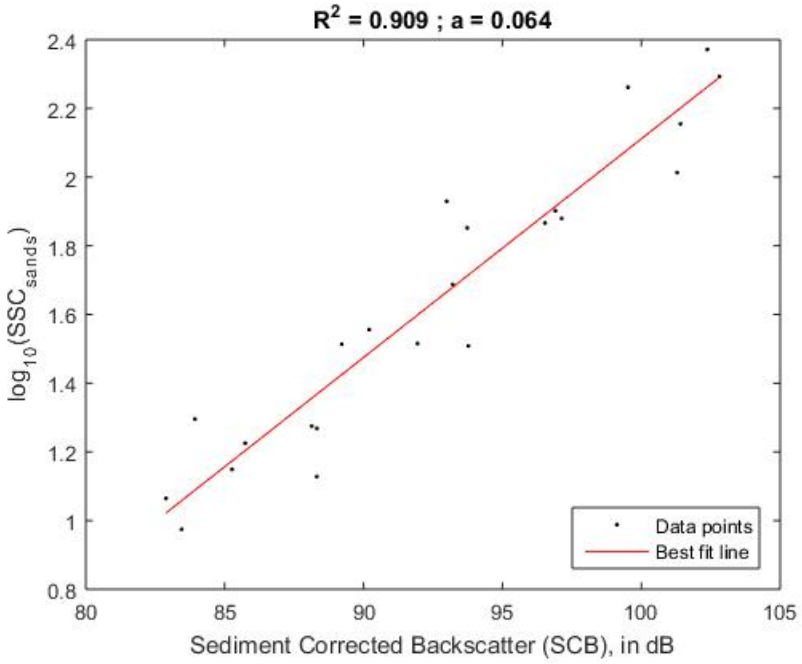

Figure 3. Calibration developed for coarse fraction concentration for the Missouri River at St. Charles, MO, July 20, 2016

Table 2. Research sites and calibration results from the Sediment Transect Acoustics software when processing data from all available verticals and calibrating to the coarse fraction [EDI, equal discharge increment method; SSC, suspended-sediment concentration; SSC_t, total suspended-sediment concentration; D50, median particle size diameter; kHz, kilohertz; ADCP, acoustic Doppler current profiler; STA, Sediment Transect Acoustics software; R^2, coefficient of determination; N/A, not applicable]

River site	Validation EDI sample SSC, average of sets if applicable (mg/L)	Percent fines	Coarse D50 (μm); volume distribution (number distribution)	Fines D50 (μm); volume distribution number distribution)	Results with 1200kHz ADCP (calibration to coarse)			Results with 600kHz ADCP (calibration to coarse)		
					STA-estimated SSC_t (mg/L)	STA calibration R^2	STA calib-ration slope	STA-estimated SSC_t (mg/L)	STA calibration R^2	STA calib-ration slope
Missouri River at St. Charles, MO	348	77	159 (90)	2[a] (1)	279	0.91	0.06	280	0.78	0.06
Sacramento River at Freeport, CA	96	43	204 (76)	11.5 (0.61)	68	0.82	0.06	67	0.81	0.06
Illinois River at Florence, IL	78	81	154 (120)	4.1 (0.18)	67	0.66	0.08	59	0.44	0.05
Missouri River at Nebraska City, NE	691	69	169 (104)	11.4 (0.21)	710	0.82	0.09	744	0.48	0.05
St. Joseph River at Napier Ave. at St. Joseph, MI	292	46	253 (114)	12.1 (0.23)	217	0.91	0.08	193	0.80	0.07
Cowlitz River at Castle Rock, WA	15	32	150[b] (150)	4[b] (4)	13	0.98	0.09	N/A[c]	N/A[c]	N/A[c]

[a]Over 50 percent of the distribution of the fines fraction was smaller than 2 μm, the smallest particle size category reported during analysis; input 2 μm as the fines D50.
[b]Did not perform detailed particle size analysis on this dataset; used assumed D50 values based on data from similar sites and historical data.
[c]600kHz ADCP data not collected at this site.

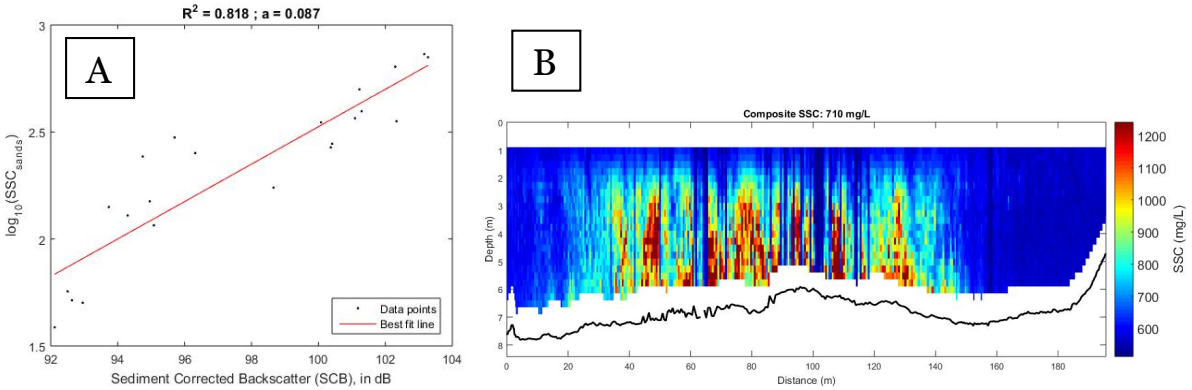

Figure 4. Calibration developed for SSC_c (A) and cross section estimates of SSC_t (B) for the Missouri River at Nebraska City, NE, May 25, 2017, showing banding and non-uniform appearance in sediment distribution

Overall, calibrations developed for SSC_c were good but were typically not adequate when calibrating to SSC_f or SSC_t. Other researchers have noted similar issues (Topping and others, 2007; Wright and others, 2010; Moore and others, 2013; Szupiany and others, 2018) indicating backscatter from coarse particles dominates the acoustic response and calibration when coarse particles are present. Additionally, some of the datasets showed that attenuation can also be dominated by coarse particles even when substantial fines are present. One example is the Sacramento River dataset (Figure 5), which showed that the backscatter in each bin is dominated by the coarse particle sizes, as expected. The sediment size contributing to attenuation, however, varied by depth in the water column and was often medium and coarse-sized sands. Figure 5A shows the particle sizes contributing to bin backscatter (top) and bin attenuation (bottom) for the point sample collected at vertical 2-0.9D near the bed. Figure 5B shows the same graphs for the point sample collected at vertical 1-0.2D near the water surface. The sample at vertical 2-0.9D contained about four times higher coarse fraction concentration and twice as high of a coarse fraction D50 than the sample at vertical 1-0.2D. This dataset shows that coarse particles can contribute a substantial amount of attenuation and that, overall, separating the acoustic response to the fines fraction in an attempt to quantify fines concentration, in the presence of coarse particles, can be problematic. As a result, the calibrations developed and presented in Table 2 were calibrations on SSC_c, but as previously mentioned, SSC_t is calculated for the cross section by adding the average fines concentrations from the point samples to the SSC_c calculated by the calibration equation. Issues associated with this approach are discussed under the Limitations section. Moore and others (2013) present an approach for estimating SSC_f using measurements of attenuation at three acoustic frequencies. This approach is not integrated in the current version of STA but may be investigated in the future.

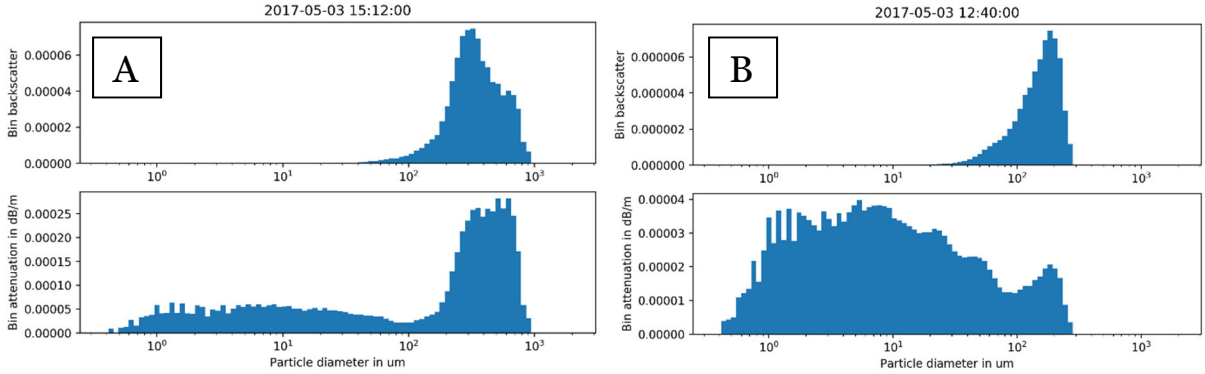

Figure 5. Graphs showing comparative contribution of sediment particle sizes on bin backscatter (top) and bin attenuation (bottom) for point sediment samples collected from (A) vertical number 2, 0.9-depth and (B) vertical number 1, 0.2-depth at the Sacramento River at Freeport, CA, May 3, 2017

Preliminary Testing on Minimum Datasets

STA was used to test various scenarios at each research site to evaluate sensitivity of calibrations and reasonable minimum datasets for estimating SSC. These scenarios included:

- the use of select verticals and combinations of verticals.
- the use of a reduced number of points collected in the water column.
- the use of different echo intensity scale factors for ADCP beams.
- the use of data from different combinations of ADCP beams (1, 2, 3, and 4).

The resulting calibrations and estimates of cross section SSC were compared to those obtained from the full dataset of five verticals and 25 sediment sampling points, using ADCP beams 3 and 4 (upstream and downstream, respectively) and manufacturer-supplied echo intensity scale factors.

The results of testing select verticals and combinations of verticals showed that selection of a minimum of two verticals, one in a more quiescent zone and one in a more turbulent, dynamic zone, together representing a wide range of sediment transport and backscatter conditions for the cross section, appears to produce calibrations that are reasonably close to those developed with data from all five verticals. Statistical comparisons of calibrations based on the full versus reduced datasets, using an analysis of covariance (ANCOVA) test, are planned to confirm initial observations.

Selection of three points within each vertical (0.4-D, 0.6-D, 0.8-D) appears to produce better calibrations than those using all available points. Data collected at 0.2-D showed unusual patterns and scatter at some sites, particularly for the 600kHz ADCP datasets, perhaps due to larger than expected near-field zones or turbulence introduced by the boat. Samples collected at 0.9-D were often within the sidelobe interference zone of both ADCPs so were not used in calibrations but could be used to validate bottom SSC estimates extrapolated by the STA software (see Plans for Future Work section).

The calibration results presented in Table 2 were based on the use of data from only ADCP beams 3 and 4. When testing sensitivity to which ADCP beam(s) is used in the calibration and associated beam echo intensity scale factors, the greatest sensitivity on results appears to be on beam used rather than the actual scale factors. Though this continues to be tested, a best

practice might be to use the average of all four ADCP beams to reduce the effect of individual beam variation.

Current Limitations of Method

As previously mentioned, calibrations developed for SSC_c were good but typically not adequate when calibrating to SSC_f or SSC_t. The inability to develop a calibration specifically for SSC_f presents a limitation of the method: particularly the ability to apply the calibration to another time period and get an estimate of SSC_t without having to collect a sediment sample. We are currently testing various approaches for obtaining a better estimate of SSC_f, including using the Topping and Wright (2007) and Landers and others (2016) side-looking approach by calculating sediment attenuation using only a small portion of the water column near the top (where little to no coarse particles are present) or the Moore and others (2013) approach of multi-frequency acoustic inversion. Until an operational, computational approach can be developed to estimate SSC_f, users of the methods described in this paper might collect a single vertical or grab sample, analyzed for concentration and percent fines. This approach is less labor intensive than taking a full EDI sample and may supply the information needed for the fines fraction. The datasets collected for this research effort were examined to evaluate the variability in the fines fraction of sediment concentrations in all point samples and verticals to assess whether a single vertical, grab, or point sample could be collected to adequately represent the fines fraction. For all sites, the coefficient of variation (CV, standard deviation divided by the mean) for fines concentration ranged from 2 to 17 percent among all point samples collected at a site, meaning variability was relatively low. CV was 10 percent or less for four out of the six sites. In comparison, CV for coarse concentrations ranged from 41 to 121 percent over all sites. We will continue to work on an approach for developing a calibration for fines, but in the meantime, collecting a single vertical (preferred) or grab/point sample in a well-mixed location may be adequate for representing the fines at sites similar to those tested.

Plans for Future Work

Researchers from the Littoral National University in Argentina have developed another software program, Acoustic Sediment Estimation Toolbox (ASET), described in Dominguez and others (in review). Methods in ASET are further described in Szupiany and others (2016; 2018) and allow for characterization of noise or undesired portions of the received signal as well as uncertainties in other terms; characteristics of the acoustic signal such as transmit power and transmit length; and a form factor representing sediment characteristics. ASET also computes estimates of sediment transport in the top and bottom unmeasured areas of the ADCP profile and cross section using different methods. The point sediment samples collected at the 0.9-D locations will be used to validate the estimates in the bottom unmeasured areas. Selected elements of ASET were incorporated into STA beta version 4.0 but additional coding and testing are needed to allow estimation of total SSC and to compare with results described in this paper. Once integrated and tested, the joined software will allow broader and more complete evaluations of these and future datasets compared to the evaluations described in this paper.

The seasonal and site-specific dependence of ADCP-based calibrations for estimating suspended sediment has been reported as a major challenge in advancement of the method (Latosinski and

others, 2014). We also plan to conduct a series of tests to apply calibrations developed on the dates in Table 2 to other time periods where cross-section, moving boat ADCP measurements have been made and validation sediment samples have been collected. This exercise will assess whether calibrations hold over different flow and sediment transport conditions. If calibrations hold over different conditions, they could be applied to any ADCP measurement (made before or after the calibration field campaign) to get a rapid estimate of SSC and suspended-sediment load (SSL) when no other sediment data are available. Additionally, we plan to apply calibrations developed at one location on a river reach to another nearby location, on the same river, to determine if calibrations could be used to accurately "map" and quantify sediment distribution in a river reach. Development of calibrations that hold over time and space and produce reasonable estimates of SSC and SSL would greatly expand the amount of sediment information available to the public and science communities and allow reporting of sediment data on demand during times when samples cannot be collected due to logistical or safety considerations.

Conclusions

The use of down-looking ADCPs to estimate SSC and SSL showed great promise at the six U.S. river sites selected. Best results were found when using data from the 1200kHz ADCPs (R^2 0.66 to 0.98, calibration slopes 0.06 to 0.09) and by calibrating to the coarse fraction of suspended sediment. Estimates of total SSC were determined by adding sampled fines concentration to the calibration-estimated coarse concentration for a site. Obtaining a calibration for fines proved problematic for all sites because of the difficulty separating backscatter and attenuation for fines in the presence of any coarse particles. STA-estimated SSC was less than validation sample SSC at all sites except one, which was expected because the methods selected for data processing in STA do not yet extrapolate SSC at the top, bottom, and edges of the river cross section where data are not reported by the ADCP. Preliminary testing on minimum datasets showed that calibrations resulting from data collected at a minimum of two verticals over a wide range of backscatter conditions, and at a minimum of three points within each vertical (0.4-D, 0.6-D, 0.8-D), are needed to produce reasonable calibrations and cross section estimates of SSC. Additional work is needed to evaluate the validity of the calibrations when applied to ADCP cross section measurements made at other times, under different sediment transport conditions, and other locations within a river reach. Additionally, work is underway to fully incorporate features in the ASET software into the STA software to allow characterization of additional variables in the acoustic data correction process and to allow extrapolation of SSC estimates in unmeasured areas. The use of down-looking ADCPs to rapidly estimate suspended-sediment concentrations and loads, while leveraging other uses of the instruments for flow measurement, has applicability for sand-bedded rivers over a wide range of sediment transport and river conditions.

Disclaimer

Use of trade, product, or firm names in this paper is for descriptive purposes only and does not imply endorsement by the U.S. Government.

References

Boldt, J.A., Czuba, J.A., Straub, T.D., Curran, C.A., Szupiany, R.N., and Oberg, K.A. 2012. "Estimation of suspended-sediment concentration from down-looking acoustic Doppler

current profilers using an acoustic backscatter calibration procedure and MATLAB-based tool," Proceedings of the Hydraulic Measurements and Experimental Methods Conference, August 12-15, 2012, Snowbird, Utah.

Boldt, J.A. 2015. "From mobile ADCP to high-resolution SSC: a cross section calibration tool," Proceedings of the 3rd Joint Federal Interagency Conference on Sedimentation and Hydrologic Modeling, April 19-23, 2015, Reno, Nevada, pp 1258-1260.

Dominguez Ruben, L.G., Szupiany, R.N., Latosinski, F.G., Lopez Weibel, C., Wood, M., and Boldt, J. in review. "Acoustic Sediment Estimation Toolbox (ASET): A software package for calibrating and processing ADCP data to compute suspended-sediment transport," submitted to Computers and Geosciences, Elsevier.

Downing A, Thorne PD, Vincent CE. 1995. "Backscattering from a suspension in the near-field of a piston transducer," Journal of the Acoustical Society of America 97(3): 1614-1620.

Edwards, T.K., and Glysson, G.D. 1999. "Field methods for measurement of fluvial sediment," U.S. Geological Survey Techniques of Water-Resources Investigations, book 3, chap. C2, 89 p.

Gartner, J.W. 2004. "Estimating suspended solids concentrations from backscatter intensity measured by acoustic Doppler current profiler in San Francisco Bay, California," Marine Geology, Elsevier, 211: 169–187.

Guerrero, M., Szupiany, R.N., and Latosinski F. 2013. "Multifrequency acoustics for suspended sediment studies: an application in the Parana River," Journal of Hydraulic Research, 51 (6): 696-707.

Guerrero, M., Ruther, N., Haun, S., and Baranya, S. 2017. "A combined use of acoustic and optical devices to investigate suspended sediment in rivers," Advances in Water Resources, Elsevier, 102: 1-12.

Landers, M.N., Straub, T.D., Wood, M.S., and Domanski, M.M. 2016. "Sediment acoustic index method for computing continuous suspended-sediment concentrations," U.S. Geological Survey Techniques and Methods, book 3, chap. C5, 63 p., http://dx.doi.org/10.3133/tm3C5.

Latosinski, F. G., Szupiany, R. N., García, C. M., Guerrero, M. and Amsler, M. L. 2014. "Estimation of concentration and load of suspended bed sediment in a large river by means of acoustic Doppler technology," Journal of Hydraulic Engineering, 140(7).

Moore, S.A., LeCoz, J., Hurther, D., Paquier, A. 2013. "Using multi-frequency acoustic attenuation to monitor grain size and concentration of suspended sediment in rivers," Journal of the Acoustical Society of America, 133: 1959-1970.

Mueller, D.S., Wagner, C.R., Rehmel, M.S., Oberg, K.A., Rainville, F. 2014. "Measuring discharge with acoustic Doppler current profilers from a moving boat," U.S. Geological Survey Techniques and Methods, book 3, chap. A-22, version 2.0, 95 p.

Schulkin, M., and Marsh, H.W. 1962. "Sound absorption in sea water," Journal of the Acoustical Society of America, 34: 864– 865.

Szupiany, R. N., Amsler, M. L., Parsons, D. R., and Best, J. L. 2009. "Morphology, flow structure, and suspended bed sediment transport at two large braid-bar confluences," Water Resour. Res., 45, W05415, doi:10.1029/2008WR007428.

Szupiany, R.N., Lopez Weibel, C., Latosinki, F., Dominguez Ruben, L., Amsler, M., and Guerrero, M. 2016. "Sediment concentration measurements using ADCPs in a large river: evaluation of acoustic frequency and grain size," Proceedings of the International Conference on Fluvial Hydraulics, 10.1201/9781315644479-243.

Szupiany, R.N., Lopez Weibel, C., Guerrero, M., Latosinki, F., Wood, M., Dominguez Ruben, L., and Oberg, K. 2018. "Estimating sand concentrations using ADCP-based acoustic inversion in a large fluvial system characterized by bi-modal suspended-sediment distributions," Earth Surface Processes and Landforms, John Wiley & Sons, Ltd, 14 p., https://doi.org/10.1002/esp.4572

Thorne, P. D. and Meral, R. 2008. "Formulations for the scattering properties of suspended sandy sediments for use in the application of acoustics to sediment transport processes," Cont. Shelf Res., 28(2): 309–317.

Thorne, P.D., Vincent, C.E., Hardcastle, P.J., Rehman, S., and Pearson, N. 1991. "Measuring suspended sediment concentrations using acoustic backscatter devices," Marine Geology, Elsevier, 98(1): 7–16.

Topping, D. J., Wright, S. A., Melis, T. S., and Rubin, D. M. 2007. "High resolution measurements of suspended-sediment concentration and grain size in the Colorado River in Grand Canyon using a multifrequency acoustic system," Proceedings of the 10th Int. Symp. on River Sedimentation, M. V. Lomonosov, Moscow State Univ., Moscow, Russia.

Topping, D.J., and Wright, S.A. 2016. "Long-term continuous acoustical suspended-sediment measurements in rivers - Theory, application, bias, and error," U.S. Geological Survey Professional Paper 1823, 98 p.

Wall, G.R., Nystrom, E.A., and Litten, S. 2006. "Use of an ADCP to compute suspended-sediment discharge in the Tidal Hudson River, New York," U.S. Geological Survey Scientific Investigations Report 2006–5055, 16 p.

Wood, M.S. 2014. "Estimating suspended sediment in rivers using acoustic Doppler meters," U.S. Geological Survey Fact Sheet 2014-3038, 4 p.

Wood, M.S., Fosness, R.L., and Etheridge, A.B. 2015. "Sediment transport and evaluation of sediment surrogate ratings in the Kootenai River near Bonners Ferry, Idaho, Water Years 2011-14," U.S. Geological Survey Scientific Investigations Report 2015-5169, 48 p.

Wright, S.A., Topping, D.J., and Williams, C.A. 2010. "Discriminating silt-and-clay from suspended-sand in rivers using sidelooking acoustic profilers," Proceedings of the Joint Federal Interagency Conference on Sedimentation and Hydrologic Modeling, June 27- July 1, 2010, Riviera Hotel, Las Vegas, Nevada, https://acwi.gov/sos/pubs/2ndJFIC/Contents/2C_Wright_03_01_10_paper.pdf.

Monitoring the Transport of Sediment in an Ephemeral Stream

David Varyu, Hydraulic Engineer, U.S. Bureau of Reclamation, Denver, CO, dvaryu@usbr.gov
Dr. Jonathan B. Laronne, Professor Emeritus, Ben-Gurion University of the Negev, Beer Sheva, Israel, john@bgu.ac.il
Dr. Daniel Cadol, Associate Professor, New Mexico Institute of Mining and Technology, Socorro, NM, daniel.cadol@nmt.edu
Robert Padilla, Supervisory Civil Engineer, U.S. Bureau of Reclamation, Albuquerque, NM, rpadilla@usbr.gov
Tony Lampert, Supervisory Civil Engineer, U.S. Bureau of Reclamation, Albuquerque, NM, alampert@usbr.gov
Kyle Stark, Ph.D. Student, New Mexico Institute of Mining and Technology, Socorro, NM, kyle.stark@student.nmt.edu
Stephen Scissons, Supervisory Hydraulic Engineer, U.S. Army Corps of Engineers, Albuquerque District, Stephen.K.Scissons@usace.army.mil
Jonathan AuBuchon, Regional Sediment Specialist, U.S. Army Corps of Engineers, Albuquerque District, Jonathan.Aubuchon@usace.army.mil
Yaniv Munwes, Owner, Yamma Hydrometric Solutions. yaniv.munwes@yamma-hydro.co.il

Abstract

Quantifying sediment delivery from tributaries is requisite for understanding fluvial characteristics and geomorphic processes of a river reach. A research station has been constructed on the Arroyo de los Piños, a tributary to the Rio Grande near Socorro, NM. This project has become a multi-agency effort with extensive collaboration. The interest generated by this research project is due to the data gaps recognized by hydraulic engineers, geomorphologists, biologists, and other researchers who work in the American Southwest and other arid regions. The site was constructed and fully operational as of May 2018. The primary components of the site include: 3 Reid-type slot samplers, 2 active pipe microphones, 1 active plate with both a microphone and a geophone, vertical-horizontal duo pipe microphones, 4 passive hydrophones, 1 seismometer, 2 ISCO pump samplers, 2 high-end turbidity sensors, 5 pressure transducers for stage, 4 rain gages throughout the basin, and a state-of-the-art signal processing/data storage system. There have been five runoff events during the 2018 monsoon season which were recorded. Preliminary results for a variety of research aspects are presented by collaborating partners at this conference.

Introduction

Quantifying the mass, size, timing, and frequency of sediment delivery from tributaries is requisite for understanding fluvial characteristics and geomorphic processes of a river reach. Sediment transport in perennial tributaries can be quantified reasonably well using standard methods; ephemeral streams prove to be more difficult. These difficulties arise from the infrequent and flashy nature of events, the effort required to obtain measurements in these often-remote areas, and varying cross section shapes during runoff events. Standard gaging

methods cannot be utilized, and safety concerns exist in sediment laden water when a runoff event does occur. An automated research station can overcome these difficulties by notifying stakeholders when an event occurs and by collecting data continuously throughout the flow event. This paper documents the installation of such a station on the Arroyo de los Piños, a tributary to the Rio Grande, located near Socorro, NM. This station directly samples bedload and suspended load, as well as indirectly monitors suspended concentration, bed load flux, and hydraulic properties using surrogate methods.

There are five other papers submitted to these proceedings (four presented orally, one as a poster) regarding the technical aspects of the Arroyo de los Piños Research Station, including data collection and preliminary analysis. This paper provides the background to the project and discusses the partnerships and collaboration that have been established in tandem with site development.

Background

In 2013, funding was provided by Reclamation's Research and Development Office to conduct a literature review regarding sediment transport in ephemeral streams. The result was an understanding of the state of the research focused on monitoring ephemeral streams (particularly related to bed load) as well as a conceptual layout for a research station that could be deployed in an arid-region river of the American Southwest (Varyu, 2013). During 2014, a new three-year proposal was developed, submitted, and funded for conducting research (Varyu, 2017). Fiscal years 2015-2017 (October 2014 – September 2017) were dedicated to site selection, developing partnerships, conducting preliminary data collection, and developing a project (design drawings, site plans, permitting, and contracting). Construction commenced and completed in the first half of fiscal year 2018, the site was fully operational by May 2018, and data collection began in earnest with five storm events in the summer/fall of 2018.

As is characteristic of the semi-arid southwest, flow in this basin is almost exclusively generated by intense localized thunderstorms associated with the North American Monsoon. A majority of precipitation falls during the monsoon season of July-October. Monsoon storms tend to be short duration and high intensity, with limited spatial extent, while winter precipitation tends to be widespread and low intensity, rarely generating runoff.

Site Selection and Development

Thirteen arroyos along the Rio Grande in New Mexico were visited in October 2014 to determine the location most appropriate for site development. This included members of the Technical Service Center (TSC) of Reclamation, the Albuquerque Area Office (AAO) of Reclamation, and Ben Gurion University of the Negev (BGU). The subsequent months involved discussion and consideration of the arroyo sites, as well as considering which additional arroyos should be visited. By mid-March 2015 the Arroyo de los Piños was deemed the most promising and three additional arroyos were identified for assessment.

The week of March 30, 2015 consisted of visiting three additional arroyos along the Rio Grande, after which the Arroyo de los Piños was selected for research. A geometric survey of the channel and bed material sampling was conducted to characterize the arroyo in the vicinity where the research station was envisioned, and the upper basin was observed to characterize the watershed. It was chosen because its bed contained sands and gravels up to large cobbles, and

because the channel had been constricted to 10 m near the confluence with the Rio Grande. An important benefit of the Arroyo de los Piños is its proximity to Socorro, NM (Figure 1) where the New Mexico Institute of Mining and Technology (NMT) is located. The Department of Earth and Environmental Sciences was contacted, and a meeting took place that same week. It was clear from the meeting that a productive partnership would come to fruition regarding the Arroyo de los Piños Research Station.

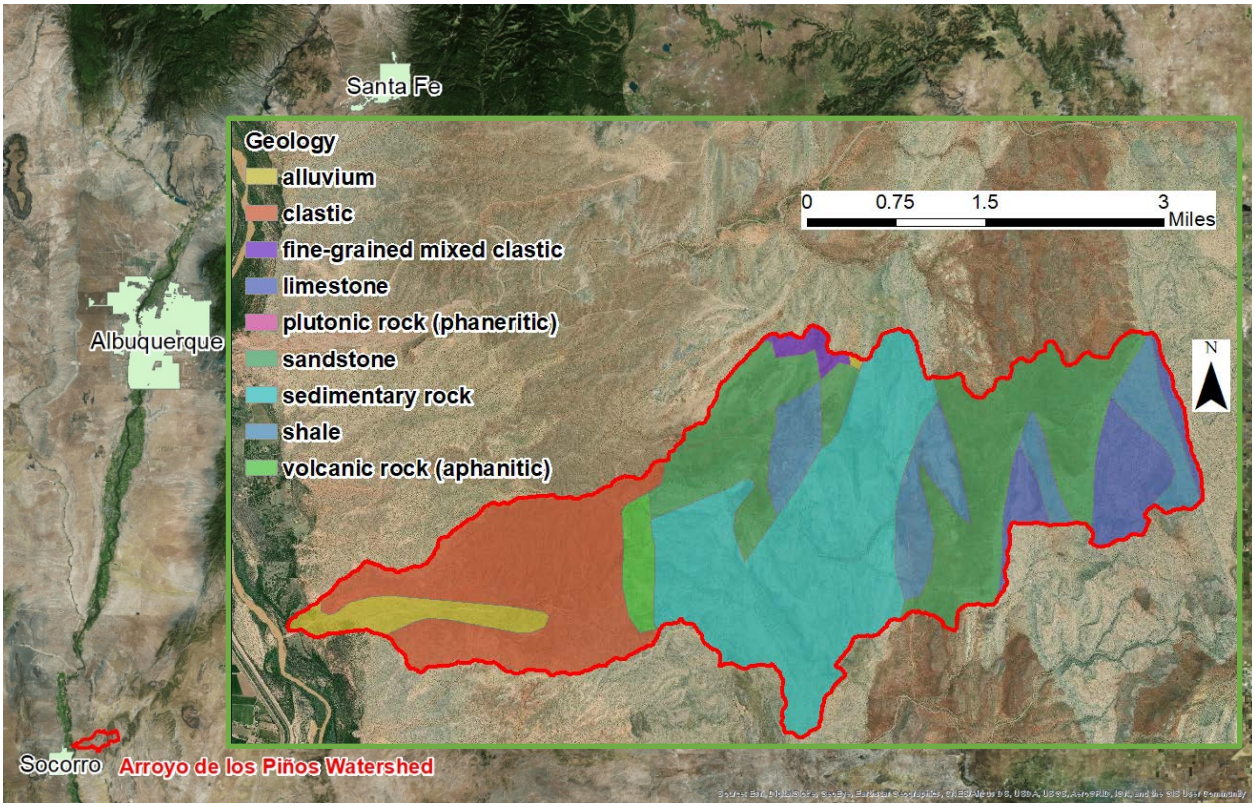

Figure 1. Location map of the research site drainage basin (red polygon), with inset of basin geology.

During the bulk of design and instrument specification (Spring 2015 – Spring 2016) NMT hired a graduate student to undertake an MSc study (Stark, 2018) on this project. Collaboration and iteration led to developing the final project description, design drawings and instrument specification. The project description and design drawings were produced by AAO (Lampert, 2016), and instrument specification was led by BGU and NMT.

The Spring of 2016 marked a new phase of the project; obtaining environmental permits, purchasing instrumentation, and broadening partnerships. In the Fall of 2016, a conference was organized by AAO that brought together a multitude of stakeholders interested in management, monitoring, and research activities occurring on the Middle Rio Grande. This useful conference provided a framework for various local, state, and federal agencies, water managers and users, as well as interested private citizens to gather and learn from each other. A presentation was made at this conference regarding the planned installation of the Piños research station which was well received and generated interest on the part of the U.S. Army Corps of Engineers' Albuquerque District (Corps). This marked the beginning of the collaboration with the Corps, which includes the Corps' Engineering and Research Development Center (ERDC). The Corps has provided financial support, technical guidance, and collected digital terrain surveys using fixed-wing aircraft. Additional device deployment is regularly being discussed as well. NMT

began manual sampling of monsoon events in Summer 2016 before the station was fully automated. Some of the items purchased during 2016 included handheld sediment samplers for suspended load (DH-48) and bed load (BLH-84); one event in 2016 provided the opportunity for gaining acumen with these manual samplers. Figure 2 presents a reach of the arroyo approximately 500 yards upstream of the research site.

Figure 2. The arroyo approximately 500 yards upstream of the research site. Photo is looking upstream (east).

Funding was secured for project construction in the Spring of 2017 and the contracting process initiated to hire a construction firm. A previous line of construction funding had been pursued, but did not materialize, leading to the delay between the design being finalized and a contract awarded to initiate construction. A contract was awarded in the spring, but construction did not begin until the fall, as there were concerns of monsoon events damaging any work that was not fully completed. This could have led to costly delays in the construction, so a decision was made to wait until after the monsoon season. Hindsight showed the wisdom in this decision, as six monsoon events occurred during the summer of 2017. Although it would have been ideal to sample these events with an automated system, they were still manually sampled by NMT. This sampling effort helped to characterize the nature of runoff events for the basin and represent the costly, time-intensive methods that the automatic station seeks to supplant. Furthermore, it provides a pre-construction dataset to which the post-construction data can be compared (Stark, 2018). Construction commenced in the fall of 2017 and was completed by the end of January 2018. The subsequent months were spent deploying the automated instruments, testing the system, and ensuring the station was prepared for the 2018 monsoon season. The 2018

monsoon season supplied continuous, very interesting and first of their kind data on five flood events. A very large flashflood occurred on 26 July, 2018, causing damage to some of the gabions on the banks and degrading the riverbed downstream of the monitoring station. This damage was repaired with grouted riprap on the bank, the horizontality of the concrete sill was secured, and concrete access steps were added by AAO in November 2018.

Site Description & Purpose

The site was constructed and fully operational as of May 2018. The primary components of the site include (Figure 3) three Reid-type slot samplers (direct measurement of bed load), two pipe microphones (bed load surrogate), one impact plate with both a microphone and a geophone (bed load surrogate), vertical-horizontal duo pipe microphones (investigating the nature of saltation in the channel), four passive hydrophones (bed load surrogate), seismometer (bed load surrogate), two ISCO pump samplers (direct measurement of suspended load), two high-end turbidity sensors (suspended load surrogate), five pressure transducers for water stage (hydraulics), 3 (a fourth to be deployed prior to 2019 monsoon season) rain gages throughout the basin (rainfall-runoff correlations), and a state-of-the-art signal processing/data storage system, including cellular transmission, allowing monitored data to be viewed in real-time. These are supplemented by manual measurements of bedload, suspended sediment concentration, and velocity.

As of 2019 surface water velocity will be determined manually using a portable SVR (Surface Water Velocimetry), thereby calculating average water velocity for all but very shallow flows (Welber et al., 2016). Surface water velocity and turbulent structures in the approach reach will be established by Large Scale Particle Image Velocimetry (Le Coz et al., 2010) using an available video camera.

The goals and methods deployed at this site have slightly evolved, with an intent of this research to provide a reliable means to quantify the mass of sediment being delivered by ephemeral, flashflood streams to a higher-order stream. It has been demonstrated that bed load flux in an ephemeral stream can be “several orders of magnitude higher than maxima measured at similar levels of stream power in perennial counterparts (Reid and Laronne, 1995). This fact is unfortunate when considering that the current state of the practice for estimating sediment yield/delivery is to apply a transport equation (developed using data from perennial streams) to an ephemeral stream’s geometry, bed material gradation, and a synthesized storm runoff hydrology for an event(s). Although a lofty goal, improving the state of the practice for quantifying sediment delivery from ephemeral streams is a necessary one, especially for the semi-arid American Southwest and similar such areas on our globe.

This research station alone will not achieve such a goal, but it will be a necessary, large piece of a larger dataset. A near-term outcome of data collected at this research station will be a relationship between acoustic impulses and bedload for the Arroyo de los Piños. Such a relationship can then be compared to other relationships already developed for other instrumented ephemeral streams (Rickenmann et al., 2014). A multi-variate regression can then be performed to assess parameters that may be used to normalize the acoustic signal vs. bedload relationship such as grain size and channel slope, basin size, elevation and slope, peak storm discharge, and/or other parameters. Following the scientific method, a hypothesis would be made for the acoustic impulse – bed load relationship in an un-instrumented basin and a test would be designed. Data during a storm event in the new basin would be collected and the

Figure 3. Overview of instrumentation. (A) Control section (view from right bank), with 3 Reid-type slot samplers and active acoustic surrogates upstream of slot openings. (B) stilling well for pressure transducer and two perforated arms housing ISCO pump sampler tubes and co-located turbidity sensors. (C) One of three up-basin rain gages to characterize rainfall-runoff relationship. (D) Control house with signal processors, data storage, and cellular data transmission. Control house also contains ISCO samplers (not shown).

hypothesis would be assessed. Self-evidently, this long-term vision is beyond the purview of the Arroyo de los Piños Research Station, but this is where the research for bedload (and total load) for ephemeral streams is headed. Ultimately, the deployment of surrogate methods can be used to reliably estimate the sediment load being delivered from ephemeral to higher order streams safely and at a reasonable cost. The use of acoustic sensors as bedload surrogates requires their deployment in the water column, with related potentials to flood damage as well as being covered by sediment. We foresee the opportunity to further advance the use of seismic monitoring of bedload with sensor deployment on river banks. Although the science of seismic monitoring postdates that of acoustic monitoring of bedload, the Arroyo de los Piños installation is also involved in this technology.

This project has become a multi-agency effort with extensive collaboration. The interest generated by this research project is due to the data gaps recognized by hydraulic engineers, geomorphologists, biologists, and other researchers who work in the American Southwest and other arid regions. As is evidenced by the author list, this project includes active participation

and collaboration by Reclamation, Army Corps of Engineers, New Mexico Institute of Mining and Technology, Ben-Gurion University of the Negev, and Yamma and Ayyeka Companies. There are many other collaborators on this project as well, including CNRS France, German Research Center for Geosciences, and the United States Geological Survey.

During the 2018 monsoon season, five bedload-producing runoff events occurred and were monitored by the instrumentation at the Arroyo de los Piños Research Station. From these events there have been approximately 81 discrete suspended sediment samples, 130 bedload samples subset from the Reid-type slot samplers, 15 manual bedload measurements, 75 manual depth and velocity measurements, and 72,000 automatically recorded measurements. The following papers are included in the proceedings and will be presented orally or as a poster presentation at this conference:

- Initial Calibration of Acoustic Pipe Microphone Sensors to Monitor Bedload During Flash Floods in the Arroyo de los Piños, NM. (Stark et al., 2019)
- The Seismic View on Sediment Laden Ephemeral Flows – Modelling of Ground Motion Data for Fluid and Bedload Dynamics in the Arroyo de los Piños (Dietze et al., 2019)
- Bedload Flux and Characteristics from Flash Floods in the Arroyo de los Piños, NM – initial results (Cadol et al., 2019)
- Initial Analysis of Suspended Sediment Concentrations During Flash Floods on the Arroyo de los Piños, NM (Laronne et al., 2019)
- Rainfall-Runoff Relationships Complementing Previous Sediment Transport Studies at the Arroyo de los Piños, New Mexico (Richards et al., 2019)
- Recent Acoustic Bedload Monitoring Field Experiments Using Hydrophones (Marineau et al. 2019)

The Arroyo de los Piños Research Station is fully operational and a suite of data is collected and analyzed during and after monsoonal storm events. The process of developing the site has been perhaps slow and steady, but now that it is operational there are years (if not decades) of data to be gathered and information to be gleaned from this site.

Acknowledgements

We thank: Micha Dietz, Cord Everetts, Florent Gilbert, Eran Halfi, Alexandre Hauet, Robert Hilldale, Bill Holmes, Michinobu Nonaka, Tim Randle, Rudolfo Bernal, Jens Turowski, and Jeb Brown, for their support in this project.

References

Cadol, D., Stark, K., Laronne, J.B., Varyu, D. and Richards, M. 2019. “Bedload Flux and Characteristics from Flash Floods in the Arroyo de los Piños, NM – Initial Results” SedHyd2019, Federal Interagency Sedimentation and Hydrologic Modeling Conference. June 2019, Reno NV.

Dietze, M., Gimbert, F., Turowski, J.M., Stark, K., Cadol, D. and Laronne, J.B. 2019. “The Seismic View on Sediment Laden Ephemeral Flows – Modelling of Ground Motion Data for Fluid and Bedload Dynamics in the Arroyo de los Piños” SedHyd2019, Federal Interagency Sedimentation and Hydrologic Modeling Conference. June 2019, Reno NV.

Lampert, A. 2016. Arroyo de los Piños: Sediment Sampling Site Project Description. Bureau of Reclamation, Upper Colorado Region, Albuquerque Area Office, Technical Services Division, Albuquerque, NM.

Laronne, J.B., Stark, D. Cadol., D., Varyu, D. and Richards, M. 2019. "Initial Analysis of Suspended Sediment Concentrations During Flash Floods on the Arroyo de los Piños, NM" SedHyd2019, Federal Interagency Sedimentation and Hydrologic Modeling Conference. June 2019, Reno NV.

Le Coz, J., Hauet, A., Pierrefeu, G., Dramais, G. and Camenen, B. 2010. "Performance of image-based velocimetry (LSPIV) applied to flash-flood discharge measurements in Mediterranean rivers," Journal of Hydrology. 394(1-2), 42-52.

Marineau, M., Wright, S., Daeuman, D., Curran, C., Stark. K., and Siemion, J. 2019. "Recent Acoustic Bedload Monitoring Field Experiments Using Hydrophones" SedHyd2019, Federal Interagency Sedimentation and Hydrologic Modeling Conference. June 2019, Reno NV.

Reid, I. and Laronne, J.B. 1995. "Bedload sediment transport in an ephemeral stream and a comparison with seasonal and perennial counterparts," Water Resources Research, 31, 773-781.

Richards, M., Cadol, D., Laronne, J.B., Varyu, D., AuBuchon, J. and Brown, S. 2019. "Rainfall-Runoff Relationships Complementing Previous Sediment Transport Studies at the Arroyo de los Piños, New Mexico" SedHyd2019, Federal Interagency Sedimentation and Hydrologic Modeling Conference. June 2019, Reno NV.

Rickenmann, D., Turowski, J., Fritschi, B., Wyss, C., Laronne, J., Barzilai, R., Reid, I., Kreisler, A., Aigner, J., Seitz, H., and Habersack, H. 2014. "Bedload transport measurements with impact plate geophones: comparison of sensor calibration in different gravel-bed streams," Earth Surface Processes and Landforms. 39, 928–942. DOI: 10.1002/esp.3499

Stark., K. 2018. A Two-Year Study of Flash Flood Characteristics in New Mexican and Israeli Ephemeral Channels. Unpublished M.Sc. thesis, Dept. Earth & Environmental Sciences, New Mexico Institute of Mining & Technology, 52 pp.

Stark, K., Cadol, D., Laronne, J.B., Varyu, D., Halfi, E., and Richards, M. 2019. "Initial Calibration of Acoustic Pipe Microphone Sensors to Monitor Bedload During Flash Floods in the Arroyo de los Piños, NM.," SedHyd2019, Federal Interagency Sedimentation and Hydrologic Modeling Conference. June 2019, Reno NV.

Varyu, D. 2017. Measuring the Transport of Sediment in an Ephemeral Stream; Project Closeout Report; ST-2017-9781-01. Bureau of Reclamation, Technical Service Center, Research and Development Office, Science and Technology Program, Denver, CO. https://www.usbr.gov/research/projects/download_product.cfm?id=2611

Varyu, D. 2013. Ephemeral Tributary Sediment Loads; Project ID 2180. Bureau of Reclamation, Technical Service Center, Research and Development Office, Science and Technology Program, Denver, CO. https://www.usbr.gov/research/projects/detail.cfm?id=2180

Welber, M., Le Coz, J, Laronne, J.B., Zolezzi, G., Zamler, D., Dramais, G., Hauet, A. and Salvaro, M. 2015. "Field assessment of non-contact stream gauging using portable surface velocity radars (SVR)," Water Resources Research. 52, 1108–1126, doi:10.1002/2015WR017906

Patterns in Gravel Bedload Transport from Impact Plates in a Laboratory Flume

Daniel G. Wren, Research Hydraulic Engineer, USDA-ARS, Oxford, MS, Daniel.Wren@ars.usda.gov
Roger A. Kuhnle, Research Hydraulic Engineer, USDA-ARS, Oxford, MS, Roger.Kuhnle@ars.usda.gov
Robert C. Hildale, Hydraulic Engineer, USBR, Denver, CO, Hilldale, Robert rhilldale@usbr.gov

Abstract

Bedload remains difficult to measure, and finding patterns in bedload transport, such as those caused by the passage of a hydrograph or from a change in sediment supply, is particularly difficult because manual sampling methods are laborious and limit temporal resolution and total monitoring time. The use of accelerometer-equipped steel plates installed in the bottom of a channel allows the impact of particles on the plates to be continuously recorded. Using a calibration process, the data can be converted to particle size, and the sum of the particle masses can be used to quantify transport rate over a range of time scales. Impact plates in a 30 m laboratory flume were used to record gravel transport over a range of antecedent shear stresses for a gravel/sand mixture. The data were processed to reveal patterns in mass transport and gravel particle size resulting from different antecedent conditions for repeated experiments with the same flow conditions. Both initial transport rate and variability in transport rate were found to be higher when starting from a screeded bed and when following flows with larger excess shear stresses.

Introduction

Temporal variability in bedload makes continuous monitoring attractive in rivers where coarse bedload may have impacts on flooding, navigation, and fisheries management. In recent years, the use of metal plates equipped with accelerometers or geophones to detect impacts of particles transported as bedload has expanded (e. g., Wyss et al., 2016; Barrière et al. 2015; and Rickenmann et al., 2014). Based on the calibration and testing of the impact plates in Kuhnle et al. (2017), which describes cooperation with the U.S. Bureau of Reclamation on research aimed at providing a calibration for instrumented plates installed in the Elwha River, a new series of experiments was focused on investigating the effect of antecedent conditions or stress history on sediment transport. The effect of antecedent flow conditions on bedload transport has been previously considered. For example, Ockelford and Haynes (2012), studied the effects of sub-critical shear stresses on the bed structure for gravel beds in an effort to explain why critical shear stresses for mobilizing gravels have been shown to increase after extended periods of flow with sub-critical shear stresses. Mao et al. (2011) identified structural difference in static and mobile armor layers, and Mao (2012 and 2018) examined the effects of flow hydrographs and stress history on sediment load. The present work is focused on the effect of antecedent conditions on sediment transport for a sand/gravel mixture, with emphasis here on gravel bedload transport.

Methods

A range of bedload transport rates for a sand/gravel mix was created in the flume at USDA-ARS-National Sedimentation Laboratory, and the signal generated by gravel particles as they impacted steel plates in the flume channel was recorded. Using procedures similar to those described in Wyss et al. (2016a) and detailed in Kuhnle et al. (2017), particle impacts were identified in the voltage signal. The data packets representing the impacts were converted to particle size based on the calibration procedure in Kuhnle et al. (2017), and the time series of particle sizes was used to find gravel load by particle size class.

The experiments were run in a tilting, recirculating 30-m x 1.22-m x 0.61-m flume with adjustable slope. The flume can recirculate water and sediment up to 80 mm in diameter. A 0.25-m thick gravel bed with a median grain diameter of 8.12 mm was screeded flat for the first experiment of this series. The bed material was a bimodal sand/gravel mixture, and the median size of the sand was approximately 0.5 mm. The gravel was 2-45 mm in diameter. The 15.9-mm thick impact plates (0.349 m x 0.501 m in the cross-channel direction) were at the same elevation as the gravel bed, 28-m from the channel origin. Each plate had a CMCP-1100 accelerometer (STI Vibration Monitoring, League City, Texas) mounted to the center of the underside of the plate. Deformation of the plate by impacts induced a voltage that was recorded at 50 kHz. The lower limit of detection for the impact plates was 4 mm gravel.

Table 1 shows the basic hydraulic parameters for the experiments, including the antecedent shear stress at the beginning of each series of experiments. Four experiments with the same shear stress are reported, but each one had a different stress history. Bed shear stress was determined from $\tau_b = \rho g h S$, where ρ is fluid density, g is acceleration due to gravity, h is water depth, and S is water surface slope. The bed shear stress data were wall corrected based on modifications of the Vanoni and Brooks (1957) method described in Vanoni (1975) with further modification by Chiew and Parker (1994), which resulted in an explicit relationship for wall friction. The first experiment was run on a screeded, randomized bed. The second experiment was begun after approximately 40 hours for a flow with approximately 6.3 Pa of shear stress. Each subsequent experiment inherited its bed from previous runs with increasing shear stresses. Note that the final series (Shear 1d) inherited the entire stress history of all previous runs. The bed was not randomized and screeded again before each set of experiments. This implies the assumption that the higher shear stresses applied before each of the low shear runs was able to create its own equilibrium bed and transport rate that was independent of previous experiments at lower shear stresses.

Table 1. Hydraulic parameters

Designation	Shear stress for antecedent condition (Pa)	Mean shear stress (Pa)	Mean depth (m)	Froude number
Shear1a	0 (screeded bed)	5.31	0.253	0.51
Shear1b	6.3	5.21	0.260	0.49
Shear1c	7.0	4.84	0.262	0.48
Shear1d	7.4	5.40	0.264	0.48

Results

Figure 1 summarizes the results obtained during the flume experiments. The first two hours of data for Shear1a (antecedent stress 0 pa) is not present because of a temporary equipment malfunction. Figure 1A shows the time series of the gravel size class centered at 6 mm (4-8 mm) for each of the antecedent shear stresses. The most evident effect of antecedent condition in Figure 1A is the period of increased load in the first 10 hours of the 0 pa (Shear1a) and 7.4 pa (Shear1d) experiments, which was likely caused by particles being exposed to the flow on beds that were not in equilibrium with flow conditions. Figure 1B shows that the mean load for the 6 mm class (calculated with the first 2 hours removed to match Shear1a) decreased across the experiments, while Figure 1C shows that the standard deviation of the load (again calculated with the first 2 hours removed to match Shear1a) decreased with increasing antecedent shear until the highest antecedent shear stress, which resulted in increased variability. This effect may have been caused by patterns in particle arrangement generated by the preceding flow, which persisted for the subsequent shear stress condition. Similar patterns were found for the 12 mm size class (8-16 mm), with higher mean loads (Figure 1E) that reflect the greater amount of the 12 mm class in the bed material. The standard deviation for the 7.4 pa antecedent condition was nearly as high as for the 0 pa condition (Figure 1F). The relative infrequency of 24 mm motion, along with the decreased load, resulted in a sparse dataset (Figure 1G). The lowest mean loads (Figure 1H) were found for the 24 mm class across the antecedent conditions, which may account for the opposite trend in standard deviation (Figure 1I) relative to the 6- and 12-mm classes.

The results contribute to efforts to understand the effects of antecedent conditions on bed load transport. For example, Mao (2018) studied the effects flood history on sediment transport and bed topography, finding that transport rates were greater on the rising limb of a flood flow hydrograph, with decreasing hysteresis for repeated hydrographs. The present work continued each flow for extended periods and adds capability for separating the bed load by particle-size class, which enables examination of preferential movement by size class. In future work, detailed measurements and analysis of bed topography and its effect on transport rate will be incorporated (e.g., Hodge et al., 2009 and Cooper and Tait, 2009).

Conclusions

Measurements of fractional transport made with impact plates showed that antecedent conditions affected the rate of gravel transport, and the effect varied across particle size classes. The effect of beginning an experiment with a screeded bed was similar to the effect of the highest shear stress antecedent condition, resulting in initially high transport rates that gradually decreased as the bed was reworked into equilibrium with the new, lower flow rate. Variability in gravel transport also appeared to be influenced by the prior stress history, with transport rates following screeded bed and high shear stress flows showing increased standard deviation relative to flows that had lower antecedent shear stress conditions.

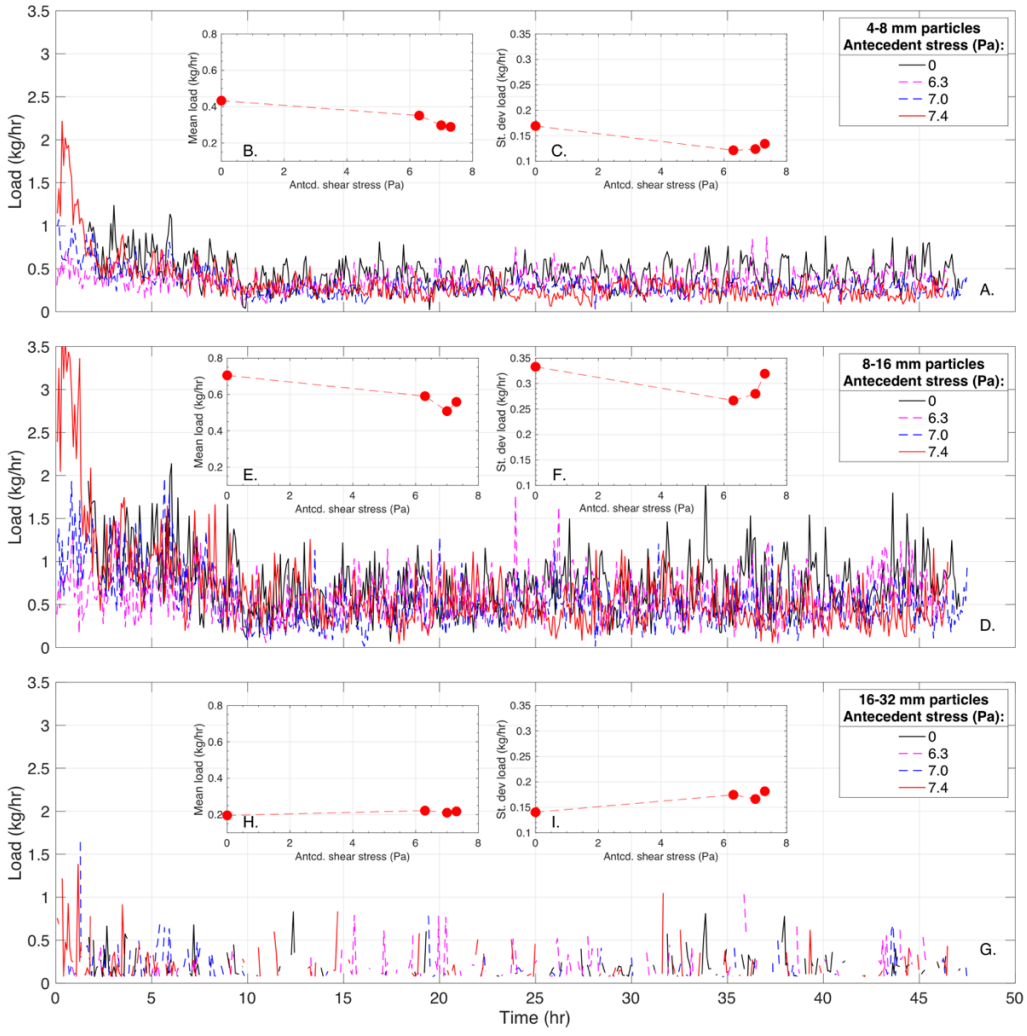

Figure 1. Fractional gravel load from impact plate experiments. A. load for the 6 mm size class (4-8 mm); B. mean load for 6 mm class; C. Standard deviation for the 6 mm size class; D. load for the 12 mm size class (8-16 mm); E. mean load for 12 mm size class; F. standard deviation for 12 mm size class; G. load for the 24 mm size class (16-32 mm); H. mean load for the 24 mm size class; I. standard deviation for the 24 mm size class.

References

Barrière, J., Krein, A., Oth, A., and Schenkluhn, R. (2015). "An advanced signal processing technique for deriving grain size information of bedload transport from impact plate vibration measurements." Earth Surface Processes and Landforms, 40(7), 913–924.

Chiew, Y. and Parker, G. (1994). Incipient motion on non-horizontal slopes. Journal of Hydraulic Research. 32(5):649–660.

Cooper, J. R., and Tait, S. J. (2009). "Water-worked gravel beds in laboratory flumes - a natural analogue?." *Earth Surface Processes and Landforms*, John Wiley & Sons, Ltd., 34(3), 384–397.

Hodge, R., Brasington, J., And Richards, K. (2009). "Analysing laser-scanned digital terrain models of gravel bed surfaces: linking morphology to sediment transport processes and hydraulics." *Sedimentology*, John Wiley & Sons, Ltd (10.1111), 56(7), 2024–2043.

Kuhnle, R. A., Wren, D. G., Hilldale, R. C., Goodwiller, B. T., and Carpenter, W. O. (2017). "Laboratory Calibration of Impact Plates for Measuring Gravel Bed Load Size and Mass." *Journal of Hydraulic Engineering*, American Society of Civil Engineers, 143(12), 06017023.

Mao, L., Cooper, J. R., Frostick, L. E. (2011). "Grain size and topographical differences between static and mobile armour layers." *Earth Surface Processes and Landforms* 36, 1321-1334. Doi:10.1002/esp2156.

Mao, L. (2012). "The effect of hydrographs on bed load transport and bed sediment spatial arrangement." *Journal of Geophysical Research* 117, F03024, doi:10.1029/2012JF002428

Mao, L. (2018). "The effects of flood history on sediment transport in gravel-bed rivers." *Geomorphology*, Elsevier B.V., 322(C), 196–205.

Ockelford, A.-M., and Haynes, H. (2012). "The impact of stress history on bed structure." *Earth Surface Processes and Landforms*, 38(7), 717–727.Kuhnle, R. A., Wren, D. G., Hildale, R. C., Goodwiller, B. T., and Carpenter, W. O. Laboratory calibration of impact plates for measuring gravel size and mass. Journal of Hydraulic Engineering. 143(12). https://doi.org/10.1061/(ASCE)HY.1943-7900.0001391. 2017.

Rickenmann, D., Turowski, J. M., Fritschi, B., Wyss, C., Laronne, J., Barzilai, R., and Habersack, H. (2014). Bedload transport measurements with impact plate geophones: comparison of sensor calibration in different gravel-bed streams. Earth Surface Processes and Landforms, 39(7), 928-942.

Vanoni, V. A. (1975). Sedimentation Engineering ASCE Manual 54. ASCE, New York.

Vanoni, V. A. and Brooks, N. H. (1957). Laboratory studies of the roughness and suspended load of alluvial streams, sedimentation laboratory report no e68. Report no., California Institute of Technology, Pasadena, CA.

Wyss, C. R., Rickenmann, D., Fritschi, B., Turowski, J. M., Weitbrecht, V., Boes, R. M., 2016. Measuring bed load transport rates by grain-size fraction using the Swiss plate geophone signal at the Erlenbach. Journal of Hydraulic Engineering, 04016003-1, doi:10.1061/(ASCE)HY.1943-7900.0001090.

Overview of Five Recent Bedload Monitoring Field Experiments Using Hydrophones

Mathieu Marineau, U.S. Geological Survey, Sacramento, CA, mmarineau@usgs.gov
Scott Wright, U.S. Geological Survey, Sacramento, CA, sawright@usgs.gov
David Gaeuman, Yurok Tribe, Klamath, CA, dgaeuman@yuroktribe.nsn.us
Chris Curran, U.S. Geological Survey, Tacoma, WA, ccurran@usgs.gov
Kyle Stark, New Mexico Tech, Socorro, NM, kyle.stark@student.nmt.edu
Jason Siemion, U.S. Geological Survey, Troy, NY, jsiemion@usgs.gov
Edward Schenk, City of Flagstaff, AZ, edward.schenk@flagstaffaz.gov

Abstract

Bedload transport rates are often desired by engineers and scientists for a variety of purposes. Obtaining useful bedload data through physical sampling, however, can be logistically challenging and expensive. Conventional bedload sampling techniques can have high uncertainty, and poor correlation of bedload transport to discharge or other easily measurable variables makes it difficult to model or predict transport rates. In recent years, there has been increased interest in surrogate monitoring techniques such as passive acoustics as a lower-cost method of collecting bedload data. Hydrophones (underwater microphones) can be used to detect the underwater sounds generated by gravel and cobble as they roll and saltate along the bed. This noise is referred to as sediment-generated noise (SGN). While the acoustic data still require calibration to physical samples, it can be used to produce a high-quality continuous record. This paper provides a brief overview and preliminary findings from five recent passive acoustic monitoring (using hydrophones) projects conducted by the US Geological Survey with other partners and cooperators, either as a stand-alone study or as part of larger sediment transport or geomorphic studies. The objectives of the passive acoustic monitoring studies were to test passive acoustic monitoring in different types of systems, determine if sediment-generated noise was correlated with bedload transport rates, and experiment with different techniques to improve correlations (such as using pairs of hydrophones). Study sites ranged from small (5-10 meters in width) channels in the Catskill Mountains of New York and a tributary creek in the Grand Canyon to a large glacially-fed river (70-meters in width) in the Cascade Range in Washington State. Bed material ranged from mixed sand and gravel to coarse cobble with small boulders. Channel slope ranged from about 0.2 percent (Trinity River, CA), to 3.5 percent (Shinumo Creek, AZ). Overall, we found that hydrophones detected SGN at all but one site; however, noise from air entrainment and water turbulence severely degraded the signal quality at two relatively steep (1.5 percent slope) cobble-bed streams. Continuous recording (versus 15-minute intervals) did not necessarily improve calibration but placing hydrophones at opposite banks helped detect lateral variability in transport and placing hydrophones at different elevations allowed improved data collection at a wider range of flows.

Introduction

Passive acoustic bedload monitoring has been an area of increasing research in recent years. This method typically uses either geophones and geoplates (e.g., Wyss et al. 2016), pipe hydrophones (Mizuyama et al., 2010) or hydrophones (e.g., Marineau et al., 2017; Geay et al.,

2017) to collect surrogate acoustic data to supplement physical bedload measurements. The advantage of using a surrogate technique is to increase the frequency of bedload measurements while also reducing the overall monitoring costs. In the studies presented here, hydrophones were used to record sounds generated by collisions of bedload particles, which are referred to as sediment-generated noise (SGN). Those acoustic data are then calibrated to transport rates from physical samples to produce continuous or near-continuous estimates of bedload transport. Passive acoustic bedload monitoring has been demonstrated in some cases to provide estimates with greater accuracy than conventional methods. However, the method is not suitable in all stream types, and there are still several issues to address before making passive acoustic monitoring an established method. These issues are generally related to underwater sound propagation and its relation to channel geometry, field installation design, and calibration. Here, we discuss preliminary results from five recent studies by the US Geological Survey (USGS) and other collaborators, as well as some of the challenges encountered.

Objectives

The objectives of these five studies generally fell into one or more of the following: 1) attempt to calibrate acoustic data to bedload measurements to determine if acoustic data can be used as a surrogate, 2) test if multiple hydrophone-recorders, more frequent sampling, and/or splitting bedload measurement transects (explained in methods) can improve calibration, and 3) explore and evaluate the passive acoustic sediment monitoring for a variety of channel types and site conditions.

Study Areas

The five study sites discussed are: Sauk River, WA; Trinity River, CA; Arroyo de los Piños, NM; Birch and Stony Clove creeks in the Esopus Creek watershed, NY; and Shinumo Creek, AZ (Figure 1). Table 1 summarizes some of the key hydraulic and hydrologic information for each site. Study areas are presented in order of stream width from widest to narrowest. The Trinity River sites are grouped together and ordered from upstream to downstream.

The Sauk River was the largest river (70-m width) monitored. The Sauk River has a gravel-cobble bed and streamflow in the Sauk River is not regulated by an upstream dam. The river is dynamic with active channel migration, gravel bars, and log jams. The largest flow of record (measured in 1855) was over 1,300 m^3/s.

The Trinity River is a gravel-bed river with a channel width of about 40 meters. Streamflow is regulated by upstream dams and controlled releases during wet years are generally limited to 340 m^3/s. Gravel injection is used to replenish gravel supply downstream of the dams (Gaeuman, 2014) and there is a long-term sediment monitoring program at four sites (acoustic monitoring took place between 2015 and 2017, but the number of sites acoustically monitored varied from 2 to 4 sites). Gravel is often injected at two locations in the river. One of those is about 1.6 km upstream from the Lewiston site (USGS Station No. 11525500) and the other is about 0.2 km upstream of the site above Grass Valley Creek (USGS Station No. 11525540).

The other study areas had smaller channels. Birch and Stony Clove creeks (tributary creeks in the Esopus Creek Watershed, NY) are about 10 m in width, with steeper gradients, and their mixed beds are mostly gravel to large cobble. Arroyo de los Piños is an ephemeral stream which is a tributary to the Rio Grande. Its bed is composed mostly of sand- to gravel-sized material and

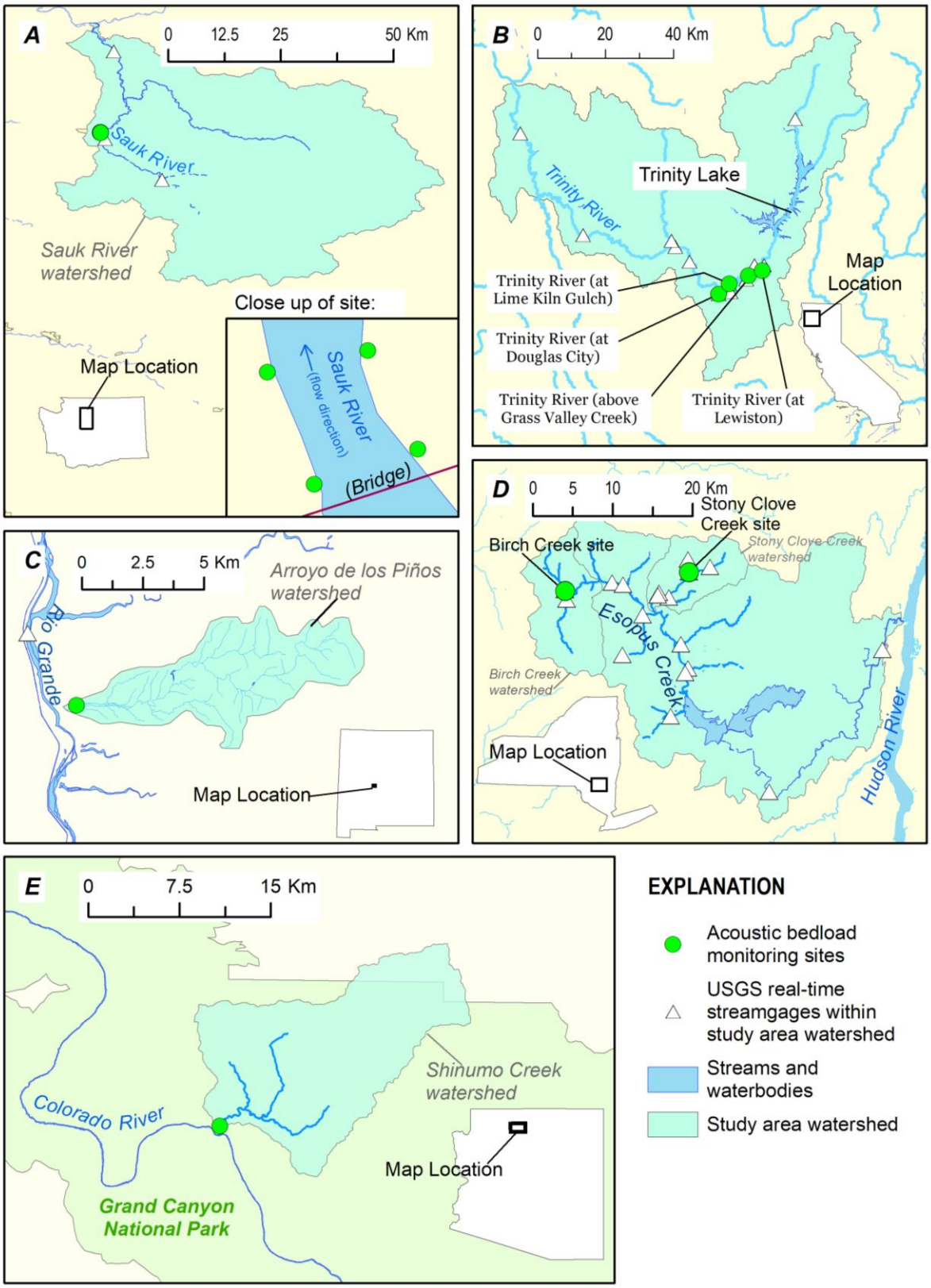

Figure 1. Study area sites: Sauk River, Washington (A), Trinity River, California (B), Arroyo de los Piños, New Mexico (C), Esopus Creek watershed, New York: Birch and Stony Clove creeks (D), and Shinumo Creek, Arizona (E).

flow events generally last only a few hours but stream depth can exceed 1 m during extreme events. Shinumo Creek, AZ, is a small gravel-cobble bed creek, tributary to the Colorado River. Following a 2015 post-wildfire debris flow (Schenk et al., 2017), the channel was filled with sand and gravel to near bank-full height, but the majority of in-channel fine sediment was evacuated in the subsequent 2 years of spring snowmelt high water (Schenk, 2018).

Table 1. Summary site information for 6 acoustic bedload monitoring sites, arranged by channel size. USGS streamgage site ID in parenthesis. D_{50} is median grain size.

Site and (streamgage ID)	Channel width (m)	Dominant bed-material sizes[a] and D_{50} [in mm]	Slope (percent)	2-year flow (m^3/s)	Drainage area (km^2)
Sauk River, Washington					
Sauk River at Darrington, WA, (12187500)	70	Sand, gravel, cobble, small boulders [–]	0.5	480	760
Trinity River, California					
Trinity River, at Lewison, CA (11525500)	40	Gravel-cobble [55–60]	0.17	170	1,860
Trinity River above Grass Valley Creek (11525540)	38	Gravel-cobble [29–72]	0.13	*unknown*	1,970
Trinity River below Lime Kiln Gulch (11525655)	43	Gravel-cobble [41–52]	0.28	195	2,100
Trinity River at Douglas City (11525854)	46	Sand, gravel, cobble [42–62]	0.3	220	2,410
Arroyo de Los Piños, New Mexico					
Arroyo de los Piños, NM	10	sand (1/3), gravel (2/3) [2.5–4]	1.3–1.7	*unknown*	32
Esopus Creek watershed, New York					
Stony Clove Creek at Janssen Road, NY (01362336)	9–10	Sand-cobble & small boulders [58–95]	1.5	*unknown*	24
Birch Creek at Big Indian, NY, (013621955)	10	Sand-cobble & small boulders [64–80]	1.6	12	32
Shinumo Creek, Arizona					
Shinumo Creek, AZ	5	Sand-gravel, boulders also present [29]	3.2–3.7	*unknown*	221

[a] Particle size classifications are defined as: sand (<2 mm), gravel (2 to <64 mm), cobble (64 to <256 mm) and boulder (256 mm or larger). –, not reported.

Methods

At each site at least one audio recorder was used with two hydrophones to record files (.wav format) at 44.1 kHz. The system, which was developed by the USGS (Marineau et al. 2015) recorded files that were 1-minute in duration and were generally collected at 15-minute sampling intervals. The newer systems (2017 and later) also supported a feature that allowed continuous (i.e. consecutive 1-minute recordings). This feature was utilized at sites during physical bedload sampling. At the Arroyo de los Piños site, runoff events only lasted a few hours, so the systems here were programmed to only record in continuous mode. The systems also used an external liquid detection sensor. The system was programmed to check this sensor (which was placed at an elevation slightly above base flow) frequently. If liquid wasn't present, the system would go to into standby mode for a set amount of time. If liquid were present

(indicating a high flow event), then the system would go into recording mode and record at the pre-programmed sampling frequency. The recording system was kept on the bank out of the water (Figure 2). Using a liquid-detection sensor to trigger recording allowed the devices to remain in the field for months on battery power.

Figure 2. Examples of hydrophone installations: Sauk River, WA (left photo), Stony Clove Creek, NY (right photo)

For the Trinity River sites, typically only one recorder was installed at a site. However, at one of the Trinity sites (Lewiston) a recorder was installed on each bank to determine if lateral variability could be detected. At Stony Clove Creek, Birch Creek and Arroyo de los Piños two recorders were installed, typically on opposing banks. At the Sauk River, four recorders were installed (one pair on each bank, separated by about 60-70 m).

Bedload samples at Trinity River, Sauk River, and Esopus Creek Watershed sites (Stony Clove Creek and Birch Creek) were collected with a TR-2 (Childers, 1999) or Elwha sampler (Childers et al., 1999) using the Equal Width Increment (EWI) method (Edwards and Glysson, 1999). Bedload samples at the Arroyo de los Piños site were collected using three slot samplers (Berkman et al, 2006). Several other sediment surrogate methods were being tested at the Arroyo de los Piños site, see Varyu et al. (2019) for details). Traditionally, bedload measurements are collected using the EWI method and consist of about 10-20 subsamples (verticals) which are composited across the entire transect to create a single bedload measurement. To capture the lateral variability in transport rates and explore ways to improve surrogate calibration, the sampling protocol was modified at the Trinity River and Sauk River. At the Trinity River, the subsamples were composited into thirds (rather than the full transect). Bedload from each side of the channel and middle could be compared to the sediment-generated noise (SGN) recorded by the hydrophone on the corresponding bank. At the Sauk River, the

mass of each subsample (wet weight) was recorded prior to compositing. This provided greater spatial resolution in the bedload.

Audio recordings were processed using discrete Fast Fourier transform (using a Hamming Window). Sound was recorded with a sampling frequency of 44.1 kHz with 16-bit integer resolution. See Marineau et al. (2016, 2017) for detailed description of audio processing. Results from a single 1-minute audio recording are in the form of a power spectral density (PSD) function which shows the sound-level pressure (in $\mu Pa^2/Hz$, which can be converted to decibels re 1V/µPa) at each frequency. Examples of PSD for various flows during an event on the Trinity River at Lewison, CA, are shown in Figure 3.

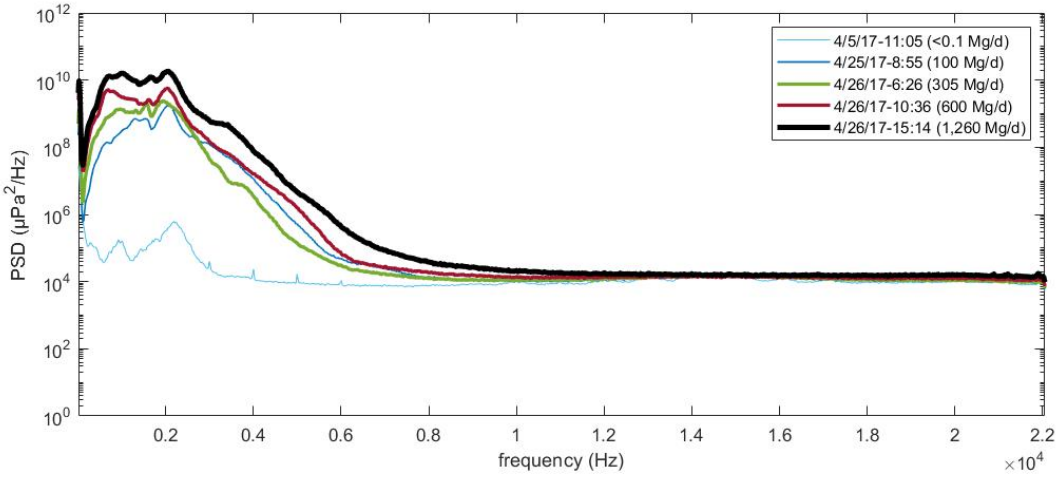

Figure 3. Examples of power spectral density (PSD) estimates under different streamflow and bedload transport conditions at the right bank of the Trinity River at Lewiston, CA.

Most of the SGN is in the lower frequency ranges (0.5 to 6 kHz). The sound level or sound pressure level for any given recording can be integrated over the entire frequency range or over a more narrowly selected frequency range to obtain a value which would then represent the SGN at that time. The values of SGN during bedload sampling can then be used to establish an empirical relation between SGN and bedload. Figure 4 in the results section shows an example time series of estimated bedload at the Trinity River at Lewiston site during controlled upstream dam releases.

The error around the bedload for the Trinity River was calculated from an experiment by GMA Hydrology Inc. (Pittman, 2018) in which six sequential vertical samples were collected at the same cross-section station over a 29-minute period (Pittman, 2018). During those six vertical subsamples, bedload ranged from 60 to 429 Mg/day.

Results

Sauk River near Darrington, Washington, WY 2018

At the Sauk River, in WY2018, several high flow events occurred, the largest was in November and was roughly 850 to 1,100 m^3/s. This is an estimate based on upstream and downstream streamgages. The event eroded a 30-m section of the right bank where the upstream right bank hydrophones were located. The same event also buried two of the three other hydrophone pairs. Hydrophones were recovered and reset or replaced in the following months (except for the

upstream right bank recorder which was completely lost). Partial records of acoustic data were available from the remaining three recorders. Generally, SGN was much higher on the left side of the river. Bedload measurements were collected on two separate occasions (February 5 and May 9) and partial acoustic records were collected over a period of several months (example shown in Figure 9). For each measurement, 2 to 4 subsamples were collected at each location across the transect. The results show that about 60 to 75 percent of the total bedload occurred at only 3 of the subsample locations, all of which were near the left side of the channel. Total bedload from the four measurements collected on May 9 varied from about 500 Mg/day to nearly 1,700 Mg/day (Figure 4). Approximately one-third of the bedload was coarse (>8 mm). During the 4-hour period of bedload sampling, stage only varied by about 5 cm and SGN did not vary substantially (Figure 5).

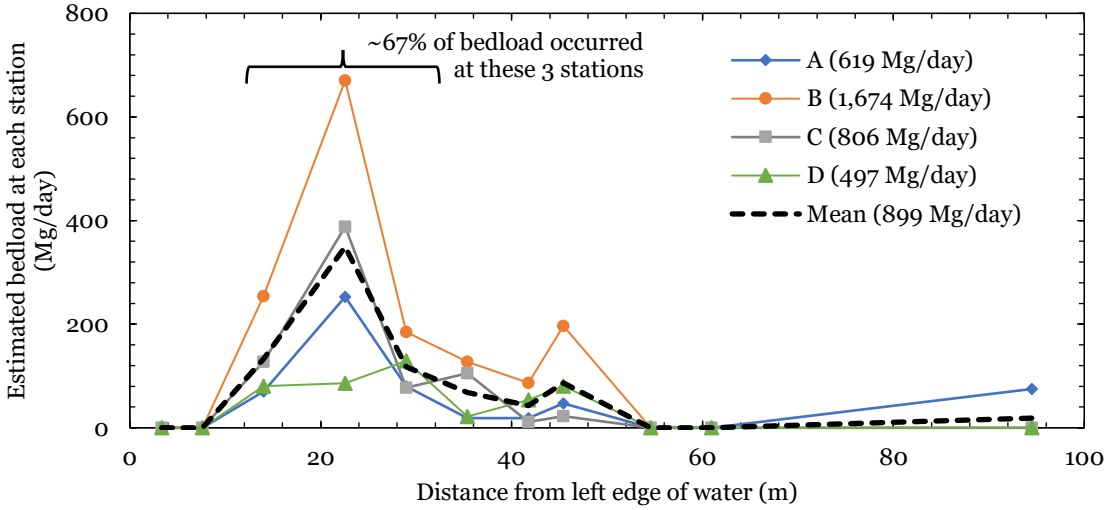

Figure 4. Repeated vertical bedload sampling across entire cross-section of Sauk River, May 9, 2018, showing temporal and spatial variability. Each station (vertical) was sampled 4 times before moving to the next station. Most of the bedload transport occurred at 3 of the sampling stations and transport rates ranged from 497 to 1,674 Mg/day.

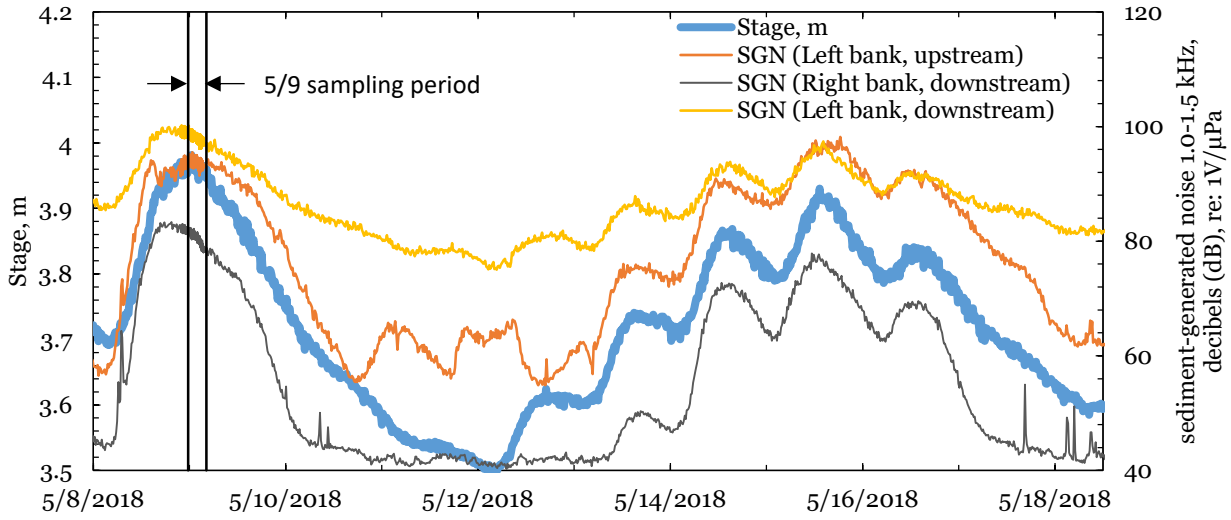

Figure 5. Time series of sediment generated noise at three locations along a short reach of the Sauk River, WA (right-bank upstream hydrophone was destroyed in an earlier flood).

Trinity River at Lewiston, California, WY 2016-2017

The Trinity River had the largest bedload sample set including multiyear results. Results (which include three other sites) from WY2015-16 can be found in Marineau et al. (2016, 2017). At the Trinity River, Lewiston site, 64 bedload samples were collected in WY2016. All stations across the transect were composited together for those samples. In the following year (WY2017), 19 bedload samples were collected with separate compositing of the left, middle, and right sections of the channel. Of those two years, streamflow discharge had the highest peak in WY2017 at 340 m^3/s. A relation was developed between the SGN on each bank and the bedload samples. Pearson's r was used as a measure of the correlation between SGN from each bank and coarse (>8 mm) bedload (Table 2). For WY2017, correlation was also measured between SGN from each bank and the bedload measured in each section of the channel. Most (67 percent) of the bedload transport occurred in the middle section while the rest was divided evenly (~16 percent) to each side.

Table 2. Correlation (measured by Pearson's r) between SGN and coarse (>8mm) bedload. Bedload measurements in WY2016 were not composited by channel section.

SGN recorder	Left Channel	Middle Channel	Right Channel	Total channel
WY2016[a]				
Left bank				0.67
Right bank				0.85
Average of both banks				0.77
WY2017[b]				
Left bank	0.61	0.75	0.56	0.86
Right bank	0.40	0.51	0.65	0.65
Average of both banks	0.56	0.69	0.61	0.82

[a] 64 bedload measurements (each transect counted as a measurement) collected; bedload transport rates ranged from 4.7 to 590 Mg/day
[b] 19 bedload measurements collected; bedload transport rates ranged from 139 to 1592 Mg/day

In WY2016, the highest correlation of total bedload was with the SGN recorded from the right bank, however, this switched in the following year. This is likely due to most of the transport occurring in the center of the channel rather than on one side. Using the acoustic record from the left bank only, a continuous record of bedload was created (Figure 6).

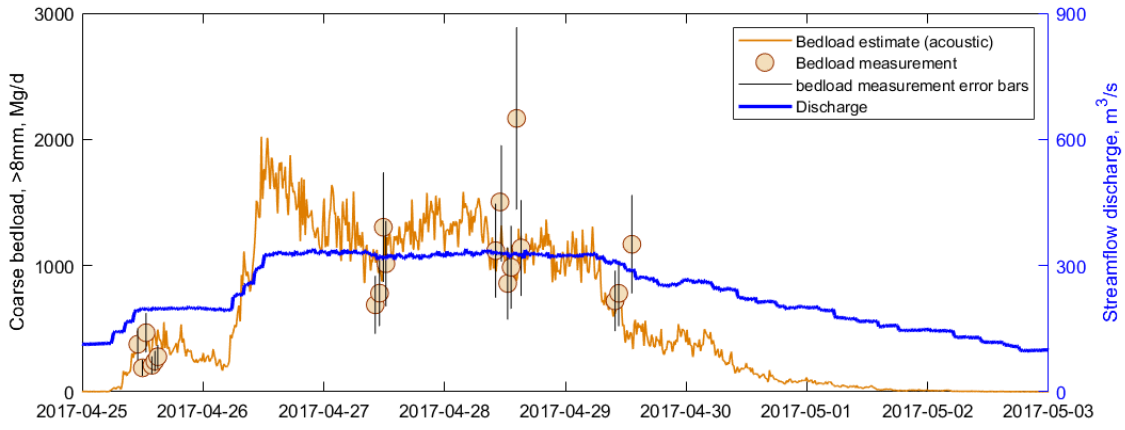

Figure 6. Example time series of acoustic-based bedload estimates with bedload measurements and streamflow discharge, Trinity River, Lewiston, CA. Vertical error bars represent standard deviation from repeated vertical sampling bedload experiment (Pittman, 2018).

The sediment transport rates (as a function of discharge) also changed over time. Figure 7 shows a plot of acoustic-based bedload transport estimates as a function of discharge, color coded by the date. Clockwise hysteresis is apparent; on the initial rising limb of the hydrograph (4/26/17-4/27/17) the transport rates were about an order of magnitude higher than on the falling limb (4/29/17-5/5/17).

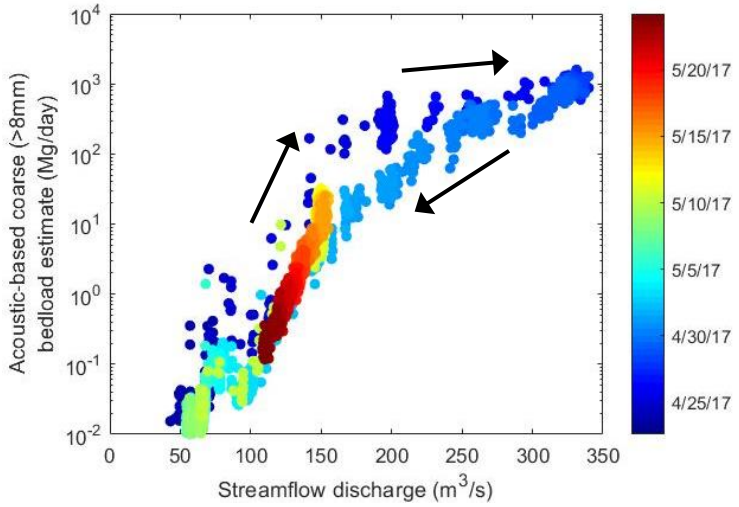

Figure 7. Acoustic-based bedload estimates vs streamflow discharge showing hysteresis and temporal variability at Trinity River, Lewiston, CA, 2017; bedload can sometimes vary by an order of magnitude for a given streamflow.

Conventional bedload rating curves were developed using streamflow discharge as the predictor variable. A comparison was made between two years of bedload data at the Lewiston site in Figure 8. The hydrophones were located at approximately the same place in both years. The plot on the left shows bedload as a function of SGN while the plot on the right shows bedload as a function of discharge. Power-law regression lines show that the empirical relation of bedload to discharge changed between these two years, whereas the relation between bedload and SGN was relatively constant.

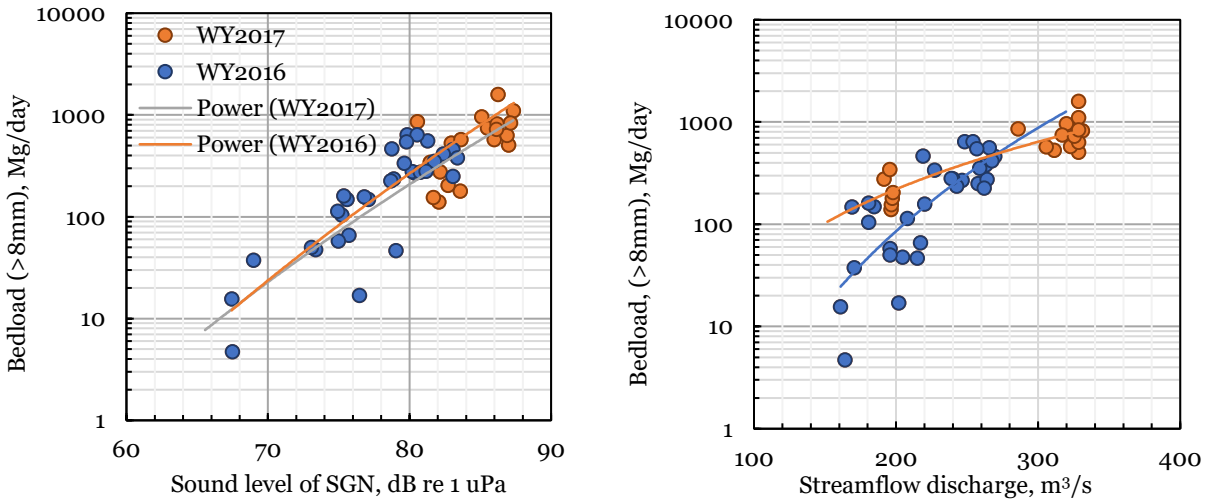

Figure 8. Comparisons of SGN vs bedload (left panel) and streamflow discharge vs bedload (right panel) for two consecutive years at same site with power-law regression lines for each year shown; Trinity River at Lewiston, CA. Gravel is sometimes injected approximately 1.6 km upstream from this site.

Arroyo de los Piños, Socorro, New Mexico, WY 2018

At the Arroyo de los Piños site, a large runoff event occurred about a week after the hydrophones were installed. One recorder (right bank) was fully operational during the event and recorded about 4 hours of audio data. Sediment samples were only collected at the very beginning of the event not collected during this event; however, other experimental surrogate methods were in operation in addition to the hydrophones (Stark et al, 2019). During this event, both hydrophones recorded a similar surge in SGN during the peak of the event (Figure 9). After that subsided, a second surge occurred only in the upper hydrophone while SGN recorded from the lower hydrophone remained relatively flat. Raw recordings from the lower hydrophones sounded muted, suggesting that aggradation had buried them during the event and subsequent scour possibly re-exposed them later.

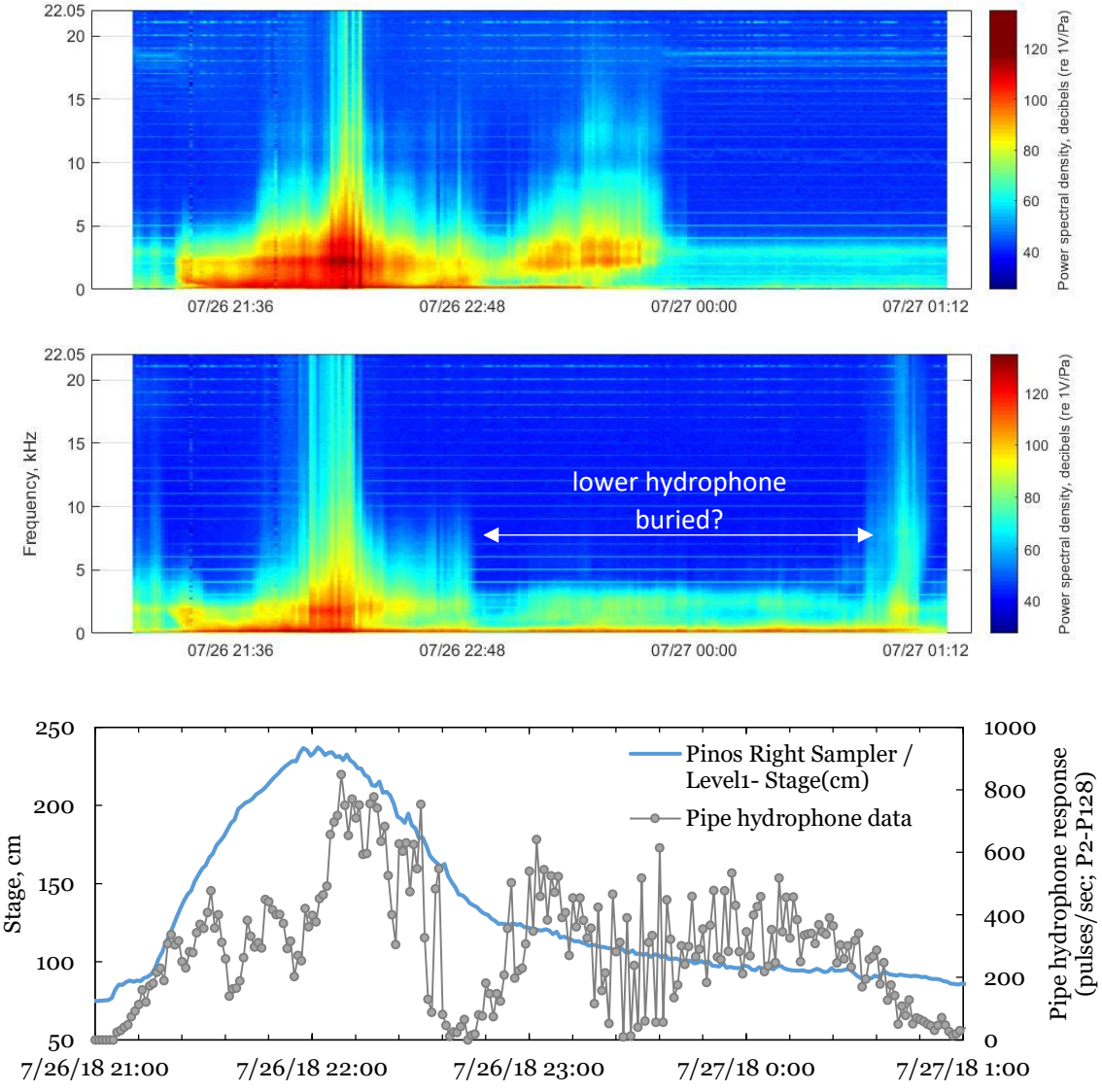

Figure 9. Acoustic data from right bank Arroyo de los Piños, NM, July 2018. Top panel is from the upper hydrophone, middle panel is from the lower hydrophone. The bottom panel shows stage and pipe hydrophone data during the same event (Stark et al. 2019).

Summary Bedload Data Collection Information

Table 3. Summary of bedload data collection information from each study

Site	Water years monitored	Bedload samples and sampler	Highest flow (m^3/s) or stage (m) during monitoring	>8 mm bedload measurement range (Mg/day)	Bedload/ SGN signal present?
Sauk River, Washington					
Sauk River at Darrington, WA	2018	6 samples using TR-2	1,120 m^3/s (estimated[a])	206–2,400 ~33% coarse[b]	Yes
Trinity River, California					
Trinity River at Lewiston	2016-17	19–64 samples using TR-2	340 m^3/s (4/26/2017)	3–1,442 ~82% coarse[b]	Yes
Trinity River above Grass Valley Creek	2015-16	14–53 samples using TR-2	283 m^3/s (5/10/2016)	4-2204 ~79% coarse[b]	Yes
Trinity River at Lime Kiln Gulch	2016	72 samples using TR-2	300 m^3/s (5/10/2016)	5-1034 ~67% coarse[b]	Yes
Trinity River at Douglas City	2015-16	13–53 samples using TR-2	314 m^3/s (5/10/2016)	19-3420 ~62% coarse[b]	Yes
Arroyo de los Piños, New Mexico					
Arroyo de los Piños, NM	2018	~27 samples per event from 3 slot samplers[d]	~ 1.6 m (7/26/2018)	[measured in kg/s·m][d] ~34% coarse	Yes
Esopus Creek watershed, New York					
Stony Clove Creek, NY	2017-18	8 samples using Elwha	35 m^3/s (7/24/2018)	1.7–38.3 ~40% coarse[b]	Yes[c]
Birch Creek, NY	2017-18	3 samples using Elwha	16.7 m^3/s (8/17/2018)	0.03–0.3 ~17% coarse[b]	No[c]
Shinumo Creek, Arizona					
Shinumo Creek, AZ	2015	1 sample using BLH-84	1.18 m (3/23/2016)	4.9 ~25% coarse[b]	Yes

[a]Discharge at the Sauk River at Darrington gage (Station No. 12187500) was discontinued July 2017. Streamflow estimate here is mean of the next upstream and downstream gages.
[b]"% coarse" is defined as the percent of the total bedload with particles having diameter >8 mm.
[c]Audio signal quality degraded by excessive water-turbulence and air-entrainment noise.
[d]Slot-samplers were used to record continuous bedload data during 4 events in WY2018, acoustic monitoring occurred during 2 of those events; bedload transport rates recorded during those events ranged from 1.0 to 16.5 kg/second-meter

Esopus Creek Watershed (Birch and Stony Clove creeks), New York, WY 2018

At the Birch and Stony Clove creek sites, the largest event in WY2017 was about a 2-year recurrence interval event. Audio recordings from that event revealed that the hydrophones detected very little SGN. However, listening to the raw audio files indicated a significant amount of noise, likely from water turbulence due to air entrainment around the large cobbles and small boulders. More testing is needed in this type of stream to determine if larger events would produce enough sediment-generated noise in the underwater soundscape for passive acoustic bedload monitoring to be useful.

Shinumo Creek, Grand Canyon National Park, Arizona, WY 2016

Shinumo Creek was one of the steepest channels monitored with hydrophones. Prior to the acoustic bedload monitoring study, the creek experienced a large post-wildfire flood which filled the channel with sediment (Schenk et al, 2017); much of it was gravel-size. The combination of readily available sediment supply and relatively steep channel (~3.5 percent slope) created conditions for sediment to be easily transported even during modest runoff events. A clear SGN signal was detected at this site during three runoff events; the largest was on 7/27/2018 with a water depth of about 1.6 meters (Table 3). The creek is located in a remote part of Grand Canyon National Park, AZ, and therefore only one bedload sample was collected during this study.

Discussion

The study on the Trinity River has provided a range of results and insights into the methods for acoustic data collection such as site selection, hydrophone placement, recorder placement, and bedload sampling protocols. The four sites on the Trinity generally have similar sized bed-material; therefore, other sites were tested to gain further insight into acoustic data collection. These other sites included a much larger, unregulated gravel-bed river, two steep gravel/cobble-bed creeks, and an ephemeral sand/gravel-bed creek. These deployments have provided valuable information on hydrophone performance in a wide range of conditions and serve as a guide for future improvements in the methods.

Location of bedload transport within the channel appears to be a significant factor in site calibration. At the Trinity River at Lewiston site most (67 percent) of the bedload transport was in the middle third of the channel and as a result, SGN did not show a particularly strong correlation to bedload in the left or right third of the channel. However, acoustic data at another Trinity River site (Marineau et al., 2017) showed a high correlation when the hydrophones were placed adjacent to the thalweg, where (presumably) most transport occurs. Alternatively, at the Sauk River, while fewer bedload measurements were collected, about 60-75 percent of the bedload occurred in only 3 subsamples, all of which were near the left bank. The SGN recorded on this side of the river was also much louder than that on the right bank. While there were not enough samples to calibrate the Sauk River acoustic data, the available data suggest that hydrophones on the left bank detected a greater portion of the bedload and that using pairs of hydrophones (i.e. one recorder on each bank) and compositing subsamples by lateral subsection of the transect may improve calibration efforts at some sites.

Hydrophone burial appears to be an issue in smaller creeks as well as larger dynamic rivers. The lower hydrophone at the Arroyo de los Piños and multiple hydrophones in the Sauk River were buried. To strike a balance between hydrophone burial during large events, and hydrophones not being submerged during low-flow events, hydrophones can be placed at two elevations along the bank: one low on the bank and another near mid-bank.

Lastly, the sampling frequency, which has typically been 15- or 20-minute intervals, was adjusted to sample continuously (every minute) at Arroyo de los Piños (due to the short-lived runoff events) and continuously at the Sauk River and Esopus creeks during sampling. In the latter two studies, the continuous audio recording was to determine if capturing all the short-term temporal variability would improve site calibration. At the Sauk, the level of SGN changed only gradually. Thus, over a 1–2-hour bedload sampling period, a 15-minute series of audio samples would have been sufficient. The bedload response and transport mechanisms will likely

vary from site to site, therefore, we recommend collecting and evaluating continuous recordings initially at a new site.

In conclusion, while results are pending for the study areas with smaller creeks, passive acoustic monitoring appears to work well for measuring sediment-generated noise in gravel-bed rivers. The findings and recommendations documented herein can be used to guide installations and sampling protocols at new sites.

References

Berkman, N., Laronne, J., Reid, I. 2006 "Benefits of design modifications to the Birkbeck bedload sampler illustrated by flash-floods in an ephemeral gravel-bed channel": Earth Surf. Process. Landforms, 32, 317-328.

Childers, D., 1999, "Field comparison of six pressure difference bedload samplers in high energy flow: U.S. Geological Survey Water Resources Investigation Report, 92-4068, Vancouver WA, 71 p.

Childers, D., Kresch, K.L., Gustafson, S.A., Randle, T.J., Melena, J.T., and Cluer, B., 1999, "Hydrologic data collected during the 1994 Lake Mills drawdown experiment, Elwha River, Washington": U.S. Geological Survey Water-Resources Investigations Report 99-4215, 115 p.

Edwards T.K., and Glysson, G.D, 1999, "Field Methods for Measurement of Fluvial Sediment": U.S. Geological Survey Techniques and Methods Book 3, Chap. C2. Reston VA, 89 p.

Gaeuman, D. 2014. "Analyses to support gravel augmentation recommendations for the Trinity River, California". Technical Report TR-TRRP-2014-1. Trinity River Restoration Program, Weaverville, California. Available at: http://www.trrp.net/library/document/?id=2197

Geay, T., P. Belleudy, C. Gervaise, H. Habersack, J. Aigner, A. Kreisler, H. Seitz, and J. B. Laronne (2017), Passive acoustic monitoring of bed load discharge in a large gravel bed river: J. Geophys. Res. Earth Surf., 122, doi:10.1002/2016JF004112.

Marineau, M.D., Wright, S.A., and Gaeuman, D., 2016, "Calibration of sediment-generated noise measured using hydrophones to bedload transport in the Trinity River, California, USA", *in*: Proc. of River Flow 2016, St. Louis, USA, 11–14 July 2016: London, Taylor & Francis, Paper 222, p. 1519–1526.

Marineau, M.D., Wright, S.A., and Gaeuman, D., 2017, "Estimating bedload transport along the gravel-bedded Trinity River using in-situ and boat-mounted hydrophones", *in* Proc. of Hydraulic Measurements and Engineering Methods, ASCE conference, July 2017, Durham, N.H., 6 p.

Marineau, M.D., Saraceno, J.F., Snyder, R., 2015. Hydrophone-based Underwater Sound Recorder, Provisional patent Number 62-147978, U.S. Patent Office

Mizuyama, T., Oda, A., Laronne, J.B., Nonaka, M., and Matsuoka, M., 2010, "Laboratory tests of a Japanese pipe hydrophone for continuous monitoring of coarse bedload", *in* Bedload-Surrogate Monitoring Technologies, USGS Scientific Investigation Report 2010 – 5091, edited by Gray, J.R., , Laronne, J.B., and Marr, J.D.G., pp. 319–335, U.S. Geological Survey, Reston, Va.

Pittman, S., 2018, "2017 Trinity River Sediment Transport Monitoring Report": GMA Hydrology, Inc., prepared for Bureau of Reclamation [Contract R14PC00122], 170 p.

Schenk, E.R. 2018. Springs flows restoring surface water features post disturbance – Shinumo Creek, Grand Canyon: 2018 Springs Ecosystem Science Symposium, Flagstaff, AZ.

Schenk, E.R., Tobin, B.W., Tanski, N., Marineau, M.D., 2017 "Determining the process of desert stream recovery following debris flow and implications of climate change" *in* GSA Annual Meeting 2017, Seattle, WA, *Abstracts with Programs.* Vol. 49, No. 6, doi: 10.1130/abs/2017AM-304328

Stark, K., Cadol, D., Laronne, J.B., Varyu, D., Halfi, E., Richards, M., 2019. "Initial Calibration of Acoustic Pipe Microphone Sensors to Monitor Bedload During Flash Floods in the Arroyo de los Piños, NM.," SedHyd2019, Federal Interagency Sedimentation and Hydrologic Modeling Conference. June 2019, Reno NV.

Varyu, D., Laronne, J.B., Cadol, D., Padilla, R., Lampert, T., Stark, K., Scissons, S., AuBuchon, J., and Munwes, Y., 2019, "Monitoring the Transport of Sediment in an Ephemeral Stream", *in* Proc. of SedHyd 2019 Federal Interagency Sedimentation and Hydrologic Modeling conference, June 2019, Reno, N.V., 6 p.

Wyss, C.R., Rickenmann, D., Fritschi, B., Turowski, J.M., Weitbrecht, V., Travaglini, E., Bardou, E., Boes, R.M., 2016, "Laboratory flume experiments with the Swiss plate geophone bed load monitoring system: 2. Application to field sites with direct bed load samples", Water Resources Research, 52, 7760–7778, doi:10.1002/2016WR019283.

Sound Localization for Sediment-Generated Noise (SGN) measurement

J.R. Rigby, Research Hydrologist, USDA-ARS, Oxford, MS, JR.Rigby@ars.usda.gov
Daniel G. Wren, Research Hydraulic Engineer, USDA-ARS, Oxford, MS, Daniel.Wren@ars.usda.gov
Praveen Panickar, CRAFT-Tech, Oxford, MS, PPanickar@craft-tech.com

Abstract

SGN is a surrogate bed-load monitoring methodology with the potential to allow economical, continuous measurement of coarse bed load in streams using passive acoustics. While the magnitude of recorded sound has been shown in some cases to be well-correlated with bed load transport, substantial work is still needed before the technique is ready for wide-spread deployment. Past efforts to develop SGN as a surrogate bed load monitoring technology have revealed that little information on underwater sound propagation in natural stream channels is currently available. Most of the work on acoustic propagation that has been done in shallow water that is directly relevant to SGN deployment has been in support of bioacoustics research, where the lack of shallow, freshwater acoustic research has been noted. Our recent efforts to address the basic processes of SGN have further highlighted the importance of understanding sound propagation in natural stream channels. Previous measurements of sound propagation in both a snow-melt driven, natural gravel-bed stream (Halfmoon Creek, CO) and a shallow sand/gravel bed stream (Goodwin Creek, MS) provided an initial step towards the goal of the proposed work but revealed many new questions relevant to SGN development. Two key problems highlighted by this preliminary work were the variable acoustic environments created by stream geometry and the production of flow-induced noise around the hydrophone. We address the source area problem by attempting to map detected SGN signals from the stream bed in real-time through the design and development of a 2-D phased hydrophone array to locate the sound sources spatially on the riverbed. Two-dimensional phased arrays have been used in many fields including aeroacoustics research for the localization of sound sources on an airframe. Such a device, suspended from a floating platform, will provide information in larger mobile bed applications of the spatial distribution of bed movement as well as a de facto measurement of the source region for SGN signals. Empirically mapping the acoustic source region would aid the development of calibration relations for SGN deployments on larger rivers.

Introduction

Accurate bed load measurement using direct measurement methods is difficult and expensive (Kuhnle and Southard, 1988; Kuhnle, 1989; Gray et al., 1991; Bunte and Abt, 2005). Passive acoustic instrumentation is well suited for remote, continuous deployment, is non-intrusive, and integrates sound from a finite area, decreasing bias caused by spatial heterogeneity of bed load transport. Challenges of using passive acoustics to measure bed load include the generally unknown size of the interrogated area of the bed and the unknown acoustic interactions of SGN with fluvial environments (Rigby, 2017). One potential means of mitigating these challenges is the

use of phased acoustic arrays for sound localization on the river bed. Such arrays can map the sound emission from the river bed in two dimensions for multiple frequencies, eliminating the uncertainty in interrogated area. This technology has the potential to provide immediate qualitative maps of bed load variability in time and space across a river cross-section from continuous monitoring. In addition, boat-mounted arrays may allow mapping bed load activity over long river reaches. Additional work may further allow calibrated phased-array monitoring for continuous, quantitative bed load measurement using SGN.

The use of phased microphone arrays for localizing aeroacoustic sources has seen increasing use in the recent past with the development of advanced data-processing algorithms. CRAFT Tech has developed an acoustic source localization (ASL) toolbox to perform frequency-domain beamforming calculations on aeroacoustic flowfields using a variety of techniques. The main beamforming program in the toolbox has been parallelized to run on multiple processors, which allows for beamforming calculations to be performed on multiple frequencies simultaneously, thereby reducing the time for these calculations. Beamforming provides the phased array system with directionality by effectively amplifying the sound from a region in space while attenuating sound from other regions. For a collection of M microphones that comprise the phased array system, the classical approach, called the delay-and-sum (DAS) beamformer consists of selecting appropriate delays, ΔM, and weights, w_M, in order to steer or focus at desired points in predefined grid region of interest. More information about the DAS procedure can be found in (Humphreys et al., 1998).

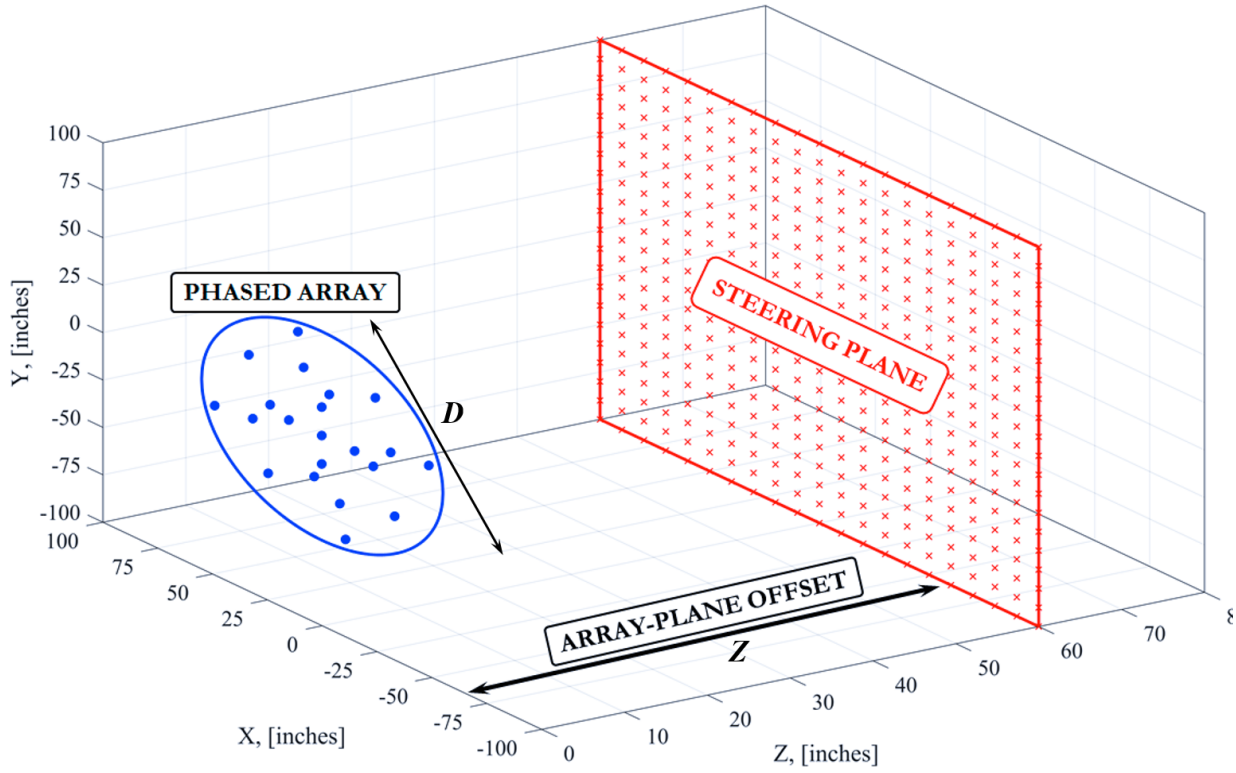

Figure 1. Schematic of hydrophone phased array system.

This project focused on developing a hydrophone-based phased array design that could be used to localize acoustic sources for underwater applications such as SGN. A schematic of the measurement setup is shown in Figure 1, where D is the aperture of the phased array, which is

located at an offset of Z meters from the steering/interrogation plane. The primary products sought in this work were the phased array design specifications including the number of hydrophones, the coordinate locations of the sensors, and theoretical beamforming performance characteristics of the array system based on the following design parameters and constraints that are considered desirable for the phased array system for SGN applications:

- Array dimension: 1 m² (approximate, to facilitate field application),
- Scan plane dimensions: 20 m (width) × 5 m (length),
- Array plane offset: 1 m – 5 m (water depth),
- Frequency range: 1 kHz – 20 kHz (expected SGN signal band),
- Nominal resolution between sources: 0.25 m (spatial resolution on the bed).

Methods

For this application two array designs were evaluated, namely the multi-arm spiral array and the Underbrink array, the latter of which is a modification/enhancement of the former to obtain better array response. The multi-arm spiral array design in based upon using a number of spirals, equally rotated about the origin (Underbrink, 2002). The procedure for determining sensor locations is to select the maximum and minimum radii, r_{max} and r_o, the number of spiral arms, N_a, the number of sensors per arm, N_m, and the spiral angle, ν. The equation for the first arm, in polar coordinates, yields sensor locations that are equally spaced on a spiral. This spiral arm is then repeated N_a times and equally rotated about the origin to yield the coordinates of the multi-spiral array.

The Underbrink array is a modified version of the multi-spiral design, wherein the sensors are placed in the center of equal-area segments. In order calculate the sensor locations, one selects the same parameters as for the multi-arm spiral array. Following this, the area of the array is divided into (N_m-1) equal area annuli, which are further divided into equal area segments, with sensors placed at the center of these segments. Finally, an inner circle of sensors is added at r_o to improve the high-frequency MSL.

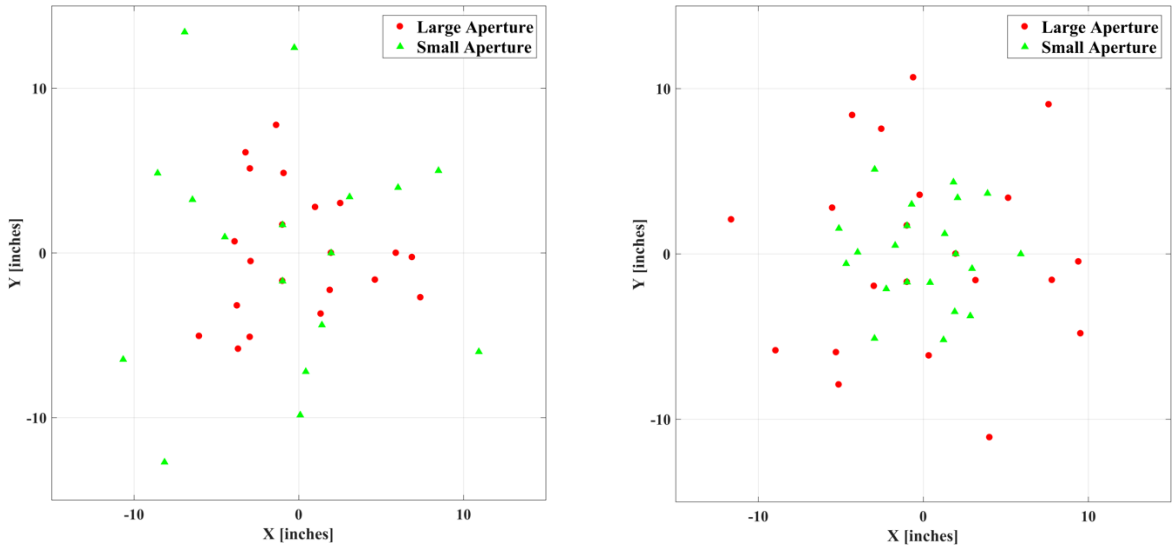

Figure 2. Candidate array designs for acoustic source localization using hydrophone sensors. Multi-spiral array (left) and Underbrink array (right) showing large and small aperture sub-arrays to cover the full frequency band of interest.

Results

After testing a number of different combinations of parameters for the multi-spiral and Underbrink array design, initial array designs for 5 m x 5 m scanning plane were constructed using 15 hydrophones with three different apertures to span the frequency range of interest from 5 kHz to 20 kHz. Updating the scanning plane dimensions to 20 m x 5 m to reflect a realistic interrogation of a river cross-section resulted in the need for a total of 21 sensors to fulfill the design specifications. With this increase in the number of sensors, the frequency range of interest could be covered using only two phased-array apertures for the multi-spiral design (D=0.40 m and 0.90 m) and the Underbrink design (D=0.30 m and 0.60 m). Figure 2 shows the sensor locations for the two array designs, each containing the sensor placements for the desired apertures. Following this, MSL calculations were performed for both array designs and all apertures to obtain the array response over the frequency range of interest; these results are shown in Figure 3. The superiority of the performance of the Underbrink array can be clearly seen over the entire range of frequencies in that this array design significantly reduces the amplitudes of the maximum sidelobes, allowing for a deterministic localization of the acoustic sources.

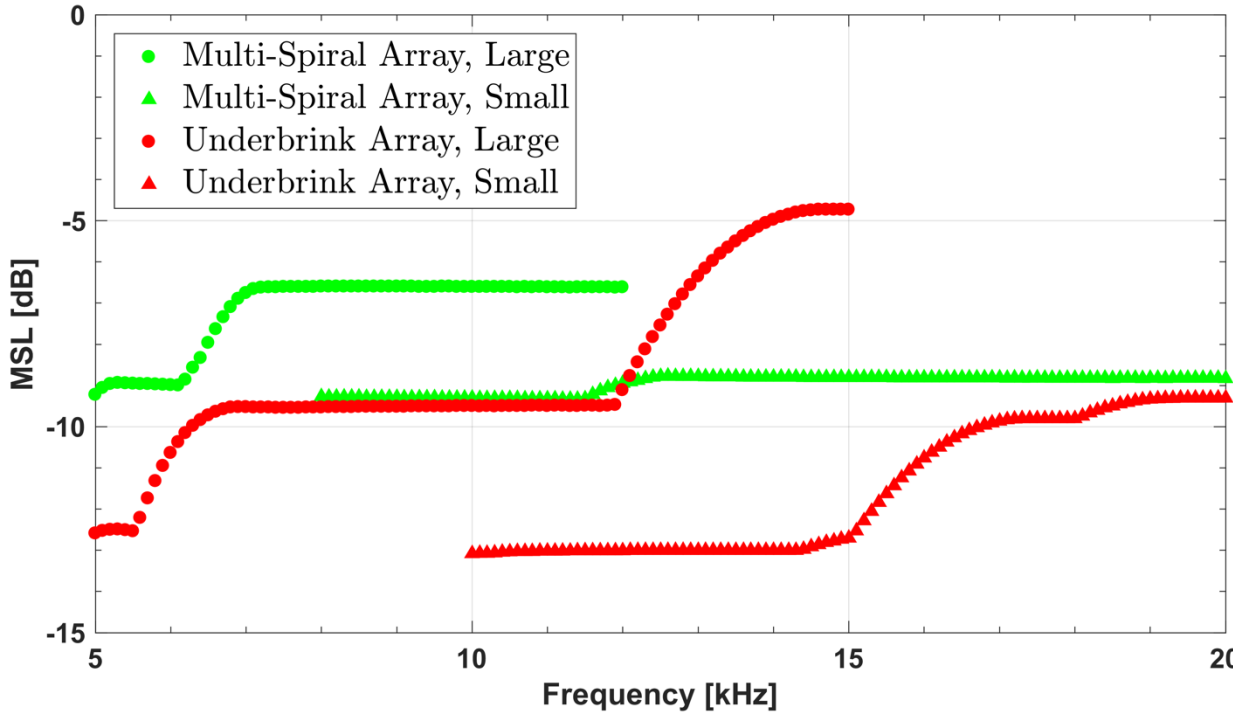

Figure 3. Results of the mean sidelobe level (MSL) calculations, which is an indicator of the dynamic range, for the different array types and apertures.

For the model results presented here, the two-dimensional phased array will be located in the Z=0 plane (water surface) and will be used to scan a rectangular XY plane that is 20×5 m² (river bed), located at Z = 4 meters (water depth). Results will be presented for four source frequencies ranging from 5 kHz – 20 kHz in steps of 5 kHz using the Underbrink array; the array aperture is

chosen based on the source frequency. To begin with, we use the traditional DAS beamforming algorithm to localize a point source located at (x,y,z)= (0,0,4) meters. Figure 4 shows the beamform maps for the ideal point source at the various frequencies. The figures on the left show surface plots, normalized by the value of the array response at the source location, and the figures on the right show the projection of the surface plots, presented as constant contour levels (in decibels). In addition to constant contour levels, these plots also show the location of the first stationary points, depicted as the dashed lines, surrounding the main peak; the MSL value is the maximum value of the array response outside this region.

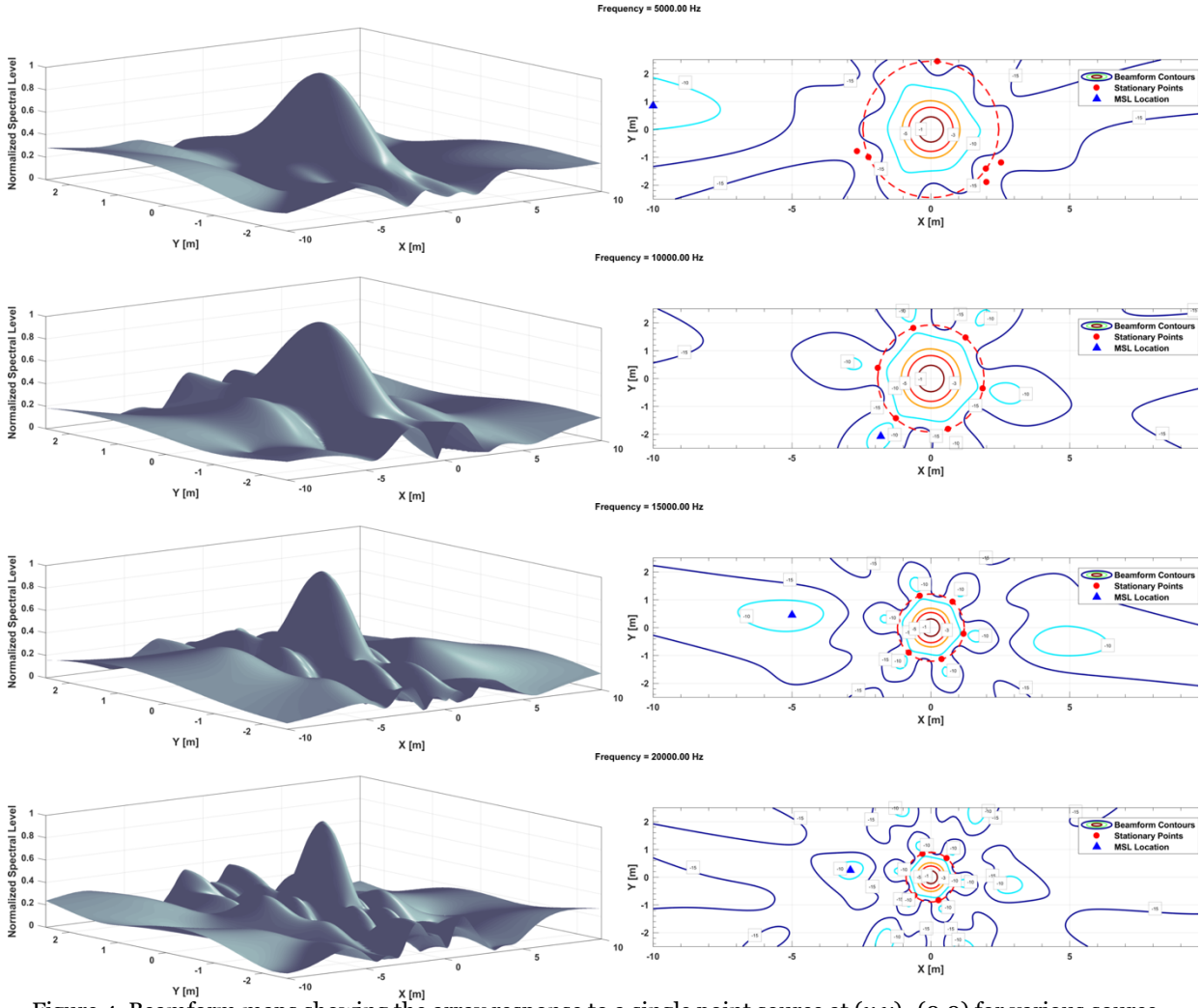

Figure 4. Beamform maps showing the array response to a single point source at $(x,y)=(0,0)$ for various source frequencies; from top to bottom: 5 kHz and 10 kHz, using array with large aperture; 15 kHz and 20 kHz, using array with small aperture.

Conclusions

We have presented the first step in a novel use of acoustic beam forming technology for application to bed load monitoring using the passive acoustics of SGN. We adapted existing

model design algorithms from aeroacoustics to design a phased array of hydrophones for underwater application. The resulting multi-spiral and Underbrink arrays provide 0.25 m spatial resolution over an interrogation plane 20 m by 5 m in up to 4 m of water depth. Such dimensions and resolution are believed to be appropriate for fluvial applications, and model results indicate the ability of the array designs to resolve sound sources on these scales. Following the design of the phased array system, we plan to build and test a prototype array using idealized sources in a laboratory setting, following which we will deploy the arrays in the field to localize acoustic sources in underwater applications.

References

Bunte, K., and Abt, S.R. (2005). "Effect of sampling time on measured gravel bed load transport rates in a coarse-bedded stream." Water Resources Research, 41, W11405, doi:10.1029/2004WR003880, 12 p.

Gray, J. R., and Gartner, J. W. (2009). "Technological advances in suspended-sediment surrogate monitoring," Water Resources Research, 45(4). doi:10.1029/2008WR007063.

Humphreys Jr., W.M.,Brooks, T. F., Hunter, W. W., and Meadows, K.R. (1998). "Design and use of microphone directional arrays for aeroacoustics measurements." AIAA Paper 98-0471, 1998.

Kuhnle, R. A., and Southard, J. B. (1988). "Bed load transport fluctuations in a gravel bed laboratory channel," Water Resources Research, 24(2), 247-260.

Kuhnle, R. A. (1989). "Bed-surface size changes in gravel-bed channel," Journal of Hydraulic Engineering, ASCE, 115(6), 731-743.

Rigby, J.R., Wren, D. G., and Kuhnle, R. A. (2016). "Passive acoustic monitoring of bed load for fluvial applications," Journal of Hydraulic Engineering, ASCE, 142(9), 02516003.

Underbrink, J.R. (2002) "Aeroacoustic phased array testing in low speed wind tunnels." *Aeroacoustic Measurements*, Ed. By T. J. Mueller, Berlin: Springer. Chapter 3, pp. 98-217, ISBN: 3-540-41757-5.

The 'Revolutionary' Potential of Passive Bedload Monitoring for River Science and Management

Peter W. Downs, Associate Professor, University of Plymouth, Plymouth, UK, peter.downs@plymouth.ac.uk
Philip J. Soar, Principal Lecturer, University of Portsmouth, Portsmouth, UK, philip.soar@port.ac.uk

Abstract

Field research into river bedload has relied largely on direct measurements using expensive sediment trapping facilities or labor intensive, potentially dangerous and time-limited active sampling. Passive, indirect measurements of particles passing an acoustic or impact sensor offer the prospect of high-resolution measurements over extended time periods from low cost, non-intrusive, portable devices. Based on recent exploratory experiences (Downs *et al.*, 2016; Soar and Downs, 2017; Downs and Soar, 2018; Downs and Soar *in prep*), we offer four observations on the extent to which such surrogate measurements do indeed offer the 'revolutionary' concept in fluvial sedimentology suggested by Gray *et al.* (2010a). The first emphasizes the degree that near-continuous data permits fresh examination of time-dependent behaviors such as instantaneous fluctuations, event-based hysteresis, selective path transport and multi-annual trends. Second, high resolution particle counts facilitate data-driven bedload estimation based on bedload entrainment theory, monitored bedload counts and a probabilistic optimization of individual particle sizes in transport. The resulting model, BLIP, provides an uncertainty-bound, indicative range of estimates, not prone to the overestimation associated with traditional bedload formulae. Continued monitoring at high resolution over multiple years with very varied flow types permits the observation that effective discharge at our site occurred consistently at sub-barfull flows indicating the importance of bedload availability along the sediment thalweg combined with network-scale replenishment during wet periods. Related, the multi-year data highlighted that discharge-bedload rating curves are not stationary and revealed the existence of a two-phase rating relationship with a consistent below-bankfull 'bulge' in rate, maximized in wet years, and appearing to relate to variations in sediment supply. Capacity-related controls were dominant only in flows above bankfull. We conclude that high resolution perspectives on coarse bedload transport emphasize the potential importance of water year type and sediment supply limitations on rates of bedload transport, and that a sensitivity-style sediment supply index could produce a valuable indication of time dependent behavior in coarse sediment transport. High resolution data from passive monitoring focuses attention on a site's 'hydrogeoclimatic' context and position in the watershed as factors determining coarse sediment dynamics and suggests that previous 'partial data' perspectives on bedload transport may have placed over-emphasis on rising limb sediment entrainment, under-emphasis on falling limb dynamics and focused on the influence of capacity controls to the detriment of supply-related controls.

Introduction

The last decade has witnessed a significant uptake in the use of passive devices for measuring river bedload. Such devices generally record either the vibration caused by bedload particles colliding with a rigid-bodied pipe, plate or column ('geophones'; for review see Rickenmann,

2017), the ambient noise of inter-particle collisions near the sensor ('hydrophones'), 'out-of-stream' seismic monitoring of coarse bedload activity (Roth *et al.*, 2014; Schmandt, *et al.*, 2017) or some combination (Downing, 2010; Froehlich, 2010; Mizuyama *et al.*, 2010). Previously, fluvial geomorphology had relied for decades on direct, active measurement of river bedload using portable or *in situ* sediment traps of various kinds. Such methods are generally expensive, labor intensive, require operation in high flow events that are potentially hazardous to the researcher, and the variability in results between samplers questions their accuracy and representativeness (Bunte *et al.*, 2004, 2014). Above all, though, most active techniques have produced data sets that are either extremely time-limited (*e.g.*, focused on high intensity sampling at the onset of an event to establish entrainment thresholds) or are of very low resolution (*e.g.*, collecting an event-total load via a pit sampler). No wonder, therefore, that Gray *et al.* (2010b, p.209) voiced concern that: "Progress in knowledge about bed load-transport processes is retarded for want of more reliable, accurate, and temporally dense bed load datasets." One might reflect that the bedload researchers of the Twentieth century deserve enormous credit for assembling a reasonably comprehensive understanding of bedload transport processes from such limited field data.

However, there are consequences of utilizing limited field data sets reinforced by multiple, controlled, flume experiments. One of the most limiting may be the presumption of *time invariant behavior* fostered by regarding bedload primarily as an energetic phenomenon, controlled primarily by shear stresses generated by river discharge. This has manifested itself in the over-riding concerns for the physics of particle entrainment, resulting from early, seminal laboratory experimentation (*e.g.*, incipient motion studies – for review see Buffington and Montgomery, 1997), and on establishing bedload transport *capacity* (recent review in Wainwright *et al.*, 2015). Conversely, very little research has been focused on the connection between network-scale sediment supply characteristics and the resulting (*i.e.*, at least partially dependent) reach-scale bedload transport, despite these connections being at the heart of a comprehensive understanding of fluvial geomorphology. At best, bedload transport is generally summarized as an average annual sediment load *potential* provided by the prevailing flow regime (*i.e.*, linked to concepts of dominant discharge, Wolman and Miller, 1960; Andrews 1980) or, where monitored, as a time-invariant sediment rating curve. Overlooking the temporal variability masked by these metrics is despite the long-standing recognition that bedload rates are subject to significant hysteresis (*e.g.*, Reid *et al.*, 1985; Mao, 2012; Gunsolus and Binns, 2018) and pulsing (*e.g.*, Nicholas *et al.*, 1995; Aigner *et al.*, 2017; Gran and Czuba, 2017) during the passage of flood hydrograph and that capacity-based sediment transport equations characteristically over-estimate sediment load by an order of magnitude or more, even in environments of apparently unlimited sediment supply (*e.g.*, Gomez & Church, 1989; Gomez 2006).

Passive monitoring of river bedload takes bedload data collection into the realm of 'big data', facilitating routine generation of datasets that are both of high resolution and spanning extended time periods and allowing, for the first time, the prospect of *data-driven* understanding of bedload dynamics in locations beyond a small number of expensively-maintained sediment gauging stations. Big data, of course, brings new challenges, such as separating the true sediment signal from the empirical noise expected with large volumes of data (*e.g.*, Rickenmann *et al.*, 2012; Downs *et al.*, 2016). However, such perspectives are exciting and the prospect for a *temporally-variable* understanding of bedload behavior (such as long-since achieved for river flow and transport of suspended sediment) would provide compelling evidence for the prescience in Gray *et al.*'s (2010a) suggestion that surrogate monitoring offers a

'revolutionary concept in fluvial sedimentology' and for the management of the world's sedimentary resources. Herein, we reflect on recent progress and, based largely on our own recent experiences (Downs *et al.*, 2016; Soar and Downs, 2017; Downs and Soar, 2018; Downs and Soar, *in prep*), offer five observations on the extent to which such surrogate measurements do indeed offer the 'revolutionary' concept in fluvial sedimentology.

Revolutionary Potential

Time Dependent Behaviors

The existence of near-continuous data permits fresh examination of time-dependent behaviors such as instantaneous fluctuations, event-based hysteresis, selective path transport and exploring and contrasting trends in bedload transport over numerous periods of interest. This permits comparison to seminal works (*e.g.*, Reid *et al.*, 1985) contextualized by flow frequency, magnitude and duration, but requires 'big data' display and processing methods. Geophones and hydrophones potentially offer great insight but bring with them intrinsic concerns for instrument accuracy and precision that are far from resolved, including such factors as deployment, grain-size dependency and transport-style effects (Rickenmann and McArdell, 2007, 2008; Turowski and Rickenmann, 2009; Gray *et al.*, 2010a; Rickenmann and Fritschi, 2010; Rickenmann *et al.*, 2012, 2014; Beylich and Laute, 2014; Tsakiris *et al.*, 2014; Kuhnle *et al.*, 2017). No instrument is perfect (not least portable sediment traps for bedload measurement!) but passive monitoring offers the prospect of achieving the balance between accuracy and practicability sought by Wilcock (2001) in enhancing understanding of sediment transport rates, while enabling routine deployment for practical applications. The primary requirement for better insight is that we can reliably distinguish the signal from the noise in large data sets.

We sought to understand time dependent behaviors using 'Benson-type' seismic impact plates (Carling *et al.*, 2002; Richardson *et al.*, 2003) installed near the mouth of the River Avon, a flashy, gravel-bed river (surface D_{50} 33 mm, bankfull water surface slope 0.0023) in South West England and characterized by an apparently abundant supply of local bed sediment sources (Downs *et al.*, 2016). Initial monitoring of a centrally-placed impact plate (May 2012 to April 2013) coincided with an exceptionally wet period, with twenty overbank events (>32 m^3s^{-1}), the maximum recorded instantaneous peak flow (124 $m^3s^{-1,}$ return period of *ca*.87 years), and nearly 1.15 M recorded impacts. In summary, results indicated a strong general correspondence between high flows and large impact counts but, at 5-minute interval discharges, demonstrated considerable scatter (R^2 = 0.38) (Figure 1A). Converting flows to a local estimate of shear stress immediately above the plate mildly worsened the explanation (R^2 = 0.33), whereas using an array of three impact plates somewhat improved the relationship to flow (R^2 = 0.49). Considerable hysteresis was observed in nearly all events, with larger events leading to greater negative (anti-clockwise) hysteresis related to a second and dominant peak of impacts during the hydrograph recession that we interpreted as pulsing of sediment delivery from upstream supplies (*e.g.*, resulting from bank erosion, surface armor disruption, network delivery). Monitoring over a 4.5 month period (late December 2012 to early May 2013) based on an array of three impact plates indicated considerable lateral variability in impacts and impact timing during the passage of a hydrograph, with one plate clearly indicating considerable late-flood transport of (from observation) finer gravels during the late stages of a flood event and presumably related to thalweg deflection as larger particles settled in the center channel.

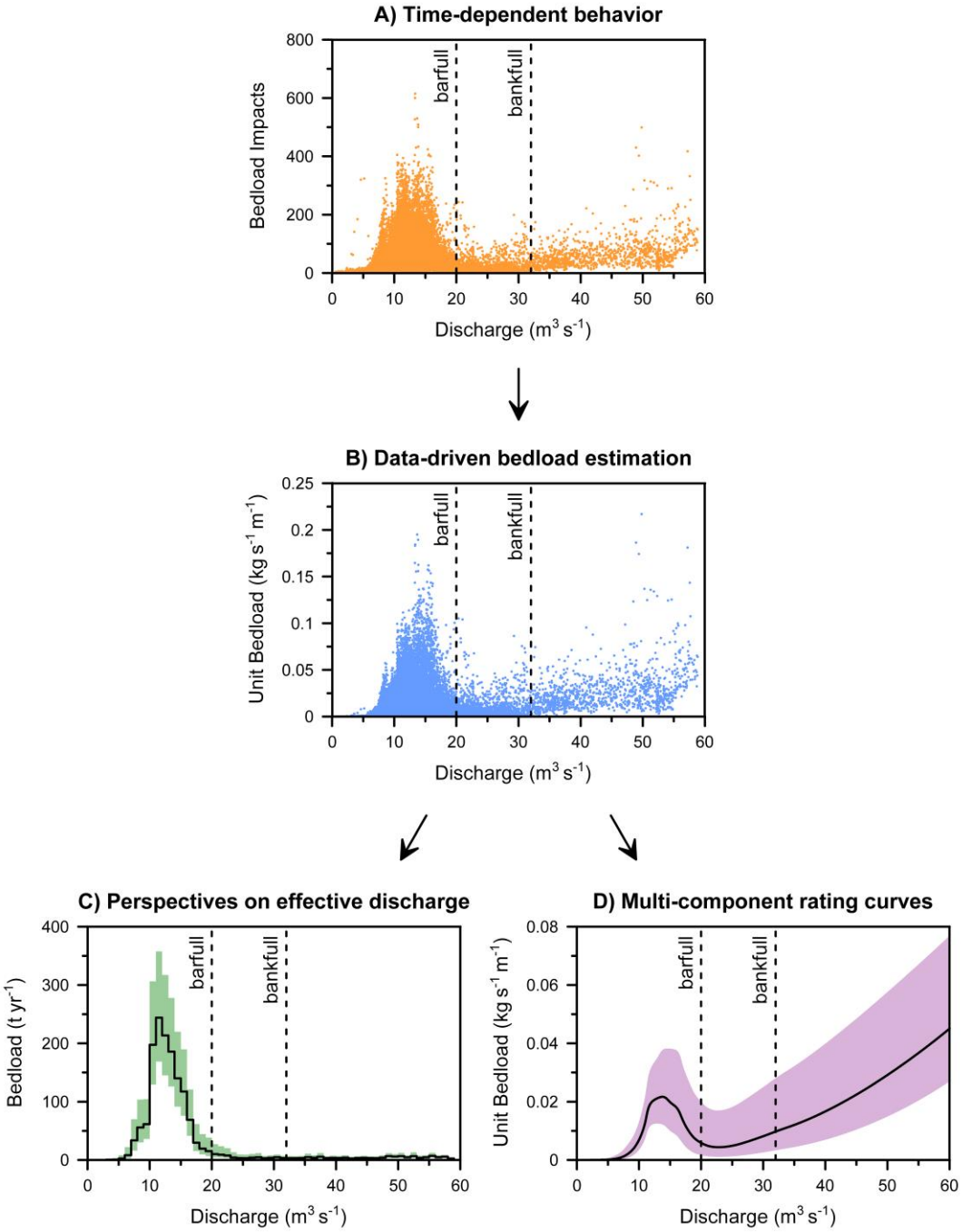

Figure 1. The revolutionary potential of passively monitored river bedload data as four observations, illustrated for WY2014 on the River Avon, Devon, UK: A) Time dependent behavior - 5-minute continuous impact counts against instantaneous discharge (zero counts omitted); B) Data-driven bedload estimation - cross-sectional bedload transport (>10 mm) over 5-minute intervals predicted from the BLIP model (average from Monte-Carlo routine); C) Perspectives on effective discharge - magnitude-frequency analysis of cross-sectional bedload at 1 m^3s^{-1} increments (with 95% prediction intervals from the BLIP model); D) Multi-component rating curves - annual relationship between instantaneous discharge and coarse bedload transport rate, revealing evidence for a two-phase rating curve comprising a supply-limited 'bulge' of transport preceding a near-linear trend at flows exceeding ≈25 m^3s^{-1} (data-driven average trend generated from LOWESS curve fitting applied to log-transformed data with 95% prediction limits from the BLIP model).

Near-instantaneous bedload transport thus appears to be partially a function of tractive force, but relates also to granular interactions, the dynamics of bedform behavior and reach- and catchment-scale variability in supply related to the intensity and duration of the multiple high flow events experienced. Inherently, the results also reflect experimental design and the performance character of the chosen plates, related particularly to the particle's striking velocity (Rickenmann and McArdell, 2007, 2008) and size-dependent recording efficiency (Rickenmann *et al.*, 2012). Testing these assumptions, an aggregation of event-total impacts from the central plate against event-volumetric discharge, implying the coarsening of experimental resolution from 5-minute periods to 32-hour periods (the average duration of the recorded flood events), considerably increased flow-impact explanation ($R^2 = 0.74$) as intra-event and stochastic bedload factors were subsumed. A similarly strong relation in event total impacts versus flow was achieved by Rickenmann *et al.* (2012, $R^2 = 0.91$), both results indicating a more ''traditional' dependency of bedload transport on energetic phenomenon only at these lengthened time bases.

Data-Driven Bedload Estimation

High-resolution recording of bedload data offers the opportunity to develop a new 'class' of bedload rate estimation that is *data-driven*, associated with the conversion of particle counts to bedload rates by combining attributes from the two traditional routes of empirical (*i.e.*, active bedload monitoring) and theory-based (*i.e.*, sediment transport equations) bedload estimation. Consistent with the inherently stochastic nature of bedload transport, we approached this task using an uncertainty-bound, probabilistic method that avoids the need for grain-size specific calibration of the plates that has proved problematic (for progress, see Barrière *et al.*, 2015; Wyss *et al.*, 2016a, 2016b, 2016c; Kuhnle *et al.*, 2017). The BedLoad from Impact Plates (BLIP) model (Soar and Downs, 2017) represents a complementary approach to bedload estimation that integrates data monitoring and theory-based sediment entrainment formulae with a probabilistic optimization of individual particle sizes in transport derived using a Monte Carlo simulation (Figure 2). The Monte Carlo component converts count data into a uncertainty-bound array of possible particle sizes in transit based on knowledge of the minimum particle size reliably detected by the plate (*ca*. 10±2 mm), the particle size distribution of the upstream channel bed provided from multiple bulk and surface samples, and time-series of local water surface elevation (derived from pressure transducer data, and related to instantaneous discharge, see Downs *et al.*, 2016) to establish bed shear stress over each plate. The impact count data are used to calibrate the model internally before each run, optimizing for the largest particle in motion at any individual flow against the Shields parameter and sediment hiding coefficient. With this constraint set and additionally accounting for the minimum detectable particle size (intrinsic to the impact plates), specific gravity and water surface slope, varying between set limits, an uncertainty bound estimation of sediment load was achieved for impact counts recorded over 5-minute durations (Figure 1B) (see Soar and Downs, 2017 for further details of the method).

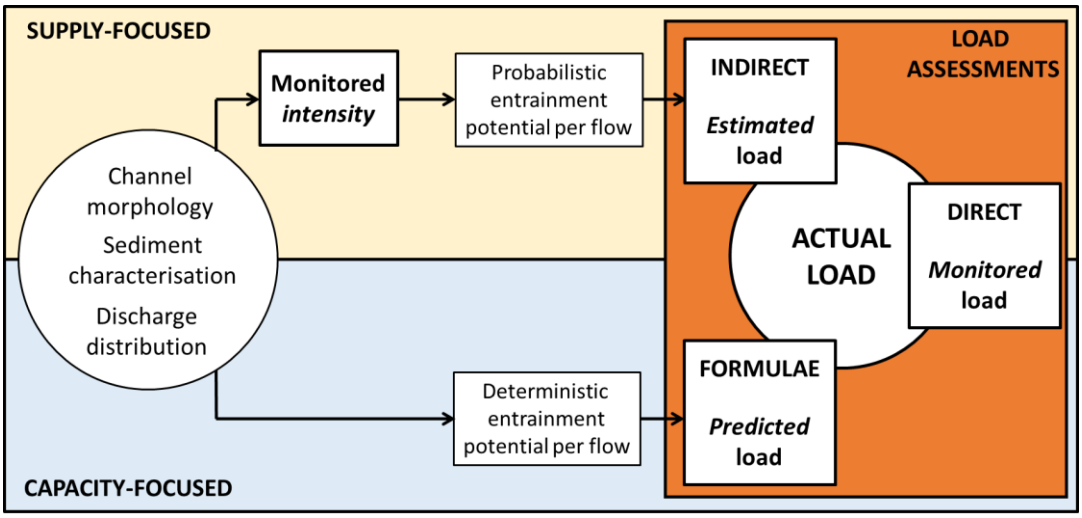

Figure 2. Relation of the BedLoad from Impact Plate (BLIP) approach for estimating coarse bedload transport to direct measurement and predictions based on tractive force theory. Modified from Downs and Soar (2018).

The resulting estimates of instantaneous bedload transport use are thus faithful to the inherently stochastic nature of bedload transport (see previous section). Because estimates are based directly on count data rather than a capacity-based estimate of transport potential, they are autogenically-moderated for local sediment supply factors, providing an illustration of how technological improvements might improve bedload transport rate estimation (Ashmore and Rennie 2012). As such, they provide a location-specific estimate that is less prone to the overestimation associated with traditional bedload formulae (Gomez, 2006). The outputs follow the resolution of the data inputs, allowing estimates of relative rates of bedload transport dynamics during rising and falling flows of flood events. When aggregated, they provide an estimate of bedload yield that is both supply- and transport-limited and consistent with annual variability in flow events, albeit acknowledging the irreducible epistemic uncertainty of bedload transport (Refsgaard *et al.*, 2007). Such estimates are conceivably the basis for annualized bedload rating curves and so provide a potentially valuable tool for informing stable channel design applications (Soar and Thorne, 2001, 2011), as baseline monitoring tool for determining sustainable river restoration (Downs *et al.*, 2011) and for predicting bedload under changing hydroclimate conditions. As the approach is model based, it is amenable to sensitivity testing for scientific purposes including, for instance, the apparent impacts of varying the Shields parameter and hiding coefficient on bedload transport rates and yields. The additional benefit of BLIP as a data-driven model is that once the performance characteristics of impact plates are better understood, the opportunity exists to add a correctional algorithm into the model to adjust for and minimize particle size-related differences in plate performance.

Continued deployment of the three-impact plate array at a cross-section of the lower River Avon provides the basis for observations on bedload variability that utilize the inherent value of longer-term data sets (Burt, 1994). Perspectives highlighted below are based on records of inter-annual bedload variability spanning Water Years (WYs) 2013 to 2017. Over this period, bedload rates (estimated via BLIP) varied across two orders of magnitude between 20 t (interquartile range: 13-33 t) and 1,854 t (interquartile range: 1,626-2153 t) within WYs that ranged from Very Wet to Very Dry classified according to flow duration curves generated from a 36-year record of flows at the gauging station.

Perspectives on Effective Discharge

Consistent with our first year of observations at the central impact plate (Downs *et al.*, 2016), the extended period of monitoring reinforced, for this site, the persistence dominant of 'bar-building' flows as the peak efficiency for sediment transport (Figure 1C). Coarse bedload transport (*i.e.*, transport of particles ≥10 mm detectable by the plates) begins at about 8 m^3s^{-1} and, during wetter years, there is a maximum cross-sectional bedload transport rate of ≈0.3 kg s^{-1} m^{-1} although transport rates rarely exceed 0.15 kg s^{-1} m^{-1}. In drier years, the maximum rate of transport is ≈0.1 kg s^{-1} m^{-1} with rates rarely exceeding 0.05 kg s^{-1} m^{-1} (Downs and Soar, 2018). Aggregated into a magnitude-frequency histogram of yields (using data-driven rather than 'potential-driven' estimates using BLIP), the results consistently indicate the influence of significant hysteresis present in the data (see above), irrespective of WY type. The influence of the characteristic spikes in bedload transport during, first, the rising limb and, second (and often dominantly), the falling limbs of the hydrograph, similar to that shown in the 'classic' active measurements of Reid *et al.* (1985), result in annual bedload yields peaking at flows that are about 0.3–0.4 of bankfull discharge (*i.e.*, ≈11–12 m^3s^{-1}). Indeed, the large majority of annual transport occurs at flows below 'barfull' discharge (20 m^3s^{-1}) and has no relationship with the bankfull discharge of ≈32 m^3s^{-1} (Downs and Soar, *in prep*.).

We interpret these results to indicate the importance of 'residual' bedload availability along the sedimentary thalweg (*i.e.*, point bar face–riffle couplets) in this channel, with the relatively lower transport rates during dry years implying the importance of upstream sediment replenishment during wet periods, and thus the critical role of sediment supply in conditioning bedload transport. At least for this site (background in Downs *et al.*, 2016), the impact of hysteretic behavior in sediment transport is sufficient to dictate the nature of effective discharge and provide a reasonable explanation for its striking and noteworthy discordance with the morphological bankfull discharge.

Multi-Component Rating Curves

Annualizing the instantaneous estimates of coarse bedload transport at this site provides the basis for generating inter-annual bedload rating curves based on high-resolution monitored data rather than on transport capacity potential. Reflecting the hysteretic nature of sediment dynamics at the site, we fitted a LOWESS-based (locally-weighted scatterplot smoothing, Cleveland, 1979) function to the data, so to more faithfully follow sediment transport estimates for the 5-minute data points (Downs and Soar, 2018, *in prep*.). The curves revealed that the relationship between discharge and coarse bedload transport rate is not stationary over time. Intriguingly, though, the curves consistently illustrated a two-phase rating relationship consisting of a below-bankfull 'bulge' that precedes an apparently tractive force-based component at flows above bankfull discharge (Figure 1D). Normalizing the curves indicated that the below-bankfull bulge is relatively less important during drier years. These plots are interpreted to imply the existence of supply-limited controls at lower flows that give way to the more commonly perceived transport-limited controls during overbank discharges.

Extending the interpretation above implies that, for the lower Avon at least, large volumes of sediment are derived from the upstream contributing area into short-residence time storage on the sedimentary thalweg during extreme flow events. After such events, storage is progressively reduced during lower magnitude 'high flow' events. Thus, during extended dry periods, the sediment available for 'below barfull' transport is reduced to the extent that the supply-related

bulge is eliminated during dry periods that exceed one WY (Downs and Soar, *in prep*). Further controls may be provided by lower virtual velocities of sediment transport in drier years which reduce the upstream length of channel capable of providing a source of coarse material, and the prospect that drier periods make the channel bed more resistant to particle entrainment as near-critical flows promote tighter particle packing, greater vertical settling and the flow parallel orientation of coarser particles (*e.g.*, Monteith and Pender, 2005; Haynes and Pender, 2007; Ockelford and Haynes, 2013).

Overall, and possibly as a function of the short-duration high-magnitude flow events at this site, it appears that sedimentary morphology is a critical component of sediment transport. While it is perhaps not surprising that annual sediment yields revealed such marked variability given the observed annual differences in flow regime experienced over the 5-year monitoring period, the capability of high resolution data to reveal both subtle and conspicuous idiosyncrasies in bedload dynamics would have been concealed by the coarse sampling frequency of direct measurement methods, and is arguably the greatest revolutionary quality of passive sensing technology.

Prospect: Time-Dependence and Antecedent Preparation in Bedload Transport

The various results above suggest that high resolution perspectives on coarse bedload transport emphasize the importance of water year type and sediment supply limitations on rates of bedload transport. The existence of such limitations indicate that coarse sediment yields are far more time-dependent than implied by analyses focused on transport-limited sediment capacities. Temporal controls on sediment availability invoke the prospect of a sensitivity-style index of sediment supply that (following Brunsden and Thornes, 1979) involves the ratio of disturbance event frequency to the intervening relaxation period. Experiments based on annual indices of aggregated flow duration over the threshold discharge for coarse bedload transport versus the volume (duration-magnitude) of 'near-critical' flows as a measure of antecedent preparation (of bed material for transport) show promise in explaining the relative magnitude of the observed 'supply bulge', and suggest that annual coarse sediment yield is intimately linked to the low-flow sediment supply characteristics of the previous year (Downs and Soar, *in prep*).

Our experiences to date with passive high-resolution monitoring of coarse bedload transport lead us to believe that earlier, 'partial data', perspectives on bedload transport may have placed over-emphasis on rising limb sediment entrainment, under-emphasis on falling limb dynamics and focused on the influence of capacity related influences to the detriment of supply-related control factors. Conversely, a big data perspective prompts attention on a site's 'hydrogeoclimatic' context and position in the watershed as part of a far more site-specific interpretation of coarse sediment transport characteristics than has previously been the case. Better understanding will require a substantial network of passive monitoring sites capable of supporting hypothesis-led reappraisals of many accepted norms in bedload transport. We suggested previously (Downs *et al.*, 2016) that high-resolution passive monitoring provided the prospect of liberty and equality in bedload monitoring and emphasize again that scientific fraternity is required to deliver the final part of Gray *et al.*'s, (2010a) revolutionary potential.

Acknowledgements

Initial research was funded by a grant from the Seale-Hayne Education Trust to the first author, while an exchange programme grant from CONICYT Chile allowed productive collaboration with Luca Mao and Ricardo Carrillo. Richard Hartley, Alex Taylor and Stephen Haley are thanked for field assistance, and Adrian Simpson and John Hosking for permission to access their land. Gauging station data was provided by the Environment Agency (Tim Shipley, Sandy Satterly and Andy Roberts). The impact plates are made by Ian Benson (iandesignandbuild@gmail.com). We are very grateful for the thoughtful review of the original submission.

References

Aigner, J., Kreisler, A., Rindler, R., Hauer, C., and Habersack, H. 2017. "Bedload pulses in a hydropower affected alpine gravel bed river," Geomorphology, 291:116-127.

Andrews, E.D. 1980. "Effective and bankfull discharges of streams in the Yampa river basin, Colorado and Wyoming," Journal of Hydrology 46:311-330.

Ashmore, P.E. and Rennie, C.D. 2012. "Gravel-bed rivers: From particles to patterns," Earth Surface Processes and Landforms 38:217–220.

Barrière, J., Krein, A., Oth, A. and Schenkluhn, R. 2015. "An advanced signal processing technique for deriving grain size information of bedload transport from impact plate vibration measurements," Earth Surface Processes and Landforms, 40: 913–924.

Beylich, A.A., and Laute, K. 2014. "Combining impact sensor field and laboratory flume measurements with other techniques for studying fluvial bedload transport in steep mountain streams," Geomorphology 218, 72–87.

Brunsden, D. and Thornes, J.B. 1979. "Landscape sensitivity and change," Transactions of the Institute of British Geographers, NS4:463-484.

Buffington, J.M., Montgomery, D.R., 1997. "A systematic analysis of eight decades of incipient motion studies, with special reference to gravel-bedded rivers," Water Resources Research 33:1993–2029.

Bunte, K., Abt, S.R., Potyondy, J.P., and Ryan, S.E. 2004. "Measurement of coarse gravel and cobble transport using portable bedload traps," Journal of Hydraulic Engineering, 130:879-893

Bunte, K., Abt, S.R., Swingle, K.W. and Cenderelli, D.A. 2014. "Effective discharge in Rocky Mountain headwater streams," Journal of Hydrology 519: 2136-2147.

Burt, T.P. 1994. "Long-term study of the natural environment: perceptive science or mindless monitoring?" Progress in Physical Geography, 18:475–496.

Carling, P.A., Benson, I. and Richardson, K. 2002. "A new instrument to record sediment movement in bedrock channels," ICCE/IAHS: Erosion and Sediment Transport Measurement: Technological and Methodological Advances, Oslo Workshop

Cleveland, W.S. 1979. "Robust locally weighted regression and smoothing scatterplots," Journal of the American Statistical Association, 74:829–837.

Downing, J. 2010. "Acoustic gravel-momentum sensor," In: Bedload Surrogate Monitoring Technologies, Gray, J.R., Laronne, J.B., Marr, J.D.G. (eds). U.S. Geological Survey Scientific Investigations Report 2010–5091. U.S. Geological Survey: Reston, VA, 143-158.

Downs, P.W., Singer, M.S., Orr, B.K., Diggory, Z.E., Church, T.C., Stella, J.C. 2011. "Restoring ecological integrity in highly regulated rivers: the role of baseline data and analytical references," Environmental Management 48:847–864.

Downs, P.W., Soar, P.J. and Taylor, A. 2016. "The anatomy of effective discharge: The dynamics of coarse sediment transport revealed using continuous bedload monitoring in a gravel-bed river during a very wet year," Earth Surface Processes and Landforms, 41:147–161.

Downs, P.W. and Soar, P.J. 2018. "Determining the dynamics of coarse bedload transport using passive indirect monitoring: time-dependent variability at event to interannual scales," River Flow 2018 - Ninth International Conference on Fluvial Hydraulics, E3S Web of Conferences, 40:05014, (https://doi.org/10.1051/e3sconf/20184005014), 7pp.

Downs, P.W. and Soar, P.J. *in prep*. "Beyond Stationarity: Influence of Sediment Supply and Antecedent Conditions on the Inter-Annual Variability of Coarse Bedload Dynamics".

Froehlich, W. 2010. "Monitoring of bed load transport within a small drainage basin in the Polish Flysch Carpathians," In: Bedload Surrogate Monitoring Technologies, Gray, J.R., Laronne, J.B. and Marr, J.D.G. (eds). U.S. Geological Survey Scientific Investigations Report 2010-5091. U.S. Geological Survey: Reston, VA, 185-194.

Gomez, B. 2006. "The potential rate of bed-load transport," Proceedings of the National Academy of Sciences, 103: 17170–17173.

Gomez, B. and Church, M. 1989. "An assessment of bed load sediment transport formulae for gravel bed rivers," Water Resources Research, 25:1161–1186.

Gran, K.B., and Czuba, J.A. 2017. "Sediment pulse evolution and the role of network structure," Geomorphology, 277:17-30.

Gray, J.R., Gartner, J.W., Barton, J.S., Gaskin, J., Pittman, S.A. and Rennie, C.D. 2010a. "Surrogate technologies for monitoring bed-load transport in rivers," In: Sedimentology of Aqueous Systems, Poleto, C. and Charlesworth, S. (eds). Wiley-Blackwell: Oxford, 46-79.

Gray, J.R., Laronne, J.B., Osterkamp, W.R. and Vericat, D. 2010b. "Bed Load Research International Cooperative – BRIC," In: Bedload-surrogate Monitoring Technologies, Gray, J.R., Laronne, J.B. and Marr, J.D.G. (eds). U.S. Geological Survey Scientific Investigations Report 2010-5091. U.S. Geological Survey: Reston, VA, 208-217.

Gunsolus, E.H. and Binns, A.D. 2018. "Effect of morphologic and hydraulic factors on hysteresis of sediment transport rates in alluvial streams," River Research and Applications, 34:183-192.

Haynes, H. and Pender, G. 2007. "Stress history effects on graded bed stability," Journal of Hydraulic Engineering, ASCE, 133:343–349.

Kuhnle, R.A., Wren, D.G., Hilldale, R.C., Goodwiller, B.T. and Carpenter, W.O. 2017. "Laboratory calibration of impact plates for measuring gravel bed load size and mass," Journal of Hydraulic Engineering, 143:06017023.

Mao, L. 2012. "The effect of hydrographs on bed load transport and bed sediment spatial arrangement", Journal of Geophysical Research, Earth Surface, 117:F03024.

Mizuyama, T., Laronne. J., Nonaka, M., Sawada, T., Satofuka, Y., Matsuoka, M., Yamashita, S., Sako, Y., Tamaki, S., Watari, M., Yamaguchi, S. and Tsuruta, K. 2010. "Calibration of a passive acoustic bedload monitoring system in Japanese mountain rivers," In: Bedload Surrogate Monitoring Technologies, Gray JR, Laronne JB, Marr JDG (eds). U.S. Geological Survey Scientific Investigations Report 2010-5091. U.S. Geological Survey: Reston, VA. 296-318.

Monteith, H. and Pender, G. 2005. "Flume investigation into the influence of shear stress history," Water Resources Research 41:W12401.

Nicholas, A.P., Ashworth, P.J., Kirkby, M.J., Macklin, M.G. and Murray, T. 1995. "Sediment slugs: large scale fluctuations in fluvial sediment transport rates and storage volumes," Progress in Physical Geography, 19:500-519.

Ockelford, A.-M. and Haynes, H. 2013. "The impact of stress history on bed structure," Earth Surface Processes and Landforms, 38:717-727.

Refsgaard, J.C., van der Sluijs, J.P., Højberg, A.L. and Vanrolleghem, P.A. 2007. "Uncertainty in the environmental modelling process e a framework and guidance," Environmental Modelling and Software, 22, 1543–1556.

Reid, I., Frostick, L.E. and Layman, J.T. 1985. "The incidence and nature of bedload transport during flood flows in coarse-grained alluvial channels," Earth Surface Processes and Landforms, 10:33–44.

Richardson, K., Benson, I. and Carling, P.A. 2003. "An instrument to record sediment movement in bedrock channels," In: Erosion and Sediment Transport Measurement in Rivers: Technological and Methodological Advances, Bogen J, Fergus T, Walling DE (eds). IAHS Publication 283, Wallingford, UK, 228–235.

Rickenmann, D. and McArdell, B.W. 2007. "Continuous measurement of sediment transport in the Erlenbach stream using piezoelectric bedload impact sensors," Earth Surface Processes and Landforms, 32:1362-1378.

Rickenmann, D. and McArdell, B.W. 2008. "Calibration of piezoelectric bedload impact sensors in the Pitzbach mountain stream," Geodinamica Acta, 21:35-52.

Rickenmann, D., Turowski, J.M., Fritschi, B., Klaiber, A. and Ludwig, A. 2012. "Bedload transport measurements at the Erlenbach stream with geophones and automated basket samplers," Earth Surface Processes and Landforms, 37:1000–1011.

Rickenmann, D., Turowski, J.M., Fritschi, B., Wyss, C., Laronne, J., Barzilai, R., Reid, I., Kreisler, A., Aigner, J., Seitz, H., Habersack, H. 2014. "Bedload transport measurements with impact plate geophones: Comparison of sensor calibration in different gravel-bed streams," Earth Surface Processes and Landforms 39:928-942.

Rickenmann, D. 2017. "Bedload transport measurements with geophones, hydrophones, and underwater microphones (passive acoustic methods)," In: Gravel Bed Rivers: Processes and Disasters, Tsutsumi, D. and Laronne, J.B. (eds). Wiley. 185–208.

Roth, D.L., Finnegan, N.J., Brodsky, E.E., Cook, K.L., Stark, C.P. and Wang, H.W. 2014. "Migration of a coarse fluvial sediment pulse detected by hysteresis in bedload generated seismic waves," Earth and Planetary Science Letters. 404:144-153.

Schmandt, B., Gaeuman D., Stewart R., Hansen S.M., Tsai V.C. and Smith J. 2017. "Seismic array constraints on reach-scale bedload transport," Geology, 45:299–302.

Soar, P.J. and Downs, P.W. 2017. "Estimating bedload transport rates in a gravel-bed river using seismic impact plates: model development and application," Environmental Modelling and Software, 90:182-200.

Soar, P.J. and Thorne, C.R. 2001. "Channel Restoration Design for Meandering Rivers," Coastal and Hydraulics Laboratory Report ERDC/CHL CR-01-1, U.S. Army Engineer Research and Development Center, Vicksburg, MS. Not in the paper

Soar, P.J. and Thorne, C.R. 2011. "Design discharge for river restoration," In: Stream Restoration in Dynamic Fluvial Systems: Scientific Approaches, Analyses and Tools, Simon, A., Bennett, S.J. and Castro, J. (eds). AGU Geophysical Monograph 194, American Geophysical Union, Washington DC, 123-149.

Tsakiris, A.G., Papanicolaou, A.N. and Lauth, T.J. 2014. "Signature of bedload particle transport mode in the acoustic signal of a geophone," Journal of Hydraulic Research 52, 185–204.

Turowski, J.M. and Rickenmann, D. 2009. "Tools and cover effects in bedload transport observations in the Pitzbach, Austria," Earth Surface Processes and Landforms, 34, 26–37.

Wainwright, J., Parson, A.J., Cooper, J.R., Gao, P., Gillies, J.A., Mao, L., Orford, J.D. and Knight, P.G. 2015. "The concept of transport capacity in geomorphology," Reviews of Geophysics, 53: 1155–1202.

Wilcock, P.R. 2001. "Toward a practical method for estimating sediment-transport rates in gravel bed rivers," Earth Surface Processes and Landforms, 26:1395-1408.

Wolman, M.G., Miller, J.P. 1960. "Magnitude and frequency of forces in geomorphic processes," Journal of Geology, 68:54-74.

Wyss, C.R., Rickenmann, D., Fritschi, B., Turowski, J.M., Weitbrecht, V. and Boes, R.M. 2016a, "Measuring bed load transport rates by grain-size fraction using the Swiss plate geophone signal at the Erlenbach," Journal of Hydraulic Engineering, 142: doi:10.1061/(asce)hy.1943-7900.0001090.

Wyss, C.R., Rickenmann, D., Fritschi, B., Turowski, J.M., Weitbrecht, V. and Boes, R.M. 2016b, "Laboratory flume experiments with the Swiss plate geophone bed load monitoring system: 1. Impulse counts and particle size identification," Water Resources Research, 52:7744–7759.

Wyss, C.R., Rickenmann, D., Fritschi, B., Turowski, J.M., Weitbrecht, V., Travaglini, E., Bardou, E. and Boes, R.M. 2016c, "Laboratory flume experiments with the Swiss plate geophone bed load monitoring system: 2. Application to field sites with direct bed load samples," Water Resources Research, 52:7760–7778.

Using Hydrologic Indices to Continuously Estimate Sediment and Mercury Concentrations

Alexandra Etheridge – U.S. Geological Survey, California Water Science Center

The use of hydrologic indices as surrogates to estimate continuous sediment and sediment-bound constituent concentration has potential for large-scale implementation. Hydrologic indices can be computed using automated processors in the U.S. Geological Survey National Water Information System Time Series (NWIS-TS) database. Hydrologic indices derived from continuous streamflow were determined to be significant predictors of total mercury concentration at two headwaters streams in a Central Idaho mining area. Streamflow derivatives were further explored as potentially significant explanatory variables for sediment surrogates in an urban stream in California. Two hydrologic index terms were used. The first index term used base flow index (BFI) to weight streamflow. The second hydrologic index term used the ratio of mean daily streamflow to daily range in streamflow (Qrange) and significantly improved model fit in one example. A Qrange index close to 1 results from any sudden increase in streamflow commonly observed in flashy urban or mountain headwaters streams. The examples where this method worked will be shown and large-scale potential applications discussed.

Sediment Yield & Fingerprinting

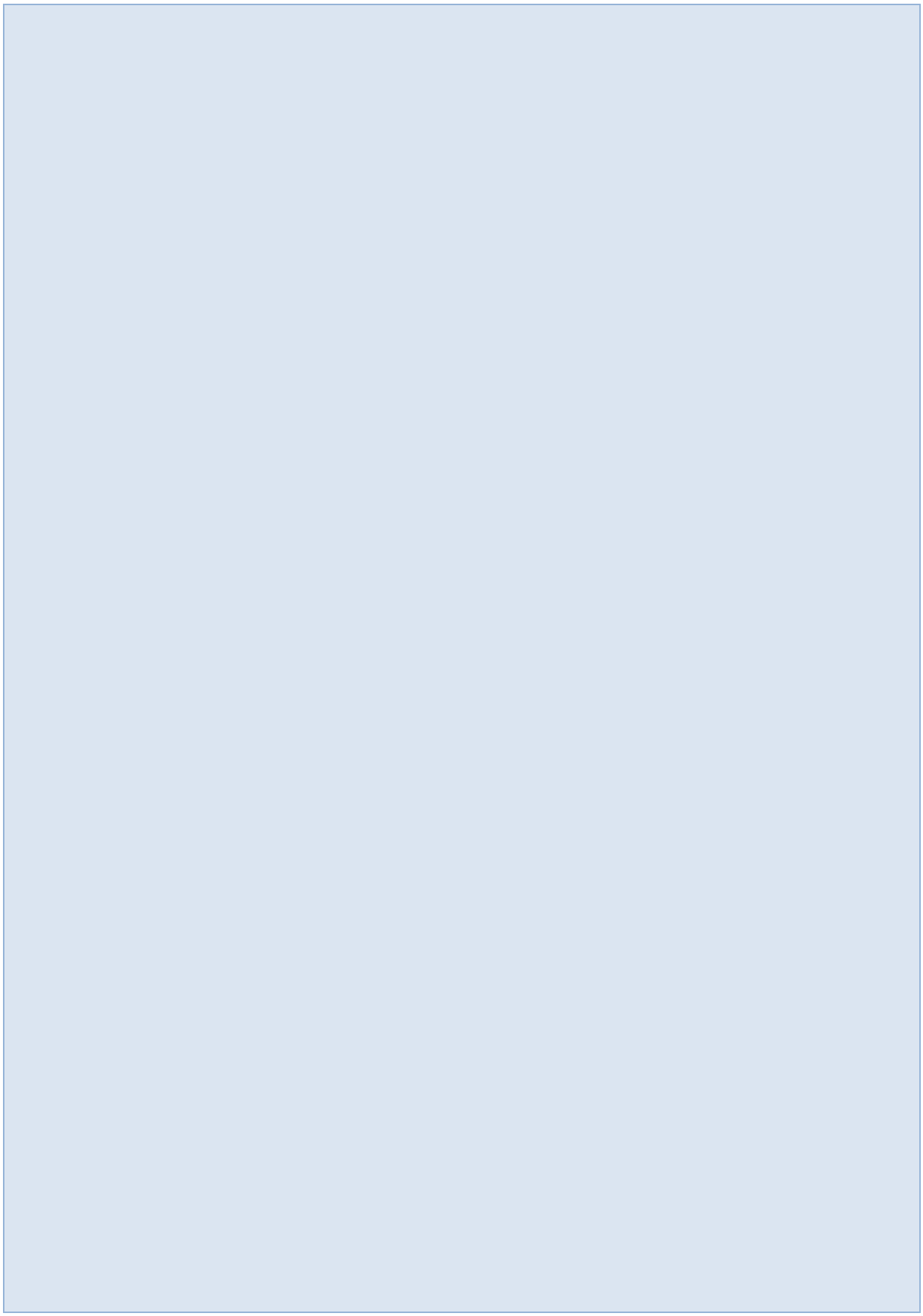

A Comparison of Five Different Methods for Validating Sediment Yield to Reservoirs in the Great Lakes

James Selegean, Hydraulic Engineer, U.S. Army Corps of Engineers, Detroit, MI, james.p.selegean@usace.army.mil
Mark Baskaran, Professor, Wayne State University, Detroit, MI, baskaran@wayne.edu
A. Kumar, Research Associate, Wayne State University, Detroit, MI ed2747@wayne.edu
Travis Dahl, Research Hydraulic Engineer, U.S. Army Corps of Engineers, ERDC Coastal and Hydraulics Laboratory, Vicksburg, MS, travis.a.dahl@usace.army.mil
John Barkach, Great Lakes Environmental Center, Inc., Farmington Hills, M 48334, jbarkach@glec.com
Fatemah Babakhani, Research Associate, Wayne State University, Detroit, MI fatemeh@wayne.edu
Calvin Creech, Hydraulic Engineer, U.S. Army Corps of Engineers, Mobile District, Mobile, AL, calvin.t.creech@usace.army.mil

Abstract

There is inherently a great deal of uncertainty in sediment yield modeling. To build confidence in the fidelity of these models, it is common to collect field data to calibrate the models and then validate the results. In this paper, we will compare the results of five different types of validation data sets across 10 different reservoirs in the Great Lakes (Figure 1). Two of the methods used radioisotopes (^{210}Pb and ^{137}Cs) to determine sediment accumulation rates. These data were obtained from multiple cores from each of the ten study reservoirs. The third method used USGS sediment gages upstream and downstream of the reservoir to calculate the sediment retained in the reservoir. The fourth method comes from a comparison of reservoir bathymetric changes over time, and the final method comes from a regional sediment yield curve that has been compiled from 61 sediment yield observations over the last century throughout the Great Lakes Basin. A comparison between and within these methods shows a large amount of variance in the measurements that are being used to validate sediment yield models.

Bathymetry and Coring

For all of the study reservoirs, post dam construction bathymetric data was collected with a SonTek M9 river surveyor. Pre-dam bathymetry was obtained from the local stakeholders. At the 10 study sites, 10-12 core samples were retrieved at the same time

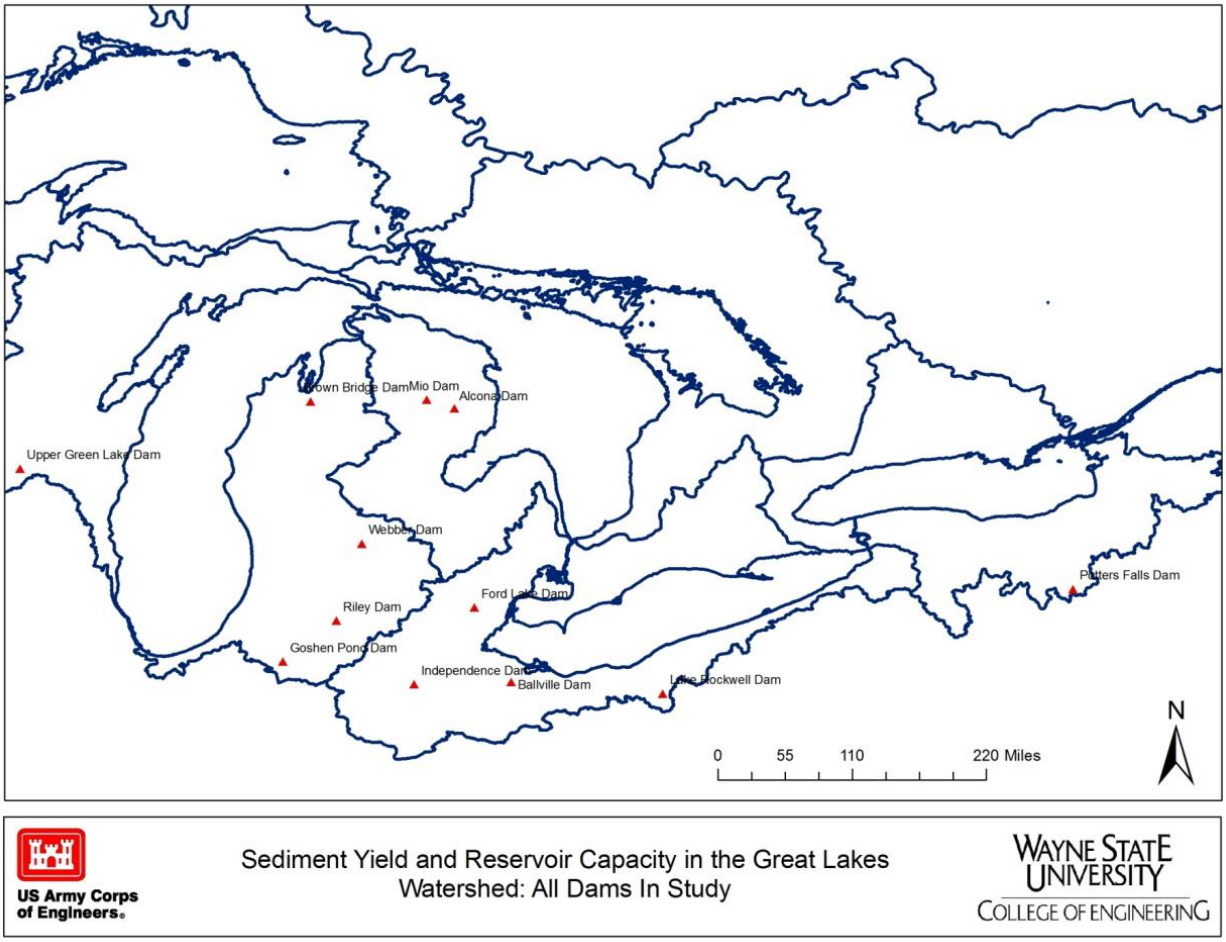

Figure 1. Map of the Study Reservoirs

as the reservoir was mapped. The core samples were removed from the reservoir bottom using the vibra-core method, frozen on site and send to the laboratory at Wayne State University for analysis of gradation, ^{210}Pb and ^{137}Cs. The frozen sediment cores were sliced while frozen into 1-cm slices for the first 10 centimeters and 2-cm slices for the rest of the sediment core.

Sediment Gages

This technique used suspended sediment data from 19 U.S. Geological Survey sediment gages to estimate sediment yield (https://waterdata.usgs.gov/nwis). The number of years of data at these gages ranged from 2 to 54 years, with an average of 15 years. Using sediment gages is a very cost-effective way to estimate sediment yield as no new field work is required. This technique is not applicable to all reservoirs in this study because there must exist sediment gage data for a number of years within the study

reservoir watershed. Assuming dams may or may not act as sediment traps, yields were calculated using both impounded and un-impounded areas.

Each sediment gage has a different period of record. The USGS sediment gages display sediment yield in tons per day. The data were summarized for each year and averaged over all the years available. In order to make comparisons among reservoirs the data were normalized by the contributing drainage area.

Total Sediment Yield Regression Curve

A sediment yield regression curve was created using 13 data points from previous U.S. Army Corps of Engineers 516(e) numerical models in Great Lakes watersheds, and a total of 48 Great Lakes Reservoirs from the Subcommittee on Sedimentation Reservoir Sedimentation (RESSED) database (fig. 2). A regression equation has been developed that relates total sediment yield in tons per year to the watershed area, in square miles based on these additional studies.

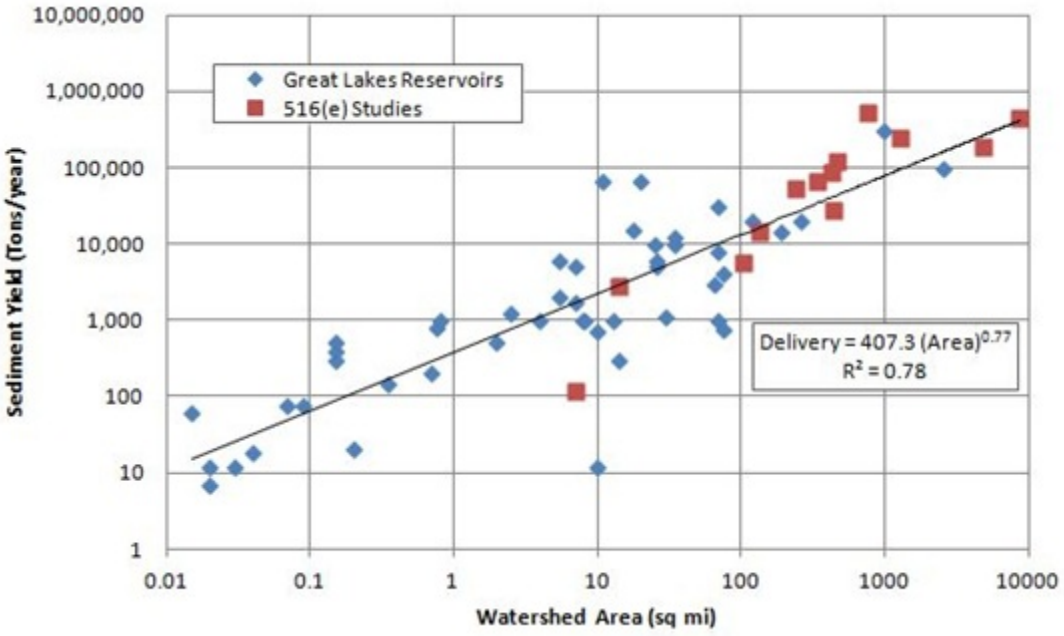

Figure 2. Great Lakes sediment yield regression curve

Stream Corridor Sources of Suspended Sediment and Phosphorus from an Agricultural Tributary to the Great Lakes

Faith A. Fitzpatrick, Research Hydrologist, USGS, Middleton, WI, fafitzpa@usgs.gov;
James D. Blount, Physical Scientist, U.S. Geological Survey, Middleton, WI, jblount@usgs.gov;
Leah E. Kammel, Hydrologist, U.S. Geological Survey, Middleton, WI, lkammel@usgs.gov;
Sarah A. Francart, Watershed Planner/GIS Specialist, Outagamie County LCD, Appleton, WI, sarah.francart@outagamie.org;
Allen C. Gellis, Research Hydrologist, USGS, Baltimore, MD, agellis@usgs.gov;
Barbara C. Eikenberry, Research Hydrologist, USGS, Middleton, WI, beikenberry@usgs.gov

Abstract

Fine-grained sediment and phosphorous are major contaminants in the Great Lakes and their tributaries. Plum Creek, Wisconsin (92 km^2), a tributary to the Lower Fox River, has a Total Maximum Daily Load (TMDL) requiring reductions of suspended sediment and phosphorus loading by 70% and 77%, respectively. In 2016-18, an integrated sediment fingerprinting and stream corridor-based sediment budget study was conducted to help quantify upland and stream corridor sources of suspended sediment and phosphorus at a loads monitoring station on Plum Creek. Sediment fingerprinting results indicated that the proportion of upland and stream corridor sources of suspended sediment in Plum Creek varied by season and the amount of runoff; however, bank and gully erosion accounted for 51% and 24% of the suspended sediment annual load, with one or both sources present in all seasons. The next most common source was roadside ditches (11%), which was also present in all seasons. Cropland and woodland sources accounted for small proportions of the suspended sediment, with cropland mainly in summer and woodland in winter, spring, and summer. Relative source proportions for sediment-bound phosphorus were similar to suspended sediment but made up less of the overall loading because on average 27% of the phosphorus load resides in the dissolved phase. Soft fine-grained streambed sediment had source signatures of mainly bank, gully, and ditches (ordered by decreasing proportion). Results from the field-based rapid geomorphic assessment supported the sediment fingerprinting results and in general showed that the amount of bank erosion increases in a downstream direction. The high proportion of sources from banks and gullies is due, in part, to a 20-km long, deeply entrenched valley and steep eroding bluffs between the majority of cropland and the Plum Creek water monitoring station.

Introduction

Plum Creek (92 km$^{2)}$ is a tributary to the Lower Fox River, Wisconsin and is located about 16 km upstream of a Lake Michigan Area of Concern (AOC) for the Lower Green Bay and Fox River (Figure 1). The Lower Green Bay and Fox River AOC is a priority area for the Great Lakes Restoration Initiative (EPA 2016). The AOC is working toward removal of beneficial use impairments for eutrophication and undesirable algae through reductions in total suspended solids (TSS) and total phosphorus (TP) loads from the top seven highest loading tributaries, including Plum Creek (WDNR 1988; 2018a). Plum Creek has almost 32 km of stream length on the Wisconsin state impaired waters list for TP and TSS (WDNR 2018b).

Plum Creek is part of the Total Maximum Daily Load (TMDL) and watershed management plan for TSS and TP in the Lower Fox River Basin (EPA 1999; Cadmus 2012). Based on the Soil and Water Assessment Tool (SWAT) modeling results, Plum Creek was estimated to produce 5,500 metric tons/yr of TSS and 14,300 kg/yr of TP, of which 95 and 94%, respectively, were contributed from agricultural land (Cadmus 2012). Agricultural land makes up 76% of the watershed area. The TMDL goals for Plum Creek are to reduce the TSS and TP loading by 70% and 77%, respectively. Sources of TSS and TP from bank erosion were not specified in the SWAT model (Cadmus 2012). However, streambank inventories of Plum Creek

in 2014 by the Outagamie Land Conservation Department indicated that 39 of the 69 km of channels inventoried had actively eroding banks, and that these banks could be contributing 45% of the annual TSS load to the stream (Francart 2017).

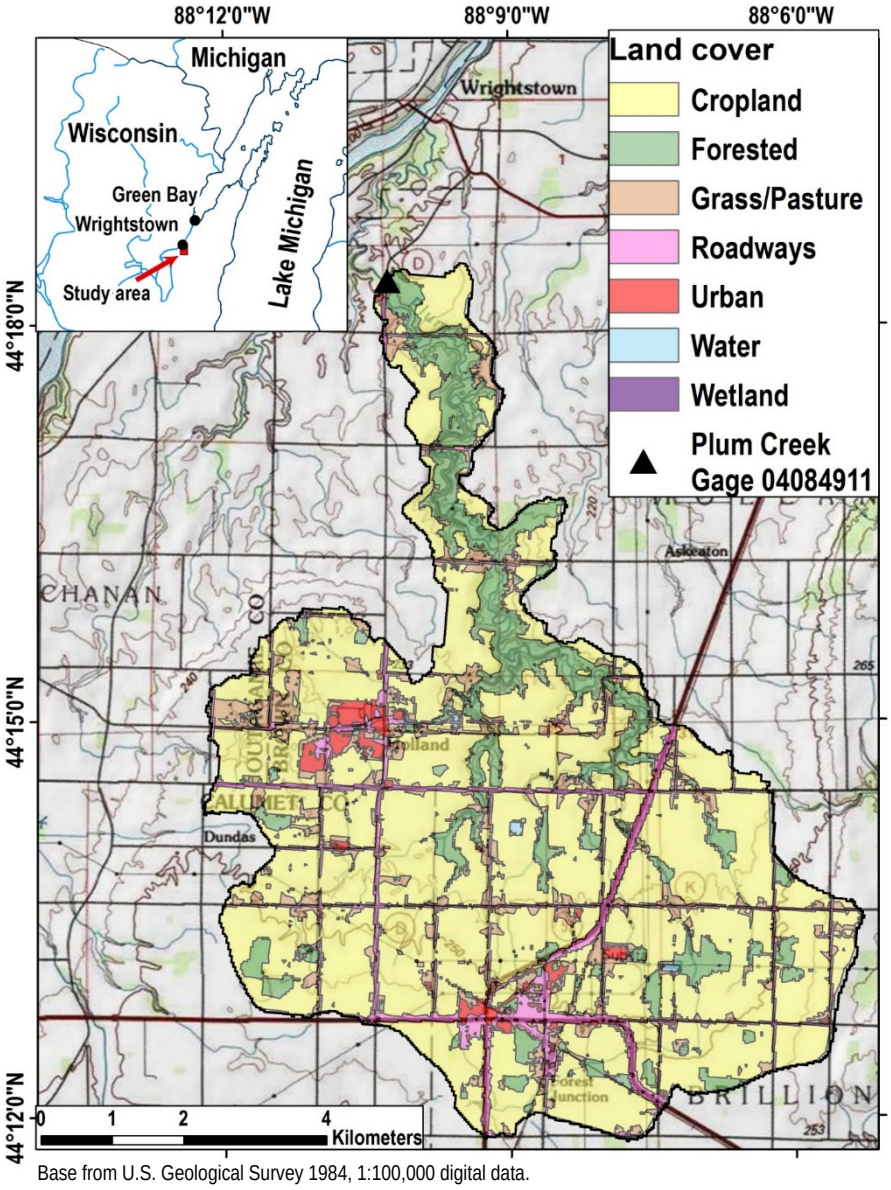

Figure 1. Location of Plum Creek study area with major land-cover categories (Homer et al. 2015)

An integrated sediment fingerprinting and stream corridor-based sediment budget study was conducted by the U.S. Geological Survey (USGS), the Wisconsin Department of Natural Resources (WDNR), and Outagamie County for Plum Creek in 2016-18 to help quantify the proportions of the TSS and TP loadings originating from stream and riparian corridor sources. The study hypothesis was that banks and possibly gullies along the stream corridor are potentially significant sources of TSS and TP. The field-based stream corridor geomorphic assessment included banks and ravines along perennial and ephemeral channels. Integration of sediment budget and source apportionment tools developed by Gellis et al. (2016) for the TMDL process helped to describe spatial and temporal patterns in sources for TSS and TP throughout the watershed compared to loads measured at a water-quality monitoring station run by the USGS and

University of Wisconsin-Green Bay (UW-GB). This report describes the major findings from the study for suspended sediment and soft bed sediment sampled from Plum Creek in 2016-18.

Study Area

Plum Creek is an eastern tributary of the lower Fox River in Outagamie County (fig 1). The watershed is in the Eastern Ridges and Lowland Physiographic Province (Martin 1965). Soils are generally silt loams, silty clay, and clay loams (Soil Survey Staff NRCS 2017). Topography is steep, and the entrenched valley is typical for Great Lakes tributaries where valleys intersect steep zones of post-glacial paleo shorelines (Fitzpatrick et al. 2006). The river enters the lower Fox River upstream of the community of Wrightstown and below Rapide Croche Dam. The drainage area upstream of the USGS streamgage on Plum Creek (04084911) is 54.3 km^2.

Land cover in Plum Creek is mainly cropland (66%), with smaller percentages of woodland (10%), grassland/pasture (10%), roads (7%), wetland (4%) and urban land (2%) (Homer et al. 2015) (Figure 1). Much of the woodland is located adjacent to Plum Creek and its tributaries, along steeply sloping valley sides. Much of the grassland is made up of rights-of-way along roads and grassy areas adjacent to subdivision or rural residential lots. There are few pastures in the watershed.

Baseline monitoring data for streamflow, TSS, TP, and dissolved phosphorus (P) have been collected by the USGS and UW-GB at the Plum Creek streamgage (USGS #04084911) since 2011 (U.S. Geological Survey, 2019). The watershed above the streamgage is 54.3 km^2 or 58.9% of the total watershed. Annual loads of TSS ranged from 3,183 metric tons (MT) in 2012 to 13,491 MT in 2017, with an annual average of 6,040 MT. Annual loads of TP ranged from 6,122 kg in 2012 to 18,691 kg in 2014, with an annual average of 12,622 kg (U.S. Geological Survey, 2019).

Methods

Integrated techniques helped to describe sources, transport, and sinks of TSS and TP throughout the watershed at a range of spatial and temporal scales. Field-based rapid geomorphic assessments (Fitzpatrick et al. 2016) were focused on field measurements of streambank erosion, gully erosion, and soft streambed sediment deposition that were used in the stream corridor sediment budget calculations. Sediment fingerprinting techniques and tools described in Gellis et al. (2016) and Gorman Sanisaca et al. (2017) were used to apportion suspended sediment and soft sediment to specific sources. Results were compared to TSS and TP loads from streamflow monitored at Plum Creek streamgage 04084911 (U.S. Geological Survey 2018).

Field-Based Rapid Geomorphic Assessments

The USGS conducted field-based rapid geomorphic assessments in Spring 2017, which included measurements of streambank and gully erosion and soft streambed sediment deposition. Data collected during the assessments were used in stream corridor sediment budget calculations. Assessments were done at 30 reaches using methods described in Fitzpatrick et al. (2016) and were in part built off the 2014 bank erosion inventory done by Outagamie County (Outagamie County Land Conservation Department 2017). Reaches for rapid geomorphic assessments were selected to represent a range of slope, valley types, stream order, and channel sizes along the stream network longitudinal continuum. The stream network and its physical characteristics were described using an overlay of WDNR streamlines and Lidar-based 3-m digital elevation model data (USGS et al., 2010). The reaches included ephemeral and perennial channels.

Annual volumes of bank erosion were estimated using field measurements of the length and height of eroding banks. Annual lateral recession rates for the eroding banks were determined from categorical rates based on indicators assembled by the Wisconsin Natural Resources Conservation Service (2015). A volume weight conversion of 1,362 kg/m^3 was used for banks and bluffs with heights greater than 1.5 m

because they were typically made up of glacial deposits (silt loams, silty clay, clay loams) (Wisconsin NRCS, 2015). For banks less than 1.5 m high and for all gullies a volume-weight conversion of 1,121 kg/m^3 was used because they were typically composed of less dense alluvium.

Estimates of annual volumes of gully erosion were based on the Ephemeral Gully Erosion Estimator for permanent gullies (Natural Resources Conservation Service 2006). Gullies included in the assessments were developed in ravines along the steep slopes of the entrenched valley sides. The ravines had punctuated sections of gully or channel erosion at knickpoints with old channels covered with sediment in between.

Soft bed sediment volumes were estimated from field measurements of length, width, and average thickness of soft sediment deposits. Sediment deposit thickness was measured using a meter stick and recording the depth of penetration. A conservative estimate of a volume-weight conversion of 800 kg/m^3 was used because of the high-water content, based on similar soft sediment samples from the silt-dominated Fever River in southwest Wisconsin (Peppler and Fitzpatrick 2018).

Sediment Source Apportionment

Source and Target Site Selection and Sampling: Sites selected for source and target sediment sampling included uplands (cropland, woodland, and ditch), stream corridors (streambanks and gullies), and streams (suspended and soft fine-grained streambed sediment). Sites designated for upland sediment source sampling were identified through geographic information system (GIS) analyses of available land use (or land cover) (Homer et al. 2015). A stratified random sampling approach was used to select 15 sites per land use type with greater than 10% areal coverage. The three major upland land cover categories included (1) cropland, (2) grassy ditches between roads and fields, and (3) woodlands. Pasture was not included because of the small number of pastures in this watershed. Similarly, urban was not included because of its low percentage in the watershed. The GIS site-selection procedure was run at least twice to select potential alternative sites in case of limited access to some sites on private land, physical or safety impediments, and land-use changes that occurred after mapping, especially if crops were in rotation with pastures. Soil samples were collected from the top 2 cm of the soil surface with a plastic hand shovel at 30 points spaced 10 m in a rectangular grid pattern. The number of transects and transect length were adjusted to stay within the areal shape of the sampled land use. The point samples, consisting of about 2 liters volume, were composited into a zip seal plastic bag. Field replicates were collected for one site in each land use category with a 1-m offset from the original sampling points.

Two stream corridor sources, banks and gullies, were included in the apportionment. Stream reaches sampled for bank and gully erosion sources were from the rapid geomorphic assessments with additional sites from Outagamie County's bank erosion inventory as needed to fill in gaps along the stream corridor. Actively eroding gullies were sampled in a similar fashion to upland soil samples, with the top 2 cm of bare eroding sediment sampled with a plastic hand shovel. The transect or grid size was adjusted to fit the eroding gully dimensions, and sampling points included both the actively eroding bottom and sides of a gully. An optimum of 30 points were sampled and composited into one bag per site. Representative samples of eroding banks were collected from the surficial 2 cm of exposed sediment from the bottom to the top of the bank face. Three to five points along each of three to six transects were sampled, depending on the height and length of the eroding bank, with a total of 15-30-point samples composited into one 4-liter plastic bag. If banks were eroding on both sides of the channel, then samples from an equal number of points were collected on both sides and composited. Field replicates were collected by side-by-side sampling of the same points.

Target samples used to source sediment included soft, fine-grained streambed sediment and suspended sediment. Soft bed sediment was sampled from the rapid geomorphic assessment reaches and was defined as having a high-water content that was not able to support the weight of a person (i.e. one would sink into the sediment when stepping in it). The sediment was collected from 15 points in one or more inundated depositional areas per reach and composited into a 1-L plastic jar. The point samples were collected with an open-ended plastic or Teflon tube and plastic spatula. Field replicates were collected by side-by-side sampling of the same points.

Suspended sediment was collected at the USGS Plum Creek streamgage from October 2016 through February 2018 at roughly one-month intervals (Table 1). An in situ suspended sediment sampler with two stacked sampling tubes was deployed downstream of the bridge crossing at the gage during ice-free months (Phillips et al. 2000; Banks et al. 2010). The sampler was left in over the winter of 2016-2017 but was lost during thick ice movement and breakup. A grab sample was collected on March 8, 2017 to catch a large runoff event associated with ice breakup. A new sampler was reinstalled in April 2017 at the same location as the lost sampler. In August 2017 a second sampler was installed upstream of the bridge crossing. The recovery from the two samplers in September and October 2017 was small and required compositing sediment from both the upstream and downstream samplers. In November 2017 each of the samplers had enough sediment for submitting separate samples for quality assurance checks. Two rain/snowmelt events in January 2018 caused water and sediment to flow over ice. Subsequent rapid drops in temperature caused sediment-laden water to freeze over the top of existing ice. The ice layers, with sediment still in suspension, were collected and thawed at the lab. The sediment melted out of the ice was processed in the same manner as the other in situ suspended sediment samples. The contents of the samplers were emptied into plastic buckets and returned to the USGS Upper Midwest Water Science Center laboratory in Middleton, Wisconsin.

Table 1. In situ suspended sediment samples and associated suspended sediment phosphorus (SS_TP) concentrations collected at the Plum Creek streamgage, October 2016-February 2018

Sample identifier	Start date	End date	Representative period	Type of sample	SS_TP (mg/kg)
--	--	--	10/1 – 10/25/2016	(Prior to project start)	--
--	--	--	10/26 – 11/21/2016	(Prior to project start)	--
03	11/22/2016	12/5/2016	11/22 – 12/25/2016	In situ passive collector	1,768
--	--	--	12/26 – 1/26/2017	River frozen	--
--	--	--	1/27 – 2/27/2017	River frozen	--
04	3/8/2017	3/8/2017	2/28 – 3/26/2017	Grab water sample late winter	1,235
--	--	--	3/27 – 4/25/2017	Sampler destroyed by ice/flood	--
06	4/26/2017	5/25/2017	4/26 – 5/24/2017	In situ passive collector	1,351
07	5/25/2017	6/26/2017	5/25 – 6/26/2017	In situ passive collector	1,084
08	6/26/2017	7/25/2017	6/26 – 7/25/2017	In situ passive collector	1,058
--	7/26/2017	8/23/2017	7/26 – 8/23/2017	Sample too small to analyze	--
09	8/24/2017	9/28/2017	8/24 – 9/23/2017	In situ passive collector[1]	1,662
10	9/28/2017	10/27/2018	9/28 – 10/27/2017	In situ passive collector[1]	1,541
11	10/28/2017	12/7/2017	10/28 – 12/7/2017	In situ passive collector	2,096
11-QA	10/28/2017	12/7/2017	10/28 – 12/7/2017	In situ passive collector[2]	2,061
--	12/8/2017	1/10/2018	12/8 – 1/10/2018	Sample too small to analyze	--
12	2/7/2018	2/7/2018[3]	1/11 – 1/27/2018[3]	Ice layers collected	3,955

[1]Composite of two sets of samplers upstream and downstream of bridge.
[2]Sampler located upstream of bridge only.
[3]Plum Creek streamgage not operating, timing of events based on partial record from nearby East River streamgage (USGS station ID 04085108) (U.S. Geological Survey, 2019)

All sediment samples except those from the in situ suspended sediment sampler were stored frozen until subsampling occurred. The water-sediment mixture from the in situ suspended sediment sampler was allowed to settle in a refrigerator at about 4° C. Clear water from the bucket was decanted until a sediment-rich slurry of generally less than 0.5 L was left. The slurry was transferred to a plastic wide mouth jar and frozen until subsampling occurred. Frozen samples were thawed prior to being subsampled. The sediment was mixed thoroughly with a plastic spatula and spread evenly into a 11- x 17- x 3-inch glass dish. The sediment was divided into 16 equal sections using a plastic knife. A random number generator was used to select subareas for processing. The remaining unsieved portion of a sample was returned to its original container and refrozen. The subsample was wet-sieved through a 63-micron polyester sieve using de-ionized water and all-plastic sieve frame and equipment using methods from Shelton and Capel (1994) and ASTM D3977-97 Method C for wet-sieving filtration (ASTM, 2002). Both the <63 and >63-micron fractions were dried at 60 degrees Celsius for 24-48 hours or until completely

dry. After drying, the <63 and >63-micron fractions were weighed to the nearest 0.1 g. If needed, the dried sample was lightly ground with a ceramic mortar and pestle. The <63-micron sieved dry sediment was placed in plastic vial(s) for shipping to analytical laboratories. The >63-micron fraction was retained at the USGS. All sample collection and subsampling equipment was washed with phosphate-free liquid detergent, soaked with 5% HCl, and rinsed with deionized water between samples.

Laboratory Analyses: Sediment samples were analyzed for a suite of 51 major and trace elements, particle size, and organic matter (loss on ignition) (Table 2). The Wisconsin State Laboratory of Hygiene used the ESS INO Method 420.0 Thermo Finnigan ELEMENT2 High Resolution ICP-MS (EPA Method 200.8) method and the milestone microwave digestion system (ESS INO IOP 550.0) for elemental analyses (Wisconsin State Laboratory of Hygiene 2016a; 2016b). (Any use of trade, firm, or product names is for descriptive purposes only and does not imply endorsement by the U.S. Government). The analyses included phosphorus in sediment. The elemental data are available on the Wisconsin State Surface Water Integrated Monitoring System (https://dnr.wi.gov/topic/surfacewater/swims/). The elemental analysis includes a near total digestion using three acids.

Particle size and organic matter determinations were completed at the U.S. Geological Survey Cascades Laboratory in Vancouver, Wash. for the less than 63-micron fraction. Organic matter content was analyzed using the I-5753 method for loss-on-ignition. Particle size determinations were completed with a SediGraph 5120 down to 1 micron. Data are available upon request from the U.S. Geological Survey Upper Midwest Science Center, Middleton, WI.

Table 2. Elemental analyses of Plum Creek source and target samples

Ag	Be	Co	Eu	Hg	Lu	Nb	Pd	S	Sn	U	Zn
Al	Bi	Cr	Fe	Ho	Mg	Nd	Pr	Sb	Sr	V	Zr
As	Ca	Cs	Ga	K	Mn	Ni	Pt	Sc	Th	W	
B	Cd	Cu	Gd	La	Mo	P	Rb	Se	Ti	Y	
Ba	Ce	Dy	Hf	Li	Na	Pb	Rh	Sm	Tl	Yb	

Source Apportionment: The Sediment Source Assessment Tool (Sed_SAT) (Gellis et al. 2016; Gorman Sanisaca et al. 2017) was used to apportion the relative contributions of five possible sources of fine-grained suspended and soft bed sediment including croplands, woodlands, roadside ditches, eroding gullies, and banks to the target samples of suspended sediment and soft streambed sediment. Sed_SAT is an automated package of statistical procedures that uses patterns in trace element concentrations to distinguish between the sediment sources. Sed_SAT uses a five-step procedure to apportion sediment sources for each target suspended or bed sample: (1) removal of outlier source samples, (2) application of particle size and organic content corrections to the source data, (3) a bracket test to test conservativeness of the tracer, (4) stepwise discriminant function analysis (DFA) to determine the tracers that best discriminate between the source types, and (5) an "unmixing model" that uses the discriminant tracers and their weighting factors as determined by DFA to determine the percent contribution of each source to the target sediment sample. The default settings for the statistical tests in Sed_SAT were applied to the Plum Creek apportionment.

While the suspended sediment target samples were collected at the watershed outlet near the USGS streamgage, the bed sediment target samples were collected throughout the watershed to determine if sediment sources varied spatially. Source samples from throughout the entire Plum Creek watershed were used in Sed_SAT to determine sediment source contributions for all target samples, meaning that for most of the bed sediment target samples the source samples were not all located within the contributing area of the sample. Source samples are assumed to be representative of the land use areas for the whole watershed, with large enough sample sizes of n=15 for cropland, ditch, and bank source groups and n=16 for woodland and gully source groups to provide robust sampling of source areas in the watershed to account for geochemical variability within each source group.

Three tests are used to assess uncertainty in the sediment fingerprinting results for each target sediment sample: (1) a confusion matrix of the DFA results, (2) a source verification test (SVT) on the unmixing model, and (3) a Monte Carlo leave-one-out cross validation. The confusion matrix demonstrates how well the final set of discriminant tracers determined by DFA distinguishes between the source groups by summarizing the percentage of source samples classified correctly to their source group compared to the total number of source samples in the group. The source verification test (SVT) is a measure of how well the final set of tracers and their weighting factors used in the unmixing model discriminates the sources. In the SVT, each of the source samples are treated as target samples and run through the unmixing model, providing a qualitative determination of how successfully the unmixing model apportions sediment to the correct sources. The Monte Carlo leave-one-out cross validation quantifies the sensitivity of the unmixing model to the removal of samples (Gellis et al. 2016). The Monte Carlo simulation was run 1,000 times, with a random sample removed from each source group for each iteration before the unmixing model was run (Gorman Sanisaca et al. 2017).

The source apportionments for the target suspended sediment samples were applied to the streamgage TSS for water year (WY) 2017 (October 1, 2016 to September 30, 2017) (U.S. Geological Survey, 2018). Monthly suspended sediment phosphorus (SS_TP) loads were calculated by multiplying the SS_TP concentrations of the in situ suspended sediment samples by the monthly TSS load. An average of the WY 2017 SS_TP concentrations was used for calculating the monthly SS_TP loads for months with missing fingerprints. Results for TSS loads from October 2017 forward were not available yet at the time of this writing (April 2019).

Stream Corridor Budgets of Erosion and Deposition

For each segment in the WDNR streamlines that made up the Plum Creek network, stream order (Strahler 1957) and slope category were identified (Table 3). Slope categories were adopted from similar geomorphic assessments done on Lake Superior tributaries that reflect potential channel bedform types (Fitzpatrick et al. 2006; 2016; Montgomery and Buffington 1997). Segments with a stream order of 1 made up most of the network with most having slopes of 0.3-1.0 percent, typical for lowland settings of post-glacial streams in the Great Lakes region. The cumulative length of streams in order 4 was larger than order 3, reflecting the long-neck funnel shape of the watershed (Figure 1).

Table 3. Number of stream segments (gray-shaded) and total stream lengths categorized by stream order and slope for Plum Creek (km, kilometer; <, less than; >, greater than)

Slope category (percent)	Stream order 1	Stream order 2	Stream order 3	Stream order 4	Total length (km)
<0.3	5	4	5	20	25.3
0.3-1.0	21	18	7	4	51.9
>1.0-2.0	9	0	1	0	9.9
>2.0	3	0	0	0	0.7
Total length (km)	42.5	20.4	10.7	14.2	87.8

Reach-scale assessment data for annual gully and bank erosion, and soft bed sediment volumes were applied to WDNR stream segments with similar slopes, valley entrenchment, stream order, and riparian vegetation in a GIS. Before the application of reach data to the segment lengths, the sediment TP concentration, included in the trace elements sample analysis, was applied to the bank and bed amounts. After the initial automatic application, the assignments were checked and adjusted if needed by hand in the GIS after further investigation with overlays of digital elevation model data for valley setting and aerial photographs for riparian vegetation, and other qualitative data and photos collected during Outagamie County's bank inventory or USGS reconnaissance. If two reaches were in the same segment category and no other differences were observable on aerial photographs, averages of the SS_TP concentrations, reach bank erosion rates, and fine sediment volume were used. The amounts of annual bank erosion and soft bed sediment volume for each segment were summed to get an estimate of the

entire stream network contribution of eroded and stored sediment and sediment-bound phosphorus in Plum Creek upstream of the USGS streamgage.

Sources of Sediment and Sediment Related Phosphorus

A multiple-lines of evidence approach was used to determine the relative amounts of potential sources of TSS and TP in Plum Creek. This approach used available and new data with emphasis on quantifying stream corridor sources.

Sediment TP concentrations in source and target samples generally ranged from about 500 to 2,000 mg/kg (Figure 2). These concentrations, which are from near total sample digestions, cannot be directly compared to typical soil P tests done by farmers for nutrient management plans, but give an idea of the relative amount of sediment TP spanning the watershed pathways from uplands and stream corridors to stream channels. Bioavailability and chemical mobilization of the TP likely varies among the sources and is the topic of an ongoing related study in Plum Creek. Highest sediment TP concentrations were from ditches and woodlands and lowest concentrations were from banks and gullies. Some of the ditches sampled were erosional while others were depositional. If depositional, the ditches likely had sediment from nearby adjoining fields as well as roads. Many of the woodland samples were from the valley bottom of Plum Creek, which has a high potential for overbank sedimentation and accumulation of leaf litter. Suspended sediment had the highest concentrations of sediment TP, suggesting that the stream sediment is becoming enriched with phosphorus as it is transported in streams. The highest sediment TP concentration, near 4,000 mg/kg, was from suspended sediment collected from an ice sample (Table 1). The suspended sediment samples were over 80% fines (silt- and clay-sized fractions) except from the ice sample which was closer to 50%. The soft bed sediment had the lowest percent fines (Figure 2).

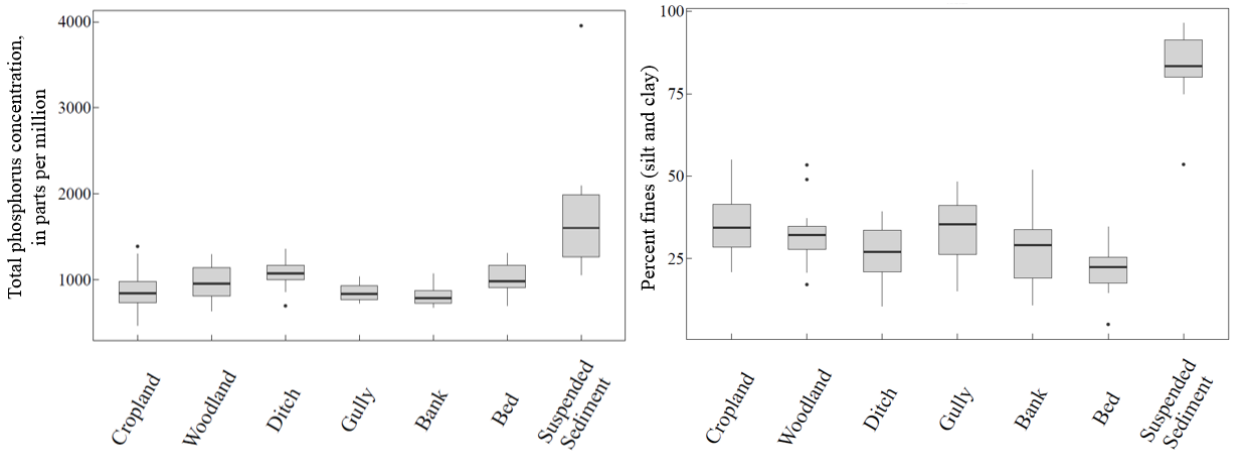

Figure 2. Total phosphorus concentrations and percent fines (silt and clay) in sediment samples from different source locations in the Plum Creek watershed. All samples were sieved to less than 63 microns prior to elemental analysis.

The sediment fingerprinting results showed that source apportionment varied among the target samples, with banks serving as the largest source of sediment on average for both suspended sediment (44%) and for bed sediment (80%) (Table 4). Suspended sediment showed substantial contributions on average from gullies (25%) and ditches (22%), with smaller proportions from woodland (7%) and cropland (2%). The source contribution to soft bed sediment was dominated by banks as well, with small average contributions from gullies (10%), and 5% or less from ditches, cropland, and woodland. Bed sediment sample 81 was the only target sample to not be corrected for organic content because the loss on ignition (LOI) analysis was not available for the sample. However, this difference did not have a negative impact on the relative error and the sediment fingerprinting results are comparable to other nearby bed sediment target samples that were corrected.

Table 4. Apportionment by relative source area and discriminant tracers (ordered by decreasing weighting factor) of suspended sediment and soft bed in Plum Creek, 2017

Sam-ple	Sample type	Cropland	Woodland	Ditch	Gully	Bank	Relative Error	Discriminant tracers
03	Suspended	0	9	15	24	52	0.534	Cr, U, Cd, Ga, Zn, Li, Mo, Sc, Ni, Mg, Ba, Ce, Nb, Mn, Fe, Ti, Na
04	Suspended	0	12	13	54	21	1.169	Cr, U, Ga, Cd, Co, Zn, Dy, Mo, Yb, Y, Ni, Pd, Sb, P, La, Ti
06	Suspended	0	0	0	0	100	0.391	Ga, Cr, U, Zn, Ho, Mo, Li, Pd, Ni, Mn, Fe, Nd, P
07	Suspended	7	9	12	29	43	0.266	Co, U, Cr, Zn, Ga, Pd, Ni, P, Fe, Pt, La, Sr, Ti
08	Suspended	15	8	13	0	63	0.228	Ga, U, Zn, Cr, Mo, Li, Ni, Pd, Y, P, Fe, Mn, Nd, Sr
09	Suspended	0	0	25	0	75	1.633	Cr, Ga, Co, U, Cd, Zn, Li, Pd, Mo, Ni, Ce, Fe, Mg
10	Suspended	0	0	19	0	81	0.413	Cr, Ga, U, Cd, Co, Zn, Li, Pd, Mo, Ni, Ce, Fe, Mg
11	Suspended	0	0	26	74	0	1.459	Cr, Ga, Co, U, Cd, Zn, Mo, Li, Ni, Mg, Fe, Pt, Ce
11Q	Suspended	0	1	45	53	0	1.403	Cr, Ga, Co, U, Cd, Zn, Mo, Li, Mi, Mg, Fe, Pt, Ce
12	Suspended	0	34	54	12	0	0.824	Cr, Ga, Co, U, Cd, Zn, Ni, Pd, Nb, Fe, Ag, La, Mg, Ti
76	Bed	0	0	5	16	78	0.063	Ga, Cr, V, Co, Zn, U, Li, Cd, Sc, Mg, Mo, Ba, Na, Nb, Ti, Fe, Th
76Q	Bed	2	0	4	27	68	0.168	Ga, Cr, Co, U, Zn, Mg, Li, Na, Sc, Mo, Ba, Nb, Ti, Fe, Th
79	Bed	0	0	0	14	86	0.430	Cd, U, Co, V, Yb, Mo, Zn, Ga, Li, P, Ni, Mn, Nb, Th, Ce, Sr
81	Bed	0	0	2	4	94	0.126	Cr, Zn, Co, Cd, Mg, Ni, Pd, U, Fe, Sm
83	Bed	0	0	0	0	100	0.488	Ho, V, U, Co, Zn, Ga, Mo, Cd, Sc, Li Ni, P Th, Pt, Nd, Ag
86	Bed	0	0	0	0	100	0.336	Ho, V, Ga, U, Zn, Mo, Li, Pd, Ni, Fe, Mn, P, Pt, Nd
87	Bed	0	0	0	0	100	0.205	Ga, Cr, Zn, U, Mo, Ni, Pd, Mn, La, Fe
89	Bed	0	0	0	31	69	0.249	Ga, Cr, Co, U, Zn, Y, V, Cd, Pd, Ni, La, Fe
90	Bed	0	0	0	0	100	0.299	Ga, Cr, Zn, V, Cd, U, Mo, Ni, Pd, Fe, Nd
91	Bed	35	8	36	20	0	0.171	U, Co, Cd, V, Zn, Mo, Ga, Sc, Mg, Li, Fe, Ni, P
92	Bed	0	0	11	0	89	0.279	Cr, Ga, U, Zn, Ho, Li, Mo, Mg, Ni, Sc, Ba, Na, Nb, Fe, Mn, Ti

Of the 51 tracers included for sediment fingerprinting analysis, 31 tracers were found to be discriminant for one or more of the target samples (Table 4). Results of the stepwise DFA found that five tracers were discriminant for all suspended sediment target samples (Cr, Ga, Ni, U, Zn) and two tracers were discriminant for all bed sediment target samples (U, Zn). Chromium was the highest weighted discriminant tracer for most suspended sediment target samples, followed by gallium. The highest weighted discriminant tracers for bed sediment target samples were more varied, with gallium the most common. The number of tracers found to be discriminant from the DFA ranged from 10 to 17, providing strong differentiation between sediment source groups.

Results from the three tests for uncertainty in the Sed_SAT procedure give overall high confidence in the sediment fingerprinting results. The confusion matrix summary indicates the percentage of source samples correctly classified by the final set of tracers in the DFA. Woodland and ditches had 100% of the samples classified correctly for the suspended sediment tracers, with nearly all samples classified correctly for cropland (98%), gully (98%), and bank (93%) (Figure 3). Soft bed sediment had similar results (not shown). The high percentage of correctly classified source samples confirmed that the stepwise DFA was successful in selecting tracers that effectively discriminated among the five source groups.

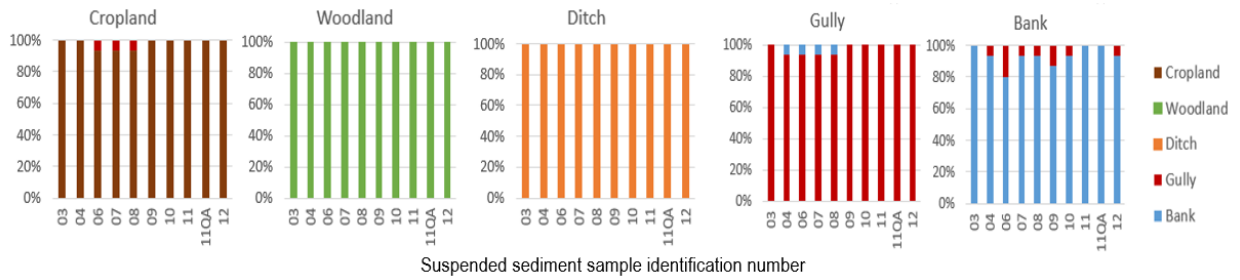

Figure 3. Summary of the confusion matrix results for target suspended sediment samples indicating the percentage of source samples correctly classified by the final set of tracers in the stepwise discriminant function analysis

The source verification test (SVT) also showed that the unmixing models were successful (Figure 4). The SVT test runs each source sample as a target sample and checks for possible misclassification as another source. The median percent contribution attributed to the correct source was greater than 75% for cropland, woodland, ditch, and banks, and was slightly lower at 67% for gullies. Most of the misclassified cropland samples were classified as woodland (9%) and most of the misclassified woodland samples were classified as cropland (10%). Ditches also showed some overlap with cropland and woodland sources, with an average of 15% of misclassified ditch samples classified as cropland and 9% classified as woodland. Gully source samples showed the greatest degree of misclassification by the unmixing model, with an average of 10% of samples classified as cropland, 12% classified as woodland, and 11% classified as bank. Most of the misclassified bank samples were classified as gully (15%). These overlaps are not unexpected among the upland sources because of the possibility that some of the land has changed land-use categories at some point in the past. Gullies physically extend from uplands to wooded slopes to banks, with the possibility of sediment coming from a mix of source categories.

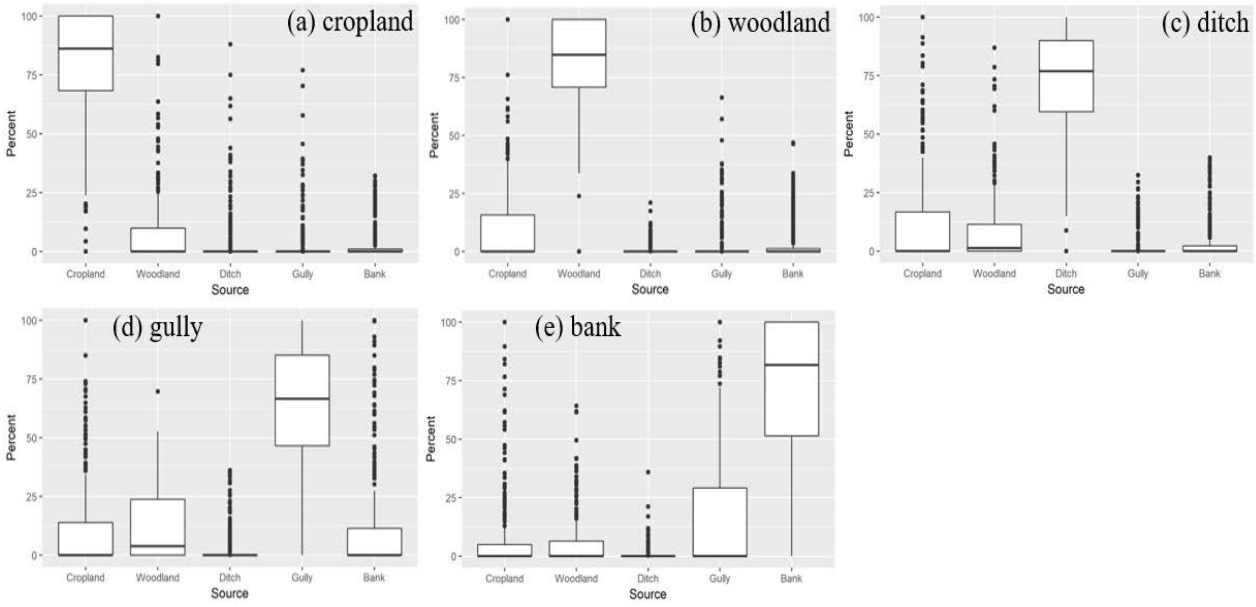

Figure 4. Source verification test results of source samples for all target sample Sed_SAT runs, (a) cropland (n=315), (b) woodland (n=336), (c) ditch (n=315), (d) gully (n=336), and (e) bank (n=315)

The Monte Carlo leave-one-out cross validation demonstrated that the unmixing models were robust and had low sensitivity to removal of individual samples for all 21 target samples except one suspended sediment sample ID 03 from December 2016. Amongst all source groups 20 of the 21 target samples had a standard deviation of the Monte Carlo iterations of less than 5%, with 8 of the target samples with standard deviations of less than 2%. Eleven of 21 target samples showed a difference of less than 10% between the unmixing model results and the maximum or minimum of any Monte Carlo iteration. The

gully and bank source apportionment results for suspended sediment sample 03 showed a high degree of variability in the Monte Carlo iterations, with gully contribution ranging from 0-53.5% (median=26.3%, standard deviation = 14.8%) and bank contribution ranging from 22-78% (median=50.0%, standard deviation=14.8%). The reasons for this sample having such high variability compared to other samples are unknown.

The results from the source apportionments for the monthly in situ suspended sediment samples applied to the Plum Creek streamgage TSS and SS_TP loads for WY 2017 (October 2016 to September 2017) are shown in Figure 5. Results for samples collected after October 2017 are shown as proportions only because the TSS loads were not yet available. The proportions of the five sources varied seasonally. The month of June had the largest loads for both TSS and SS_TP. Bank sources dominated in the months of May, June, July, September and October. Gully sources were present in March, June, November, and the January 2018 ice sample. Ditch sources were present in all months except May and seemed to increase through the fall and winter months of 2017-18. Woodland sources were present in March, June, July, and the January 2018 ice sample. The January 2018 ice sample had the highest proportions of ditch and woodland sources. The replicate sample from November indicated that the same sources were identified but that source proportions varied by about 20 percent. The proportion of the total TSS and SS_TP loads for WY 2017 without fingerprints was 22% and 25%, respectively, with the majority missing from the April sample when the river was still frozen. The March grab sample, and the May and July in-situ samples had similar loads, but different source proportions, further illustrating the need for capturing sediment during all seasons, including cold-season runoff events.

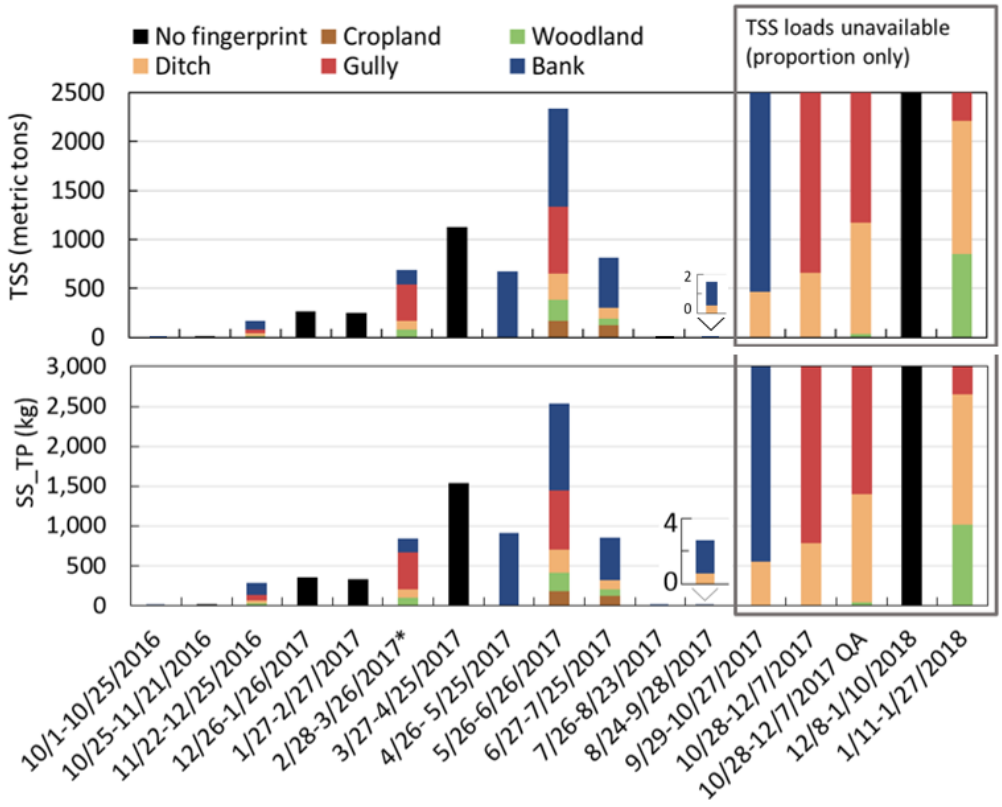

Figure 5. Temporal distribution of source apportionment to suspended sediment at the Plum Creek streamgage, October 2016 to January 2018.

The annual loads for WY 2017 for sediment and phosphorus were compared among the streamgage water monitoring, sediment fingerprinting, and stream corridor budget approaches (Figure 6). The water monitoring based TSS and TP loads at the streamgage from WY 2017 were similar to the average for 2011-17, which were 1.5 to 2.1 times the baseline TMDLs. The particulate portion of the water TP load was 73% for 2011-17 and 68% for WY 2017. In contrast, the calculated SS_TP load from the in-situ sediment

samples was 53% of the water TP load in WY 2017, even though the suspended sediment TP concentrations are from near total digestions. Applying the fingerprinting apportionments, the sources of TSS were predominantly from banks (51%), gullies (24%), and ditches (11%), with smaller amounts from woodland (8%) and cropland (6%). The relative proportions of sources of SS_TP (assuming SS_TP makes up 53% of the water TP load) are bank (28%), gully (13%), and ditch (6%), with smaller amounts from woodland (4%) and cropland (3%). Completion of WY 2018 load calculations and fingerprinting apportionments will give more perspective to the magnitude of potential sources during the fall and winter events with frozen ground conditions.

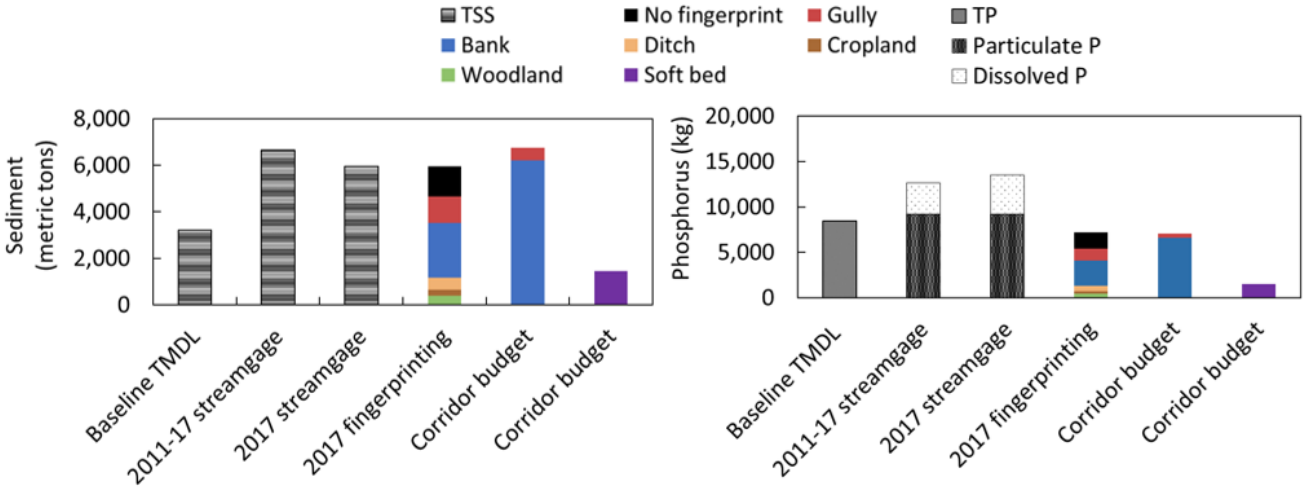

Figure 6. Comparison of annual loadings of sediment and phosphorus from streamgage monitoring, sediment fingerprinting, and stream corridor budgets for Plum Creek.

Sediment and phosphorus loads from the stream corridor budget for bank and gully erosion were within the same order of magnitude as the fingerprinting results (Figure 6). Annual loads of bank erosion from the stream corridor assessment were similar to the WY 2017 TSS loads and comprised 49% of the water TP loads. The bank erosion estimates include coarse-grained sediments that would contribute to an unknown, unmeasured bedload at the streamgage. Part of the eroded bank and gully sediment is also deposited in overbank areas, which was not measured as part of this study. The amount of fine-grained soft bed sediment stored in the stream network is 24% of the WY 2017 TSS and 11% of the water TP load, indicating that a relatively small amount of sediment and sediment-bound phosphorus is deposited in channels relative to the amount eroded.

The spatially distributed apportionment results from soft bed sediment samples throughout the stream network give further insights into the distribution of sources of TSS and SS_TP along the stream corridor (Figure 7). Banks and secondarily gullies were the main sources of soft bed sediment along the entrenched valley of the main stem. However, the most upstream bed sample, located on a first-order tributary upstream of the entrenched valley, had predominantly cropland, ditch, and gully sources. This observed shift in dominant sediment source is likely more representative of the western and southern parts of the watershed dominated by cropland and drained by first and second order stream channels upstream of the entrenched valley.

Bank erosion and soft bed sediment deposition, calculated by stream length, also supported the sediment fingerprinting results (Figure 8). The amount of bank erosion and soft sediment deposition was highly variable from reach to reach. Annual bank erosion loadings ranged from about 0 to 500 metric tons/km/yr for sediment and 0 to almost 400 kg/km/yr for sediment P. Soft sediment deposition ranged from about 0 to 105 metric tons/km for sediment and about 0 to 40 kg/km for sediment P. In general, sediment and sediment P loads would be expected to increase in a downstream direction because bank heights typically increase and slopes typically decrease with increasing stream size. However, for streams like Plum Creek that intersect multiple post glacial lake shorelines and lake plains, the valley width and slope can vary over short distances. The anomalously high loads from bank erosion were from reaches with active bluff erosion where the channel is impinging on a steep valley side. Chances for bluff erosion

remain high along the entire main stem of Plum Creek because the meander belt width is the same as the valley width. The large disparity between amounts of bank erosion and soft bed sediment storage are indications that most of the sediment coming from upland and bank erosion is transported downstream.

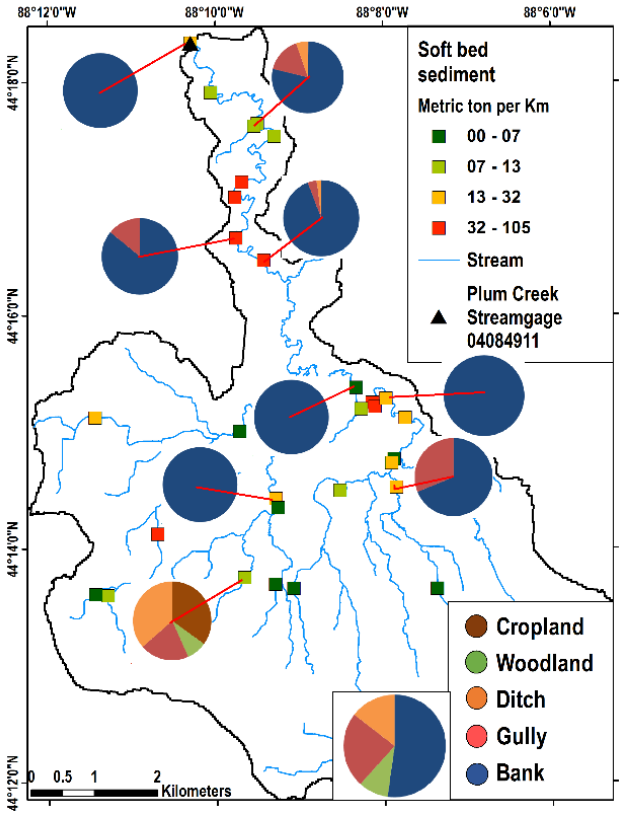

Figure 7. Spatial distribution of source apportionment to soft streambed sediment in Plum Creek.

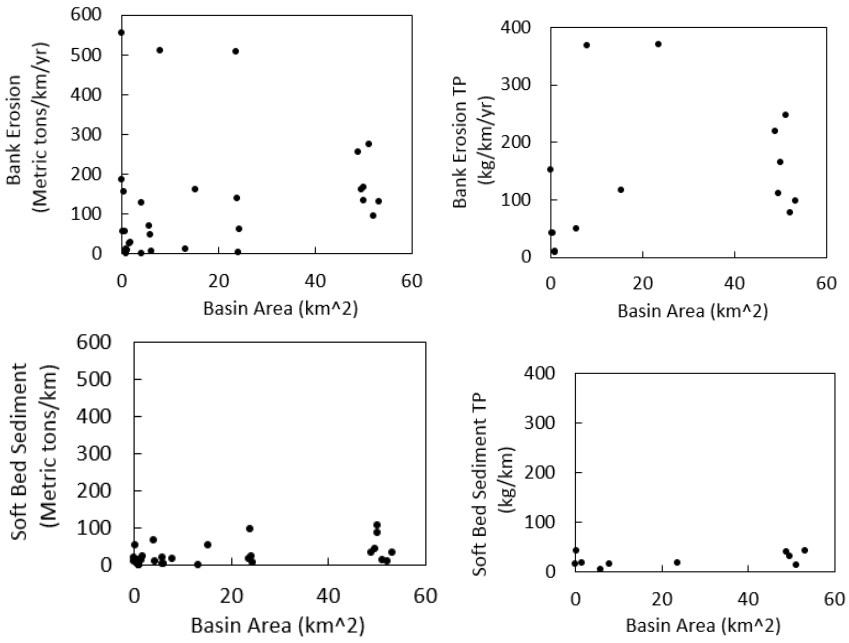

Figure 8. Reach-based bank erosion loading and fine sediment deposition for Plum Creek.

Summary and Conclusions

An integrated sediment fingerprinting and stream-corridor budget approach was helpful for understanding the seasonal and spatial distributions of sources of suspended sediment and sediment-related phosphorus in Plum Creek. The streamgage monitoring of TSS, TP, and dissolved P made it possible to quantify, on a monthly basis, the highly varying distribution of sources of suspended sediment and sediment-bound P. The fingerprinting technique was successful at discriminating between bank, gully, ditch, cropland, and woodland sources. Stream corridor budget estimates of bank and gully erosion supported the sediment fingerprinting results. Annual sediment-budgeted calculated loads of bank and gully erosion were similar to the WY 2017 TSS load and about 52% of the water TP load. The proportion of cropland source of TSS was low (6%), likely because of Plum Creek's geomorphic setting with a long-neck funnel-shaped watershed and the preponderance of bank and gully erosion in the 18-km stretch of main stem in the lower half of the watershed. In addition, cropland-derived sediment entering roadside ditches and mixing with road-derived sediment may form the unique ditch source signature. The fingerprinting-derived contribution of bank and gully erosion was potentially 41% of the water TP load at the streamgage. The proportions of bank and gully sources are likely different for cold season runoff events based on a few, difficult to collect, winter samples. The relatively low amount of soft bed sediment stored in the channels, about 24% of the annual load TSS and 11% of the annual load of TP, are an indication that most of the fine-grained sediment eroded from the watershed is transported past the streamgage. The results from this study indicate that upland and stream corridor conservation techniques are needed for reducing sediment and runoff in accordance with TMDL goals for stream TSS and TP reductions. Conservation techniques to reduce TP likely will differ for dissolved and particulate portions, and cold-season runoff events likely will require targeted sampling. Finally, additional study is required to better understand instream interactions of particulate and dissolved P phases.

References

American Society for Testing and Materials (ASTM). 2002. D3977-97, Standard Test Methods for Determining Sediment Concentration Samples, Method C, online at http://www.astm.org/cgi-bin/SoftCart.exe/DATABASE.CART/REDLINE_PAGES/D3977.htm?E+mystore.

Banks, W.S.L., Gellis, A.C., Noe, G. 2010. "Sources of fine-grained suspended sediment in Mill Stream Branch watershed, Corsica River basin, a tributary to the Chesapeake Bay, Maryland, 2009," Proc. 2nd Meeting of the Joint Federal Interagency Conference, Las Vegas, NV.

Cadmus. 2012. Total maximum daily load and watershed management plan for total phosphorus and total suspended solids in the lower Fox River Basin and Lower Green Bay. The Cadmus Group report.

Fitzpatrick, F.A., Peppler, M.C., DePhilip, M.M., and Lee, K.E. 2006. Geomorphic characteristics of Duluth-area streams. U.S. Geological Survey Scientific Investigations Report 2006-5029.

Fitzpatrick, F.A., Ellison, C.A., Czuba, C.R., Young, B.M., and McCool, M.M. 2016. Geomorphic responses of Duluth-area streams to the June 2012 flood, Minnesota. U.S. Geological Survey Scientific Investigations Report 2016-5104.

Francart, S. 2017. Plum Creek sediment budget study: Fox-Wolf Watershed Alliance. http://fwwa.org/2017/07/13/plum-creek-sediment-budget-study/.

Gellis, A.C., Fitzpatrick, F.A., and Schubauer-Berigan, J. 2016. A manual to identify sources of fluvial sediment. EPA ORD Technical Manual.

Gorman Sanisaca, L., Gellis, A.C., and Lorenz, D.L. 2017. Determining the sources of fine-grained sediment using the Sediment Source Assessment Tool (Sed_SAT). U.S. Geological Survey Open-File Report 2017-1062.

Homer, C.G., Dewitz, J.A., Yang, L., Jin, S., Danielson, P., Xian, G., Coulston, J., Herold, N.D., Wickham, J.D., and Megown, K. 2015. "Completion of the 2011 National Land Cover Database for the conterminous United States-Representing a decade of land cover change information," Photogrammetric Engineering and Remote Sensing, 81(5):345–354.

Martin, L. 1965. The Physical Geography of Wisconsin. University of Wisconsin Press, Madison, Wis., p. 33.

Montgomery, D.R. and Buffington, J.M. 1997. "Channel reach morphology in mountain drainage basins," Bulletin of the Geological Society of America, 109: 596–611.

Natural Resources Conservation Service. 2006. Estimating soil loss from gully erosion, ephemeral or classic: https://www.nrcs.usda.gov/Internet/FSE_DOCUMENTS/stelprdb1075520.xlt

Outagamie County Land Conservation Department. 2017. Outagamie County land & water resource management plan 2017. Outagamie County Land Conservation Committee, Appleton, WI, https://datcp.wi.gov/Documents/OutagamieCountyLWRMPlan.pdf

Peppler, M.C. and Fitzpatrick, F.A. 2018. Collection methods, data compilation, and lessons learned from a study of stream geomorphology associated with riparian cattle grazing along the Fever River, University of Wisconsin Platteville Pioneer Farm, Wisconsin, 2004–11. U.S. Geological Survey Open-File Report 2016–1179.

Phillips, J.M., Russell, M.A., and Walling, D.E. 2000. "Time-integrated sampling of fluvial suspended sediment: a simple methodology for small catchments," Hydrological Processes, 14(14):2,589–2,602.

Shelton, L.R. and Capel, P.D. 1994. Guidelines for collecting and processing samples of stream bed sediment for analysis of trace elements and organic contaminants for the National Water-Quality Assessment Program. U.S. Geological Survey Open-File Report 94–458.

Soil Survey Staff, Natural Resources Conservation Service (NRCS), United States Department of Agriculture. 2017. Soil Survey Geographic (SSURGO) Database for Brown, Outagamie, Calumet, and Manitowoc Counties, Wisconsin. Available online. Accessed 25 March 2017.

Strahler, A. N. 1957. "Quantitative analyses of watershed geomorphology," Transactions American Geophysical Union Journal, 38(6):913–920.

Wisconsin Department of Natural Resources (WDNR). 1988. Lower Green Bay Remedial Action Plan for the Lower Fox River and Lower Green Bay Area of Concern, Madison, WI, Wisconsin Department of Natural Resources, PUBL-WR-175-87 REV 88.

Wisconsin Department of Natural Resources (WDNR). 2018a. Remedial Action Plan Update for the Lower Green Bay and Fox River Area of Concern, April 2018, Madison, WI, Wisconsin Department of Natural Resources.

Wisconsin Department of Natural Resources (WDNR). 2018b. Wisconsin Water Quality Report to Congress, 2018. Madison, WI, Wisconsin Department of Natural Resources EGAD #:3200-2018-36

Wisconsin Natural Resources Conservation Service (NRCS). 2015. Streambank erosion. U.S. Department of Agriculture Field Office Technical Guide.

Wisconsin State Laboratory of Hygiene. 2016a. Inductively coupled plasma-emission spectrometry high resolution mass spectrometry (EPA Method 200.8, SW846-Method 6020B): Wisconsin State Laboratory of Hygiene EHD Metals Department, EHD METALS METHOD.420.0, Rev. 1, July 2016, 22 p.

Wisconsin State Laboratory of Hygiene. 2016b. Digestion of solid samples for inductively coupled plasma spectrophotometry (ICP) (EPA SW846, Section 3050B): Wisconsin State Laboratory of Hygiene EHD Metals Department, EHD METALS METHOD 550.0, Rev. 6, March 2015.

U.S. Environmental Protection Agency (EPA). 1999. Protocol for developing sediment TMDLs, 1st Edition. EPA Report 841-B-99-004, Office of Water (4503F), United States Environmental Protection Agency, Washington D.C. 132 p.

U.S. Environmental Protection Agency (EPA). 2016. Great Lakes Restoration Initiative Report to Congress and the President, Fiscal Year 2016. https://www.glri.us/sites/default/files/fy2016-glri-progress-report-to-congress-and-president-20170803-35pp_0.pdf.

U.S. Geological Survey (USGS). 2019. Water data for the Nation., https://waterdata.usgs.gov/nwis.

U.S. Geological Survey (USGS), Brown County WI, Green Bay Metropolitan Sewerage District, Ayres Associates, Inc. 2010. Brown County WI LiDAR 2010: Brown County Land Information Office. https://www.co.brown.wi.us/departments/page_a7c50fe306ac/?department=85713eda4cdc&subdepartment=89ce08984445/.

Tracking Phosphorus and Sediment Sources and Transport from Fields and Channels in Great Lakes Restoration Initiative Priority Watersheds

Tanja N. Williamson, Research Hydrologist, OH-KY-IN Water Science Center, USGS, tnwillia@usgs.gov
Faith A. Fitzpatrick, Research Hydrologist, WI Water Science Center, USGS, fafitzpa@usgs.gov
Diana L. Karwan, Assistant Professor, Dept. of Forest Resources, Univ. of Minnesota, dlkarwan@umn.edu
Randall K. Kolka, Research Soil Scientist, USDA Forest Service Northern Research Station, rkolka@fs.fed.us
Edward Dobrowolski, Hydrologist, OH-KY-IN Water Science Center, USGS, edobrowo@usgs.gov
James Blount, Physical Scientist, WI Water Science Center, USGS, jblount@usgs.gov **Ethan D. Pawlowski**, Graduate Student, Dept. of Forest Resources, Univ. of Minnesota, pawlo026@umn.edu

Introduction

Western Lake Erie is one of several freshwater ecosystems that have experienced record-high harmful algal blooms (HABs) in the last two decades, with notable issues occurring in 2008, 2011, 2014, and 2015 (Ho & Michalak, 2015; Michalak et al., 2013). These HABs have been linked to a combination of nutrient loads, specifically abundance, stoichiometry, and bioavailability of nitrogen (N) and phosphorus (P); algal and mussel populations; high spring runoff; and climate patterns that enable long residence times of algae in warm, calm conditions that extend from late spring into mid-fall (Ho & Michalak, 2017; Michalak et al., 2013; Zhang et al., 2016). For example, large precipitation events in late winter and spring of 2011 resulted in relatively high daily-mean streamflow from the Maumee River resulting in high loads of dissolved reactive phosphorus, also known as orthophosphate (PO^4; orthoP) (Michalak et al., 2013). Examination of historical abundance of HABs has shown that a high proportion of interannual variability can be linked to orthoP, especially high spring orthoP loads and decadal scale loading within Lake Erie (Ho & Michalak, 2017; Scavia et al., 2016). This is exacerbated by the sediment-bound pool of P (sed-P) in western Lake Erie and organic matter decay (Zhang et al., 2016), which may release P over multiple years as a result of resuspension, redoximorphic conditions, and biological processes in this shallow lake environment (Søndergaard et al., 2003). High total annual discharge directly correlates with high total P (TP) annual loads (Han et al., 2012). The implications are that minimizing spring P loading, while also limiting the overall contribution of P to the system, is key to minimizing blooms (Ho & Michalak, 2017; Scavia et al., 2016; Zhang et al., 2016).

Non-point sources, like cropland, animal operations, and septic systems, contribute a majority of TP delivered to western Lake Erie by the Maumee River (Han et al., 2012). On average, the western Lake Erie basin receives 60% of the TP load for the whole lake and 66% of the orthoP (Dolan & Richards, 2008); orthoP loads average 30% of the TP load to Lake Erie (Scavia et al., 2016). Agricultural watersheds export the most TP, combining sed-P with orthoP (Han et al., 2012). Fine-grained sediment is considered among the most significant of pollutants because in addition to transporting excess nutrients, especially P, and hydrophobic pesticides, fine-grained sediment physically degrades aquatic habitat by burying substrate and attenuating light

(Lowrance et al., 2006). However, in some cases, best management practices (BMPs) that successfully address sediment and sed-P, like conservation tillage, have been linked to increased dissolved nutrients, such as orthoP (Fanelli et al., 2019; Michalak et al., 2013). This further complicates the implementation of BMPs and underscores the need for quantifying how individual BMPs relate to both proportional and absolute contributions of sediment and TP to stream systems and larger water bodies like the Great Lakes.

Another complication in understanding the seasonal contribution of sediment and sed-P from agricultural landscapes to the stream system is identifying how material is eroded and transported from fields and how movement of sediment and sed-P differs as a function of field management. At the edge-of-field scale, distinguishing surficial erosion from erosion that extends deeper into the soil profile can help document and quantify the benefits of individual BMPs, including tile-drainage, conservation tillage, grassed waterways, and cover crops. Fallout radionuclides, such as cesium-137 (^{137}Cs), unsupported lead-210 ($^{210}Pb_{xs}$), and beryllium-7 (^{7}Be), have proved useful for this distinction. In particular, the 54-d half-life of ^{7}Be makes it appropriate for estimating surface erosion on short-term time scales (Ryken et al., 2018b), including removal and transport of surface soil from agricultural fields (Blake et al., 1999). Beryllium-7 is naturally occurring in precipitation as a consequence of cosmic ray spallation of N or oxygen (Blake et al., 1999) and provides an ability to examine short-term erosion because of its short half-life combined with a propensity for rapid, stable adsorption to soil particles at the surface that are the first to come in contact with precipitation (Ryken et al., 2018a). The concentration of ^{7}Be in precipitation can significantly vary geographically, among storms, and even during individual storms (Walling, 2013). Beryllium-7 is generally concentrated near the soil surface (organic litter layer and top 0.5-1 cm) in both cultivated and “undisturbed” soils (Walling, 2013). Comparison of the ^{7}Be signature of sediment leaving individual fields with different BMPs provides information on how the proportion of eroded material differs between near-surface and deeper soil sources as a function of current field conditions (Blake et al., 1999).

Sediment source tracking provides a direct method to quantify suspended sediment, and consequently sed-P, sources by identifying a minimal set of properties (or fingerprint) that uniquely defines individual sources of sediment in the basin (Gellis & Walling, 2013). Sediment source tracking can be applied on a range of temporal scales, focusing on individual storms (Cashman et al., 2018), seasonal patterns (Crain et al., 2017), and annual synopses (Williamson et al., 2014). Sediment source tracking has been successfully used to discriminate both provenance (Collins et al., 1998) and land use, including differentiating active cropland from both pasture land and retired cropland (Crain et al., 2017; Williamson et al., 2014). Sediment source tracking can also help distinguish sediment from roadside ditches, gullies, and streambanks (see Fitzpatrick et al., this volume). Knowing more about when and from where suspended sediment is being transported provides an opportunity to understand how seasonal variability in nutrient and sediment loads might relate to land use -- key information for resource managers. Moreover, quantifying the effects of independent BMP implementation on sediment and nutrient movement provides a mechanism of isolating and valuing the potential of these BMPs to help reach nutrient and sediment reduction targets.

The study-design described here is for the Black Creek, IN basin (12-digit hydrologic unit code [HUC-12] 041000050104; USGS Site ID 04183038), a tributary to the Maumee River that has been identified as a significant contributor to nutrient and sediment loads (Robertson & Saad, 2011). In October 2015, long-term, continuous streamflow and water-quality monitoring began along Black Creek (32 km^2 at the gage; Figure 1). This watershed-scale monitoring is supplemented by edge-of-field monitoring of a pair of agricultural fields in the basin where discharge and water quality of both surface runoff and tile-drain flow are being monitored.

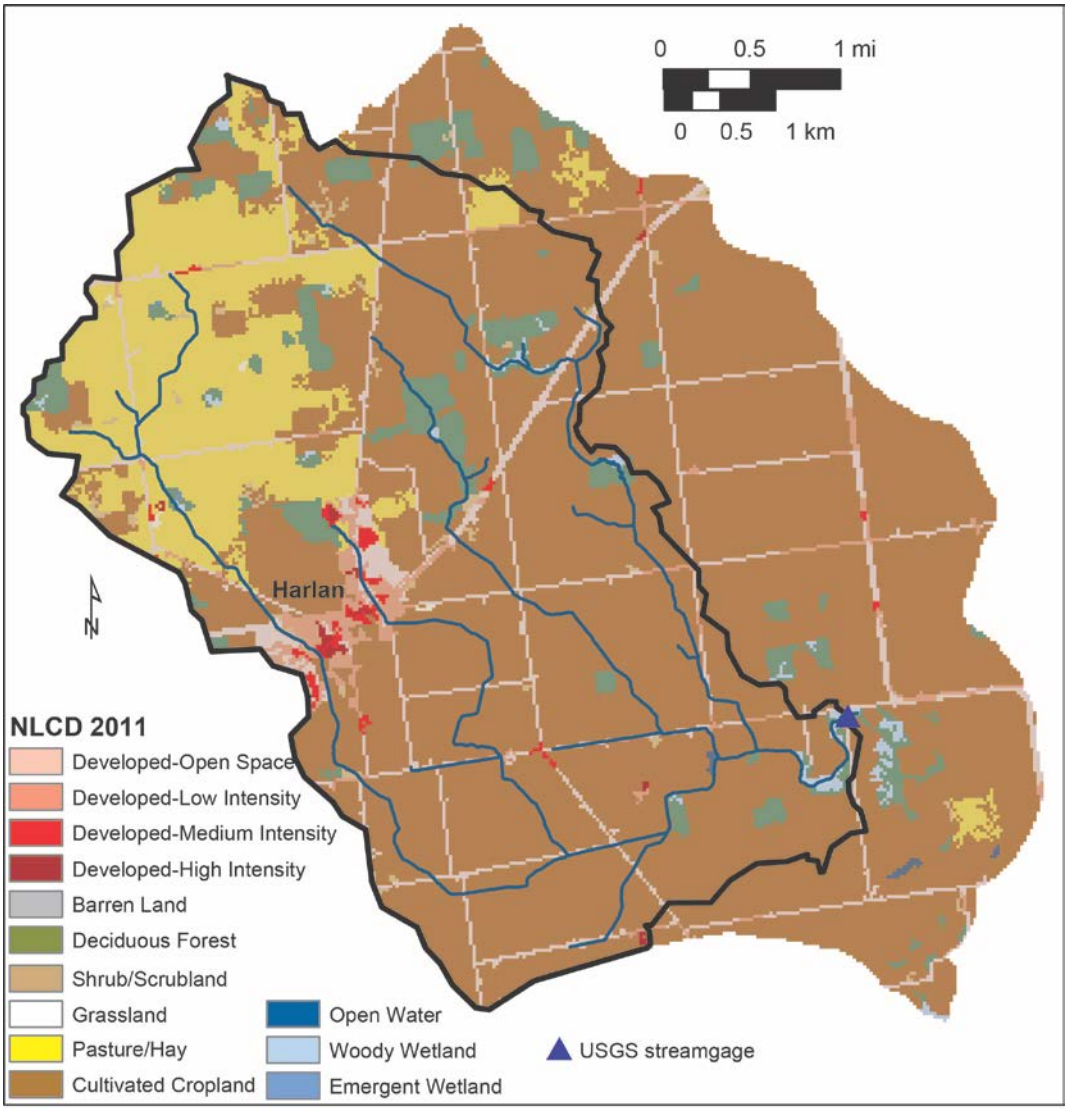

Figure 1. Black Creek basin, Indiana. The population center is Harlan, Indiana. Land cover is shown for the entire basin, a tributary to the Maumee River. The black outline and stream network shows the basin that is sampled by the USGS streamgage (Site ID 04183038).

Edge-of-field monitoring included three years when these fields were managed the same way (pre-BMP), and is continuing through a period after adoption of a new BMP (cover crop) on one of the fields in November 2018. In addition, sediment source tracking is being combined with ^{7}Be sampling to apportion sources of sediment from these agricultural fields both before and after implementation of the cover-crop BMP; these fields are bounded by forest and a road that are additional potential sources of sediment. Sediment source tracking and ^{7}Be analysis at the edge-of-field site was combined with sediment source tracking for the Black Creek basin during the 2018 water year to differentiate the seasonal contribution of cropland sediment from that derived from developed areas, forested patches, and pastures. Microbial source tracking began in January 2019 at the Black Creek gage to complement the sediment source tracking. Our objective is to provide local resource managers, including the Allen County Soil and Water Conservation District, local residents, US Department of Agriculture's (USDA) Natural Resources Conservation Service (NRCS), and the US Environmental Protection Agency (USEPA) information on:

- the variability of sources of sediment and sed-P during the year, especially during the March to July period of concern;
- the relation between agricultural-management practices and subsurface versus surface flow paths of nutrients and sediment;
- the contribution of non-cropland sources to nutrient and sediment loads in the basin.

Parallel work is also underway in Plum Creek, WI (HUC-12 040302040204, USGS Site ID 04084911), a tributary of the Lower Fox River, with a focus on similar land uses and the construction of a grassed waterway as the BMP being evaluated.

Study Design

As part of the Great Lakes Restoration Initiative (GLRI), sediment and microbial source tracking is being combined with P and sediment monitoring in stream water within two study watersheds identified as major contributors of P to the Great Lakes (Robertson & Saad, 2011): the 50 km^2 Black Creek, Indiana in the Maumee River basin (Lake Erie) and the 90 km^2 Plum Creek in the Lower Fox River basin (Lake Michigan). Details below focus on aspects of the Indiana site. The Lower Fox site is discussed elsewhere in these proceedings (see Fitzpatrick et al.).

Multiple tracking methods are being used and adapted for best results in these watersheds, including a suite of trace elements for overall source apportionment in addition to the short-term fallout radionuclide ^{7}Be for high-flow event-based transport on fields and in stream channels. Tile-drain connectivity to the surface is of critical interest in the Black Creek watershed, as both nutrients and sediment are transported through tile systems (e.g. Cuadra & Vidon, 2011; Vidon & Cuadra, 2011; Williamson et al., 2019); this is less of a concern in the Plum Creek basin, where the steep topography precludes the need for sub-surface drainage. Microbial source tracking has been integrated in the Black Creek basin because of the abundance of active horse pastures alongside confined animal operations that include poultry, swine, and cattle.

Sediment Source Tracking: Upland sources were sampled during July and August 2017 throughout the Black Creek basin upstream of the gage (Table 1), including sites close to 1st thru 5th order streams (Horton, 1945). Fifteen samples were obtained for each source type, with multiple source types sampled at the same general location when possible to limit the potential for localized differences in parent material to obscure the land-use signature. For each of the four land-use type sources (cropland, pasture, forest, and roads), the top 1-2 cm of soil material was composited along a total transect of 250 m, with one sample collected every 10 m, usually along five parallel lengths; roads were sampled along a 150-m transect, collecting from both sides and the center. Fields sampled included corn, soybean, wheat, and alfalfa under traditional tillage and conservation tillage and a combination of fertilizer and manure management. Roads included both those within and outside the population center of Harlan, IN. Because previous researchers have shown that streambanks generally contribute a majority of the material carried as suspended sediment in both agricultural and rural/suburban environments (Cashman et al., 2018; Gellis & Noe, 2013; Lamba et al., 2015), low and middle streambanks were also sampled from both sides of a stream for a 100-m length. Streambanks were sampled at sites that included streams bounded by a combination of the land-use source types and riparian environments. Sampling and laboratory materials used for both upland source samples and sediment samples were plastic to avoid any potential for metal contamination.

Table 1. Upland area and land use[1] distribution for each sampling site.

Site	Area	Cropland	Pasture	Forest	Developed	Stream Length[2]
	km^2	%				km
Black Creek	34.5[3]	66	20	6	8	260
Western Tributary	5.85	19	65	5	11	52
Eastern Tributary	5.56	66	17	11	6	60
BMP field	0.25	66	0	34	0[4]	NA
Control field	0.15	100	0	0	0[4]	NA

[1]Land use from NLCD 2011 (Homer et al., 2012) – roads are grouped with developed areas; [2]stream length calculated from National Hydrography Database (U.S. Geological Survey et al., 2009); [3]area upstream of USGS gage; [4]a road divides these two fields, so each has the potential to receive surface runoff from the road.

Each source sample was sub-sampled at the USGS Kentucky Sediment Laboratory, where material was wet sieved to remove particles larger than 63 micrometers in diameter, freeze dried, and sent for trace metal (Table 2) and carbon-form analysis (USGS Central Region Mineral Laboratory schedules 3a, 3b, and 17; https://minerals.usgs.gov/science/analytical-chemistry/) in addition to stable isotope analysis of total carbon (TC) and TN (USGS Reston Stable Isotope Laboratory schedule 1832) of the fine-grained sediment. An additional sub-sample was sent to the USGS Cascades Volcano Observatory Sediment Laboratory, where particle-size distribution was analyzed using an x-ray absorption particle-size analyzer (SediGraph III) to obtain a mean particle diameter by mass (d_{50}).

Table 2. Indicators used for fingerprint analysis of sediment denoted by Name (Symbol).

Silver (Ag)	Cobalt (Co)	Lanthanum (La)	Phosphorus (TP-s)	Tantalum (Ta)	Yttrium (Y)
Aluminum (Al)	Chromium (Cr)	Lithium (Li)	Lead (Pb)	Terbium (Tb)	Ytterbium (Yb)
Arsenic (As)	Cesium (Cs)	Lutetium (Lu)	Rubidium (Rb)	Tellurium (Te)	Zinc (Zn)
Barium (Ba)	Copper (Cu)	Magnesium (Mg)	Sulfur (S)	Thorium (Th)	Zirconium (Zr)
Beryllium (Be)	Iron (Fe)	Manganese (Mn)	Antimony (Sb)	Titanium (Ti)	
Bismuth (Bi)	Gallium (Ga)	Molybdenum (Mo)	Scandium (Sc)	Thallium (Tl)	Nitrogen (TN-s), $\delta^{15}N$
Calcium (Ca)	Hafnium (Hf)	Sodium (Na)	Selenium (Se)	Uranium (U)	Carbon (TC-s), $\delta^{13}C$
Cadmium (Cd)	Indium (In)	Niobium (Nb)	Tin (Sn)	Vanadium (V)	Organic C (OrgC)
Cerium (Ce)	Potassium (K)	Nickel (Ni)	Strontium (Sr)	Tungsten (W)	Carbonate C (CO3)

-s: sediment; δ: delta

Suspended sediment was collected monthly (Table 3) from two passive samplers (also known as Walling Tubes; Phillips et al., 2000) that were installed upstream of the USGS gage on Black Creek. Suspended sediment was also collected at two smaller, parallel tributary sites (Western and Eastern Tributaries) with drainage areas of approximately 6 km^2 and different land-use distributions (Table 1). Each of these in-situ, passive samplers was placed along the thalweg, at the water surface during low flow with the opening submerged, to provide a flow-integrated sample that included both low-flow and stormflow conditions. Black Creek is a 5th order stream and each of the sampled tributaries are 4th order streams. Passive samplers at the Black Creek gage were removed after the November 2017 sampling and replaced at the end of February 2018 because the stream was covered with ice; the tributaries continued to flow. Soft sediment from the stream bottom was collected along a 50-m transect centered on the passive samplers before they were installed in August 2017. This provided a second type of time-integrated sediment sample focused on sediment accumulation on the bottom of the channel. Suspended sediment was also collected from the edge-of-field site by placing a passive sampler immediately downstream of the flume that concentrates overland flow for the surface-runoff and water-quality monitoring. Sediment from the passive samplers and soft-bottom sediment, both of which are considered "target" samples, was processed similarly to the source material. Passive

samplers usually contained stream water in addition to suspended sediment; these samples were rinsed into buckets using additional native water and then allowed to settle to isolate the sediment. In the case of the edge-of-field site, samplers were generally rinsed with deionized water. In two cases, these samplers were rinsed with pumped groundwater, and in one case, stream water from one of the tributary sites was used, so this sample was only analyzed for particle size analysis (PSA) and not metal or nutrient abundance. For several months, there was not enough material from the edge-of-field site for all of the laboratories and, therefore, particle size will be estimated using data from other months.

Table 3. Monthly collection and aggregation of suspended sediment at each site

	2017				2018												2019								
Site	S	O	N	D	J	F	M	A	M	J	J	A	S	O	N	D	J	F	M	A	M	J	J	A	S
Black Creek	↔	↔	x				x	x	x	x	x	x	x												
Western T.	↔	↔	x	↔	↔	x	x	x	x	x	x	x	x												
Eastern T.			x	↔	↔	x	x	x	x	x	x	x	x												
BMP Field			x		x*	x[1]	x[1]	x[1]	x[1]	x		x[1]		x		x		x		B		B		B	

T. – tributary; ↔ multiple months were composited to have enough sample for lab analyses; *used only for particle size analysis (PSA); [1]not enough material for PSA; B bi-monthly sampling planned for the second year at the edge-of-field site only

The Sediment Source Assessment Tool (SedSAT; Gorman Sanisaca et al., 2017) was used for source apportionment. SedSAT includes preliminary steps for data normality checks, data transformations, and handling non-detect data. Indicator values can be adjusted as a function of median particle size and organic carbon abundance (OrgC); this addresses differences in surface area which may affect the abundance of different indicators. A bracket test eliminates any indicators for which the target sample exceeds the range of the upland source samples. Sources are apportioned through individual runs for each target sample. A linear discriminant function analysis (DFA) evaluates each indicator in order to identify those that best separate the source categories; additional indicators are incorporated if they improve this separation at a significance level of 0.01. Once each indicator has been evaluated and ranked for the contribution to discrimination of sources, a mixing model uses the relation among these indicators to apportion the original source samples, providing a confidence level for target sample apportionment; this mixing model is run as a Monte Carlo analysis with 1000 iterations. The fluvial target sample is then evaluated using the same mixing model, again using a Monte Carlo analysis with 1000 iterations.

For this *preliminary work*, data were only adjusted by the OrgC, but final results will also incorporate adjustment using median particle size. Source data and target data for the tributaries and edge-of-field monitoring will be published as a USGS Data Series when all analyses have been completed. Data for the Black Creek gage site will be published on the National Water Information System (NWIS) as per USGS fundamental science practices.

Characterization of Soil Erosion at Edge-of-Field Site Using ^{7}Be: To evaluate the effect of a cover crop on field erosion, ^{7}Be is being used to characterize surface erosion at paired fields (BMP and control) at the edge-of-field site. ^{7}Be activity is being measured in:

- the soil profile sampled before a precipitation event,
- rainfall for a discrete period, and
- sediment from field runoff corresponding to the same precipitation period.

To maximize the likelihood of enough overland flow to provide an adequate volume of sediment, precipitation events that extend over a series of days have been targeted.

Beryllium-7 is a naturally-derived radionuclide tracer mainly delivered to the soil surface in precipitation (Kaste et al., 2002). In soils, the ^{7}Be activity density (becquerel per kilogram; Bq/kg) is generally highest at the surface and decreases exponentially with depth. Overall, ^{7}Be binds strongly to surface soils and sediments, with some variation due to organic content and soil or sediment grain size and surface area (Ryken et al., 2018a). Beryllium-7 has been shown to rapidly and stably bind to arable (drained) soils like the Aqualfs (U.S. Department of Agriculture - Natural Resource Conservation Service [USDA-NRCS], 2016) at the Indiana edge-of-field site (Ryken et al., 2018a), with potentially higher sorption to the finer-grained Aquolls that define the preferential flowpaths in these fields (Ryken et al., 2018b). Due to its strong binding affinity and short half-life, ^{7}Be provides a means of differentiating surface soil from that below the surface (Walling, 2013). The ^{7}Be activity of suspended sediment in runoff from the field can be compared to the established field inventory (pre-precipitation activity resulting from previous event(s) and decay since previous event(s)) and that in the precipitation event, indicating whether sediment is majorly derived from the surface or from deeper soil erosion. Conceptually, if the ^{7}Be activity in the suspended sediment is relatively high, then surface erosion is the dominant source of the suspended sediment because this material came in contact with precipitation because of its location at the top of the soil profile and/or its contact with event precipitation while traveling in suspension. Conversely, if the ^{7}Be activity in the suspended sediment is lower than that in the baseline soil, then rilling and gully erosion deeper into the soil profile (of material that has no ^{7}Be activity) is contributing to sediment at the edge-of-field collection point. At the edge-of-field site, this ^{7}Be signature can be combined with the suspended-sediment concentration to understand if the abundance of eroded material is a function of how erosion is occurring and enables quantification of surface versus deeper erosion processes. Additionally, a mass balance can be performed on an event timescale to determine the net surface erosion during storm events.

Spring, summer, and fall events were monitored for surface erosion in 2018; winter (snow) events were not sampled because precipitation coming into contact with the soil surface must be from discrete events and these sites experience snowpack accumulation and melt that integrates multiple storms. Suspended sediment was collected in the same type of passive sampler used for sediment source tracking; three passive samplers were placed at the edge-of-field outlet. Both the BMP and the control field were sampled for each event; this is being repeated in 2019 now that the cover-crop BMP is in place. The first year of data, with both fields managed the same way, will illustrate if the fields undergo similar surface erosion for each of the sampled events. The second year of sampling will provide an ability to assess the effect of the BMP on surface erosion and how that relates to suspended-sediment concentration and proportional contribution from cropland relative to adjacent forest and roads.

Previous work at the Indiana edge-of-field site has shown a difference in tile-drain connectivity between the paired fields as exhibited by consistent differences in duration, magnitude, and water quality of tile-drain discharge, especially sediment, orthoP, and TP concentrations (Williamson et al., 2019). Consequently, ^{7}Be is also being analyzed for composited field runoff collected as part of the general edge-of-field monitoring. This is only being attempted for storms that produce a large volume of runoff from both overland and tile-drain samples; no precipitation or baseline soil samples are being collected. The hypothesis is that the ^{7}Be analysis will distinguish material derived from surface erosion, that may be delivered to the tile system by unintentional exposure to the surface, from deeper soil material entering through weak or broken connections in this aged, clay, tile-drain system.

Beryllium-7 activity is being measured at the University of Minnesota short-term radionuclide lab via gamma-ray spectrometry on high-purity germanium gamma-ray spectrometers

(Canberra Broad Energy and Canberra Coaxial type detectors). Solids and sediments are oven dried (55°C) for 48 hours before being analyzed. Liquid samples, including rainfall, tile-drain effluent, and overland flow, are first precipitated onto ion-exchange resins before analysis by the methods of Karwan et al. (2016). The ^{7}Be activity density (Bq/kg) associated with suspended sediments and soils and the activity concentration (Bq/L) in precipitation, was computed based upon the multi-channel peak area centered at 477.7 keV; background was computed for each sample using the 5-channels bracketing each peak and an empty counting vessel. Efficiency of the ^{7}Be peak was determined through interpolation between known peaks (Lead-210 at 46.5 keV, Americium-241 at 59.5 keV, Cadmium-109 at 88.0 keV, Cobalt-57 at 122.1 keV, and Cesium-137 at 661.7 keV) in a mixed isotope standard (Eckert & Ziegler Analytics, Atlanta, GA). The detectors used in this project have been previously calibrated with ^{7}Be standard reference material (Eckert & Ziegler Analytics, Atlanta, GA) added to both the ion exchange resins and characteristic suspended sediment. Correction for interference from the ^{228}Ac peak centered at 478.3 keV was based on the methods of Landis et al. (2012).

Preliminary Results and Integration of Tracer Methods

Preliminary results from the Black Creek basin show that critical indicators of sediment source include: Zr, W, TN-s, Mo, OrgC, TC-s, TP-s, Mg. Together, these indicators discriminate the five sources to a confidence of 91% (Figure 2). Similar to Williamson et al. (2014), both TP-s and carbon forms were identified as critical indicators, reflecting expected differences in nutrient abundance among these five environments (Figure 3), with the highest TP-s on active cropland and the highest OrgC on forested land and roads. This source discrimination is being used in a mixing model (Gorman Sanisaca et al., 2017) to apportion sediment among the different land uses on a seasonal time step. For example, the first aggregated sample for the Black Creek gage site, including September and October 2017, is derived mainly from streambank (39%) and pasture (33%) sources, combined with 18% cropland and 11% roads – there was no apparent contribution from forested land (Figure 4).

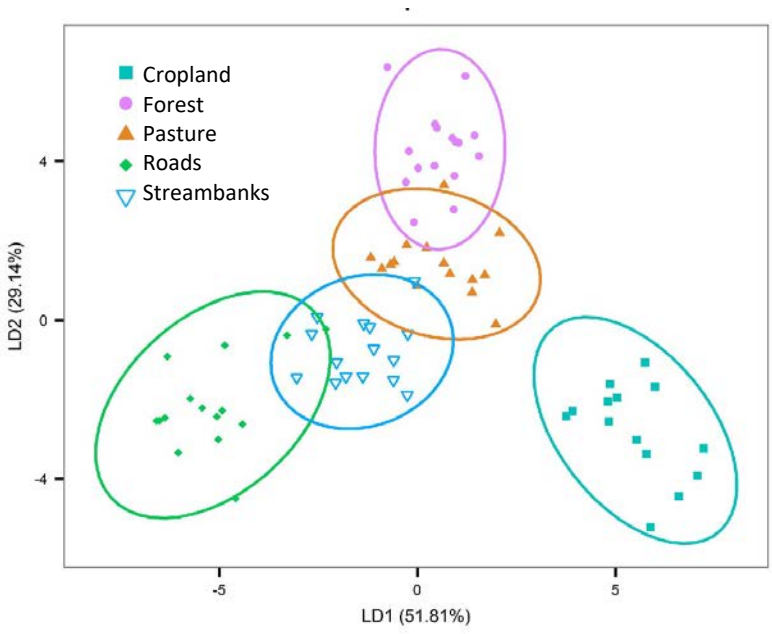

Figure 2. Preliminary source discrimination for September-October sediment from Black Creek gage site. LD1 is the indicator that provides the most differentiation (51.81%) among the sources - this is Zirconium. LD2 is the next most differentiating indicator - Tungsten. Eight critical indicators were identified.

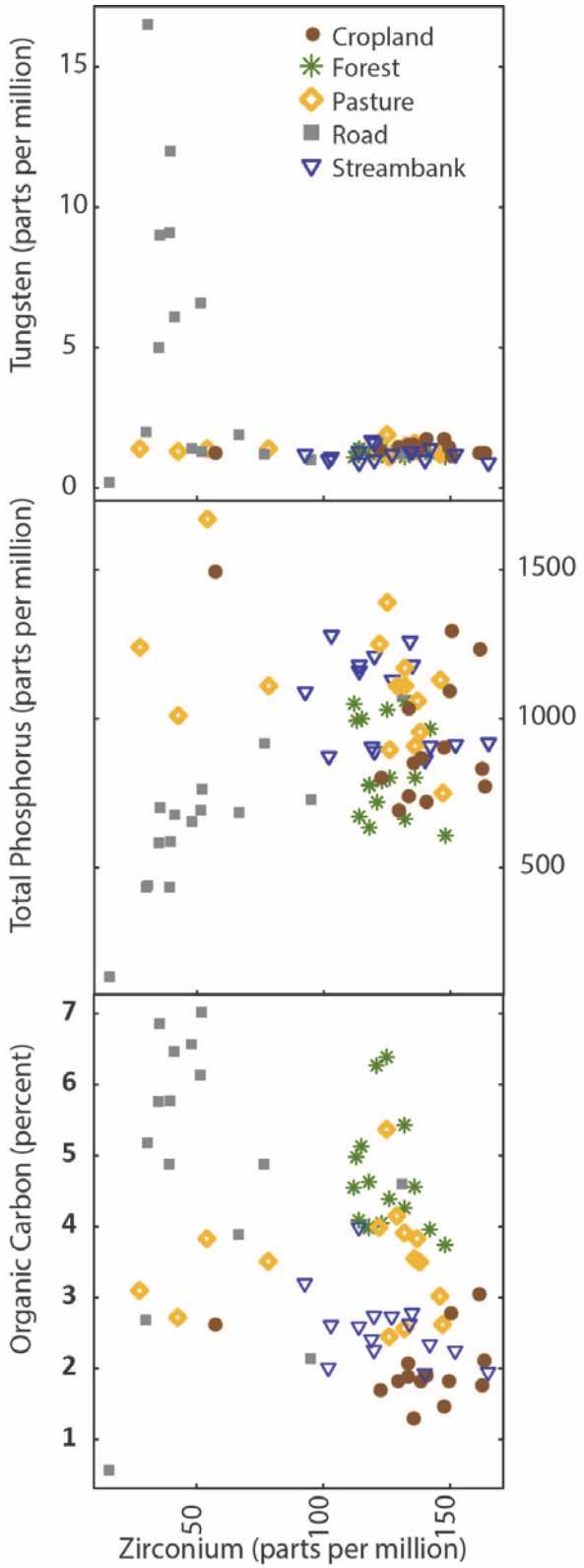

Figure 3. Concentrations of indicators. Preliminary analysis identified zirconium and tungsten as the two indicators that best separate the sources. Organic carbon and total phosphorus in sediment significantly improve this differentiation; their relative abundance reflects what we would expect from these five environments.

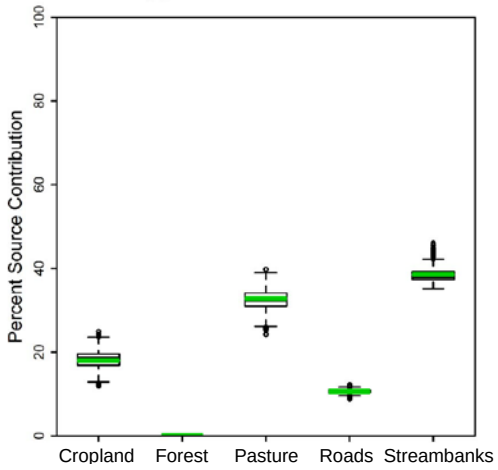

Figure 4. Preliminary source allocation for sediment from September-October 2017 Black Creek gage site.

When active erosion off the agricultural fields is considered, preliminary results show that ^{7}Be activity density in suspended sediment is similar from both the control and the pre-BMP field at the Indiana edge-of-field site, indicating similar erosion processes. The soil inventories from before the event show a range of depth profiles from the two fields, with ^{7}Be accumulation in organic matter at the soil surface and almost no ^{7}Be activity below the surface soil (Figure 5). A preliminary difference between the Black Creek, IN and Plum Creek, WI fields is in the baseline ^{7}Be profile. This difference reflects field management: the Indiana site is no-till and the Wisconsin site is conventional tillage, resulting in direct contact of precipitation with an irregular surface, exposed soil in cracks, and clods of soil that are left at the surface. Over time, this results in ^{7}Be being incorporated deeper into the soil at the Wisconsin site, with a more gradual decrease in ^{7}Be activity over the plow-layer depth.

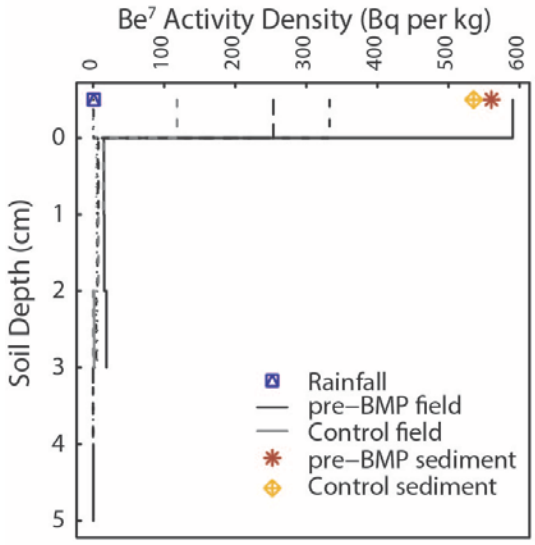

Figure 5. Preliminary ^{7}Be results from the Indiana edge-of-field sites for the 3/30/2018 event. Pre-event cores indicate ^{7}Be is only in the organic-litter layer and very near the surface in the soil profiles in these fields, with no ^{7}Be measurable below 5 cm. Differences among individual cores could be due to particle size and organic matter content differences as well as gamma counting differences for low-mass organic samples on the top of the profiles.

Summary

The strength of this sediment source tracking study lies in the inclusion of a pre-BMP period, including paired edge-of-field sites in Indiana that will enable ongoing comparison between BMP and control conditions. At the field scale, this will provide information on how the cover-crop BMP changes the source of sediment in both overland and tile-drain flow at the Indiana edge-of-field site, in addition to how it changes the abundance of overland flow and concentration of suspended sediment. Incorporation of ^{7}Be analysis will help document how BMP implementation alters both surface and deeper-soil erosion as a function of storm type and field conditions. The ability to quantify the effect of individual BMPs in terms of sediment source, abundance, and link to nutrient concentrations will provide a way of valuing these field-management strategies to water quality in both the focus basins of Black Creek, IN and Plum Creek, WI as well as the western Lake Erie and Lake Michigan basins.

References

Blake, W. H., Walling, D. E., & He, Q. (1999). Fallout beryllium-7 as a tracer in soil erosion investigations. *Applied Radiation and Isotopes, 51*(5), 599-605. doi:https://doi.org/10.1016/S0969-8043(99)00086-X

Cashman, M. J., Gellis, A., Gorman Sanisaca, L., Noe, G., Cogliandro, V., & Baker, A. (2018). Bank-derived material dominates fluvial sediment in a suburban Chesapeake Bay watershed. *River Research and Applications, 34*(8), 1032-1044. doi:10.1002/rra.3325

Collins, A. L., Walling, D. E., & Leeks, G. J. L. (1998). Use of composite fingerprints to determine the provenance of the contemporary suspended sediment load transported by rivers. *Earth Surface Processes and Landforms, 23*(1), 31-52. doi:doi:10.1002/(SICI)1096-9837(199801)23:1<31::AID-ESP816>3.0.CO;2-Z

Crain, A. S., Cherry, M. A., Williamson, T. N., & Bunch, A. R. (2017). *Multiple-source tracking: Investigating sources of pathogens, nutrients, and sediment in the Upper Little River Basin, Kentucky, water years 2013–14* (2017-5086). Retrieved from Reston, VA: http://pubs.er.usgs.gov/publication/sir20175086

Cuadra, P. E., & Vidon, P. (2011). Storm nitrogen dynamics in tile-drain flow in the US Midwest. *Biogeochemistry, 104*(1), 293-308. doi:10.1007/s10533-010-9502-x

Dolan, D. M., & Richards, R. P. (2008). Analysis of late 90s phosphorus loading pulse to Lake Erie *Checking the Pulse of Lake Erie* (pp. 79-96).

Fanelli, R. M., Blomquist, J. D., & Hirsch, R. M. (2019). Point sources and agricultural practices control spatial-temporal patterns of orthophosphate in tributaries to Chesapeake Bay. *Science of The Total Environment, 652*, 422-433. doi:https://doi.org/10.1016/j.scitotenv.2018.10.062

Gellis, A., & Noe, G. (2013). Sediment source analysis in the Linganore Creek watershed, Maryland, USA, using the sediment fingerprinting approach: 2008 to 2010. *Journal of Soils and Sediments, 13*, 1735-1753. doi:10.1007/s11368-013-0771-6

Gellis, A. C., & Walling, D. E. (2013). Sediment Source Fingerprinting (Tracing) and Sediment Budgets as Tools in Targeting River and Watershed Restoration Programs *Stream Restoration in Dynamic Fluvial Systems* (pp. 263-291): American Geophysical Union.

Gorman Sanisaca, L. E., Gellis, A. C., & Lorenz, D. L. (2017). *Determining the sources of fine-grained sediment using the Sediment Source Assessment Tool (Sed_SAT)* (2017-1062). Retrieved from Reston, VA: http://pubs.er.usgs.gov/publication/ofr20171062

Han, H., Allan, J. D., & Bosch, N. S. (2012). Historical pattern of phosphorus loading to Lake Erie watersheds. *Journal of Great Lakes Research, 38*(2), 289-298. doi:https://doi.org/10.1016/j.jglr.2012.03.004

Ho, J. C., & Michalak, A. M. (2015). Challenges in tracking harmful algal blooms: A synthesis of evidence from Lake Erie. *Journal of Great Lakes Research, 41*(2), 317-325. doi:https://doi.org/10.1016/j.jglr.2015.01.001

Ho, J. C., & Michalak, A. M. (2017). Phytoplankton blooms in Lake Erie impacted by both long-term and springtime phosphorus loading. *Journal of Great Lakes Research, 43*(3), 221-228. doi:https://doi.org/10.1016/j.jglr.2017.04.001

Homer, C. H., Fry, J. A., & Barnes, C. A. (2012). *The National Land Cover Database* (2012-3020). Retrieved from Reston, VA: http://pubs.er.usgs.gov/publication/fs20123020

Horton, R. E. (1945). Erosional development of streams and their drainage basins: hydrophysical applications of quantitative morphology. *Bulletin of the Geological Society of America, 56*, 275-370.

Karwan, D. L., Siegert, C. M., Levia, D. F., Pizzuto, J., Marquard, J., Aalto, R., & Aufdenkampe, A. K. (2016). Beryllium-7 wet deposition variation with storm height, synoptic classification, and tree canopy state in the mid-Atlantic USA. *Hydrological Processes, 30*(1), 75-89. doi:doi:10.1002/hyp.10571

Kaste, J. M., Norton, S. A., & Hess, C. T. (2002). Environmental Chemistry of Beryllium-7. *Reviews in Mineralogy and Geochemistry, 50*(1), 271-289. doi:10.2138/rmg.2002.50.6

Lamba, J., Thompson, A. M., Karthikeyan, K. G., & Fitzpatrick, F. A. (2015). Sources of fine sediment stored in agricultural lowland streams, Midwest, USA. *Geomorphology, 236*, 44-53. doi:https://doi.org/10.1016/j.geomorph.2015.02.001

Landis, J. D., Renshaw, C. E., & Kaste, J. M. (2012). Measurement of 7Be in soils and sediments by gamma spectroscopy. *Chemical Geology, 291*, 175-185. doi:https://doi.org/10.1016/j.chemgeo.2011.10.007

Lowrance, R., Isenhart, T. M., Gburek, W. J., F.D. Shields, J., P.J. Wigington, J., & Dabney, S. M. (2006). Landscape management practices. In M. Schnepf & C. Cox (Eds.), (pp. 271-317): Soil and Water Conservation Society.

Michalak, A. M., Anderson, E. J., Beletsky, D., Boland, S., Bosch, N. S., Bridgeman, T. B., . . . Zagorski, M. A. (2013). Record-setting algal bloom in Lake Erie caused by agricultural and meteorological trends consistent with expected future conditions. *Proceedings of the National Academy of Sciences*. doi:10.1073/pnas.1216006110

Phillips, J. M., Russell, M. A., & Walling, D. E. (2000). Time-integrated sampling of fluvial suspended sediment: a simple methodology for small catchments. *Hydrological Processes, 14*(14), 2589-2602. doi:10.1002/1099-1085(20001015)14:14<2589::aid-hyp94>3.0.co;2-d

Robertson, D. M., & Saad, D. A. (2011). Nutrient Inputs to the Laurentian Great Lakes by Source and Watershed Estimated Using SPARROW Watershed Models1. *JAWRA Journal of the American Water Resources Association, 47*(5), 1011-1033. doi:10.1111/j.1752-1688.2011.00574.x

Ryken, N., Al-Barri, B., Blake, W., Taylor, A., Tack, F., Bodé, S., . . . Verdoodt, A. (2018b). Impact of soil hydrological properties on the 7Be depth distribution and the spatial variation of 7Be inventories across a small catchment. *Geoderma, 318*, 88-98. doi:https://doi.org/10.1016/j.geoderma.2017.12.036

Ryken, N., Al-Barri, B., Blake, W., Taylor, A., Tack, F. M. G., Van Ranst, E., . . . Verdoodt, A. (2018a). Rapid and irreversible sorption behavior of 7Be assessed to evaluate its use as a catchment sediment tracer. *Journal of Environmental Radioactivity, 182*, 108-116. doi:https://doi.org/10.1016/j.jenvrad.2017.11.018

Scavia, D., DePinto, J. V., & Bertani, I. (2016). A multi-model approach to evaluating target phosphorus loads for Lake Erie. *Journal of Great Lakes Research, 42*(6), 1139-1150. doi:https://doi.org/10.1016/j.jglr.2016.09.007

Søndergaard, M., Jensen, J. P., & Jeppesen, E. (2003). Role of sediment and internal loading of phosphorus in shallow lakes. *Hydrobiologia, 506*(1), 135-145. doi:10.1023/B:HYDR.0000008611.12704.dd

U.S. Department of Agriculture - Natural Resource Conservation Service [USDA-NRCS]. (2016). Soil Survey Geographic (SSURGO) Database for Allen County, IN. Retrieved September 13, 2017, from Soil Survey Staff, Natural Resources Conservation Service, United States Department of Agriculture https://websoilsurvey.sc.egov.usda.gov/App/WebSoilSurvey.aspx

U.S. Geological Survey, U.S. Department of Agriculture, & Natural Resources Conservation Service. (2009). *Federal guidelines, requirements, and procedures for the national Watershed Boundary Dataset*. Retrieved from http://nhd.usgs.gov/

Vidon, P., & Cuadra, P. E. (2011). Phosphorus dynamics in tile-drain flow during storms in the US Midwest. *Agricultural Water Management, 98*(4), 532-540. doi:https://doi.org/10.1016/j.agwat.2010.09.010

Walling, D. E. (2013). Beryllium-7: The Cinderella of fallout radionuclide sediment tracers? *Hydrological Processes, 27*(6), 830-844. doi:doi:10.1002/hyp.9546

Williamson, T. N., Christensen, V. G., Richardson, W. B., Frey, J. W., Gellis, A. C., Kieta, K. A., & Fitzpatrick, F. A. (2014). Stream Sediment Sources in Midwest Agricultural Basins with Land Retirement along Channel. *Journal of Environmental Quality, 43*(5), 1624-1634. doi:10.2134/jeq2013.12.0521

Williamson, T. N., Dobrowolski, E. G., Meyer, S. M., Frey, J. W., & Allred, B. J. (2019). Delineation of tile-drain networks using thermal and multispectral imagery—Implications for water quantity and quality differences from paired edge-of-field sites. *Journal of Soil and Water Conservation, 74*(1), 1-11. doi:10.2489/jswc.74.1.1

Zhang, H., Boegman, L., Scavia, D., & Culver, D. A. (2016). Spatial distributions of external and internal phosphorus loads in Lake Erie and their impacts on phytoplankton and water quality. *Journal of Great Lakes Research, 42*(6), 1212-1227. doi:https://doi.org/10.1016/j.jglr.2016.09.005

Stream Restoration

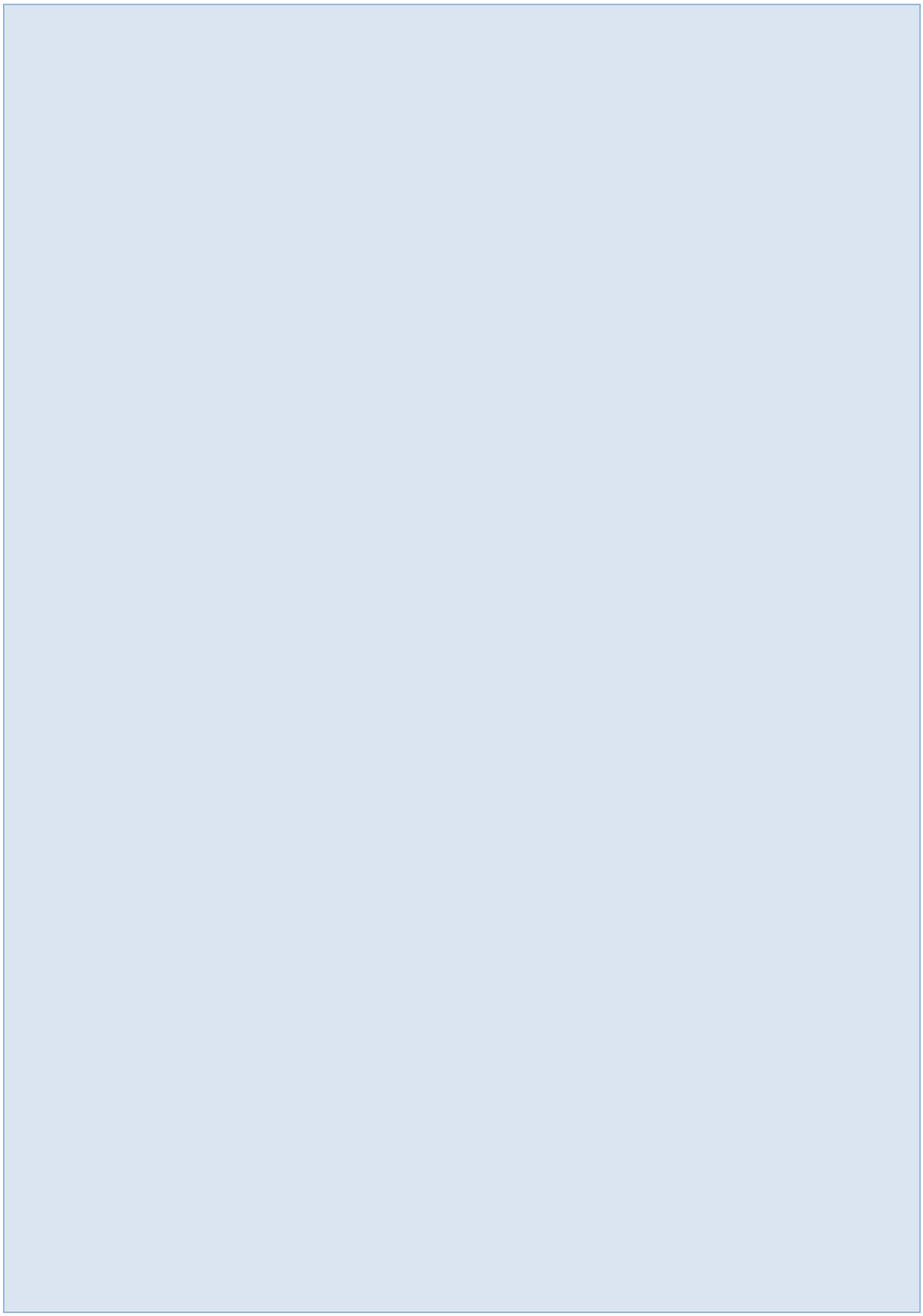

Application and Case Study of Sediment Augmentation on the Clackamas River, Oregon

Geoff Hales, P.G., Geologist, McBain Associates, Arcata, CA, geoff@mcbainassociates.com
Mindi Curran, G.I.T., Geologist, McBain Associates, Arcata, CA,
mindi@mcbainassociates.com

Extended Abstract

Channel restoration via sediment augmentation in the Clackamas River basin is being conducted by Portland General Electric Company to help restore geomorphic processes below key hydroelectric facilities on the mainstem Clackamas River (2,430 km^2 drainage area) and on the Oak Grove Fork (a major tributary, 370 km^2 drainage area). Measurable geomorphic changes to both the Clackamas River and Oak Grove Fork have been attributed to facilities operations (e.g., sediment trapping, flow regulation), and include changes in channel geometry, sediment supply, grain size, and bed elevation (McBain et al. 2001, Wampler and Grant 2003; McBain and Trush 2004). The overarching sediment augmentation program goal at both locations is to resupply sediment to help restore geomorphic processes and channel form under the contemporary flow regime using a portion of the historic sediment supply. It is expected that sediment augmentation will result in restorative and beneficial geomorphic, biological, and water quality changes.

Variations in geology and natural basin sediment yield and flow regime between the mainstem Clackamas River and Oak Grove Fork requires different augmentation scales and strategies, and provides a unique opportunity to compare augmentation and monitoring methods under the same program. The Clackamas River sediment augmentation site is located below River Mill and North Fork Dams, at 93 m elevation in the eastern Willamette Valley (45.300927°, -122.354126°). Annual peak flows typically occur in fall or winter and are rainfall or rain-on-snow events ($Q_{2.0}$ = 702 cms). The Oak Grove Fork augmentation sites (n=2) are located approximately 56 km upstream of the mainstem augmentation site, at 450 m and 625 m elevation, and are located below Lake Harriet Dam (45.077034°, -121.974364°). Annual peak flows typically occur as winter rainfall and spring snowmelt events ($Q_{2.0}$ = 28.3 cms). Natural sediment yield on the Oak Grove Fork is small compared to the mainstem Clackamas River (9.1 t/km^2/yr and 92 t/km^2/yr, respectively) (McBain and Trush 2002, Wampler and Grant 2003).

Sediment augmentation in the basin began at both sites in 2016. Sediment for the Oak Grove Fork augmentation is screened to a specific particle size distribution ranging from 101 mm – 10 mm, and is added directly to the wetted channel. Sediment is placed along the bank at two sites, approximately 6 km apart, where recruitment begins immediately. Placement at the upstream site is in a steep canyon and sediment is added via chute, forming a temporary cone, and placement at the downstream site is along a vertical cutbank where sediment is placed by excavator, forming a prism. In contrast, mainstem Clackamas River augmentation sediment is mined from an adjacent upslope terrace and is not screened or washed prior to placement. This results in both coarse and fine sediment being placed and a substantially broader particle size range, with the largest particles (D_{max}) up to 256 mm. Mainstem sediment augmentation occurs during summer, when sediment is placed on a dry bedrock shelf adjacent to the channel where it is recruited during fall and winter high flow events. Annual augmentation volumes between the two locations differ by up to two orders of magnitude, e.g., August 2018 augmentation volumes were 470 t on the Oak Grove Fork and 18,200 t on the mainstem Clackamas River.

The placement sites are visited several times annually to observe augmentation pile evolution in response to peak flow events. On the Oak Grove Fork, sediment recruitment has occurred as expected and no changes to the placement strategy have been made. Conversely, sediment augmentation pile behavior on the mainstem Clackamas River has required some finessing to optimize augmentation pile recruitment. The inaugural (2016) augmentation pile placement showed little recruitment following the first peak flow events (up to $Q_{1.4}$), while modeling suggested sediment mobility thresholds should have been met. Based on observations during these peak flow events, the pile was reshaped to a configuration that increased its hydraulic exposure and resulted in greater sediment recruitment during subsequent similar magnitude peak flows. This active, adaptive management has been a critical component to the early success at this location. Subsequent placements have followed this strategy and are showing improved sediment recruitment and downstream transport.

Differences in scale between the two locations also allows for a range of monitoring techniques to track downstream transport, deposition, and resulting geomorphic response. While monitoring objectives for both the Oak Grove Fork and the mainstem Clackamas River focus on evaluating augmentation-related geomorphic changes, site size and scale requires different data collection and analytical methods. The Oak Grove Fork monitoring reach is a 2 km-long wadable channel, allowing data collection to be ground-based. Geomorphic monitoring objectives focus on tracking downstream transport and deposition, which are accomplished by (a) annual reconnaissance to identify and document downstream deposition distance, which is aided by a unique-lithology visual tracer gravel added to the augmentation mix (5 percent), and (b) high resolution ground-based photogrammetry and Digital Elevation Model (DEM) differencing to measure depositional volumes and patterns, compare results to sediment transport model predictions, and evaluate whether geomorphic objectives are being met (Curran 2017).

In contrast, monitoring on the much larger mainstem Clackamas River is conducted over a 10 km reach, and requires a boat. A pre-augmentation “baseline” monitoring program was conducted from 2011-2013 that focused on documenting pre-project conditions in downstream areas determined most likely to be influenced by sediment augmentation (Wampler and Grant 2003, PGE and McBain and Trush 2011). Monitoring resumed in 2017 and is repeating the baseline monitoring so comparisons can be made to (1) evaluate how augmented sediment is routing and depositing downstream, (2) evaluate resulting geomorphic, biological, and water quality changes, and (3) assess whether adverse effects are occurring as a result of sediment augmentation that require corrective action. Like the Oak Grove Fork, monitoring objectives on the mainstem Clackamas River include assessing geomorphic change from DEM differencing, but the larger channel requires data collection using a combination of aerial LiDAR and boat-based channel bathymetry to capture surfaces. Additional mainstem geomorphic monitoring evaluates the overall abundance and composition of alluvial features, including bar frequency and particle size distribution, bedrock exposure, and side channel entrance flow thresholds.

While still early in the program, monitoring has already documented successful sediment recruitment, transport, and downstream deposition from each augmentation location, showing a positive start to meeting program objectives. Success can be attributed to both natural recruitment and routing, and (on the mainstem Clackamas River) active adaptive management of the augmentation pile by observing pile response to multiple peak flow events and reshaping the pile to maximize the opportunity for sediment to be recruited and transported downstream. Data collection for a full evaluation of geomorphic and biological objectives is underway and a data synthesis and program review are scheduled for 2022.

References

Curran, M. 2017. Application of Agisoft Photoscan and sediment transport modeling for the analysis of sediment wave propagation succeeding gravel augmentation, Oak Grove Fork of the Clackamas River, Oregon. Master's thesis. Humboldt State University, Arcata, CA.

McBain and Trush, Inc. 2002. Sediment yield analysis for the Oak Grove Fork and upper mainstem Clackamas River above North Fork Reservoir. Portland General Electric Company.

McBain and Trush, Inc. 2004. Synthesis of geomorphic, vegetation, and instream flow studies, Oak Grove Fork Project, Oak Grove Fork and Clackamas River upstream from North Fork Reservoir, Appendix D: sediment transport capacity modeling, Oak Grove Fork subreaches 1F and 1G. Portland General Electric Company.

McBain, S., W. Trush, G. Hales, P. Wampler, G. Grant. 2001. Geomorphic setting summary report for the mainstem Clackamas River and Oak Grove Fork of the Clackamas River. Portland General Electric Company.

Portland General Electric Company (PGE) and McBain and Trush, Inc. 2011. Gravel augmentation plan for the Clackamas River below River Mill Dam, Clackamas River Project (FERC 2195), License Appendix A, Condition 8(i). Prepared for the Federal Energy Regulatory Commission, April 19, 2011.

Wampler, P. J., and G. Grant. 2003. Final report, geomorphic changes resulting from River Mill Dam operations. Portland General Electric Company.

Applied Science and Design Strategies in Cranberry Bog and Wetland Restoration

Martin Melchior, Regional Director, Inter-Fluve, Madison, WI
mmelchior@interfluve.com
Nick Nelson, Geomorphologist, Inter-Fluve, Cambridge, MA
nnelson@interfluve.com
Glorianna Davenport, Director, Tidmarsh Farms and Living Observatory, Manomet, MA gid@media.mit.edu
Evan Shulman, President, Tidmarsh Farms and Living Observatory, Manomet, MA, evan@tykhe.biz
Alex Hackman, Massachussetts Division of Ecological Restoration, Boston, MA
alex.hackman@state.ma.us

Introduction

Retired cranberry culture operations present a unique opportunity for wetland and stream restoration. For stream restoration in these low-gradient wetland systems, the design risks associated with many river restoration projects, including flooding, incision, erosion and damage to installed materials are minor or non-existent. Design challenges instead include fine sediment transport, subsidence, challenging construction conditions, and determination of proposed ground water and surface water elevations as they relate to wetland inundation, stream temperature, and successful plantings. Combining the scientific data into functional hydraulic models to propose a designed channel geometry, frequency of wetland inundation, and channel slope is critical to project success. Synthesizing this information into a constructible design package requires creativity and an understanding of the capabilities and limitations of construction equipment in the bog environment. This extended abstract discusses two critical projects in the history of cranberry bog restoration in Massachusetts, the Eel River Restoration in Plymouth, and the Tidmarsh Farms/Beaver Dam Brook restoration in Manomet. This abstract will focus on critical design data needs, design strategies incorporated and implementation strategies used to date.

Site Geology and Geomorphology

Plymouth township contains over 700 kettle hole bogs. During the last glaciation over 9,000 years ago, glacial outwash streams from the receding Buzzard's Bay lobe glacier inundated fractured ice blocks with large amounts of sand and gravel. At both Eel River and Tidmarsh Farms, the melting ice blocks left behind a series of large depressions, or kettles, surrounded by kames and kame delta deposits. These kettle holes eventually filled with accumulating peat and began to have active surface water drainage to the nearby Atlantic Ocean. The Eel River and Tidmarsh sites occupy the headwaters of their respective stream systems that flow through these kettle hole peatlands.

Site History

Historic maps from the 1830s to the 1850s show both Eel River and Tidmarsh as natural wetlands, but little detail available regarding their history prior to 1830. Maps of both the Eel River and Tidmarsh project sites show a meandering stream running through low gradient and apparently treeless or partially forested wetlands, suggesting that a stream did run through both bog systems. However, it is unknown whether the mapped channel is a natural channel or constructed. Ditching and draining of wetlands was common in the Plymouth area following European settlement, and it is possible that a channel was excavated or manipulated. Given the amount of steady groundwater flow from the cranberry bog complex, and early maps that show a channel through the bog complex, it is highly likely that a small natural stream system, either single or multi-thread, did flow through the peatlands. Many of Plymouth Township's peat bogs were Atlantic white cedar swamps prior to European settlement. Logging of white cedar was widespread and could have occurred within the bog complexes as far back as the 1600s, but no records were found.

Commercial cranberry production began in earnest in Cape Cod around 1820. By the 1870s, many of Plymouth's kettle hole bogs had been converted to cranberry culture and have remained so ever since. More recently, cranberry prices have dropped, and some less productive bogs are being retired. Cranberries are grown on wetlands, which are often covered in a layer of coarse sand to help stimulate optimal root and vine growth, forcing uprights and providing stability for harvest. Most cranberry bogs in southeastern Massachusetts sit atop kettle bogs and fen peatlands. Eel River and Tidmarsh Farms, like most bog complexes, consist of a series of dikes and dams with operating headgates to control water levels in the bogs. Cranberry bogs often have a main trunk channel, a perimeter drainage channel, and cross ditches spaced 40-60 feet across and measuring about 24 inches in top width (Figure 1). Bog owners place sand in increments of no more than 1 inch, typically every 3-4 years.

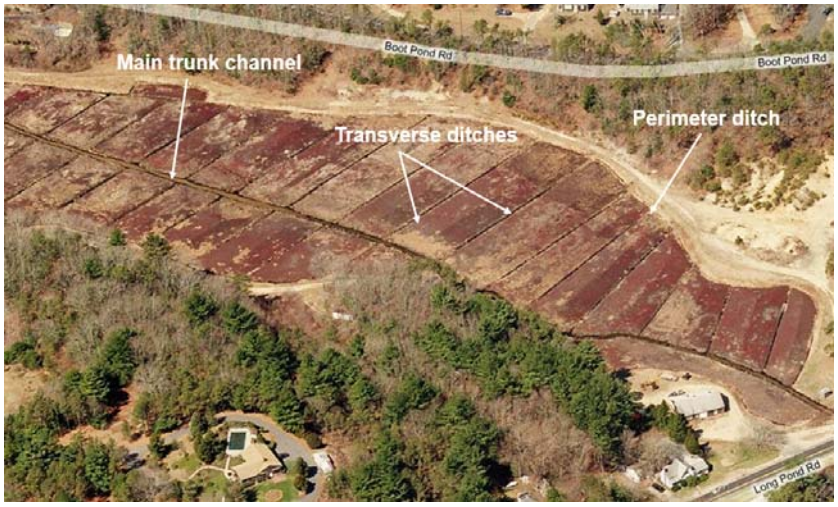

Figure 1. Cell 2 of the Eel River cranberry bog complex showing the central trunk channel, transverse ditches and perimeter ditches

Eel River and Tidmarsh were farmed continuously from the late 1800s to just prior to restoration. In 2003, the Cape Cod Cranberry Growers Association (CCCGA) raised awareness to Washington, DC Natural Resources Conservation Service (NRCS) officials to allocate more money to Massachusetts for the Wetlands Reserve Program (WRP) to help cranberry growers retire bog acreage that was difficult to manage or was located in environmentally sensitive areas. The Town of Plymouth worked with landowners, the NRCS and various funders to purchase the Eel River Property, and in 2007 began investigating restoration options. The Tidmarsh Farm owners partnered with the Town of Plymouth, NRCS, Fish and Wildlife Service and the Audubon Society to transfer ownership of the Tidmarsh Farms bogs, a complex that had once produced over 1% of Ocean Spray's annual crop.

Data Collection

For both the Eel River and Tidmarsh projects, topographic survey data were collected in order to create a 0.5ft (0.15m) contour basemap for design grading in AutoCAD Civil 3D. Ground survey data were integrated with available LiDAR data to create a basemap that included wetland and stream surfaces as well as surrounding topography. In order to determine the depth of peat accumulations within the bogs, ground penetrating radar and probes were used. At Eel River, a ground penetrating radar profile was produced using a sled mounted ground penetrating radar unit. At Tidmarsh Farms, several profiles and cross-sections were collected by staff from both UMass-Amherst and the NRCS. Metal rod probes were used to verify peat depths of less than 15 feet around the outer margins of the bogs.

To quantify the depth of the sand layer in each bog cell, a steel rod was driven through the sand until the peat layer was contacted. Probe locations were recorded with a portable GPS-RTK unit.

Groundwater elevations were measured using piezometers at both project sites, with water depth readings being taken manually at regular intervals ranging from weeks to months. Stream flow data was monitored periodically, both by manual flow meter measurements and by continuously monitoring pressure transducers related to a stage-discharge relationship.

In order to gauge the chemical conditions for peatland restoration, water quality samples were taken at various locations throughout the bog complex. Shallow test pits were excavated and groundwater samples collected and submitted to a state approved laboratory for analysis of metals, nutrients, pH, salinity and conductivity. YSI probes were used to collect field data to augment laboratory results. Soil samples were collected from test pits in each bog cell. Samples were collected from both the sand layer and the underlying peat layer. Laboratory analysis included pH, organic content, nutrients, calcium, magnesium, ammonium and nitrate, metals, polyaromatic hydrocarbons, DDT and derivatives, and organo-chlorine pesticides and herbicides.

Design Strategies

Eel River Restoration Project

The Eel River project began in 2005, with design completed and construction starting in 2009. The first step in the design process for Eel River was the development of project

performance criteria. Early in the design process, ideas regarding project performance criteria were solicited from the many participating project partners. Individual performance criterion suggestions were tallied and refined through the concept design process. The following table shows a summary of the performance criteria listed in order of frequency of identification by project partners during preliminary design meetings.

Table 1. Project performance criteria for the Eel River project

Dam removal / fish passage restoration
Stream restoration / fish habitat improvement
Bog restoration (at least a part of the total area)
Diverse wetland habitat restoration, including Atlantic white cedar
Educational opportunities / interpretive signs
Walking trails

The design team considered these criteria and incorporated them into the concept designs. Numerical design criteria were generated from the performance criteria, and guided the design through final revisions. Inter-Fluve completed the project concept and final designs, with Atlantic white cedar restoration expertise provided by Keith Underwood, Meadowview Biological Station, and Dr. Aimlee Laderman, of the Swamp Research Center, Woods Hole.

The channel design for the Eel River headwaters was founded on removal of fish passage barriers, restoration of free-flowing conditions, and creation of a self-sustaining, geomorphically functioning stream system that would support bridle shiner (*Notropis bifrenatus*), brook trout (*Salvelinus fontinalis*) and mottled sculpin (*Cottus bairdi*) populations found in Eel River. Analog stream reaches within 20 miles of Plymouth were examined through analysis of aerial photos and ground reconnaissance, and were used to help define both planform geometry and bank and floodplain morphology. Meander planform geometry was based on analog conditions derived from several non-forested stream systems. Floodplain and bank conditions at nearby Red Brook were used to inform channel cross-sectional form and structure use. Large wood was used to define channel boundaries, create complex fish habitat, provide basking habitat for waterfowl and herptiles, and provide nurseries for sapling trees. Hydraulic modeling (1D HEC-RAS) included multiple iterations of channel planform (and thus slope) and cross-section to refine the channel design. Modeling was used to evaluate water surface elevations and determine channel bed material size in immobile, grade controlling riffles.

Cranberry culture had added between 1.5 and 2.5 feet of sand on top of the historic peat, and the groundwater with control gates and berms removed would be well below the existing sand surface, making wetland plant establishment impossible. Wetland restoration thus required a decision to either remove the placed sand or simply raise the groundwater elevation. A combination approach was used in which grade controlling riffles were installed at critical locations to impound groundwater, and peat material was disturbed and mixed with sand to liberate the historic seed bank. The final design included partial excavation of the sand layer, removal of contaminated peat soils and mixing of peat and sand through microtopography grading.

Because it was not possible given project budgets to accurately estimate final groundwater levels for the proposed grading condition, the grade controlling riffles were constructed such that they could be lowered or raised if the resultant groundwater level needed manipulation. The project site has been monitored by the Town of Plymouth and Massachussetts Department of Ecological Restoration, and to date, no adjustments have

been made. The project also included seepage berms intended to collect surface drainage from surrounding slopes, retain it and meter out flow slowly, thus attenuating stream flow and wetland groundwater fluctuations. Because of the predominance of surrounding sand soils, this treatment may have been redundant to the attenuating characteristics of the existing geology and wetlands.

A summary of project design attributes is given in shown in the list below:

- Removal of seven control dikes and operating gates
- Removal of a 15ft high stone dam and preservation of historic artifacts
- Creation of 6,000 feet of meandering wetland stream channel
- Creation of 500 feet of gravel riffle-pool channel
- Creation of 1,200 feet of boulder step-pool channel
- Installation of 1,200 pieces of large wood
- 20 acres of diverse minerotrophic fen restoration
- 20 acres of Atlantic white cedar swamp restoration
- Wildlife passage culvert installation
- Sphagnum moss seeding and restoration
- Native fen plant establishment
- Eastern box turtle habitat creation
- Custom Atlantic white cedar growing operations
- Fish spawning and rearing habitat
- Raptor perch installation
- Interpretive signage
- Walking trails

Tidmarsh Farms/Beaver Dam Brook Restoration Project

The Tidmarsh Farms project began to develop in 2009, as Eel River was in construction. At 400 acres, the Tidmarsh project site is nearly ten times the size of the Eel River site, but had nearly identical project performance criteria. In addition to the criteria listed for Eel River, the Tidmarsh site included fish passage and habitat creation for native blue back herring (*Alosa aestivalis*) and alewife (*Alosa pseudoharengus*). The Tidmarsh site is much lower in elevation than Eel River, at between 8-15 feet above sea level. The project included 250 acres of wetland restoration and 20,000 feet of stream channel restoration, including fish passage restoration for blueback herring, American eel and alewife. This project incorporates the Living Observatory, a collaboration among the project owners, Massachusetts Division of Ecological Restoration, MIT, various universities and project partners in which remote sensing techniques are incorporated into visitor experience to both monitor ecological recovery and educate the public regarding cranberry bog restoration.

A summary of project design attributes is given in the list below:

- Removal of ten control dikes and operating gates
- Removal of a 15ft high earthen berm dam and concrete spillway
- Creation of 20,000 feet of meandering wetland stream channel
- Installation of a fish passage bridge for maintenance access
- Installation of a fish passage culvert for property access

- Installation of more than 3,000 pieces of large wood
- 250 acres of diverse minerotrophic fen restoration
- 40 acres of Atlantic white cedar swamp/red maple swamp restoration
- Native fen plant establishment
- Eastern box turtle habitat creation
- Custom Atlantic white cedar and native plant growing operations on site
- Fish spawning and rearing habitat for alewife and herring
- Raptor perch installation
- Walking trails

Implementation

The Eel River project was constructed in 2009-2010. The Tidmarsh project was constructed from 2015-2017. Construction included removal of drainage berms and establishment of dewatering channels to manage water during construction. Channel and wetland construction was completed using low pressure track equipment sometimes limited to working from large plastic or wooden mats. Channel material was excavated, and large wood placed at the same time. Following channel construction, microtopography grading was completed. The historic drainage channels were buried and slopes were graded. Seeding of disturbed sand areas was limited to the graded areas around the perimeter, while the wetlands were allowed to revegetate from native seed bank. Several thousand native plant plugs were installed and thousands of trees and shrubs were planted, but these represented a small percentage of the total wetland area.

Project Monitoring

The Eel River project has met the design criteria and performance criteria listed above. Within the first two years of construction, the dormant seed bank germinated across the entire project site, and plant biologists identified over 105 native plant species that were not planted during construction. This welcome result was expected to a lesser degree, and the degree of dormant seed bank regeneration helped to minimize planting costs at Tidmarsh and other future cranberry bog restoration sites. Since construction, the Plymouth gentian, a regionally endangered wildflower, has been observed numerous times. The target fish species have been found on site since construction, and fish habitat complexity continues to develop. Atlantic white cedar trees have grown to over 10 ft (3 m) in ten years, a rate of almost 1.0ft (0.3 m) per year, and began producing cones at year two, and seedlings in year three post construction.

Both during and after construction, the Eel River project provided valuable information relating to design treatments and construction methods. Groundwater levels were high toward the end of construction, due to the perimeter ditches and many of the transverse ditches being filled early in the project. Although helpful in determining the proper depth of microtopography, the high water complicated construction. To keep groundwater levels low during construction of the Tidmarsh project, the perimeter ditches and transverse ditches were filled toward the end of the construction timeline.

Grading of the Eel River site impacted the design and sequencing of the Tidmarsh project also. Differential settling near the lower elevations along the Eel River channel margin caused ponding in two of the bog cells, which although a short-term phenomenon, caused concern regarding warming of water. Channel levee features were added to the Tidmarsh site design to account for differential settling following construction.

Immediately following construction of the Eel River channel, the project site experienced the wettest spring on record, which caused numerous springs to form along the valley sides bordering the project. This cold spring water traveled across open, unvegetated sand and warmed the main channel considerably until water levels receded and the springs disappeared. For the Tidmarsh project, thermal imaging (UMass Amherst) of spring sources and fiberoptic temperature monitoring of stream temperature identified active spring areas prior to design, which allowed the design team to design small tributaries and concentrate spring flow in defined channels, minimizing surface movement of water and solar exposure.

Migrating alewife and blueback herring have been documented in the upper Eel River system, the first time these fish have accessed the headwaters since the 1790s. These same species have also been observed during spawning migration runs into the Tidmarsh system, utilizing existing and constructed ponds for spawning.

Acknowledgements

There were, and are, many people involved in the planning, design and implementation of these historic projects. Project partners who have participated in funding and project planning include the Town of Plymouth (David Gould and Kim Tower), Massachusetts Division of Ecological Restoration, NRCS, The Nature Conservancy, American Rivers, Mass Office of Coastal Zone Management (Wetland Restoration Program and Massachusetts Bays Program), Mass DEP, Mass Fish and Game, Eel River Watershed Association, US Fish and Wildlife Service, Audubon Society, NOAA and the US Army Corps of Engineers.

Assessment of Stream Health in the Catalpa Creek, Mississippi

John J. Ramirez-Avila, Assistant Professor, Mississippi State University, Mississippi State, MS, jjr149@msstate.edu
Bradley Richardson, Graduate Research Assistant, Mississippi State University, Mississippi State, MS, bmr380@msstate.edu
Sandra L. Ortega-Achury, Research Associate, Mississippi State University, Mississippi State, MS, slo51@msstate.edu
James L. Martin, Professor, Mississippi State University, Mississippi State, MS, jmartin@cee.msstae.edu

Abstract

Restoration and maintenance of healthy stream ecosystems have become important objectives of natural resources management. Macroinvertebrates are useful indicators of stream health because they respond to many kinds of pollution, including chemical pollution and physical disturbance to the landscape surrounding the stream, wetland structure, and hydrology. Research focused on the identification and assessment of habitat, water quality, and flood hazards processes along the main channel and tributaries of Catalpa Creek is advanced in order to support the implementation of the water management plan for the Catalpa Creek watershed. Results should identify general stream health, macroinvertebrate community tolerance, and restoration mitigation needs for tributaries of Catalpa Creek. In order to address research aims, a combination of methods has been performed including field reconnaissance, detailed sampling, and laboratory analysis. As an indicator of stream health, a pollution tolerance index rating, based on the quantification and qualification of identified macroinvertebrates, has been determined for each site along the studied reaches. Preliminary results indicate that biological monitoring using macroinvertebrates is a suitable option to meet the needs of Catalpa Creek watershed management, and help improve water quality evaluation in Mississippi streams.

Introduction

Biological assessment methods using macroinvertebrate community structure are valuable tools in the monitoring of lakes, rivers, and stream health. (Hawkes, 1979). Aquatic macroinvertebrates live on, under, and around rocks and sediment on the bottom of lakes, rivers, and streams, and can be used as bioindicators in standard water quality management (Hellawell, 1986). Macroinvertebrates are organisms large enough in size to be caught with a net, or retained on a sieve with a mesh size of 250 μm to 1,000 μm. These organisms can be seen with the naked eye, and are considered to be fairly immobile. With these considerations, the organisms can be useful in determining water quality in the lakes, rivers, and streams (Richardson et al., 2017).

A majority of macroinvertebrates dwell on the bottom, or near the bottom of the stream. These bottom dwelling, or benthic, organisms indicate the biological health of streams and other waterbodies. Different types of macroinvertebrates have different survival requirements. Some require cooler temperatures, relatively high dissolved oxygen levels, or niche habitats. Others

can survive in less ideal conditions, with low dissolved oxygen levels or increased fine sediment levels in the stream.

The easiest and most common method to evaluate these parameters is the Pollution Tolerance Index (PTI) (Lewis, 2014). This method measures the overall health status of aquatic systems with macroinvertebrates. The PTI method splits the macroinvertebrates into four separate groups dependent upon their pollution tolerance and ranks stream health by assigning a numeric score -- the higher the score, the more diverse and desirable the stream health. (Lewis, 2014). Group are numbered 1 through 4, with Group 1 representing the best water quality, and hence least tolerant species. Specifically:

- Group 1 macroinvertebrates are completely intolerant to pollution and hence is the best water quality. This group can only thrive in pollution-free environments with good water quality. Thus, the water needs to be cold, and the habitat more shaded. Higher dissolved oxygen levels and non-turbid waters, with a neutral pH (6.5 - 7.5), are also required. Examples of Group 1 macroinvertebrates are stoneflies, mayflies, and caddisfly larva.

- Group 2 macroinvertebrates are slightly more pollution tolerant than Group 1. These organisms can survive in a wide variety of water quality. Organisms in Group 2 are more tolerant to turbid waters and low dissolved oxygen levels. Examples of these organisms are the damselfly, dragonfly, crayfish, clams and mussels.

- Group 3 macroinvertebrates are fairly pollution tolerant. These organisms can tolerate much lower dissolved oxygen and pH levels. The shade requirement is not as important compared to Group 1, as the organisms can survive in warmer waters. Examples of Group 3 organisms include midge larvae, leeches, blackfly larvae, and flatworms.

- Group 4 macroinvertebrates are very pollution tolerant. Organisms that thrive in this group can live in muddy waters that are nearly stagnant. They require minimal dissolved oxygen, and can survive in a wide range of pH levels. Examples of Group 4 organisms are the aquatic worm, blood midge larvae, and left handed snail. This group of macroinvertebrates indicates high pollution levels.

This focus of this study is the identification and assessment of habitat, water quality, and flood hazard processes along the main channel and tributaries of Catalpa Creek in order to support the implementation of a water management plan for the Catalpa Creek watershed. Preliminary results identify general stream health and macroinvertebrate community tolerance, while future extended results will guide identification of restoration mitigation needs for tributaries of Catalpa Creek.

Methods

A combination of methods including field reconnaissance, detailed sampling, and laboratory analysis have been completed for an unnamed tributary to Catalpa Creek. The study site is within the Red Bud-Catalpa Creek Watershed in Oktibbeha County, MS, located in the northeast

region of Mississippi. It is a part of the Tombigbee River Basin and spans 11,706 ha with 50 km of mainstream length. The watershed covers part of the Mississippi State University (MSU) campus, the MSU HH Leveck Research facility and dairy farm, as well as some private lands. Once primarily prairie, the land currently includes 44% hay production/pasture land, 10% cultivated crops, 9% development, and 8% wetland/open water (Ramirez-Avila et al. 2016).

Preliminary results represent initial findings from an unnamed tributary surveyed as part of the study. The tributary drains a 0.6 square mile area, which is 87.3 % developed and 33.7% impervious. The length of the longest flow path is 1.7 miles and it has maximum and minimum basin elevations of 403 ft and 327 ft, respectively (Wilkinson et al., 2018). The studied reach runs very close to the MSU College of Veterinary Medicine and is surrounded by frequently mown grass for the majority of its length and a small segment of forested riparian zone for the upstream portion (Figure 1). Therefore, runoff containing pollutants, as well as the transition in habitats, could be affecting macroinvertebrate populations. For the analysis, this reach has been split into six segments as outlined in Figure 1.

Figure 1. Location of biological monitoring segments along headwater tributary of Catalpa Creek.

Macroinvertebrate collection along the study reaches was performed on February 23 (winter), April 6 (spring), and August 28 of 2018. A dip net was used to collect twenty representative samples along the length of each segment. Material was collected by "jabbing" the net in locations where macroinvertebrates were expected to occur (Figure 2). Locations include vegetated areas submerged in water along the banks, leaf packs, and woody material present within the stream. When the flow was adequate, the dip net was placed on the stream bed, and bed material was mechanically disturbed to release attached and buried material which then flowed into the net. Once twenty representative samples of the segment were collected, the net was then emptied into a plastic bag and preserved with 10% Formaldehyde solution. Each sample was washed in the lab through a 600-micron sieve (to remove sediment and fine material), and then distributed across a tray. Using forceps, macroinvertebrates were then surveyed from the sample and identified using an Accu-Scope (Figure 3). Once the sample was completely surveyed, the macroinvertebrates were separated into Groups 1 through 4, and quantified based on their respective taxa. A pollution tolerance index was then created according to the Hoosier Riverwatch Biological Monitoring protocol (2017)(Figure 4).

Figure 2. Biological assessment along tributaries

Figure 3. Macroinvertebrates identification

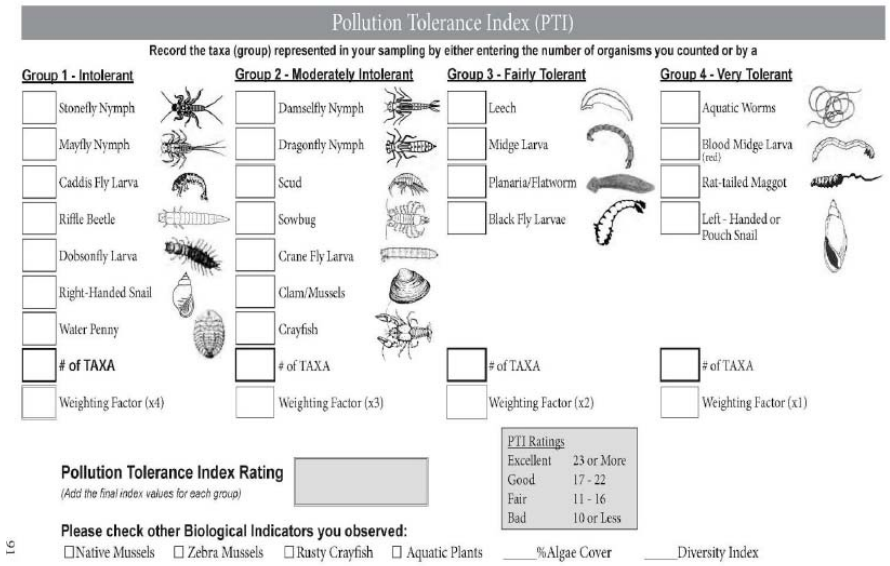

Figure 4. Biological Monitoring Datasheet

Preliminary Results and Discussion

The studied tributary indicates acceptable, and in many segments, excellent pollution tolerance index ratings through time, based on macroinvertebrate presence and diversity (Table 1). The average number of individuals collected during the summer season 2018 (34) was higher than the numbers in spring 2018 (30) and winter 2018 (27). Fair ratings in some segments (Table 1) could infer that a lack of macroinvertebrates in these stream segments could be caused by an absence of habitat either due to insufficient flow or inadequate substrate. When water levels were adequate, and there was organic material within the stream, macroinvertebrate populations were present and diverse enough to indicate low pollution levels.

Although most of the samples indicate “excellent” or “good” water quality conditions, a large proportion of our macroinvertebrates are “fairly tolerant” or “very tolerant” to pollution. Diversity in the studied reaches is good, including the presence of some intolerant species (Figure 6). However, abundance of different groups would need to be reported in addition to diversity, in order to determine any direct impact on macroinvertebrate populations caused by polluted runoff from cattle farms (high in nitrogen and phosphorous) or urban areas (high in hydrocarbons).

There does appear to be a difference in specific macroinvertebrate abundance (mayflies) between forested and grassed riparian zones due to the increased habitat that grasses provide. In order to improve the conclusions of this study, the temporal and spatial variability of macroinvertebrate analysis will be extended.

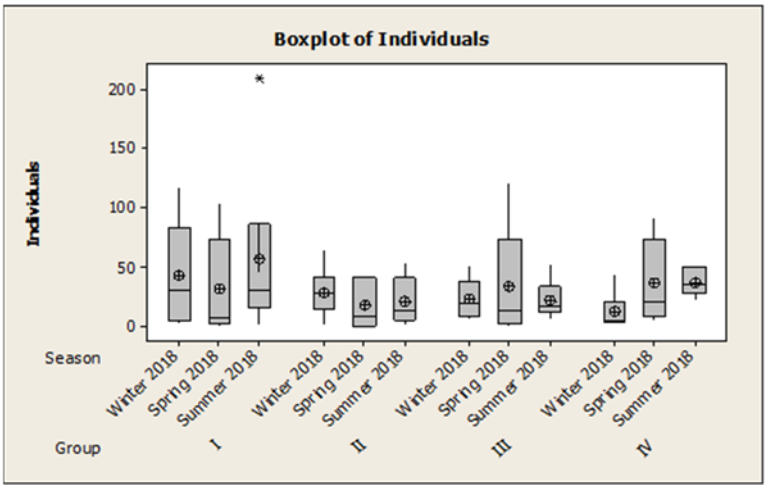

Figure 5. Seasonal variation of macroinvertebrate communities

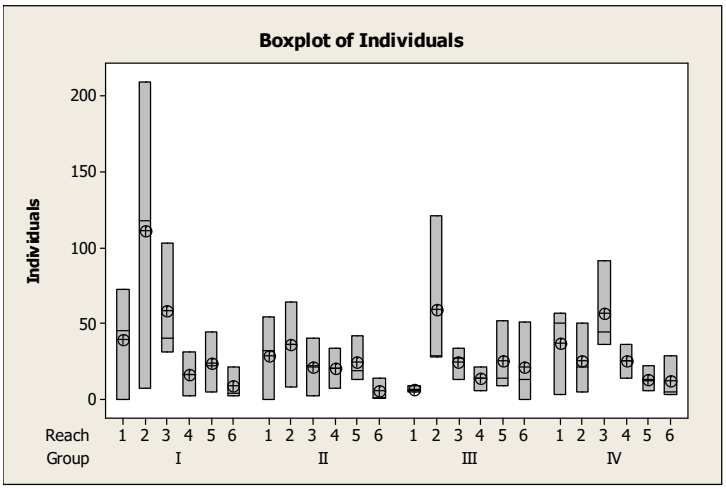

Figure 6. Spatial variation of macroinvertebrate communities

Table 1. Pollution Tolerance Index for CT

Stream Segment	Feb. 2018		Apr. 2018		Aug. 2018	
	PTI	Rating	PTI	Rating	PTI	Rating
1	23	Good	5	Fair	27	Excellent
2	27	Excellent	27	Excellent	33	Excellent
3	23	Excellent	27	Excellent	26	Excellent
4	22	Good	35	Excellent	20	Good
5	20	Good	29	Excellent	28	Excellent
6	13	Fair	12	Fair	22	Good

References

Hawkes, H. A., & De Pauw, N. (1979). Biological Monitoring of River Quality. River Water Quality Monitoring and Control. W.J. Walley & S. Judd (Eds). Aston University, Birmingham, 87-111.

Hellawell, J. M. (1986). Biological Indicators of Freshwater Pollution and Environmental Management. London, UK: Elsevier Applied Science Publishers.

Indiana Department of Environmental Management. 2017. Volunteer Stream Monitoring Training Manual 2017. 168 pp. https://www.in.gov/idem/riverwatch/files/volunteer_monitoring_manual.pdf (Accessed May 2, 2019)

Lewis, K. (2014). Pollution Tollerance Index. Judy Creek Stream Ecology. https://sites.nd.edu/bios21202/macroinvertbrates/pollution-tolerance-index/ (Accessed May 2, 2019)

Richardson, B. M., Pounders, D., & Walker, R. (2017). Sampling Macroinvertebrates to Monitor Stream Health. 1-7. Mississippi State University.

Ramirez-Avila, J., Schauwecker, T. J., & Czarnecki, J. M. P. (2016). Catalpa Creek Watershed Planning, Restoration, and Protection Project. In Conference: XIX Conferenza Nazionale de lla Società Italiana degli Urbanisti (SIU). Catania, Italy.

Wilkinson, H.; B. Spiller; N. Forbes; S. L. Ortega-Achury; J. J. Ramirez-Avila. (2018). The Effects of Forested Riparian Zones on Stream Conditions. 2018 World Environmental and Water Resources Congress 2018. 318-326

Ecohydraulic Design of Salmonid Habitat Enhancement Projects in the Central Valley, California

Chris Hammersmark, Ph.D., P.E., Director, cbec eco engineering, 519 Seabright Ave, Suite 102, Santa Cruz, CA 95062, c.hammersmark@cbecoeng.com, 916-668-5236
Ben Taber, P.E., cbec eco engineering, 2544 Industrial Blvd., West Sacramento, CA 95691, b.taber@cbecoeng.com, 916-231-6052
John Hannon, U. S. Bureau of Reclamation - Bay-Delta Office, Science Division, 801 I Street, Suite 140, Sacramento, CA 95814, jhannon@usbr.gov, 916-414-2413
Lilly Allen, Sacramento Water Forum, 1330 21st Street, Suite 103, Sacramento, CA 95811, lallen@waterforum.org, 916-808-1998

Abstract

In the last eleven years, concerted efforts led by agencies including the U.S. Bureau of Reclamation, U.S. Fish and Wildlife Service, California Department of Fish and Wildlife, NOAA Fisheries, Sacramento County Parks and the Sacramento Water Forum have resulted in a suite of aquatic habitat enhancement projects in the lower American River which runs through the greater metropolitan area of Sacramento, California. These projects have focused on the creation and enhancement of spawning and juvenile rearing habitats for Central Valley steelhead and Fall-run Chinook salmon. The ecohydraulic design approach employed incorporates topographic/bathymetric/hydraulic surveys, development and application of detailed multidimensional hydrodynamic models which are then combined with locally derived habitat suitability indices to estimate the amount of potential habitat and sediment mobility calculations to evaluate the potential longevity of project features.

The habitat enhancement projects are needed to support habitat that was lost due to the construction of Folsom and Nimbus Dams, which are components of the Federal Central Valley Project. These dams block access to the vast majority of the habitat once available to anadromous fishes in the American River watershed, as well as interrupt the transport and delivery of sediment to the lower American River, where it once replenished riffles used for the development of redds utilized for spawning. Though the vast majority of water originating in the watershed still flows down the lower American River, the sediment does not. This has led to a coarsening of the bed due to the winnowing of fine sediment. Habitat project features include the enhancement and/or creation of spawning riffles at locations where high amounts of spawning was historically documented, creation or reconnection of secondary and tertiary channels, gravel augmentation, construction of floodplain benches, and the placement of large woody material in the channel, banks and floodplains. In some cases, the projects include the placement of large cobble and boulder material in the main channel in an effort to raise water levels and re-wet previously disconnected side channels.

The ecohydraulic design process includes comprehensive bathymetric and topographic surveys, surface development, hydraulic surveys/measurements, and development of detailed two-dimensional hydrodynamic and habitat suitability models. Outputs from the hydrodynamic model for a wide variety of flow conditions are used to estimate salmonid spawning and rearing habitat suitability for proposed design configurations, as well as to assess the potential mobility of the placed sediment. The design process follows an iterative approach where the amount of

habitat created is optimized for a given amount of spawning sized material and excavation (set by the project budget) and the potential for mobility of the project features.

The material for the gravel augmentation efforts has been supplied from a variety of sources including purchase from nearby aggregate producers, excavation and onsite sorting from adjacent terraces distal from the current river channel, as well as material that is generated from the excavation of side channels and floodplain benches included in the project design. Many of the projects have been designed such that a cut-fill balance is achieved within the project footprint. When locally sourced, the material too fine to be used for gravel augmentation to riffles is used to improve the texture of floodplain surfaces to improve native plant recruitment, establishment and growth. The material that is too coarse to be used for gravel augmentation is used to fortify areas of the design that are expected to experience high shear stresses and subsequent transport of the placed appropriately size spawning gravels.

Extensive post-project physical and biological monitoring has occurred at these sites, which has documented the utilization of the sites by salmonids at various life stages in a variety of hydrologic conditions (i.e., critically dry through wet years), as well as the rate of degradation (i.e., erosion of sediment from the spawning areas). This post-project monitoring data has been used to enhance the design process and project complexity in subsequent years. Enhancements to the design process resulting from the post-project monitoring include refinement of habitat suitability curves, inclusion of increasing amounts of large wood, addition of secondary and tertiary channels for rearing and spawning habitat, and refinement of and experimentation with the size of the sediment placed in spawning areas.

The projects have substantially contributed to the limited amount of habitat used by anadromous salmonids at multiple freshwater life stages. As examples of the success of this ongoing project, the Nimbus Basin project was home to 926 documented redds (24% of all redds documented within the lower American River in that year) in the first spawning season following construction. 91% of these redds occurred in locations that were predicted to be medium or high-quality spawning habitat by the habitat suitability modeling effort. The Lower Sailor Bar project was home to 514 documented redds (14% of all redds documented within the lower American River in that year) in the first spawning season following construction. 79% of these redds occurred in locations that were predicted to be medium or high-quality spawning habitat by the habitat suitability modeling effort.

Effect of Increasing Bed Material Storage on Bed Relief and Rearing Habitat in a Reach of the Trinity River, California

David Gaeuman, Geomorphologist, Yurok Tribe, Fisheries Dept., Weaverville, CA, dgaeuman@yuroktribe.nsn.us
Aaron Martin, Habitat Restoration Biologist, Yurok Tribe, Fisheries Dept., Willow Creek, CA, yurokfish@gmail.com
Nicholas A. Som, Statistician, U.S. Fish and Wildlife Service, Arcata, CA, nicholas_som@fws.gov

Introduction

The physical habitat characteristics of streams are the result of the interactions between topographic structures that generate a spatially-variable hydraulic field that, in turn, create topographic relief via sediment erosion and deposition. The availability of sediments for fluvial redistribution is therefore a critical factor for maintaining physical habitat quality. In gravel-bed streams, the dominant aquatic habitat features are predominantly composed of non-cohesive bed material ranging from sand to cobbles. These coarse sediment fractions are the building blocks for the bars and riffles that drive variations in flow depth, velocity, and direction that constitute the diversity in meso- and micro-scale habitats needed to support the range of species and life stages present in the aquatic ecosystem (Petts and Maddock 1996; Kondolf and Wilcock 1996; Stanford et al. 1996; Richter et al. 1997; Milhous 1998; Ock et al. 2015).

Dams can alter downstream physical conditions in part by cutting off the supply of bed-material sediments from upstream. If stream flows downstream from a dam are occasionally competent to transport the more mobile gravel sizes on the bed, these sizes will be exported downstream, leading to bed coarsening, decreased bed mobility, and decreases in both bed relief and physical habitat diversity (Williams and Wolman, 1984; Lisle et al. 1993; Church, 1995; Viparelli et al. 2011). In such cases, habitat restoration effort may include adding gravel-sized sediments to the stream reaches downstream from dams. Generically called gravel augmentation, this practice is intended to replenish the supply of alluvial materials that comprise bars and riffles and support the processes of scour and fill that build and renew those topographic features (Sklar et al. 2009; Venditti et al. 2010; Gaeuman 2012; Humphries et al. 2012; Gaeuman 2014).

Despite its potential for ecological benefit there is also a risk for gravel augmentations to produce unfavorable outcomes. There is evidence that large increases in sediment supplies can cause pools and other relatively deep areas to fill, resulting in a general flattening of the stream bed and decreases in physical habitat diversity (Lisle 1982; Madej 1999; Bartley and Rutherfurd 2005; Madej and Ozaki 2006; Yarnell et al. 2006; Madej and Ozaki 2009; Zunka et al. 2015). Bars, pools, and other structural features that contribute to physical habitat quality are therefore likely to be most fully developed in reaches with intermediate sediment supplies, as qualitatively illustrated in Figure 1.

If correct, this “intermediate supply” hypothesis implies that resource managers should attempt to identify the unique sediment supply rate that will maximize morphologic complexity in the stream reach under consideration. The current state of the science, however, provides little guidance on how to achieve that objective, as the optimal supply rate presumably depends on a host of details regarding the geomorphic and hydrologic characteristics of the system being considered (Lisle et al. 1997; Sklar et al. 2009; Humphries et al. 2012; Gaeuman et al. 2017).

Herein we describe the effects of gravel augmentations and associated changes in bed material storage on channel morphology and salmonid rearing habitat in a reach of the Trinity River of northern California. This reach is located downstream from a pair of dams that have sequestered bed material from the upper watershed since 1960 but has been receiving repeated gravel augmentations since 2011.

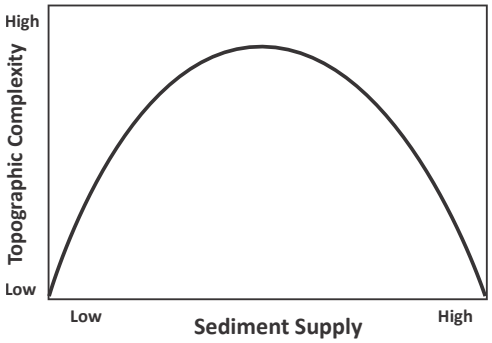

Figure 1. Hypothesized relationship between topographic complexity and sediment supply. Adapted from Yarnell et al. (2006).

Study Area

The data presented herein were collected in a straight reach of channel extending 440 m downstream from a gravel augmentation point near the upstream end of the Lowden Ranch reach of the Trinity River, which is located about 10 km downstream from Lewiston Dam in northern California (Figure 2). This study area spans the same reach of river as the response zone and the distal zone discussed by Gaeuman et al. (2017) and approximately the same reach as zones 3 through 6 that Gaeuman (2014) used to develop a gravel budget for 2010-2011. The Trinity River is gravel-bedded with typical channel widths in the vicinity of the study reach between about 30 and 45 m and a mean annual flood of about 180 m^3/s under current dam operating rules. Restoration flow releases from Lewiston Dam are implemented each spring by the Trinity River Restoration Program (TRRP), a multi-agency partnership charged with restoring anadromous salmonid populations in the river. The magnitude of the flow releases depends on precipitation during the preceding winter, as well as year-specific management objectives. Three types of primary objections are typically considered when designing release hydrographs – maintaining water temperatures within a range suitable for salmonid survival, encouraging the establishment of riparian vegetation on floodplain surfaces, and redistributing bed material to create and maintain the topographic complexity that supports diverse physical habitat for all salmonid life stages. See Gaeuman (2014) for a more detailed description of the Trinity River, the Lowden Ranch reach, and TRRP.

Because the dams eliminate all bed material supplies from the upstream catchment, TRRP manages gravel supplies in the river. Gravel management in the Lowden Ranch reach includes gravel augmentations that have been implemented four times at the upstream end of the Lowden Ranch reach (G_{LR}) since 2011 (Figure 2; Table 1). All four augmentations were performed in conjunction with the annual spring flow release peaks listed in Table 1. The three augmentations prior to 2017 were high-flow gravel injections (gravel pushed into the channel on the rising limb of the flood peak), whereas in 2017 the gravel was placed in the center of the channel a few days before the start of the rise. The particle size distribution of the injected gravel was similar to that of the bed surface in the reach, particularly for size fractions larger than the

median. Pebble counts indicate that the median and 90th percentile particle sizes of the injection material are about 60 and 116 mm, respectively, whereas the same percentiles for the bed surface are 55 and 118 mm. The bed surface material, however, had a finer tail than the injection gravel.

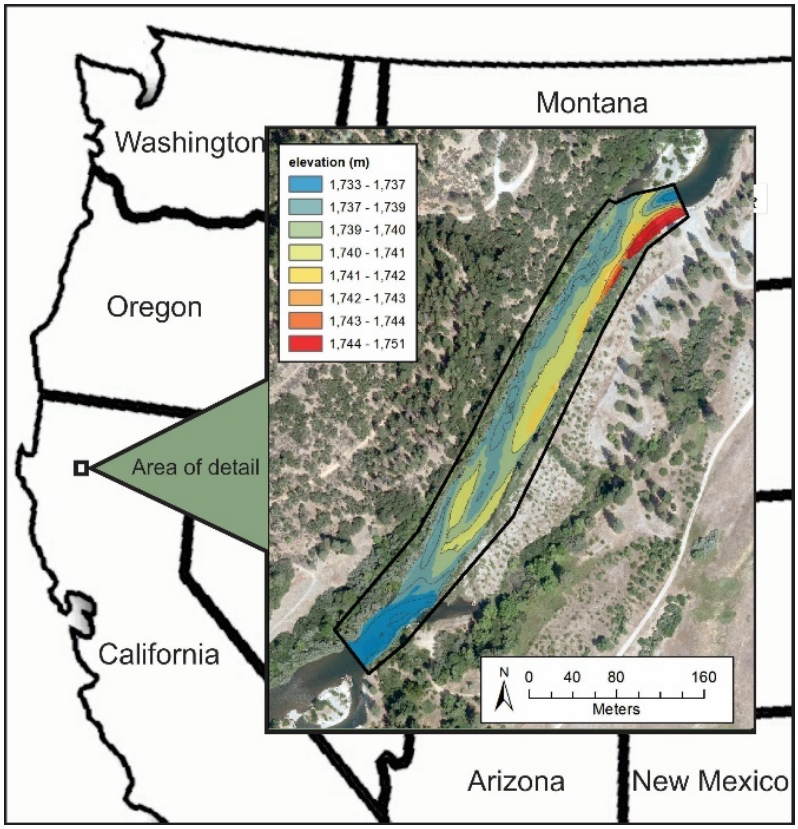

Figure 2. Map of the Lowden Ranch reach showing the analysis extent outlined in black and 2017 bed topography.

Table 1. Peak discharges released from Lewiston Dam and gravel augmentation volumes in the Lowden Ranch reach since 2011. All peaks listed occurred during annual spring flow releases except for the 2014 peak. Units of m^3 refer to volumes of stockpiled gravel whereas m^3* are volumes adjusted to substrate-equivalent bulk density (Gaeuman 2014). Topographic survey types are sonar (S), conventional ground surveys (CG), and multibeam sonar (MS).

Year	Time Interval	Q_{pk} (m^3/s)	G_{LR} (m^3, m^3*)	Topo Surveys
2010		212	0	S, CG
2011	2010-11	348	1570, 1413	S, CG
2012		175	0	--
2013		130	0	--
2014		98	0	--
2015	2011-15	250	520, 467	MS, CG
2016	2015-16	272	1225, 1102	MS, CG
2017	2016-17	340	1070, 963	MS, CG

Methods

The aim of this investigation is to explore how changes in channel morphology caused by flow and gravel management have affected salmonid habitat downstream from a gravel augmentation point. Current efforts to restore the Trinity River fishery are based on the hypothesis that a variable flow hydrograph coupled with adequate bed material supplies will support the development of complex channel morphology that meets the needs of all salmon life stages (USFWS and HVT 1999).

Assessing Channel Morphology

Active channel morphology within the study reach is represented at five points in time (Table 1) with data obtained from repeated topographic surveys consisting of sonar combined with conventional ground-based surveys. A 2010 survey of the site included sonar collected with dual boat-mounted transducers supplemented with conventional surveys along the channel margins (Table 1). In 2011, channel topography was obtained with an array of 2 or 3 boat-mounted transducers and supplementary conventional surveys. Sonar data collected in 2015, 2016, and 2017 were obtained with a Norbit iWBMSc multibeam system featuring 256 sonar beams sampling at up to 40 Hz. Small amounts of conventional survey data were collected in each of those years to fill in topography along the channel margins. Each of the five active channel surveys were superimposed on valley topography obtained with an airborne terrestrial LiDAR survey conducted in 2016, creating five terrain models with different channel configurations but identical overbank topography.

We computed year-to-year changes in bed material storage within the study reach as the difference in streambed elevations between successive terrain models. The effects of recent management actions on topographic variability within each of the analysis zones were evaluated with time series of depth statistics at a reference discharge of 113 m^3/s. Water surface elevations at that discharge were estimated using SRH-2D, a 2-dimensional hydraulic model developed at the Bureau of Reclamation's Technical Services Center (Lai 2010), and the 2016 terrain model. Subtracting each of the five terrain models from the modelled 2016 water surface yielded a time series of five depth distributions for each analysis zone. The mean, standard deviations, and selected quantiles of depths derived from those distributions are discussed below.

Three types of error potentially contribute to the uncertainty in bed elevations and sediment volume changes derived from topographic survey data. These are 1) random errors in the elevation data, 2) systematic bias in the elevation data, and 3) uncertainty in the bulk densities of the substrate and augmented gravel. Random errors are considered first.

Gaeuman (2014) presents an extensive uncertainty analysis suggesting that the total uncertainty in individual elevations due to all sources of random error in the data used in this study is less than 0.1 m. These survey errors are assumed to be independent and randomly distributed. The expected error over n random, mutually independent elevation measurements is equal to the standard error of the estimate, which is defined by the expected error divided by $n^{0.5}$ (Hamilton 1990), which tends to zero in the limit of $n \rightarrow \infty$. Uncertainty due to random errors therefore have negligible net effect on the mean bed elevations or volumetric changes estimated over large portions of the study area where the topography is characterized by large numbers of survey points (Grams et al. 2013; Gaeuman 2014). In the present case, the dataset with the fewest measurement within the analysis area (the 2010 survey) contains on the order of 10^5 individual

survey points. This value of n coupled with individual random errors of 0.1 corresponds to a standard error of about 0.0003 m. Values of n for all other years are much larger and so yield smaller standard errors. Random errors therefore usually have a negligible effect on the bed material storage changes and depth statistics computed for this study. Exceptions occur only in the 2010 survey, which includes some local areas where the survey density is sparse enough to potentially generate non-negligible interpolation errors. That source of uncertainty is accommodated in the Gaeuman (2014) gravel budget, which is used to derive the 2011 bed material storage volumes presented herein.

However, survey measurements are also subject to systematic bias between different surveys. Denoted herein by ε_b, bias is expressed by a non-zero expected error that persists regardless of the magnitude of n. Possible sources of survey bias include various errors associated with equipment dimensions or set-up, such as imperfect measurement of GPS antenna offsets, as well as issues with instrument calibration or parameterization. Because ε_b applies uniformly to the entire survey, it is propagated to total uncertainty in the estimated difference in sediment volumes between two surveys:

$$\delta V_b = A\varepsilon_b \quad (1)$$

where δV_b is the total volumetric uncertainty over an area A (Grams et al. 2013, Gaeuman et al. 2017).

Bias accumulates in proportion to the area being considered, so even a relatively small value of ε_b can eventually produce large uncertainties when accumulated over a large study area. It is therefore a critical factor in any assessment of geomorphic change. Gaeuman (2014) reported that the potential survey-to-survey bias associated with arrays of vertical transducers used prior to 2015 was empirically estimated at 0.012 m, whereas tests with the multibeam system used in 2015 suggested a potential bias of less than 0.01 m (Gaeuman et al. 2017). Careful analysis of the 2017 multibeam data, however, revealed a systematic bias of about 0.015 m between the 2016 and 2017 surveys. The source of the relative bias in the 2017 data could not be identified, but one possibility is that, although the same model of multibeam sonar was deployed in 2015 through 2017, the equipment was rented and the actual units supplied by the vendor may have differed. The bias detected in the 2017 data was corrected, and the larger value for ε_b (0.015 m) was used to compute the uncertainty margins for volumetric changes after 2015.

Uncertainty in the difference between the estimated bulk density of the substrate and the bulk density of the augmented gravel is assumed to be ± 10%, as suggested by Gaeuman (2014).

Rearing Habitat Assessment

Although the importance of habitats such as spawning riffles and pools for adult holding are recognized, TRRP habitat assessments focus on the availability of rearing habitat for juvenile salmon (Goodman et al. 2014). Salmon fry (≤ 50 mm in length) and presmolts (50–100 mm) are generally found in shallow, low velocity areas where their limited swimming ability is sufficient to maintain position, and where proximity to the substrate and/or vegetative cover offers micro-habitats in which to rest and hide from predators (Chapman and Bjornn 1969; Everest and Chapman 1972; Shirvell 1990). These rearing areas are frequently found along channel margins, in side channels, and near topographic features that promote hydraulic complexity. This linkage between rearing habitat availability and channel morphology makes it a useful proxy for

evaluating TRRP's overall success in promoting the development of a more complex aquatic environment.

Various methods for assessing salmonid habitat availability have been proposed, including meso-habitat classification (Bisson et al. 1982), habitat suitability indices (Bovee 1982), and bioenergetic models (Rosenfeld 2003). Despite their differences, the various methods generally recognize that the quality of physical habitat used by juvenile salmonids is a function of three primary factors: water depth, flow velocity, and proximity to cover (Bjornn and Reiser 1991; Hardy et al. 2006). The extent of cover in a stream reach, however, depends to a large extent on the status of riparian development and the recruitment of woody debris. As those factors are largely independent of the morphological changes we wish to assess, we neglect the role of cover in the habitat assessment presented below. Instead we consider "hydraulic rearing habitat," which we define solely in terms of flow depths and flow velocities.

The first step in exploring how hydraulic rearing habitat has responded to morphologic changes in the Lowden reach is to estimate flow depths and depth-averaged flow velocities throughout the reach over a range of discharges for each terrain model. Those hydraulic variables were determined for discharges of 8.5, 12.7, 19.8, 28, 42.5, and 56.6 m^3/s using SRH-2D. This range of discharges was selected to span the range of frequent flows in this reach of river during the winter months when juvenile salmon are present: 8.5 m^3/s is equal to the winter baseflow released from Lewiston Dam from mid-October through mid-April (Goodman et al. 2018). Due to its proximity to the dam, tributary accretions in the Lowden reach are usually small, so that the larger modelled flows are rarely exceeded until the annual spring high flow release begins at the end of April. The 2-d model mesh used extends several channel widths upstream and downstream from the study reach, and within the active channel consists of elements averaging 1.25 m^2 in area. The main channel bed was assigned a Manning's roughness values of 0.03, whereas sparsely- and densely-vegetated overbank areas were assigned roughness values of 0.045 and 0.06, respectively.

As no single metric can be expected to represent hydraulic rearing habitat quality with absolute accuracy, we chose to assess the availability of hydraulic rearing habitat with two metrics based on distinctly different approaches. The first of these, denoted DV (for depth-velocity), is a simple binary metric computed as the sum of the areas where flow depths and depth-averaged velocities meet habitat suitability criteria for juvenile salmonids. Substantial effort has been directed toward identifying and validating the hydraulic conditions preferred used by juvenile salmonids in the Trinity River. Based on observations in the stream, areas in which depths and velocities are less than 0.61 m and 0.15 m/s are considered suitable for rearing salmon fry, whereas depths and velocities less than 1 m and 0.24 m/s are considered suitable for rearing presmolt (Goodman et al. 2014). It was determined that the probability of observing fish under these hydraulic conditions is 16 times higher than in areas with larger depths or velocities.

The second metric used to evaluate hydraulic rearing habitat is based on a generalized linear statistical model that relates the maximum carrying capacity for juvenile Chinook salmon to variations in depth, velocity, and distance to cover, coupled with consideration of natural variations in the spatial and temporal distribution of juvenile fish (Som et al. 2018). This habitat model was generated from an extensive dataset collected within a section of the Trinity River that includes the study area for this analysis. A detailed description of the model is beyond the scope of this paper, so interested readers are referred to Som et al. (2018) for information regarding the data and Bayesian hierarchical method used to develop the model. Because the present analysis considers only the hydraulic factors that contribute to rearing habitat, we

selected a constant distance to cover of 0.3 m for all habitat calculations herein. Due to this implementation decision, the model output does not represent an actual capacity. Rather it should be regarded only as a relative index of hydraulic rearing habitat quality, which we refer to as hydraulic habitat quality (HHQ).

Results

Bed Material Storage Changes

Repeated gravel augmentations produced consistent increases in bed material storage in the study reach. By the time of the 2017 survey, the storage volume had increased by an estimated 1992 m^3 relative to the storage level prior to the first gravel augmentation in 2011 (Figure 3). These results are consistent with the findings of a similar analysis presented by Gaeuman and Boyce (2018), but it should be noted that the boundaries of the analysis area for that study differs slightly from the boundaries used herein. Bed material storage increased at an approximately constant annual rate throughout the study period.

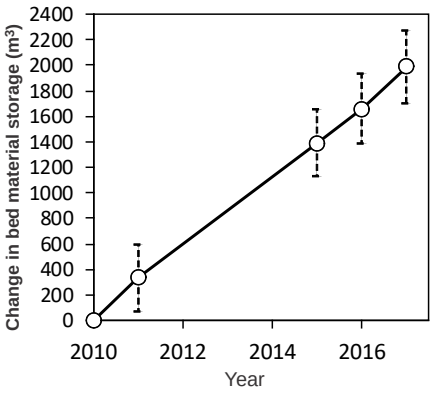

Figure 3. Cumulative changes in bed material storage since 2010.

Changes in Bed Relief

Increased bed material storage and the redistribution of bed material produced year-to-year changes in the distribution of depths at the reference discharge level (h_r). The most striking change occurred between 2010 and 2011 when the shallow end of the distribution became shallower and the deep end of the distribution became deeper (Figure 4a). For example, the 10th-percentile depth (h_{10}) decreased by 0.33 m and the 90th-percentile depth (h_{90}) increased by 0.15 m. Metrics of topographic variability, such as the standard deviations of h_r (σ_h) or the inter-decile range ($R_d = h_{90} - h_{10}$), reflect this shift toward more extreme depths between 2010 and 2011, with σ_h and R_d increasing by 39% and 57%, respectively (Figure 4b). Depths near the median (h_{50}), however, remained nearly constant.

Topographic changes after 2011 were more modest, particularly at the deeper end of the distribution. Some depth percentiles near the shallower end of the distribution continued to decrease through 2016, but the net increases in σ_h and R_d between 2011 and 2016 were just 9% and 5%. Slight fluctuations in depth percentiles near h_{50} during that period had relatively little impact on these measures of topographic relief.

The general trend toward greater topographic relief during the first four years switched after 2016 when h_{10} increased by 0.13 m, producing decreases in σ_h and R_d. At its peak in 2016, R_d was 66% larger than its initial 2010 value, whereas in 2017 it was just 48% larger than the 2010 value and smaller than the values for any of the intervening years (Figure 4b). Likewise, σ_h fell from a peak value in 2016 that was 51% larger than σ_h in 2010 to a 2017 value just 40% larger than 2010. In another shift from previous years, h_{50} decreased by about 0.08 m and depths spanning about the 20th- through the 65th-percentiles equaled or exceeded their minimum values of all five years.

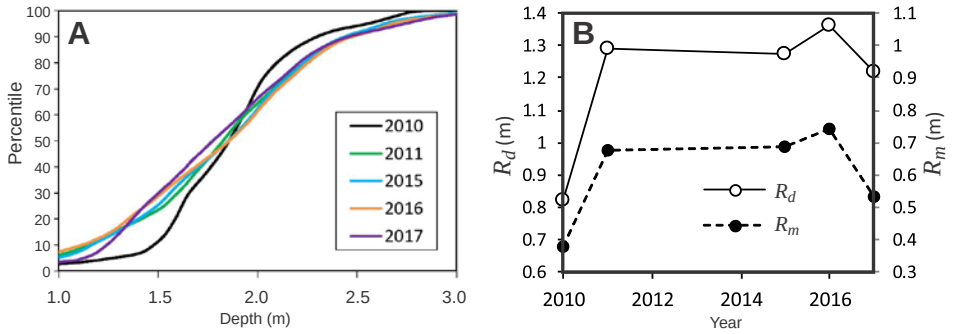

Figure 4. A) Cumulative frequency histograms showing depth percentiles at five points in time, and B) values of R_d and R_m computed for different years.

The changes in bed relief as measured by σ_h and R_d were driven by changes in h_{10}. The dominant role of the shallow tail of the depth distribution is evident when comparing R_d with the alternative metric R_m, which we define as ($h_{50} - h_{10}$). The trace of R_m plotted in Figure 4b correspond closely with the trace of R_d, confirming that the increases in R_d observed between 2010 and 2016 were primarily due to aggradation in the topographically highest parts of the channel and that decreasing relief after 2016 was due to erosion in those same areas. In other words, changes in the elevations of bar crests have influenced topographic variability within this reach to a much greater extent than have elevation changes in pools or thalweg areas.

Hydraulic Rearing Habitat

Plots of DV for the six modeled flows, each of the five years, and both juvenile salmon size classes versus discharge (Figure 5) show a tendency for DV and HHQ values to be relatively large at the baseflow discharge of 8.5 m^3/s and to decline with discharge to a minimum at an intermediate discharge before increasing again as discharge approaches the maximum modeled value of 56.6 m^3/s. Habitat availability as measured by DV reaches an absolute minimum for fry at 19.8 m^3/s in all years, whereas for presmolt the minimum is reached at discharges ranging from 19.8 to 56.6 m^3/s. Minima for HHQ also range from 19.8 to 56.6 m^3/s for both juvenile size classes. The concave up curvature of these flow-to-habitat profiles is typical of flow-to-habitat relationships in the Trinity River and is attributed to increasing flow velocities as discharges increase above baseflow but remain confined to the low-flow channel, whereas the increases in rearing habitat availability observed at higher discharges is due to rapid increases in wetted area as the bank slopes and lowest portions of the riparian zone begin to inundate (USFWS and HVT 1999).

Flow-to-habitat curves can indicate a meaningful improvement in rearing habitat availability in several ways. The most obvious indication would be an upward translation of the entire curve, corresponding to larger values of the habitat metric at all flows. Alternatively, biologically significant improvements in habitat availability also correspond to increases in the minimum habitat values on the curve, particularly if they correspond to discharges that are sustained for long durations during the January through mid-April juvenile-rearing season. Such low points at frequent flow levels are the weak links that potentially limit the productivity of the reach. In the case of Lowden Ranch, the frequency and duration of flows greater than 8.5 m^3/s during that period decline rapidly with increasing discharge, so that flows greater than 20 m^3/s occur less than 5% of the time and have a negligible impact on salmonid juveniles using the Lowden reach in most years.

Comparing the flow-to-habitat curves between years, it is immediately apparent that the absolute minimum values of both habitat metrics and both juvenile size classes are attained by the 2010 curves at a discharge of 19.8 m^3/s (Figure 5). The 2010 curves also invariably reach the lowest values of both habitat metrics for all years at 8.5 and 12.7 m^3/s. The 2017 curves, on the other hand, have the lowest habitat values at moderately large to large discharges and rival 2010 for the lowest values at 19.8 m^3/s (DV) or over all discharges equal to or lower than that level (HHQ). In short, rearing habitat availability in 2010 was relatively poor throughout the range of smaller discharges that are frequent in this reach, whereas habitat availability also tended to be low in 2017, especially at discharges of 19.8 m^3/s or more. In contrast, habitat availability was consistently close to the maximum value at all discharges in 2011 and 2015, regardless of which metric is considered. The 2016 habitat availability curves occupy an intermediate position slightly below the 2011 and 2015 curves and above the 2017 curve at most discharges.

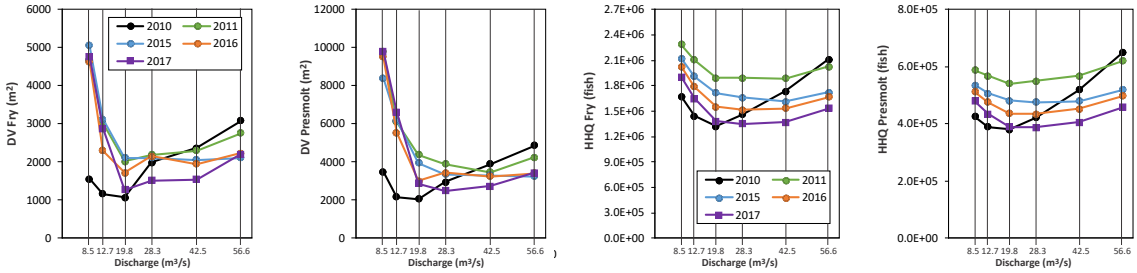

Figure 5. DV (left) and HHQ (right) flow-to-habitat curves for each juvenile size class.

Storage and Topographic Relief

All measures of bed relief discussed herein increased substantially with increasing bed material storage between 2010 and 2011, but subsequent larger increases in storage had comparatively little effect on any of the relief metrics. A plot of R_d as a function of storage suggests that the relationship could be interpreted as a step-like function that increases rapidly to a maximum, then remains constant over the range of data considered (Figure 6). That possibility is modeled in the figure with a scaled exponential distribution that fits the observed data with $R^2 = 0.94$ (for comparison, R^2 obtained from a linear least-squares fit is 0.47). A step function, however, cannot accommodate the possibility that bed relief may eventually begin to decrease as bed material storage continues to increase, as is suggested by the decreased relief observed in 2017 when the storage volume was largest. That possibility is modeled in the figure with a quadratic function that fits the data with $R^2 = 0.76$.

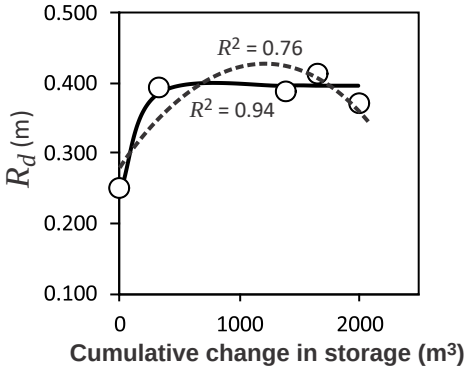

Figure 6. R_d as a function of bed material storage.

Topographic Relief and Rearing Habitat

Plots of DV and HHQ for both juvenile size classes versus R_d suggest a positive correlation with topographic variability for discharges of 8.5, 12.7, and 19.8 m^3/s (Figure 7). These discharges span the range of frequent flows that have the greatest significance for juvenile rearing in the study area. The strength of those relationships, however, depend to a large extent on one data point (2010) with exceptionally low values of R_d and low habitat metric values. The other four data points are clustered at substantially higher values of all metrics. The distribution of points in Figure 7 suggest that the topographic differences between 2011 and later years are too small to produce detectable differences in the rearing habitat metrics.

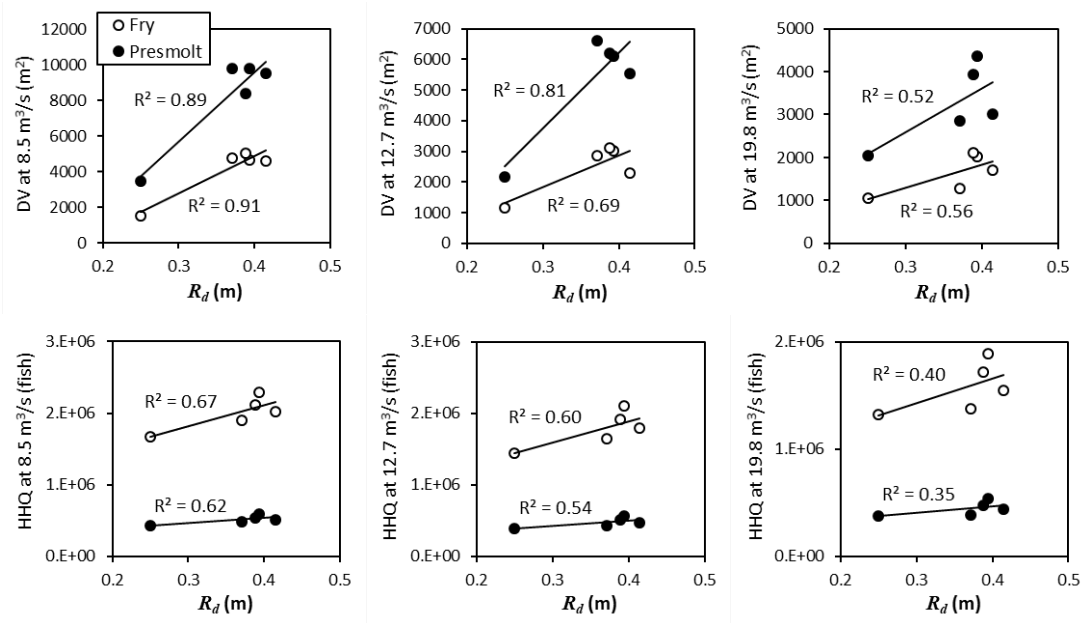

Figure 7. Plots of DV and HHQ for both juvenile size classes and discharges less than 20 m^3/s with linear least-squares relationships shown.

Similar plots of R_d versus DV and HHQ for the higher, less frequent discharges show virtually no correlation between relief and the habitat metrics except at the highest flow of 56.6 m^3/s (Figure 8). At that flow, rearing habitat availability appears to be inversely correlated with bed relief.

Again, the apparent correlation depends on the separation between the 2010 data points and the remaining years, which are clustered within a limited range of R_d.

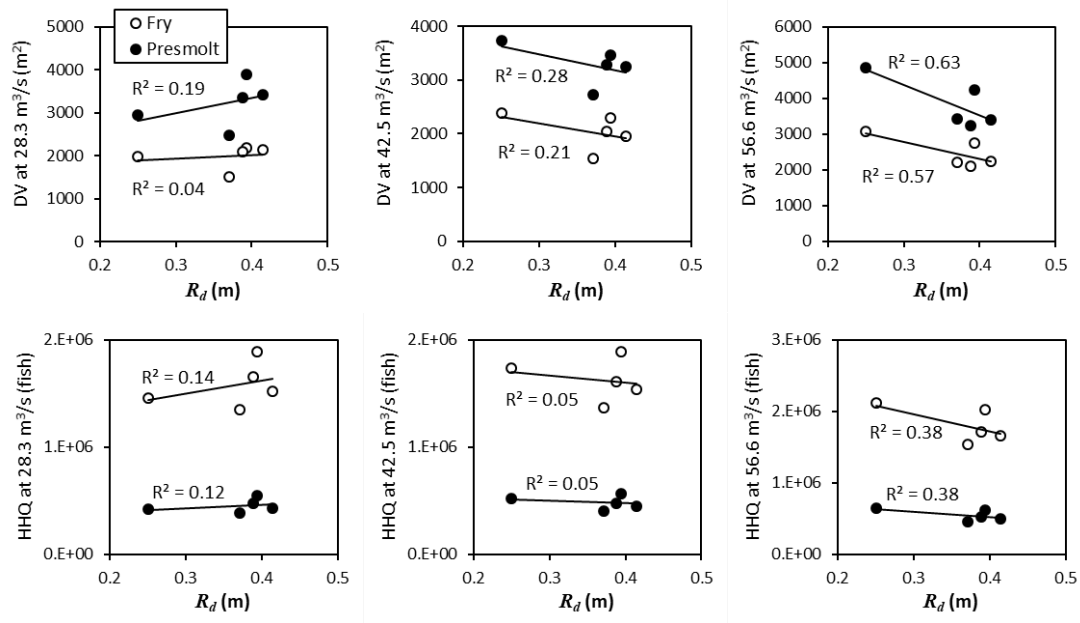

Figure 8. Plots of DV and HHQ for both juvenile size classes and discharges greater than 20 m^3/s with linear least-squares relationships shown.

Discussion

Repeated gravel augmentation at the upstream end of the study reach resulted in consistent increases in bed material storage over 7-year period. The increases in storage are associated with an initial increase in topographic relief within the active channel, followed by smaller changes in later years. That result could be interpreted in terms of a sediment "saturation" hypothesis in which increasing sediment supplies are thought to increase bed relief up to a point, after which additional increases in the sediment supply have little effect on bed topography. The largest change in bed relief over the final 6 years of the study, however, consists of a decrease in bed relief between 2016 and 2017, despite (or perhaps because of) the continued accumulation of bed material during that time interval. The fact that the two years with the least topographic relief correspond to the years with the smallest and largest bed material storage volumes is consistent with the intermediate supply hypothesis described by Yarnell et al. (2006), which posits that topographic variability is greatest when sediment supplies are neither too small or too large.

Some of the mechanisms by which changing sediment supplies alter topographic relief can be inferred from changes in the distribution of flow depths in the study reach. The initial large increase in relief observed in 2010-2011 was the result of bar growth and, to a lesser extent, bed scour in deeper portions of the channel. A smaller increase in relief in 2015-2016 was almost entirely due to an increase in the heights of bar crests, whereas the decrease in relief in 2016-2017 was associated with erosion of the bar crests. Topographic changes in 2016-2017 also included aggradation in regions of intermediate depth, so that the 2017 channel contained wider but slightly lower bars than were present in 2016. Bed elevations in the deepest parts of the channel remained relatively constant through time, possibly because the study reach is almost perfectly straight and so lacks bends or other structures associated with the formation of deep

pools that have the potential to fill and scour. It is likely that changes at the deep end of the depth distribution will contribute more significantly to changes in bed relief metrics in other reaches.

The availability of rearing habitat for juvenile salmon at low discharges increased markedly with the increase in bed relief between 2010 and 2011. These habitat improvements were likely due to the development of larger bars that create eddies and local backwater zones that provide suitable hydraulic conditions. Habitat metrics remained larger than their 2010 levels through the later years of the study, resulting in moderately strong positive correlations between bed relief and habitat availability. The range of topographic conditions over the later years is too small, however, to conclude that the apparent correlations are reliable.

The apparent correlation between bed relief and rearing habitat observed at low flows becomes extremely weak or entirely absent when discharge increases beyond about 20 m^3/s. We hypothesize that the correlation is lost when flow over the bars that generate eddies and backwater zones at lower discharges becomes deep and fast enough to eliminate many of those low-velocity hydraulic features. Once the bars are fully washed out, their presence in the channel may result in decreased habitat availability, leading to the apparent inverse correlation between bed relief and rearing habitat that emerges at the highest modeled flow of 56.6 m^3/s. Assuming this result is real, it can potentially be explained as the consequence of reduced conveyance for moderately large in-channel flows. Flow begins to spread onto the floodplain adjacent to the study reach at discharges near 113 m^3/s, and most of the floodplain area is inundated when discharges exceed about 240 m^3/s. Thus, a flow of 56.6 m^3/s is still well within the bankfull channel even though it is between 3 and 6.7 times larger than typical flows during the months when juvenile salmon are in the Lowden Ranch area. In the absence of well-developed bars, a flow of that magnitude can be conveyed over the full width of an approximately rectangular channel. As bars develop, the channel becomes more triangular in cross section, and conveyance is progressively restricted to a narrower thalweg area with higher flow velocities. This potential negative influence of in-channel bars on rearing habitat availability at moderately high flows may reverse, however, as discharge continues to increase to higher levels not considered in this study. Any reduction in channel conveyance will encourage floodplain inundation at lower discharges than otherwise, greatly increasing of the availability of productive rearing habitat in overbank areas (Sommer et al. 2001).

Conclusions

Increasing bed material storage or bed material storage in a stream reach does not necessarily result in an increase in topographic relief or geomorphic complexity. Topographic monitoring in conjunction with repeated gravel augmentations in the Trinity River demonstrate that the first of several gravel augmentations increased bed relief, but subsequent augmentations did not and the maximum level of bed material storage in the reach coincided with a decrease in topographic relief. These findings are consistent with the hypothesis that geomorphic complexity is greatest when sediment is supplied to a reach at an intermediate rate.

Topographic relief is correlated with juvenile salmon rearing habitat availability at some discharge levels, but not at others. Habitat within the active channel is positively correlated with relief when discharge in the study reach is near the regulated winter baseflow level.

The correlation disappears as discharge increases to approximately 3 times the regulated winter baseflow level, and a negative correlation appears to emerge as discharge approaches 6 times the baseflow level. Habitat availability at the higher discharges likely depends on channel planform characteristics and the morphology of the upper banks and floodplain rather than on bed topography.

Year-to-year differences in channel morphology within the study reach were relatively subtle for four of the five years analyzed, so the correlations obtained between topographic variability and rearing habitat availability are heavily dependent on the difference between the metrics computed for a single year versus those of the remaining four years. Additional studies with reaches spanning a wider range of morphologies are needed to assess the relationship between topographic factors and habitat quality with greater confidence.

References

Bartley, R. and Rutherfurd, I. 2005. "Measuring the reach-scale geomorphic diversity of streams: application to a stream disturbed by a sediment slug," River Research and Applications, 21:39-59.

Bisson, P.A., Nielson, J.L., Palmason, R.A., and Grove, L.E. 1982. "A system of naming habitat types in small streams, with examples of habitat utilization by salmonids during low stream flow," In: Acquisition and utilization of aquatic habitat inventory information, Edited by N.B. Armantrout, American Fisheries Society, Bethesda, Md. pp. 62–73.

Bjornn, T.C. and Reiser D.W. 1991. "Habitat Requirements of Salmonids in Streams," In: Influences of Forest and Rangeland Management on Salmonid Fishes and Their Habitats, Edited by W.R. Meehan, American Fisheries Society Special Publication, 19, 83-138.

Bovee, K.D. 1982. "A guide to stream habitat analysis using the instream flow incremental methodology," Instream Flow Information paper 12, U.S. Fish and Wildlife Service, Office of Biological Services, FWS/OBS-82/26.

Chapman, D.W. and Bjornn, T.C. 1969. "Distribution of salmonids in streams," In: Symposium on Salmon and Trout in Streams, Edited by T.G. Northcote, HR MacMillan Lectures in Fisheries. Institute of Fisheries, University of British Columbia, Vancouver, BC.

Church, M. 1995. "Geomorphic response to river flow regulation: Case studies and time-scales," Regulated Rivers: Research and Management, 11:3-22.

Everest, F.H. and Chapman, D.W. 1972. "Habitat selection and spatial interaction by juvenile chinook salmon and steelhead trout in two Idaho streams," Journal of the Fisheries Board of Canada, 29(1):91-100.

Gaeuman D. 2012. "Mitigating downstream effects of dams," In Gravel-bed Rivers: Processes, tools, environments, Edited by M. Church, P. Biron, and A.G. Roy, Chichester, John Wiley & Sons, 563 pp.

Gaeuman D. 2014. "High-flow gravel injection for constructing designed in-channel features," River Research and Applications, 30:685-706, doi:10.1002/rra.2662.

Gaeuman D., Stewart R.L., Schmandt B. and Pryor, C. 2017. "Geomorphic response to gravel augmentation and high-flow dam release in the Trinity River, California", Earth Surface Processes and Landforms, 42:2523-2540, doi:10.1002/esp.4191

Gaeuman, D. and Boyce, J. 2018. “Effects of gravel supply on gravel bar morphology and physical habitat in a reach of the Trinity River, California, USA,” Proceedings of the 12th International Symposium on Ecohydraulics, Aug. 19-24, 2018, Tokyo, Japan.

Goodman, D.H., Som, N.A., and Hetrick, N.J. 2018. “Increasing the availability and spatial variation of spawning habitats through ascending baseflows,” River Research and Applications, 34:844-853.

Goodman D.H., Som N.A., Alvarez J., and Martin, A. 2014. “A mapping technique to evaluate age-0 salmon habitat response from restoration,” Restoration Ecology, 23(2):179-185.

Grams, P.E., D.J. Topping, J.C. Schmidt, J.E. Hazel, Jr., and M. Kaplinski. 2013. “Linking morphodynamic response with sediment mass balance on the Colorado River in Marble Canyon: Issues of scale, geomorphic setting, and sampling design,” Journal of Geophysical Research, 118(2):361-381, doi:10.1002/jgrf.20050.

Hamilton, L.C. 1990. “Modern data analysis: a first course in applied statistics,” Brooks/Cole Publishing Company, Belmont, CA, 684 pp.

Hardy, T.B., Shaw, T., Addley, R.C., Smith, G.E., Rode, M., and Belchik, M. 2006. “Validation of Chinook fry behavior-based escape cover modeling in the lower Klamath River,” International Journal of River Basin Management, 4(3):169-178.

Humphries R., Venditti, J.G., Sklar, L.S., and Wooster. J.K. 2012. “Experimental evidence for the effect of hydrographs on sediment pulse dynamics in gravel-bedded rivers,” Water Resources Research, 48, W01533, doi:10.1029/2011WR010419.

Kondolf, G.M. and Wilcock, P.R. 1996. “The flushing flow problem: Defining and evaluating objectives,” Water Resources Research 32:2589-2599.

Lai, Y.G. 2010. “Two-dimensional depth-averaged flow modeling with an unstructured hybrid mesh,” Journal of Hydraulic Engineering 136(1):12-23.

Lisle, T.E. 1982. “Effects of aggradation and degradation on riffle-pool morphology in natural gravel channels, Northwestern California,” Water Resources Research 18(6):1643-1651.

Lisle, T.E., Iseya, F. and Ikeda, H. 1993, “Response of a channel with alternate bars to a decrease in supply of mixed-size bed load: a flume experiment,” Water Resources Research, 29(11):3623-3629.

Lisle, T.E., Pizzuto, J.E., Ikeda, H., Iseya, F., and Kodama, Y. 1997. “Evolution of a sediment wave in an experimental channel,” Water Resources Research 33:1971-1981.

Madej M.A. 1999. “Temporal and spatial variability in thalweg profiles of a gravel-bed river,” Earth Surface Processes and Landforms, 24(12):1153-1169.

Madej, M.A. and Ozaki. V. 2006. “Channel response to sediment wave propagation and movement, Redwood Creek, California, USA,” Earth Surface Processes and Landforms, 21:911-927.

Madej, M.A. and Ozaki, V. 2009. “Persistence of effects of high sediment loading in a salmon-bearing river, northern California,” In Management and restoration of fluvial systems with broad historical changes and human impacts: Geological Society of America Special Paper 451, Edited by L.A. James, S.L. Rathburn, and G.R. Whittecar, pp. 43-55.

Milhous, R.T. 1998. “Modelling of instream flow needs: The link between sediment and aquatic habitat,” Regulated Rivers: Research and Management 14:79-94.

Ock, G., Gaeuman, D., McSloy, J., and Kondolf, G.M. “Ecological functions of restored gravel bars, the Trinity River, California,” Ecological Engineering, 83:49-60.

Petts, G.E. and Maddock, I. 1996. “Flow allocation for in-river needs,” In: River Restoration, Edited by G.E. Petts and P. Calow, Blackwell Science, London.

Richter, B.D., Baumgartner, J.V., Wigington, R., and Braun, D.P. 1997. “How much water does a river need?” Freshwater Biology 37:231-249.

Rosenfeld, J. 2003. “Assessing the habitat requirements of stream fishes: An overview and evaluation of different approaches,” Transactions of the American Fisheries Society, 132:953-968.

Shirvell, C.S. 1990. “Role of instream rootwads as juvenile coho salmon (Oncorhynchus kisutch) and steelhead trout (O. mykiss) cover habitat under varying streamflows,” Canadian Journal of Fisheries and Aquatic Science, 47(5):852-861.

Sklar, L.S., Fadde, J, Venditti, J.G., Nelson, P., Wydzga, M.A., Cui, Y. and Dietrich, W.E. 2009. “Translation and dispersion of sediment pulses in flume experiments simulating gravel augmentation below dams,” Water Resources Research 45, 10.1029/2008WR007346.

Som, N.A., Perry, R.W., Jones, E.C., De Juilio, K., Petros, P., Pinnix, W.D., and Rupert, D.L. 2018. “N-mix for fish: estimating riverine salmonid habitat selection via N-mixture models,” Canadian Journal of Fisheries and Aquatic Science, 75:1048-1058.

Sommer, T.R., Nobriga, M.L., Harrell, W.C., Batham, W., and Kimmerer, W.J. 2001. “Floodplain rearing of juvenile chinook salmon: evidence of enhanced growth and survival,” Canadian Journal of Fisheries and Aquatic Science, 58:325-333.

Stanford, J.A., Ward, J.V., Liss, W.J., Frissell, C.A., Williams, R.N., Lichatowich, J.A., and Coutant, C.C. 1996. “A general protocol for restoration of regulated rivers,” Regulated Rivers: Research and Management 12:391-413.

USFWS and HVT (United States Fish and Wildlife Service and Hoopa Valley Tribe). 1999. “Trinity River Flow Evaluation Study,” Report to the Secretary of the Interior, US Department of the Interior, Washington, D.C.

Venditti J.G., Dietrich W.E., Nelson P.A., Wydzga M.A., Fadde J., and Sklar L. 2010. “Effect of sediment pulse grain size on sediment transport rates and bed mobility in gravel bed rivers,” Journal of Geophysical Research, 115, F03039, doi:10.1029/2009JF001418.

Viparelli E., Gaeuman D., Wilcock P.R., and Parker G. 2011. “A model to predict the evolution of a gravel bed river under an imposed cyclic hydrograph and its application to the Trinity River,” Water Resources Research 47, W02533, doi:10.1029/2010WR009164.

Wu, W., He, Z., Wang, S.S.Y, and Shields, F.D., Jr. 2006. “Analysis of aquatic habitat suitability using a depth-averaged 2-D model,” Proceedings of the Joint 8th Federal Interagency Sedimentation Conference and 3rd Federal Interagency Hydrologic Modeling Conference, April 2–6, Reno, Nevada.

Williams, G.P. and M.G. Wolman. 1984. “Downstream effects of dams on alluvial rivers,” US Geological Survey Professional Paper 1286, 83 pp.

Yarnell S.M., Mount J.F. and Larsen E.W. 2006. “The influence of relative sediment supply on riverine habitat heterogeneity,” Geomorphology, 80:310-324.

Zunka, J.P.P., Tullos, D.D. and Lancaster, S.T. 2015. “Effects of sediment pulses on bed relief in bar-pool channels”, Earth Surface Processes and Landforms, doi:10.1002/esp.3697.

Evaluating and Developing Multi-Purpose Riverine Projects: An Example from the Middle Rio Grande

Jonathan AuBuchon, Regional Sediment Specialist, U.S. Army Corps of Engineers, Albuquerque, NM, Jonathan.Aubuchon@usace.army.mil
Robert Padilla, Supervisory Hydraulic Engineer, U.S. Department of the Interior, Bureau of Reclamation, Albuquerque, NM, rpadilla@usbr.gov

Abstract

Fluvial systems like the Middle Rio Grande (MRG) are inherently complex given its geology and characteristics as a semi-arid southwest river. Developing a cohesive framework for multi-disciplinary teams to integrate their expertise and analytical tools in a project development process is challenging due to the dynamic, uncertain, and complex nature of the riverine environment. The MRG has undergone both geologic, hydro-climate, and anthropogenic driven morphological changes resulting in the need to perform river maintenance to ensure effective water and sediment delivery, meeting socio-economic needs in the MRG valley. The observed morphological responses have also affected endangered species and their habitats. The U.S. Department of the Interior, Bureau of Reclamation (Reclamation) has evolved its project planning processes to balance sometimes conflicting needs of satisfying socio-economic and ecological needs in the semi-arid southwest. The methodology presented herein describes the framework for a robust decision making process by which project alternatives are formulated and analyzed comparatively, culminating in a preferred alternative for implementation. The procedure builds upon lessons learned in other fluvial systems and provides guidance based on MRG experiences through the alternative formulation, analysis, and selection process.

Developing goals, identifying constraints, formulating alternatives, defining specific project objectives, and systematically evaluating the alternatives involves two distinct steps. The first step is at a conceptual or appraisal level and is more qualitative than quantitative. This first step culminates in the formulation of potentially suitable alternatives. The second step includes the development and analysis of those potentially suitable alternatives in a systematic and holistic manner. This second step is typically more quantitative in nature, culminating in the development of a feasibility level or 30% project scope for the potentially suitable alternatives. This step also results in the selection of a preferred alternative. These two steps are preceded by an assessment(s) providing understanding of the underlying physical processes and environmental conditions occurring in the fluvial system.

Background

In the early to mid-1900s the MRG transported an estimated 30 to 40 million tons of sediment annually (Finch and Tainter 1995). This quantity of sediment created large geomorphic changes causing severe flooding, loss of water, damage to riverside facilities, and the loss of productive farmlands because of high water tables. This led to the Flood Control Acts (Acts) of 1948 (P.L. 80-858) and 1950 (P.L. 81-516) which established the MRG Project. Reclamation was authorized at this time to perform maintenance on the MRG. Essential maintenance performed by Reclamation is described in more detail in Reclamation's Plan and Guide (2007; 2012a), but generally includes ensuring channel capacity, protection of adjacent infrastructure, and effective transport of water and sediment between Velarde and Caballo Dam, New Mexico. An

international treaty with the Republic of Mexico for delivery of water and the 1939 Rio Grande Compact, which regulates the distribution of Rio Grande water among the states of Colorado, New Mexico, and Texas also affects the MRG Project and associated essential maintenance activities. These maintenance actions provide a socio-economic service to the MRG valley, however, they also tend to limit the degrees of freedom the MRG has to adjust. Maintenance activities have evolved since the Flood Control Acts to include Federal responsibilities under the 1973 Endangered Species Act (ESA), including habitat requirements mandated by the 2016 Biological Opinion (USFWS 2016) for work on the MRG. Consequences of not performing these activities include substantial damage to riverside facilities, loss of water, and loss of endangered species habitat.

Habitat restoration work on the MRG also provides a socio-economic value by creating features that have aesthetic and recreational value along with the underlying ecosystem services function. There are circumstances where this type of work may conflict with maintenance needs that protect riverside facilities and ensure water and sediment can be conveyed downstream effectively. For instance, the creation of bank terraces and backwater embayments on the MRG restores a vital connection between the river and its floodplain. This helps dampen the flood peaks for some flows, encourages riparian vegetation that provides a level of bank stability that protect riverside facilities, and locally raises groundwater levels. These features also spread water out, make the effective transport of water and sediment less efficient, and potentially provide an avenue for fluvial adjustments of the channel to cause lateral migration of the banks towards riverside facilities. It is in considering both the socio-economic and ecological needs that a balance must be struck. Given that balancing these needs occurs within a complex and dynamic MRG, a multi-disciplinary team decision making process for formulating and evaluating alternatives has been developed and refined over the years on the MRG. This alternative analysis process that encompasses both the socio-economic and ecological needs along the MRG is further described in the following sections.

General Concepts and Preliminary Assessments

The river system and its processes, substrate, biota, and their dynamic inter-relationships provide challenges for multi-disciplinary teams in predicting channel conditions and responses to river projects. Key to the success and development of potentially suitable alternatives is to assess the underlying physical processes that are occurring within the fluvial system. Wohl et al. (2006) emphasizes understanding of the physical processes in the development of alternatives in order to provide a more self-sustainable river system, which helps with resiliency (Parsons and Thoms 2018). This understanding requires at least a basic understanding of the geology, fluvial geomorphology, sediment, hydrology, and hydraulics for the reach in which work is being pursued (Biedenharn et al. 1997; Watson et al. 1999; NRCS 2007a; Niezgoda et al. 2014). These assessments require the continuous or periodic collection of field data and an understanding of the history of channel conditions and trends to help assess changes that are occurring. On the MRG periodic data collection efforts are analyzed for current morphological trends on a project by project basis that considers the local fluvial area (Harris and AuBuchon 2016; Holste 2017). Larger geomorphic reaches are also evaluated on the MRG (Klein et al. 2018; Harris et al. 2018) to provide a system wide assessment. This process helps identify dominant processes occurring throughout a connected ecosystem (Wohl et al. 2015), allowing the potential for multiple projects to work with a river's self-sustaining processes. These studies coupled with collections of historical channel changes and anthropogenic influences on the MRG (Graf 1994; Scurlock 1998; MEI 2002; Massong et al. 2010; Makar and AuBuchon 2012; and Makar 2015) provide a framework for understanding potential fluvial system responses to proposed projects.

An understanding of the ecology within a fluvial system and the inter-dynamics, such as vegetation growth and biological activity (e.g. beaver and other animal burrows in the streambank), that influence the fluvial system (Cramer 2012) is also important. This also entails the consistent collection and analysis of field data. On the MRG, biological studies have focused on the needs of endangered species (e.g., Siegle et al. 2013; Tetra Tech 2014; Baird 2016; and Bachus and Gonzales 2017). There are a fewer broader and more holistic studies that have been pursued such as Crawford et al. (1993) and Mortensen et al. (2019) to help link observed biological changes with morphological, hydrologic, hydraulic, and sediment changes. Reclamation has also been working towards developing ecological function criteria (Reclamation, unpub. data, 2017) to help assess desirable morphological features for different life stages of endangered species. This helps to target better habitat improvement projects. Habitat suitability indexing, such as Harris (2017), have also been found to be useful on the MRG to identify potential Rio Grande silvery minnow habitat. Similar analysis would benefit an evaluation of habitat improvement potential during evaluation of alternatives. These types of evaluations, however, require an understanding of the ecological needs for a given biota (this may vary by life stage as well).

Finally, to successfully formulate alternatives, an understanding of available and appropriate river treatment methods are needed. These form a working "toolbox" from which to pull ideas during the brainstorming session that occurs as part of the alternative analysis process. There are a variety of resources and training courses available that help fill this toolbox. While not an extensive list, some useful references include NRCS (2007a), Baird and Makar (2011), Reclamation (2012a; 2012b; 2015), Baird et al. (2015), Baird (2016), Lagasse et al. (2016), Newbury (2016), Reclamation and USACE (2016), Sholtes et al. (2017), and Yochum (2018). These references provide guidance on a variety of river treatment methods.

Given the breadth of information required to conduct an alternative analysis, a multi-disciplinary team is needed along with a robust alternative analysis process. On the MRG there is a desire to ensure that both socio-economic and ecological considerations are developed and integrated together as alternatives are evaluated in terms of their effectiveness and costs. The alternative analysis allows the multi-disciplinary project team the flexibility and innovation required to integrate these diverse and sometimes conflicting needs. The goal being to make sound and defensible decisions, working towards a more self-sustaining and resilient system (Parsons and Thoms 2018).

Assuming data collection and reach assessments have been conducted, the alternative analysis process would then progress in two distinct steps. Both of these steps would involve a multi-disciplinary team. The first step, identified as alternative formulation, is a conceptual or appraisal assessment that develops and clearly articulates the goal(s), scope, and constraints of the project. A brainstorming session, based on the experience and knowledge obtained from previous projects and literature reviews, is then conducted to identify mutually exclusive, suitable alternatives. A suitable alternative implies that the team would formulate an alternative that meets a project's agreed upon goals/objectives, developed by the multi-disciplinary team, and that the alternative is realistic and achievable. The second step involves the analysis and rating of the suitable alternatives. During this step, the team develops an evaluation framework centered on engineering effectiveness, ecosystem function, and economic criteria. The second step is quantitative in nature, culminating in the development of a feasibility level (30% level of scope development) scope for the suitable alternatives. This step also typically results in the selection of a preferred alternative. Each of these steps is described in more detail in the sections below, including a listing of key work steps and a schematic diagram of the work process.

Step 1 – Formulation of Alternatives

The formulation of alternatives is the first step of a robust alternative analysis process. The formulation of potentially suitable alternatives begins after a general understanding of the underlying physical processes and environmental conditions is obtained, as previously described. The formulation of potentially suitable alternatives is more of an appraisal (i.e. conceptual or order of magnitude for cost) level assessment that begins by forming a multi-disciplinary team. This team works by consensus to develop and clearly articulate the goal(s), scope, and constraints of the project (Biedenharn et al. 1997; Watson et al. 1999; IPMP 2002; NRCS 2007a; Skidmore et al. 2011; Martin et al. 2016; Wohl et al. 2015; Sholtes et al. 2017). The goal(s) need to convey the value and intent of the desired work. This should be clearly and succinctly stated so others can readily grasp the project's vision and desired outcome. From this effort the project's scope is developed, which includes defining the purpose and need for the planned project. The team should also consider the potential consequences and impacts of not doing the project. Ideally the scope and effect of the project's benefits would be greater, or at least proportional, to the potential consequences and impacts of not doing the project. Potential project constraints are also identified to help refine the goal(s) and project scope. Constraints include verifying that there is legal (land use), statutory, and fiscal authority to pursue the project and identifying any limitations related to this authorization. These constraints may also be identified for other reasons, such as cultural, recreational, etc.

Ideally the multi-disciplinary team provides the expertise or understanding to make the background assessments described earlier or has the capability to collect and analyze additional data to provide this level of expertise in support of a project's alternative formulation. From this body of knowledge, alternatives can be proposed through a brainstorming exercise that would satisfy the stated goal(s), purpose and need of the project, and objectives. If an alternative is proposed that doesn't solve the problem (would not meet the goal(s) or objectives and is not within the identified constraints) then this alternative should be screened out from further evaluation.

The multi-disciplinary team may include primary stakeholders, such as landowners, as part of the team. One of the keys to working with a multi-disciplinary team is to keep a level of independence among the team for analyzing and rating alternatives. The desire in an alternative analysis is to have each team member provide feedback and ask challenging questions about the proposed alternatives, rather than relying on the opinions of one or two team members (Nemeth 2014). It is easy for teams, especially ones that work well together or with teams under significant time constraints, to rely on others in the team, instead of critically evaluating the proposed alternatives against the agreed upon goals, objectives, and constraints. As an example, one MRG project north of Albuquerque had to be redesigned at construction because not all concerns of the primary stakeholder were thoroughly expressed to the multi-disciplinary team during the alternative analysis process even though the team included members from the primary stakeholders. While not foolproof, developing clear and succinct goals, purposes, and needs during the alternative formulation process and having a team environment in which concerns can be brought forward and discussed is helpful to minimize potential problems experienced further down the planning road.

Involving the experience and expertise of construction personnel during this assessment may also be useful to understand which identified constraints can be overcome through utilization of an appropriate construction technique, such as minimizing damage to riparian vegetation by using amphibious excavators or employing specialized planting techniques, such as Longstem

and Tallpots (NRCS 2007b; Dreesen et al. 2002), to increase viability of vegetation and aid in the bank stability in a more arid climate.

Alternatives should also be assessed if they will work with the dominant physical processes that are identified from the background assessments described previously. This in essence checks if the proffered alternative works with the identified physical processes. This can provide a further screening of alternatives, but would be dependent upon the originally stated goal(s) and objectives. For example, the reach of the MRG upstream of Elephant Butte Reservoir experiences loss of channel capacity concerns due to sediment deposition within the channel. This has created a main channel system perched above the adjacent floodplain. In this situation large sustained runoff events have caused the river's sediment load to entirely block the active channel, forcing all of the water into the floodplain, creating socio-economic concerns about loss of water for downstream users. Previous reach responses have focused on removing the sediment mechanically after an observed blockage. This alternative, while effective in the short term, works against the dominant physical processes that have created a perched channel condition and continue to cause sediment deposition. In an effort to provide a more sustainable approach, an alternative analysis (Holste 2014) identified an option to relocate the channel to a lower point in the floodplain further to the east. The relocation option provides an opportunity for the fluvial system to respond and self-adjust without continuous intervention. This alternative also provides more space between the infrastructure at risk when the river floods. The additional space allows the channel to self-adjust, facilitating the natural successional development of both morphological and vegetative features. Over the long term the continued deposition of sediment will result in perched conditions. The perched channel conditions will not, however, be as constrained due to the increase of available space for the river to adjust. Due to the goals associated with this alternative, monitoring of this project is geared to assess the increased resiliency and diversity that results from the channel relocation.

Screening alternatives at the appraisal level (e.g. proof of concept, meets purpose and need, works with the dominant physical processes, etc.) helps minimize the time required to perform the next phase of the alternative analysis process — the evaluation of alternatives. Identified alternatives for evaluation at a feasibility level (30% scope development) should be mutually exclusive so that their effects may be quantified and independently assessed. Based on experience in the MRG, having between 3-5 alternatives is sufficient to identify an initial array of alternatives and helps provide an efficient and timely alternative screening step. For example, some MRG projects (Lopez and AuBuchon 2012; Tetra Tech 2012) identified six or more alternatives. This extends the time needed to evaluate alternatives and results in a more laborious selection process to differentiate between similar alternatives. In hindsight, the number of alternatives should have been reduced by grouping together alternatives with the same function. For example, some of the MRG sites had different iterations of indirect bank protection like bendway weirs (low, flat structures perpendicular to the flow), rock vanes (sloped structures perpendicular to the flow), or a combination of bendway weirs and rock vanes. If these had been evaluated as a single transverse feature alternative, less time would have been spent during evaluation, facilitating a quicker transition into design.

When combining alternatives to form mutually exclusive options, it is important to remember that the purpose of the alternative analysis process is to assess the suitability of any given alternative to achieve the project goal(s). The design phase of the work, which is outside the scope of an alternative analysis, would delve into the details, such as the specific transverse feature type to provide an adequate design for the above example (Biedenharn et al. 1997; NRCS 2007a; Yochum 2018). Information developed during the alternative analysis phase, such as project goal(s), scope, objectives, constraints, etc. should also be carried into the design phase.

Key Work Steps: The following alternative formulation steps are provided as an outline for a project team conducting an alternative analysis for a specific site or reach. These steps are also illustrated graphically in Figure 1.

1. Form a project team
    a. Identify disciplines needed (engineering, biology, geomorphology, etc.)
    b. Start small, but add expertise as needed (such as addressing concerns related to lands or cultural resources).
2. Identify overarching goal(s)
    a. Why is this work being pursued?
    b. What is the intent/vision of the project?
    c. Develop the goal statement with cognizance of authority (see work step 4).
3. Identify the project's scope and intended outcome
    a. Includes the purpose and need statements.
    b. The scope and effect of the project's benefits would be greater, or at least proportional, to the potential consequences and impacts of not doing the project.
4. Identify constraints
    a. What is not allowed?
        i. Limits of disturbance, including site access
        ii. Limits of type of activities
        iii. Seasonal restrictions
        iv. Safety
        v. Anticipated site conditions
    b. Are there authority limitations (legal, statutory, and/or fiscal) to do the work?
    c. Are there are any other stakeholders that may have authority/jurisdiction to perform or to influence aspects of the work?
5. Brainstorm to obtain a list of mutually exclusive alternatives
    a. Based on reach understanding of fluvial geomorphology, including information on geology, sediment, hydrology, and hydraulics.
    b. Based on reach understanding of ecology and biota.
    c. Based on knowledge of river methods, suites of methods, track record for method application, and construction techniques that would help achieve the project goal(s).
    d. Useful to have around 3-5 mutually exclusive alternatives.
    e. Include the "no action" scenario (e.g. cost or effects of doing nothing).

Step 2 – Evaluation of Alternatives

The evaluation of each alternative formulated by the multi-disciplinary team is the second step. These alternatives are developed and analyzed to approximately the 30% design and planning level. This provides a means to rank each alternative, helping the multi-disciplinary team select a preferred alternative to implement.

The multi-disciplinary team generates an evaluation framework to objectively analyze the alternatives. The evaluation process relies on the multi-disciplinary team to determine the evaluation criteria. The evaluation criteria may be weighted by the team towards criteria that is considered more important to achieving the defined project goals and objectives. In general, there are three categories/factors of evaluation criteria used on the MRG: engineering effectiveness, ecosystem function, and economics (Biedenharn et al. 1997).

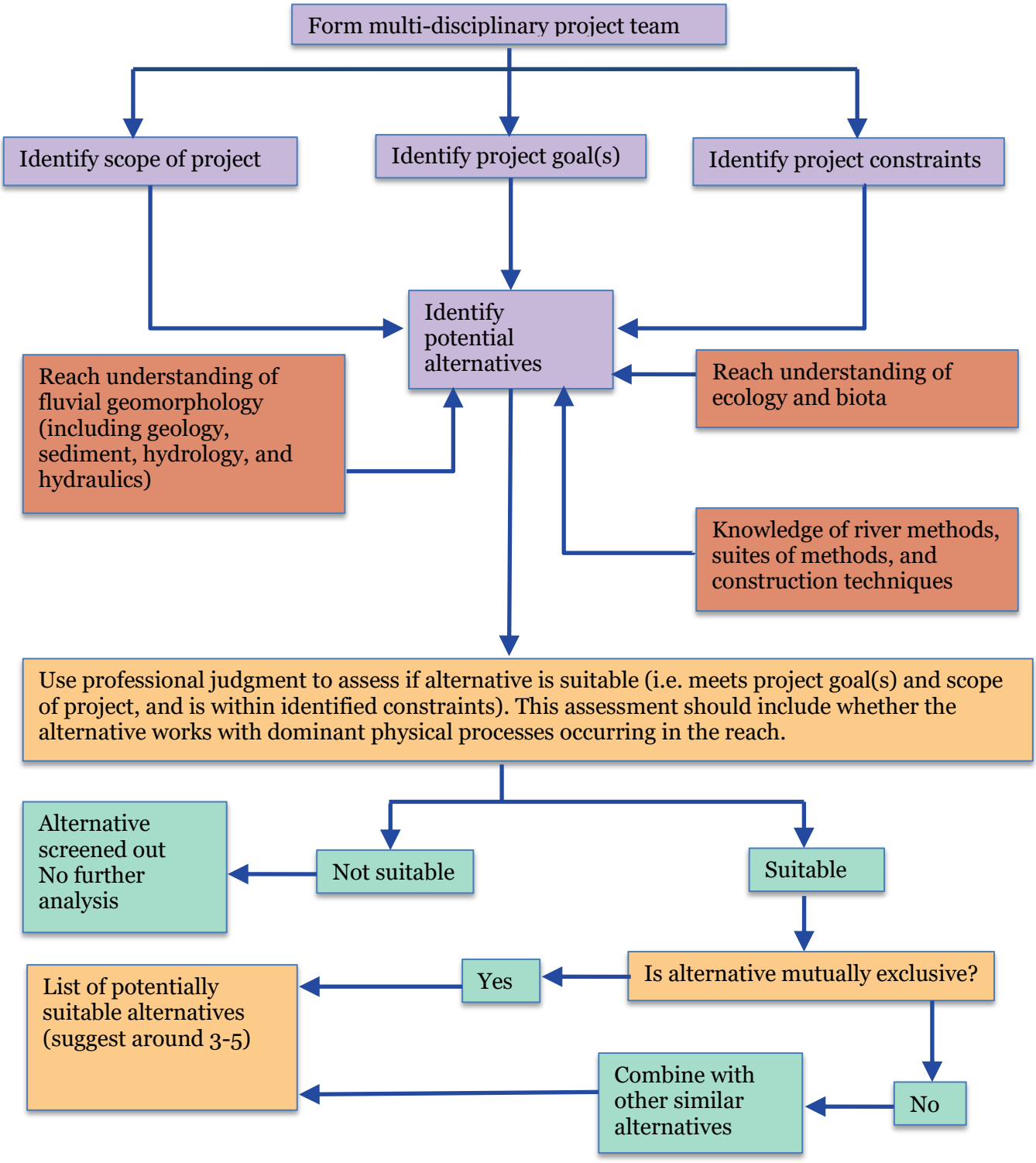

Figure 1. Flowchart of alternative analysis process – Formulation of Alternatives

1. *Engineering effectiveness* – This factor subset may include the following: function, public safety, constructability, reliability, adaptive management, design life, recurring maintenance, levee integrity, hydraulic capacity, sediment transport, and/or water delivery.
2. *Ecosystem function* – This factor subset may include the benefits and effects to the following: fish, bird, general wildlife, wetlands, riparian vegetation, and/or habitat diversity. General environmental considerations related to the Endangered Species Act (ESA), Clean Water Act (CWA), National Historical Preservation Act (NHPA), and National Environmental Policy Act (NEPA) may also be included.
3. *Economics* – This factor subset may include the following: implementation cost, maintenance cost, level of adaptive management, recreation and aesthetics, service life, and/or environmental compliance cost related to the laws listed in the ecosystem function evaluation criteria.

The intent of the three categories is to appropriately balance the needs of a project with sound engineering, environmental, and economic considerations consistent with satisfying socio-economic and ecological criteria. Implicit in the assessment of the first two evaluation criteria categories is an understanding of the geomorphic response. A geomorphic approach (working with the underlying physical processes) helps inform the team of how the fluvial system functions and responds to a given alternative. Both upstream and downstream effects of an example should be considered, given the current understanding of the current reach morphology. Generic morphological responses to changes in width, slope, sinuosity, sediment supply, etc as stated by Lane (1954) and Schumm (1969; 1977) are useful in assessing potential morphological changes. Changes from any particular action should be assessed both downstream and upstream when considering an alternative, as these responses may precipitate additional future remedial actions.

It should also be kept in mind that sometimes similar projects may have different morphological responses due to the complex and dynamic interplay of the riparian corridor processes. As an example, two side channel installations on the MRG, both north of Albuquerque (Bio-West 2005; Holste et al. 2012) resulted in different effects to the construction of inundated floodplains. One project (Bio-West 2005) created a side channel to realign a meander bend that threatened infrastructure. The intent of the side channel was to re-connect the river to the lower portion of the meander. The project accomplished this purpose, but the side channel also widened by eroding through an abandoned floodplain terrace. The widening brought additional sediment into a supply limited reach of the MRG and allowed for trees to fall naturally into the river. While the widening through the abandoned terrace had been foreseen, the random addition of trees created morphological variability, while the addition of sediment augmented the formation of an inset floodplain. The overall effect was the creation of additional habitat benefits (increased diversity) not foreseen in the alternative analysis evaluation.

A different side channel project (Holste et al. 2012) was conducted at another location on the MRG to also create floodplain habitat. A side channel was constructed through an existing floodplain terrace to facilitate water moving through the terrace at lower discharges. A small backwater embayment was constructed off this side channel to develop floodplain habitat. After construction, the side channel incised and abandoned the backwater embayment, resulting in lower inundation frequencies than originally expected based on the design. Beavers moved in a few years later and constructed a dam across the side channel, increasing the inundation frequency and facilitating a greater connection to the floodplain. These two MRG projects demonstrate the dynamic nature of the complex interplay between hydrologic, morphologic, and biologic interactions.

Evaluating the potential morphological adjustments and likely future maintenance actions helps in assessing both the long term cost implications and the ecological benefits. The geomorphic response is evaluated under one or more of the described factor subsets for engineering effectiveness or ecosystem function (side channel example). If the geomorphic response of a particular factor subset in engineering effectiveness or ecosystem is considered by the multi-disciplinary team to be critical to a project goal (e.g. improve sediment transport), that factor subset could be weighted more than other criteria within the corresponding engineering effectiveness or ecological function categories.

Objectives are then developed from the goal(s), scope, and constraints, through the use of the three evaluation criteria categories stated previously. Objectives need to be tied directly to the stated project goal(s) and are used after the project is constructed to monitor its success. Objectives need to be specific, measurable, achievable, relevant, and time-bound (i.e. SMART) (Skidmore et al. 2011; Kenney et al. 2012). Objectives may focus on an optimal condition (maximizing a desirable condition or minimizing an undesirable condition), be used to provide additional screening, or help to achieve the least damaging scenario (maximize the minima or minimize the maxima) (IPMP 2002).

Specific metrics are then developed for each objective. While objectives describe what is measured, the metrics tie to the objective and specifically describe how the measurement of an alternative will occur. They can be qualitative and/or quantitative. There may be a one to one or a one to many relationship between the objectives and their corresponding metrics. Metrics may involve professional judgment, modeling, or cost estimating. These metrics may be used later in the project when it is implemented as part of monitoring and adaptive management associated with the performance of the project.

It is the metric results that are used by the team to independently review and evaluate each alternative. Typically this is done within areas of expertise. For example, biologists on the team would evaluate the objectives associated with ecosystem function for each alternative, while engineers would evaluate the objectives associated with engineering effectiveness and economics.

Once independent discipline assessments are performed then the team reconvenes and collectively evaluates all alternatives, taking into account all of the objectives and their associated metrics until a consensus on a preferred alternative is reached. This method of using an expert panel to arrive at a consensus, after an independent assessment, is similar to the “Delphi method” (Prakash 2004), but without the stricter adherence to the assessors anonymity.

The independent and subsequent team evaluations of alternatives may use a linear scoring function approach (IPMP 2002), also known as valuation methods (Martin et al. 2016), to rank the overall preference of alternatives. The linear scoring function involves a process wherein each objective is assigned a weight and all objectives are assigned a numerical value indicating how well or poorly that objective was met. This is done for all of the alternatives. The individual product of the objective weight and the objective score are then summed to obtain a value for that alternative.

Alternatively, a more holistic or interactive approach (Martin et al. 2016), based on professional judgment and transitive ordering may be used. Transitive ordering refers to preferentially ordering alternatives based on the overall composite picture (or holistic view) of the metric results (IPMP 2002). This may be accomplished through expert elicitation from appropriate

team members that relies on professional judgment or by iteratively comparing each alternative to each other to provide a relative ranking.

Both the holistic approach and the linear scoring function approach involve a level of uncertainty which requires the use of professional judgment that may or may not be explicitly defined. The final ranked alternatives are then evaluated by the multi-disciplinary team to choose a preferred alternative based on a group consensus. The preferred alternative may be a single or composite grouping of alternatives that are chosen. For example, a MRG project north of Albuquerque (Tetra Tech 2012) identified a combination of bank protection, floodplain lowering, and vegetation planting as the preferred alternative. All of these were originally considered as separate potential alternatives to meet the identified socio-economic and ecological needs.

Key Work Steps: The following alternative evaluation steps are provided as an outline for a project team conducting an alternative analysis at a specific site or reach. These steps for an alternative evaluation are also illustrated graphically in Figure 2.

1. Identify objectives
    a. Develop objective statements that tier off of the defined project goal(s).
    b. These are directly linked to the defined goals and scope of the project and must consider the identified constraints
    c. Need to follow SMART guidance: Specific, Measurable, Achievable, Relevant, and Time-bound (Skidmore et al. 2011).
    d. Should provide a means for monitoring post-project success.
    e. Should get at the implications of doing (or not doing) an action.
    f. Objectives may be tied with project success criteria.
2. Define evaluation metrics for each objective
    a. Describe how measurement will occur
    b. Qualitative or quantitative
    c. 1 to 1 or 1 to many relationship
    d. May involve professional judgment, modeling, and/or cost estimating
3. Develop an evaluation framework
    a. The evaluation framework includes the metrics assigned to each objective. Metrics may be developed on a one to one (one alternative to one metric) or one to many (one alternative to two or more metrics) correlation with an objective.
    b. Objectives should be based on three evaluation criteria
        i. Engineering Effectiveness
        ii. Ecosystem Function
        iii. Economics
    c. The framework may include assigning a weight for each objective and the conversion of the metric to a consistent numerical scale for evaluating each objective (linear scoring function approach).
    d. The framework may be defined more loosely and based on professional judgment (holistic approach).
4. Evaluate alternatives based on the evaluation framework
5. Develop identified alternatives to approximately the 30% design and planning level and no more
    a. Includes rough plan view sketch.
    b. Includes typical details.
    c. Includes at least a conceptual description of all perceived alternative elements.
    d. Approximate volumetric calculations.

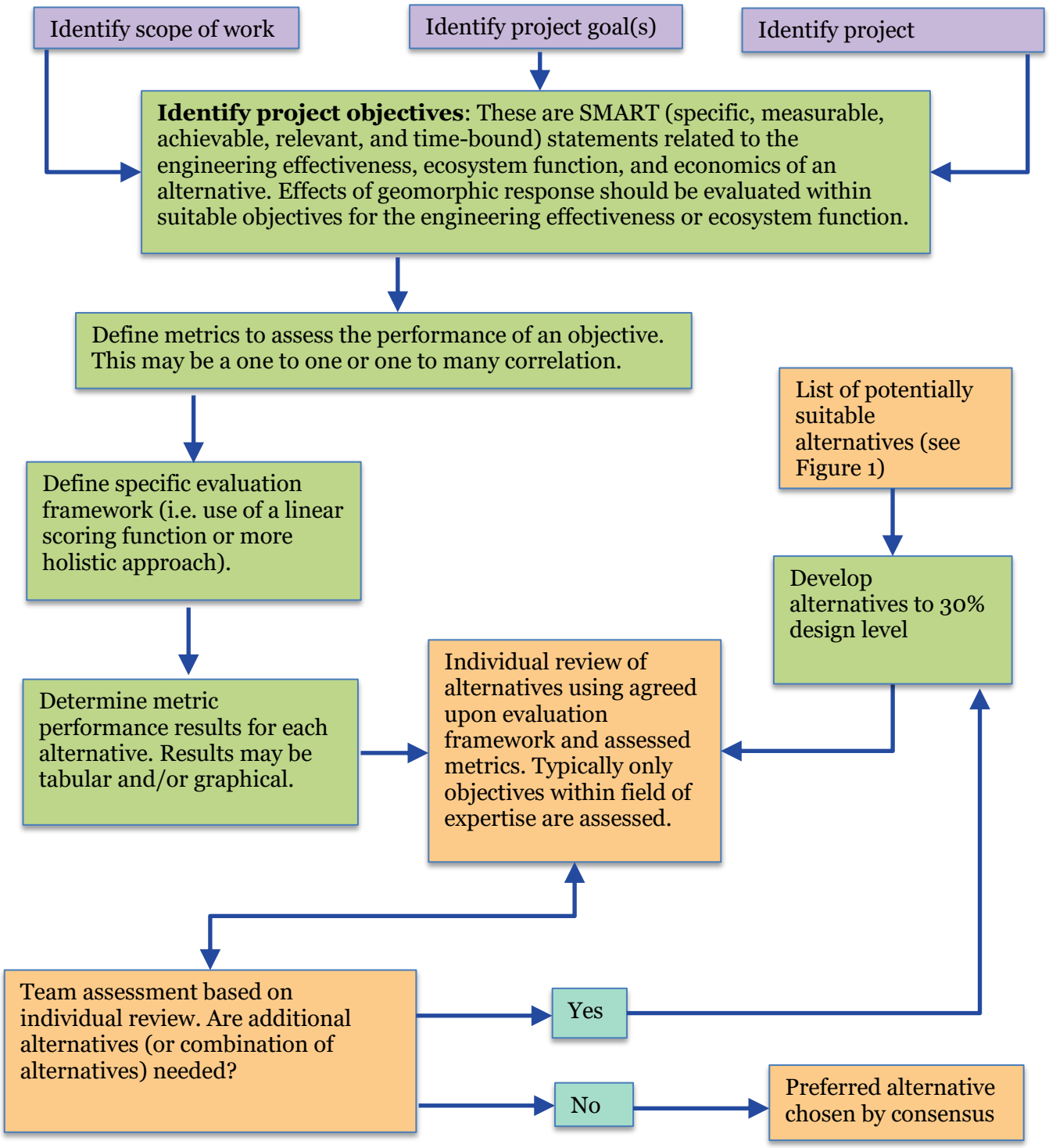

Figure 2. Flowchart of alternative analysis process – Evaluation of Alternatives

6. Project Team review
    a. Assess alternative evaluations
    b. Assess if there are benefits to grouping two or more of the alternatives (or aspects of those alternatives)
    c. Assess if additional alternatives are needed, but were overlooked previously.
    d. Repeat steps 4–6, if needed.
7. Choose a preferred alternative by consensus.

Conclusions

A framework for multi-disciplinary teams working on the MRG has been developed to assess and evaluate the socio-economic and ecological impacts of potential alternatives. The process has been refined over the years and is geared towards identifying alternatives that work with the river to re-establish or promote self-sustaining processes for increased resiliency to the extent possible. The methodology described the framework developed on the MRG, building on techniques developed on other fluvial systems and on lessons learned from MRG experience. The procedure provides guidance through the alternative formulation, analysis, and selection process. This alternative process is preceded by data collection and assessment(s) providing understanding of the underlying physical processes and environmental conditions occurring in the fluvial system. For work on the MRG, developing goals, identifying constraints, formulating alternatives, defining specific project objectives, and systematically evaluating the alternatives involves two distinct steps. The first step is at a conceptual or appraisal level and is more qualitative than quantitative. This first step culminates in the formulation of potentially suitable alternatives. The second step includes the development and analysis of those potentially suitable alternatives in a systematic and holistic manner for comparative analysis. This second step is typically more quantitative in nature, culminating in the development of a feasibility level or 30% project scope for the potentially suitable alternatives. This step also results in the selection of a preferred alternative by the multi-disciplinary team. In addition the team may undertake an additive approach where separate alternatives are combined or partially combined to get a preferred alternative that satisfies multiple goals and objectives.

Acknowledgement

The projects described in this report were conducted by Reclamation's Albuquerque Office, New Mexico. Jonathan AuBuchon, currently with U.S. Army Corps of Engineers, participated in these projects while employed with Reclamation at the Albuquerque Office. The ideas presented are based on the project principles espoused by others (see citations throughout the paper) and on informal discussions among project team members that have helped to identify steps to improve the alternative analysis process. The present work does not necessarily reflect the position of Reclamation or the U.S. Army Corps of Engineers.

References

Bachus, J. and Gonzales, E. 2017. Technical Note – Habitat Targets for BDA Realignment Pilot Modeling Analysis. U.S. Department of the Interior, Bureau of Reclamation, Albuquerque Area Office, Albuquerque, NM.

Baird, D. 2016. Rio Grande Silvery Minnow Habitat Restoration Design Review. U.S. Department of the Interior, Bureau of Reclamation, Technical Service Center, Denver, CO.

Baird, D. and Makar, P. 2011. Middle Rio Grande Endangered Species Collaborative Program River and Habitat Restoration Methods Workshop. U.S. Department of the Interior, Bureau of Reclamation, Technical Service Center, Denver, CO.

Baird, D., Fotherby, L., Klumpp, C.C., and Scurlock, S.M. 2015. Bank Stabilization Design Guidelines. U.S. Department of the Interior, Bureau of Reclamation, Technical Service Center, Denver, CO.

Biedenharn, D.S., Elliott, C.M., and Watson, C.C. 1997. The WES Stream Investigation and Streambank Stabilization Handbook. U.S. Army Corps of Engineers, Waterways Experiment Station (WES), Vicksburg, MS.

Bio-West. 2005. Middle Rio Grande Project Cochiti Priority Site: Draft Alternatives Analysis. Bio-West for Reclamation, Logan, UT.

Crawford, C.S., Cully, A.C., Leutheuser, R., Sifuentes, M.S., White, L.H., and Wilber, J.P. 1993. Middle Rio Grande Ecosystem: Bosque Biological Management Plan. Middle Rio Grande Biological Interagency Team, University of New Mexico, Albuquerque, NM.

Cramer, M.L ed. 2012. Stream Habitat Restoration Guidelines. Co-published by the Washington Departments of Fish and Wildlife, Natural Resources, Transportation and Ecology, Washington State Recreation and Conservation Office, Puget Sound Partnership, and the U.S. Fish and Wildlife Service, Olympia, WA.

Dreesen, D., Harrington, J., Subirge, T., Stewart, P., and Fenchel, G. 2002. Riparian Restoration in the Southwest–Species Selection, Propagation, Planting Methods, and Case Studies. So. National nursery proceeding – 1999, 2000, and 2002, eds. R.K. Dumrose, L.E. Riley, and T.D. Landis, USDA Forest Service, Rocky Mountain Research Station, Ft. Collins, CO.

Finch, D. and Tainter, J.A., ed. 1995. Ecology, Diversity, and Sustainability of the Middle Rio Grande Basin. U.S. Department of Agriculture, Rocky Mountain research Station, Ft. Collins, CO.

Graf, W.L. 1994. Plutonium and the Rio Grande: environmental change and contamination in the nuclear age. Oxford University Press, New York, NY.

Harris, A. 2017. Technical Note: Bosque del Apache National Wildlife Refuge Pilot Project: Habitat Suitability Indexing for Rio Grande Silvery Minnow. U.S. Department of the Interior, Bureau of Reclamation, Albuquerque Area Office, Albuquerque, NM.

Harris, A. and AuBuchon, J. 2016. Arroyo de las Cañas Geomorphic, Hydraulic, and Sediment Transport Analysis. U.S. Department of the Interior, Bureau of Reclamation, Upper Colorado Region, Albuquerque, NM.

Harris, A., Klein, M., and Bui, C. 2018. Angostura Dam to Montaño Bridge: Geomorphic and Hydraulic Analysis. U.S. Department of the Interior, Bureau of Reclamation, Albuquerque Area Office, Albuquerque, NM.

Holste, N. 2014. BDANWR Sediment Plug and River Restoration Project: Alternatives Analysis Synthesis Report. Department of the Interior, Bureau of Reclamation, Albuquerque Area Office, Albuquerque, NM.

Holste, N. 2017. Geomorphology and Sediment Transport of Bosque del Apache Pilot Project. U.S. Department of the Interior, Bureau of Reclamation, Denver Technical Service Center, Denver, CO.

Holste, N., AuBuchon, J., and Bui, C. 2012. San Ildefonso Priority Site Alternatives Analysis Report. U.S. Department of the Interior, Bureau of Reclamation, Albuquerque Area Office, Albuquerque, NM.

IPMP. 2002. Leadership for Guiding Complex Problem-Solving and Decision-Making Efforts. Institute for Participatory Management and Planning (IPMP), Monterey, CA.

Kenney, M.A., Wilcock, P.R., Hobbs, B.F., Flores, N.E., and Martinez, D.C. 2012. "Is urban stream restoration worth it?" Journal of the American Water Resources Association, 48(3), 603-615.

Lagasse, P.F., Clopper, P.E., Thornton, C.I., Shields, F.D. Jr., McCullah, J., and Spitz, W. 2016. NCHRP Report 822: Evaluation and Assessment of Environmentally Sensitive Stream Bank Protection Measures. National Cooperative Highway Research Program, Transportation Research Board, Washington, D.C.

Lane, E.W. 1954. The Importance of Fluvial Morphology in Hydraulic Engineering. U.S. Department of the Interior, Bureau of Reclamation, Denver, CO.

Lopez, S. and AuBuchon, J. 2012. Santo Domingo Priority Sites Alternative Analysis Report. Department of the Interior, Bureau of Reclamation, Albuquerque Area Office, Albuquerque, NM.

Klein, M., Herrington, C., AuBuchon, J. and Lampert, T. 2018. Isleta to San Acacia Geomorphic Analysis. U.S. Department of the Interior, Bureau of Reclamation, Albuquerque Area Office, Albuquerque, NM.

Makar, P. 2015. Lower Reach Conditions and Strategies. U.S. Department of the Interior, Bureau of Reclamation, Denver Technical Service Center, Denver, CO.

Makar, P. and AuBuchon, J. 2012. Channel Conditions and Dynamics of the Middle Rio Grande. U.S. Department of the Interior, Bureau of Reclamation, Upper Colorado Region, Albuquerque, NM.

Martin, D.M., Hermoso, V., Pantus, F., Oiley, J., Linke, S., and Poff, N.L. 2016. "A proposed framework to systematically design and objectively evaluate non-dominated restoration tradeoffs for watershed planning and management." Ecological Economics, 127 (2016), 146-155.

Massong, T., Makar, P., and Bauer, T. 2010. "Planform evolution model for the Middle Rio Grande, NM. Department of the Interior, Bureau of Reclamation, Albuquerque Area Office and Denver Technical Service Center." Published in the Proceeding of the 2nd Joint Federal Interagency Conference, Las Vegas, NV.

MEI, 2002. Geomorphic and Sedimentologic Investigations of the Middle Rio Grande between Cochiti Dam and Elephant Butte Reservoir. Mussetter Engineering Inc., for New Mexico Interstate Stream Commission, Albuquerque, NM.

Mortensen, J.G., Dudley, R.K., Platania, S.P., and Turner, T.F. 2019. Rio Grande Silvery Minnow Biology and Habitat Syntheses Final Report. University of New Mexico for U.S. Department of the Interior, Bureau of Reclamation, Albuquerque, NM.

Nemeth, M.S. 2014. "Effects of information cascades on collaborative decision-making in river engineering projects on the Rio Grande." International Journal of River Basin Management, DOI:10.1080/15715124.2014.928303.

Newbury, R. 2016. Stream Restoration Hydraulics: Project Casebook. Canadian Rivers Institute, https://www.newbury-hydraulics.com, accessed January 23, 2018, Lake Country, British Columbia, Canada.

Niezgoda, S.L., Wilcock, P.R., Baker, D.B., Mueller, J., Castro, J.M., Curran, J.C., Wynn-Thompson, T., Schwartz, J.S., and Shields, F.D. Jr. 2014. "Defining a stream restoration body of knowledge as a basis for national certification." J. Hydraul. Eng., 140 (2), 123-136.

NRCS. 2007a. Part 654 Stream Restoration Design National Engineering Handbook. U.S. Department of Agriculture, Natural Resources Conservation Service. Washington, D.C.

NRCS. 2007b. Deep Planting – The Ground Water Connection: Guidelines for Planting Longstem Transplants for Riparian Restoration in the Southwest. National Resources Conservations Service, Los Lunas Plant Material Center, Los Lunas, NM.

Parsons, M. and Thoms, M.C. 2018. "From academic to applied: operationalizing resilience in river systems." Geomorphology, 305 (2018), 242-251.

Prakash, A. 2004. Water Resources Engineering: Handbook of Essential Methods and Designs. American Society of Civil Engineers (ASCE), Reston, VA.

Reclamation. 2012a. Middle Rio Grande River Maintenance Program Comprehensive Plan and Guide. Department of the Interior, Bureau of Reclamation, Albuquerque Area Office and Denver Technical Service Center, Albuquerque, NM.

Reclamation. 2012b. Middle Rio Grande River Maintenance Program Comprehensive Plan and Guide, Appendix A: Middle Rio Grande Maintenance and Restoration Methods.

Department of the Interior, Bureau of Reclamation, Albuquerque Area Office and Denver Technical Service Center, Albuquerque, NM.

Reclamation. 2015. Joint Biological Assessment Middle Rio Grande Project and San Juan-Chama Project, NM, Part III – Proposed Action and Effects: River and Infrastructure Maintenance and Restoration. Department of the Interior, Bureau of Reclamation, Bureau of Indian Affairs, and Non-Federal Water Management Agencies, Albuquerque, NM.

Reclamation and USACE. 2016. National Large Wood Manual: Assessment, Planning, Design, and Maintenance of Large Wood in Fluvial Ecosystems: Restoring Process, Function, and Structure. U.S. Department of the Interior, Bureau of Reclamation, Boise, ID and the U.S. Army Corps of Engineers, Research and Development Center, Vicksburg, MS.

Scurlock, D. 1998. From the Rio to the Sierra: An Environmental History of the Middle Rio Grande Basin. U.S. Department of Agriculture, Forest Service, Rocky Mountain Research Station, Fort Collins, CO.

Schumm, S.A. 1969. "River metamorphosis." Journal of the Hydraulics Division, American Society of Civil Engineers, No. HY1, Proc. Paper 6352, 255-273.

Schumm, S.A. 1977. *The Fluvial System*. The Blackburn Press, John Wiley and Sons, NY.

Sholtes, J.S., Ubing, C., Randle, T.J., Fripp, J., Cenderelli, D., and Baird, D.C. 2017. Managing Infrastructure in the Stream Environment. Advisory Committee on Water Information Subcommittee on Sedimentation an Environment and Infrastructure Working Group. Department of the Interior, Bureau of Reclamation, Denver, CO.

Siegle, R., Ahlers, D., Ryan, V. 2013. Southwestern Willow Flycatcher Habitat Suitability 2012 – Middle Rio Grande, NM. Department of the Interior, Bureau of Reclamation, Denver Technical Service Center and Albuquerque Area Office, Denver, CO.

Skidmore, P.B., Thorne, C.R., Cluer, B.L., Press, G.R., Castro, J.M., Beechie, T.J., and Shea, C.C. 2011. Science Base and Tools for Evaluating Stream Engineering, Management, and Restoration Proposals. U.S. Department of Commerce, National Oceanic and Atmospheric Administration, Springfield, VA.

Tetra Tech. 2012. Middle Rio Grande River Maintenance Projects San Felipe Pueblo Reach Priority Sites Phase II: Alternative Analysis Report. Tetra Tech for Reclamation, Albuquerque, NM.

Tetra Tech. 2014. Final Report Ecohydrological Relationships along the Middle Rio Grande of New Mexico for the Endangered Rio Grande Silvery Minnow. Tetra Tech, Inc. for the U.S. Army Corps of Engineers, Albuquerque District, Albuquerque, NM.

USFWS. 2016. Biological and Conference Opinion for Bureau of Reclamation, Bureau of Indian Affairs, and Non-Federal Water Management and Maintenance Activities on the Middle Rio Grande, New Mexico. U.S. Department of the Interior, Fish and Wildlife Service, Albuquerque, NM.

Watson, C.C., Biedenharn, D.S., and Scott, S.H. 1999. Channel Rehabilitation: Processes, Design, and Implementation. U.S. Army Corps of Engineers, Engineer Research and Development Center, Vicksburg, MS.

Wohl, E.E., Bledsoe, B.P., Merritt, D.M., and Poff, N.L. 2006. "River restoration in the context of natural variability." Stream Notes, Stream Systems Technology Center, Rocky Mountain Research Center, U.S. Department of Agriculture, Forest Service, Ft. Collins, CO.

Wohl, E., Lane, S.N., and Wilcox, A.C. 2015. "The science and practice of river restoration." Water Resour. Res, 51, 5974-5997, doi:10.1002/2014WR016874.

Yochum, S.E. 2018. Guidance for Stream Restoration. U.S. Department of Agriculture, National Stream and Aquatic Ecology Center, Ft. Collins, CO.

Floodplain Reconnection on Butano Creek - Design, Implementation and Results from the First Season

Chris Hammersmark, Ph.D., P.E., Director, cbec eco engineering, 519 Seabright Ave, Suite 102, Santa Cruz, CA 95062, c.hammersmark@cbecoeng.com, 916-668-5236
Ben Taber, P.E., cbec eco engineering, 2544 Industrial Blvd., West Sacramento, CA 95691, b.taber@cbecoeng.com, 916-231-6052
Jarrad Fisher, Project Manager, San Mateo Resource Conservation District, 80 Stone Pine Road, Suite 100, Half Moon Bay, CA 94019, jarrad@sanmateorcd.org, 650-712-7765

Abstract

Butano Creek, the largest tributary to Pescadero Creek, drains 23 sq. mi. (60 sq. km.) of the Santa Cruz Mountains, San Mateo County, California, U.S.A. Located in the lower portion of the watershed is the rural agricultural community of Pescadero, and the Pescadero Creek Estuary, which provides habitat for a number of threatened and ESA listed animal species including California red-legged frog (Rana draytonii), San Francisco garter snake (Thamnophis sirtalis tetrataenia), tidewater goby (Eucyclogobius newberryi), coho salmon (Oncorhynchus kisutch), and steelhead (Oncorhynchus mykiss).

Analysis completed by the San Francisco Bay Regional Water Quality Control Board has documented that land management activities (primarily logging, tilling and road building) and channel management practices (primarily channel straightening, riparian vegetation clearance and large wood removal) in the last two centuries have doubled sediment inputs and disconnected channels from their floodplains through incision, virtually eliminating floodplain sediment storage (SFBRWQCB In prep.). This increased sediment load has led to the system being listed at impaired for sediment under the Clean Water Act. Incision and floodplain disconnection not only eliminated sediment storage in the valley but also transformed floodplain storage areas into sources substantially contributing to elevated sediment loads. The delivery of this additional sediment load to the lower watershed has resulted in substantial channel aggradation in the very low gradient, downstream reaches of Butano Creek, which has resulted in chronic flooding of adjacent agricultural areas as well as Pescadero Creek Road, which provides the primary access and egress to the rural community of Pescadero. This channel aggradation has both restricted access/passage to the Butano Creek watershed by salmonids, and has also been linked to poor water quality in the Pescadero Creek Estuary, which has suffered nearly annual mortality events for aquatic species (also called fish kills) present in the estuary for over two decades. Poor water quality conditions in the Estuary are a result anoxia resulting from sheet flow across the marsh plain, subsequent flow through decomposing vegetation, as well as artificially created depressions that don't mix. When the sand bar that forms the bar-built estuary breaches (naturally or unnaturally) poor quality water in the adjacent marsh plain is drawn into the lagoon. The lack of a defined channel both results in sheet flow across the marsh plain as well as a lack of an egress pathway for fish trying to escape poor water quality conditions

Removal of large wood, channel incision, and floodplain disconnection are the main drivers of a significant reduction in the complexity and function of aquatic habitats that are home to a number of sensitive and ESA-listed species. Channel change and sediment budget analyses revealed that, historically, the lowland valley functioned as a wet meadow and included an extensive well-connected floodplain that provided a diverse array of habitats. This extensive floodplain also provided sediment storage upstream of the Pescadero Creek Estuary, which is a key nursery habitat for juvenile, anadromous fish.

A feasibility study for restoration of Butano Creek, commissioned by the San Mateo Resource Conservation District, was completed in 2014. While operating within the constraints present, the study identified a number of possible solutions to the elevated sediment load and the plethora of impacts that it drives (e.g., chronic road flooding, reduced fish passage, simplification of aquatic habitats, poor water quality in the estuary resulting in fish kills, etc.). This effort, led by cbec inc. eco engineering, identified several potential actions including:

- implementation of upland sediment control activities to reduce the amount of sediment delivered to the project area;
- reconnection or restoration of floodplains to absorb sediment and flood water energy, thereby reducing transport of sediment to downstream reaches;
- creation of additional flow capacity at Pescadero Creek Road, through construction of a new bridge/causeway, and/or channel dredging; and
- restoration or creation of a stable and open channel to provide habitat connectivity for salmonids and other aquatic species from Butano Creek upstream of the road downstream into the lagoon.

The focus of this presentation is on the first project implemented to reconnect and restore floodplains along Butano Creek.

A project implemented in the summer and fall of 2016enhances channel habitat and reconnects the floodplain along a roughly one-mile (1.6 km) reach of Butano Creek and restores approximately 100 acres (~40.5 hectares), or approximately 10%, of the historical floodplain of Butano Creek. The project was led by the San Mateo Resource Conservation District, funded by the California Department of Water Resources Urban Stream Restoration Program, and located on land owned and managed by the Peninsula Open Space Trust.

The design of the project was informed by the results of a detailed topographic survey of the reach, and the development of a two-dimensional hydrodynamic model (SRH-2D). The local (reach-scale) intent of the project was to provide physical features that would roughen the channel, force channel aggradation, limit channel capacity, and therefore increase floodplain inundation and sediment deposition. The pre-project channel capacity ranged from the magnitude of a 5-10-yr recurrence interval event, while the design resulted in floodplain inundation in flows at approximately a 1.5-yr recurrence interval event. Reducing the channel capacity further was not possible without generating flood impacts to nearby insured structures.

Project elements include a roughened channel/rock ramp grade control structure, two constructed engineered log jams, two jams constructed by induced recruitment of live bankside alders into the channel, and bankside berm breaches. Each of these features is described in greater detail below.

The roughened channel/rock ramp raised the channel thalweg by approximately 5 feet, providing grade control to limit future incision, and also limiting the channel conveyance capacity. This rock ramp has a slope of ~4.25% and includes seven structural rock ribs (built of 1-2 ton quarry rock) with 1 foot (0.3 m) elevation drop between each, with the remainder of the structure comprised of an engineered streambed material mixture which was generated through onsite blending of quarry products and locally soured streambed material. The engineered streambed material was engineered to resist movement up to a 25-yr return interval flow event, making it a stable feature through typical flows.

The two porous engineered log jams are keyed into one of the channel banks and span approximately two thirds of the channel. They are constructed from five Coast redwood and Douglas fir logs ranging from 24-36 inches (0.6-0.9 m) in diameter, two of which with rootwads attached. The logs are pinned together, as well as ballasted with two 4-ton rocks to provide stability.

Two additional log jams were constructed through the recruitment of seven to nine alder trees rooted near the top of the creek channel banks. The perimeter of each root wad was excavated and then the stems were toppled across the channel forming a simple jam, intended to catalyze the recruitment of additional stream wood. Efforts were made to keep many roots intact such that the alder trees would continue to live and therefore not degrade/decompose as rapidly.

A berm that appears at least partially unnatural is present along the left bank, presumably resulting from previous channel relocation efforts. This berm further limits floodplain connectivity. The result of this berm is that a higher flow rate is required to achieve the initiation of floodplain inundation. Bankside berm breaches (also referred to as connector channels), which emulate natural crevasses, were implemented in two locations (upstream of the rock ramp and upstream of one of the engineered log jams) connecting the main channel to the adjacent floodplain. These connector channels allow for floodplain connectivity at lower discharges/stages.

Analysis of the monitoring results of the first few flow seasons is underway and include: channel bed and floodplain morphology (via ground-based LiDAR), channel habitat type, groundwater level changes and floodplain inundation/off channel habitat increase. Topographic monitoring of the channel bed has documented both scour and deposition resulting from the project. The volume of in-channel, pool habitat increased by a factor of 20, although a net depositional trend was documented. Regrettably the survey effort was unable to cover much of the floodplain due to thick riparian vegetation. Consequently, although floodplain deposition was observed in these areas sedimentation rates could not be quantified. Shallow groundwater elevations adjacent to the project reach increased by over 4 feet, bringing it in much closer proximity to the floodplain surface. Additional results will be discussed during the presentation.

References

SFBRWQCB (San Francisco Bay Regional Water Quality Control Board). In preparation. Pescadero-Butano Watershed Sediment TMDL and Habitat Enhancement Plan. Staff Report.

Geomorphic Response to Gravel Injection, Channel Restoration and Peak Flows in Clear Creek, CA

Aaron (Smokey) Pittman, Fluvial Geomorphologist, McBain Associates,
Placerville, CA, smokey@mcbainassociates.com

Abstract

The impoundment-induced coarse sediment deficit and concomitant reduction in habitat quality in Clear Creek below Whiskeytown Dam has been well documented by various investigators (Coots 1971, McBain and Trush 2001). Clear Creek is located in northern California, in the transition between the Klamath Mountains (a bedrock gorge) and the Central Valley (an unconfined, alluvial reach). Historic gravel mining and gold dredging resulted in large scale channel and floodplain disturbance in the alluvial reach. Whiskeytown Dam, closed in 1964, impacted all downstream reaches with flow regulation. Effects of the impaired flow regime and reduced coarse sediment supply include: an overly simplified channel, riffle coarsening, fossilization of alluvial features, reduced rates of channel migration, reduction of fine sediment supply for overbank deposition, and reduction in the amount and quality of spawning gravels for available for anadromous salmonids. Infrequent dam spills winnow, but lacking sediment input, do not replace mobile bed sediments. In some reaches, reduced coarse sediment supply, compounded by gravel or gold mining, resulted in incision to bedrock and a loss of channel dynamism and floodplain connectivity.

Restoration efforts to address habitat degradation include temperature-control flow releases, gravel injection, channel realignment and floodplain grading and extensive riparian planting. The focus for many projects is on geomorphic-process restoration (e.g. bed scour and redeposition related to gravel injection). Restoration of a “natural” channel and floodplain, in combination with gravel injection and appropriate flow releases, is intended to initiate and sustain sediment transport processes thereby enhancing ecological function. A “natural” channel in this case is defined as one whose physical structure and interaction with the contemporary flow/sediment regime approximates the pre-dam condition, albeit at a smaller scale. Gravel injection is intended to replace the pre-dam sediment supply and hydrograph manipulation (coupled with naturally occurring uncontrolled spills and below-dam tributary floods) was intended to replace impaired hydrograph components (e.g. winter peaks and spring runoff). Efforts to manipulate the hydrograph have been limited to spring pulse flows (on the order of 800 cfs), much lower than the intended gravel-mobilizing flows of at least 3,000 cfs (McBain and Trush 2001, Stillwater 2013). Gravel injection sites have been developed at 15 locations. Most injection sites provide passive gravel recruitment during high flows, e.g. lateral berms and talus cones. Over 200,000 tons of gravel have been added over 20 years resulting in dramatic (orders of magnitude) increases in below-dam spawning habitat.

Controlled pulse flows are limited to a maximum of 1,200 cfs by the dam’s outlet works, though 800 cfs is more typical due to operational constraints. Spring pulse flows, implemented since 2009, were developed for biological considerations related to anadromous salmonids. For context, the post-dam 1.5-year event is 2,240 cfs. Since the large floodplain restoration projects were designed to flow overbank at 3,000 cfs (the 2.0-year event) and since the channels were designed to become active at this threshold (e.g. channel will migrate and form new alluvial features), the 800 cfs pulse flows were assumed to provide minimal geomorphic benefit (e.g. scour and re-deposition of coarse sediment). During drought years however, it became apparent that these relatively minor flows (much smaller than the average annual post-dam peak flow) were

capable of fulfilling a vital function in the restoration of Clear Creek: the mobilization and redistribution of injected gravel. Spring pulse flows mobilized lateral berms and talus cones but had little effect on most placed riffles. This capacity to perform geomorphic work is especially pronounced in the near-dam reaches, where floodplain and channel restoration have not occurred, only gravel injection. This paper will explore the role of gravel injection in two very different geomorphic settings: the confined, near-dam reach and the unconfined, alluvial central valley reach where extensive channel and floodplain restoration has been implemented.

The near-dam reach (the first two miles below Whiskeytown Dam) is fairly confined (relic floodplains are about as wide as the active channel) is bedrock controlled (riffle crests are keyed to bedrock) and is steered by topography (channel alignment parallels valley walls). Pre-gravel injection, the reach exhibited quasi-alluvial characteristics in the form of skeletal point bars, coarse riffles and persistent gravel lobes associated with favorable hydraulic settings (e.g. high flow eddies below islands). Due to its proximity to the dam, the ambient coarse sediment load into the reach is essentially zero (tributary contribution is minimal). Gravel injection occurs via a large talus cone immediately below the dam and at several riffles along the two-mile reach where gravel is placed directly in the channel. Riffle supplementation provides immediate benefit in the absence of high flows (fish utilize the placed gravels). Both strategies contribute to the longer-term goal of providing coarse sediment for fluvial redistribution.

The large channel/floodplain restoration projects occur downstream in unconfined, low gradient reaches and (in their restored state) are largely governed by purely alluvial processes. A sinuous channel has been realigned away from shallow clay pan through areas of deeper (though highly disturbed) valley sediments and is free to migrate within a broad floodplain. Ambient coarse sediment load into the restoration reach has been enhanced by removal of a relict dam (liberating >60,000 cubic yards of stored mixed sediments) and by ongoing upstream gravel augmentation. The hydrologic setting for the downstream reaches is notably different, due to tributary accretion. Floods (as high as 12,000 cfs) occur even when flows in the upper reach remain near base-level (200 cfs). A very steep, confined bedrock gorge separates the two reaches.

Gravel injection in the floodplain reach was accomplished via a massive (75,000 tons) “transfusion” during construction of the downsized (3,000 cfs capacity) channel. Large segments (pool tails and riffles) were blanketed with spawning sized gravels (1 to 5 inch), which set the stage for fluvial redistribution. Immediately following construction of the first phase (2002), fall run Chinook Salmon (*Oncorhynchus tshawytscha*) began to spawn in the placed gravels. Five flow events in Water Year (WY) 2003 exceeded the channel capacity (and designed bed mobility) threshold of 3,000 cfs and a prolonged dam spill exceeded 3,000 cfs for over 36 hours in April. The channel evolved into a slightly longer, more sinuous alignment, creating new alluvial features (medial and point bars) as it migrated. Tracer gravel studies showed the riffle crests to be 100 percent mobile at flows exceeding the design threshold (Graham Matthews & Associates, 2004). All of these dynamic responses were aligned with the geomorphic performance objectives for the new channel. Nonetheless, the restoration team remained concerned that without additional sediment supply, the highly active channel might return to its previously degraded state so an adaptive gravel injection program was developed.

An average of 5,000 tons per year was injected via a talus cone in a bedrock gorge 1.6 miles upstream of the floodplain restoration project. The ambient supply coming into the reach increased as liberated dam sediments and injected gravels arrived: upstream pools partially filled and bars increased in height and area (Graham Matthews and Associates 2016). Other injection sites (lateral berms and riffle supplements) were developed within the project footprint to enhance key sites where incision to claypan (an undesirable response) began to occur in areas of higher shear stress (steeper riffles and along the outside of bends). During low water years, the

spring flow dam releases (~800 cfs) mobilized nearly all of the lateral berms within the project (some gravels remained perched on higher surfaces). As evidenced by topographic differencing, riffles immediately below injection sites (on the order of hundreds of feet) aggraded and claypan exposures were at least partially buried. During higher flow water years, the signature of injected gravel was not clearly detectable as gravels were absorbed into the overall channel response to high flow events, but the channel continued to respond in a favorable manner: highly dynamic bars changes, limited claypan exposure, continued planform evolution. Based on annual geomorphic monitoring results, managers assumed that the annual injections (approximately 1,700 tons per year) were making a positive contribution. Annual injections continue through this writing.

Gravel injection in the floodplain reach is clearly beneficial, but in the upstream reach, where no large-scale restoration was performed, the role of gravel injection is most compelling. In this reach, the large talus cone at the dam and three riffle-supplement injection sites have "recharged" (gravel-coated a significant portion of the bed) nearly the entire two-mile reach. This recharge was for the most part achieved under a highly regulated flow regime, as compared to the lower reaches. Since 2003 only two very brief peak flow events (1,000 to 2,000 cfs) have exceeded the typical spring flow release magnitude of 800 cfs. The importance of these relatively small events cannot be overstated from a geomorphic recovery perspective. Without them, only a small percentage of the two-mile reach would likely have been recharged. Gravel injection response relative to flow events has been carefully tracked with spawning gravel area mapping, topographic surveys, aerial photo analysis, bar mapping and visual channel condition (composition and function) assessments.

In addition to creating spawning habitat, gravel injections have induced positive geomorphic changes which represent a shift in the trajectory of Clear Creek's geomorphic response to impoundment. Alluvial form and function have been enhanced as highly dynamic and complex bar sequences develop along gravel "waves" as injected gravels propagate downstream. Scour and deposition associated with these waves disrupts riparian colonization which had evolved into a robust state under the post-dam flow regime. Sand delivery from the few below-dam tributaries, while modest in terms of annual contribution, interacted with the bank vegetation to create berms. These riparian berms not only "lock up" gravels available for transport, they contribute to channel confinement, increasing water velocities and impacting juvenile salmonid habitat quality. Gravel waves cause mechanical disruption to riparian areas as well as divert flow (as a function of bar height) toward banks causing undercutting, lateral scour and channel migration.

Complex flow patterns develop across depositional bedforms which benefit aquatic organisms by promoting heterogeneous hydraulic conditions: increasing hyporheic flow and changing flow depth, velocity and direction. Armored features become more mobile as finer particles infiltrate and "lubricate" bars and riffles. Increased floodplain connectivity occurs as the result of gravel waves decreasing channel capacity and forcing stream flow up out of the channel onto adjacent surfaces. Raising the near-channel water table also appears to increase alder mortality, further reducing riparian confinement and increasing woody debris loading which in turn increases the degree of mechanical disruption; high flows with a high woody debris component are more effective at disrupting established riparian vegetation.

The primary geomorphic recovery goals on all of the below-dam reaches of Clear Creek require high flows and sediment contributions as the agents of change (McBain and Trush 2001). Efforts to establish a high flow release program (Stillwater 2016) similar to the program implemented on the Trinity River (U.S. Department of the Interior and U.S. Bureau of Reclamation, 2000), have to date proven unsuccessful. Despite the lack of a high flow management program, carefully planned gravel injection, coupled with relatively small pulse flows has proven highly successful in

aiding the recovery of floodplain/channel restoration projects and offsetting the progressive near-dam channel degradation by restoring a suite of beneficial sediment-related geomorphic processes.

References

Coots, M. 1971. Unpublished California Department of Fish and Game data, Millard Coots. Redding, California.

Graham Matthews & Associates, 2004: "Clear Creek Geomorphic Monitoring, WY2003 Annual Report." Report submitted to Western Shasta Resource Conservation District, Anderson, California.

Graham Matthews & Associates, 2016: "Clear Creek Geomorphic Monitoring, WY2015 Annual Report." Report submitted to US Fish and Wildlife Service, Red Bluff, California.

McBain and Trush, 2001. "Geomorphic Evaluation of Lower Clear Creek, Downstream of Whiskeytown Reservoir." Report submitted to Clear Creek Restoration Team.

Stillwater Sciences. 2013. "Clear Creek Environmental Water Program: Core Monitoring and Adaptive Management Plan." Prepared by Stillwater Sciences, Berkeley, California for U.S. Fish and Wildlife Service, Red Bluff, California.

U.S. Department of the Interior (DOI) and U.S. Bureau of Reclamation, 2000. Record of Decision, Trinity River Mainstem Fishery Restoration Final Environmental Impact Statement/Environmental Impact Report (EIS/EIR), December 2000.

How to Make Meadow Restoration Work for California's Mountain Frogs?

Karen Pope, Research Wildlife Biologist, USDA Forest Service, Pacific Southwest Research Station, Redwood Sciences Lab, Arcata, CA 95521, kpope@fs.fed.us, 707-825-2957
Sarah Yarnell, Research Hydrologist, UC Davis, Center for Watershed Sciences, Davis, CA 95616, smyarnell@ucdavis.edu, 530-320-4688
Jonah Piovia-Scott, Assistant Professor, Washington State University, Vancouver, WA 98686, jonah.piovia-scott@wsu.edu, 360-546-9657

Introduction

Intensive land uses have transformed many of the Sierra Nevada's low gradient streams and meadows from multi-thread channels with annually inundated floodplains into single-thread, incised channels that store less water and have reduced habitat quality for a diverse suite of meadow-associated wildlife (Kattlemann 1996, Loheide et al. 2009). Recovery of the beneficial functions of these systems has become a priority in California's water infrastructure plans. The increased commitment to upper watershed stream and meadow restoration has facilitated a dramatic increase in the pace and scale of mountain meadow restoration projects (Drew et al. 2016). However, many of the techniques being implemented by the restoration industry are failing to accomplish restoration objectives, or are not meeting natural reference standards (Pope et al. 2015). An overarching goal of stream and meadow restoration projects is to recover self-sustaining ecological systems and the dynamic processes that support them. In spite of this, common design approaches often include channel form and stability criteria that prevent the dynamic physical processes that support biodiversity (Arscott et al. 2002, Ward et al. 2002, Florsheim et al. 2008). In order to achieve long-term sustainability, a process-based design approach that allows for natural changes in channel condition through time and thus sustains critical ecological functions may be warranted.

Understanding the relationship between hydrologic processes in meadows and the focal taxa that use meadows can provide insight into not just ways to create habitat features in restoration projects, but also insight to which physical processes maintain those habitat features. Among the organisms that inhabit montane meadows, amphibians are particularly sensitive. Meadows may serve as refugia for amphibians, including the declining Sierra Nevada yellow-legged frog (*Rana sierrae*) and Cascades frog (*R. cascadae*), due to their complex and varied habitat conditions. Therefore, the processes that create habitat heterogeneity in meadows may be directly linked to habitat conditions that support these sensitive amphibians. We evaluated the relationship between meadow hydrological conditions and habitat use by these frogs to understand the conditions that promote population persistence. Our specific objectives were to (1) describe important hydrologic, geomorphic, and thermal processes pertinent to meadow restoration that create and maintain habitat for focal amphibian species; (2) evaluate the effectiveness of common meadow restoration approaches in improving native amphibian habitat; and (3) provide recommendations for prioritizing likely restoration sites and incorporating specific design elements to enhance conditions for focal amphibians.

Methods

We monitored surface and ground water patterns and habitat use by Cascades frogs at three reference meadows in the northern Sierra Nevada/southern Cascades between 2014 and 2017. We also assessed two meadows that had been restored using a pond-and-plug technique and

one that used beaver dam analogs (BDAs). When Cascades frogs were found, data were collected on numbers, life stage, and size. The location of each observed frog, group of larvae, or egg mass was recorded using GPS, and habitat measurements including water temperature, water depth, flow, substrate, percent emergent vegetation, and canopy cover were taken at the site. Within the meadows occupied by Cascades frogs, we used this local habitat data associated with individual frogs and egg masses to describe the characteristics of habitats used by frogs.

To relate surface and ground water conditions with important frog habitats, we collected detailed topographic and hydrologic data. We collected overlapping aerial imagery from a set altitude with a 3D Robotics Solo quadcoptor with a Canon S100 camera. Ground control points were surveyed during flights with a Topcon GPS-RTK system (Hiper Lite and Hiper V models) with centimeter accuracy. Agisoft Photoscan Professional software was used to stitch and rectify the imagery and create digital surface elevation models with 2-5 cm resolution of the three meadows. We mapped surface water pathways on the ground using a Trimble Pathfinder Pro GPS that allows accurate measurements to below 30 cm horizontally. In 2015, we established transects of ground water monitoring wells at each meadow, and we installed staff gauges in the primary stream channel at the top and bottom of each meadow and in channels bisected by well transects. After summarizing the hydrologic data collected for each meadow, we related core frog habitats with the underlying hydrology of the meadow in a GIS framework. We compared the surface elevation models created from the drone imagery with groundwater elevation raster layers developed from the measured well data to assess ground water flow patterns and elevation change relative to topography both spatially and temporally.

Results

In the three focal meadows that supported Cascades frogs, a common hydrological theme was the presence of a variety of consistent, but shallow, aquatic habitats; including channels, pools, springs, and fens that provide habitat for all life stages from eggs to adult frogs throughout the year, even in drought conditions. Another commonality was off-channel, still water habitat with minimal canopy cover for breeding. These shallow, surface water pools were often augmented by groundwater spring input to extend the hydroperiod well into the summer, allowing tadpoles to successfully metamorphose (Figure 1a). Pool temperatures were warmed by the sun but moderated by the cool spring water input (Figure 1b). Within meadows, all life stages of Cascades frogs occurred most often in locations with minimal (0-25%) canopy cover and avoided areas with high shading. Adult frogs tended to occur in the more fluvially active channels and juvenile frogs resided in secondary channels and oxbows. In general frogs avoided the more stable, densely vegetated meadow flats.

Our assessment of the restored meadows found that one of the pond-and-plug meadows provided appropriate off-channel breeding pools with connection to groundwater, but the pools were often near the larger and deeper borrow pit ponds that also provided habitat for detrimental invasive species including American bullfrogs (*Lithobates catesbeianus*) and brook trout (*Salvelinus fontinalis*). At the second pond-and-plug restoration site, although neither native nor non-native frogs were found, several of the borrow pit ponds supported static habitat conditions (permanent, still water with rooted floating vegetation) known to be more suitable for bullfrogs than native frogs (Figure 2a). We did not find any shallow off-channel pool habitat with extended hydroperiods known to be preferred by Cascades frogs for breeding. The meadow restored with BDAs created appropriate shallow backwater pool habitats behind the dams that could serve as breeding habitat and refuge from brook trout for Cascades frogs (Figure 2b). However, without seasonal maintenance of the dams, the ponds were observed to drain too

quickly in the summer. Once maintenance occurred, juvenile Cascades frogs were observed using the backwater pools.

Discussion

Our study revealed that restoring habitat for native amphibians requires restoring a diversity of aquatic habitat conditions from shallow pools with consistent still water for eggs and larvae to fluvially active stream channels for adults. While raising the water table and thereby increasing the amount of surface water and length of the hydroperiod are part of the solution, restoration of physical processes and associated heterogeneity is also important. Meadows that have some degree of consistent groundwater input should be high priority for restoration and conservation as they may be more likely to provide wet meadow habitat despite varying climatic conditions. Within meadows, locations where low gradient depressions and high water table intersect could be targets for breeding pool enhancement. Meadow alterations that create novel deep, permanent ponds may be colonized by non-native species rather than target native species. In-channel structures such as BDAs seem promising for creating appropriate shallow, backwater pool areas, but they require maintenance. In general, meadow restoration guided by a process-based approach and focused on creating habitat heterogeneity over both time and space will provide greater potential suitability for native frog species with varied life histories and life stages.

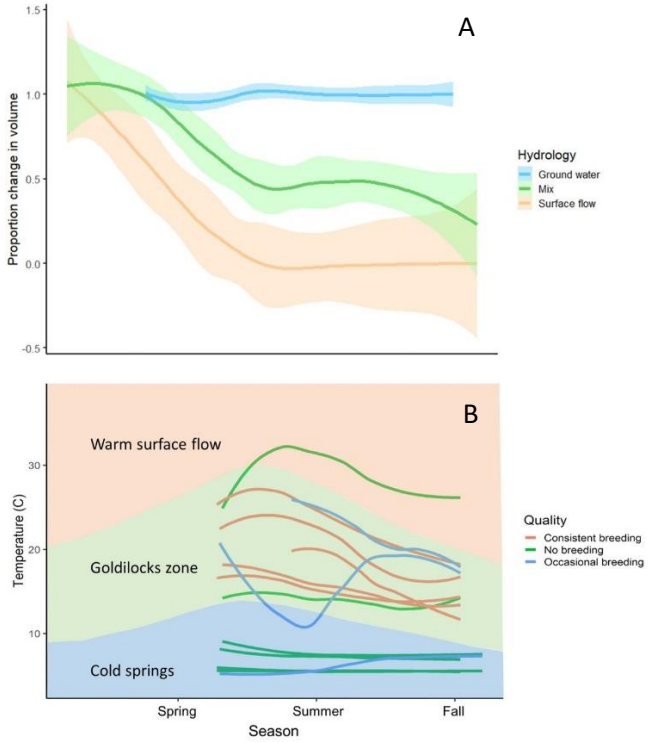

Figure 1. Schematic representation of the change in volume, or dry down rates, over time for three main types of off-channel pools in meadows (A). Spring-fed groundwater pools (blue line) tend to remain stable over the course of the dry season while surface water pools (orange line) quickly dry down. Pools with a mix of surface water and spring water (green line) decrease in volume but tend to stay stable at a base rate driven by the spring flow. (B) Water temperatures at pools where Cascades frogs consistently breed (red lines) tend to be moderate compared to pools where they occasionally (blue lines) or never (green lines) breed. Lines are overlaid on colored polygons representing water temperatures of the pool types shown in A.

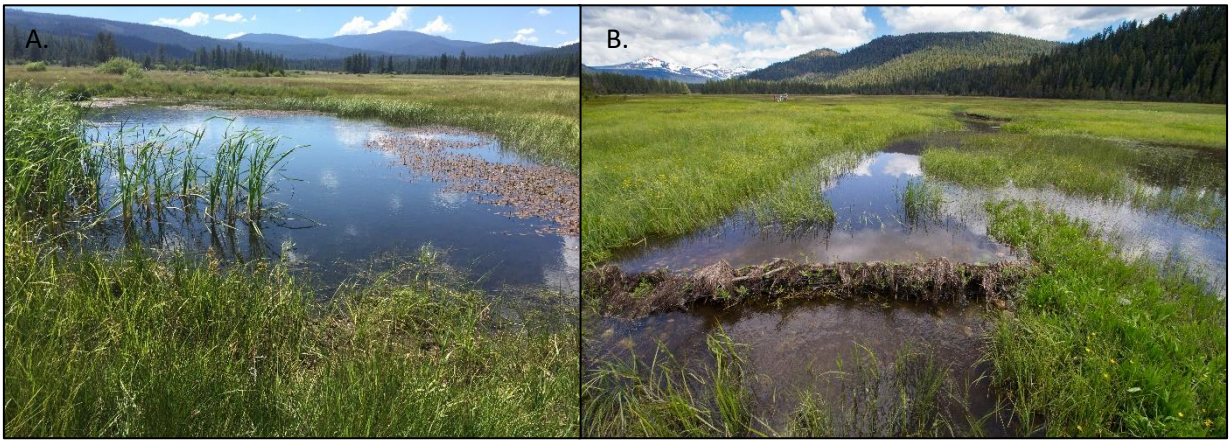

Figure 2. Deep, still water off-channel pond in a meadow restored with the pond-and-plug technique (A) compared to a shallow, backwater pool associated with biogenic instream structures such as beaver dam analogs (B).

References

Arscott, D. B., K. Tockner, D. van der Nat, and J. V. Ward. 2002. Aquatic habitat dynamics along a braided alpine river ecosystem (Tagliamento River, Northeast Italy). Ecosystems 5:802-814.

Drew, W. M., N. Hemphill, L. Keszey, A. Merrill, L. Hunt, J. Fair, S. Yarnell, J. Drexler, R. Henery, J. Wilcox, R. Burnett, K. Podolak, R. Kelley, H. Loffland, R. Westmoreland, and K. Pope. 2016. Sierra Meadows Strategy. The Sierra Meadows Partnership, https://meadows.ucdavis.edu/files/Sierra_Meadow_Strategy_full_report_SHAREABLE_mid.pdf.

Florsheim, J. L., J. F. Mount, and A. Chin. 2008. Bank erosion as a desirable attribute of rivers. Bioscience 58:519-529.

Kattlemann, R. 1996. Hydrology and water resources. Pages 855-920 *in* Sierra Nevada Ecosystem Project: Final report to Congress, vol. II, assessments and scientific basis for management options. University of California, Davis, California.

Loheide, S. P., R. S. Deitchman, D. J. Cooper, E. C. Wolf, C. T. Hammersmark, and J. D. Lundquist. 2009. A framework for understanding the hydroecology of impacted wet meadows in the Sierra Nevada and Cascade Ranges, California, USA. Hydrogeology Journal 17:229-246.

Pope, K. L., D. S. Montoya, J. N. Brownlee, J. Dierks, and T. E. Lisle. 2015. Habitat conditions of montane meadows associated with restored and unrestored stream channels of California. Ecological Restoration 33:61-73.

Ward, J. V., K. Tockner, D. B. Arscott, and C. Claret. 2002. Riverine landscape diversity. Freshwater Biology 47:517-539.

Increasing Freedom Space and Sustainability on the Rio Grande through Channel Realignment

Nathan Holste, Hydraulic Engineer, Bureau of Reclamation, Denver, CO, nholste@usbr.gov
Aubrey Harris, Hydraulic Engineer, Bureau of Reclamation, Albuquerque, NM, aharris@usbr.gov
Brian Hobbs, Project Manager (Biologist), Bureau of Reclamation, Albuquerque, NM, bhobbs@usbr.gov

Abstract

A channel realignment project on the Rio Grande demonstrates the benefits of applying the freedom space concept to river management. Freedom space is defined as the minimum space needed for fluvial and ecological function of the river system. River engineering has historically focused on water delivery, flood control, and infrastructure to the detriment of biodiversity, ecosystem services, and fluvial processes. Providing space for the river to migrate and flood accomplishes both engineering and environmental goals. The Rio Grande is a useful case study for this strategy because it has been heavily altered and constrained. In the early 1900s, the active channel was up to one mile wide and the floodplain corridor was several miles wide. Currently, the active channel is less than 500 ft wide and the floodplain corridor is less than 0.5-miles wide for the majority of the Middle Rio Grande. Formerly active river processes of erosion, deposition, flooding, lateral migration, and channel avulsion are significantly diminished in the contemporary environment. Increasingly dense, riparian vegetation (both native and invasive) also limits channel planform adjustment. Despite this evolution toward a more static channel, there are continued conflicts between human stakeholders and the ecosystem services provided by the river. In the project reach near Socorro, NM the channel typically does not have the minimum space required for essential geomorphic processes to occur. The constrained channel has created a perched condition where overbanking flows are disconnected from the river and the main channel can become completely plugged with sediment. Under historical conditions prior to intervention there would eventually be an avulsion, but under current practices the sediment plug is removed to protect the spoil levee. A channel realignment project is currently being constructed to create a managed avulsion, simulating what would have occurred under natural flow and sediment conditions. Realigning the river away from a levee to a wide, well-connected floodplain provides a functional corridor where the river can adjust over time with fewer constraints on ecological and fluvial processes.

Introduction

Motivation and Background

River engineering has often emphasized the core functions of water delivery, flood control, and infrastructure protection. Design and construction activities in the river corridor have focused on these components at the expense of a more holistic view of the river that incorporates ecosystem services, sustainability, and resiliency. Riverine infrastructure typically has not considered impacts to the stream environment, and designs did not account for stream processes and fluvial hazards (Sholtes, et al. 2018). Since the 1990s, river management has more

frequently recognized a hydrogeomorphic approach that provides space for rivers to migrate and flood. This emphasis on the health of the river system has the added benefit of reducing risks associated with erosion and flooding (Biron, et al. 2014). The hydrogeomorphic strategy for addressing both engineering and environmental goals is exemplified by a current channel realignment project on the Rio Grande.

Makar and AuBuchon (2012) summarize the historical changes on the Middle Rio Grande (MRG), which provides context for the channel realignment project. During the late-nineteenth and throughout the twentieth century, the MRG was transformed from a natural stream into a heavily managed river system, with the rate and magnitude of anthropogenic impacts steadily rising since the start of larger-scale diversions and expansion of European settlers during the late 1800s. The natural tendency for the river is to migrate and shift position across the valley during flood events, while depositing sediment in the main channel and overbank areas. This sediment deposition and shifting river channel impacted infrastructure and water use, especially as engineering-centered, water resource development and exploitation on the MRG increased during the early 20th century. Significant negative impacts to the MRG in New Mexico include: surface-flow withdrawals, grazing, flood control and diversion dams, levees, and channelization. Geomorphic changes are also driven by episodic floods and droughts. There has been an overall reduction in peak flows and sediment loads since about 1950. The integrated outcome of these events has been a trend of channel narrowing, vegetation encroachment, and an overall simplification of the channel geometry and planform as the river has become less dynamic. These geomorphic trends have led to corresponding declines in aquatic and terrestrial habitat for native species and long-term reduction in the capacity of the MRG to meet the demands placed upon it by humankind through provision of ecosystem services.

As with many rivers, flow modifications (flood control and water delivery) and infrastructure on the MRG have reduced opportunities for restoring active riverine processes. A unique opportunity exists in a section of the MRG where the channel is near a spoil levee to the west and is perched above a relatively wide floodplain to the east. A river realignment project has been developed to move the channel further from infrastructure constraints and reconnect it to the lower-lying, eastern floodplain. One of the channel realignment project goals is to promote long-term effective conveyance of water and sediment through the reach (Holste 2014). Inherent within this goal is allowing for sustainable geomorphic processes that allow the river to adjust to the water and sediment supply. Ecological resilience is improved by allowing the river system to withstand and recover from disturbance events, in addition to responding more naturally to gradual changes (Seavy et al. 2009). Realigning the channel to a well-connected, less confined floodplain should reduce future potential conflicts between the environment and anthropogenic needs.

Project Area

The realignment project is located on the MRG in south-central New Mexico (Figure 1). This reach is near Socorro, NM, about 80 miles south of Albuquerque, NM, and about 50 miles north of Elephant Butte Dam. Most of the project is within the Bosque del Apache National Wildlife Refuge (BDANWR), which is managed by the United States Fish and Wildlife Service (USFWS). This area of the river is generally known as the Socorro Reach, and spans about 20 miles from the Highway 380 Bridge to the San Marcial Railroad Bridge. MRG River Miles (RM) for the channel realignment are from RM 86 at the upstream end to RM 79 at the downstream outlet. Specific concerns associated with this reach include: river drying during periods of low flow,

breaches of the non-engineered levee during flood events, overbank flows that are disconnected from the main channel, stranding of aquatic species, loss of channel diversity and complexity, and loss of native riparian vegetation.

Figure 1. MRG channel realignment project location map (from ESRI reference map)

Historical Context and Channel Evolution

Environmental extremes have been documented for centuries within the Rio Grande watershed, such as alternating drought cycles that were contrasted with large flood events (Scurlock 1998, Lagasse 1980, Berry and Lewis 1997). This dynamic hydrologic regime limited vegetation encroachment and maintained a wide, braided channel that shifted position during high flows. Nelson et al. (1914) provide an account of the Rio Grande's historical characteristics:

"The low average gradient of the river accounts for the deposition of a large part of its heavy load of sediment during flood periods. These consist mainly of fine sand, silt, and clay. The river channel through the area varies in width from one-eighth to 1 mile. The bottom of the channel forms a wide, sandy flat with banks averaging 2 to 2 ½ feet above the river bed. The stream

current shifts its course from one side of the channel to the other at frequent intervals, depending upon the deposition of material within its bed...The greatest deposition from the river occurs during flood periods when the water overflows areas covered with grass and brush."

Nelson et al.'s (1914) description highlights the large floods that were common in the early 1900s, the wide shallow nature of a channel that often migrated, and the relative low density of mature vegetation in the geomorphically-active part of the floodplain. These traits can be observed in Figure 2(a), an aerial photo of the realignment project area from 1935. In addition to the 1935 main channel location, evidence of former channel locations to the west is apparent. Crevasse splays, meander scars, and other patterns of fluvial erosion and deposition across a wide swath of the floodplain can be seen in the photograph. Figure 2(b) shows that a spoil levee has cut off most of the formerly active floodplain. The 1918 and 2012 channel planform outlines are shown in both images to illustrate the dramatic channel and active-floodplain narrowing that has occurred. Also, orange hatching in the figure represents areas where the 1918 channel planform is outside the bounds of the 1950's constructed spoil levee. Lateral mobility of the river has been constrained in addition to reduction in the active floodplain area.

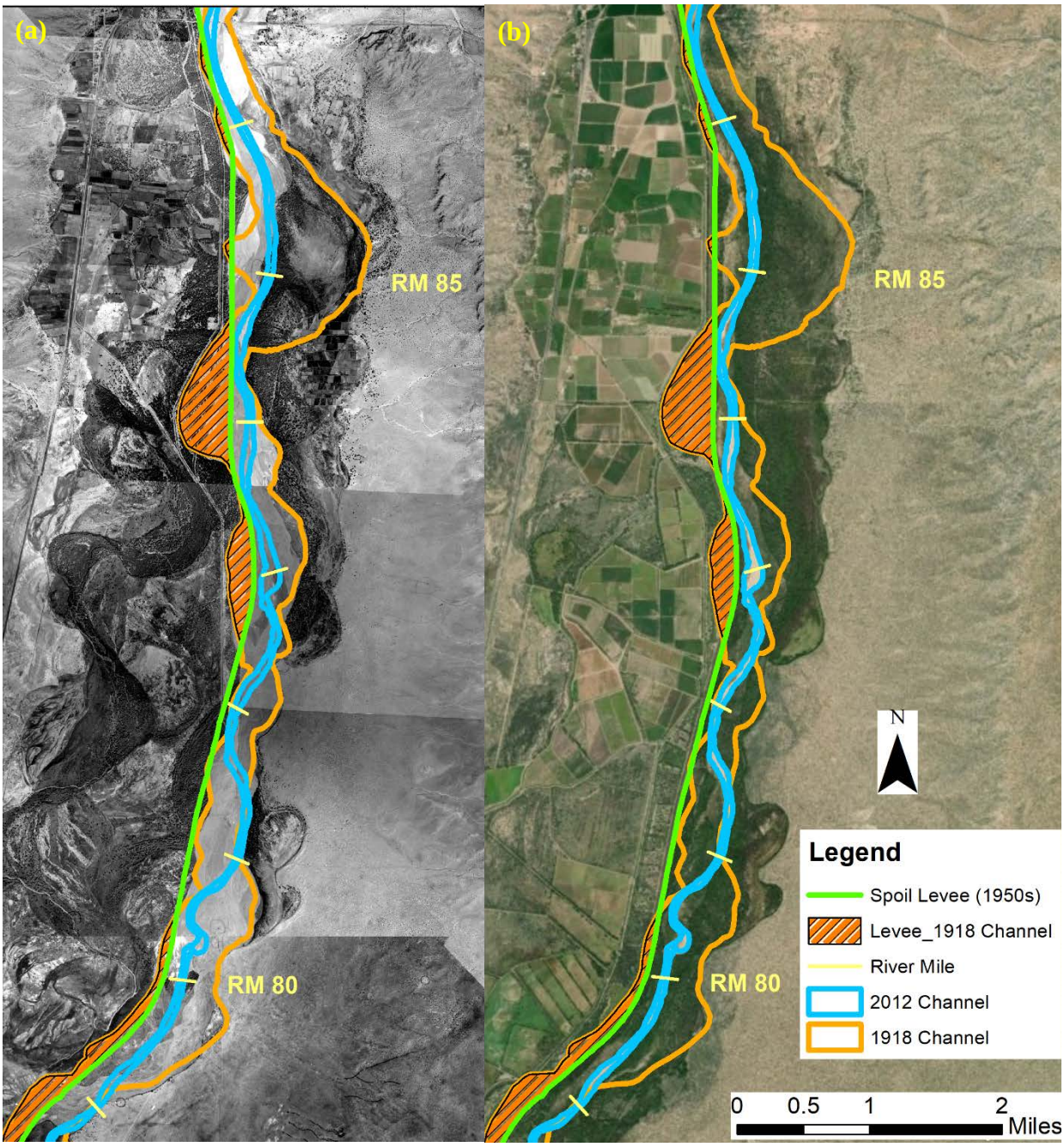

Figure 2. Comparison of 1918 (orange) and 2012 (blue) channel planform with spoil levee (green) shown for reference. Areas where the 1918 channel is beyond the subsequently constructed spoil levee are represented by orange hatching. Background imagery is from (a) 1935 and (b) 2014. Formerly active channel locations to the west of the spoil levee have been converted to irrigated fields. Evidence of active channel migration and avulsions can be seen across the entire 1935 floodplain.

Over the last one hundred years the dominant planform trend has been channel narrowing and vegetation encroachment, so that the current river is a relatively narrow, single-thread channel with a fixed position (Figure 3). The primary drivers of channel width are the magnitude of peak flows and the ratio of peak flows to mean annual flow (Knighton 1998). Prior to 1950, floods over 10,000 cfs were relatively common, occurring once every two or three years on average.

Since 1950, flows have not exceeded 10,000 cfs at San Marcial (USGS Gage 08358300 and 08358500). Figure 4 demonstrates how the channel narrowing trend relates to the reduction of peak flows. Gage records also indicate that the frequency of channel drying has been reduced in recent years in addition to the reduction of peak flows. Channel drying may have contributed to controlling excessive vegetation encroachment in the past, since low flows in the river provide water that irrigates vegetation adjacent to the channel. Historical flow variability, coupled with high sediment loads, created significant in-channel and riparian diversity. Opportunities for renewal of the riparian community were provided when the wide, multi-threaded channels were relocated by avulsions or lateral migration (Tetra Tech 2014).

The 1980s are the most recent time period where significant channel widening was observed in the project reach. Although peak flows during the 1980s were controlled, there were several years of high volume, long duration spring snowmelt runoff events that caused channel widening between the late 1970s and mid-1980s. Floodplain vegetation clearing practices during the 1960s and 1970s also contributed to subsequent channel widening. Conversely, during relatively large spring snowmelt runoff events in recent years (2005, 2008, and 2017) significant channel widening was not observed. This is likely due to the presence of extensive mature vegetation adjacent to the channel and throughout the floodplain. Current flood peaks no longer have the energy required to scour established riparian vegetation.

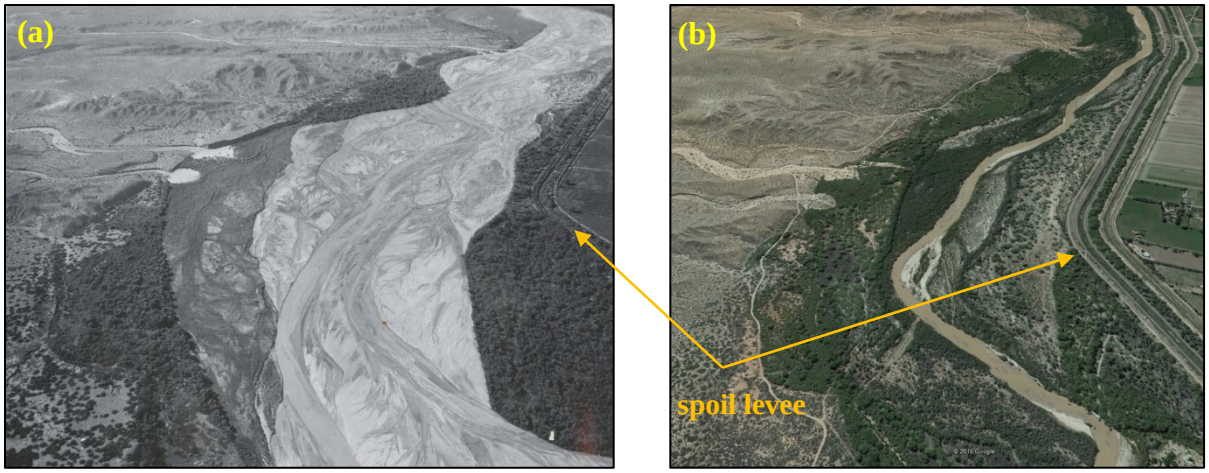

Figure 3. Comparison of oblique aerial imagery looking downstream at RM 101 for (a) 1953 and (b) 2013. The 1953 wide and braided channel has transitioned to a narrow, single thread channel. The spoil levee was constructed in 1952 at this location.

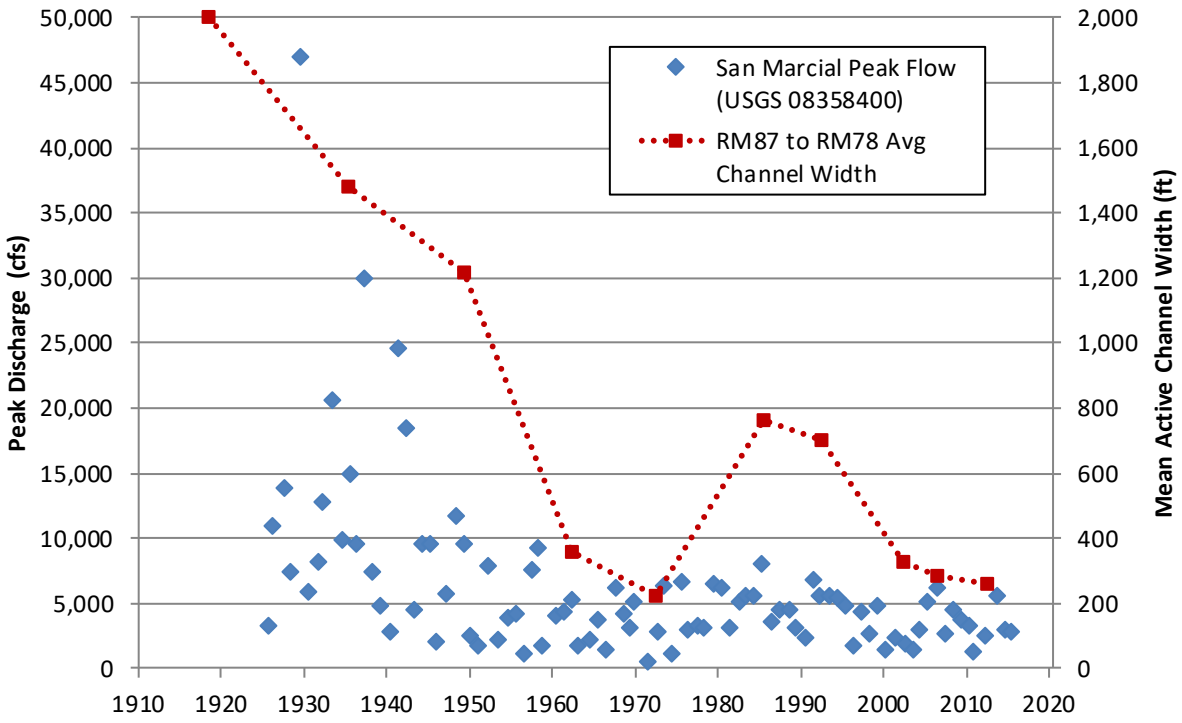

Figure 4. Annual peak flow and reach-averaged active channel width over time. Widening in 1980s occurred in response to several large spring runoff events, even though peak discharge was controlled by upstream dams. San Marcial gage is at RM 69, downstream of the study reach.

Existing Conditions and Sediment Plugs

The sediment transport in the project reach is predominantly capacity limited in which sediment supply exceeds transport capacity. However, this is a general trend and is highly variable both spatially and temporally. Deposition occurs as the excess sediment cannot be carried downstream by the river, thereby raising the channel bed elevation over time. The part of the floodplain accessible by the river also experiences aggradation (to a lesser degree) as overbank flow deposits fine-grained silt and clay sediments. The greatest deposition typically occurs in overbank areas adjacent to the main channel. These vegetated banks are zones of high roughness where there is a significant reduction in flow velocity that induce deposition of sediment carried from the main channel during high flows. In this manner, there is a tendency for the elevation of the channel bed and banks to rise faster than floodplain areas further from the river, creating a perched channel. As channel migration has been limited, areas of sediment deposition are increasingly concentrated within the river and its banks, rather than being spread out across the floodplain.

A perched channel causes floodplain surface water to be disconnected from main channel flows during flood events. Aquatic species are often stranded as flows recede because there is no return path back to the main channel. Additionally, the disconnected flows cause increased water losses and reduced sediment transport capacity. Seepage flows are lost from the river channel to nearby irrigation drains, groundwater, and low elevation areas. Channel perching has

also been identified as one of the primary factors associated with sediment plug formation (Park 2013, Tetra Tech 2010).

In addition to the general long-term aggradational trend, sediment has plugged the channel five times since 1990 in the Socorro Reach. Sediment plugs are the result of rapid and severe local channel aggradation. A higher concentration of sediment is transported near the bed, so that when overbanking occurs at the top of the water column a disproportionate volume of sediment is left in the main channel. Holste (2014) summarized the channel characteristics that contribute to sediment plugs: backwater effects (reservoir pool, bridge, abrupt bends), narrow or constricted channel, low channel slopes (or sudden reduction in slope), limited main channel hydraulic and sediment transport capacity, and a perched channel. A high magnitude, long duration spring snowmelt runoff event is also required for a sediment plug to occur. Sediment plugs are driven by overbanking flow and the associated sediment transport imbalance caused by the channel characteristics listed above. This sediment imbalance must persist over some minimum duration for a plug to form; sediment plugs have not formed during flashy monsoon events. The most recent sediment plug occurred in 2017 within BDANWR. This event demonstrates that the geomorphic and sediment conditions required for a plug are still present in this reach.

Figure 5 provides example photographs of a sediment plug that occurred during the spring snowmelt runoff of 2008. Historically, a new flow path would have developed, bypassing the old plugged channel as the entire river flow overbanked. Eventually, a new channel would become established thus creating a full avulsion and resetting the river (Massong et al. 2010). With the current vegetation levels, it would likely take several years or even decades for a natural avulsion to occur. Vegetation would need to die off through drowning or other means before it could be uprooted by scour from high flow events. It is possible that a breach of the western spoil levee would occur before a natural avulsion to the east.

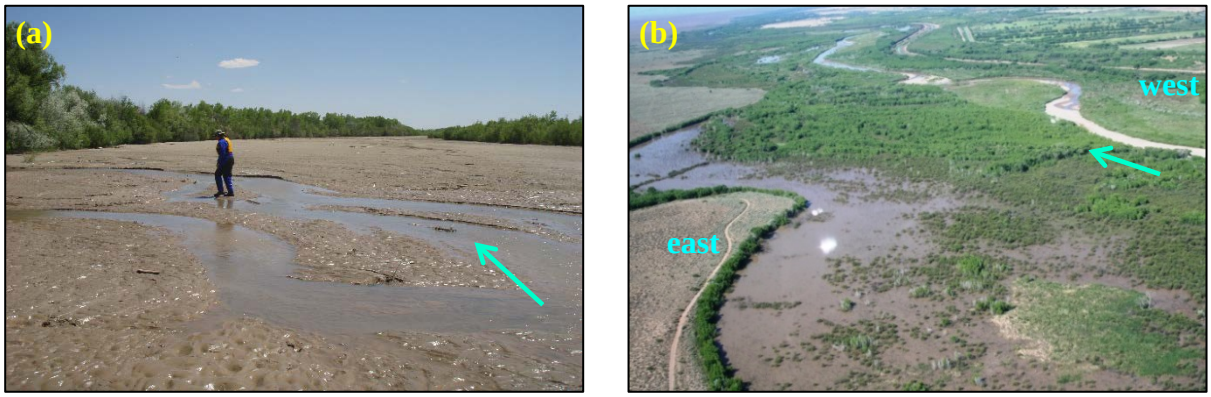

Figure 5. Sediment plug photos from 2008 (a) June 3, 2008 looking downstream: main channel is filled with sediment and all flow (3,700 cfs) is forced around the plug into floodplain (b) July 4, 2008 looking downstream: flows have receded (1,600 cfs), the sediment plug has grown upstream, and a large volume of water remains ponded in the east floodplain.

Massong et al. (2010) developed a planform evolution model for the MRG that describes the various channel conditions from the historical wide, braided channel to the current narrow,

single thread, plugged channel (Figure 6). For the previous five sediment plugs, a pilot cut has been excavated through the plug to restore flow and sediment continuity in the main channel. The pilot channels have been effective for this purpose, but, along with the heavily vegetated floodplain, have also inhibited geomorphic processes and natural channel evolution. Since about 1990, the river has essentially been confined to planform stages A4 and A5. Historically, larger flows and the unconfined, less densely vegetated floodplain have transitioned the channel from A5 to A6 and eventually back to Stage 1. It is this process that the realignment project is attempting to follow. Modern conditions necessitate that construction equipment, rather than high flow, provides the energy to move the river through Stage A6 to Stage 1. Although the as-built conditions will resemble Stage 1, the realignment will still be governed by the geomorphic drivers of reduced flow and sediment. Movement between the first three stages is expected with a preference for Stages 3 and A4. Ideally, the unconfined floodplain setting and increased distance from infrastructure will provide the river more freedom to move between stages with reduced maintenance and intervention.

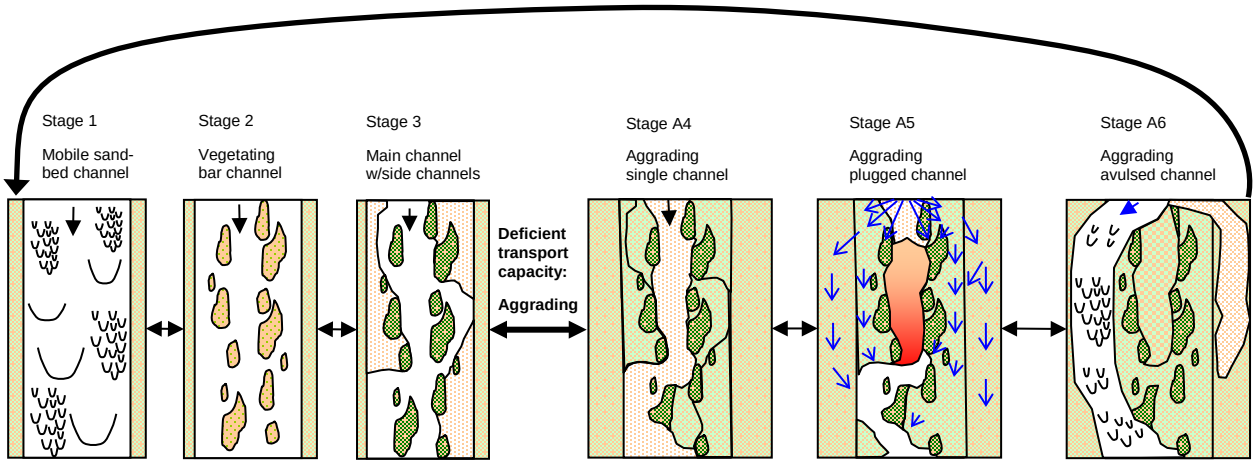

Figure 6. Rio Grande planform evolution model (modified from Massong et al. 2010). Existing channel is "stuck" between Stages A4 and A5 as sediment plugs that form are subsequently excavated. Realignment project "re-sets" the river to Stage A6 and then Stage 1 by creating a managed avulsion.

Channel Realignment

Design Concept

The realignment design attempts to work with the river's geomorphic and historical tendencies by creating a channel avulsion. The overall philosophy is to remove unnecessary constraints and allow for the natural riverine processes of channel migration, deposition, and flooding. It is not a project goal to maintain the newly constructed channel dimensions, but to allow for channel adjustment and habitat development while reducing negative impacts to infrastructure and water delivery. Habitat conditions are expected to improve as opportunities are provided for geomorphic processes to revitalize certain aspects of the historical environment, at least for a period of time. River maintenance activities are also expected to reduce significantly because the channel will be able to transport water and sediment to Elephant Butte Reservoir without the need to excavate pilot channels.

Figure 7 shows the plan view location of the realignment, along with cross sections of the existing topography. The perched channel is apparent in the cross sections that show how any overbanking flow from the current channel will contact the non-engineered spoil levee. This places the levee at risk for geotechnical failure any time there is an extended duration of water ponding against the levee. Also, there are several locations where the levee constrains the lateral migration of the existing channel. The realignment is essentially a managed avulsion that uses vegetation clearing to establish a path for the new river channel through the east floodplain and away from the levee. In addition to the main corridor of complete vegetation removal, adjacent stands of non-native vegetation will be cleared in select areas to provide variability to the planform morphology. Most of the excavation associated with the realignment will occur at the inlet and outlet areas to facilitate a connection to the existing channel. There is a section in the middle of the project near RM 82 where the channel cannot be realigned because of an archaeological site and location of the east mesa. The downstream phase of the project will be implemented first and then monitored before constructing the upstream phase.

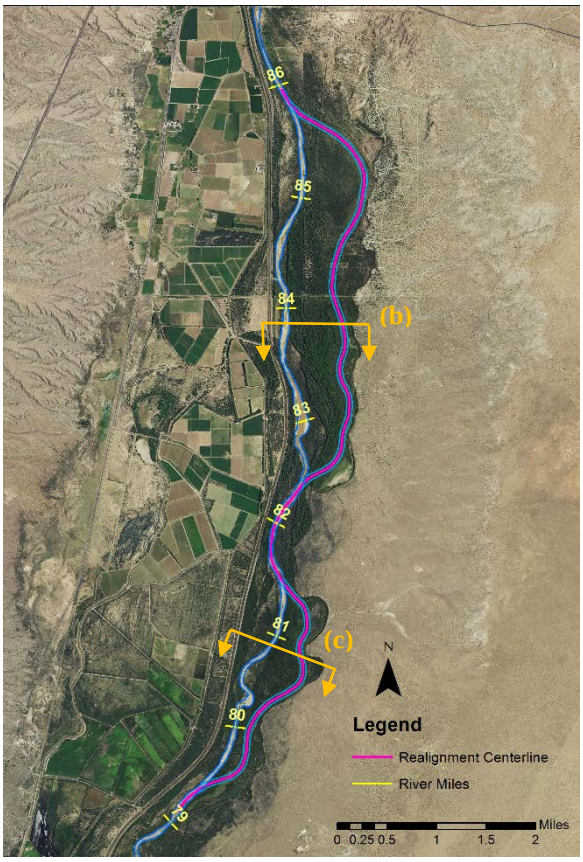

(a) Realignment map

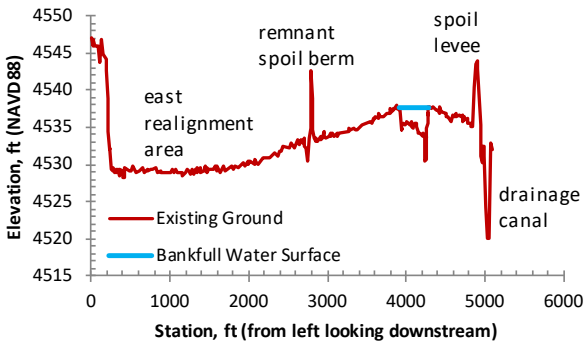

(b) Cross section near RM 84

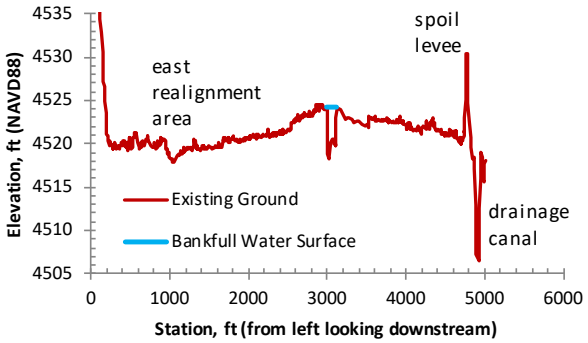

(c) Cross section near RM 81

Figure 7. Channel realignment location and associated cross section topography. Existing channel bank is perched 5 – 10 ft above low point in east floodplain.

Freedom Space

The channel realignment project applies the "freedom space" concept proposed by Biron et al. (2014). Freedom space is defined as the minimum space needed for fluvial and ecological function of the river system. Biron et al. (2014) advocate for this approach as a sustainable river management strategy to increase the resiliency of river systems. Similar terms that have been proposed and applied to river management include "making space for water," "room for the river," "river corridor," "erodible corridor," and "fluvial territory." These programs typically focus on either channel mobility, creation of a riparian corridor or flood risk management.

The important insight of the freedom space concept of Biron et al. (2014) is the integration of wetlands, mobility, and flood zones. Mobility space is based on short- and long-term channel migration, areas of high avulsion potential, and the geomorphic function of the river. The mobility zone is generally defined as the area that will be occupied by the river considering lateral erosion, migration, and the meander belt width. Flooding space is based on inundation at flows of various return intervals, and also interpretation of morphological landforms and riparian wetlands to account for connectivity between groundwater and surface water. Biron et al. (2014) define the minimum freedom space as the combined zone of short-term mobility space and high frequency flooding space. This represents the minimum space needed for hydrogeomorphic and ecological processes to operate effectively in a river. For a longer time period, the functional freedom space is defined as the combined zone of long-term mobility space and medium frequency flooding space. This represents the corridor needed for the river's essential fluvial and biotic processes.

Channel realignment in this part of the Rio Grande provides a significant increase in freedom space. Figure 8(a) represents the mobility space for the project reach by measuring the distance between the channel bank and spoil levee. The existing channel has three locations, for a total distance of about one mile, where the distance to levee is less than 1.2 times the channel width. This ratio of 1.2 times the channel width corresponds to the smallest distance for minimum freedom space that was found in any of the rivers studied by Biron et al. (2014). Essentially, the Rio Grande in the project area does not have the minimum freedom space needed for a naturally-functioning river system to develop and self-maintain. The realignment channel increases the average distance to levee ratio from 3.1 to 9.2. The lowest ratio for the realigned channel is 4.5, although the middle section that could not be relocated remains close to the levee at a ratio of 1.2 over a distance of 1,000 ft.

Figure 8(b) represents the flooding space for the existing and realigned channel. Results from a one-dimensional hydraulic model were used to analyze when overbanking flows first contacted the levee at cross sections throughout the project reach. The average flow required to contact the spoil levee is 3,500 cfs for the existing channel, which is the approximate flow with a 2-year return period. Realigning the channel increases the average flow required to contact the levee to 18,000 cfs, which has not occurred since 1942 (before current water management operations and dams). Only 30% of the reach would still be susceptible to levee risk at flows below 10,000 cfs. Flooding and overbanking flow is an important fluvial geomorphic process for fish spawning and rearing and the scour and seeding of vegetation. The realignment will allow these processes to be unrestricted by the levee. Increased freedom space for the realigned channel meets engineering goals of infrastructure protection and reduced maintenance costs, while

simultaneously addressing ecological goals of removing constraints and increasing dynamism in natural hydrogeomorphic and ecological systems.

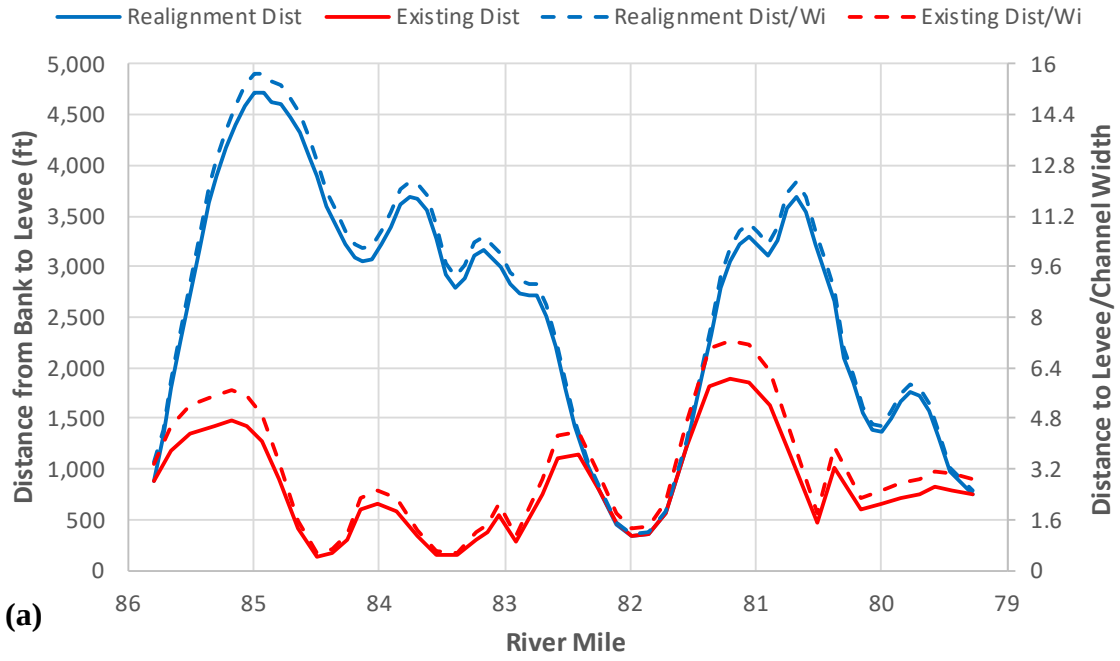

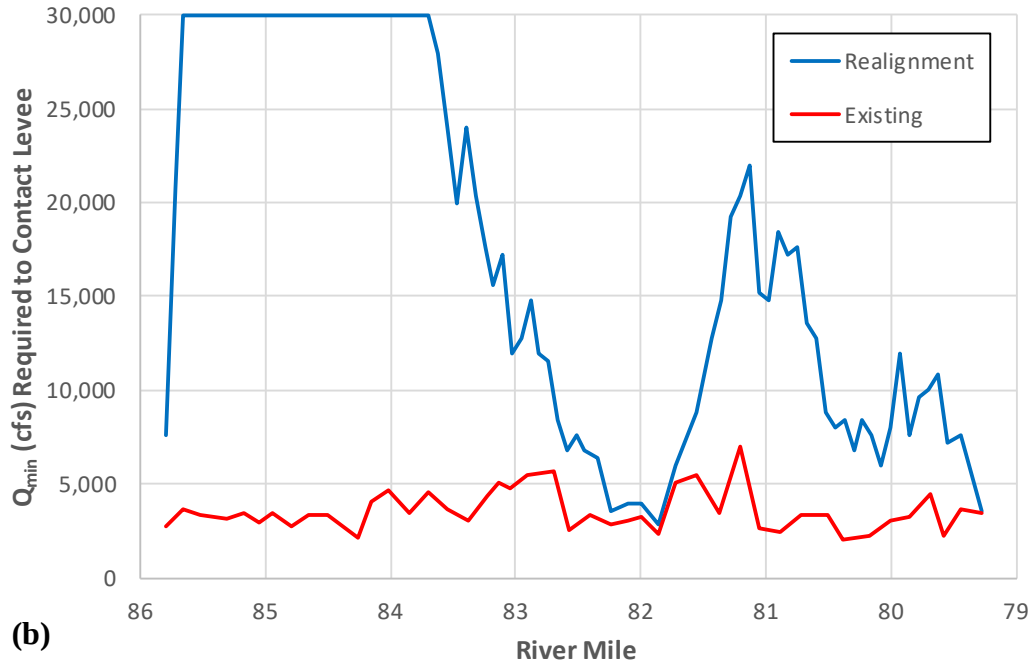

Figure 8. (a) Comparison of distance from channel to spoil levee for existing conditions and realignment. Secondary y-axis is the ratio of levee proximity to channel width. Realignment increases average distance to width ratio from 3.1 to 9.2. (b) Comparison of minimum discharge required to contact spoil levee for existing conditions and realignment. Discharges above 30,000 cfs are not shown and are assumed at this value for plotting purposes (RM 85.7 to RM 83.7). Realignment increases average discharge from 3,500 cfs (2-yr return period) to more than 18,000 cfs. River could not be realigned near RM 82 because of archaeologic and geologic features in this area.

Summary and Conclusions

The existing channel morphology is a result of the interaction between water discharge, sediment load, geology, vegetation, infrastructure, and anthropogenic actions. Over the last one hundred years, the historically wide, braided, and dynamic channel has narrowed to a relatively fixed position with a simplified morphology. Infrastructure has further limited active geomorphic processes. Specific concerns associated with the existing Rio Grande conditions include: reduced water deliveries, river drying during periods of drought, breaches to the non-engineered levee during flood events, overbank flows that are disconnected from the main channel, stranding of aquatic species, loss of channel diversity and complexity, and loss of native riparian vegetation. A combination of artificially-reduced flood peaks and sediment loads, together with the effects of anthropogenic lateral constraints and river channelization, do not provide the same opportunity to rework the channel as occurred historically.

The realignment project on the Rio Grande restores some of the river's lost freedom space and demonstrates that multiple project goals can be met through a holistic design approach that emphasizes balance between fluvial geomorphic and vegetation-led, ecological processes. Removing constraints and providing freedom to the river will allow for channel adjustment within a well-connected floodplain. The degree of adjustment and morphological dynamics will be driven by the upstream flow and sediment conditions. A managed avulsion (realignment) attempts to restore, at least for a period of time, some of the dynamic geomorphic processes that used to occur on the historical Rio Grande. Existing channel conditions do not meet the criteria for minimum freedom space. That is, the minimum space needed for the natural hydrogeomorphic and ecological processes of a river. The realigned channel provides a functional space for a river corridor where the integral fluvial processes can occur. Incorporating the freedom space concept in river management planning and design has provided a means to reduce threats to infrastructure while improving the health and function of the fluvial system.

References

Berry, K. and Lewis, K. 1997. Historical Documentation of Middle Rio Grande Flood Protection Projects, Corrales to San Marcial. U.S. Army Corps of Engineers, Albuquerque District, Albuquerque, New Mexico. Contract No DACW47-94-D-0019, Delivery Order # 0006.

Biron, P.M., Buffin-Bélanger, T., Laracque, M., Choné, G., Cloutier, C.-A., Ouellet, M.-A., Demers, S., Olsen, T., Desjarlais, C., and Eyquem, J. 2014. "Freedom Space for Rivers: A Sustainable Management Approach to Enhance River Resilience," Environmental Management 54(5):1056–1073.

Holste, N. 2014. BDANWR Sediment Plug and River Restoration Project: Alternatives Analysis Synthesis Report. Bureau of Reclamation, Upper Colorado Region, Albuquerque Area Office, Technical Services Division, Albuquerque, NM.

Knighton, D. 1998. Fluvial Forms and Processes: A New Perspective. Arnold, London, England and Oxford University Press, New York, New York.

Lagasse, P.F. 1980. An Assessment of the Response of the Rio Grande to Dam Construction – Cochiti to Isleta Reach. Technical Report for U.S. Army Corps of Engineers, Albuquerque District, Albuquerque, NM.

Makar, P., and J. AuBuchon. 2012. Channel Conditions and Dynamics of the Middle Rio Grande. Bureau of Reclamation, Technical Service Center, Denver, Colorado, and Upper Colorado Region, Albuquerque Area Office, Albuquerque, NM.

Massong, T.M., Makar, P.W., and Bauer, T.R. 2010. “Planform Evolution Model for the Middle Rio Grande, New Mexico,” In Proceedings of the 2nd Joint Federal Interagency Conference on Sedimentation and Hydrologic Modeling, June 27 – July 1, 2010, Las Vegas, NV.

Nelson, J.W., Holmes, L.C., and Eckmann, E.C. 1914. Soil Survey of the Middle Rio Grande Valley Area, New Mexico. U.S. Department of Agriculture, Bureau of Soils, Washington, DC.

Park, K. 2013. Mechanics of Sediment Plug Formation in the Middle Rio Grande, New Mexico. Ph.D. Dissertation, Colorado State University, Fort Collins, CO.

Scurlock, D. 1998. From the Rio to the Sierra: An Environmental History of the Middle Rio Grande Basin. General Technical Report RMRS-GTR-5. U.S. Department of Agriculture, Forest Service, Rocky Mountain Research Station, Fort Collins, CO.

Seavy, N.E., Gardali, T., Golet, G.H., Griggs, F.T., Howell, C.A., Kelsey, R., Small, S.L., Viers, J.H., and Weigand, J.F. 2009. “Why Climate Change Makes Riparian Restoration More Important than Ever: Recommendations for Practice and Research,” Ecological Restoration 27(3):330-338.

Sholtes, J.S., Ubing, C., Randle, T.J., Fripp, J., Cenderelli, D., and Baird, D.C. 2018. “Managing Infrastructure in the Stream Environment,” Journal of the American Water Resources Association 54(6):1172–1184.

Tetra Tech. (2010). River Mile 80 to River Mile 89 Geomorphic Assessment and Hydraulic and Sediment Continuity Analyses. Prepared for the Bureau of Reclamation, Albuquerque, NM.

Tetra Tech. (2014). Ecohydrological Relationships along the Middle Rio Grande of New Mexico for the Endangered Rio Grande Silvery Minnow. Contract No. WP912PP-08-D-0009-0-20, Task Order 20, Task 5. Prepared for U.S. Army Corps of Engineers, Albuquerque District, Albuquerque, NM.

Large Wood Helicopter Loading Project on the South Fork Trinity River, Northern California

David (DJ) Bandrowski, Civil Engineer, Yurok Tribe, Weaverville, California, djbandrowski@yuroktribe.nsn.us
Aaron Martin, Habitat Restoration Biologist, Yurok Tribe, Willow Creek, California, amartin@yuroktribe.nsn.us
Josh Smith, Natural Resource Specialist, Watershed Research and Training Center, Hayfork, California, josh@thewatershedcenter.com
Eric Wiseman, Restoration Specialist, Yurok Tribe, Weaverville, California, ewiseman@yuroktribe.nsn.us

Executive Summary

The South Fork Trinity River (SFTR) the largest un-dammed river in the State of California is a federally designated wild and scenic river for much of its length, and is a keystone watershed that supports one of the last remaining populations of wild spring-run Chinook Salmon (Oncorhynchus tshawytscha) within the Klamath River basin. However, this culturally and economically valuable salmon species has seen a dramatic decline in the SFTR with population estimates declining from an average of over 10,000 fish prior to 1965 to a low of only 15 observed fish in 2017. This realization motivated the Yurok Tribe and Watershed Research and Training Center (WRTC) to take action to halt the decline and implement a unique in-channel restoration project. The project entailed utilizing a helicopter to transport and place whole trees within a 5 mile reach of the river. This paper describes the planning, design, implementation and monitoring involved in completing the project.

The culmination of over two years of planning, analysis, and design resulted in the implementation of the project in September of 2018. This was a coordinated effort between the Yurok Tribe, the WRTC, and several state and federal agencies. The project's objective was to increase and improve reach-scale ecosystem and geomorphic processes. A total of 309 whole trees were flown into 57 specific design locations in the SFTR on both US Forest Service and private lands. The whole trees were placed in un-anchored arrangements designed to interact with hydraulic forces to induce scour pools, create habitat complexity, provide instream cover, promote floodplain connectivity, and enhance thermal refugia.

The project's design work integrated a wide-range of technologies including Unmanned Aircraft Systems (UAS) and survey grade GPS equipment. This technology was used to collect and develop detailed aerial imagery and Digital Terrain Models (DTMs) using a photogrammetric process called Structure for Motion (SfM). 2D-Hydrodynamic models utilizing the DTMs were developed for existing and design conditions to evaluate river hydraulics and support design calculations. In addition, a quantitative monitoring plan was developed to evaluate the physical change of the river, the movement of placed whole trees due to high flow events and the biological response of the anadromous fish populations.

Introduction

Project Overview

The overarching objective of the project is to increase wild spring-run Chinook Salmon (Oncorhynchus tshawytscha) populations by improving habitat and water quality (thermal refugia) through the augmentation of large wood. Large wood (whole trees with root balls and canopy structure intact) were placed in designed arrangements at key locations within proximity to cold water tributary confluences, groundwater seeps, or geomorphic key points. The large wood was designed to interact with hydraulic forces to induce scour pools, create habitat complexity, sort sediments, provide instream cover, and promote floodplain connectivity. The following are the specific project goals:

- Goal 1: Restore and enhance South Fork Trinity River Spring Run Chinook and SONCC Coho salmon habitat within the project reach; Improve adult holding and migration habitat conditions; Improve juvenile rearing habitat conditions; Improve adult spawning habitat conditions; Improve ecosystem function for in-stream and floodplain habitats.
- Goal 2: Restore and enhance South Fork Trinity River geomorphic processes within the project reach; Increase in-channel complexity and floodplain connectivity; Increase pool frequency, residual depths, and resiliency; Increase hydraulic and hydro-geomorphic function; Increase stream bed topographic heterogeneity and sustainability.
- Goal 3: Restore and enhance South Fork Trinity River Water Quality within the Project Reach; Improve water quality conditions for Spring Run Chinook and SONCC Coho salmon; Increase the spatial and temporal cold water retention; Increase the quality of in-channel thermal refugia Areas; Increase groundwater hyporheic exchange zones.

Large wood is a critical element and driver for the interplay between ecosystem health, in-stream habitat complexity, and geomorphic processes in gravel bed rivers (Montgomery and Abbe. 2006). Strategic implementation of large wood arrangements can enhance thermal resiliency for salmon to migrate through and hold in the SFTR, as well as promote the habitat complexity required by juvenile salmon for successful rearing and emigration.

Process-based large wood loading of salmon streams has been shown to improve salmon rearing and salmon spawning habitats (Roni et al. 2014). In stream large wood provides a critical source of available cover that both rearing juvenile and adult salmon readily utilize to avoid predators. Research from Washington found juvenile Coho production increased in stream reaches where more complex wood structures were installed compared to simple log structures (Cederholm et al. 1997), and in off-channel habitats (Peterson and Reid 1984). Similar projects implemented in the Lower Klamath (Terwer Creek and Hunter Creek) have resulted in increased pool frequencies and volumes, instream habitat complexity, and development of off-channel habitats vital to juvenile survival. Large wood inputs into the stream channel provide morphological variability that causes sorting of sediments; finer sediments are aggraded in zones that promote riparian plant growth, medium sediments deposited in zones promoting spawning habitat for adult fish, and hydrologic scouring is promoted in zones deepening the stream channel to form pool habitat that is typically selected by rearing juvenile salmonids (McHenry et al. 2007). Instream large wood also promotes hydrologic variability and in turn provides velocity refugia for overwintering juvenile salmonids as well as groundwater down/upwelling leading to cooler and more oxygenated water.

Project Background: From the SFTR's headwaters in the Yolla Bolly Wilderness, it flows in a northerly direction for ninety-two miles before joining the mainstem Trinity River near Salyer in Trinity County. The SFTR basin, at 980 square miles, drains approximately 34% of the Trinity River watershed and 6% of the entire Klamath Basin. The SFTR provides suitable habitat for Upper Klamath Trinity River (UKTR) spring- and fall-run Chinook salmon, summer- and winter-run Klamath Mountain Province (KMP) Steelhead trout, and pacific lamprey (Borok and Jong. 1997). Activities such as timber harvest, road construction, mining, fire suppression, and stream diversion have modified streamflow and natural erosion processes and altered stream channels in the river basin. Forest fires, flood events, and climate change have further exacerbated these activities. This has resulted in severely degraded aquatic habitat in the form of impaired water quality, altered sediment supply, and altered hydrologic function within the entire SFTR basin (Chilcote et al. 2013).

Declines in both spring Chinook and Coho salmon in the SFTR have been attributed to both natural and anthropogenic disturbances as indicated above. In 1964, LaFaunce estimated that 11,604 adult spring chinook salmon were holding in the SFTR (CDFG, 1967) while over the past decade the run size has averaged approximately 200 fish (SFTR Spring Chinook Subgroup, TRRP, Fish Work Group, 2013). It was estimated that 127 adult Coho individuals entered the SFTR in 1985 and only 99 adults returned in 1990 using in-stream weirs to trap and count migrating fish (Jong and Mills, 1992). Recent efforts to document the presence of Coho salmon in the SFTR watershed has focused on summer surveys in historically utilized mainstem reaches and tributaries. The last record of juvenile Coho salmon in the SFTR watershed was 2009 in lower Corral and Eltapom Creeks. Coho salmon within the SFTR are included in the Southern Oregon Northern California Coast (SONCC) Evolutionary Significant Unit (ESU) and have been federally listed as threatened under the Endangered Species Act since 1997. Similar efforts to obtain ESA protected status for spring-run Chinook salmon within the Upper Klamath and Trinity Rivers (which includes the SFTR) is currently under review by the National Marine Fisheries Service.

The project was a collaborative effort by several federal and state agencies including: US Forest Service (USFS), National Oceanic and Atmospheric Administration (NOAA), National Marine Fisheries Service (NMFS), US Army Corps of Engineer (USACE), and California Department of Fish and Wildlife and California State Water Resources Control Board. The project was funded through the North Coast Resources Partnership Proposition 84 Grant and the Bureau of Reclamation - Trinity River Restoration Program (TRRP) Watershed Grant

Project Location: The project area is located on the SFTR, approximately 4 miles upstream of the town of Hyampom, in Trinity County, California. The downstream boundary of the project is Lat.: 40.581055°, Long.: -123.440665° while the upstream boundary of the project is Lat.: 40.581055°, Long.: -123.440665°. The project is within Sections 1, 11-14, and 24 in Township 02N, Range 06E Humboldt Meridian. The project occurs on a combination of private and federally managed lands. This includes six private parcels owned by four separate private landowners and six public parcels managed by solely by the USDA Forest Service, Shasta-Trinity National Forest The project is at approximately 1,500 feet in elevation. Figure 1 below shows the map of the project area.

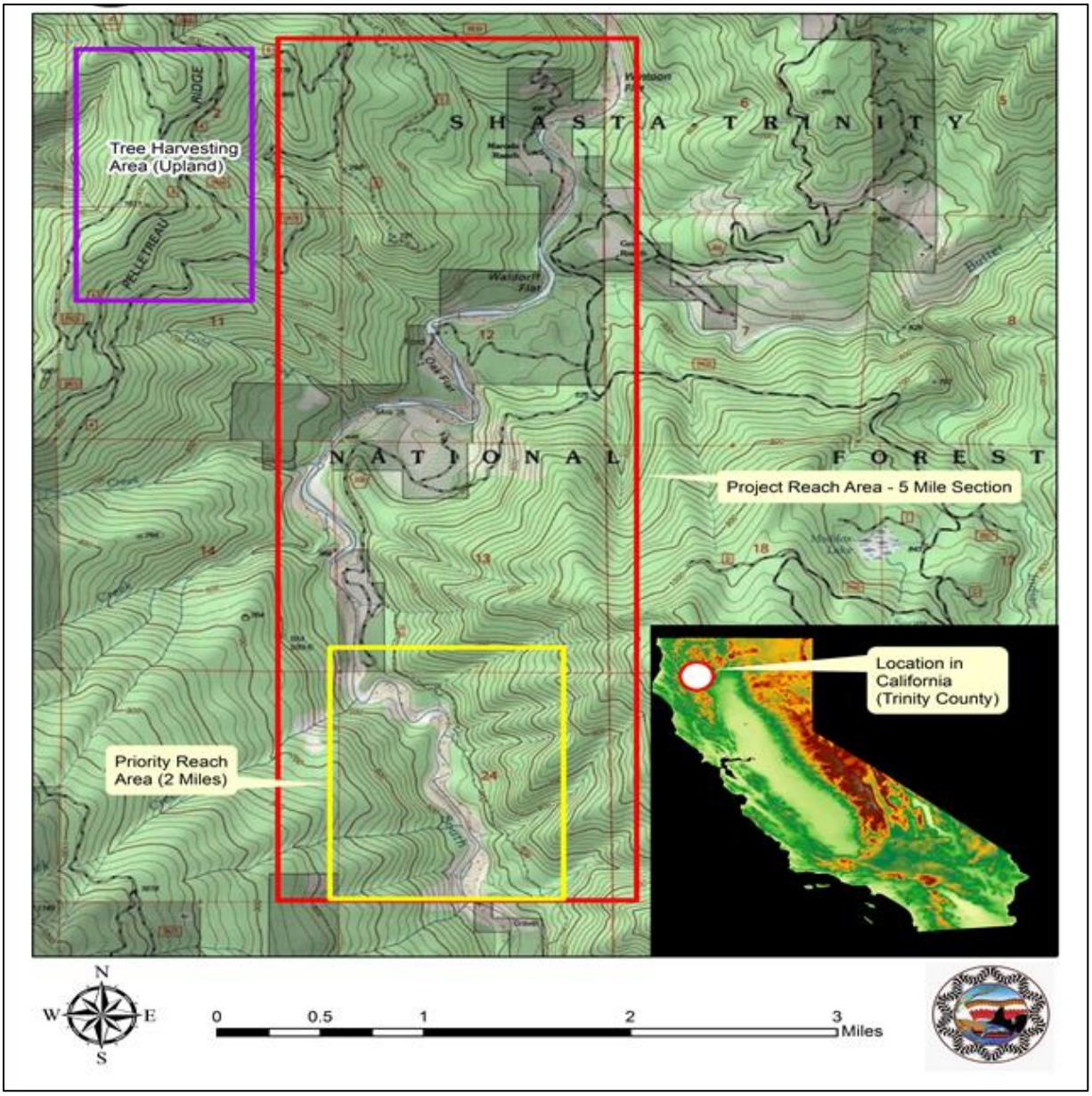

Figure 1. Map of the South Fork Trinity River Showing the Total Project Reach vs. the Priority Reach

Project Description: A total of 309 whole trees, with canopy and root structures were placed at 57 locations along a 5-mile long reach. Over 70% of the trees were placed within the upstream 2 mile section of the project, referred to as the Priority Reach (Figure 1). The trees were sourced and staged on private timber property owned by Trinity Timberlands LLC., under an emergency timber operations permit due to 2015 wildfire damage. The whole tree source area is located approximately one mile upslope of the downstream end of the project boundary (Figure 1). Whole trees were harvested and staged during the months of July and August 2018 using tracked excavator and dozer equipment. The majority of trees harvested were Douglas Fir, a small number of them included Tan Oak, Madrone and Ponderosa Pine.

Tree placement flight operations were conducted during the week of September 24, 2018 by Columbia Helicopters and included three days of implementation. Whole trees were transported from the upland staging area and set in place using a Columbia model 234 Chinook CH-47D helicopter. The helicopter flew to predetermined locations in the Project Reach and set the trees in strategic design arrangements based on field direction of onsite design team (Figure 2 – left). Trees placements were designed using a combination of field and modeling tools to determine the best locations for each structure.

Two types of tree placements were used in the project; 1) Habitat Structures and 2) Geomorphic Structures. Habitat structures were defined as simple arrangements to promote juvenile rearing and adult holding habitat. Geomorphic structures were defined as aggregate (complex wood jams) to interact with the rivers hydraulics to promote natural geomorphic evolution processes. Typical arrangements for this project entailed anchoring the rootwad end of the tree on the bank next to a suitable anchor point such as between large boulders or existing live trees. For whole tree aggregate, which have multiple trees at a single site, trees were placed in architectural arrangement to increase the longevity of promote natural river processes. (Figure 2 – right)

Figure 2. Example Photos showing Chinook Helicopter Flight and Large Wood Geomorphic Structure Placement

Baseline Data Collection

Overview

Physical and biologic monitoring was conducted prior to project implementation and will continue to be monitored over time after project implementation to determine project effectiveness. Pre-construction monitoring using Columbia Habitat Monitoring Program (CHaMP) methodology was used to develop baseline physical and biological indices. Monitoring has included repeated aerial photo collection, development of Digital Terrain Models, cross-sectional surveys, long profile thalweg surveys, channel unit habitat mapping, snorkel surveys, temperature monitoring, and benthic macroinvertebrate sampling.

Aerial Drone Mapping: Remote piloted Unmanned Aerial Systems (UAS) or drones were used extensively to collect key baseline photography and GPS information that was used to create high-resolution aerial imagery for aid in the planning, design, and monitoring process. The entire 5 mile reach was photographed at an altitude of 400 feet above river level using an average of 70% overlap. A total of 53 Control points were established as "X" locations painted on open areas along the river and referenced into high precision horizontal and vertical (XYZ) control using Northing, Easting, and Elevation from the RTK-GPS equipment. Approximately 3500 photos were taken across the 5 mile reach and integrated into Structure for Motion (SfM) software called AgiSoft. Through high resolution photogrammetry workflow, various algorithms produce a dense point cloud that is used to build a Digital Terrain Model (DTM) and georeferenced aerial image.

Physical Surveys: Topographic surveys were conducted in strategic locations using a combination of survey grade and mapping precision GPS instruments to collect baseline physical data within the Priority Reach (the furthest upper-stream 2-mile reach of the project). Prior to implementation, 3-D topographic surveys of the channel profile within the Project Reach were performed. Permanent cross sections and thalweg profiles were established in the area by the US Forest Service (USFS) in 1998. We reoccupied the USFS's cross sections where possible and thalweg surveys and also established new cross sections to document pre-project geomorphic conditions and to help document changes over time. Survey Grade Trimble R10 Global Navigation Satellite System (GNSS) - Real-Time Kinematic (RTK) - Global Positioning System (GPS) Equipment, commonly referred to as RTK-GPS. All surveys conducted on the site were performed using a consistent coordinate system, the North American Datum (NAD – 83 US Foot) State Plane, California Zone 1. A total of nine cross-sections pre-project were surveyed across the river channel and floodplain area within this reach. The cross-sections were established with monuments on each side of the river using rebar and caps. Topography points including ground shots, rebar monuments, bathymetric riverbed, water surface, and other features were collected per cross-section at key locations near the designed large wood structures. The cross-sections will be re-occupied and repeated to determine the amount of physical change and topographic evolution that has occurred. Figure 3 below shows an example cross-section surveyed in August of 2018 prior to the implementation of the project.

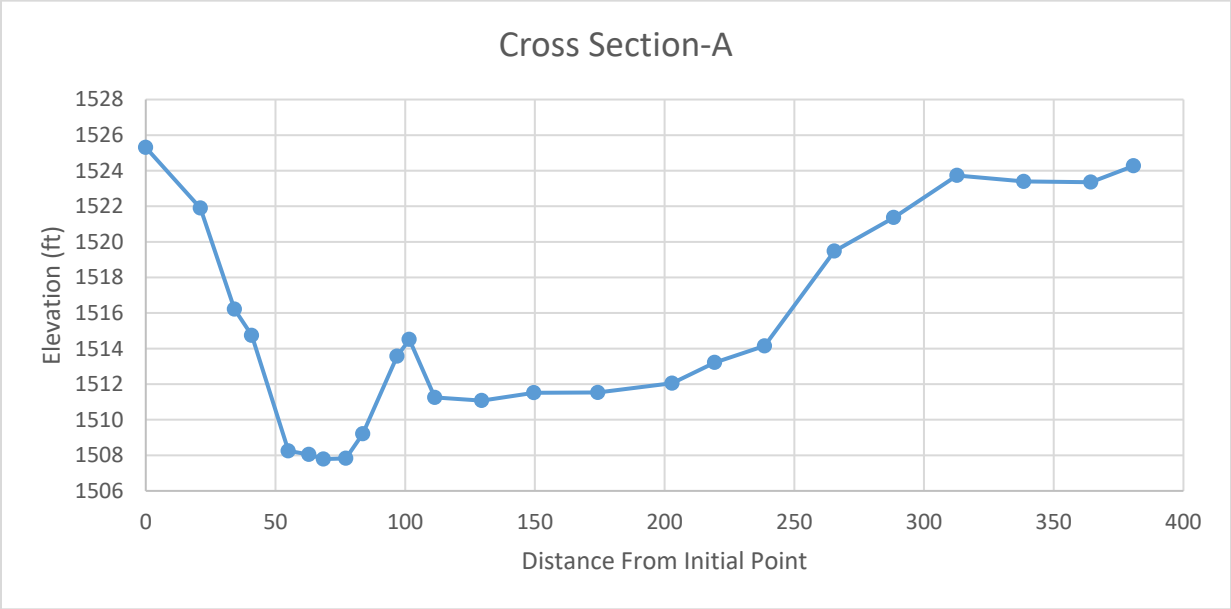

Figure 3. Example Topographic Cross-Section Survey within the Priority Rach

A long profile thalweg survey was conducted pre-project within the priority reach to document the deepest part of the river along the flow path. Measurements of the water surface and the depth of the river were taken using RTK-GPS along thalweg grade breaks to map the changing depths of the channel. Depth measurements were taken using a survey stadia rod by in-river divers due to the depth and flow of the river. Some examples of where thalweg points are measured are the tops and bottoms of riffles and rapids and the different depths of a pool. Thalweg mapping was supplemented with mapping the wetted edges of the channel by using a Trimble Pro Series Receiver 6H #98850 and TruPulse 360 R laser rangefinder to measure the horizontal distance to the wetted edge. The survey data collected was analyzed, plotted, and graphed. Figure 4 below shows the thalweg profile survey across the 2-mile priority reach. The total vertical drop is 40 feet (Elevation 1510 to 1470) across the 10,500 feet river length. The channel grade of this section of river is approximately 0.3% slope. The thalweg profile mapping will be repeated to monitor and document the topographic evolution over time based on the hydraulic forces acting on the large wood elements.

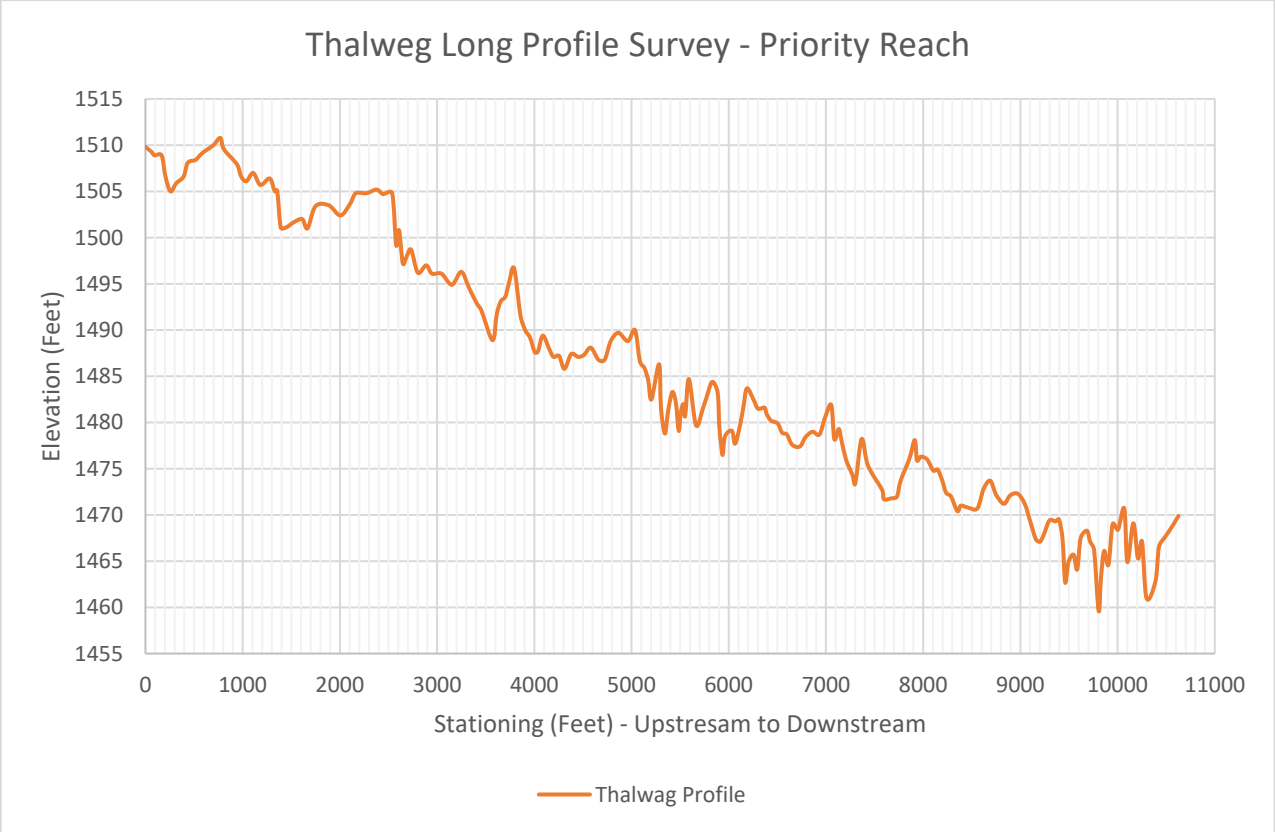

Figure 4. Thalweg Profile of the South Fork Trinity River – Priority Reach

Photographic monitoring:

There were four photographic monitoring points from geo-referenced and flagged or tagged locations were established prior to implementation to further document baseline and post-project habitat conditions. Photographs will be obtained throughout the project's duration and at various flow levels to improve our ability to assess the effectiveness of the project.

Biological Surveys:

Direct Observation Method: Both the juvenile and adult salmonid surveys will follow protocols defined in the publication "Underwater Methods for Study of Salmonids in the Intermountain West" (https://www.fs.fed.us/rm/pubs_int/int_gtr307.pdf). Minor deviations to the protocol will be made in order to better understand if performance standards are being met at the reach scale as well as to better understand habitat preferences of salmonids at the microhabitat scale.

Biological monitoring through direct observation techniques was conducted to determine juvenile fish habitat use and relative abundance within the Project Reach during the summer of 2018. Direct observation surveys for adult salmonids in the Project Reach was conducted during the annual interagency SFTR summer snorkel survey effort which occurred in late August of 2017 and 2018. This particular SFTR survey has been performed annually since 1978, and can provide a historical reference to base reach scale response. These surveys will occur separately but within the same period as the juvenile fish surveys.

Water Temperature:
Water temperatures have be monitored above, within, and downstream of the Project Reach using deployable continuous recording water temperature sensors (OnSet HOBO water temperature Pro V2 data logger). Water temperature data has been collected the summer prior to implementation, during implementation, and for three continuous years following project implementation. The temperature sensors will be checked, deployed, and maintained by following the US EPA recommended best practices (U.S. Environmental Protection Agency 2014). In addition to continuous monitoring via deployable sensors, we also intend to perform post-implementation aerial drone overflights with a thermal imaging sensor to record the precise location and extent of critical thermal refugia areas.

CHaMP:
This protocol was developed by the Columbia Habitat Monitoring Program (CHaMP) and includes a complete set of data collection and analysis methods. It is a method of monitoring effectiveness of instream habitats. Methodologies employed in the project reach include; Channel Unit Classification, Estimating Instream Juvenile Salmonid Abundance Using Snorkeling, Measuring Large Woody Debris, Channel Unit Substrate Composition, and Thalweg Profile,. A suite of analysis were performed as outlined in the protocol.

Benthic macroinvertebrate (BMI) collection and analysis:
Macroinvertebrates were collected on 7/7/2018 and 8/18/2018 and using Surface Water Ambient Monitoring Program (SWAMP) by certified SWAMP specialist Carrieanne Lopez of the Regional Water Quality Control Board. Jon Lee Consulting, an original member of the California Aquatic Macroinvertebrate Laboratory network (CAMLnet) and an active member of CAMLnet's current morph, SAFIT, analyzed samples. Jon Lee Consulting analyzed the 2018 BMI samples to a 500-count subsample, SAFIT Taxonomic Level 1a, metric and IBI calculation.

Environmental Compliance

Overview

Throughout a two-year period, environmental analysis was conducted to meet compliance requirements with several state and federal agencies in order to implement the project. Environmental consultation was coordinated with the National Oceanic Atmospheric Administration (NOAA), US Forest Service (USFS), US Army Corps of Engineers (ACOE), CA Department of Fish and Wildlife (CDFW), CA Department of Forestry and Fire Protection (CAL FIRE), and CA State Water Resources Control Board (SWRCB). Below is a summary of the environmental permit process for the project.

USFS, ESA Section 7 Compliance: Applied for project inclusion under the NOAA Arcata Restoration Center Biological Opinion (BO) in May 2017. Project accepted for inclusion and granted BO coverage in June 2017. Project modifications in January 2018 included adding SFTR stream segments on USFS managed land. A revised application was submitted to NOAA Fisheries to include these USFS lands and extend BO coverage to this agency in March 2018. The revised application was approved in April 2018.

USFS, Wild and Scenic Rivers (WSR) Act - Section 7(a) Analysis : This requires the river-administering agency to evaluate the effects of a federally assisted water resources project proposed within a WSR corridor on the river's free-flowing condition, water quality and an individual river's designated Outstandingly Remarkable Values (ORVs). Congressional intent was for the rivers included in the National System be managed to as near natural state as reasonably possible; eliminating activities such as rip-rapping stream banks, channelization, construction of dams and other facilities, or other activities which may alter the natural appearance and function of the river. The USFS therefore, as the river administering agency, has the responsibility to determine whether the proposed project would have a direct and adverse effect on the river's free-flowing condition, water quality, and the SFTRs ORVs. A WSR Section 7(a) analysis was completed in August 2018 that showed the Project would not have a "direct and adverse" effect on any of these criteria. On September 13, 2018, the USFS Region 5 Forester, Randy Moore, issued a formal determination stating as much and allowed the Project to proceed.

ACOE, Nationwide 27 Permit: This permit provides Federal Section 10 Rivers and Harbors Act and Section 404 Clean Water Act (CWA) permit coverage. The project application was originally submitted in April 2017. An amendment package was submitted in April 2018 to; include USFS lands within the project area and remove the cable yarding/accelerated recruitment method from the project description. Permit issued in June 2018.

State Water Resources Control Board, General 401 Water Quality Certification for Small Habitat Restoration Projects (SHRP): A Notice of Intent (NOI) was submitted to the SWRCB in June 2018 in order to comply with the terms of, and obtain coverage under, the General 401 Order for the Project. As the project size is less than 5 acres and 500 feet of linear disturbance it therefore qualifies for a CEQA Categorical Exemption 15333. The North Coast Regional Water quality Control Board issued a Notice of Applicability (NOA) on July 23, 2018 for coverage under the State Water Resources Control Board General 401 Water Quality Certification for the Project (WDID: 1A170535WNTR, CW-835381)

CaDFW, Habitat Restoration and Enhancement Act (HREA) Project Approval: State level approval authority that provides California Endangered Species Act (CESA) and 1600 Lake and Streambed Alteration Agreement (LSAA) project coverage. HRE Act project approval is linked to the SWRCB 401 SHRP permit. Directly following project 401 certification from the SWRCB in July, a Section 1653 application was submitted to the CaDFW. On September 6, 2018, the CDFW determined that the NOA, NOI and related species protection measures were consistent with HREA as the Project meets the conditions set forth in Fish and Game Code 1653 for authorizing the Project (Consistency Determination No. 1653-2018-024-001-R1).

Design Process

Overview

The project was designed over a two-year period using various in-field and remote sensing analysis techniques to determine the best location for the placement of the large wood structures. A multi-disciplinary team to determine best locations for habitat and geomorphic placements and architectural arrangements completed field reconnaissance surveys. Low altitude aerial drone surveys were conducted across the 5-mile reach to map the pre-construction project area and to develop a topographic digital terrain model (DTM) using Structure for Motion (SfM) workflow process. Additional analyses were conducted including hydraulic modeling, stability calculations, and risk assessment to evaluate the design parameters of each of the wood structures. Throughout the design process, standard guidelines and scientific literature were followed based on the method and approach documented in the National Large Wood Manual (BOR and ERDC, 2016).

Field Design Surveys: A multi-disciplinary team made up of a fisheries scientist, civil engineer, and natural resource specialist performed detailed design surveys across various hydro periods to determine the highest priority locations of wood placements, a total of 57 wood structure locations were identified. The surveys were conducted using high precision RTK-GPS equipment to determine locations of each wood structure in relation to the rivers hydraulic patterns and existing riparian features. Wood structures were positioned to take advantage of the existing river features including: standing trees, boulders, tributary confluences, and other riparian elements along the river corridor.

Design Drawings: Field reconnaissance data and the detailed results from each of the design surveys were digitized into AutoCAD drawings. A detailed architectural design was developed in the field for each of the 57 wood placement locations, detailing the locations and quantity of each type of wood element including size, species, orientation, sequencing, anchor strategies, and overall design objective. GPS information was transferred into the AutoCAD Civil 3D environment and overlaid onto aerial drone photography. Various iterations of refinement were performed to insure that each structure was in the best location to insure that it would perform and function to promote the physical process. Two types of placements were designed for the project; 1) Habitat Structures and 2) Geomorphic Structures. Habitat structures were defined as placements to primarily promote juvenile rearing and adult holding and geomorphic structures were defined as arrangements that were used to interact with the rivers hydraulics to promote natural river processes and geomorphic evolution. Figure 5 below shows and example drawing sheet showing the design of the wood structures for both Habitat and Geomorphic structures.

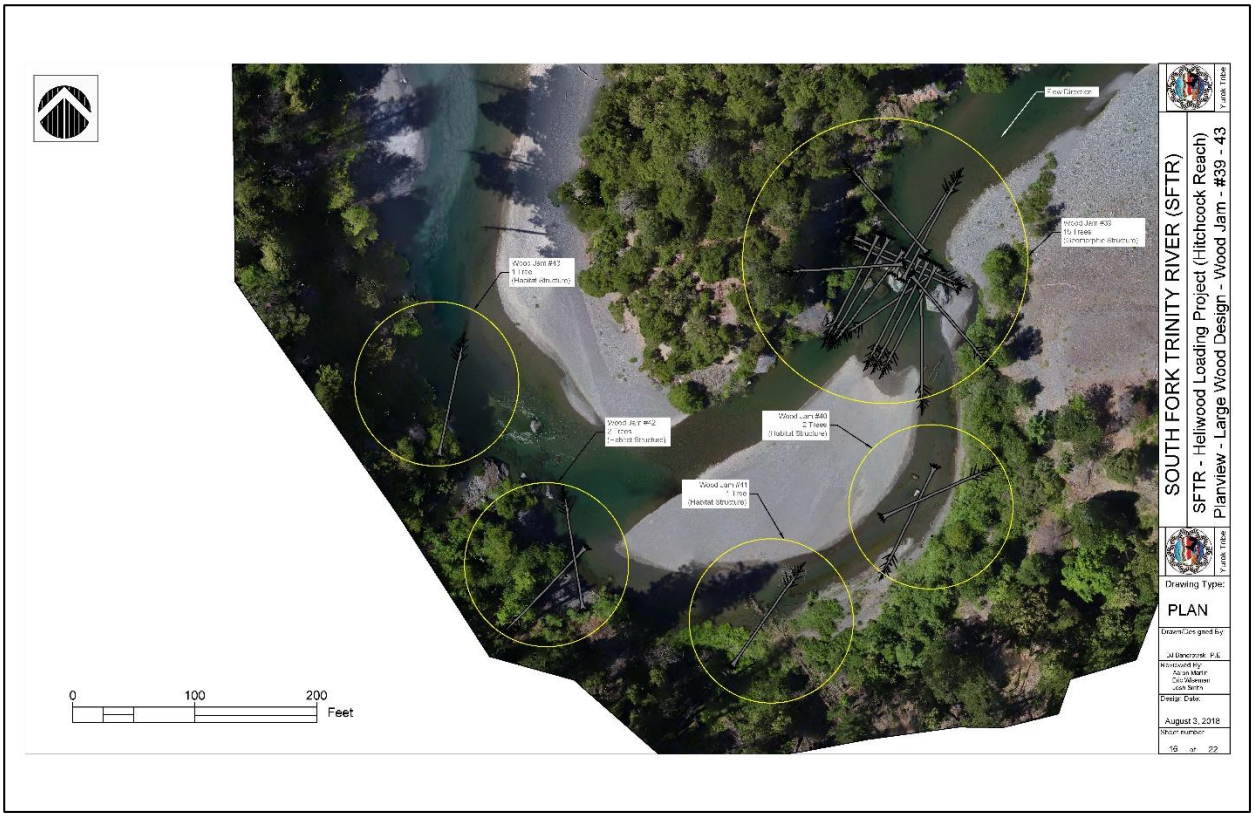

Figure 5. Example Design Drawing of both Habitat and Geomorphic Wood Structures

Modeling and Analysis: For the design of the project a preliminary set of analysis was performed to document the projects design intent. A pre and post construction 2D-hydraulic model was developed utilizing the aerial imagery and associated DTM. The model was constructed using SRH-2D and SMS workflow. Initial model was developed using a course mesh and calibrated to the low flow water surface condition that was visible in the aerial imagery and cross-referenced to the USGS gauge records. The approximate flow discharge during the aerial imagery flight was approximately 35-40 CSF which corresponded well with the initial model calibration results. The base flow model condition was refined to a densified mesh with a grid cell size of approximately 4ft. by 4ft. dimensions using Aquaveo SMS software version 12.3.4. Several higher discharge models were developed in the asbuilt terrain conditions using SRH-2D to evaluate velocity, water elevation, flow depth, surface inundation extents, and other hydraulic parameters. These results were used to calculate wetted cross-sectional area at a range of flows to determine hydraulic conditions acting at various design locations and structural patterns.

Figure 6 below shows example hydraulic model results from SRH-2D/SMS software output at 5,000 CFS within the priority reach at as-built terrain conditions. Flow is from right to left and from bottom to top of page. Velocity is shown as Feet per second (FPS).

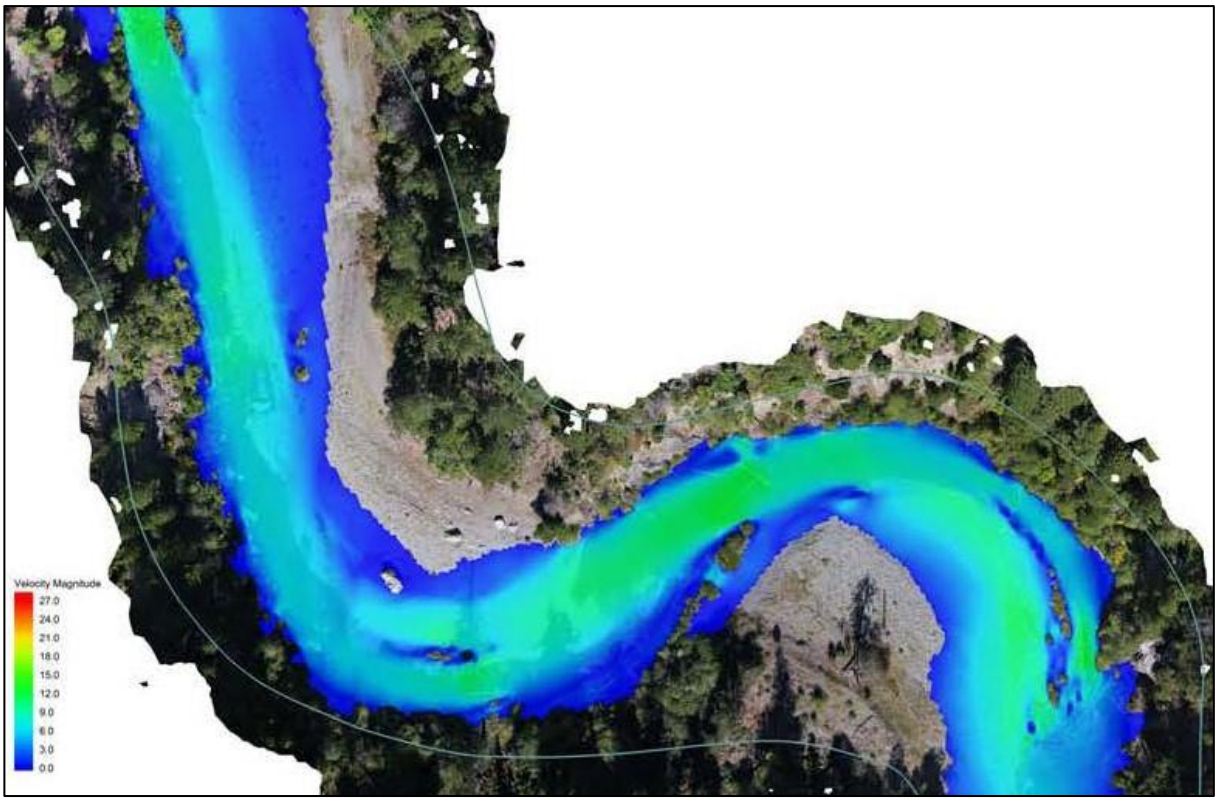

Figure 6. 2D Hydraulic Model Output on Asbuilt Conditions at 5,000 CFS

Hydraulic information from the 2D Hydraulic model was used to evaluate the stability of the design conditions at a combination of structure types at a range of flow conditions. The flow range and correspondent hydraulic parameters that was used for evaluation was from base flow condition at 35 cfs to approximately 10,000 cfs. Large wood design structure types evaluated ranged from simple 1 or 2 log habitat type placements to multi-tree geomorphic complex systems. Force-balance stability calculations for large wood structures are not advanced enough to determine exact stability but are often used to evaluate sensitivity at a range of flows rather than absolute values. Stability is evaluated based on a factor of safety determined by the type of project which is typically 1.5 to 2.0. Initial force-balance stability calculations were evaluated to determine at what flows the wood structures would become mobilized.

The stability evaluation method and associated calculations used were from the Computational Design Tool for Evaluating the Stability of Large Wood Structures Proposed for Stream Enhancement (Rafferty 2013). The spreadsheet looks at cross-sectional inputs at the project location, hydraulic information, wood dimensions/orientation/location and other factors to determine forces acting against each wood element. Initial calculations were performed on a sub-set of both habitat and geomorphic type structures. Simple single or double structure types habitat structures results showed that they were stable from base flow at 35 cfs to around 2,000 cfs. More complex multi-log structures that were pinned together in trees or behind boulders were stable between 35cfs and 5,000 cfs. Some of the structure types depending on anchoring techniques were stable to 10,000 cfs. All wood structures were anchored using natural techniques including woven into existing trees, boulders, and dense vegetation with the riparian corridor. These type of natural ballasting and anchoring techniques are difficult to evaluate the exact counteracting forces against vertical and horizontal forces from the rivers hydraulics.

Although based on field observations and visual evaluation of natural conditions, wood elements can often be stable at conditions that calculations cannot predict. The results of the modeling has determined that after 10,000 cfs all types of structures will deform and become unstable. At this flow natural recruitment will begin the process of geomorphic evolution which is consistent with project goals and objectives. Figure 7 below shows the free body diagram of the forces that are acting on each wood element (Rafferty 2013).

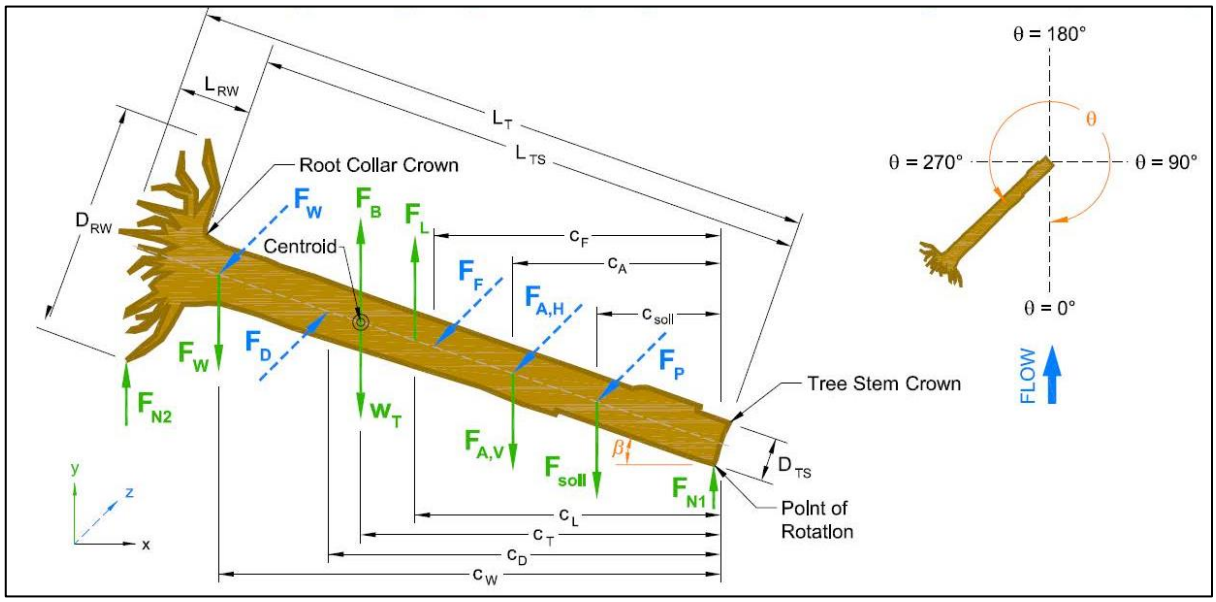

Figure 7. Typical Log/Rootwad Free Body Diagram with Forces

A detailed risk assessment was also performed for the site to evaluate project risk associated with wood mobility in relation to property, infrastructure, and public safety. The overall infrastructure and property risk of the project follows a method described by Bureau of Reclamation through a set of risk-based guidelines (Bureau of Reclamation, 2014). The method considers both the stream response potential (stream type, hydrologic regime, bank erosion and sour, etc.) and the infrastructure/property characteristics (in-stream and floodplain infrastructure, land use). The infrastructure and property risk scored "LOW" for the project. The public safety risk for each designed large wood structure was assessed using the Risk Matrix method that considers both recreational use characteristics (frequency of use, skill level, access, etc.) and the structure characteristics (channel type, structure location, egress potential, sight distance, etc.). The public risk score is "LOW" for all large wood structures. Public risk is further mitigated by limiting construction to natural materials (wood and sediment) and specifically avoiding use of artificial fasteners (cables, bolts, and anchors). Artificial fasteners are often used to increase the short-term stability of large wood structures but pose a significant public safety risk in the long term. Artificial fasteners create a dangerous tangle of cables and sharp points as the large wood structure slowly degrade and become mobile. Figure 8 below shows the results of the risk analysis for property and infrastructure characteristics.

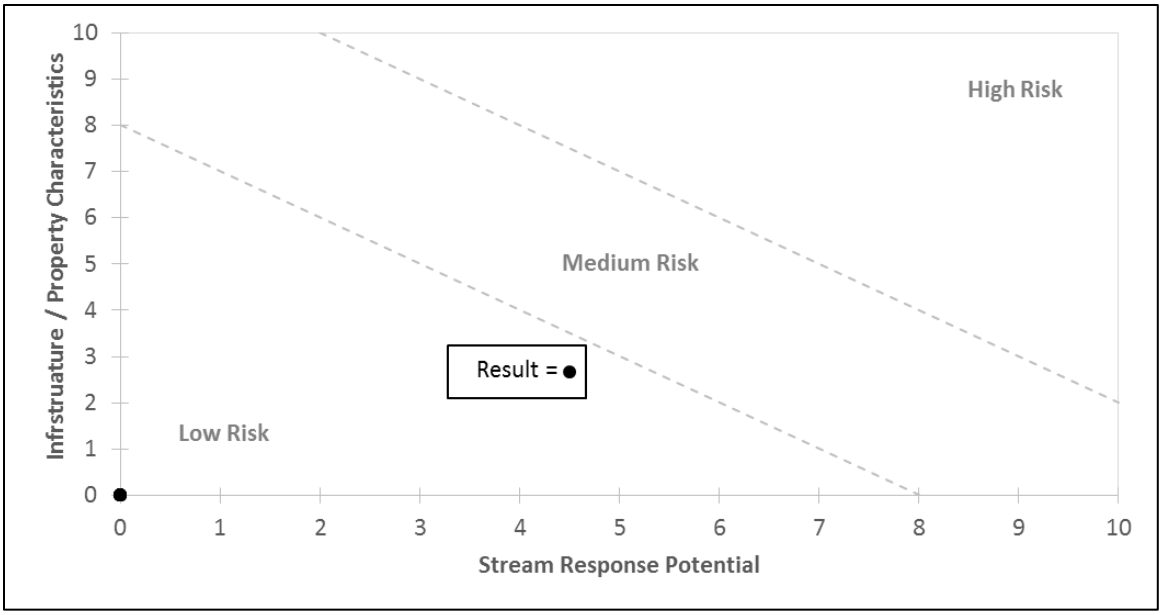

Figure 8. Risk Assessment Matrix Results for Property and Infrastrucutre

Implementation

Overview

Implementation activities including two phases; 1) whole tree harvesting in the upland area; and 2) helicopter placement of the harvested trees into the river. All implementation activities took place in July through October 2018. All operations were performed safely and free of any issues or incident. The project was constructed according to the design scope and within regulatory requirements. Below is a detailed summary of each phase describing the implementation activities.

Tree Harvesting: All the trees used on the project were harvested from an upland area just west of the project boundary on Pelletreau Ridge, approximately 1 mile from the downstream end of the project and 5 miles from the upstream end of the project. The harvesting location was on private lands owned by Trinity Timberlands LLC and was permitted under an emergency exemption due to forest fire damage from the 2015 "Johnson" wildfire. The State of California Department of Forestry and Fire Protection issued the emergency harvesting permit on 8-23-17 and was valid through 8-22-18. Harvesting operations began on July 2, 2018 as completed on August 8, 2018. Whole tree harvesting was performed using a tracked excavator in-order to remove the rootwad from the ground and keep the entire tree whole. A John Deere 2554 Forestry Excavator was used for the harvesting operations due to the reinforced cab to protect the operator from potential safety hazard of falling trees. In addition, a CAT D7R tracked dozer was used to support the harvesting operation by building temporary access roads, providing fire protection, and to assist the excavator with tree removal and transport. Heavy equipment operators from the Yurok Tribe executed all tree harvesting and decommissioning activities across an approximately 6-week period. Harvesting operations were coordinated with regulatory agencies, and operators worked closely with the Registered Professional Forester

(RPF), Licensed Timber Operator (LTO) and other support team to insure compliance and fire safety persuasions were achieved.

The RPF team did an excellent job of marking the units for a sustainable harvest and the LTO and Yurok Tribe's equipment operators did an exemplary job of minimizing impacts so in many ways the unit was left better than it was encountered.

All trees harvested were stockpiled and inventoried according to date, weight, length, diameter, and species. A specialized excavator mounted scale was used to measure the trees weight to determine appropriate lift capacity and limitations by the helicopter. After harvesting activities were completed, a ground crew developed a detailed map and inventory of the entire harvesting and stockpile area in preparation for the helicopter operations. Each tree was flagged according to a color categorization based on weight. Trees with a weight less than 10,000 were categorized white, between 10,000 and 15,000 blue, and greater than 15,000 were pink.

Tree Placement: All 309 trees were flown into place during three days of flight operations between September 25 and 27, 2018. A total of 20 hours of flight time was used across the three days of operations. The implementation team consisted of 15 crewmembers from Columbia Helicopters, 3 staff from the Yurok Tribe, and 3 staff members from the Watershed Research and Training Center (WRTC). Additional behind the scenes support was received from various partners including private landowners, and State/Federal regulatory agencies.

Columbia Helicopters mobilized to the project on Monday, September 24 and staged their equipment at the Hyampom Airport. Columbia operations team was broken into four groups; 1) flight crew (pilot/co-pilot); 2) in-river ground crew (4 laborers); and 3) upland ground crew (2 laborers and foreman); 4) ground support crew at the airport (mechanic and 6 additional support staff). Additional Columbia support included fuel truck, equipment trailer, job trailer, and two mechanic trucks.

The in-river ground crew consisted of two teams of four people. Each team was broken into two laborers from Columbia Helicopters paired with two technical staff from the Yurok Tribe and WRTC. The two teams divided the reach in half and were responsible for the final design details of each placement locations. Columbia's in-river ground team provided logistical, safety and communication support and between the helicopter pilot and the design team on the ground. The final design locations of each tree placement were determined real-time in the field according to on-site conditions and constraints based on flight logistics and operation limitations. The ground team used bright multi-color flagging to signal to the pilot the location and orientation of each tree placement. Each bright colored flagging was wrapped around a large rock that was used to weight the signaling flags (referred to as blobs) so that they did not blow away from the rotor wash. The helicopter pilot carried each tree using a 300-foot long-line that was connected to each tree using 5/8 inch choker cables. At the end of the long-line, a hooking mechanism controlled by the pilot would release the choker cable and tree as one unit at the location identified by the ground crews. The maximum operating weight of the Chinook Helicopter is 20,000 pounds including fuel, crew, and long-line load. Most trees placed were approximately 7 to 10,000 lbs. and therefore the helicopter often was able to place 2-3 trees per placement cycle.

Each placement cycle (turns) took on average 10 minutes, which included load time at the upland area, flight time to placement location, drop sequence of the trees, and return flight back

to upland staging area. Therefore, the helicopter was able to get in approximately 6 turns in per hour. The longest distance between the tree stockpile within the upland harvesting location and the priority reach was approximately4-5 miles flight distance. The flights turns were predominantly completed in this upper section, although some of the placements were near the stockpile location, which decreased flight time and increased efficiency of the turns.

The stockpile area was the location where each tree had to be secured by an individual 5/8 inch choker cable and manually hooked to the helicopter's long-line by the upland ground crew. This aspect of the operation had the most safety risk and having good communication between the pilot and the ground crew is critical.

Additional items: During a several month period following project implementation, ¾ inch natural fiber manila rope was used to bind approximately 10% of placed trees together, particularly geomorphic and habitat wood jams that we felt were slightly more unstable or prone to floating.

Whitewater kayaker safety outreach has been conducted including posting to online kayaker/rafter forums, outreach to local communities, sign posting at major hubs (Post Office, Restaurants, etc.) and outreach to key landowners up and downstream of the project.

A landowner specific outreach event was held in the nearby community of Hyampom during December of 2018. We met at the Hyampom Community Center and held a slideshow of the project. We discussed the reasons for the project, the methods and monitoring outlined in this report, and discussed the evolution of the project over time. Approximately 25 local landowners attended the event.

Post-construction Documentation: Once all the trees were placed, a four-week data collection effort was initiated to document each of the structures as-built architecture and detailed location and attributes. Several data collection methods were used to document these characteristics including: 1) post-construction aerial imagery flight; 2) physical marking tags placed on each of the wood elements; 3) Geo-referencing and attributing each wood element using GPS; 4) ground and oblique aerial photos of each wood structure. The following were attributes collected for each wood element including: Tag number identifiers, GPS Location (Northing/Easting), species, diameter (DBH), length, rootwad location, and log orientation.

Post-construction, low-altitude aerial drone flights were conducted across the full 5-mile project reach. Similar SfM workflow and methodology was used for the as-built flight as was for the design flight. Updated control points were used to geo-reference the project reach and were incorporated into the photogrammetry software (Agi-Soft Photoscan). Detailed high-resolution as-built Imagery and Digital Terrain Model was developed using SfM workflow. As-Built flight was conducted during low base flows of approximately 35 cfs.

Additional as-built design attributes were documented according to anticipated evolution characteristics for each of the structures. Field based assessments were conducted by the design team in October of 2018 to determine a ranking for the following attributes: structural stability, scour potential, mobility potential, and racking potential. Based on field assessment the design team determined which structures should be lashed using rope to add stability. All of this information was added to Geo-referenced shapefile of each wood element to develop a

comprehensive baseline tool for monitoring the project evolutionary response. Based on the post construction data collection, as-built design documentation was developed to determine baseline conditions for future monitoring and analysis. As-built designs were developed using AutoCAD software with data integration from post-construction aerial photography and field GPS data. As-built plan set and associated GIS shapefiles was developed for each of the 57 wood structures to document the final architectural arrangements. 2D-Hydraulic models and force-balance calculations were also re-developed for the as-built conditions to document structural stability and evolution potential. SRH-2D and SMS modeling software and workflow was used to perform the hydraulic modeling based on as-built DTM. The hydraulic models were developed primarily to evaluate post-construction velocity results at various flows to inform stability calculations. The results of the modeling and calculations performed indicate that the wood structures are semi-stable at discharges between 2,000 to 5,000 cfs but show that all wood structures will deform and become be entrained at higher discharges above the 10,000 cfs threshold. This documented wood mobility is designed to drive fluvial processes and allow for long-term geomorphic evolution to promote key physical and biological response. Figure 9 below is a pre and post implementation aerial imagery documenting the comparison before and after the wood placements within the Project Reach.

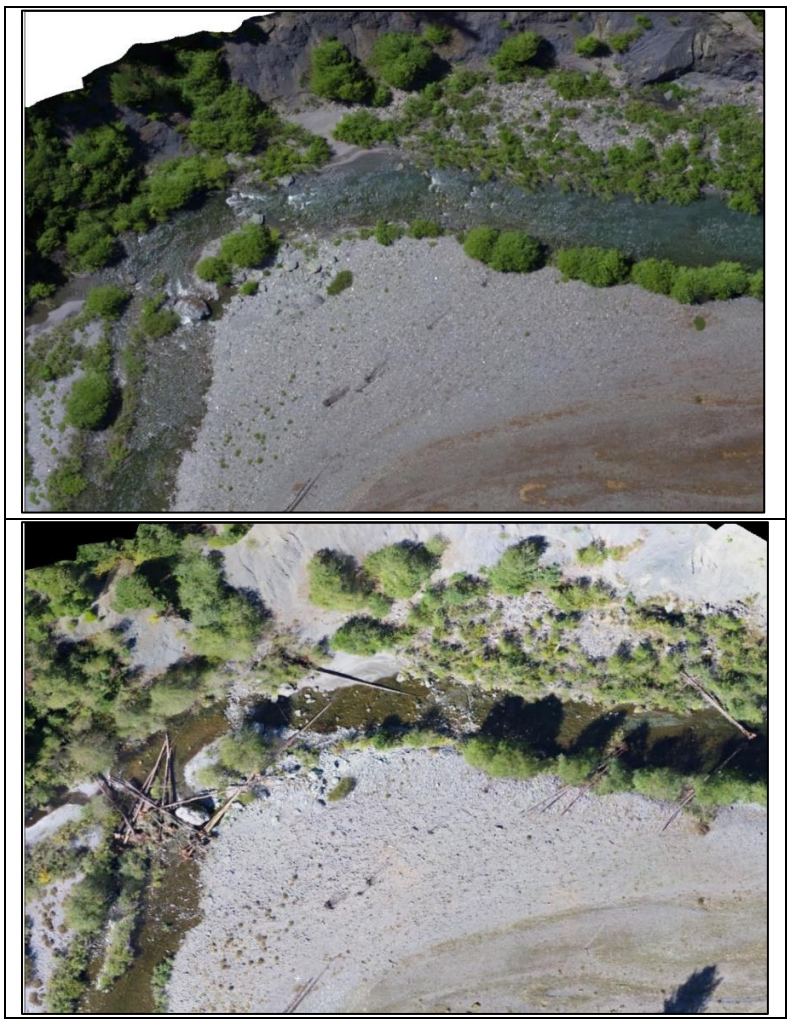

Figure 9. Aerial Imagery Comparison between Pre and Post Project Implementation

References

Borok, Sara L. and Jong, Howard W. (1997) *Evaluation of salmon and steelhead spawning habitat quality in the South Fork Trinity River Basin, 1997.* Sacramento, CA, California Department of Fish and Game, (Inland Fisheries Division Administrative Report, 97-8)

Bureau of Reclamation, M. Knutson and J. Fealko, 2014. Large Woody Materials Risk Based Guidelines. Pg. 14-25.

Bureau of Reclamation and U.S. Army Engineer Research and Development Center (USBR and ERDC), 2016. National Large Wood Manual: Assessment, Planning, Design, and Maintenance of Large Wood in Fluvial Ecosystems: Restoring Process, Function, and Structure.

Chinook, S.F.T.R.S. and Chilcote, S., 2013. Spring Chinook in the South Fork Trinity River: recommended management actions and the status of their implementation.

McHenry, M., Pess, G., Abbe, T., Coe, H., Goldsmith, J., Liermann, M., McCoy, R., Morley, S. and Peters, R., 2007. The physical and biological effects of engineered logjams (ELJs) in the Elwha River, Washington. *Report to Salmon Recovery Funding Board and Interagency Committee for Outdoor Recreation, Port Angeles, WA*, p.82.

Montgomery, D.R. and Abbe, T.B., 2006. Influence of logjam-formed hard points on the formation of valley-bottom landforms in an old-growth forest valley, Queets River, Washington, USA. *Quaternary Research*, *65*(1), pp.147-155.

Rafferty, M., 2013. Development of a Computational Design Tool for Evaluating the Stability of Large Wood Structures Proposed for Stream Enhancement. Masters of Science Thesis, Colorado State University.

Roni, P., Beechie, T., Pess, G. and Hanson, K., 2014. Wood placement in river restoration: fact, fiction, and future direction. *Canadian Journal of Fisheries and Aquatic Sciences*, *72*(3), pp.466-478.

Stage Zero Stream Restoration in California

Jared McKee, **Hydrologist**, USFWS, Elk Grove, CA, (jared_mckee@fws.gov)
Damion Ciotti, USFWS, Auburn, CA, (damion_ciotti@fws.gov)

Introduction

Project Description

The U.S. Fish and Wildlife Service (Service) in partnership with Placer Land Trust (PLT) started a stream and floodplain restoration project along Doty Ravine Creek in 2014. The goals of the project involved shifting the reach from an incised single thread reach with threshold/erosional instream processes to a Stage 0 reach with active depositional processes instream and across the floodplain (Cluer and Thorne 2013).

The 1-mile reach and 50 acre floodplain is part of the habitat preserve and rangeland owned and managed by PLT. Doty Creek is in the Feather River watershed and is critical habitat for steelhead.

Design

Design Criteria

Site design was guided by newly developed and broadly applicable general criteria based on existing ecological standards and process based principles for fluvial restoration (Beechie et al., 2010; Palmer et al., 2005). These criteria assure restoration actions and design are ongoing, adaptive, aimed at increasing space for fluvial action and restoring sediment and stream (dis)connectivity (Ward et al., 2002; Wohl et al., 2018). These criteria are presented and discussed as general tools for any fluvial restoration project that seeks to pursue process-based ecological restoration at a landscape scale and in a cost and time effective way.

Implementation

Adapting Management and Infrastructure

While the project area remains in active grazing for 2 months a year, limiting livestock access allowed for the development of a robust riparian area throughout the floodplain. Levee removal increased floodplain connectivity and increased instream deposition. Cessation of lethal beaver removal encouraged instream deposition and accelerated floodplain connectivity.

Instream Actions

Instream restoration investments by the Service for Doty Ravine are relatively low (less than $10,000) and include hand placed wood jams, beaver dam support structures, and beaver dam analogues (Pollock et al., 2014).

Conclusion

Results

In three years, approximately 30 acres of floodplain evolved from a single thread channel dominated by oak and grassland to a permanently flooded Stage 0 condition with highly complex stream and wetland morphology. Cost of habitat restoration through bio-geomorphic process was an order of magnitude lower when compared to a traditional construction-based stream restoration. The result is a fully connected floodplain with multiple flowpaths, heterogeneous water depth and velocities, and dynamic full gradient wetland throughout the year providing multi-species benefits and ecosystem services.

Tracking the habitat creation by bio-geomorphic process with the help of streamflow estimates and site surveys helps guide adaptive management and design and communicate actions, costs and outcomes to stakeholders (Figure 1).

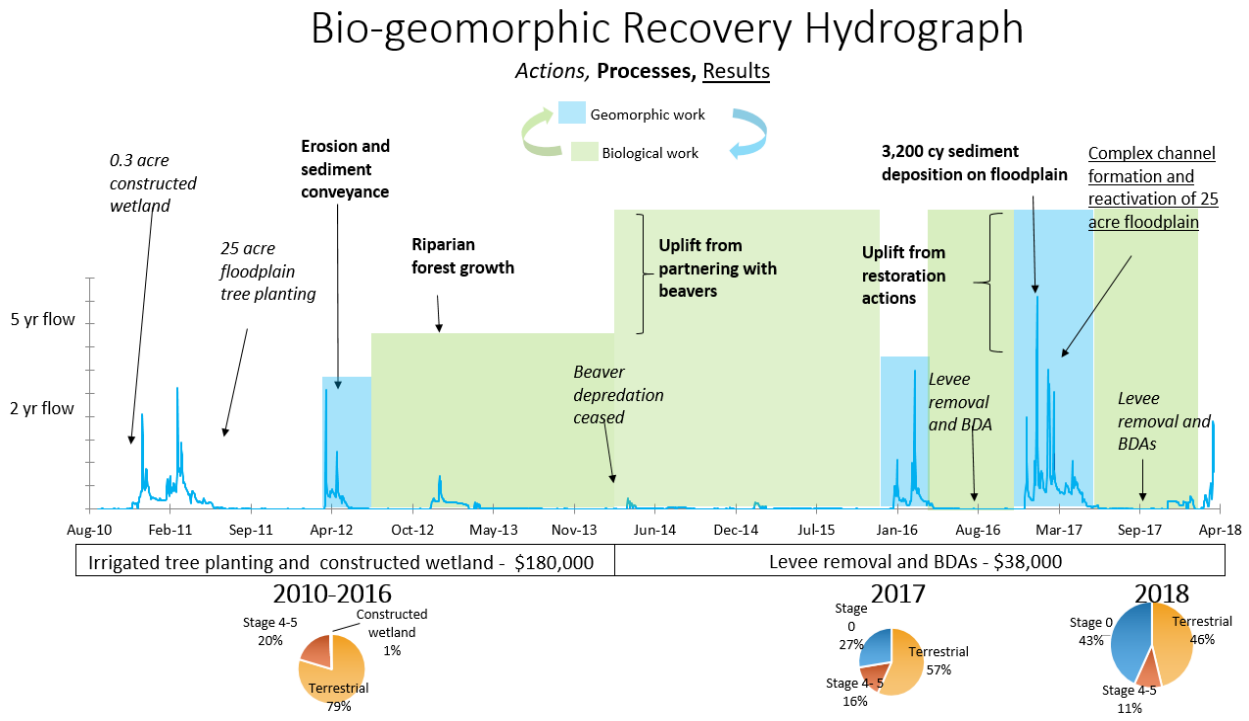

Figure 1. Bio-geomorphic process based recovery tracking with hydrograph

Discussion

The project provides the Service and PLT with an ideal demonstration of maximum stream restoration with minimum intervention. Basic habitat indicators such as channel length increased by a magnitude. The project does not involve stream channel reconstruction beyond the use of hand placed wood jams intended to nudge inherent process to create more beneficial habitat and satisfy stream and floodplain form objectives. The livestock continue to access the project for an average of 2 months a year with no apparent deleterious effects on habitat.

References

Beechie TJ, Sear DA, Olden JD, Pess GR, Buffington JM, Moir H, Roni P, Pollock MM. 2010. Process-based principles for restoring river ecosystems. BioScience 60: 209–222.

Cluer B, Thorne C. A stream evolution model integrating habitat and ecosystem benefits. River Research and Applications. 2014 Feb 1;30(2):135-54.

Palmer MA, et al. 2005. Standards for Ecologically Successful River Restoration. Journal of Applied Ecology 42-2: 209–217.

Pollock, M. M., T. J. Beechie, J. M. Wheaton, C. E. Jordan, N. Bouwes, N. Weber, and C. Volk. 2014. Using Beaver Dams to Restore Incised Stream Ecosystems. Bioscience 64:279-290.

Wohl, E.; Brierley, G.; Cadol, D.; Coulthard, T.J.; Covino, T.; Fryirs, K.A.; Grant, G.; Hilton, R.G.; Lane, S.N.; Magilligan, F.J.; et al. Connectivity as an emergent property of geomorphic systems. Earth Surf. Process. Landf. 2018.

Ward JV, Tockner K, Arscott DB, Claret C. Riverine landscape diversity. Freshwater Biology. 2002 Apr 1;47(4):517-39.

Partnering with Nature's River Restorers for Sustainable River Management

C. R. Thorne, Chair of Physical Geography, University of Nottingham, UK
colin.thorne@nottingham.ac.uk
M. F. Johnson, Assoc. Professor, School of Geography, University of Nottingham, UK
J. M. Castro, Project Leader, US Fish and Wildlife Service, Vancouver WA

Extended Abstract

River management based entirely on physics-based science has proven to be unsustainable, evidenced by the fact that the problems river management is intended to solve (e.g. flood hazards, poor water quality, channel instability) have patently not been solved, while long-term deterioration in aquatic environments continues to reduce the capacity of rivers to go on meeting the expanding needs of society (Gilvear et al. 2016). In response to this emerging truth there has, over the past two decades, been a shift in river management towards restoration. However, at least to date, ecological, morphological and societal benefits achieved using this approach have been underwhelming (Palmer et al. 2014). We believe this is because restoration over-relies on the same physics-based science as past management; focusing on analysis of the power of flowing water in relation to the resistance offered by channel boundary sediments and attempting to design stable, alluvial channels.

This form of analysis has long been characterised by Lane's Balance (Lane 1956), a visual representation of how imbalance between stream power and sediment load leads to aggradation or degradation. It is now possible to solve the governing equations of water flow and sediment transport in multiple dimensions and over long reaches and periods, yet the focus of physics-based analyses remains in-bank flows along single-thread channels with straight or meandering planforms. This despite the fact that we now know meandering streams with bankfull discharge return periods of 1.5 or 2 years were not prevalent prior to human modification of natural streams and are, in fact, often the legacy of historical, anthropogenic river engineering for hydro-power, flood control or land drainage (Walter and Merritts, 2008). In light of this revelation, innovative restoration approaches are challenging the orthodoxy that single-thread, meandering channels necessarily constitute the best 'target' morphology (Cluer & Thorne, 2014). Practitioners propose instead that rivers with functional floodplains and adequate sediment supplies are better served by restoration of multi-channel, anastomosed planforms that better represent pre-disturbance forms and are fully-connected to the surrounding, wetland-floodplain systems (Powers et al. 2018).

If future river management and restoration is to reverse long-standing declines in river functions, it is necessary to re-envisage what it means to design a channel, focusing less on balancing water and sediment flows and more on situating channels within complex channel-wetland-floodplain corridors that support balanced and healthy biomes. We define this as *Biomic River Restoration*. Our new vision of a biomic river can be illustrated by amending Lane's Balance to acknowledge and incorporate the influence of life in the river on the balance between aggradation and degradation (Figure 1).

Biomic restoration recognises that biological processes interact with alluvial processes, with direct consequences for both the physical form of the river and its response to disturbance. Organisms work constantly to improve their own life chances and those of their species (Darwin, 1859). This endows disturbed natural fluvial systems with a self-healing capacity, driven by successional processes that follow a major disturbance to facilitate ecological recovery that, in turn, promotes physical recovery to a new, dynamically meta-stable state (Castro and Thorne, in press). It is vital that the rivers we manage and restore are resilient in

an increasingly uncertain future. This requires restoration outcomes that are adaptable not only to changes in the flow and sediment regimes, but also to changes in local, catchment and regional land-use. Adaptive capacity is maximised when restoration creates fluvial and ecological systems that correspond and co-evolve, building resilience to disturbance however the future unfolds.

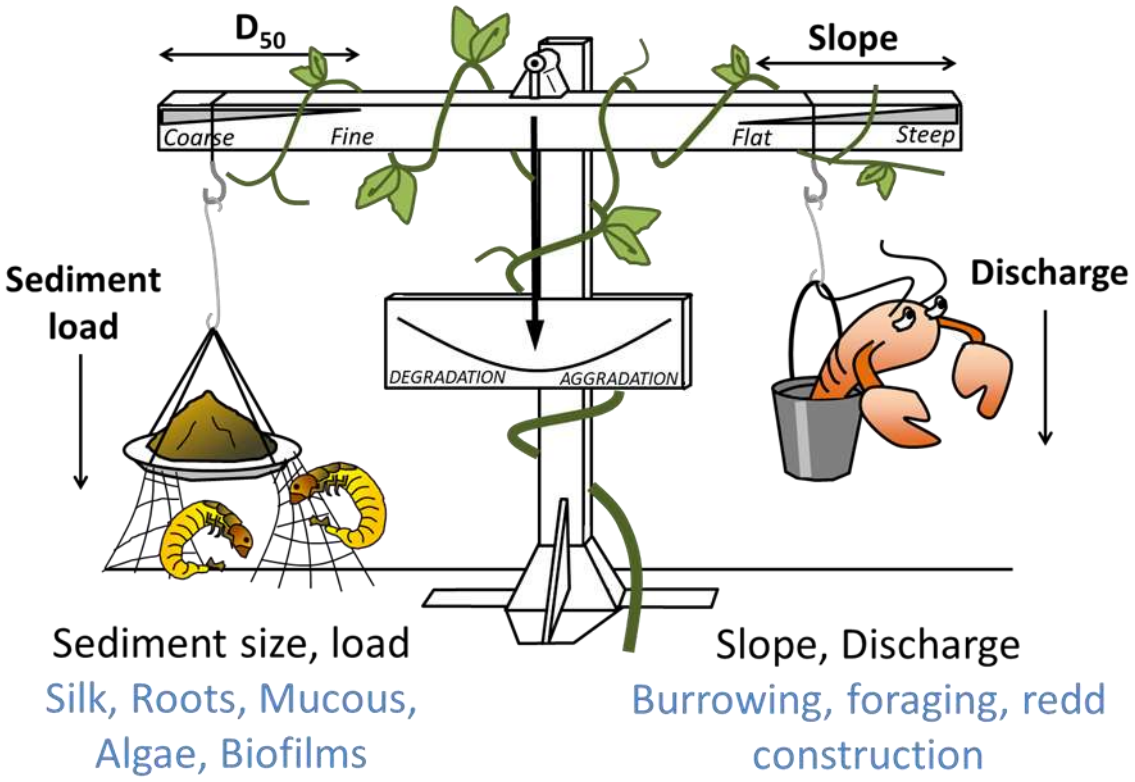

Figure 1. Lane's Balance (1955) has been used as a visual representation of the physics-based paradigm of equilibrium, degradation and aggradation in alluvial rivers for over 60 years. It describes how stable channels occur where sediment load and size are balanced by stream power. Here, we propose an alteration, which represents the important roles that the river's ecosystem also play in determining stable channel form.

Elements of the biomic approach are already in practice. For example, re-introduction of trees and large wood to resist erosion and store sediment in alluvial channels are established restoration techniques [Roni et al. 2014]. However, there is still a tendency to use wood as a 'natural' alternative to concrete or riprap when stabilising a naturally retreating bank. The natural interplay between vegetation, channel form and channel dynamics is more subtle than this; riparian tree species co-evolved with river planforms, as evidenced by sedimentological data showing that, until vegetation with substantial root systems colonised the land, most rivers were wide, sheet flows with braided planforms (Davies and Gibling, 2010). Only after the global spread of trees during the Devonian and Carboniferous periods did rivers develop gradually-shifting, meandering and anastomosed patterns; an association that was interrupted by the Permian-Triassic extinction (when over 90% of life, including plant life was obliterated and following which rivers reverted to sheet-braiding for about 5 million years). Multi-thread planforms then predominated until valley-bottom forests were cleared and rivers were confined to single channels by humankind during the last few centuries.

The influences of some macrofauna, such as cattle, beaver and salmonid fish on fluvial processes have also been recognised for some time. However, the impacts of these organisms are often regarded as atypical, being responsible for localised departures from normative, alluvial forms attributable solely to flowing water. Actually, the impacts of animals on fluvial processes are anything but localised – they are pervasive and fully integrated into the fluvial

system, because animal life in rivers is naturally abundant and diverse, and many animals are known to alter river conditions purposefully. While the biogeomorphic effects and restorative utilities of trees and large mammals are gaining recognition, the influence of small animals is rarely considered, despite their ubiquity in temperate and tropical streams. More research is needed, but early indications are that the biogeomorphic impacts of these organisms are also significant. For example, in gravel-bed rivers, natural densities of caddisfly larvae can increase the critical fluvial shear stress required to mobilise bed sediments by 33 to 45% (Johnson et al. 2009), reducing the frequency and magnitude of bed material motion.

Perhaps the best demonstration of the significance of animals to river forms and processes occurs when organisms are either extirpated, or introduced outside their native ranges. Under these circumstances, biogeomorphic impacts tend to be negative. For example, extirpation of wolves from Yellowstone National Park lead to a trophic cascade that resulted in system-wide river widening because riparian willows were overgrazed by an explosion in the elk population (Beschta and Ripple, 2006). In the UK, deleterious burrowing into the beds and banks of rivers by invasive Signal Crayfish demonstrates the vulnerability of rivers and ecosystems to damage by introduced species (Rice et al. 2014). Mismanagement of river biomes has potentially disastrous geomorphological implications and, in these cases, managing the cause of the problem by restoring balance in the ecosystem provides the only sustainable, long-term solution.

Nature's river restorers work 24/7, 365, without pay and, if they appear to work as if their lives depended on it, they do - because it does. However, they do have fundamental needs, including a liveable flow regime, space to work, a ready supply of suitable food, and support from life lower in the trophic system.

It is impractical to attempt to restore the natural, pre-disturbance flow regime in all but a relatively small number of rivers and, in any case, climate change means future flow regimes will differ from those of the past. Fortunately, native species evolve to tolerate and thrive under naturally-variable conditions and therefore, providing a liveable flow regime in regulated rivers usually requires only that seasonal patterns of instream and overbank flows are approximated (Hall et al. 2009). The biomic approach further requires conserving or restoring a river's capacity to absorb and recover from extreme events, by giving it sufficient room to flood, to entrain, transport and deposit sediment, to allow riparian vegetation to establish on new surfaces, and to recruit large wood from trees growing on gradually eroding banks (Kondolf, 2011).

Nature's river restorers cannot do their work without a functional food web. In this context, it is necessary to recognise that it is the microbial community that underpins provisioning of the biome, by creating, cycling and recycling the chemicals, nutrients and minerals that enable primary production to support the food web (Mendoza-Lera & Datry 2017). Additionally, the role of the 'Hidden Half of Nature' in supporting the immune systems of plants and animals is increasingly recognised (Montgomery and Biklé, 2015). Sterile sediments often used to rebuild floodplains and create in-channel features all too often create lifeless, abiotic matrices. Vibrant microbial communities are necessary to support the higher lifeforms needed to restore degraded fluvial and floodplain environments, and failure to consider this when restoring rivers is likely to impede success.

Unless rivers are being truly re-wilded, the range of higher lifeforms necessarily involved in delivering successful restoration outcomes include ourselves, and there certainly remains a role for suitably qualified, human restoration engineers, especially those with an appreciation of the social and biomic, as well as hydrological and morphological contexts, of their designs. Recognising this, we propose that river restoration engineers and designers who take a holistic view of the river and watchfully partner with Nature's river restorers are

more likely to deliver resilient river futures than designers who continue to rely on the physics-based analyses used to inform most restoration designs to date.

References

Beschta, R.L. and Ripple, W.J., 2006. River channel dynamics following extirpation of wolves in northwestern Yellowstone National Park, USA. *Earth Surface Processes and Landforms*, 31(12), 1525-1539.

Castro, J.M. & Thorne, C.R. 2019. *River Research and Applications*. doi.org/10.1002/rra.3421

Cluer, B.J. and Thorne, C.R. 2014. A stream evolution model integrating habitat and ecosystem benefits. *River Research and Applications*, *30*(2), 135-154.

Darwin, C. 1859. *On the Origin of Species*. London, John Murray, 502p.

Davies, N.S. and Gibling, M.R. 2010. Cambrian to Devonian evolution of alluvial systems: the sedimentological impact of the earliest land plants. *Earth-Science Reviews*, 98(3-4), 171-200.

Gilvear, D.J., Greenwood, M.T., Thoms, M.C. and Wood, P.J. (eds.). 2016. *River Science: Research and Management for the 21st Century*. Chichester, Wiley-Blackwell, 416p.

Hall, A.A., Rood, S.B. and Higgins, P.S. 2011. Resizing a river: A downscaled, seasonal flow regime promotes riparian restoration. *Restoration Ecology*, 19(3), 351-359.

Johnson, M.F., Reid, I., Rice, S.P. and Wood, P.J. 2009. The influence of net-spinning caddisfly larvae on the incipient motion of fine gravels: An experimental field and laboratory flume investigation. *Earth Surface Processes and Landforms*, 34, 413-423.

Kondolf, G.M. 2011. Setting goals in river restoration: when and where can the river "heal itself"?, *Stream restoration in dynamic fluvial systems: scientific approaches, analyses, and tools*, 194, 29-43.

Lane, E.W. 1955. Importance of fluvial morphology in hydraulic engineering. *Proceedings of the American Society of Civil Engineers,* 81, 1 – 17.

Mendoza-Lera, C. and Datry, T. 2017. Relating hydraulic conductivity and hyporheic zone biogeochemical processing to conserve and restore river ecosystem services. *Science of the Total Environment*, 579, 1815-1821.

Montgomery, D.R. and Biklé, A. 2015. *The Hidden Half of Nature: The Microbial Roots of Life and Health*. New York, WW Norton & Company, 320p.

Palmer, M.A., Hondula, K.L. and Koch, B.J. 2014. Ecological restoration of streams and rivers: shifting strategies and shifting goals. *Annual Review of Ecology, Evolution, and Systematics*, 45, 247-269.

Rice, S.P., Johnson, M.F., Mathers, K. Reeds, J. and Extence, C. 2016. The importance of biotic entrainment for base flow fluvial sediment transport. *Journal of Geophysical Research: Earth Surface*, 121, 890–896.

Roni, P., Beechie, T., Pess, G. & Hanson, K. 2014. Wood placement in river restoration: fact, fiction, and future direction. *Canadian Journal of Fisheries and Aquatic Sciences*, 72, 466–478.

Walter, R.C. and Merritts, D.J. 2008. Natural streams and the legacy of water-powered mills. *Science* 319, 299–304.

Stage 0 Restoration Projects in Oregon, USA

[1]Paul Powers, Fisheries Biologist, U.S. Forest Service, Deschutes National Forest, Oregon.
ppowers@fs.fed.us

Abstract

Stream restoration is often based on the creation or recreation of a single-thread, meandering channel with a bankfull discharge return period of 1.5 or 2-years. The channel is designed to achieve "sediment-balance", that is a condition in which the sediment supplied from upstream and local sources is transported downstream (Lane's balance). This is appropriate in 'sediment transport or transfer' valley types, but not in depositional valley types, which are net sediment sinks. There is now overwhelming geologic, historical, empirical and theoretical evidence that natural, sediment sink reaches are characterized by multi-threaded channels that are fully connected to wetland-floodplain complexes. Within the Pacific Northwest Region (PNW) of the Forest Service (USFS), restoration practitioners have been implementing a process-based, unconfined valley restoration approach referred to as "Stage 0".

Introduction

The Stage 0 methodology breaks away from traditional stream restoration approaches that focus on creating a stable channel pattern, profile and dimension through the balance of the mean annual sediment load (Lane's balance) to maintain the constructed in-channel habitats. In contrast, the Stage 0 methodology used by the USFS in PNW, is based on the pre-manipulation state (Stage 0) defined in the Cluer and Thorne Stream Evolution Model (Cluer and Thorne 2013). This restoration methodology uses historic valley surfaces and geomorphic controls, referred to as the Geomorphic Grade Line (GGL), as the target elevation of both the low flow shallow groundwater elevation and base flow wetted area (Powers et al. 2018). The primary goals of Stage 0 design are maximum floodplain connectivity at all discharge levels and the ability of the river valley to adjust and shape itself in response to watershed scale drivers. Rather than designing channels that are connected to the floodplain at a channel forming discharge, valley surfaces are activated and maintain a base flow water surface that is at or near the valley floor elevation. The fluvial valley is then able to develop a complex network of anastomosing flow paths, wetlands, vegetated islands, and diverse aquatic habitats in response to watershed and valley scale process drivers. The continued evolution of the river valley including aquatic habitats and riparian vegetation are in response to watershed drivers and not predetermined. Flow paths and riparian forests are allowed to develop and be lost through time as the site responds to disturbance, sediment (bedload and suspended) sorting and colonization of biological drivers.

Completed restoration projects are able to perform the valley scale processes identified in Roni and Beechie 2013, take advantage of dynamic food wed mosaics (Bellmore et. al 2013, 2015, 2017), and are resilient and able to adapt to large disturbances such as fires, floods, and changing conditions driven by climate change. Stage 0 projects provide the greatest amount of resiliency to fluvial systems while providing exceptionally rich, complex and diverse habitats.

Within the PNW Region of the Forest Service, adoption of the Stage 0 restoration approach began on the arid, east side of the Cascade Mountain Range. The earliest projects of this type were designed and implemented in low order streams flowing through headcut/degraded meadow systems. The rapid succession of wetland features and attributes (shallow groundwater recharge, recovery of wetland obligate vegetation, wetlands and anabranch channels) observed in these early projects prompted restoration specialists to expand this approach to larger, bedload dominated stream systems on a variety of landscapes ranging from lacustrine valleys in the Oregon Coast Range, to moderate gradient valleys in the West Cascades and East Cascades (1-2%), to high gradient valleys in the Klamath Basin (6%). The same general approach was followed on all of these landscapes, which included the elimination of anthropogenic confining features and transport channels within depositional valley types and restoration of a depositional environment. These projects rely on the development and construction of a depositional valley as opposed to the design and construction of a "balanced" channel. These project types restore fluvial processes and in turn restore ecological benefits that have been largely lost in many river systems.

Historical evidence underpinning this approach will be presented and case studies used to demonstrate how GIS-based, terrain analysis can be used to differentiate pre- and post-disturbance surfaces and support restoration design.

This presentation briefly illustrates how depositional environments have been altered, discusses how LiDAR is being used to identify historic geomorphic features during Stage 0 design and shows a series of before and after photos of recently completed projects in Oregon.

References

Bellmore et al. 2013. The floodplain food web mosaic: a study of its importance to salmon and steelhead with implications for their recovery. Ecological Applications, 23(1), pp. 189-207. The Ecological Society of America

Bellmore et al. 2015. Spatial complexity reduces interaction strengths in the meta-food web of a river floodplain mosaic. Ecology, 96(1), 2015, pp. 274-283. The Ecological Society of America

Bellmore et al. 2017. Incorporating food web dynamics into ecological restoration: a modeling approach for river ecosystems. Ecological Applications, 27(3), 2017, pp 814-832 by the Ecological Society of America.

Cluer B. and C. Thorne. 2013. A stream evolution model integrating habitat and ecosystem benefits. River Research and Applications 30: 135-154.

Powers, P., Niezgoda, S., and M. Helstab. *2018.* A Process Based Approach to Restoring Depositional River Valleys to Stage 0, an Anastomosing Channel Network. River Research and Applications 35: 3-13.

Roni, P. and Beechie, T. 2013. Stream and watershed restoration: a guide to restoring riverine processes and habitats. Wiley-Blackwell, Hoboken, NJ. 300 pp.

'Stage Zero' Restoration of Whychus Creek, Oregon: Monitoring Results and Lessons Learned

Mathias Perle, Program Manager, Upper Deschutes Watershed Council, Bend OR
Lauren Mork, Program Manager, Upper Deschutes Watershed Council, Bend OR
Colin Thorne, Professor, University of Nottingham, UK colin.thorne@nottingham.ac.uk

Extended Abstract

Background

Whychus Creek is the focus of multi-year, collaborative restoration efforts that support increased numbers of anadromous and resident fish, improved stream habitat and expanded biodiversity. In 2016, project partners led by the Upper Deschutes Watershed Council (UDWC - https://www.upperdeschuteswatershedcouncil.org), broke ground on the first mile of a six-mile restoration project along Whychus Creek on land owned by the Deschutes Land Trust (DLT - https://www.deschuteslandtrust.org) (Figure 1).

Project proponents are committed and focused on restoring the physical, chemical and biological processes necessary to establish and support a resilient and productive stream ecosystem for the long-terms benefit of fish, wildlife and water quality (Beechie et al. 2013, Bellmore et al. 2013). The approach to restoration adopted by the UDWC and its partners is founded on established principles of process-based stream restoration (Beechie et al. 2010, Roni and Beechie 2012) but also employs key principles of ecological restoration (e.g., McDonald et al. 2016). We focus on addressing the historic root causes of channel and ecological degradation: channel straightening and simplification to support agricultural activites, which led to channel incision and disconnection of the stream from its floodplain. We do this by filling-in the incised channel, re-activating the historical floodplain, and planting the restored reach with native riparian and obligate wetland species. In this approach to stream restoration, we look beyond the channel, to restore natural connectivity within the channel-wetland-floodplain system. The aim is to recover plants and animal assemblages floodplain-wide, and allow natural erosion, deposition, and avulsion processes to create, maintain and support resilient instream, wetland, washland and floodplain habitats that support all life stages of target fish and wildlife species. We intend to recreate ecosystems that are as self-sustaining and as resilient as possible to the impacts of future changes in climate and watershed land-use.

Project design and implementation in Whychus Creek also seeks to explore the degree to which optimum ecologically productive stream conditions can be achieved in practice. Our approach stems from a paper by Cluer and Thorne (2014) in which they propose the Stream Evolution Model (SEM). Their analyses suggest that the highest values for hydro-morphological attributes and ecosystem benefits are associated with 'Stage 0' (the pre-disturbance condition) in the incised channel evolutionary sequence. It follows that, when an incised stream is restored, the greatest ecological uplift possible given the remaining site and watershed constraints is attained when the stream is reset to its pre-incision condition – that is, restored to 'Stage 0'.

Post-project monitoring was designed to: support evaluation of the ecological outcomes of this restoration approach; to inform future phases of restoration at Whychus Creek; and, to establish how well 'Stage 0' restoration works in practice.

Project monitoring, ongoing since 2014, includes evaluating a wide range of physical and biological metrics including groundwater, channel morphology, habitat (especially for target and ESA-listed fish species), water temperature, primary productivity, macroinvertebrates, plant community presence/assemblages/extent, and fish usage (Table 1).

Monitoring Results

The pre-restoration, single-threaded, statically-stable channel was incised below the historical floodplain by about 10 feet. It had been relocated along the valley-right toe slope and in Figure 2 it is marked by a line of trees on the far side of the valley floor in the upper photograph. Restoration involved filling-in the incised channel and lowering the valley floor in places, to fully reconnect the stream and its floodplain. Immediately following these actions multiple, dynamically-adjusting anabranches developed (see center photograph in Figure 2). Within 2 years, the post-restoration, braided system had evolved and vegetated into an anastomosing planform, as shown in the lower photograph in Figure 2. This transformation led to very large increases in instream habitat quantity and complexity, with a 187% increase in wetted area at base flow, a 443 % increase in the number of habitat units, and a 429% increase in number of pools. Sediment sampling has revealed a reduction in the percentages of cobbles and boulders (which constituted most of the channel substrate prior to restoration) and increases in the percentages of gravel, sand and silt.

Reconnection of the stream and its floodplain has resulted a rise in the water table from about 7 ft below the valley floor to less than 2 feet - a rise sufficient to create multiple ponds and seasonally flooded areas and support rapid colonization of the project reach by a wide array of riparian and wetland vegetation. Plant assemblages show a predominance of native over non-native and invasive species.

Macroinvertebrate data show abundances in side channels well above that in unrestored reaches with simple, single-thread geometries while EPT taxa richness post restoration remains as high as that in unrestored reaches. The results of measurements of primary productivity reveal the existence of multiple, micro-biological hotspots in side channels that are not found in an unrestored, incised control reach. Anadromous fish usage data collected in Fall 2018 indicate an 321% increase in juvenile steelhead and redband trout (*Oncorhynchus mykiss*) density per unit area over pre-project density, while Chinook (*Oncorhynchus tschawytscha*) juvenile density per unit area was 800% higher in the restored reach than in the adjacent control reach.

Lessons Learned

Monitoring results establish that, to date, the project is either achieving or exceeding 15 out of its 19 success criteria (Table 1). On this basis, only two years after construction, this 'Stage 0' restoration is delivering the physical, habitat, and biological uplift hoped for from a fully connected channel-wetland-floodplain system. Notwithstanding this, four performance parameters appear to be sub-optimal and we are learning lessons about what success looks like in a 'Stage 0' restoration.

Channel bed elevations remain within +/- 2 ft of the Geomorphic Grade Line (GGL) which is the target long profile, but there remains a risk that one anabranch might scour unacceptably - capturing an ever increasing percentage of the overall flow. If monitoring reveals such a trend, adaptive management with partners will identify what potential actions could be taken to prevent renewed degradation so prevent an incised, single-thread channel from disconnecting the stream from its floodplain. One year post-project, the area of riparian and wetland vegetation had increased by approximately 5 acres (or 20%) over that in the pre-project area. It is trending toward the target increase of ≥20 acres. The lesson learned here is that despite

riparian planting and recolonization by riparian species, it takes additional time for riparian and wetland plants to become established, mature, and abundant. That said, progress towards this success criterion is substantial and ongoing.

While both the number of pools and the diversity of pool habitats have increased, maximum pool depths are slightly lower than in the control reach. It is anticipated that maximum pool depths will increase through time as anabranches evolve naturally and scour and deposition processes continue to promote pool formation. The finding that the extent of bed substrate dominated by fines (sand and silt) has increased generated concerns amongst some stakeholders, due to the risk of fish eggs being smothered. Despite this concern, gravel redds (depressions in the stream bed created by salmon into which eggs are deposited) have been detected in the 'Stage 0' reach, suggesting the presence of suitable spawning habitat in the project. Also, fine-grained bed materials provide excellent habitat for midges, which are a vital food for fish during their alevin and fry life stages.

A broader lesson learned is that the complexity and valley wall to valley wall extent of fully-connected channel-wetland-floodplain systems created by restoration to 'Stage 0' (see Figure 2) is difficult to adequately describe using conventional, channel-centric, and ground-based monitoring methods. At Whychus Creek, UDWC is expanding the scope of monitoring to capture novel parameters such as 'patch complexity' and, in judging success, we are coming to rely on measures of diversity and variability as much as on traditionally used measures of central tendency. In short, we are interested in parameter ranges and standard deviations as well as spatially- or time-averaged mean, median or modal values.

The findings of our intensive monitoring efforts provide vital insights (reported above) needed to evaluate the benefits and risks of 'Stage 0' restoration and assess whether improvements in long-term productivity, diversity and resilience justify the short-term disruption caused when the fluvial system and valley floor are re-set to their pre-disurbance condition.

References

Beechie, T.J., Sear, D.A., Olden, J.D., Pess, G.R., Buffington, J.M., Moir, H., Roni, P. and Pollock, M.M. 2010. Process-based Principles for Restoring River Ecosystems. *BioScience* 60: 209-222.

Beechie, T.J., Imaki, H., Greene, J., Wade, A., Wu, H., Pess, G., Roni, P., Kimball, J., Stanford, J., Kiffney, P. and Mantua, N. 2013. Restoring Salmon Habitat for a Changing Climate. *River Research and Applications* 29: 939-960.

Bellmore, J.R., Baxter, C.V., Martens, K. and Connolly, P.J. 2013. The floodplain food web mosaic: a study of its importance to salmon and steelhead with implications for their recovery. *Ecological Applications* 23 (1): 189-207.

Cluer B.J. and Thorne, C.R. 2013. A Stream Evolution Model Integrating Habitat and Ecosystem Benefits. *River Research and Applications* 30(2), 135-154. DOI: 10.1002/rra.2631.

Roni, P. and Beechie. T.J. (2012). *Stream and Watershed Restoration: A Guide to Restoring Riverine Processes and Habitats*. Wiley-Blackwell.

McDonald, T., Gann, G., Jonson, J. and Dixon, K. 2016. International standards for the practice of ecological restoration–including principles and key concepts.(Society for Ecological Restoration: Washington, DC, USA). *Soil-Tec, Inc.,© Marcel Huijser, Bethanie Walder*.

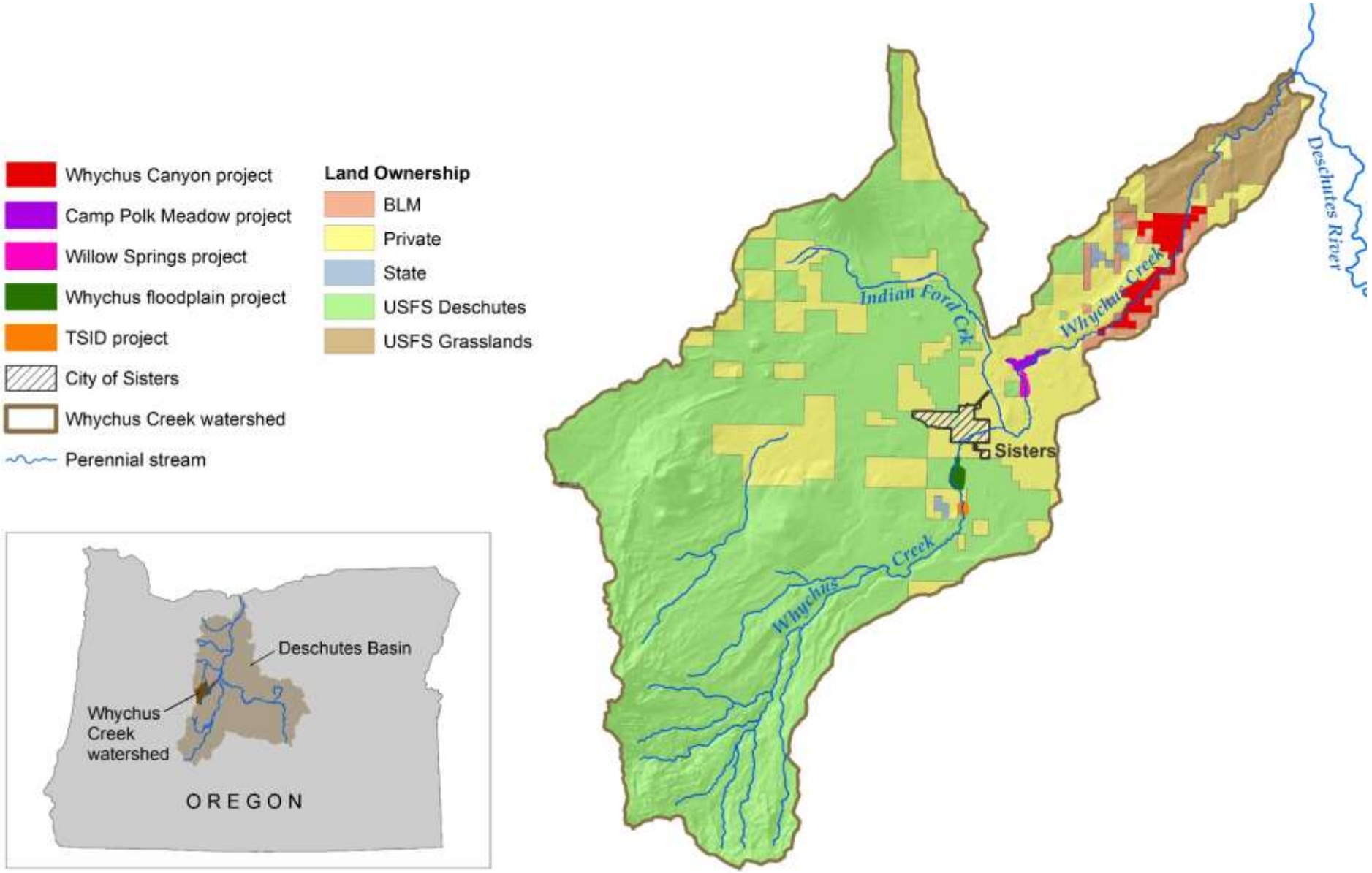

Figure 1. Project location maps.

Figure 2. Project Implementation (pre-restoration (2015), immediately post-construction (2016) and 2-years post-construction (2018).

Table 1. Monitoring outcomes to date. Green crosses indicate outcomes that currently achieve or exceed project success criteria.

Results (at baseflow)

PHYSICAL

Groundwater

- Depth +

Channel morphology

- Number of channels +
- Channel elevation + / -
- Total channel length +
- Ratio of primary : secondary +
- Total wetted area +

Stream temperature

- July rate of change +

Geomorphic units / habitat

- Total number of units +
- Number of types of units +
- Percent riffle +
- Percent pool +
- Pool number, types, area, dimensions + / -
- Pieces of wood +
- Substrate sizes, proportions + / -

BIOLOGICAL

Riparian and wetland vegetation

- Area + / -
- Species richness and type +

Algae and plankton

- Species richness and abundance +

Macroinvertebrates

- Taxa richness and abundance +

Fish

- Juvenile density +

Summary of Current Rio Grande Silvery Minnow Habitat Restoration Design and Application

Robert S. Padilla, Supervisory Civil Engineer, Albuquerque Area Office, U.S. Bureau of Reclamation, rpadilla@usbr.gov
Ari Posner Physical Scientist, Albuquerque Area Office, U.S. Bureau of Reclamation, aposner@usbr.gov
Drew C. Baird, Hydraulic Engineer, Technical Service Center, U.S. Bureau of Reclamation, Denver, CO. dbaird@usbr.gov

Abstract

Due to population decline and reduction of historical habitat range, the Rio Grande Silvery Minnow (silvery minnow) is a Federal and State listed endangered species. Currently the silvery minnow populations inhabit approximately 10 percent of their historical range. Declining silvery minnow population is attributed to the geomorphic and habitat effects resulting from: 1) upstream dam, levee and diversion dam construction, 2) river channelization, 3) effects of water withdrawals on river flows, and 4) changing climate. Habitat restoration has been undertaken to protect and improve the status of the silvery minnow while simultaneously protecting existing and future regional water uses.

The purpose of this paper is to review, summarize, and briefly evaluate the types of habitat restoration projects implemented on the Middle Rio Grande, in terms of their site selection, design criteria, and supporting analysis. We include the latest information on silvery minnow ecology, habitat, and food source needs which informs habitat restoration planning and design. Morphological changes on the Middle Rio Grande include channel narrowing, incision and disconnection of the main channel from its historical floodplain, habitat fragmentation, and channel width and depth homogeneity. Ecological and project specific design criteria, habitat restoration methods and limitations, site and technique selection, design analysis, and post project silvery minnow use, and general channel response are described. Habitat restoration has often involved lowering floodplain and channel features to provide spawning and rearing habitat. Suspended sediment is deposited on lowered floodplain and channel surfaces reducing their design life. We describe preliminary available information on project effectiveness and sustainability such as habitat usage, and channel response. We close by discussing monitoring and post project evaluation needed to provide vital information on sustainability for effective planning and implementation of additional habitat restoration.

Introduction

The decline of native fish communities, even past extirpation of indigenous species, has been well-documented (Platania 1991). Because of population decline and reduction of historical habitat range, the Rio Grande silvery minnow (silvery minnow) is a Federal and State (New Mexico and Texas) listed endangered species (Federal Register [FR] 1994; New Mexico Department of Game and Fish [NMGF] 1996). Currently the silvery minnow populations

inhabit approximately 10 percent of the historical range (Bureau of Reclamation [Reclamation] 2015).

Declining silvery minnow populations are generally attributed to the geomorphic and habitat effects of: 1) upstream dam, levee and diversion dam construction, 2) river channelization, and 3) effects of water withdrawals on river flows (Bestgen and Platania 1991; Swanson et. al. 2011). Ideally, diverse and suitable riverine habitat would be accomplished by the channel dynamics of fluvial erosion and depositional processes using the available sediment and hydrology. However, both sediment supply and peak flows have been reduced due to upstream reservoir construction (Jemez Canyon, Cochiti, Galesteo Creek, and Abiquiu Dams) resulting in the loss historical channel dynamics. The Middle Rio Grande Endangered Species Collaborative Program (MRGESCP) was created to protect and improve the status of the listed species (Tetra Tech 2004) while simultaneously protecting existing and future regional water uses. Many habitat restoration projects have been undertaken by the MRGESCP on the Middle Rio Grande. The primary purpose of this report is to review, summarize and briefly evaluate site selection, design criteria and analysis for habitat restoration projects on the Middle Rio Grande by the MRGESCP and by Reclamation.

A focused literature review of silvery minnow ecology, habitat, and food source needs is included to provide the latest knowledge for site selection and habitat restoration design. There is a considerable amount of published information documenting the need for restoration, site selection, habitat needs and environmental compliance. Some preliminary but not conclusive information is available on project effectiveness and sustainability.

Rio Grande Silvery Minnow Biology and Habitat Needs

Biology

Silvery minnows produce numerous semi-buoyant non-adhesive eggs typical of the genus *Hybognathus*. (Platania and Altenbach 1998, Platania 2000). Most spawning occurs during the spring runoff peaks during the months of May and June when water temperature generally exceeds 18-24˚ C (64 to 75˚ F) (Dudley and Platania, 1997). The minimal magnitude of flow peak necessary to stimulate spawning is not well defined. A 24-hour flow increase from about 430 cfs to about 1,200 cubic feet per second (cfs) on May 19, 1996, apparently stimulated a spawning event (Tetra Tech, 2014). As such, “spring runoff peak flows that overbank the floodplain and creates seasonally important larval habitat in May and June are strongly correlated with higher silvery minnow density as measured in the fall” (FWS 2013).

Semi-buoyant eggs have been observed to drift until they are entrained in low-velocity habitats (e.g., backwaters, channel edges and inundated bars and floodplains), or hatch about 24 to 72 hours post fertilization depending on water temperature (Platania 1995, 2000; Reclamation 2015). Newly hatched larvae are observed to passively drift for another approximately 3 days until their air bladders develop whereupon they are thought to actively seek low-velocity habitats (Platania and Altenbach 1998; Medley and Shirey 2013). River channels that are entrenched and narrowed due to reduction in sediment load and flood peaks have disconnected floodplains that offer minimal low velocity floodplain habitat for egg/larval retention. These conditions “exacerbate the likelihood that newly spawned eggs and hatching larvae will remain continuously exposed to strong river currents, minimizing their potential survivorship” (Tetra Tech 2014). Both the spawning and egg drift indicate that floodplain connectivity is a primary need for population recruitment.

Research by Shirey (2004) and Cowley et al., (2006) have shown that silvery minnow consumes diatoms largely found in soft fine sediment substrate. In addition to diatoms, other primary food sources appear to be algae and small invertebrates (Shirey et al. 2008). Most available algae and diatoms for silvery minnow consumption are believed to occur in low velocity habitats, in vegetated lateral zones – i.e., areas with emergent vegetation, backwater or slackwater areas and along bank lines especially with overhanging vegetation (FWS 2010).

Habitat Needs

In general, the species is most often found in low velocity and low depth habitat with silty and sandy substrate with suitable temperatures and nearby available food supply. Habitat criteria for adults includes flow depths less than 60 cm (2.0 ft.) and velocities less than 40 cm/s (1.3 ft./s), while juveniles require flow depths less than 50 cm (1.6 ft.), and velocities less than 30 cm/s (1.0 ft./s). Larvae habitat is less than 5 cm/s (.16 ft./s) velocity and less than 15 cm (o.5) flow depth. "Shallow areas in the floodplain during inundation and recession produce habitats with increased water temperatures which promotes improved local food availability and subsequently faster larval growth rates" (Mortensen, et al., 2019). Thus, the best main channel and floodplain (off channel) habitat for silvery minnows include areas that have a diversity of connected, relatively low-velocity flows with shallow depths.

Habitat Design Criteria

Ecological Criteria

Design criteria are centered on habitat needs of the silvery minnow. The FWS (2010) has determined that the silvery minnow habitat needs include backwaters, shallow wide channels, pools, and varying depth and velocity habitat all of which are necessary for each of the particular life history stages in the appropriate seasons. They identify that eddies created by debris piles, pools, backwaters or other refugia habitat provide a wide range of depth and velocities. Low velocity areas of sand and silt substrate in proximity to bank lines have been shown to provide food sources (FWS 2003; FWS 2010; Scholle 2015). Specific habitat needs organized by life history and seasons are summarized by Baird (2016) and Mortensen et al. (2019):

- Spawning and egg retention (April-June). The primary concern during spring runoff is having suitable conditions to produce eggs and provide for retention and development of eggs and larvae. High flows to create river-floodplain connectivity, and during low flow years low velocity and flow depth areas in the main channel are needed.
- Larval and juvenile development (June-October). This season usually produces beneficial main channel conditions due to the warm temperatures and low flows, but river drying imposes a severe threat to the silvery minnow in the contemporary environment.
- Over-wintering (November-March). Low velocity areas less than 1.3 ft./s and depths less than 1.5 ft. These are the characteristics of the most commonly occupied habitats, while habitat for the feeding and development is about the same depth (1.5 ft./s) but slower velocity on the order of 0.5 ft./s. Having areas of reduced velocity to reduce energy demands as well as providing areas of refuge from predation (SWCA 2008; FWS 2010) are often provided by in-stream debris piles.
- Adult (year round). Increased flow to support spawning between April 15 and June 15. Deeper and cooler habitat to act as refugia during drought periods, and plentiful food

supply, refuge from predation, and shading to escape higher summer water temperatures.

River Flow Criteria

For design purposes, the above flow depth, velocity and food sources need correlation to flow rates and flow durations for lateral river-floodplain connectivity to benefit reproduction and larval development. Due to flow variability, creating connectivity surfaces that inundate under a range of suitable flows is necessary. FWS (2013) developed a working hypothesis to correlate the magnitude of the spring runoff peak, peak flow duration, and the duration of overbank flooding with average silvery minnow population densities observed in the fall (October). Higher magnitude spring flows with longer peak flow and overbank flow duration results in more silvery minnows in the fall population surveys (Tables 1 and 2). The Coefficient of Determination for the relationships in Table 1 and Table 2 are about 0.78.

Table 1. Correlated Relationship between Spring Runoff Peak Flow Magnitude and Average Silvery Minnow Density Observed in the Fall (FWS 2013)

Discharge (cfs)	Approximate Fall Population/100 m^2 (1080 ft^2)
1,600	~ 1.5 silvery minnow
2,000	~3.0 silvery minnow
3,750	~5.0 silvery minnow

Table 2. Correlated Relationship between the Duration of Overbank Flooding (days of peak discharge > 2,500 cfs at the USGS Central Bridge Gage) and average Silvery Minnow Density Observe in the Fall (FWS 2013).

Duration of Peak Flow > 2,500 cfs	Approximate Fall Population/100 m^2 (1080 ft^2)
13	~1.5 silvery minnow
28	~3.0 silvery minnow
41	~5.0 silvery minnow

MEI (2006b) reported that based on experience in the reach near Albuquerque, NM, 25 days (6.8 percent exceedance value on the mean daily flow duration curve) of floodplain inundation provides for optimum egg retention and larval recruitment. In this reach the 25-day exceedance flow is about 4,000 cfs. Thus, floodplain surfaces that inundated at or below 4,000 cfs would provide suitable lateral floodplain connectivity. This does not account for the risks associated with drier flow years where spring flows do not reach those levels. To address this risk MEI (2006b) divided the annual flow volumes into dry, normal and wet years. 25-day exceedance values from dry, normal and wet year flow duration curves were 1,400, 3,500, and 5,600 cfs respectively. In summary, creating surfaces with lateral floodplain connectivity that are inundated during spring runoff for a minimum number of days benefits silvery minnow reproduction and larval development. Given the risk associated with hydrologic variability and potential temporal and spatial changes in riverbed elevation, creating surfaces that are inundated under a range of suitable flows is necessary. The minimum flow ranges used for site selection and design appear to be somewhere between 1,500 and 2,000 cfs (Tetra Tech 2014;

FWS 2013). Since 2014 there has been an emphasis on creating surfaces inundated at lower discharges corresponding to low flow years when few silvery minnows' are sampled (Posner, 2019). Using the probability of May-June flows for low flow years with corresponding low populations of silvery minnows, it was determined that the 50% exceedance design discharge was about 300 cfs. Surfaces excavated for construction design for inundation at about 300 cfs will be inundated more frequently than sites with higher design discharges and will also experience more sediment deposition.

The habitat value of connected surfaces can be enhanced by adding secondary channels and embayments within lowered areas to create more bankline habitat and associated food sources. Excavating or otherwise creating locally irregular bank lines upstream and downstream near restoration projects also provides food sources and local cover. In addition, including large wood at restoration projects increases availability of overwintering habitat with increased source of food.

Habitat Restoration Techniques and Lessons Learned

Ideally, restoration would be accomplished by the channel dynamics of fluvial erosion and depositional processes using the available sediment and hydrology to promote bars, islands, backwaters, slack waters, complex channel edge habitat, and floodplain connectivity. The extensive native and non-native vegetation on the bars has provided root structure which precludes redistribution of sediment observed during flows like the long-duration, high flows in 2005 (MEI 2006a). As a result, mechanical intervention is necessary to "redistribute sediment mass" (MEI, 2006a). Restoration techniques recommended for the Middle Rio Grande (Table 3) are taken from Tetra Tech (2004), SWCA (2008) and Baird and Makar (2011). Lessons learned are a collection of observations by individuals as reported by Baird and Makar (2011) and Habitat Restoration Workgroup (HRW 2014) and should be considered valuable but are initial or preliminary findings only. Figure 1 shows the creation of bankline benches technique (see Table 3). Limited post project monitoring indicates restored habitats provide beneficial silvery minnow floodplain habitat (Magana, 2012; SWCA 2014). Large wood can provide important low flow habitat because of the low velocity downstream habitat. Terrace, bank, and island lowering has been shown to provide good silvery minnow habitat for various life stages especially when there are surfaces created that are inundated at different discharges. Bank line embayments, and the entrance to side channels appear to be the techniques that require the most frequent maintenance (about every 1-2 years) (Table 3).

Bank lowered areas also provide good habitat and generally vegetation growth occurs during the first year. This increases the rate of subsequent sediment deposition and may need maintenance every 2-4 years depending on the magnitude and duration of peak flows (Table 3). A more complete description of maintenance of river restoration sites is given in Baird (2016).

Site and Restoration Technique Selection

Site selection can be individual sites that meet specific management objectives or a longer reach approach such that nearby sites are compatible and the interaction between sites is considered. A longer reach approach comprising multiple sites is recommended for maximum habitat benefits and to consider upstream and downstream effects and effects on multiple sites. Site and restoration technique selection are influenced by channel morphology and sediment transport at a reach scale.

Table 3. Restoration Techniques Recommended for the Middle Rio Grande (Tetra Tech 2004; and Baird and Makar 2011)

Technique	Description	Benefits of Technique	Lessons Learned
Passive restoration	Flow regulation could be used to provide higher-magnitude peak flows to accelerate channel processes when water is available. Use of alternative means of channel maintenance to allow where possible opportunities for the river to regain a more natural condition.	Can lead to increased sinuosity (continuation of current bank erosion) and allows opportunity for the development of bars, islands, side channels, sloughs, and braided channels for the development of complex and diverse habitat.	Highly dependent on post-project hydrology.
Large Wood	Placement of trees, root wads, stumps or branches	Creates slow-water habitats for all life stages, provide refugia habitat backwater nutrients, and food sources such as algae.	Can cause downstream sediment deposition filling the slow-water habitat. Life span and sustainability is unknown. Rootwads buried along the ephemeral (Los Lunas) channel provided high flow side channel habitat.
Removal of lateral confinements	Elimination of structural features that reduce bank erosion potential such as jetty jacks.	Creates wider channel and floodplain with more diverse and low velocity habitat	Removal can result in widening of the river and a more dynamic channel. Amount of bankline erosion is dependent upon flow duration, flow patterns and adjacent vegetation and root density. Best if combined with another technique, such as vegetation clearing and bank destabilization.
Creation of bank-line backwaters and embayment	Areas excavated into the banks, bars and high flow side channels to create slackwater habitat, where water from the main channel provides inundation during mid- range and peak flow events.	Retain drifting silvery minnow eggs and juveniles. Provide more complex channel edge habitat. Provide larvae and juvenile development habitat and enhance food supplies	Has provided habitat. Lower entrance elevations provide more habitat value but also more opportunity for sediment deposition. Generally, embayments have a short life span (1-2 years) depending on hydrology. Backwaters often tend to be effective for long periods than embayments.
Island and bar clearing and destabilization	Removal of vegetation by root plowing or raking, disking, and mowing to mobilize the feature during high flows	Creates more complex habitat, channel widening, increased opportunity for backwaters, pools and eddies of variable low velocity and low depth habitat.	Highly dependent on post-project hydrology to mobilize destabilized feature. Difficult to remove established root structure to the extent needed to create instability and erosion of island or bar. Riparian vegetation can regrow unless sediment mobilization can be sustained by river flows.
High-flow side (ephemeral) channels	Channels or areas excavated on islands or bank attached bars such that they carry flow during high river discharge events. Can be constructed for a variety of mid- to high-range flows.	Connect flood plain and the main channel, low velocity and depth habitat for egg and larval development during high flow periods.	Downstream portion can function as a backwater even when ephemeral channel entrance fills with sediment. Maintenance of the channel mouths are likely to be an important element to keep the channel functioning. Using woody debris, log jam, or small riprap structures placed downstream of the inlet can create a zone of flow acceleration to reduce inlet sediment deposition. Inclusion of embayment's can enhance side channel habitat

Technique	Description	Benefits of Technique	Lessons Learned
			benefit. Terraced banks can enhance habitat benefits and diversity.
Creation of bankline benches	Removal of vegetation and excavation of soils along the main channel bankline to create benches that are inundated at a range of medium to large discharges.	Provides shallow water habitat at a range of discharges for spawning, and increased egg/larvae retention.	Inundated bankline benches provided good silvery minnow habitat including spawning, egg retention, and nursery habitat for a variety of flows. Emergent vegetation helped create low velocities. Lower benches experienced some deposition at lower inundation levels. Appear to be able to function for various runoff years. Life- span depends on hydrology and sediment deposition.
Island/Bar modification and lowering	Removal of vegetation and excavation from islands or bars. Create shelves or benches on islands or bars to increase inundation frequency for a large range of discharges.	Provide increased spawning areas, and improved egg/larvae retention. Enhance floodplain connectivity.	Inundated island and bank-attached bars provided good silvery minnow habitat including spawning, egg retention, and nursery habitat for a variety of flows. Emergent vegetation helped create low velocities. Terraced bars and islands experienced some deposition at lower inundation levels. Islands appear to be able to function for various runoff years. Life- span depends on hydrology and sediment deposition. Terracing provides habitat at variable flow rates enhancing silvery minnow use.
Main channel widening	Excavation of banks and lateral expansion of active channel	Intended to reduce average flow velocity, reduce sediment transport capacity and increase lower velocity and shallow depth habitat.	No information on lessons learned is available.

Geomorphic, Hydraulic, and Sediment Analysis

For some reaches geomorphic, hydraulic and sediment analysis may be needed prior to selecting sites, restoration technique, design and implementation. A description of geomorphologic analysis is beyond the scope of this report. For more information on geomorphic principles and assessments, readers are referred to existing publications such as Schumm (2005) and Kondolf and Piegay (2003) among many others. A description of local bar evaluation is included in the next section. Hydraulic analysis may involve either a one-dimensional or two-dimensional hydrodynamic model to characterize inundation surfaces, velocities, depths, and flow patterns.

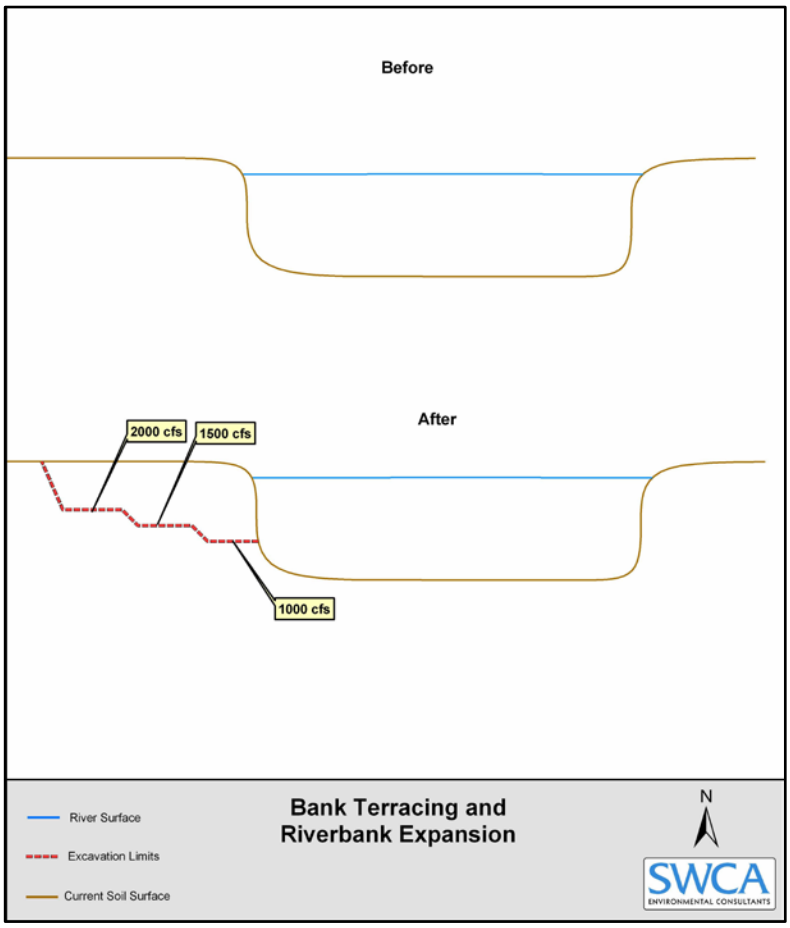

Figure 1. Bank Bench (SWCA 2008) showing surfaces for excavation to the water surface elevation of 1,000, 1,500, and 2,500 cfs river flows. See Table 7 below for a description of creating bankline benches habitat restoration technique.

Site Selection

Site selection for habitat restoration to provide floodplain connectivity is dependent upon the relative site elevation and current frequency and duration of inundation, site availability, and the presence or absence of infrastructure related constraints. Initial screening for site selection is based on identifying and classifying river islands and bank attached bars to distinguish those bars

currently providing functioning habitat, and those having conditions most conducive for connectivity.

Mid-channel and bank attached bars provide restoration opportunities based on how frequently they are inundated. MEI (2006a) classified bars on the Middle Rio Grande according to the following characteristics (Ashley 1990; Germanoski 1989):

- Mid-channel or bank-attached
- Vegetated or un-vegetated
- Subaerial or sub-aqueous
- Stationary or mobile
- Fine-grained (sand and finer) or coarse-grained (gravel or coarser).

Based on these characteristics, time sequential aerial photography, and field observations, a hierarchical bar classification was developed (Table 4) (MEI 2006a).

Table 4. Hierarchical Bar Classification for the Middle Rio Grande

Bar Type	Location	Elevation	Subaqueous or Subaerial	Perennial Vegetation
Linguoid*	Mid-channel	Bed	Subaqueous	No
Braid	Mid-channel	Level-1,**	Subaerial	No
Alternate	Bank-attached	Level-1,	Subaerial	No
Mid-Channel	Mid-channel	Level-1,2***	Subaerial	Yes
Bank-Attached	Bank-attached	Level-1,2	Subaerial	Yes

*Submerged, migrating tongue-shaped bars
**Level 1 is above the bed level and emergent during low flows.
***Level 2 bars experience sediment deposition and vertically accrete. Level-1 bars have emergent vegetation and Level-2 have high hydraulic roughness created by perennial vegetation.

Bars that are devoid of vegetation such as linguoid, and braid mid-channel, and alternate bank-attached bars (Table 3) provide current silvery minnow habitat and do not need restoration. Bars with perennial vegetation about a few years old are generally lower elevation than bars with more mature perennial vegetation that have likely experienced vertical accretion due to sediment deposition. Bars with older vegetation would likely require more sediment removal to provide floodplain connectivity than younger vegetated bars. Typically, mid-channel and bank attached Level 2 bars are “inundated about every 3 to 5 years and for durations of less than 5 days per year in the post-Cochiti Dam period. Level 2 bars therefore are primary candidates for restoration” (MEI 2006b). Initial site selection can be accomplished by field mapping of mid-channel and bank attached bar vegetation. Initial screening and site classification may also be based on management decisions that restoration is needed in a particular reach.

In summary, site selection involves these steps (slightly modified from MEI (2006b)):

- Review potential sites
- Classify potential bars
- Determine site availability
- Review infrastructure constraints
- Develop design criteria
- Hydrologic Analysis
  - Inundation duration-(13 (FWS, 2013) to 25 day (MEI, 2006a) or more
  - Determine exceedance flows for inundation targets
    - Dry, wet and normal flow ranges (Section 3.1)
- Site Selection and design discharge (dry, wet and normal flow ranges)
- Convert design/site selection discharge to water surface elevations and determine sites that are inundated for various flows using a hydraulic model (HEC-RAS, SRH-2D).
- For reach scale site selection, the results of the hydraulic model can be used to determine flood plain connectivity acreages for the desired discharge and associated inundation duration.

Restoration Technique Selection

After site selection, restoration technique identification should be accomplished. While there is not a definitive methodology to determine the most applicable restoration technique, selection should consider several factors such as: 1) types and size of sites available, 2) cost, 3) reach or sub-reach based biological needs, and 4) anticipated habitat value. Preliminary results and lessons learned (Table 4) indicate that nearly all restoration techniques improve habitat and are viable. Larger sites provide opportunity for multiple techniques that provide a range of habitat types for spawning, egg/larvae retention, and larval and juvenile development. Larger sites could include terrace, bank and island lowering, ephemeral high flow side channel with embayments and large wood along the high flow side channel. In general, and based on preliminary evaluation (Baird and Makar 2011; HRW 2014) it appears habitat value is relatively high for terrace, bank, and island lowering when restored surfaces are at multiple elevations for inundation over a range of flows. Constructing sloping surfaces that drain to the river could also provide suitable habitat and may help to avoid and minimize stranding of silvery minnow when flows recede depending on the presence and location of sediment deposition. Placement of large wood and embayments enhances side channel habitat value. For a description of long reach selection criteria, see SWCA (2008).

Design Analysis

It is assumed in this section, that geomorphic and sediment analysis, hydrology and hydraulic analysis needed for site selection and technique selection have already taken place. There are specific types of analysis for designing each restoration technique. At the design analysis stage, the hydrology used for site selection will remain the same. The same HEC-RAS, or SRH-2D model should be applied with some adjustment if needed to use final design flows and topography. Many elevations for lowered surfaces have been designed to coincide to the elevation of a selected discharge rather than a velocity or depth. This approach reduces effort for model application. Should velocity and depth be of greater interest for a particular design then a 2-dimensional depth averaged hydraulic model such as SRH-2D could be used. A one-dimensional sediment transport model, or a sediment continuity analysis, would assist in the design by indicating if the reach of

interest has tendency for erosion or deposition. At a site-specific scale, a two-dimensional, mobile bed sediment transport model of the restoration design would provide information about the likely or potential channel evolution.

Due to local sediment transport conditions, riverbed elevations changed from measurements used in design, resulting in side channels and floodplain connectivity surfaces being inundated at different flows than planned during project design. In addition, the fixed bed assumption of most hydraulic models creates uncertainty. To account for these uncertainties a factor of safety of additional inundation flow depth or reducing the design discharge can be used. For example, bankline bench elevations corresponding to the water surface elevation for 250, 1,000, 1,500, and 2,500 cfs accounts for hydrologic variability. Using a range of discharge values ensures that some of the restored habitat will be usable for dry, normal or wet years. Lowering surface elevations 0.5 or 1.0 ft. below the design water surface elevation is also a means to provide safety factor to account for bed elevation changes.

In summary, to create the opportunity for reproduction and larval and juvenile development, the risks associated with survey errors, hydrologic variability, and the fixed bed hydraulic calculation assumption are accounted for by:

- Reducing the design flow rate used to determine the elevation of excavation, or
- Reducing the design surface elevation and
- Using variable (three different elevations corresponding to 3 different spring runoff flows) surface elevations.

Post Project Silvery Minnow Use and Channel Response

Limited results of measured habitat usage indicate that the silvery minnow use lateral exchange floodplain habitats (e.g.., Magana 2012; SWCA 2014). Large wood can provide important low flow and over wintering habitat because of the low downstream velocity. Jetty removal can result in bank erosion in areas devoid of trees, or where tree roots have low density. Terrace, bank, and island lowering has been shown to provide floodplain silvery minnow habitat (Magaña 2012; SWCA 2014). While bank line embayments and side channels provide egg retention (Massong et al. 2005), these techniques experience more rapid sediment deposition than other features in Table 3. Maintenance as frequent as every 1-2 years may be needed for these habitat restoration features to remain available for inundation during spring runoff peaks.

Bank lowered areas also provide good habitat and generally vegetation growth occurs during the first year increasing the rate of subsequent sediment deposition and may need maintenance every 2-4 years depending on the magnitude and duration of peak flows. Currently monitoring studies do exist that document silvery minnow occupation at habitat restoration sites (e.g., Magaña 2012; SWCA 2014). However, these reports do not provide monitoring and evaluation of geomorphic channel response. Thus, these limited monitoring evaluations do not provide a broad evaluation of the effectiveness of habitat restoration on the Middle Rio Grande. Furthermore, observations of effectiveness and lessons learned in Table 3 are a collection of individual observations reported by Baird and Makar (2011) and HRW (2014) and can only be considered initial or preliminary findings. These initial observations indicate that most restored sites experience sediment deposition and vegetation re-growth after the first few years depending on the level of inundation (HRW 2014). Additional biological and geomorphic monitoring is needed to understand channel response and silvery minnow use to improve future habitat restoration project value.

Description of effectiveness monitoring and evaluation is outside the scope of this report. Publications by SWCA (2014) provide a summary of habitat restoration effectiveness monitoring steps. Effectiveness monitoring for geomorphic channel response should include repeated light detection and ranging (LiDAR), transects and other surveys of the main channel and habitat restoration site to document sediment deposition or erosion in relationship to flow conditions. Pre-project, as built, and several years of annual post project surveys are recommended. Side channel, backwater and embayment sediment deposition should be documented along with local vegetation. Aerial photography may also be used to provide data for determining geomorphic response.

Summary and Recommendations

Silvery minnows produce numerous semi-buoyant non-adhesive eggs mostly during spring runoff peaks during May or June. Spring runoff peaks that inundate floodplain overbanks are strongly correlated with higher silvery minnow densities measured during fall population monitoring. Silvery minnow spawning and egg drift indicate that lateral floodplain connectivity is a primary need for population recruitment. The species is most often found in low velocity and low depth habitat with silty and sandy substrate with nearby available food sources. Depending on the life stage, highest quality depth habitat is 1.5 ft. or less with mean velocities ranging from 1.5 down to near 0 ft./s. Low velocity areas of sand and silt substrate in proximity of bank lines or emergent vegetation provide food sources.

Habitat restoration projects should focus on increasing overbanking flows through lateral connectivity as well as simulating those features within the main channel where possible (e.g. islands). Systematic monitoring is needed to determine sediment deposition rates in addition to the vegetation and silvery minnow presence or absence monitoring. Geomorphic monitoring including repeat LiDAR, cross section surveys, field descriptions of sediment deposition patterns photographs, and analysis. Geomorphic monitoring should be correlated to habitat monitoring by teaming together biologists, ecologists, geomorphologists and hydraulic engineers. Opportunities to improve habitat restoration longevity, minimize future maintenance needs, determine optimum maintenance timing, and determine tradeoffs between maintaining current habitat restoration sites and developing new habitat restoration sites can be accomplished by evaluating geomorphic response.

References

Ashley, G.M. 1990. Classification of Large-Scale Bedforms: A New Look at an Old Problem. *Journal of Sedimentary Petrology* 60:160-172.

Baird, D.C., 2016, Rio Grande Silvery Minnow Habitat Restoration Design Review. U.S. Department of the Interior, Bureau of Reclamation, Technical Service Center, Sedimentation and River Hydraulics Group, 86-68240, Report No. SRH-20-2016-19.

Baird, D.C., and P.W. Makar. 2011. Middle Rio Grande Endangered Species Collaborative Program River and Habitat Restoration Methods Workshop. Sedimentation and River Hydraulics Group (86-68240) Report SRH-2011-03, Bureau of Reclamation, Technical Service Center, Denver, Colorado.

Bestgen, K.R., and S.P. Platania. 1991. Status and Conservation of the Rio Grande Silvery Minnow (*Hybognathus amarus*). The Southwest Naturalist 36, pp 186-193.

Cowley, D.E., P.D. Shirey, and M.D. Hatch. 2006. Ecology of the Rio Grande Silvery Minnow (Cyprinidae: *Hybognathus amarus*) Inferred from Specimen's collected in 1874. *Reviews in Fisheries Science*, 14:111-125.

Dudley, R.K., and S.P. Platania. 1997. Habitat Use of the Rio Grande Silvery Minnow. Submitted to Bureau of Reclamation, Albuquerque Area Office, Albuquerque, New Mexico.

Federal Register (FR). 1994. Final Rule to List the Rio Grande Silvery Minnow as Endangered, 59:138:36988-36995. U.S. Department of the Interior, Fish and Wildlife Service. Effective August 19, 1994.

FWS. 2003. Biological and Conference Opinions on the Effects of Actions Associated with the Programmatic Biological Assessment of Bureau of Reclamation's Water and River Maintenance Operations, Army Corps of Engineers' Flood Control Operation, and Related Non-Federal Actions on the Middle Rio Grande, New Mexico. U.S. Department of the Interior, Fish and Wildlife Service, Albuquerque, New Mexico.

FWS. 2010. Rio Grande Silvery Minnow (*Hybognathus amarus*) Recovery Plan, First Revision. Albuquerque, New Mexico.

FWS. 2013. draft, unpublished document. Hydrologic Objective. U.S. Department of the Interior, Fish and Wildlife Service, Albuquerque, New Mexico.

Germanoski, D. 1989. unpublished Ph.D., dissertation. The Effects of Sediment Load and Gradient on Braided River Morphololgy. Colorado State University, Fort Collins, Colorado, pp 407.

Habitat Restoration Workgroup (HRW). 2014. draft unpublished document. Recovery Implementation Restoration Planning. Middle Rio Grande Endangered Species Act Collaborative Program.

Kondolf, G.M. and H. Piegay (eds.). 2003. Tools in Fluvial Geomorphology. John Wiley & Sons, Hoboken, New Jersey.

Magaña, H.A. 2012. Habitat Use of the Rio Grande Silvery Minnow (*Hybognathus amarus*) During a Long-Term Flood Pulse in the Middle Rio Grande. *Environ Biol Fish* (95:201-212.

Makar, P. 2010. Channel Characteristics of the Middle Rio Grande, NM, Department of the Interior, U.S. Bureau of Reclamation, SRH-2011-05, Technical Service Center, Denver, CO.

Massong, T., Porter, M., Bauer, T., 2005. Design Improvements for Constructed Rio Grande Silvery Minnow Nursery Habitat, Department of the Interior, Bureau of Reclamation, Upper Colorado Region, Albuquerque Area Office.

Medley, C.N., and P.D. Shirey. 2013. Review and reinterpretation of Rio Grande silvery minnow reproductive ecology using egg biology, life history, hydrology, and geomorphology information. Ecohydrology 6(3):499-513.

Mortensen, J.G., Dudley, R.K., Platania, S.P., and Turner T.F., 2019. Rio Grande Silvery Minnow Habitat Synthesis, Draft report, Prepared for U.S. Bureau of Reclamation, Albuquerque Area Office, Contract G-01802-01.

Mussetter Engineering, Inc (MEI). 2006a. Evaluation of Bar Morphology, Distribution and Dynamics as Indices of Fluvial Processes in the middle Rio Grande, New Mexico. Prepared for the New Mexico Interstate Stream Commission and Middle Rio Grande Endangered Species Act Collaborative Program, New Mexico.

Mussetter Engineering, Inc (MEI). 2006b. Middle Rio Grande Restoration, Phase II, Site Selection and Development of Decision Analysis Tool to Estimate Cut and Fill Volumes and Distribution of Habitat. Report prepared for the New Mexico Interstate Stream Commission.

New Mexico Department of Game and Fish (NMGF). 1996. List Threatened and Endangered Species, Title 19, New Mexico Administrative Code, Chapter 33, Part 1 (19NMAC 33.1).

Platania, S,P. 1991. Fishes of the Rio Chama and Upper Rio Grande, New Mexico, with preliminary comments on their longitudinal distribution, *The Southwest Naturalist* 36, 186-193.

Platania, S.P. 1995. Reproductive Biology and Early Life-History of Rio Grande Silvery Minnow, *Hybognathus amarus*. Report under Purchase Order DACW47-94-P-0462, prepared for U.S. Army Corps of Engineers, Albuquerque District, Albuquerque, New Mexico. 30 pages.

Platania, S.P. and C.S. Altenbach. 1998. Reproductive Strategies and Egg Types of Seven Rio Grande Basin Cyprinids. *Copeia* 3:559-569.

Platania, S.P. 2000. Effects of four water temperature treatments on survival, growth, and developmental rates of Rio Grande silvery minnow, *Hybognathus amarus*, eggs and larvae. Report to the U.S. Fish and Wildlife Service, Albuquerque, New Mexico.

Posner, A. 2019. Rhodes Property Bank Lowering Aquatic Habitat Creation, U.S. Department of the Interior, Bureau of Reclamation, Albuquerque Area Office, Technical Services Division.

Reclamation. 2015. Joint Biological Assessment, Bureau of Reclamation, Bureau of Indian Affairs, and Non-Federal Water Management and Maintenance Activities on the Middle Rio Grande, New Mexico. Albuquerque, New Mexico.

Scholle, S. 2015. Effects of stream edges on algal biomass in the middle Rio Grande. Master's Thesis, University of New Mexico, Albuquerque, New Mexico.

Shirey, P. D. 2004. Foraging Habits and Habitat Utilization of Rio Grande Silvery Minnow (Hybognathus amarus) as Inferred by Diatom Frustules. Thesis Submitted to the Graduate School in Partial Fulfillment of the Requirement for the Degree Master of Science, Major Subject: Wildlife Science, New Mexico State University, Las Cruces, New Mexico.

Shirey, P. D. Cowley, and R. Sallenave. 2008. "Diatoms from gut contents of museum specimens of an endangered minnow suggest long-term ecological changes in the Rio Grande (USA). Journal of Paleolimnology 40:263-272.

Schumm, S.A., 2005, River Variability and Complexity, Cambridge University Press, New York, NY.

Swanson, B.J., G.A. Meyer, and J.E. Coonrod. 2011. Historical Channel Narrowing along the Rio Grande near Albuquerque, New Mexico, in response to Peak Discharge Reductions and Engineering: Magnitude and Uncertainty of Change from Air Photo Measurements. *Earth Surface Processes and Landforms* 36:885–900.

SWCA. 2008. Isleta Reach Riverine Restoration Project, Environmental Assessment. Prepared for the New Mexico Interstate Stream Commission, Albuquerque Office by SWCA Environmental Consultants, Albuquerque, New Mexico.

SWCA. 2014. Middle Rio Grande Endangered Species Collaborative Program Habitat Restoration Effectiveness Monitoring: 2010-2012. Prepared for the U.S. Army Corps of Engineers—Albuquerque District. SWCA Environmental Consultants, Albuquerque, New Mexico.

Tetra Tech EMI. 2004. Habitat Restoration Plan for the Middle Rio Grande, Prepared for Middle Rio Grande Endangered Species Act Collaborative Program Habitat Restoration Subcommittee, Albuquerque, New Mexico.

Tetra Tech. 2014. Ecohydrological Relationships along the Middle Rio Grande of New Mexico for the Endangered Rio Grande Silvery Minnow. Final report prepared for the U.S. Army Corps of Engineers, Albuquerque District, Albuquerque, New Mexico.

The Potential for Restoring Thermal Refuges in Rivers for Cold-Water Fishes

Joel Sholtes, Instructor, Colorado Mesa University, Department of Engineering, Grand Junction, CO, jsholtes@coloradomesa.edu
Caroline Ubing, Hydraulic Engineer, Bureau of Reclamation, Denver, CO, cubing@usbr.gov
Michael Knutson, Hydraulic Engineer, Bureau of Reclamation, Boise, ID, mknutson@usbr.gov
Ian Wilson, Fish biologist, Confederated Tribes of the Umatilla Indian Reservation, La Grande, OR, ianwilson@ctuir.org
Justin Nielsen, Hydraulic Engineer, Bureau of Reclamation, Boise, ID, jnielsen@usbr.gov

Introduction

Human impacts to rivers have resulted in increased water temperatures (Caissie, 2006; Justice et al., 2016). This threatens cold-water aquatic species such as salmonids and reduces their viability by influencing fitness and fecundity (Konecki et al., 1995, Schindler, 1998), resulting in localized extirpation of certain species and overall reduction in available habitat and fish production basin wide (Batin et al., 2007; Ruesch et al., 2012). If cold-water aquatic species recovery programs are to meet their long-term goals, they must consider mitigating the impacts of warming waters with “thermal restoration” and creation of thermal refuges. Thermal refuges are defined as discrete patches of habitiat within a river corridor where temperatures are different (warmer in winter, cooler in summer) relative to surrounding water (Torgersen et al., 2012). Thermal restoration has two primary mechanisms: (1) reducing solar insolation by reducing channel width-to-depth ratios and increasing shading by riparian vegetation, and (2) enhancing exchange of surface-subsurface water (i.e., hyporheic flow) within the channel bed, banks, and floodplain. We focus on the latter mechanism studying how restoration can mediate hyporheic flow, which can result in decreased and buffered temperatures in main and side channels. Currently, there is little documentation of the ability of and degree to which physical channel and floodplain restoration can mitigate the impacts of warming at different scales.

We present a conceptual model of how river restoration practices can bring about thermal restoration and create thermal refugia from the reach, meander wavelength, and geomorphic unit scales. An initial analysis of pre- and post-restoration temperature and groundwater monitoring data from a reach-scale restoration project in the Grand Ronde River basin, Oregon indicates that meander- and geomorphic unit-scale thermal refuges can be achieved but that reach-scale reductions in or buffering of temperature may be difficult to demonstrate. We outline our next steps to evaluate how water and temperature fluxes within the hyporheic zone are mediated by channel and floodplain restoration at these three scales.

Background

Hyporheic exchange is the mixing of surface water in the channel and shallow groundwater in the hyporheic zone across the streambed (Kasahara and Wondzell, 2003; Arrigoni et al., 2008; Tonina and Buffington, 2009). Research has documented thermal flux between water in the hyporheic zone and river channel (i.e., Poole et al., 2008). To understand the influence hyporheic exchange has on surface water temperatures as well as how restoration measures might influence this, we must understand temperature cycles of both channel and hyporheic water. Second, we must understand how these two reservoirs are hydrologically connected.

Temperature in stream surface water follows a sinusoidal pattern on a daily time period (Hatch et al., 2006). Arrigoni et al. (2008) describe the influence of hyporheic exchange on stream surface water in terms of cooling, buffering, and lagging this temperature pattern at various time scales (Figure 1). Cooling indicates a difference in mean temperature between hyporheic outflow and surface water. Buffered cycles demonstrate an attenuation in the temperature range (dampened peaks and troughs) but no change to mean temperature. Finally, lagging indicates a change in timing or phase of the temperature pattern. Studies have shown that hyporheic exchange at reach scales (1-5 km) effectively buffers and lags diel and annual temperature cycles. A net cooling effect is rarely observed outside of local groundwater or hyporheic outflow zones where reach-scale hyporheic flow paths may exist (Poole et al., 2008) or where regional groundwater may be mixing with the alluvial aquifer (Arrigoni et al., 2008). Along a reach, there may be numerous short and medium hyporheic flow paths in which buffering and lagging occurs and but only a relative small number of longer flows paths where cooling might occur. Therefore, from a thermal flux standpoint, only a small amount of water might actually be cooled resulting in negligible changes to the temperature of the main channel flow.

The magnitude of temperature lagging is dependent on the length of the flow path connecting surface water with the hyporheic zone. The flow path length directly correlates to the residence time within the alluvial or floodplain aquifer. Short flow paths (1 m to 10 m) are typically created by changes in longitudinal gradient such as along the longitudinal profile of a pool-riffle stream

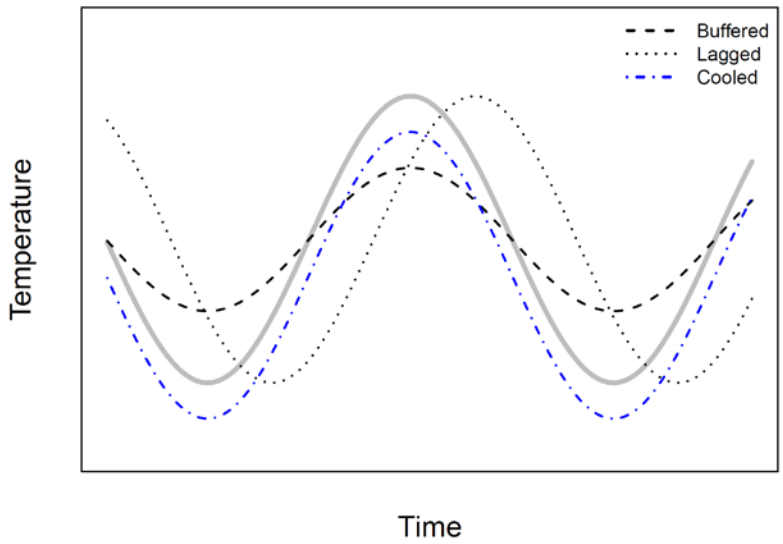

Figure 1. Representation of buffering (black dashed lines), lagging (black dotted line), and cooling (blue dash-dot line) of diurnal surface water temperature pattern compared to a standard (thick grey) after Arrigoni et al. (2008).

(Harvey and Bencala, 1993; Hester and Gooseff, 2010). Hyporheic flow entering the channel bed from a short flow path (feet or tens of feet) may alter the daily temperature range and phase compared to the main channel. These patterns are most evident in spring channels, compared to side channels or the main channel (Arrigoni et al., 2008). Therefore, cooler water may re-emerge during the hottest time of day, while warmer water surfaces at night if the lagging offsets the phase of the diurnal temperature pattern at the appropriate time scale.

Medium and long flow paths (100 m to 2000 m) are created by the channel planform and preferential flow paths across the flows alongside channel beds or abandoned channel beds (i.e., channel sinuosity, meander migration, and avulsion over time; Wroblicky et al., 1998). Restoration techniques to create medium and long flow paths include planform re-alignment, side channel construction, and coarsening of subsurface material (Hester and Gooseff, 2010). Longer flow paths buffer and lag temperature cycles at longer time periods such as weeks and months. Water re-emerging from long flow paths can cool summer surface water temperatures or provide warm refuge in the winter. Any associated mean temperature changes will be localized for long flow paths given the relatively small contribution they represent to flow in the main channel(s) (Poole, et al., 2008).

Evidence of buffered, lagged, and cooled water temperatures has been documented on a channel and floodplain restoration site on Catherine Creek, a tributary to the Grande Ronde River. Hourly temperature data monitored in surface water in the main channel and in an “alcove” adjoining the main channel show all these elements (Figure 2). An alcove may serve as an outlet for a side channel rejoining the main channel. It may also be a deeper feature excavated into the floodplain with a surface connection to the main channel. This may indicate that the alcove receives hyporheic flow from longer flow paths originating further upstream at this site.

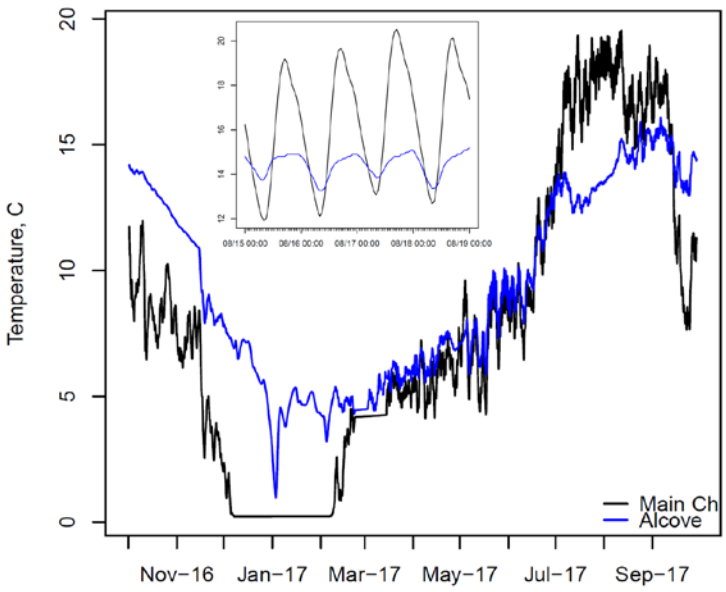

Figure 2. Plot of annual- and daily-scale surface water temperature patterns from a constructed restoration site on Catherine Creek, a tributary to the Grande Ronde River. Main Channel surface temperatures plotted in black and alcove (off-channel feature with surface connection) in blue. Annual time series averaged over a centered 30-day window. Lower average temperature and buffered and lagged pattern indicate potentially longer flow paths sourcing the flow in this alcove. Data from the Confederate Tribes of the Umatilla Indian Reservation: http://gis.ctuir.org/.

Problem Statement

Based on the knowledge of how hyporheic flow lags, buffers, and cools surface water temperatures, are we able to design restoration features that enhance hyporheic exchange and provide thermal refuge for target fish species? First, we must understand how current restoration techniques influence hyporheic exchange. For example, are sharp meander bends coupled with large wood structures facilitating subsurface flow? If the hyporheic exchange is occurring, are water temperatures effectively lagged to provide cooler temperatures during the peak ambient temperature or during the hottest months of the year? Second, can we refine our stream rehabilitation techniques to optimize hyporheic flow path lengths to provide thermal refuge? Finally, are these measures creating thermal refuges in a manner that benefits target species at pertinent seasons and life stages?

To investigate the above questions, we are studying a channel and floodplain restoration project where temperature of surface and subsurface water along with groundwater level are being monitored before and after project construction. These monitoring data will be used to investigate the patterns in surface, subsurface, and spring or side channel water near expected hyporheic flow outlet points in comparison to main channel. Groundwater monitoring well level and temperature data coupled with surface water level and temperature data will help inform where and by how much hyporheic exchange has been influenced as a result of the restoration measures. Biological monitoring will be conducted during warm water seasons to evaluate the presence and density of target species near expected hyporheic flow outlets compared to other areas within the study reach.

Study Area

Our study area, the Bird Track Springs restoration project is located on the upper Grande Ronde River in north eastern Oregon (Figure 3). The project reach is primarily snow melt fed, having an average annual peak discharge of 900 ft^3/s. It is located at approximately 3,100 ft above mean sea level where it experiences extreme swings in seasonal temperature. The study reach currently has relatively low sinuosity (1.2) and average high flows are limited to the main channel, which has a high width to depth ratio and limited riparian vegetation. Low flow in the late summer and winter seasons coupled with these seasonal temperature swings results in high water temperatures in the summer and limited ice-free areas in the winter within the study area. These conditions, especially during the summertime, are a primary concern for salmonid productivity in this region (Torgersen et al., 2012; Justice 2017).

The restoration project goals include an overall increase in the geomorphic complexity of the reach including an increase in sinuosity along the mainstem and the generation of multiple perennial and intermittent side channel flow paths (Figure 4). These constructed flow paths will distribute flow across a broader expanse of the floodplain with the objective of increasing the potential for hyporheic flow as well as a greater variety of habitat conditions for the target species. Smaller-scale features such as alcoves and enhanced longitudinal profile complexity (pools and riffles) may also serve to enhance hyporheic exchange. Inclusion of hundreds of large wood structures across the study area add to the geomorphic complexity of the system. Finally, a

riparian revegetation effort will establish shading and provide new sources of large wood to recruit over the long term.

This restoration project is part of a greater effort in the Upper Columbia River Basin to restore habitat for threatened and endangered salmonid species across their life cycles under commitments of the Bonneville Power Authority, the Bureau of Reclamation, and the Army Corps of Engineers outlined in the 2008 Federal Columbia River Power System Biological Opinion (NOAA Fisheries 2008) and subsequent Supplemental Biological Opinions in 2010 and 2014 (NOAA Fisheries, 2014). The primary project sponsor is the Confederated Tribes of the Umatilla Indian Reservation and the lead design team is the Bureau of Reclamation, Pacific Northwest Regional Office who developed the design in coordination with the project sponsor, the consulting engineer Cardno Entrix, and a host of stakeholders (Bureau of Reclamation, 2017).

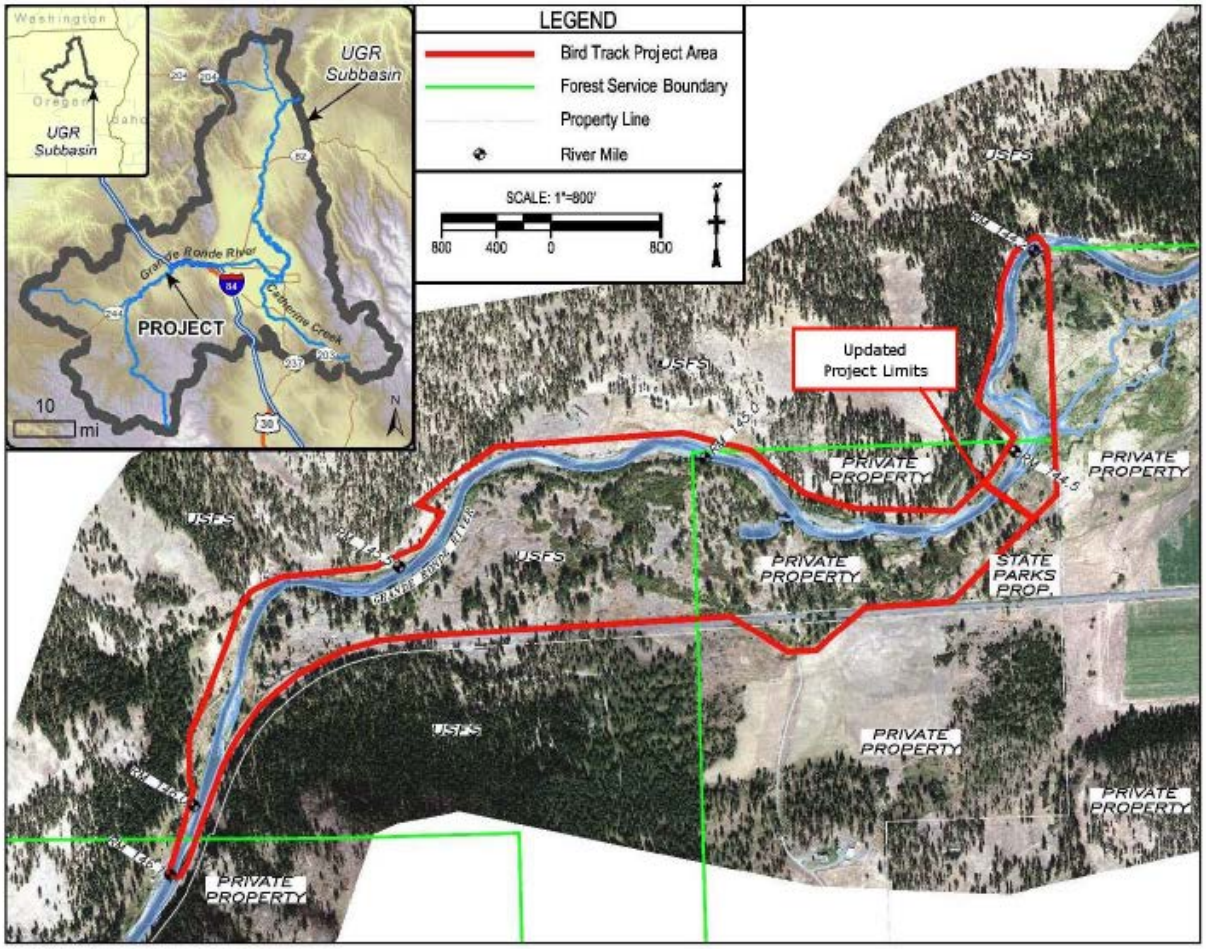

Figure 3. Overview map of study area project. From the Bird Track Springs Basis of Design Report (2017).

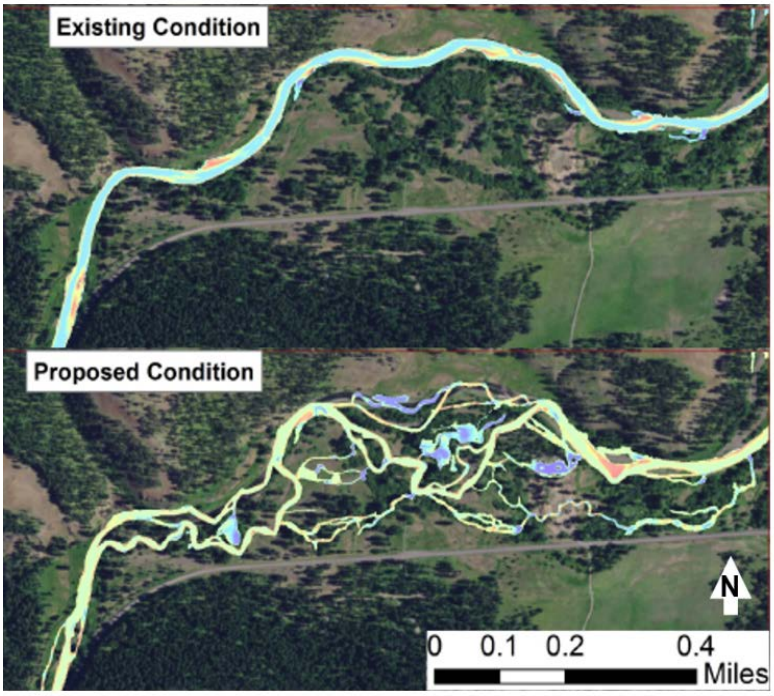

Figure 4. Bird Track Springs project reach showing modeled summer and winter high flow (900 cfs) for existing (top) and proposed (bottom) topographies. From Reclamation (2017).

Data and Methods

Temperature and water level monitoring equipment have been deployed by the Confederated Tribes of the Umatilla Indians personnel across the study area to monitor surface and groundwater stage and temperature (Figure 5). Monitoring data from these sensors collected at hourly intervals before and after restoration construction will be used to make inferences about hyporheic flow paths and to document any lagging or buffering of water temperature at locations of predicted hyporheic outflow. Hydraulic modelling conducted to aid in project design as well as the location of constructed design features like side channels and alcoves will inform predicted outflow locations. Temporary piezometers with stage loggers will be deployed within the main and side channels to evaluate geomorphic unit-scale hyporheic flow (Wondzell, 2006). Spot measurements of surface water temperatures made with a hand-held temperature probe will also be used to identify potential outflow locations. The restoration construction is currently underway and scheduled to be completed by the end of 2019.

Groundwater monitoring wells with 1-inch diameters were installed in 11 locations across the study area (Figure 5). Onset HOBO© U20L-004 pressure and temperature sensors have been deployed in the study area. Onset HOBO© Pendant 64k or TidbiTv2 loggers set to record at 1-hour intervals have been deployed to monitor temperature. One temperature logger was installed within a human-made pond intersecting the alluvial aquifer, referred to as Jordan Cr. Ranch. Each year prior to deployment temperature probes are tested in an ice bath and verified with an NIST certified thermometer.

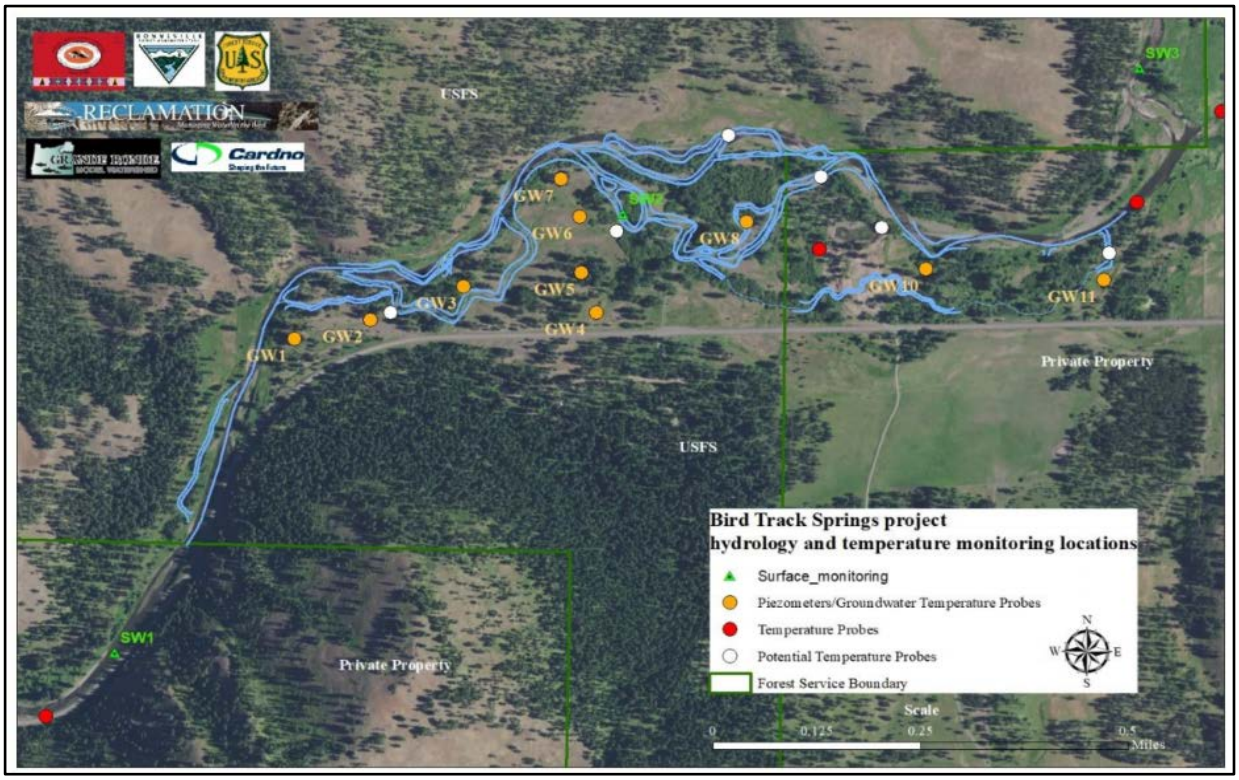

Figure 5. Groundwater level and temperature and surface water level and temperature monitoring locations on the study area. Map from the Confederated Tribes of the Umatilla Indian Reservation (2019).

In this paper we present on a preliminary analysis of main stem and groundwater temperature patterns. Future work will consider the changes in temperature and water level patterns brought on by restoration work. Using time series analysis, we will fit multiparametric sinusoidal functions to temperature time series and compare buffer (amplitude), lag (phase), and average temperature parameters among various monitoring locations sited to observed temperatures at the following types of locations (Figure 6):

1. expected hyporheic inflow locations (surface);
2. floodplain groundwater at along a transect through a meander bend (Figure 5, GW4 to GW7) (subsurface); and,
3. expected hyporheic outflow locations associated with constructed features such as alcoves and side channels (surface).

Time series analysis will allow for statistical comparison of diurnal temperature patterns to discern whether an ecologically significant change has occurred as a result of the restoration project.

Data from surface water stage loggers deployed in the main and side channels will be compared to groundwater stage to develop an understanding of hydraulic gradient and flow rates within the floodplain aquifer. We will evaluate the difference in temperature and elevation of surface and groundwater patterns at daily to seasonal time scales to characterize the influence of restoration at the reach to geomorphic unit scales. Employment of a two-dimensional

groundwater model, such as MODFLOW (Langevin et al., 2018), will be considered to aid in comparing potential hyporheic flow paths prior to and after restoration (Poole et al., 2008). This model would be parameterized with existing subsurface seismic surveys, a LiDAR digital elevation model, and existing 2-D surface hydraulic model-generated surfaces at key flow rates. Temperature and groundwater stage monitoring will be coordinated with planned post-restoration fish monitoring to evaluate if the observed temperature refuges are providing ecologically beneficial temperature and flow patterns.

Figure 6. Existing (blue) and constructed (yellow) low flow planform of Bird Track Springs study area with hypothesized hyporheic flow paths.

Surface-Groundwater Temperature Analysis

Annual Temperature Trends

Main channel temperature values from November 2017 through December 2018 in the study area exhibited a larger range compared to groundwater temperature values (Figure 7). During the summer, main channel water temperature is much warmer than all measured groundwater temperatures. Main channel temperature peaks during July and August with values reaching as high as 23°C, far exceeding the preferred temperature range of juvenile Chinook salmon (10 to 15.6°C, Yanke et al., 2004). Temperature values exceed the 15.6°C upper extent of the preferred temperature range approximately 80 days within the period of record. The DEQ standard of 17.8°C (ODEQ, 2000) was exceeded over 50 days. In contrast, winter main channel water temperature values are lower than groundwater temperature values from October through April. From November to January, stream water temperature values hover around 0°C, occasionally dipping below freezing.

Ground water temperature values are buffered and lagged compared to main channel water temperature values. During the summer, groundwater temperature values are consistently lower than stream temperatures, peaking between 10°C and 16°C, within the DEQ standard threshold of 17.8°C. Peak groundwater temperature occurs in September, lagged from main channel

temperatures by nearly two months. During July and August, ground water temperature is at least 10°C lower than stream temperature. Conversely, ground water temperature values range from 7 to 13°C between November and January. We can conclude that increased hyporheic flow has the potential to cool water in the main channel during the summer and warm surface water temperature during the winter if hyporheic exchange can be enhanced by restoration treatments.

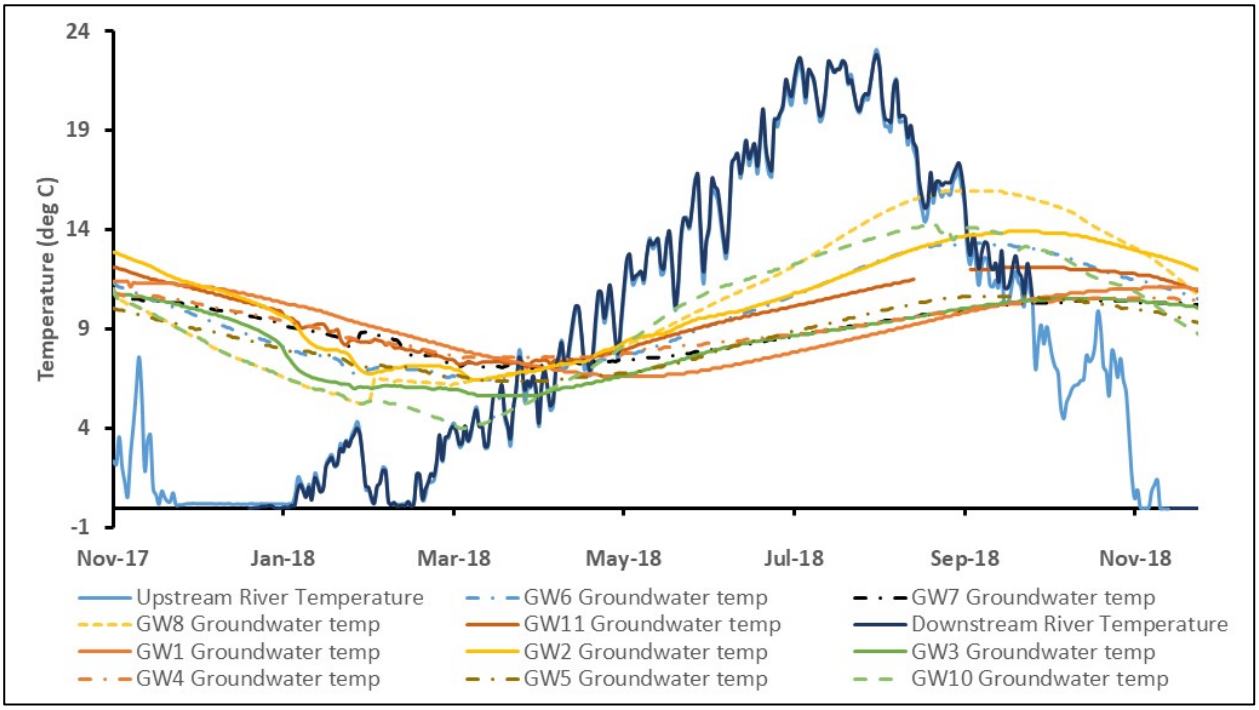

Figure 7. Annual stream water and ground water temperature trends (data provided by CTUIR).

A comparison of average daily data from groundwater wells 4 and 7 (GW4 to GW 7, Figures 5 and 8) reveals that distance from the main channel has a negligible impact on groundwater temperature values and patterns despite differing water level patterns. Wells GW4 to GW7 follow a transect perpendicular to the existing channel starting with GW7 at 140 ft from the main channel centerline to GW4 at 880 feet from the centerline. Groundwater temperature values between the two sites were comparable, differing by ±0.5°C (Figure 8). Therefore, distance from the main channel did not have a noticeable impact on groundwater temperature.

Diel Temperature Trends

Stream temperature data indicate strong diel patterns during the summer months (Figures 9 and 10). Main channel diel temperature ranges are more than 10°C between peak and minimum values. The peak temperature occurs between 16:00 and 18:00 while the coolest time is between 7:00 and 9:00. As seasonal temperatures cool, the variation throughout the day decreases until it is less than 1°C during the coldest months (December and January).

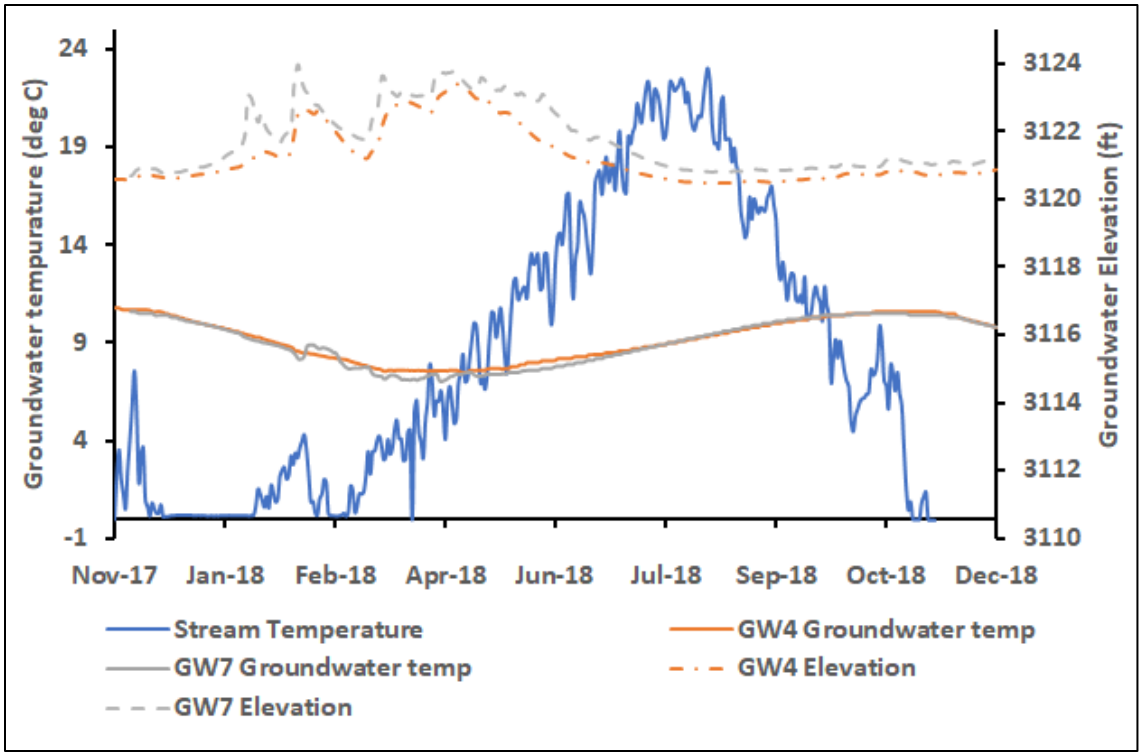

Figure 8. Groundwater temperature and level were compared at GW4 and GW7 to determine if distance from the river had an impact (data provided by CTUIR).

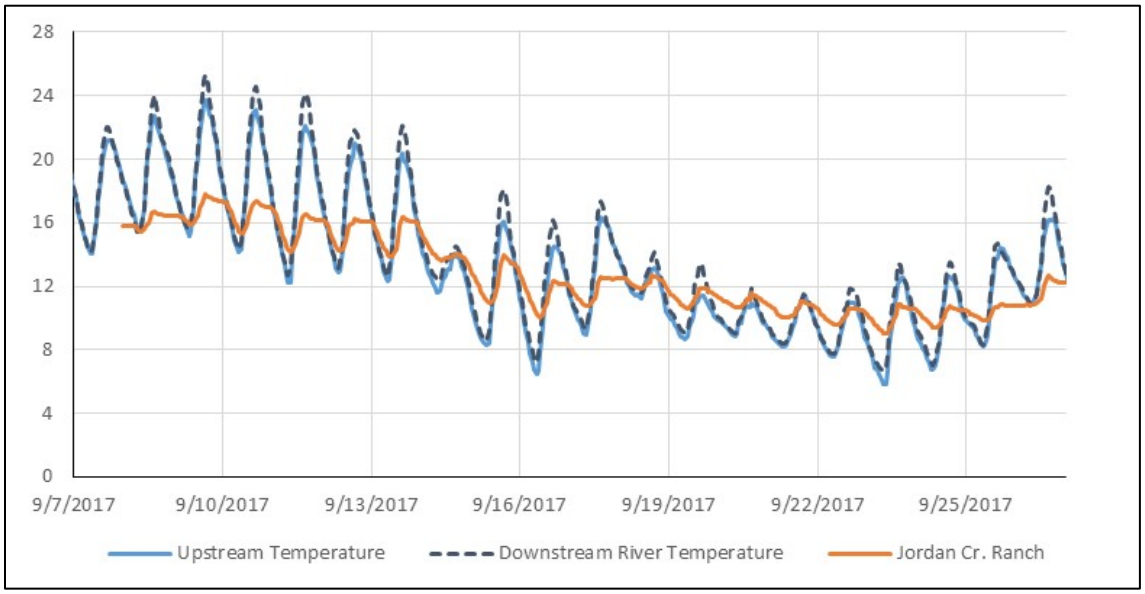

Figure 9. Diel stream temperature patterns (data provided by CTUIR). Downstream temperatures are slightly higher than those observed upstream, confirming that warming is occurring within the project reach. Buffering occurs within a pond fed by the alluvial aquifer (Jordan Cr Ranch).

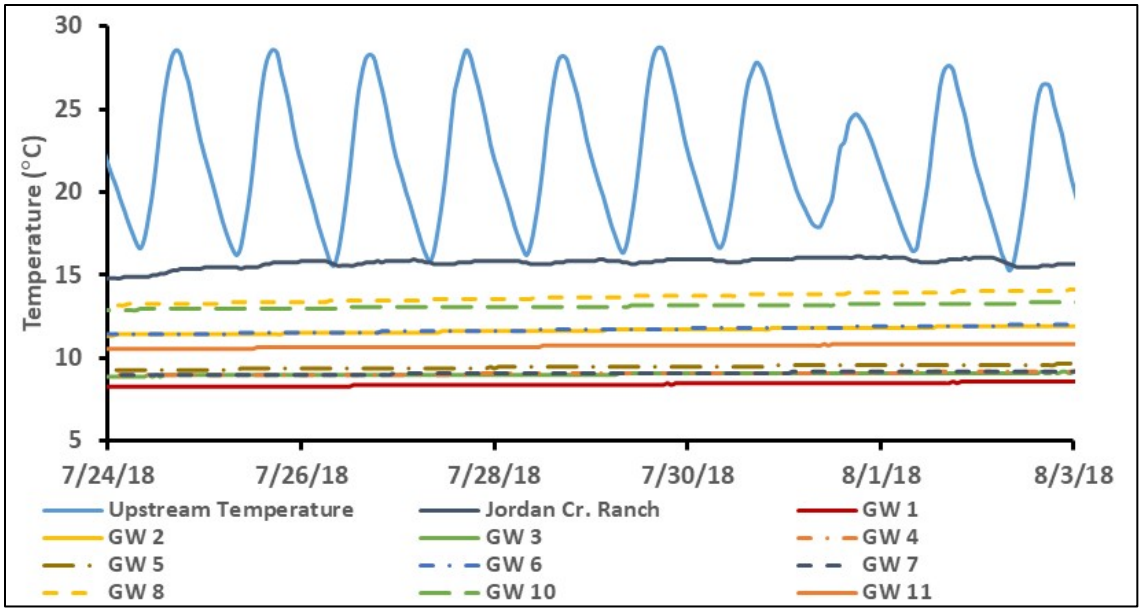

Figure 10. Diel temperature trends within the Bird Track Springs project area during the summer of 2018 (Data provided by CTUIR).

Data indicate that warming occurs from upstream to downstream of the study reach. Higher temperature values were typically recorded at the downstream logger, which is 0.4°C higher on average over the study period. This is likely due to absorption of solar radiation throughout the broad, shallow, minimally shaded channel. The temperature differential between the two gages is evident during peak daily temperature, where the downstream logger can be almost 2°C higher. At the coolest time of day, the upstream temperature logger reads a slightly lower temperature (<1°C).

Groundwater temperature loggers and piezometers recording hourly data were installed in November of 2017. These data show a strong annual trend (Figure 7), but no diel trend (Figure 10). If restoration efforts can increase interaction between surface and groundwater, daily stream temperature values may be buffered or lagged, at least at the local scale where hyporheic outflow occurs. This effect has been observed at other restoration sites in the area (Figure 2) as well as the study site. Data show temperature buffering in the Jordan Cr. Ranch pond. In September 2017 (Figure 9), temperature values ranged from 9°C to 18°C in the pond as opposed to the main channel, where temperature ranged from 6°C to 25°C during the same timeframe. The diel range in temperature is typically less than 2°C in the cold-water pond. A cooling effect is noticeable during the summer of 2018 at this site (Figure 10). Water within the pond maintains a temperature within 14°C to 17°C whereas the main river channel ranges from 15°C to 29°C, temperatures that can be lethal to fish (Becker, 1973). The restoration design will include side channel and pond habitat whose goal is to connect to and interact with the buffered and lagged temperatures of the alluvial aquifer as is observed in this pond.

Conclusion and Next Steps

Comparative temperature time series analysis on a similar and nearby restoration project has resulted in indirect evidence of enhanced hyporheic flow paths resulting in thermal refuge (Figure 2). Analysis of annual- and diel-scale temperature patterns at the study site indicate buffering and lagging of temperatures in the alluvial aquifer compared to the main channel. Additional temperature and stage monitors will be installed to study the influences of geomorphic unit to planform-scale restoration measures on temperature and hyporheic flow patterns (Figure 6). After project construction at the end of 2019, we will continue monitoring surface and groundwater temperature and stage over the next year to compare with the prior years of pre-construction monitoring data. Biological monitoring will be mobilized during the summer of 2020 and continue through 2022. We will also explore the potential of groundwater modelling to aid in interpretation of our observations.

References

Arrigoni, A. S., Poole, G. C., Mertes, L. A. K., O'Daniel, S. J., Woessner, W. W., & Thomas, S. A. 2008. "Buffered, lagged, or cooled? Disentangling hyporheic influences on temperature cycles in stream channels," Water Resources Research, 44(9), 1–13.

Battin, J., Wiley, M.W., Ruckelshaus, M.H., Palmer, R.N., Korb, E., Bartz, K.K. and Imaki, H. 2007. "Projected impacts of climate change on salmon habitat restoration. Proceedings of the national academy of sciences," 104(16), pp.6720- 6725.

Becker, C. D. 1973. "Food and growth parameters of juvenile Chinook salmon, Oncorhynchus tshawytscha, in central Columbia River," U S National Marine Fisheries Service Fish Bulletin. 71 (2), 387-400.

Bureau of Reclamation. 2017. "Basis of Design Report: Draft Final (95%) Bird Track Springs Habitat Improvement Project," Boise, ID. 81p.

Caissie, D., 2006. "The thermal regime of rivers: a review," Freshwater biology, 51(8), pp.1389-1406.

Harvey, J. W., and K. E. Bencala. 1993. "The effect of streambed topography on surface-subsurface water exchange in mountain catchments," Water Resources Research, 29, 89–98, 1993.

Hatch, C.E., Fisher, A.T., Revenaugh, J.S., Constantz, J. and Ruehl, C., 2006. "Quantifying surface water–groundwater interactions using time series analysis of streambed thermal records: Method development," Water Resources Research, 42(10).

Hester, E.T. and Gooseff, M.N. 2010. "Moving beyond the banks: Hyporheic restoration is fundamental to restoring ecological services and functions of streams," Environmental Science and Technology. 44(5): 1521-1525.

Justice, C., White, S.M., McCullough, D.A., Graves, D.S. and Blanchard, M.R., 2017. "Can stream and riparian restoration offset climate change impacts to salmon populations?" Journal of Environmental Management, 188, pp.212-227.

Kasahara, T. and Wondzell, S.M. 2003. "Geomorphic controls on hyporheic exchange flow in mountain streams," Water Resources Research, 39(1), pp.SBH-3.

Konecki, J.T., Woody, C.A. and Quinn, T.P. 1995. "Temperature preference in two populations of juvenile coho salmon, Oncorhynchus kisutch," Environmental Biology of fishes, 44(4), pp.417-421.

Langevin, C.D., Hughes, J.D., Banta, E.R., Provost, A.M., Niswonger, R.G., and Panday, Sorab, 2018. "MODFLOW 6 Modular Hydrologic Model," version 6.0.3: U.S. Geological Survey, https://doi.org/10.5066/F76Q1VQV

NOAA's National Marine Fisheries Service (NOAA Fisheries). 2008. "Endangered Species Act - Section 7 Consultation Biological Opinion and Magnuson-Stevens Fishery Conservation and Management Act Essential Fish Habitat Consultation: consultation on remand for operation of the Federal Columbia River Power System, 11 Bureau of Reclamation Projects in the Columbia Basin and ESA Section 10(a)(1)(A) Permit for Juvenile Fish Transportation Program," NMFS, Portland, Oregon.

NOAA's National Marine Fisheries Service (NOAA Fisheries). 2014. "Endangered Species Act Section 7(a)(2) Supplemental Biological Opinion," NWR-2013-9562. NMFS, northwest Region, Portland, Oregon. 610p.

ODEQ (Oregon Department of Environmental Quality). 2000. "Upper Grande Ronde River Sub-Basin Total Maximum Daily Load (TMDL)," Oregon Department of Environmental Quality, Water Quality Division, Portland, Oregon.

Poole, G. C., O'Daniel, S. J., Jones, K. L., Woessner, W. W., Bernhardt, E. S., Helton, A. M., ... Beechie, T. J. 2008. "Hydrologic spiralling: the role of multiple interactive flow paths in stream ecosystems," River Research and Applications, 21, 14. https://doi.org/10.1002/rra.1099

Ruesch, A.S., Torgersen, C.E., Lawler, J.J., Olden, J.D., Peterson, E.E., Volk, C.J. and Lawrence, D.J. 2012. "Projected climate-induced habitat loss for salmonids in the John Day river network, Oregon, USA," Conservation Biology, 26(5), pp.873-882.

Schindler, D.W. 1997. "Widespread effects of climatic warming on freshwater ecosystems in North America," Hydrological Processes, 11(8), pp.1043-1067.

Tonina, D. and Buffington, J.M., 2009. "Hyporheic exchange in mountain rivers I: Mechanics and environmental effects," Geography Compass, 3(3), pp.1063-1086.

Torgersen, C., Ebersole, J., & Keenan, D. 2012. "Primer for identifying cold-water refuges to protect and restore thermal diversity in riverine landscapes," EPA scientific guidance handbook. Seattle, WA. 91p. https://doi.org/EPA 910-c-12-001

Wroblicky, G. J., M. E. Campana, H. M. Valett, and C. N. Dahm. 1998. "Seasonal variation in surface-subsurface water exchange and lateral hyporheic area of two stream-aquifer systems," Water Resour. Res., 34, 317– 328, 1998.

Wondzell, S. M. (2006). "Effect of morphology and discharge on hyporheic exchange flows in two small streams in the Cascade Mountains of Oregon, USA," Hydrological Processes 20, pp. 267–287.

Yanke, J.A., B.C. Jonasson, F.R. Monzyk, S.M. Nesbit, A.G. Reischauer, E.S. Van Dyke, R.W. Carmichael. 2004. "Investigations into the Early Life History of Naturally Produced Spring Chinook Salmon and Summer Steelhead in the Grande Ronde River Subbasin," Oregon Department of Fish and Wildlife, La Grande, Oregon.

The Stream Evolution Triangle

Janine Castro, Project Leader, US Fish and Wildlife Service, Vancouver WA, janine_m_castro@fws.gov.

Colin Thorne, Chair of Physical Geography, University of Nottingham, Nottingham UK, colin.thorne@nottingham.ac.uk.

Extended Abstract

River restoration science is firmly rooted in the fields of geology, hydrology, and engineering, yet the objective of many stream restoration projects is biological recovery. Lane's stream balance equation from the mid-1950s described the relationship between the amount of stream flow, the slope of the channel, and the amount and caliber of sediment, but it did not incorporate the influence of biology (Lane 1955). Stream classification systems and channel and stream evolution models utilized in river restoration design today (Montgomery and Buffington 1993; Rosgen 1996; Schumm *et al.* 1984; Simon and Hupp 1986; Cluer and Thorne 2014) still do not explicitly include biology as a primary driver for stream process and morphology. To correct this imbalance, we place biology equal to both geology and hydrology, forming a triad that dictates stream morphology and evolution.

The Stream Evolution Triangle (SET) is a new approach to understanding stream evolution. The SET broadly integrates geology, hydrology, and biology, to support improved understanding of potential morphological "stream evolution stages" at the reach scale - following either natural or anthropogenic disturbance. In determining stream morphology, the SET treats the relative influences of geology, hydrology, and biology on an equal basis, recognizing that a stream may be dominated by any of these three drivers depending upon its landscape setting and geographic location. Consequently, within the SET it is possible to delineate process-domains, stream types, and evolutionary stages associated with many well-established stream classification systems (Figure 1).

Rather than a deterministic approach, the SET recognizes that similar events can result in various stream morphologies, while dissimilar events can result in a single, dominant stream type. The probability of a particular future state is dependent on the relative influences of geology, hydrology, and biology. The SET represents dynamic morphological evolution through time, recognizes that rates of change are variable through both spatial and temporal dimensions, and that evolution has numerous potential trajectories. With the SET, we frame a conceptual thinking space comprehensive enough to encompass a wide range of process-drivers, transitory stream forms, and evolutionary pathways, but simple enough to allow for creative thinking and rapid evaluation of both established and new ideas (Jackson *et al.* 2000).

The originality of the SET is its unequivocal recognition of biology as a process driver, from which improved understanding of the reach-scale dynamic-response mechanisms follow. Thus, the SET widens the lens through which hydraulic engineers, hydrologists, and geomorphologists perceive rivers, from one based primarily on physics-based science, to one that incorporates biological processes. In the SET, the balance between hydrology and geology as conceptualized by Lane (1955) forms the base of the triangle, along which biological influence is minimal. The addition of biology, which forms the apex of the SET - where biology is the dominant driver - creates two additional axes, thus allowing for the full incorporation of an array of stream types that includes forms reliant on biological processes. For example, the influence of vegetation, and particularly trees, on stream morphology is documented in the sedimentary record, where a

relationship exists between the evolution of vegetation in stream systems and planform transitions from braided to meandering and anastomosed (Davies and Gibling 2009). To further support this contention, there is evidence in the geologic record of an abrupt change from meandering back to braided planforms in South African rivers following a mass extinction event about 250 million years ago, during the Permian-Triassic transition, which essentially eliminated vegetation from the landscape for approximately 5 million years (Ward *et al.* 2000).

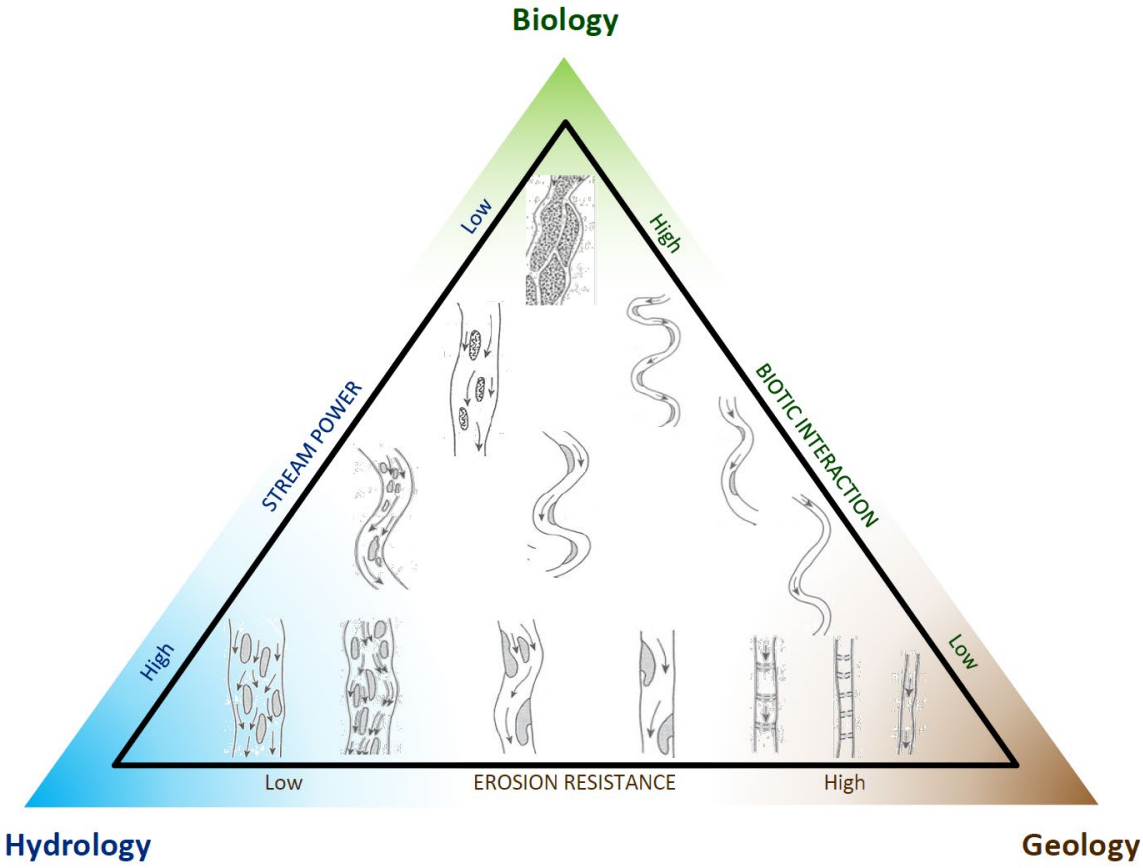

Figure 1. The Stream Evolution Triangle (SET) with planform patterns defined by Schumm (1985) illustrating typical morphologies expected to occur in different process domains. The SET represents the relative influences of geology (erosion resistance), hydrology (stream power), and biology (biotic interaction). From Castro and Thorne (2019).

Potential utility of the SET in stream restoration planning and design stems from improved understanding and explanation of morphological "stream evolution stages", which provides insights into appropriate restoration strategies to counter adverse impacts from past disturbance, while building resilience to future disturbance. The SET can do this because stream evolution is not framed as a deterministic sequence of stages. Fluvial geomorphology acknowledges that disturbance may result from a variety of natural events or human actions that affect watershed runoff, sediment discharge, or the channel's morphology and erosion resistance (Knighton 1998). In river management and restoration, channel response resulting from vegetation removal or loss has been understood for decades (Thorne *et al.* 2010). More recently, disturbances that impact connectivity in stream/floodplain systems are receiving increasing attention (Wohl *et al.* 2018), while the significance of changes to watershed, stream, and aquatic ecology due to climate change is now well-established (Atkinson *et al.* 2018).

The SET reveals that, for post-disturbance recovery to be robust and enduring, some degree of biological uplift is essential, and re-establishment of a healthy and functional ecosystem (represented by upward migration in the SET) depends on the rate of biological recolonization compared to the frequency of physical or biological disturbance (Shafroth *et al.* 2002). The SET can aid understanding in both the impact of a disturbance and recovery at the reach and system-scales, because it represents causal relationships between changes in the process-drivers and the types of disturbance, morphological response, and evolutionary trajectory that result. In this context, restoration of disturbed streams should facilitate either recovery to the pre-disturbed condition or evolution to a new and resilient morphology. Either pathway involves biological uplift. What restoration should not seek to do is lock a disturbed stream into an artificially stabilized form using engineered structures.

Rapid biological uplift achieved through full reconnection of the channel/floodplain network is illustrated by Whychus Creek, Oregon. The unrestored, incised channel plots near the Geology corner (Figure 2a) due to its erosion resistant bed and banks. Intentional filling of the incised channel, as part of a 'Stage Zero' restoration, reconnects the stream to its floodplain, and moves the system towards the Hydrology corner immediately following construction (Figure 2b). Natural colonization by aquatic, wetland and riparian plants and animals then shifts Whychus Creek towards the Biology corner (Figure 2c), following a path along the Hydrology-Biology edge of the triangle.

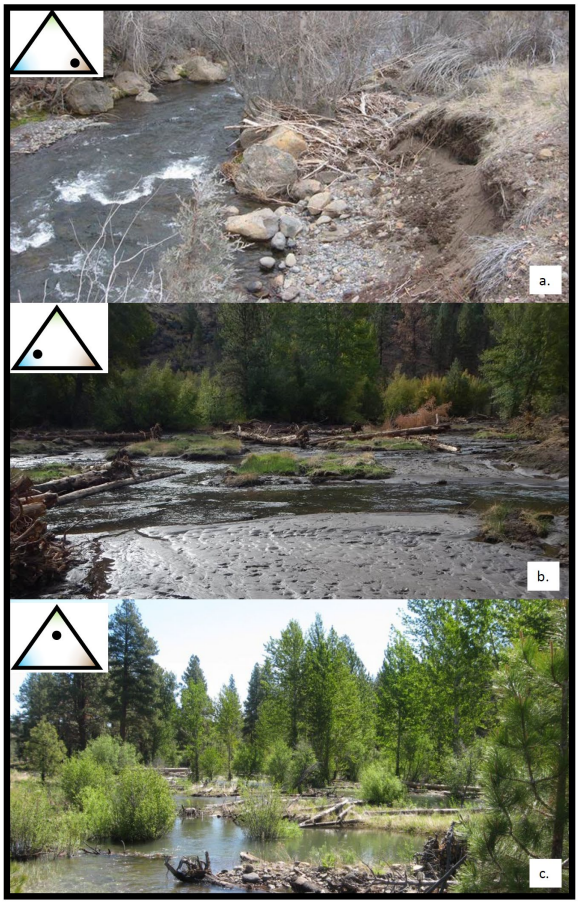

Figure 2. Whychus Creek, Oregon, restoration project phases over one year. Photos courtesy of Paul Powers, from Castro and Thorne (2019).

In summary, the purpose of the SET is to create an expansive 'thinking space'. It is not intended to exclude or supersede any existing stream classification systems or evolutionary models. However, the foundations of existing classifications and models implicitly assume that river form is derived from physical interactions between flow, sediment, and channel boundary materials, which limits their explanatory capability, given the significant effects of biota in many of our stream systems. Hence, in the SET, we cast biology as an equal partner with geology and hydrology, forming a triad that dictates stream morphology, drives morphological adjustment, and directs the paths along which disturbed streams evolve. The SET thus recognizes that the form, function, and evolutionary trajectory of a river system may be dominated by a single driver, a pair of drivers, or (more commonly) some combination of all three, depending on the watershed and land management contexts.

References

Atkinson, C.L., Allen, D.C., Davis, L. and Nickerson, Z.L. 2018. Incorporating ecogeomorphic feedbacks to better understand resiliency in streams: a review and directions forward. *Geomorphology*, 305, 123-140.

Castro, J.M. and Thorne, C.R. 2019. The stream evolution triangle: integrating geology, hydrology, and biology, *River Research and Applications*, DOI: 10.1002/rra.3421.

Cluer, B.L. and Thorne, C.R. 2014. A stream evolution model integrating habitat and ecosystem benefits, *River Research and Applications*, 30(2),135-154.

Davies, N.S. and Gibling, M.R. 2009. Cambrian to Devonian evolution of alluvial systems: the sedimentological impact of the earliest land plants, *Earth-Science Reviews*, 98(2010),171-200.

Jackson, L.J., Trebitz, A.S. and Cottingham, K.L. 2000. An introduction to the practice of ecological modelling, *BioScience*, 50(8), 694-706.

Knighton, D. 1998. *Fluvial Forms and Processes: A New Perspective*. London: Routledge.

Lane, E.W. 1955. Design of stable channels, *Transactions of the American Society of Civil Engineers*, Paper No. 2776, 1234-1279.

Montgomery, D. and Buffington, J. 1993. Channel classification, prediction of channel response, and assessment of channel condition, Report TFW-SH10-93-002 for the SHAMW committee of the Washington State Timber/Fish/Wildlife Agreement, Seattle WA: University of Washington, 84 p.

Rosgen, D.L. 1996. *Applied River Morphology*, Pagosa Springs, Colorado: Wildland Hydrology.

Schumm, S.A. 1985. Patterns of alluvial rivers, *Ann. Review Earth Planet. Sci.*, 13, 5-27.

Schumm, S.A., Harvey, M.D. and Watson, C.C. 1984. Incised channels: morphology, dynamics, and control, *Water Resources Publications,* Littleton, CO.

Simon, A. and Hupp, C.R. 1986. Geomorphic and vegetative recovery processes along modified Tennessee streams: an interdisciplinary approach to disturbed fluvial systems. *Forest Hydrology and Watershed Management*, *IAHS-AISH Publ.167.*

Shafroth, P.B., Stromberg, J.C. and Patten, D.T. 2002. Riparian vegetation response to altered disturbance and stress regimes, *Ecological Applications*, 12(1), 107–123.

Thorne, C.R., Soar, P.J., Skinner, K.S., Sear, D.A. and Newson, M.D. 2010. Investigating, characterising and managing river sediment dynamics, In, *Guidebook of Applied Fluvial Geomorphology*, Sear, D.A., Newson, M.D. and Thorne, C.R. (eds), London: Thomas Telford, pp 120–195.

Ward, P.D., Montgomery, D. and Smith, R. 2000. Altered river morphology in South Africa related to the Permian-Triassic extinction, *Science*, 289, 1740-1743.

Wohl, E., Brierley, G., Cadol, D., Coulthard, T.J., Covino, T., Fryirs, K.A., Grant, G., Hilton, R.G., Lane, S.N., Magilligan, F.J. and Meitzen, K.M. 2018. Connectivity as an Emergent Property of Geomorphic Systems, *Earth Surface Processes and Landforms*, published online, DOI: 10.1002/esp.4434.

Water Quality

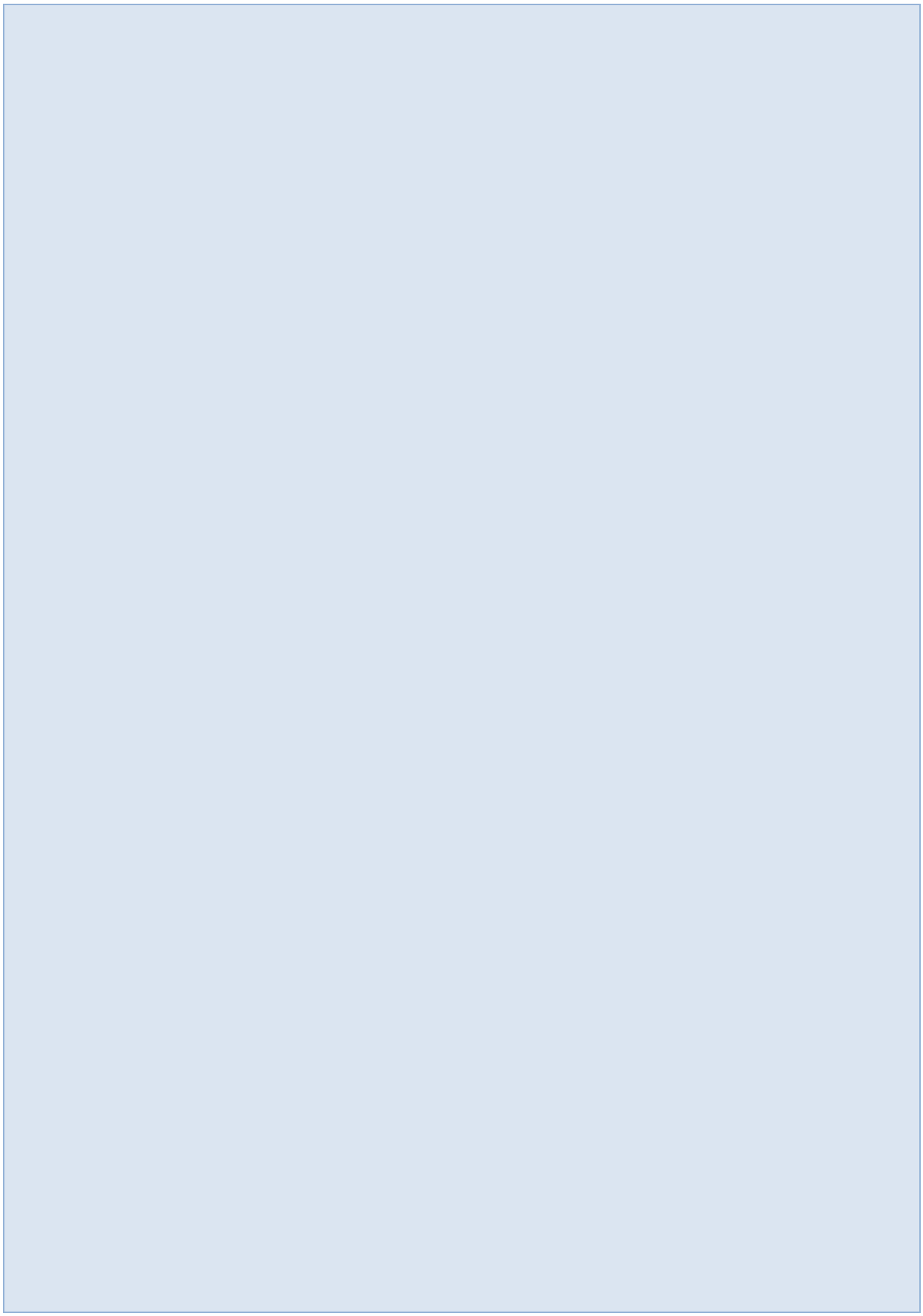

A 2D Depth-Averaged Water Quality Model: Coupling of SRH-2D and NSMI

Yong G. Lai, Hydraulic Engineer, Bureau of Reclamation, Denver, CO, ylai@usbr.gov
Joel Sholtes, Instructor, Colorado Mesa University, Grand Junction, CO, jsholtes@gmail.com
Zhonglong Zhang, Research Professor, Department of Civil and Environmental Engineering, Portland State University, Portland, OR, zhonglong.zhang@erdc.dren.mil

Abstract

Acceptable water quality values have been established by government regulators; they impose constraints on the allowable discharges into streams and reservoirs. Existing tools based on low-order modeling simplify a stream to a simple line with limited spatial distribution of inputs and poor representation of the relevant processes. In this study, a two-dimensional (2D) depth-averaged water quality model is developed by coupling with the flow model SRH-2D and the plug-in water quality module NSMI. SRH-2D is a 2D depth-averaged flow and sediment transport model developed at the Bureau of Reclamation. The 2D model incorporates data with both lateral and longitudinal geographic extents rather than lumping heterogeneous spatial results into a point-to-point or uni-directional representation. NSMI is a water quality module developed at the US Army Corps of Engineer (USACE) and distributed as a dynamic linked library. NSMI simulates aquatic dissolved oxygen, carbonaceous biological oxygen demand, nitrogen and phosphorus cycles, and algae biomass with simplified processes and minimum state variables. The technical details are described along with the coupling approach adopted. The new water quality model is tested and verified at the Lower Minnesota River. Good results are obtained.

Introduction

Water quality constituents and contaminants are introduced into aquatic systems through both natural means and human activities. The U.S. Environmental Protection Agency (EPA) and State EPAs have developed water quality standards for the nation's impaired waterbodies. In order to more fully understand the factors affecting water quality and to control water quality to meet these water quality criteria, numerical modeling tools have been widely used to evaluate and predict the fate and transport of contaminants and water quality constituents in the environment. Water quality models are often coupled with existing hydrologic and hydraulic (H&H) models for environmental analysis or water quality forecasting. Existing tools are mostly based on low-order modeling, simplifying a stream to a simple line with limited spatial distribution of inputs and poor representation of the physics of the processes. The limited spatial extents restrict the usefulness of low-order modeling for such features as agricultural returns, gravel pits, groundwater upwelling, side channel activation, and streamside vegetation. It also imposes a limitation on fish habitat assessment and reoperation outside the range of the calibration datasets. Differing levels of H&H models have been adopted over the last three decades and discussed by Bahadur et al. (2013). The water quality models using the multi-dimensional spatial representation are still limited.

In the area of stream and reservoir models, however, two-dimensional (2D), depth-averaged H&H models have been mature; examples include HEC-RAS (HEC, 2010), AdH (Berger et al., 2012), and SRH-2D (Lai, 2008). There is a need to extend these models to include water quality modeling capabilities to advance the state-of-the-art. Recognizing this need, the Environmental Quality Technology Research Program at the U.S. Army Corp of Engineers (USACE) sponsored research and development into water quality and contaminant simulation modules designed to be coupled to the general H&H models. The final products of these efforts are the NSM, CSM and HgSM modules (Zhang and Johnson, 2016a; b).

In this study, an effort is reported to develop a 2D water quality model that couples a 2D depth-averaged H&H model (SRH-2D) and the USACE water quality module NMSI. This new 2D water quality model is named SRH-WQ. The hydrodynamic model SRH-2D was developed at the Bureau of Reclamation (Lai 2008; 2010). The 2D model incorporates data with both lateral and longitudinal geographic extents rather than lumping results into a point-to-point or uni-directional representation. The objective is to improve the representation of spatial features where low-order models resort to empiricism for a lumped treatment. Better representation of processes leads to increased predictability and accuracy and higher confidence. The water quality module NSMI (Nutrient Simulation Module I) was developed at the US Army Corps of Engineer (USACE), Engineering Research and Development Center (Zhang and Johnson, 2016a). It was designed to simulate aquatic dissolved oxygen, carbonaceous biological oxygen demand, nitrogen and phosphorus cycles, and algae biomass with simplified processes and minimum state variables.

In the following, the numerical techniques are presented on the coupling of the hydrodynamic and water quality models. The development focuses on the model robustness and ease-of-use for engineering applications. The new model, SRH-WQ, is tested and verified by applying it to the Lower Minnesota River.

The Numerical Model

The details of the numerical model SRH-2D may be found in Lai (2008; 2010) and are not repeated herein. Basically, water flows in streams and reservoirs are assumed to be relatively shallow so that the effect of vertical motion is negligible. The three-dimensional Navier-Stokes equations are vertically averaged to obtain a set of depth-averaged 2D flow equations which are the well-known St. Venant or dynamic-wave equations. SRH-2D simulates the flow hydrodynamics so that the hydraulic variables such as water stage and depth, velocity components, and bed shear stress are predicted at any point in a 2D horizontal space and at any time for the simulation duration.

The water quality constituents, solids or chemical species are moving through the waterbody and they are described by the unsteady 2D shallow-water transport equation. The scalar transport equation is written in a general form for any constituent as:

$$\frac{\partial hC}{\partial t}+\frac{\partial hUC}{\partial x}+\frac{\partial hVC}{\partial y}=\frac{\partial}{\partial x}\left(hD\frac{\partial C}{\partial x}\right)+\frac{\partial}{\partial y}\left(hD\frac{\partial hC}{\partial y}\right)+S \qquad (1)$$

In the above, C is the depth-averaged value of the scalar, $D=\frac{\upsilon_t}{\sigma_C}$ is the diffusivity, and σ_C is the Schmidt number. If the scalar is a water quality constituent, C is the depth-averaged volume

concentration (m^3/m^3) and *hC* is the scalar volume per unit bed area. The volume concentration (*C*) may be converted to the mass concentration in kilograms per unit volume by multiplying *C* with the density of the constituent.

Equation (1) is discretized similarly to that used by SRH-2D (Lai, 2010). That is, the finite volume method is adopted in space and the implicit method is used in time. The 2D mesh may assume a polygonal mesh cells which are the most flexible among mesh options. What is special in the above equation (1) is the treatment of the source term as it can be very large, potentially leading to numerical instability and solution inaccuracy. Two options are developed in the present study.

The first is the linearization method for which the source term is linearized according to the following equation:

$$S = Su - Sp\,C \tag{2}$$

where *Su* represents all those treated explicitly and *Sp* includes all treated implicitly. This method is highly suitable for some scalars. For example, the source term of temperature may be expressed as $k(T_{eq} - T)$ where T_{eq} represents the equilibrium temperature and *k* is the rate of recovery.

The second method adopts the operator splitting technique reported by Savant and Berger (2012). That is, equation (1) is split into two separate procedures:

$$\frac{\partial hC}{\partial t} + \frac{\partial hUC}{\partial x} + \frac{\partial hVC}{\partial y} = \frac{\partial}{\partial x}\left(hD\frac{\partial C}{\partial x}\right) + \frac{\partial}{\partial y}\left(hD\frac{\partial hC}{\partial y}\right) \tag{3}$$

$$\frac{\partial hC}{\partial t} = hS(C,t) \tag{4}$$

The first equation (3) is the convection-diffusion equation with zero source term which may be viewed as a typical hyperbolic initial value problem. The implicit numerical procedure is used to obtain an intermediate solution C_* from the prior-time solution C_n. Since an implicit scheme is used, a very large time step may be used. The second equation (4) is a typical non-linear ordinary differential equation, and we follow the procedure of Savant and Berger (2012) to obtain the solution C_{n+1} at the new time when C_* is known. The embedded fifth-order Runge-Kutta (RK5E) numerical integration scheme is adopted, combined with the use of the adaptive time-stepping. A detailed description of RK5E procedure and program was provided by Cash and Karp (1990) and Press et al. (1992) and not repeated herein. The use of the operator splitting technique has the advantages that the set of water quality equations for all transported state variables are solved simultaneously, which takes into account the complex nonlinear interactions among state variables.

Finally, the source terms in (1) for all water quality state variables are yet to be determined; they are computed by the NSMI module. The source terms of all state variables are represented as nonlinear, complex functions within NSMI. These functions are governed by physical, chemical and biological processes. Detailed descriptions are documented in the report of Zhang and Johnson (2016a); only a brief summary is provided below.

Vertically averaged water temperature is a key state variable simulated by SRH-WQ. It is an important water quality measure by itself. Most water quality hydrochemistry parameters are functions of temperature which affects most biological and chemical reactions. In general, temperature is included solved. The temperature module applies the energy balance equation in each mesh cell. Heat inputs and outputs at the water surface and at the water-sediment interface are included. Simulated heat exchanges at the water surface include: (a) solar radiation, (b) atmospheric radiation, (c) back radiation from water to atmosphere; (d) evaporation/condensation (latent heat); and (e) heat conduction (sensible heat). Direct heat inputs/outputs through the open flow boundaries are treated separately through the boundary conditions in solving the temperature transport equation.

The aquatic eutrophication is simulated by NSMI using simplified hydrochemistry processes and a minimal number of state variables. It computes biochemical reactive processes affecting state variables within each mesh cell. Time rate of production (source) or destruction (sink) of a constituent for each state variable is computed by NSMI; it is the source term of equation (1). NSMI includes up to 16 state variables to simulate water quality within a waterbody. These state variables include algae, nitrogen and phosphorus cycles, carbon cycle, carbonaceous biochemical oxygen demand, dissolved oxygen, and pathogens within a water column. NSMI does not simulate benthic sediment processes through sediment diagenesis; such a simulation requires the use of another module named NSMII. The 16 state variables of NSMI are as follows:

- 3 nitrogen cycle variables: organic nitrogen, ammonium, and nitrate (OrgN; NH4; NO3)
- 2 phosphorus cycle variables: organic phosphorus and inorganic phosphorus (OrgP; TIP)
- 3 carbon cycle variables: particulate and dissolved organic carbon and dissolved inorganic carbon (POC, DOC, DIC)
- 2 algae variables: benthic algae (A_b) and floating algae (Ap -phytoplankton)
- 6 other variables: dissolved oxygen (DO); carbonaceous biochemical oxygen demand (CBOD); particulate organic matter (POM); sediment particulate organic matter (POM2); pathogens (PX); and alkalinity(Alk)

Among the 16 state variables, only 14 state variables are transported by SRH-WQ since A_b and POM2 are within the sediment layer, not in the water column.

In addition to the above 16, a benthic sediment layer variable used by NSMI is the sediment oxygen demand (SOD). SOD is the rate of oxygen consumption by the benthic sediments and is a user input. The pH of the water column is also an important factor because some chemical processes are initiated only after the water column exceeds certain pH thresholds. The pH of the water column determines the solubility and biological availability of chemical constituents such as nutrients (nitrogen, phosphorus and carbon) and heavy metals (lead, copper, cadmium, etc.). The pH affects the ionization and hydrolysis of organic chemicals which have effects on chemical fate and the degree of chemical toxicity to biota. The pH is computed in NSMI based on DIC and alkalinity.

A typical SRH-WQ simulation proceeds as follows. First, SRH-2D is used to simulate water flow in a stream and/or reservoir without considering the water quality processes. Such a flow simulation has been carried out routinely for numerous water resource projects. Simulated flow variables such as water depth, velocity and bed shear stress are saved to memory at user-

specified time intervals. Also saved are the model domain and 2D mesh information. These flow simulation results are inputs to SRH-WQ. Next, SRH-WQ is used to simulate the physical and biochemical processes represented by the water quality state variables. The transport module simulates the physical processes of advection and dispersion of all state variables, along with inflows and outflows represented by these variables across open boundaries. The 2D transport module is responsible for transport represented by these state variables throughout the model domain. The internal sources and sinks at each water quality mesh cell are computed using NSMI. In the final step, SRH-WQ writes out simulated state variables, along with other dependent, derived and pathway variables, at a user-specified time interval so that the model results may be graphically processed for interpretation and application. A typical water quality simulation may involve more than 20 state variables and 50 dependent, derived and pathway variables. The WQ simulation thus requires a large number of input parameters and significant computer memory, storage and computing resources.

Results and Discussion

SRH-WQ model was tested and verified by applying it to the Lower Minnesota River, MN where a plethora of water quality observations exist. Water quality data were available at multiple locations so that the new model may be demonstrated with a practical stream.

Background

The Lower Minnesota River simulated herein comprises the lower 37 miles of the Minnesota River up to its confluence with the Mississippi River upstream of St. Paul, MN. A variety of tributaries enter the river within this segment, along with point source discharges from waste-water treatments plants as well as a withdrawal and discharge from a power generation plant (Figure 1). This segment of river suffers from low dissolved oxygen levels associated with nitrogen and phosphorus loading from point and non-point sources and subsequent algae production. It also exhibits high levels of turbidity, fecal bacterial contamination, as well as mercury and PCBs (MPCA, 2008). As such, Total Maximum Daily Load (TMDLs) and load allocation studies have been developed for various water quality constituents for the study area (MPCA 2004, 2007). Many main stem and tributary gages exist within the study area providing hydraulic and water quality model boundary condition, calibration, and validation data. These are documented in Smith et al. (2012).

A number of hydraulic and water quality models have been developed and applied for the river section. These include a one-dimensional HEC-RAS hydraulic model coupled with the NSMI (Zhang and Johnson, 2014), as well as a 2D coupled hydraulic and water quality model CE-QUAL-W2 (Smith et al., 2012). Both models have been calibrated and validated as documented in the above-referenced reports.

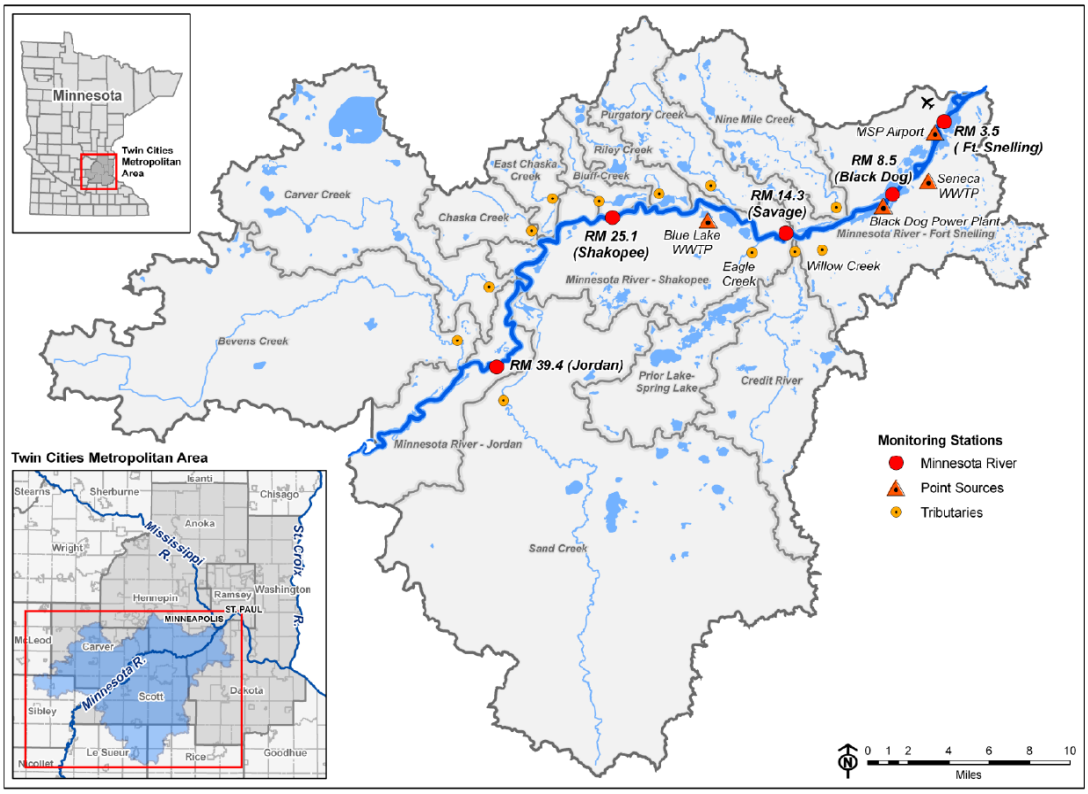

Figure 1. Overview map of lower Minnesota River study area (figure from the Metropolitan Council Environmental Services, St Paul, MN).

Flow Modeling

Flow simulation is carried out first with SRH-2D using the 2D mesh provided by the creators of the W2 model (Smith et al., 2012). The topographical data are not altered. This mesh was generated from HEC-RAS model cross-sections coupled with 10-meter resolution above-water elevation data. Tributary channels are artificially-represented as straight trenches moving flow directly from the mesh boundary to the main channel. A portion of the mesh is shown in Figure 2.

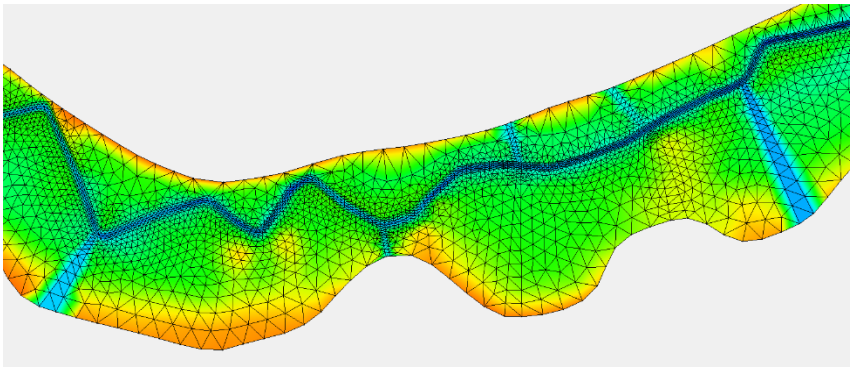

Figure 2. An example of river and floodplain bathymetry with 2D mesh and artificial tributary trenches.

Manning's roughness coefficient is the only recommended calibration parameter for the SRH-2D flow modeling. The RAS model used four roughness zones to represent the land use types:

the main stem and tributary channels (n = 0.025 to 0.03), riparian area (n = 0.05), overland area (n = 0.05), and islands (n = 0.06). SRH-2D needs to adopt a different set of roughness coefficient as a 2D model needs typically less roughness. After the unsteady flow test of three sets of roughness coefficient, the final calibrated SRH-2D set is as follows: a constant n = 0.02 in the main stem and tributary channels and the same values as the RAS model in other areas. This set of *n* values minimized the root mean square error of modeled and measured discharge and stage over several calibration points within the model. No calibration is carried out to vary n spatially as we find that the water quality results are insensitive to the flow roughness although flow variables themselves are.

Boundary conditions for SRH-2D modeling include the time series discharge data at the upstream and tributary inflows. At the confluence with Mississippi, stage time series data are used. These data are extracted from the existing W2 and RAS models. Most data are daily values. Stage and discharge gages located within the study area are used for model calibration and validation. Data sources for these boundary conditions and internal gauge locations are described in detail in Smith et al. (2012).

The unsteady flow simulation starts on January 1, 2004 and ends in January, 2006, a two-year simulation. The time step used for the simulation is one second.

The SRH-2D flow simulation results are compared with available gauge results. Two gages are within the model domain: a USACE/National Weather Service stage gage on the Minnesota River at Savage (SAVM5; RM 13) and a USGS stage and discharge gage on the Minnesota River at Ft. Snelling (05330920; RM 3.5). Comparisons of SRH-2D model outputs and observations are provided in Figures 3 and 4. The model run visually shows a reasonable fit between observations and predictions with the exception of stage at the Savage gauge. Here, stage is over-predicted. This may be due to an inaccurate representation of the river bathymetry within the provided mesh. Note that stage is also under-predicted for peak flows at the upstream model boundary and predicted well at the Fort Snelling gage. This may be influenced by model boundary conditions and should not be weighted heavily.

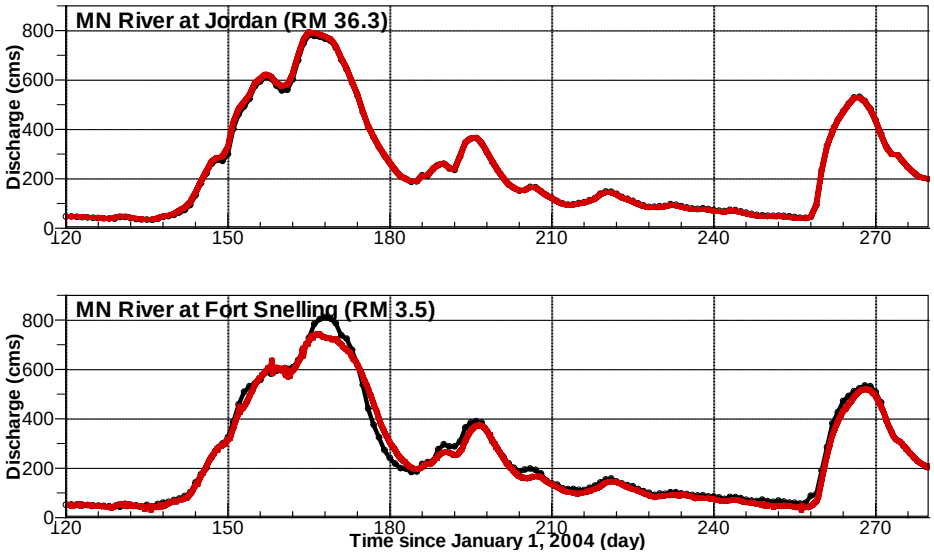

Figure 3. Daily average discharge comparison. Red: SRH-2D; Black: Observation.

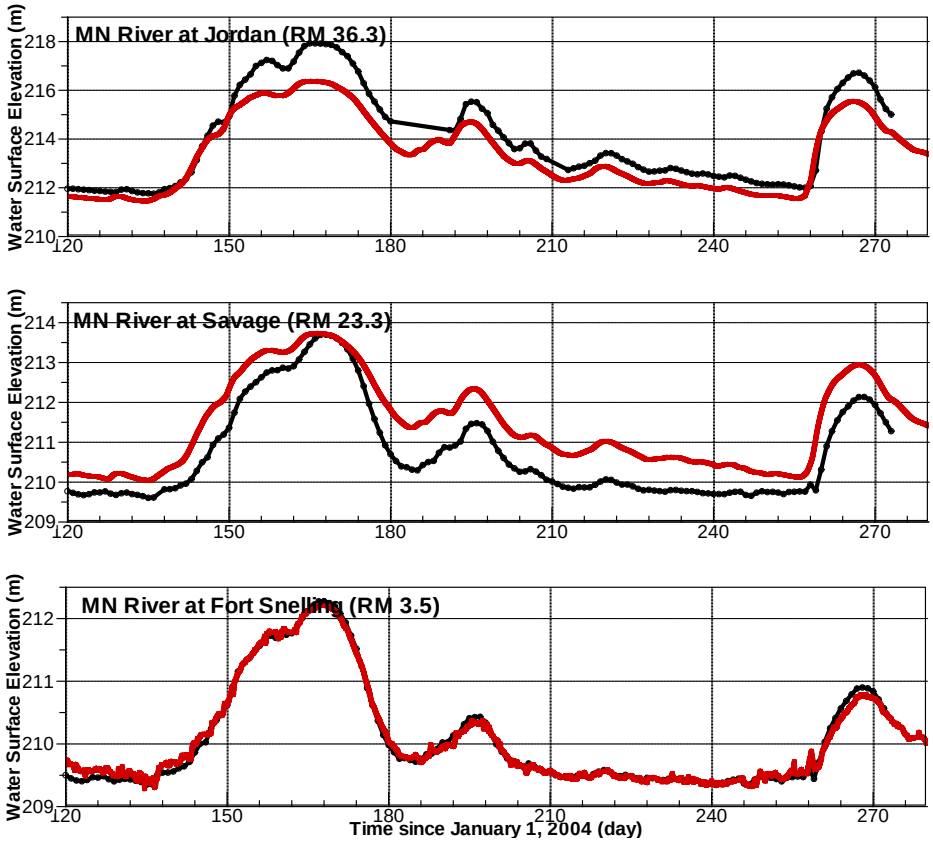

Figure 4. Daily average water surface elevation comparison: Red: SRH-2D; Black: Observation.

Water Quality Modeling

The water quality modelling requires additional water quality boundary conditions at all inflow open boundaries in connection with all transported water quality state variables. These data are available and derived the same as those used by Smith et al. (2012). At the study site, observational data are also available for water quality model calibration and validation at some river stations (discussed below). The primary input data include observations of mainstem, tributary, and point source temperature; meteorological data; nutrient concentrations; biological oxygen demand; and suspended sediment related data. A detailed description of these is omitted herein as it has been done by Smith et al. (2012). Key water quality monitoring stations are listed in Table 1 where the SRH-WQ results are compared with the measured data.

Table 1. Water quality monitoring station names, river miles and the corresponding SRH-WQ monitoring lines.

Name	Symbol	Monitoring Line	River Mile
Shakopee	sh	5	25.1
Savage	sv	1	13
Calibration Site	rm11.5	6	11.5
Black Dog	bd	7	8.5
Fort Snelling	sn	3	3.5

The results presented below include the SRH-WQ model run from January 1 to June 7, 2004. A temperature-only run is conducted from January 1, 2004 to March 8, 2005. The simulated temperature is compared with the observed data at the five monitoring stations in Figure 5. It is seen that the prediction is reasonably good. Increased divergence occurs as one moves further downstream from River Mile (RM) 30.4, the model inlet at Jordan, MN, to RM 3.5 at Fort Snelling. With the exception of hourly temperature data available at RM 11.5, temperature observations had approximately weekly frequencies making validation difficult. Nevertheless, SRH-WQ reproduces observed temperature trends. The comparison of other simulated water quality state variables with the observed values is shown in Figures 6-8. It is seen that the water quality model results are also relatively good in comparison with the measured data.

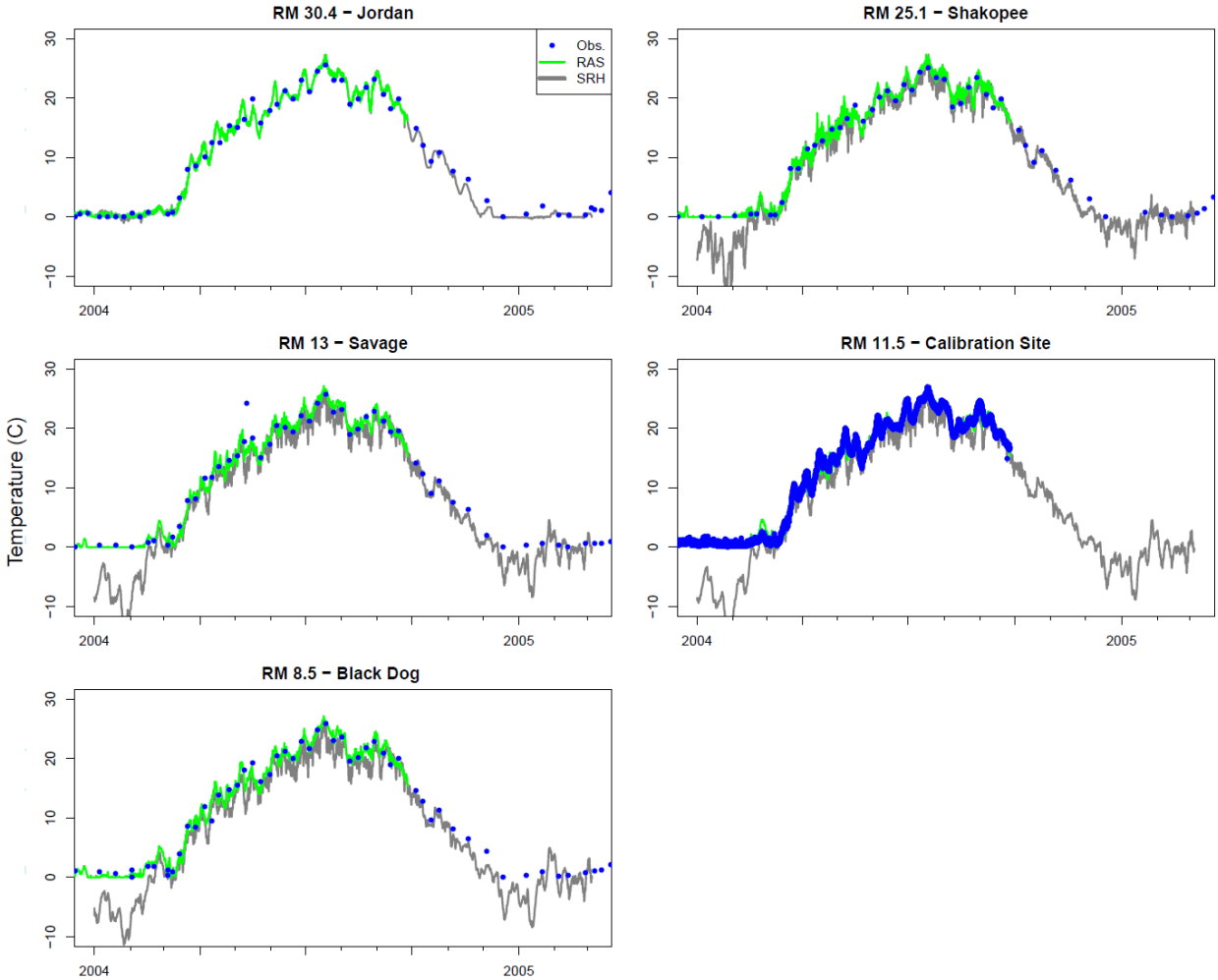

Figure 5. Comparison of simulated and observed temperature for various monitoring stations (HEC-RAS model results are also included for comparison).

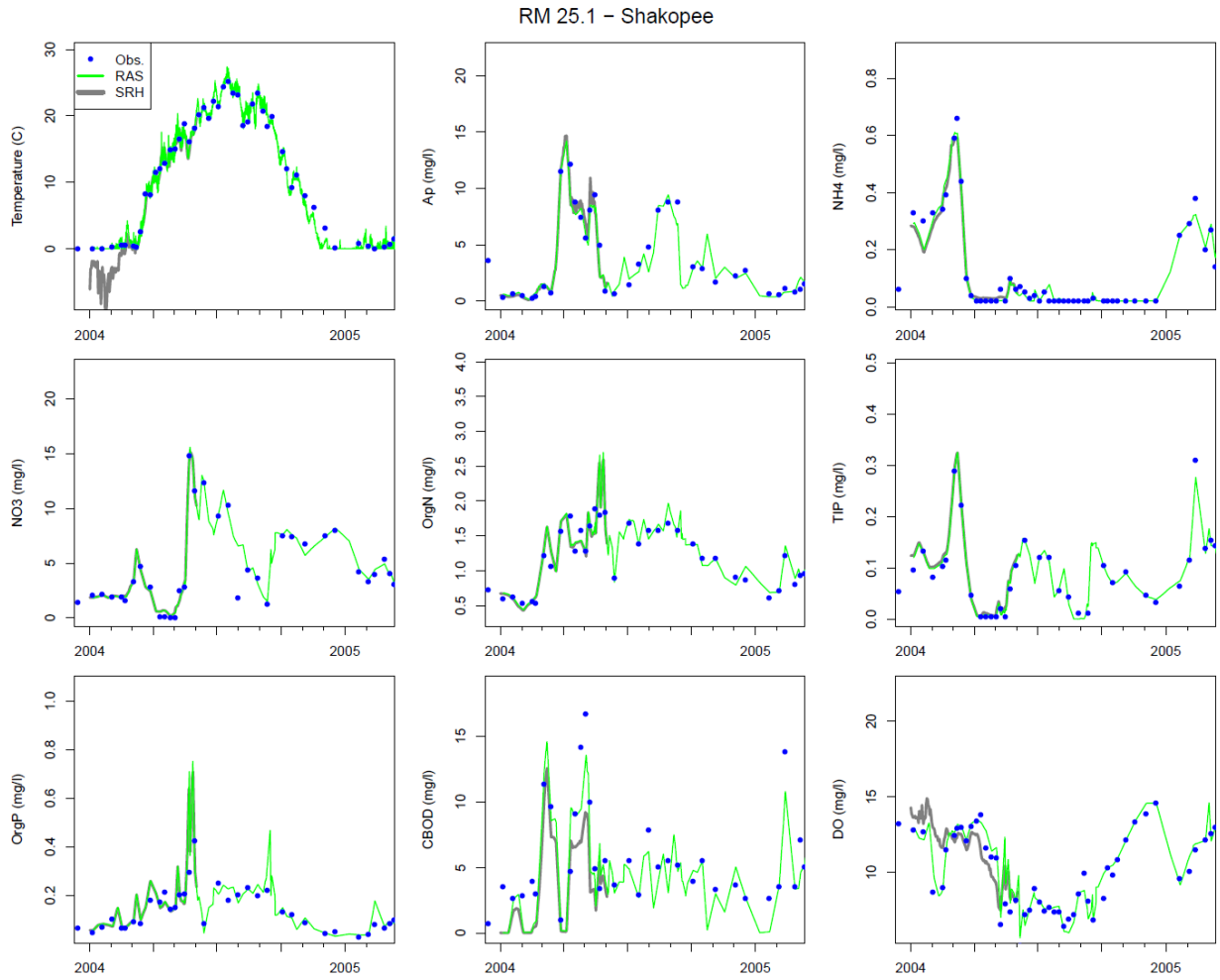

Figure 6. Comparison of simulated and observed water quality parameters for the Shakopee Station.

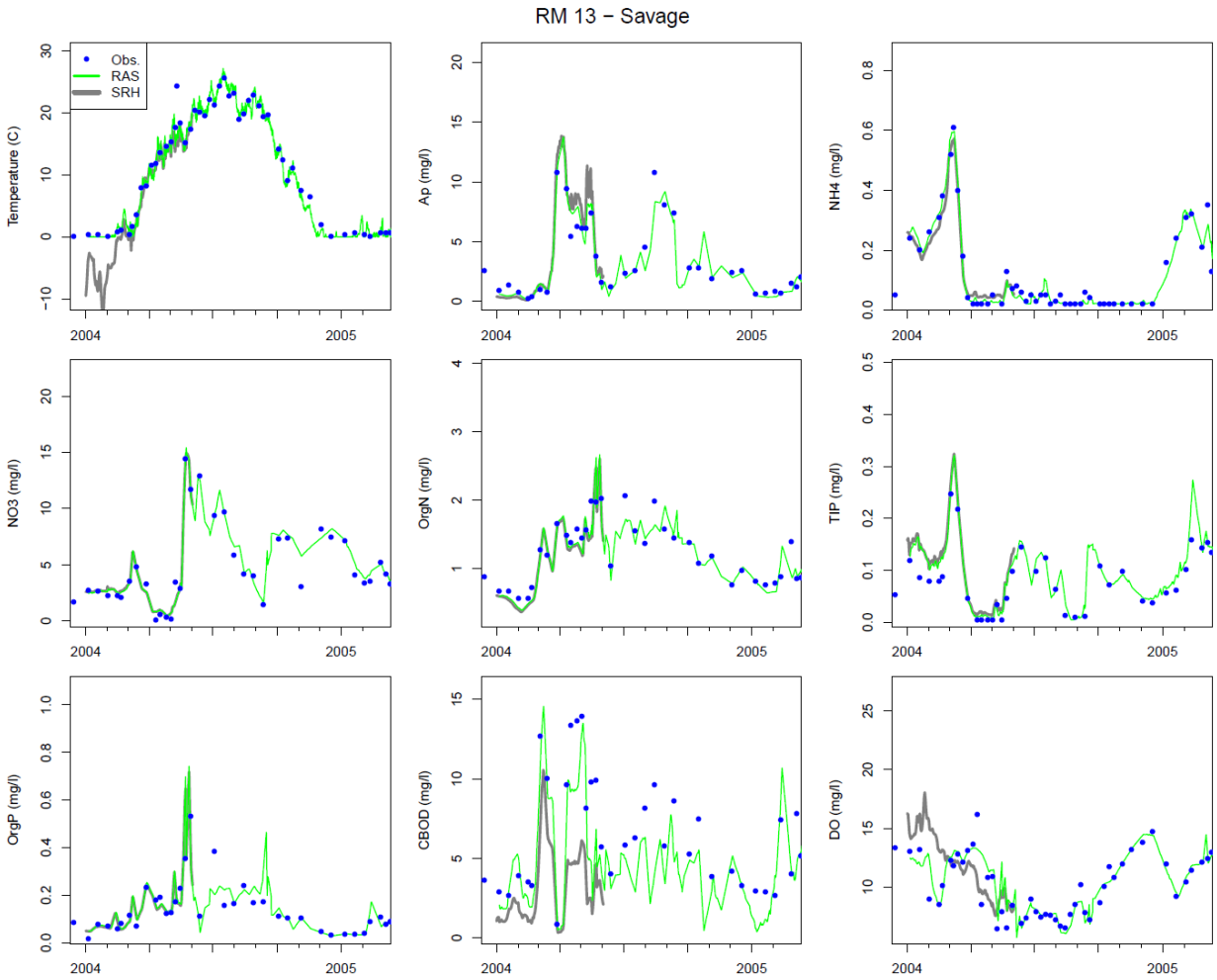

Figure 7. Comparison of simulated and observed water quality parameters for the Savage Station.

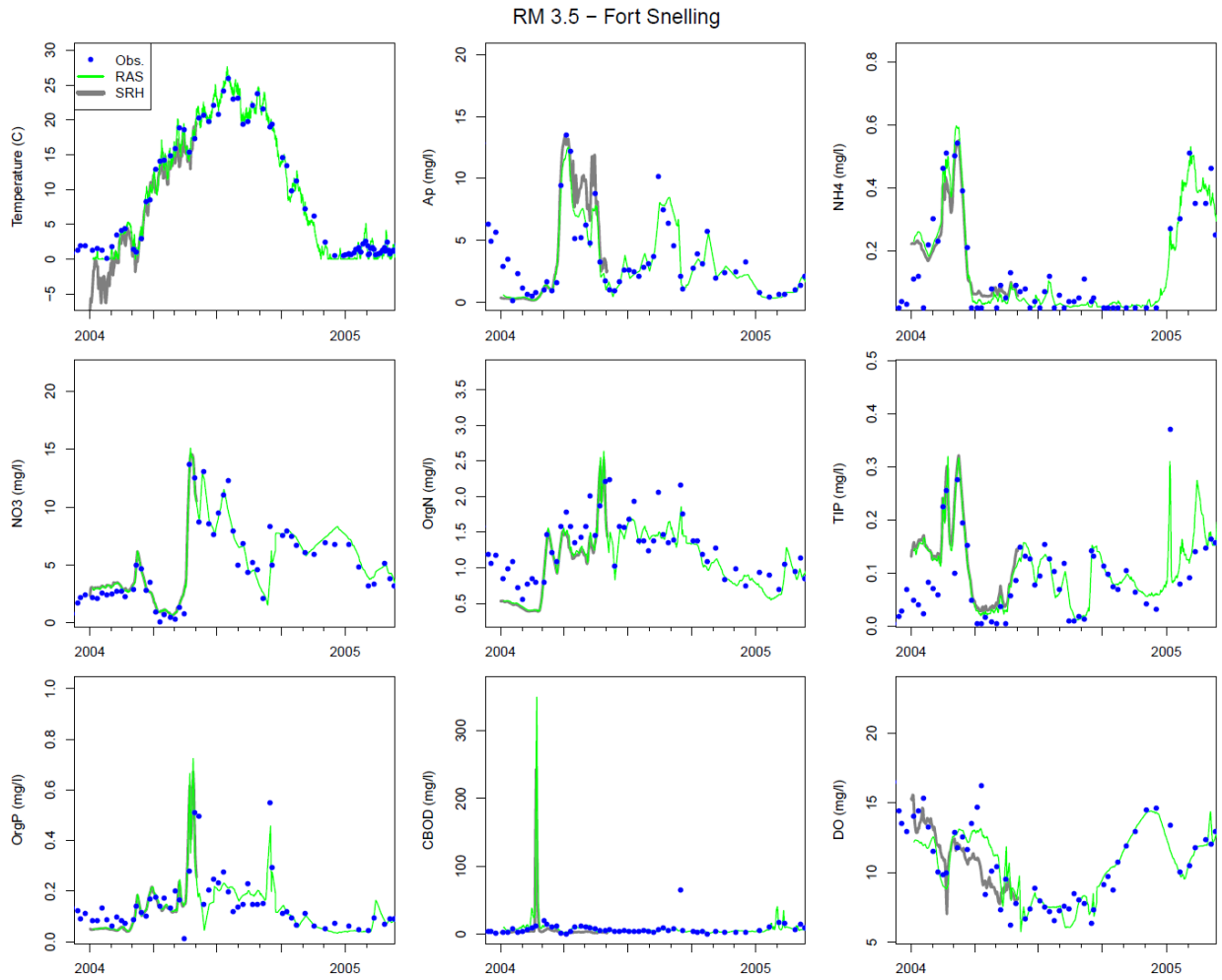

Figure 8. Comparison of simulated and observed water quality parameters for the Fort Snelling Station.

For a quantitative comparison, goodness-of-fit (GOF) metrics for all modeled variables are produced. Table 2 presents the quantitative comparison at the Fort Snelling station. Tables such as Table 2 are also produced at other monitoring stations; but they are omitted due to the paper length limitation, as well as that they do not contribute to new insight with regard to the conclusions.

These follow the various GOF metrics proposed by Krause et al. (2005). Model predictions and observations were all scaled to daily average values for comparison. These GOF metrics are mean error (ME), absolute mean error (AME), root mean square error (RMSE), the Nash-Sutcliffe efficiency (NSE), and the slope-weighted coefficient of determination (R^2) as defined in Krause et al. (2005) and implemented within R (R Core Team, 2016) using the hydroGOF package (Zambrano-Bigiarini, 2014). Note that an NSE value of unity indicates a perfect agreement between predictions and observations.

Table 2. Goodness-of-fit metrics comparing water quality observations at Fort Snelling.

Fort Snelling - SRH-WQ									
	T	Ap	NH4	NO3	OrgN	TIP	OrgP	CBOD	DO
n	22	22	21	22	22	22	22	22	22
ME	-2.54	0.17	0.01	0.42	-0.23	0.05	0.00	5.77	-0.51
AME	2.82	1.21	0.05	0.64	0.30	0.05	0.05	13.42	1.60
RMSE	11.89	0.78	0.04	1.95	1.10	0.24	0.01	27.06	2.40
NSE	0.74	0.81	0.85	0.95	0.44	0.34	0.38	-88.37	0.39
meanData	8.25	3.95	0.20	3.14	1.27	0.08	0.14	7.67	11.42
meanModel	5.71	4.11	0.21	3.56	1.04	0.13	0.14	13.44	10.91
bR^2	0.77	0.82	0.80	0.97	0.66	0.60	0.62	0.03	0.42

Concluding Remarks

A new water quality model, SRH-WQ, has been developed. The WQ model is coupled to the 2D depth-averaged flow model SRH-2D for the mesh, geometric information, and the flow variables. The water quality state variables have their own transport equations which are solved within the 2D depth-averaged framework. The source terms of the water quality equations are treated with the linearization method or the operator-splitting method. With the operator-splitting, the 5th order Runge-Kutta scheme is applied. SRH-WQ adopts the following strategy: (a) water quality is decoupled from the flow model so that an independent flow simulation may be performed; (b) an implicit finite-volume discretization on an unstructured polygonal mesh so that the model may achieve robustness and flexibility; and (c) linked to USACE water quality models so that both models (SRH-WQ and NSM) may be developed independently.

The performance of the new SRH-WQ model was demonstrated by simulating the water quality issues on the 37-mile lower Minnesota River. In particular, the coupling strategy was verified between SRH-WQ and NSMI. Model results are compared with the available observation data. SRH-WQ produces reasonable resolutions.

Acknowledgement

We thank Dr. David Smith and his colleagues at the U.S. Army Corp of Engineers, Engineer Research and Development Center, Vicksburg, MS for providing us with the model mesh, input data and calibration and validation data for the lower Minnesota River case.

References

Bahadur, R., D. E. Amstutz, and W. B. Samuels. 2013. “Water contaminant modeling – a review of the state of the science,” J. Water Resource and Protection, 5:142–155.

Berger, R. C., J. N. Tate, G. L. Brown, and G. Savant. 2012. Adaptive hydraulics user’s manual: Guidelines for solving two-dimensional shallow water problems with the adaptive hydraulics modeling system. Vicksburg, MS: U.S. Army Engineer Research and Development Center. http://chl.erdc.usace.army.mil/Media/1/2/7/8/AdH_Manual-4.201.pdf.

Cash, J.R. and Karp, A.H. 1990. A variable order Runge-Kutta method for initial value problems with rapidly varying right-had sides.” Trans. Math. Software, 16(3): 201-222.

HEC, Hydrologic Engineering Center. 2010. HEC-RAS river analysis system user's manual version 4.1. U.S. Army Corps of Engineers, Institute for Water Resources, Hydrologic Engineering Center, Davis, CA.

Krause, P. Boyle, D. P., Base, F. 2005. Comparison of different efficiency criteria for hydrological model assessment. *Advances in Geosciences*, European Geosciences Union, 5, pp.89-97.

Lai, Y.G. 2008. SRH-2D Theory and User's Manual version 2.0, Technical Service Center, Bureau of Reclamation, Denver, CO.

Lai, Y.G. 2010. "Two-dimensional depth-averaged flow modeling with an unstructured hybrid mesh," J. Hydraulic Engineering, 136(1), 12-23.

MPCA, Minnesota Pollution Control Agency. 2008. Clean Water Act Section 303(d). Total Maximum Daily Load List. St. Paul, MN.

MPAC, Minnesota Pollution Control Agency. 2004. Lower Minnesota River Dissolved Oxygen Total Maximum Daily Load Report. St. Paul, MN.

MOCA, Minnesota Pollution Control Agency. 2007. Minnesota River, Metropolitan Reach, Load Allocation Study Summer Field Survey Using Sonde-Equipped Buoys: Summary of the Minnesota Pollution Control Agency's Sonde/Buoy Field Work in Support of the Metropolitan Council's Lower Minnesota River Modeling Project's Two Field Surveys of the Summer of 2006. St. Paul, MN.

Press, W.H., Teukolsky, S.L., Vetterling, W.T., and Flannery, B.C. 1991. Numerical Recipes in C: The art of scientific computing, 2nd Ed., Cambridge Univ. Press, Cambridge, U.K.

R Core Team. 2016. *R: A Language and Environment for Statistical Computing*. R Foundation for Statistical Computing. Vienna, Austria. https://www.R-project.org/

Savant, G and Berger, R.C. 2012. Adaptive time stepping – operating splitting strategy to couple implicit numerical hydrodynamic and water quality codes. J. Environmental Engineering 138(9): 979-984.

Smith, D.L., Threadgill, T.L., Larson, C.E. 2012. Modeling the Hydrodynamics and Water Quality of the Lower Minnesota River Using CEQUAL-W2: A Report on the Development, Calibration, Verification, and Application of the Model. U.S. Army Corps of Engineers, ERDC/EL TR-12-12. 196p.

Zambrano-Bigiarini, M. 2014. *hydroGOF: Goodness-of-fit functions for comparison of simulated and observed hydrological time series*. R package version 0.3-8. https://CRAN.R-project.org/package=hydroGOF

Zhang, Z., Johnson, B.E. 2014. Application and Evaluation of the HEC-RAS-Nutrient Simulation Module (NSM I). ERDC TN-EMRRP-SR-47, U.S. Army Engineer Research and Development Center, Vicksburg, MS.

Zhang, Z., Johnson, B.E. 2016a. Aquatic Nutrient Simulation Modules (NSMs) Developed for Hydrologic and Hydraulic Models. ERDC/EL TR-16-1, U.S. Army Engineer Research and Development Center, Vicksburg, MS.

Zhang, Z., Johnson, B.E. 2016b. Aquatic Contaminant and Mercury Simulation Modules Developed for Hydrologic and Hydraulic Models. ERDC/EL TR-16-8, U.S. Army Engineer Research and Development Center, Vicksburg, MS.

Process-Based Modeling of Upland Erosion and Salt Load in the Upper Colorado River Basin

S. Kossi Nouwakpo, Research Assistant Professor, University of Nevada, Reno, NV, snouwakpo@cabnr.unr.edu

Mark Weltz, Rangeland hydrologist, USDA Agricultural Research Service, Reno, NV, mark.weltz@ars.usda.gov

Colleen Green, USDI Bureau of Land Management, Denver, CO, chgreen@blm.gov

Ken McGwire, Research Associate Professor, Desert Research Institute, Reno, NV, ken.mcgwire@dri.edu

Awadis Arslan, Research scientist, Natural Resources and Environment Sciences, University of Nevada, Reno, NV, aarslan@unr.edu

Introduction

The Colorado River is a vital municipal, agricultural and ecological resource in the United States and Mexico but is susceptible to detrimental salinity levels. The U.S. Bureau of Reclamation estimates that damages due to salinity of the Colorado River are estimated at $385 million per year. Over 55% of sediment and salts entering the Colorado River is of natural origin with a significant contribution from accelerated soil erosion on federal rangelands.

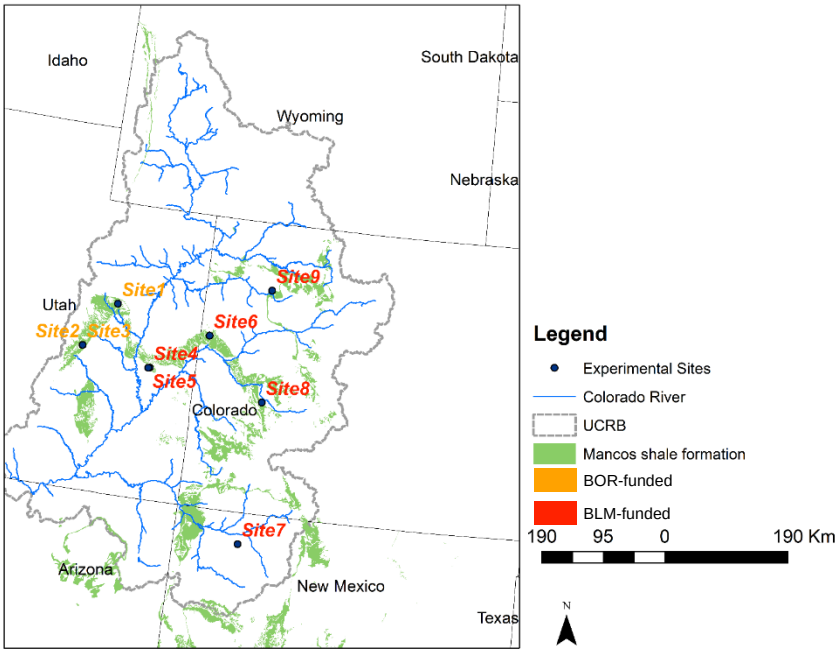

Figure 1. Map of the Upper Colorado River Basin (UCRB) showing the Mancos shale geologic formation and experimental sites funded by the U.S. Bureau of Reclamation (BOR) and the Bureau of Land Management (BLM).

High salt transport in these rangelands is imputed to a marine geologic history of the area resulting in salt-rich geologic formation. One such geologic formation is the Mancos shale (Figure 1) which has been described as one of the dominant sources of salt transport to the Colorado River. Knowledge on salt pickup and transport processes is limited to a few studies linking salt transport to soil erosion. As a consequence of this knowledge gap, no tool exists to satisfactorily predict salt load to surface waters in the Upper Colorado River Basin (UCRB). In this study, we aim to develop parameter estimation equations that are valid on saline rangeland sites for use in the Rangeland Hydrology and Erosion Model (RHEM).

Methods

RHEM was specifically developed by the U.S. Department of Agriculture to predict runoff and erosion on Rangelands. The model predicts runoff and erosion using physically-based flow routing, detachment and transport equations. The parameters of which are derived from estimation equations developed from rangeland data to reflect rangeland conditions. Because the original data used to develop RHEM did not include any saline or sodic (high in sodium) soils, new experimental data was collected at saline and sodic sites of the UCRB to test current RHEM equations and develop better parameter estimation functions. Data from rainfall simulation experiments at 9 sites in the UCRB (Figure 1) were used to develop these predictive equations. At each experimental site, rainfalls of intensities corresponding to the 2-, 10-, 25- and 50-year return frequency for the area were simulated at a rate of 1 event per plot, resulting in a total of twelve plots per site. Plot dimensions were 6 m x 2 m. During each rainfall event, traditional soil erosion measurement data (runoff rate and volume, soil loss and sediment concentration) were collected along with information on soil salinity and sodicity represented by Electrical Conductivity EC and Sodium Adsorption Ratio (SAR).

New equations for estimating the soil effective hydraulic conductivity (Ke) and the splash and sheet erodibility (Kss) on saline and sodic soils were developed. A Markov Chain Monte Carlo optimization was used to find the best Ke and Kss values that minimized error in runoff and soil loss prediction respectively. These optimum Ke and Kss values were then compared to current compared to the values of these parameters estimated by current RHEM equations by calculating corrective terms as differences and ratios between optimum and estimated values. The corrective terms were then regressed against vegetation characteristics and soil physiochemical properties to identify statistically significant factors controlling deviations of saline/sodic sites from RHEM parameter-estimation equations. The new Ke and Kss equations for saline / sodic sites were constructed by combining predictive equations for the corrective terms with the original RHEM parameter-estimation equations. Runoff and soil loss prediction performances of the new equations were compared to the original RHEM equation and evaluated with the Nash-Sutcliff Efficiency (NSE), the coefficient of determination (R^2) and the percent bias (PBIAS). Model performance was evaluated on 36 calibration plots and 36 validation plots originating from 6 of the 9 experimental sites. Data from the remaining 3 sites were used for independent validation.

Results and discussion

Differences between the equations for estimating the effective hydraulic conductivity (Ke) and the splash and sheet erodibility (Kss) on saline/sodic rangelands and the original RHEM equations for Ke and Kss are shown in in Table 1. Overall the effective hydraulic conductivity was amplified on saline / sodic sites compared to that predicted by the original RHEM Ke estimation equation. The splash and sheet soil erodibility was a function of the soil Sodium Adsorption Ratio SAR.

The performance of the newly developed saline RHEM equations for Ke and Kss are compared to the original RHEM equations in Figures 2 and 3 for the calibration data. Overall, the new Ke and Kss equations improved runoff and soil loss predictions as evaluated by all performance metrics.

Table 1. Estimation equations for the effective hydraulic conductivity (Ke) and the splash and sheet erodibility (Kss) used by the Rangeland Hydrology and Erosion Model (RHEM) on non-saline and saline / sodic sites. Parameters *a* and *b* are fitting parameters, *basal* and *litter* are the ground cover fraction occupied respectively by the base of plants and by litter. *SAR* is the Sodium Adsorption Ratio.

Parameter	Original RHEM	Saline / sodic sites
Effective hydraulic conductivity	$Ke = a\exp\left(b\left(basal + litter\right)\right)$	$Ke = a\exp\left(1.554b\left(basal + litter\right)\right)$
Splash and sheet erodibility	$Kss = Kss_{RHEM}$	$Kss = Kss_{RHEM} + \left(642.4\ SAR\right)$

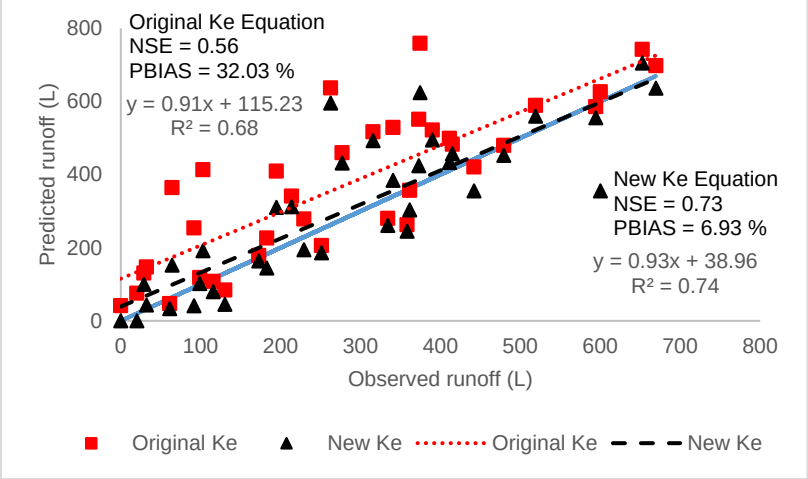

Figure 2. Observed vs. predicted runoff on 36 rainfall simulation calibration plots using current RHEM parameter estimation

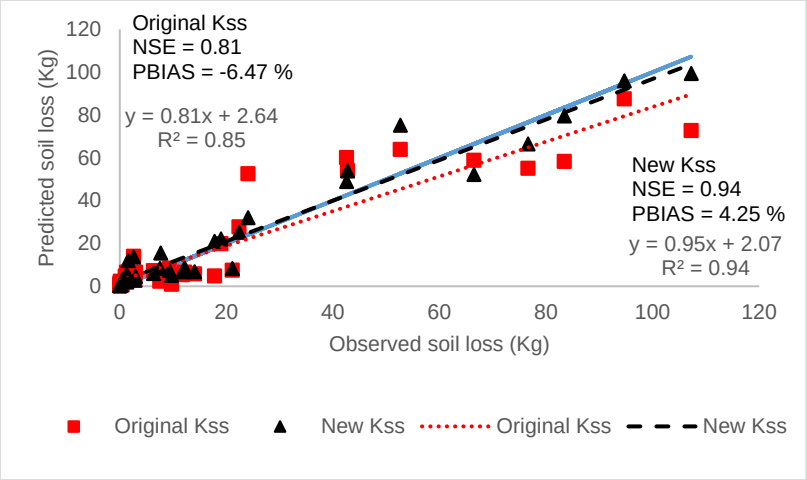

Figure 3. Observed vs. predicted soil loss on 36 rainfall simulation calibration plots using current RHEM parameter estimation equations

Performance improvements observed on the calibration data were sustained on the validation data (Figures 4 and 5).

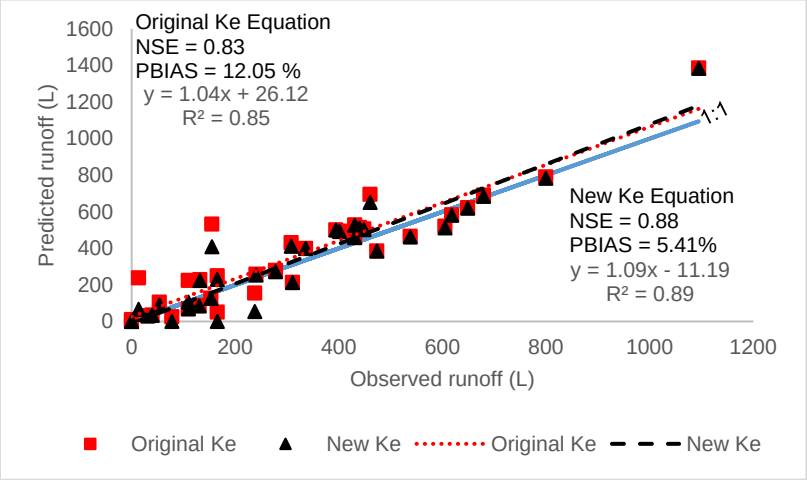

Figure 4. Observed vs. predicted runoff on the 36 validation data points using the current and the newly developed estimation equation for the hydraulic conductivity Ke

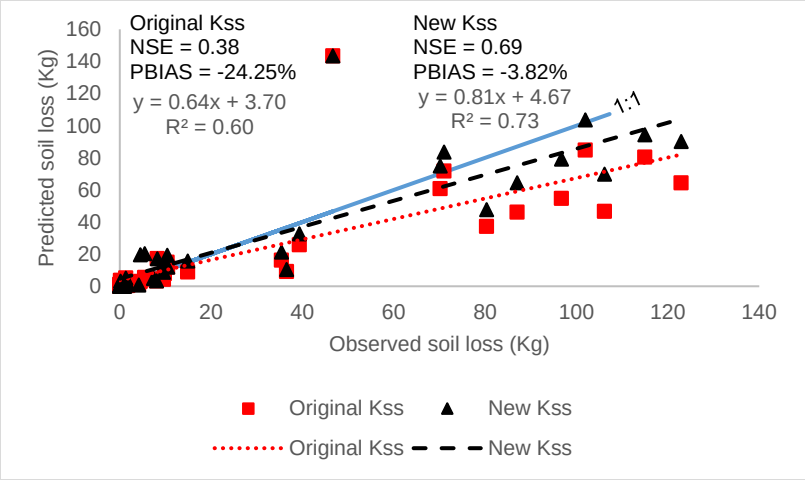

Figure 5. Observed vs. predicted soil loss on the 36 validation data points using the current and the newly developed estimation equation for the sheet and splash erodibility, Kss

A strong linear relationship was found between soil loss and total dissolved solids (a measure of salinity) in runoff with a coefficient of determination of 0.94.

$$TDS = 2.36 \times SL + 0.99$$

where TDS (10^{-3} kg) is the total dissolved solids and SL is the soil loss (kg).

With this model, soil loss data predicted with RHEM on saline / sodic sites were used to calculate TDS content in runoff (Figure 6). As shown in Figure 6, the TDS values calculated from soil loss data modeled with newly developed equations closely matched the 1:1 line when plotted against observed TDS values.

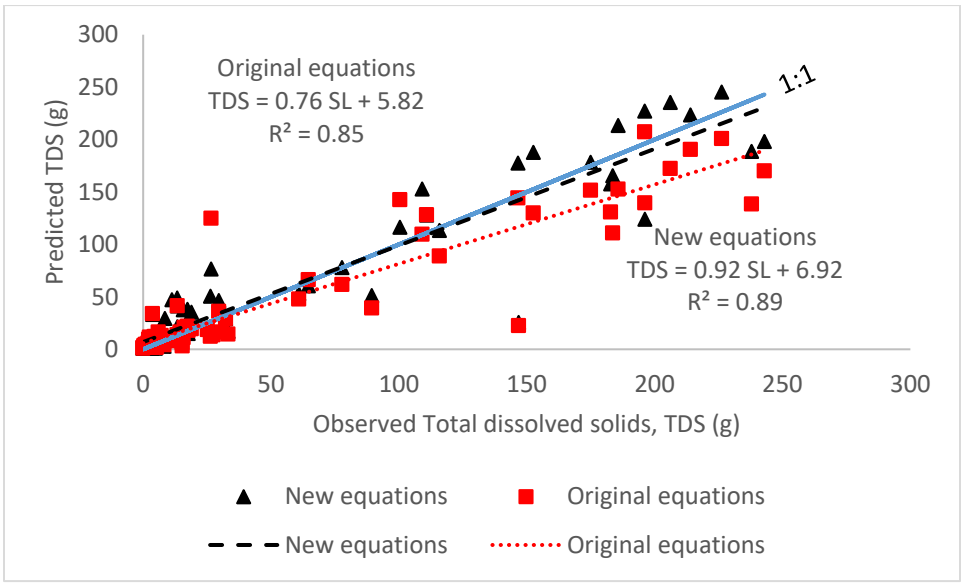

Figure 6. Observed vs. predicted total dissolved solids (TDS) on the 72 data points using the current and the newly developed estimation equations for Ke and Kss

Summary and Conclusions

The newly developed equations for the effective hydraulic conductivity and the splash and sheet erodibility adequately captured infiltration, runoff and erosion processes on saline rangelands. The performance of the RHEM model at predicting runoff and soil loss was improved with the usage of the new equations compared to the original equations. Overall, the effective hydraulic conductivity was greater on these saline rangelands compared to that predicted by the non-saline RHEM equation. Erosion was overall greater on these rangelands and was a positive function of the Sodium Adsorption Ratio. A linear function between soil loss and total dissolved solids in runoff was used to predict salt load from soil loss data. These new equations will be integrated in a new version of the RHEM model to provide a tool for land and water resource managers to evaluate erosion, runoff and water quality on salt-affected rangelands.

Runoff Water Quality from Rainfall Simulation on Different Salinity Alkalinity Levels of Rangeland Plots

Awadis Arslan, Research scientist, Natural Resources and Environment Sciences, University of Nevada, Reno, NV, United States, aarslan@unr.edu

Sayjro Nouwakpo, Research Faculty, Soil and environmental sciences, University of Nevada, Reno, NV, United States, snouwakpo@cabnr.unr.edu

Mark Weltz, Research Leader / Rangeland hydrologist, USDA Agricultural Research Service, Reno, NV, United States, Mark.Weltz@ARS.USDA.GOV

Kenneth McGwire, Associate professor, Desert Research Institute Earth and Ecosystem Sciences, Reno, NV, United States, ken.McGwire@dri.edu

Abstract

Overland flow from rainfall excess on salt affected rangeland soils is associated with transport of salts dissolved from the surface layer of the soil to surface water reservoirs causing water quality deterioration. In an attempt to quantify the amounts of salts leaving the soil profile with time, rainfall simulation experiments were conducted on three sites in the upper Colorado River basin having different levels of soil salinity and sodicity. Simulation water was applied at four intensities replicated 3 times on two sites and at one intensity repeated 12 times on one site, after measuring slope, canopy cover and other runoff-erosion parameters to determine the effect of intensity, canopy cover, slope, and soil salinity and alkalinity on the concentration of ions in runoff water transported at sequential time intervals. The Electrical Conductivity of saturated paste (EC_e) of the soils ranged between 3.04 and 8.90 dS/m and the Exchangeable Sodium Percentage (ESP) was between 0.18 and 27.67. The concentrations of major ions in the simulation water and runoff water were determined at close intervals during each event. The results show changes in cation and anion concentrations with time. We obtained polynomial fit with high coefficient of determination for each cation and anion in single runs that describe the pattern of changes in concentration with time, which differ from one ion to another. The Average EC of the runoff water ranged between 0.59 and 1.74 dS/m and Sodium Adsorption Ratio (SAR) between 0.43 and 5.71 which reflect the initial soil salinity and alkalinity of the sites.

The results improve understanding of the exchange reactions between the simulation water and soil surface during the simulation process, predicting water quality of the reservoirs accumulating runoff water and the possible effects of using the stored runoff water on soil properties, irrigated crops productivity, and quality irrigated with such water quality. Results of this study will improve existing models such as Rangeland Hydrology and Erosion Model (RHEM) for predicting the possible deterioration of surface water quality as results of rainfall on salt affected soils and suggest management practices of such soils to reduce their negative impact on surface water.

Introduction

Overland flow from rainfall excess on salt affected rangeland soils is associated with transport of salts dissolved from the surface layer of the soil to the surface water reservoirs causing water quality deterioration. Salinity-control efforts have largely focused on reducing anthropogenic sources of dissolved-solids, especially irrigation of agricultural lands while nearly half of the salt concentration in the river system comes from natural sources (Kenney et al. 2009). This suggests a significant potential to further reduce dissolved-solids loading to the Colorado River through land- and water-management activities on rangelands. It is well documented that on rangelands the amount, kind, and distribution of vegetation and ground cover are often the only factors that can be cost-effectively manipulated to alter surface runoff and soil erosion.

To assess the state-of-knowledge on rainfall/runoff-driven salt pickup and transport processes from rangeland, a bibliographic search (Gagnon et al. 2014) and synthesis (Weltz et al. 2014) was first conducted covering salt transport processes. This revealed a strong emphasis on water erosion and subsurface hydrological processes as the main driving mechanisms of salt delivery to surface waters. This state-of-knowledge exploration identified experimental understanding of salt pickup and transport processes as a key knowledge gap that needs to be addressed.

Normalized and standardized inorganic data from 648 water samples in southeastern Piceance Basin, Colorado were separated by Albrecht and Thyne (2007) into five statistically distinct groups, representing water facies, using hierarchical clustering. One cluster was low Total Dissolved Solids (TDS), Ca-Mg-HCO_3 water consistent with natural background. Other clusters showed "impacted" signatures: high Fe-Mn, high TDS Na-Cl or high TDS Na-SO_4-HCO_3. Grouping can also be applied when looking at soil salinity and alkalinity levels. Each soil group has specific solubility-precipitation, adsorption-desorption and runoff-sedimentation behavior that take place upon rainfall or through evapotranspiration processes. Typically, all chemical reactions are classed into two groups; one group with sufficiently fast and reversible reactions such as the exchange reaction (Gharaibeh et al. 2011) models the equilibrium reactions, and the other group with slower and /or irreversible reactions characterizes the kinetically dominated reactions (Rubin 1983).

The dominant ions in the salts affected soil are Ca^{2+}, Mg^{2+}, Na^{+}, K^{+}, Cl^{-}, NO_3^{-}, SO_4^{2-}, and HCO_3^{-}. The amount of each constituent depends on the kinds and amounts of the minerals and organic matter in the soil solid phase, the kind and activity of the vegetation, and the source of applied rain or simulation water (Soil Survey Investigations Report No. 45 2011; U.S. Salinity Laboratory Staff 1954). Fresh simulation water or rainwater that contacts vegetation before infiltration through the soil surface may dissolve some of the cations and anions from the rangeland canopy cover (stem flow or released through fall). Infiltrated water redistributes cations and anions through the soil. Water also penetrates the soil surface directly without contacting the plant canopy (free throughfall) and reacts with the soil's solid components. Some of which dissolve readily and others dissolve slowly soluble and slightly soluble salts (Crockford et al. 1996; Kruszyk et al. 2015; Levia Jr and Frost 2006). To assess salt mobility with runoff, the concentration of major cations and anions in the simulation water, runoff water, soil saturated extract and on the colloidal surfaces (exchangeable part) have to be determined before each simulation.

Zwikel et al. (2007) analyzed the effects of soil microenvironments and climatic conditions on the temporal dynamics of salt concentrations and found that mainly Na^{+} and Cl^{-} concentration

responded rapidly to changes in rain intensity and quantity, soil moisture, and temperature. There is minimal peer reviewed literature that directly document salt mobilization and transport from rangelands (Gagnon et al. 2014). This research aims at: (1) quantifying and qualifying runoff from saline-alkaline rangelands at short time intervals and (2) describing the changes in runoff water concentration with time from straight line curve fit.

Methods

Study Area: Three sites in the Mancos Shale geologic formation were selected to conduct rainfall simulation experiments. These sites were selected for their contrasting slope ranges and differences in soil intrinsic properties. The Price site is located near the city of Price, UT at an elevation of 1649 m (Figure 1a, Figure 2). This soil is encountered on back slopes of hilly landforms with slopes ranging from 0.6 to 10%. The mean annual precipitation at the city of Price for the period of 1968-2005 was 239 mm, while average snowfall for the same period was 513 mm (WRCC, 2015). The soil was classified based on the Natural Resources Conservation Service (NSSH Part 618. 2017) as very slightly saline non-alkaline (EC_e = 2.77 dS/m and ESP = 0.19) (Figure 3). Vegetation at the Price site is a shrub-dominated ecosystem, with a mix of perennial grasses and forbs.

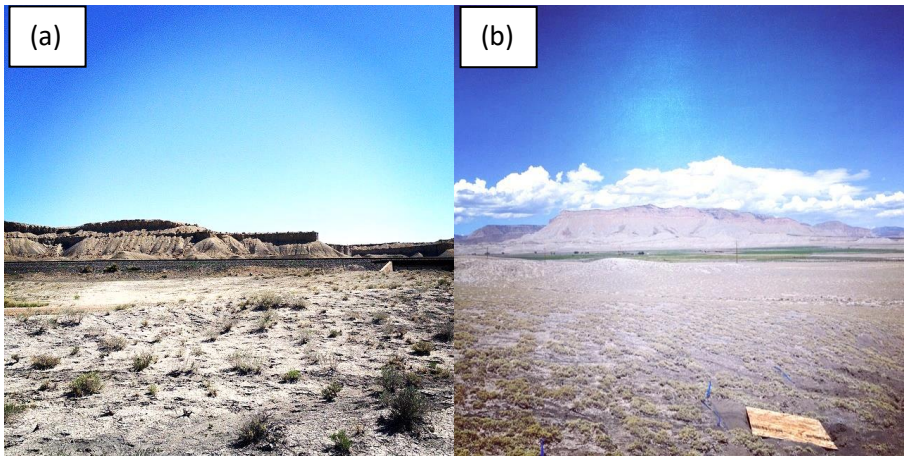

Figure 1a-b. Photos from Price (a) and Ferron (b) field sites.

The Ferron sites (Dry X and Dry X-II) are located near the city of Ferron, UT at an elevation of 1893 m (Figure 1b, Figure 2). The predominant soil type at Ferron is mapped as a complex of Chipeta soil series and Badland areas. This soil is associated with hilly landforms and is encountered on backslopes ranging from 11.4% to 24.5% at Dry X site and from 14.5% to 17.8% at Dry X-II. Mean annual precipitation and average snowfall measured at Ferron, UT between 1948 and 2005 were respectively 215 mm and 688 mm (WRCC, 2015). The observed vegetation at Ferron was solely dominated by *Atriplex corrugata* – mat saltbush. Regarding salinity and alkalinity, the soil at Dry X is moderately saline and alkaline (EC_e = 8.05 dS/m and ESP = 27.67), and Dry X-II is also moderately saline and alkaline (EC_e = 8.90 dS/m and ESP = 19.01) (NSSH Part 618. 2017) (Figure 3).

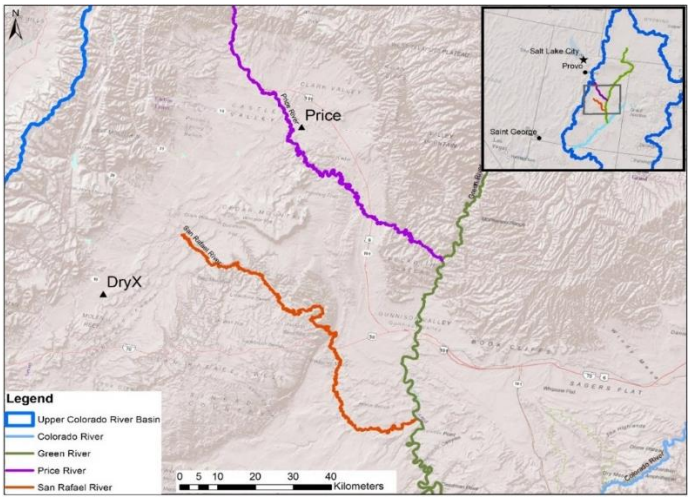

Figure 2. Map of the field sites relative to rivers in the Upper Colorado River Basin.

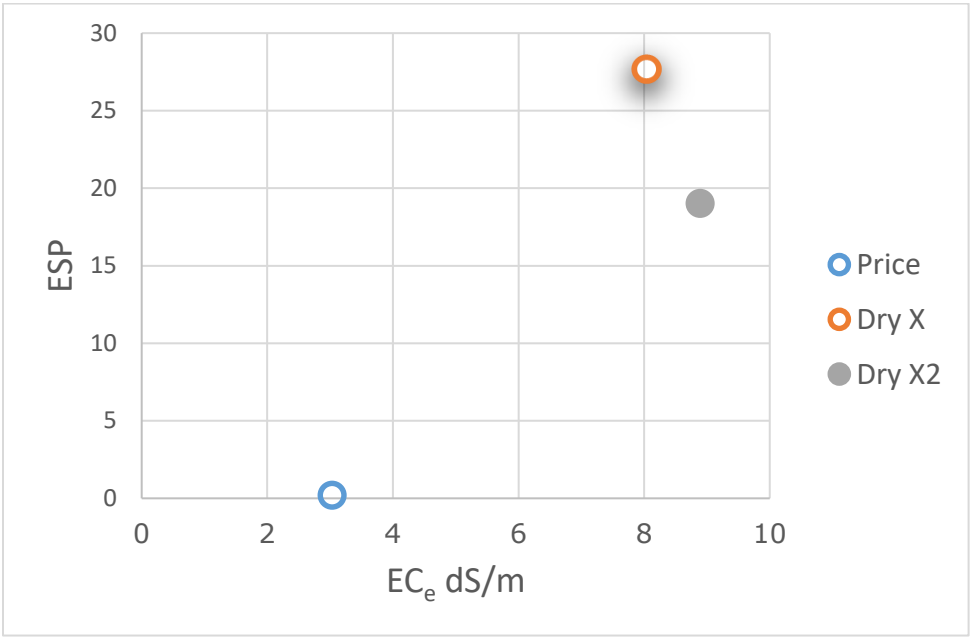

Figure 3. Electrical Conductivity of soil saturated extract (ECe dS/m) and exchangeable sodium percentage (ESP) of the field sites in the Upper Colorado River Basin.

Experimental setup: On the Price and Dry X experimental sites, a series of rainfall simulations were conducted on 6 m x 2 m erosion plots to quantify sediment and salt transport processes during rainfall-driven erosion processes. Erosion and hydrologic responses were assessed by measuring soil loss, runoff and solute transport under four rainfall intensities corresponding to return periods of 2 (44.1 mm/hr), 10 (80 mm/hr), 25 (114.4 mm/hr) and 50 (135.9 mm/hr) years. Intensities were calculated based on the 15-minute depth return frequencies published in the National Oceanic and Atmospheric Administration (NOAA) Atlas 14 (Bonnin, et al., 2006). On each plot, a single rainfall event was applied to ensure the capture

of the process of salt efflorescence (Bowles, et al., 1982, Riley, et al., 1982) whereby a salt crust is left at the soil surface by evaporation. Each rainfall intensity on each site was replicated three times.

In the Dry X-II experiment, three hillslopes were identified at the study site to represent low (L, canopy cover < 5%, average = 2.39%), medium (M, 5% < canopy cover < 19%, Average = 9.09%) and high (H, canopy cover > 19%, average = 22.41%) vegetation covers. Only the 25 year return period intensity of 114.4 mm/hr was applied to all plots. Potential hillslopes were selected by visually identifying three contrasting densities of *Atriplex corrugata* on the site. Four plots were selected on each hillslope. Ground and vegetation cover on each plot were assessed using a laser point frame (VanAmburg, et al., 2005). This data was collected on a 0.5 m x 0.1 m grid (or 220 sample points) per plot and provided information on canopy cover, litter cover, rock content and the fraction of bare ground (Table 1).

A Walnut Gulch Rainfall Simulator (WGRS) (Paige, et al., 2004) was used in this study (Figure 4). The WGRS is an oscillating nozzle type simulator with four Veejet 80100 nozzles (Spraying systems, Inc., Wheaton, Ill.) mounted in-line on a central boom. As recommended by Paige, et al. (2004), a nozzle height of 2.44 m was used in this study to achieve raindrop energy within the range encountered during natural rainfall events.

Figure 4. Walnut Gulch Rainfall Simulator operation at Dry X and DryX-II, Utah.

At the downslope end of the plot, a runoff collection pan conveyed runoff into a supercritical flume where a Teledyne 4230 flow meter (Isco, Inc., Lincoln, NE) measured discharge at a rate of four samples per minute. This automated discharge measurement was validated with periodic manual timed-sampling of runoff rate.

Experimental protocol: When runoff reached the collection pan, the time-to-runoff was recorded. At Price, rainfall was stopped after 15 minutes of runoff had occurred while at Ferron (Dry X and Dry X-II), rainfall continued until a trendless real-time hydrograph was observed for ten minutes, marking steady state conditions.

During each rainfall simulation, time-stamped runoff samples were also collected for sediment concentration and water salinity analysis (TDS) in addition to the concentration of cations and anions. Sampling was done at a frequency of one sample / minute for the first three minutes and every three minutes there on. Sediment concentration samples were collected in 1 L bottles which were immediately weighed to get water and sediment weights and oven-dried to get sediment mass used for concentration calculation. Water quality samples were collected in 50 mL centrifuge tubes immediately acidified with a hydrochloric acid solution and refrigerated to maintain the integrity of the liquid phase chemical speciation.

Pre-rainfall soil samples were collected on control plots. The control plots provided information on pre-simulation soil characteristics, since sampling in the rainfall plots would affect the flow and erosion. Soil samples were then placed in a beaker with distilled water to perform a saturated water extract using the immiscible displacement method (Mubarak and Olsen, 1976). The extraction was analyzed for the anions Cl^-, NO_2^-, NO_3^-, and SO_4^{2-} using the Dionex Ion Chromatography (IC) System (Thermo Fisher Scientific, Inc., Waltham, MA). The extraction was analyzed for the cations Ca^{2+}, Mg^{2+}, Na^+, and K^+ using TruSpec Atomic Absorption Spectroscopy (Leco Corporation, Saint Joseph, MI). Ammonium acetate exchangeable cations (Ca^{2+}, Mg^{2+}, Na^+, K^+) also were analyzed using TruSpec Atomic Absorption Spectroscopy. Ammonium (NH_4^+) for Cation Exchange Capacity (CEC) and the KCl extractable solutions (NH_4^+/NO_3^-) were analyzed using Lachat Quikchem Flow Injection Analyzer System (Hach Company, Loveland, CO). The pH of 1:2 ratio of soil : ½ M $CaCl_2$ solution was determined using a ph/mV/˚C meter (Oakton Instruments, Vernon Hills, IL) and the EC was quantified using a Model 2052 Portable EC Meter (VWR International, Radnor, PA).

Runoff water was collected and analyzed from the simulation plots (12 m^2). The concentrations of major cations and anions in the simulation water and runoff water were determined by Truspec Atomic Absorption Spectroscopy and Dionex IC.

Results and Discussion

Initial sites characteristics: The average pre-simulation sites characteristics in Table 1 show that the surface soil at Price is considered very slightly saline non-alkaline clay texture while Dry X and DryXII soils are moderately saline alkaline silt loam according to NSSH Part 618, Subpart A (2017). All soils contain small amounts of gypsum (3.5 to 4.8%) that have a positive effect on the runoff water quality. The presence of the slightly soluble gypsum was confirmed by acetone test (Soil survey Investigations report No. 45, Version 2, February 2011) and determined quantitatively by dissolution and measurement of SO_4^{2-} in the dilute extract. The predominance of calcium and sulfates (Khechai and Daoud, 2016) of the saturated soil extract required special selection of ions determination method and calculation procedures (Arslan, A., 1995; Arslan and Dutt, 1993; Khechai and Daoud, 2016). The slopes are 6.44, 16.01 and 19.17% and the canopy cover values are 8.74, 11.30 and 21.85% for Price, Dry XII and Dry X respectively. It is clear that the selected sites cover wide ranges of slope, canopy cover, EC_e and

ESP that will have different effects on runoff water quality and quantity (the objectives of the study). Applying ammonium acetate method for exchangeable cations (suitable for Western USA for non-saline conditions) produced exchangeable cations/CEC values ranged between 4.66 and 6.05. That is because the soils have different levels of salinity and contain gypsum.

Table 1. Average site vegetation and soil characteristics.

Site	Price, Utah	Dry X, Utah	Dry XII, Utah
Ecological site		Desert shallow Loamy	Desert shallow Loamy
Canopy cover %	8.74	21.85 (saltbush dominated)	11.30 (saltbush dominated)
Bare Soil %	88.90	74.77	86.56
Soil Series	Persayo loam	Chipeta-Badland complex	Chipeta-Badland complex
Surface texture	Clay	Silt loam	Silt loam
Slope %	6.44	19.17	16.01
EC_e (dS/m)	3.04	8.05	8.90
ESP	0.18	27.67	19.01
CEC ($cmol_c/kg$)	9.19	14.74	11.10
EX-Cations ($cmol_c/kg$)	55.61	68.66	60.78
% gypsum	4.80	4.36	3.50
Plant species	Many species	*Atriplex corrugata*	*Atriplex corrugata*
Longitude	-110.61	-111.12	-111.12
Latitude	39.60727	38.97317	38.97317

* according to NSSH Part 618, Subpart A 2017

Evolution of runoff water chemistry: The average amounts of the applied simulation water, presented in Table 2, ranged between 1100.24 and 1371.60 L (The lowest value for the lowest salinity and alkalinity soil, Price). Average runoff water volume were 272.28, 328.8 and 480.68 L for Price, Dryx and Dry XII respectively, which constituted 25, 28 and 35% of the simulation water. Average simulation water EC ranged between 0.44 and 0.52 dS/m with a very small % CV between sites (8.38 %). The differences in simulation water EC between sites is small because they are from the same basin. Average EC of runoff water in the three sites ranged between 0.58 and 1.71 dS/m with a large % CV between sites (48.22%), that reflected the wide range of EC_e of the soils in these sites (3.04 to 8.90 dS/m) and the wide range of ESP (0.18 to 27.67). The runoff/simulation ratios reflect site properties, where it was smallest (0.25) in price which had the smallest slope, EC_e and ESP values. The values of runoff/ simulation ratio were higher in Dry X and Dry XII which had higher EC_e, ESP, and slope. Table 2 show a deposit of 205.39 g of salts in the soil from the applied simulation water in price. The amount of deposited salts decreased to 91.84 g/plot in Dry X, while 46.47 g/plot salts removed from the soil in Dry XII and moved with runoff water.

The SAR of runoff water remained almost the same as the simulation water SAR value (0.43) in Price because of the Low soil ESP value (0.18) although the EC_e of the soil was relatively high (3.04 dS/m). That is because the salinity of the saturated extract resulted from the small amount of gypsum (4.8 %) in price soil. The SAR of runoff water values in Dry X and Dry XII were higher than the simulation water because the ESP values of the soils were high.

Table 2. The Quality and Quantity of simulation and runoff water

Site	Sim (L)	RO (L)	RO/Sim	EC Sim (dS/m)	EC RO (dS/m)	Salts removd (g/plot)	SAR Sim	SAR RO
Price	1100.24	272.28	0.25	0.44	0.59	-205.39	0.43	0.43
Dry X	1181.10	328.80	0.28	0.48	1.20	-91.84	0.48	2.53
Dry XII	1371.60	480.68	0.35	0.52	1.71	46.47	0.52	6.29
Average	1217.65	360.58	0.29	0.48	1.17	-83.59	0.48	3.08
stds	139.32	107.78	0.05	0.04	0.56	126.13	0.04	2.97
%CV	11.44	29.89	18.09	8.38	48.22	-150.90	9.06	96.41

*Values are average of 12 simulations

Salt mobility and transport processes, the concentration of major cations and anions in the simulation water, and runoff water, depend on many factors such as soil chemical and physical properties, simulation water intensity and quality, topography, surface roughness, canopy cover and its types. For better understanding the transport processes, we will present the concentration of cations and anions in the runoff water at close intervals that will help modelers in their difficult task of predicting runoff water after finding suitable pedotransfer functions from large data sets.

It is worth showing examples of the changes in ion concentration in runoff water with time from one site (Dry X) to follow the trends of these changes from the average runs at the selected sites. As it is clear in Figures 5 and 6, the concentration of all measured major ions in the runoff water was higher than simulation water except for Mg^{2+}. The increase or decrease in ion concentration in the runoff water is the result of fast reactions between the simulation water and the precipitated salts on the canopy, the soluble and slightly soluble salts in soil, and the exchangeable ions of the soil exchange sites (Kruszyk et al. 2015; Levia Jr and Frost 2006). These reactions are reversible and tend towards equilibrium. The concentration of Ca^{2+} and Mg^{2+} in the runoff water started low and increased with time, while that of Na^{+} started high and decreased with time (figure 5). This can be explained by the fast solubility of Na-containing salts in the soil such as NaCl and slower solubility of Ca^{2+} and Mg^{2+}containing salts such as gypsum (Bharmoria et al. 2012; Lebedev and Kosorukov 2017).

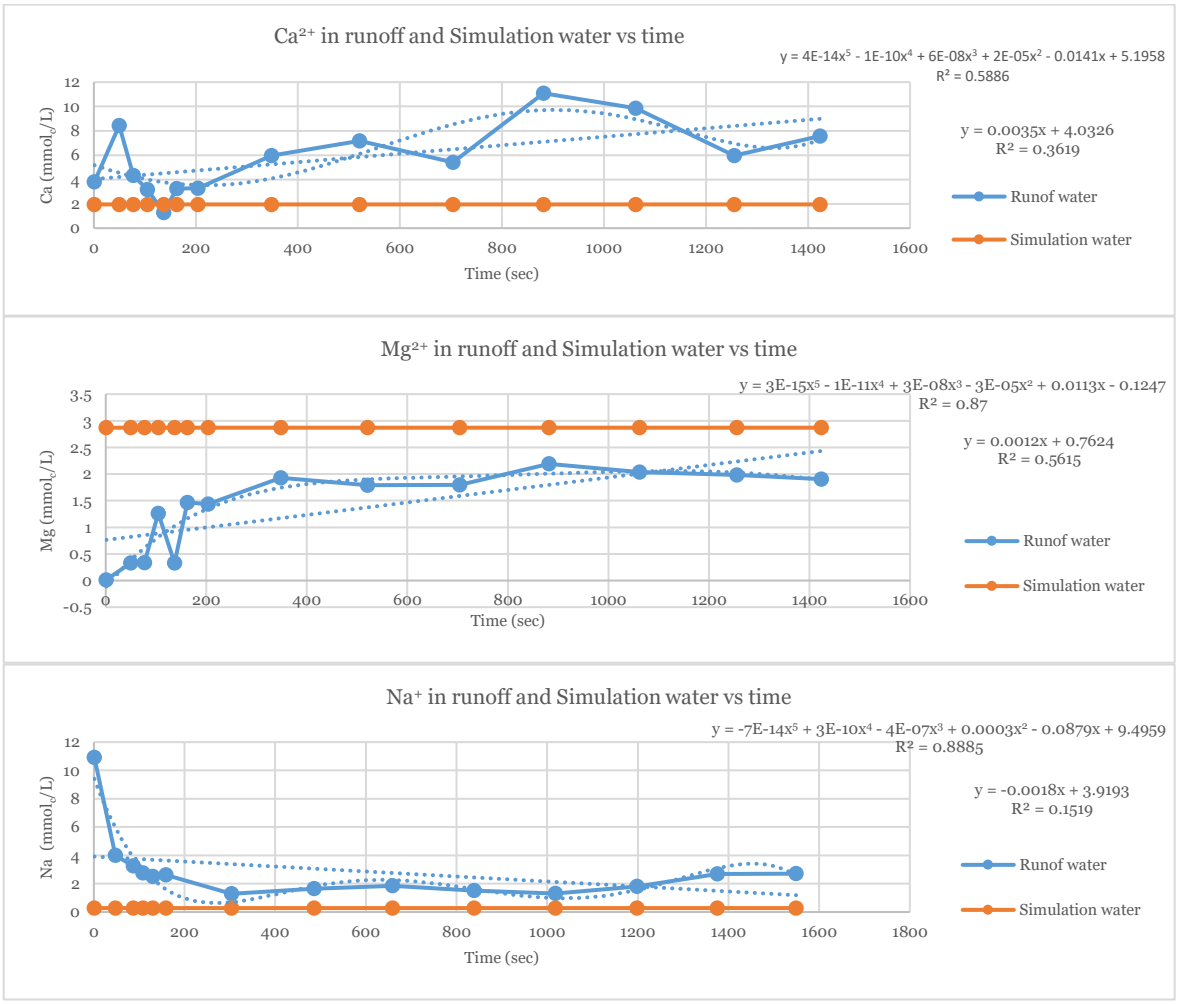

Figure 5. Concentration of Ca^{2+}, Mg^{2+} and Na^{+} in the simulation water and runoff water for run 1 at Dry X with straight line and polynomial fits.

The Cl^- in Figure 6 has a trend similar to that of Na^+ which can be explained by the higher and faster solubility of Cl^- containing salts compared with SO_4^{2-}. The high concentration of Ca^{2+} and SO_4^{2-} in the runoff water resulted from the dissolution of gypsum from the soil that is limited in water and slower than the solubility of NaCl (Bharmoria et al. 2012; Lebedev and Kosorukov 2017).

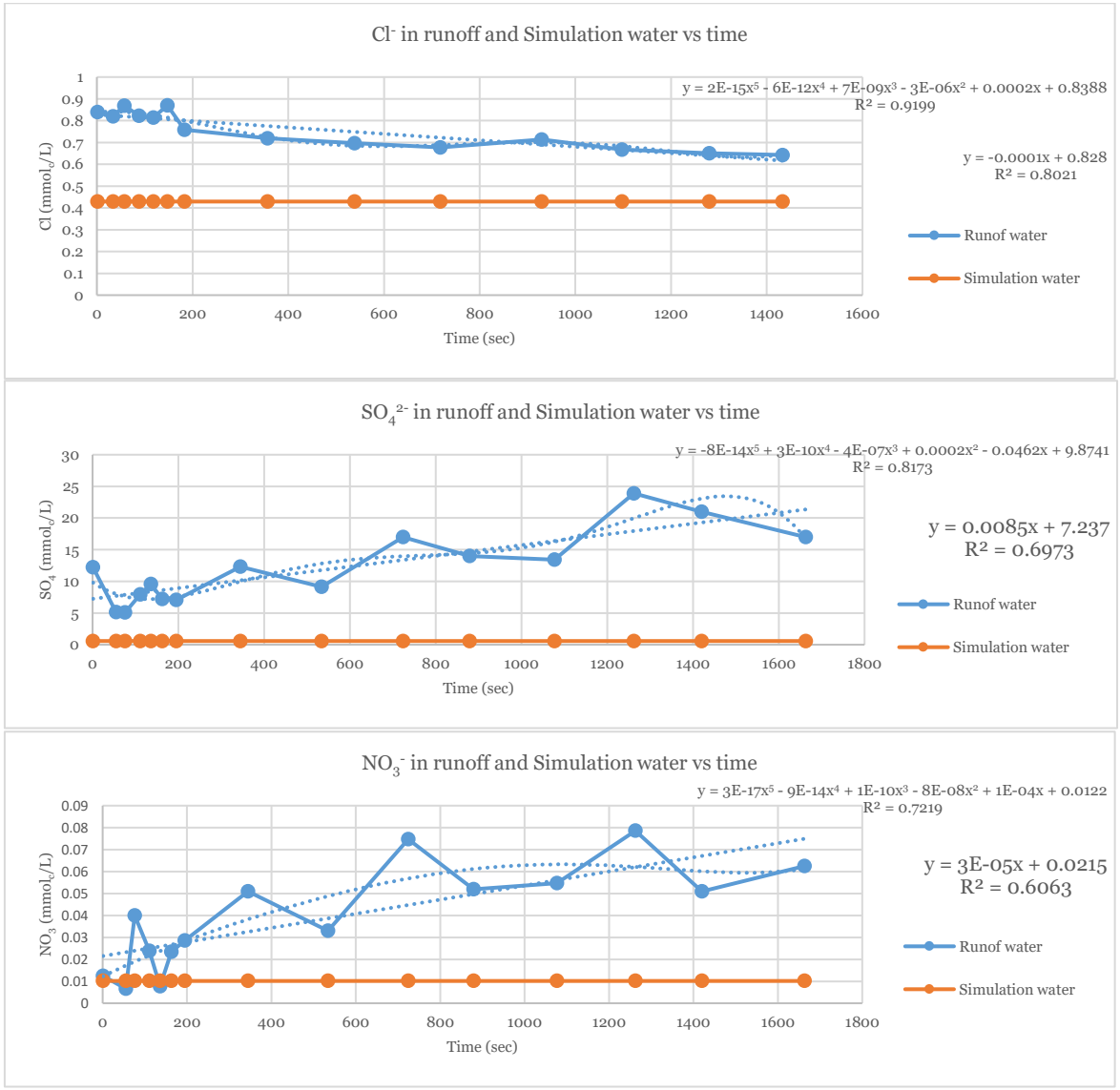

Figure 6. Concentration of Cl^-, SO_4^{2-} and NO_3^- in the simulation water and runoff water for run 1 at Dry X with straight line and polynomial fits.

The values of EC and SAR in runoff water are higher than simulation water (Figure 7). Their values reflect runoff water content of soluble of Na^+, Ca^{2+} and Mg^{2+} ions. The presented results show that even less than one hour of simulation duration is capable of extracting some plant nutrients from the soil such as NH_4^+ and NO_3^- from the soil (Figure 6) which might be higher and more important from croplands. The fast reactions between simulation water and soil, cause runoff water quality deteriorated and its suitability for irrigation, municipal and industrial use decreased resulting from increased EC, NO_3^- content in addition to SAR (Figure 6 & 7). The higher SAR values at the start of the runoff are the results of higher concentration of Na^+ compared with Ca^{2+} and Mg^{2+} because of the higher speed of Na^+ reaction and slow gypsum solubility. The presence of gypsum in the upper 11 cm of the soil is a good source of Ca^{2+}, which will maintain low ESP value and preserve the soil from fast deterioration from high Na^+ content that increase the ECe and SAR values.

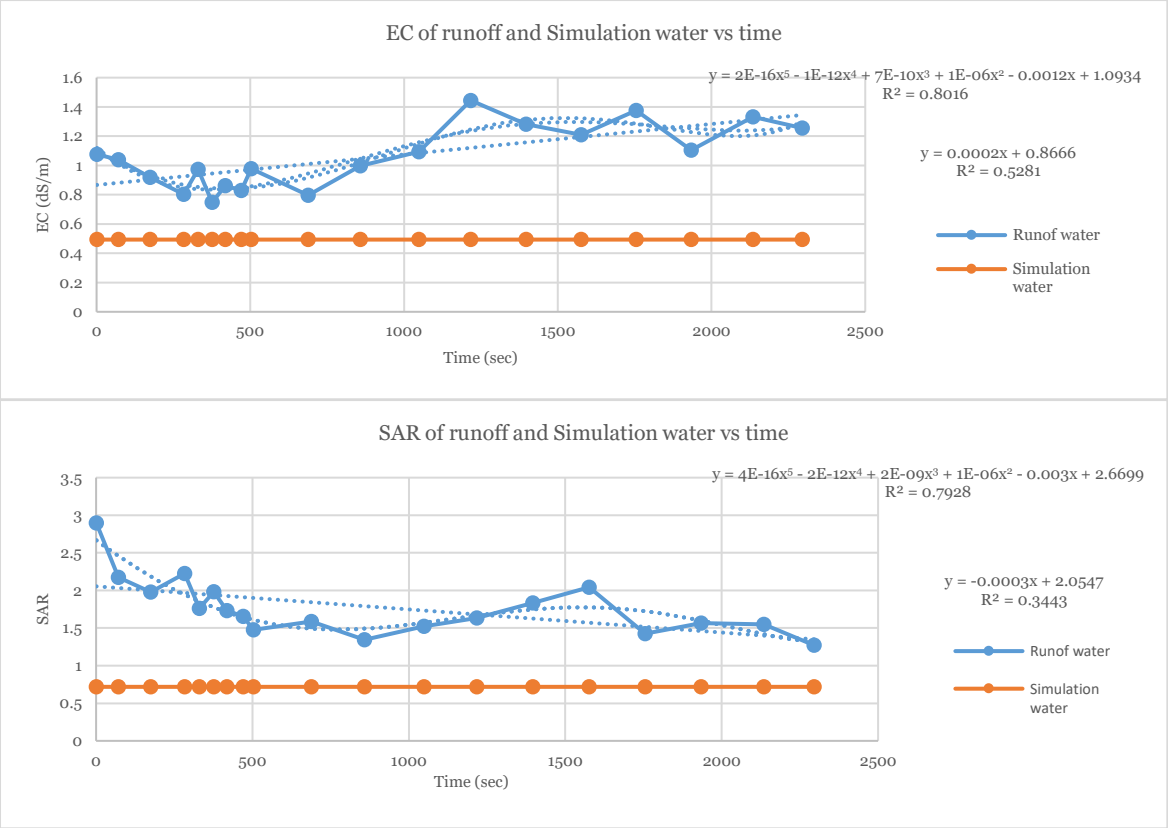

Figure 7. Total Dissolved Solids and Sodium Adsorption Ratio of the runoff water and simulation water for run 1 at Dry X with straight line and polynomial fits.

Implication of transport processes on runoff water quality: The monovalent cations (Na^+ and Cl^-) moved with runoff water from the studied plots before divalent cations
(Ca^{2+} Mg^{2+} and $SO4^{2-}$) produced high SAR values in early runoff water which decreased with time (Figure 7). The solubility of the precipitated salts on saltbush leaves by simulation water is another source of Na^+ that contributes to Na^+ concentration of runoff water. It is well known that Na^+ contributes to SAR and could appear in runoff water as well as the SAR of the soluble part that cause soil and surface water deterioration. The contribution of Na^+ from the vegetation cover deteriorates surface water quality that requires especial consideration in the selection of revegetation plant species and management of rangelands.

The higher plant nutrient concentrations (NH_4^+ and NO_3^-) in runoff water compared with simulation water are other signs of surface water reservoirs deterioration where the fertility of surface soil declines in addition to increasing the possibility of growing algae in surface water reservoirs. The presence of gypsum in the surface soil contributes positively to surface water quality by reducing The SAR of surface water and the soluble part in the soil in addition to the ESP of the exchangeable part of the soil. Our results show that gypsum content of the soil should be added to soil properties for their salinity-alkalinity classification in addition to EC_e and ESP (or/and SAR) because of the significant contribution of Ca^{2+} and SO_4^{2-} to the system.

Although higher coefficients of determination can be obtaining from fourth and fifth fitting polynomial equations of the single runs, runoff water ions concentration versus time for

example (Figure 5 and 6), the trend of concentration change with time does not describe the correct changes, and the coefficient of determination values decrease when we put many runs together. That is because the driving forces controlling the chemical reactions between the liquid and solid phases in the system (slope, covers, soil physical and chemical properties, hydrological parameters, etc.) are not the same even with the use of the same simulation intensity. In our analysis we utilized the average straight-line equation of each site to describe the behavior from the intercept and slope of the regression line where each slope and intercept is derived from 12 runs in the same site. The values of the average straight line's slope, intercept and coefficient of determination of the concentration of ions in runoff water, EC and SAR, with time for the sites are presented in Table 3. The positive slope value means increasing the value with elapsed runoff time, while negative slope value means decreasing the value with elapsed runoff time. The intercept is the value at the start of runoff that gives an idea about the magnitude. The slope and intercept values for K^+, NH_4^+, and NO_3^- are small which means that their contributions to the EC of runoff water are small and does not change dramatically with time.

The increase of Ca^{2+} and Mg^{2+} concentration in runoff water in Price, Dry X and Dry XII, respectively, mean increasing sources of these cations in the same trend, which is clear from the EC_e values, exchangeable Ca^{2+} and Mg^{2+} in addition to gypsum content of these soils. The positive slope describes the release of Ca^{2+} and Mg^{2+} which requires time for the reactions to take place. The Na^+ concentration in runoff water shows a decrease with time (negative slope) in Price and Dry XII while the slope in Dry X is small and positive that can be attributed to the higher ESP value (higher supply of Na^+ from the soluble part and exchange sites), which lasted for a long period. The slope of SAR value is negative, too, in all sites which is an indication of lower quality runoff water at the initiation of runoff and improving the quality with time.

Table 3. The slope, intercept and coefficient of determination of straight line regression of the concentration of ions ($mmol_c/l$), SAR and EC (dS/m) of the runoff water with time.

	Price			Dry X			Dry XII		
Parameter	slope	intercept	r^2	slope	intercept	r^2	slope	intercept	r^2
Ca^{2+} ($mmol_c/l$)	-0.00110	4.21	0.11	0.00239	4.73	0.42	0.00536	5.65	0.52
Mg^{2+} ($mmol_c/l$)	0.00019	1.20	0.15	0.00039	0.89	0.48	0.00086	1.17	0.48
Na^+ ($mmol_c/l$)	-0.00005	0.64	0.13	0.00013	4.37	0.18	-0.00302	7.50	0.13
K^+ ($mmol_c/l$)	-0.00008	0.22	0.28	0.00002	0.06	0.25	-0.00027	0.63	0.24
NH_4^+ ($mmol_c/l$)	-0.00001	0.02	0.39	0.00000	0.19	0.36	-0.00001	0.01	0.31
NO_3^- ($mmol_c/l$)	0.00000	0.02	0.12	0.00002	0.06	0.25	0.00004	0.10	0.47
SO_4^{2-} ($mmol_c/l$)	-0.00150	5.25	0.16	0.00581	7.22	0.43	0.00890	13.42	0.54
Cl^- ($mmol_c/l$)	-0.00001	0.46	0.03	-0.00008	0.80	0.38	-0.00030	0.98	0.38
SAR	-0.00009	0.44	0.11	-0.00051	2.83	0.12	-0.00158	3.57	0.31
EC (dS/m)	-0.00010	0.60	0.10	0.00027	1.05	0.41	0.00034	1.50	0.39

Summary and Conclusions

We conducted rainfall simulation scenarios in three sites covering different salinity, alkalinity, cover, slope, simulation intensities to characterize runoff water quality by following the concentration of ions in runoff water. The concentration of cations and anions in the runoff water were higher than that of simulation water except for Mg^{2+} because of its high concentration in the simulation water compared with other ions especially that of Ca^{2+} in normal waters. The importance of the EC and SAR values derives from their effect on the structural stability of the soil and infiltration rate upon using the collected runoff water behind

dams and reservoirs for crop production, municipal and industrial uses, in addition to reestablishment of deteriorated rangelands (Rengasamy and Marchuk 2011; Marchuk 2013).

The results improve our understanding of the governing processes and contribute in developing routines to computer simulation predictions under saline conditions. Mimicking the changes in ions concentration in runoff water will improve the prediction of existing models such as Rangeland Hydrology and Erosion Model (RHEM) the concentration of cations and anions in runoff water and hence possible deterioration of surface water quality resulting from rainfall on salt affected soils.

These results are considered provisional pending additional research that includes more variations in soil types, slopes, and vegetation communities before a global solution can be identified to predict runoff water quality and quantity. Modelling runoff, erosion and solute transport in the vadose zone and ground water recharge is not an easy task especially under saline alkaline conditions because of the complicated system and the large number of driving parameters that require large datasets. However, predicting runoff water quality enables the RHEM user to suggest the most appropriate use of runoff water and management practices of such water on soils in order to reduce their negative impact on surface water and soil.

Acknowledgment

This study was conducted as a collaborative effort between the U.S. Department of Agriculture (USDA) Agricultural Research Service and the University of Nevada, Reno. USDA is an equal opportunity provider and employer. Mention of a proprietary product does not constitute a guarantee or warranty of the product by USDA or the authors, and it does not imply its approval to the exclusion of the other products that also may be suitable. The authors which to thank the Bureau of Land Management for financial support of a research program to understand and predict salt transport process on western rangelands.

References

Albrecht, T.R. and Thyne. G. 2007. Distinguishing natural and anthropogenic sources of water quality variability, southeastern Piceance Basin, Colorado. Geological Society of America 39: 46-46. ISSN: 0016-7592.

Arslan, A., 1995. A computer program to express the properties of gypsiferous soils. Canadian Journal of Soil Science. 459- 492.

Arslan A. and Dutt, R. 1993. Solubility of gypsum and its prediction in aqueous solutions of mixed electrolytes. Soil Science. Vol 155:1, 37- 47.

Bharmoria, P., Gupta, H., Mohandas, P.K., Ghosh, V.P. and Kumar, A. 2012. Temperature Invariance of NaCl Solubility in Water: Inferences from Salt–Water Cluster Behavior of NaCl, KCl, and NH4Cl. The Journal of Physical Chemistry116:11712-11719.

Bonnin, G.M., Martin, D., Lin, B., Parzybok, T., Yekta, M. and Riley, D. 2006. Precipitation-frequency atlas of the United States. NOAA atlas, 14. Pp. 295.

Crockford, R.H., Richardson, D.P. and Sageman, R. 1996. Chemistry of rainfall, throughfall and stemflow in a eucalypt forest and a pine plantation in South-eastern australia: 2. Throughfall. Hydrological processes, 10:13-24.

Gagnon, S.R., Sears, J.R.L., Makuch, J.R., Rossi, C.G., Nouwakpo, S.K., Weltz, M.A. and Frasier, G. 2014. Salinity Mobilization and Transport: Hydrologic and Aeolian Processes and Remediation Techniques for Rangelands: A Selected Bibliography. Reference Briefs Series no. SRB 2014-01. National Agricultural Library Cataloging Record Pp. 372.

Gharaibeh, M.A., N. I. Eltaif, and Albalasmeh, A.A. 2011. Reclamation of highly calcareous saline sodic soil using atriplex halimus and by-product Gypsum. International Journal of Phytoremediation, 13:873–883.

Kenney, T.A., Gerner, S.J., Buto, S.G. and Spangler, L.E. 2009. Spatially referenced statistical assessment of dissolved-solids load sources and transport in streams of the Upper Colorado River Basin. USGS Scientific Investigations Report. U.S. Geological Survey, Reston, Virginia. Pp. 50.

Khechai, S. and Daoud, Y. 2016. Characterization and Origin of Gypsum Rhizoliths of Ziban Oases Soil-Algeria. World Applied Sciences Journal 34 (7): 948-955.

Kruszyk, R., Kostrzewski, A. and Tylkowski, J. 2015. Variability of throughfall and stemflow deposition in pine and beech stands (C zarne Lake catchment, Gardno Lake catchment on Wolin Island). Instytut Geografii Gospodarki Przestrzennej UJ. Krakow 85-102. doi:10.4467/20833113PG.15.027.4628.

Lebedev, A.L., and Kosorukov, V.L. 2017. Gypsum solubility in water at 25°C. Geochemistry International. 55(2):2015-210. ISSN 0016-7029.

Levia Jr, D. F. and Frost, E.E. 2006. Variability of throughfall volume and solute inputs in wooded ecosystems. Progress in Physical Geography 30(5)605-632.

Mubarak, A., and Olsen, R.A. 1976: Immiscible displacement of the soil solution by centrifugation. Soil Science Society of America Journal 40(2):329-331.

National Soil Survey Handbook NSSH Part 618. 2017. Soil Properties and Qualities Subpart A – General Information. United States Department of Agriculture. Pp 87.

Paige, G.B., Stone, J.J., Smith, J.R. and Kennedy, J.R. 2004. The walnut gulch rainfall simulator: A computer-controlled variable intensity rainfall simulator. Applied Engineering in Agriculture 20:25-31.

Marchuk, A. 2013. Effect of cations and structural stability of salt-affected soils. pH D sissertation. School of Agriculture, Food and Wine. The University of Adelaide. Pp. 153.

Rengasamy P., and Marchuk, A. 2011. Cation ratio of soil structural stability (CROSS). Soil, land care and environmental research . Soil Research 49:280–285.

Rubin, J. 1983. Transport of reacting solutes in porous media, relation between mathematical nature of problem formulation and chemical nature of reactions. Water Resources Research 19:1231-1252.

Soil Survey Investigations Report No. 45. 2011. United States Department of Agriculture. Natural Resources Conservation Service. National Soil Survey Center. Lincoln, Nebraska. Pp 530.

U.S. Salinity Laboratory Staff. 1954. Diagnosis and improvement of saline and alkali soils. USDA Handb. 60. U.S. Gov. Print. Office, Washington, DC.

VanAmburg, L., Booth, D., Weltz, M. and Trlica, M. 2005. A laser point frame to measure cover. Rangeland ecology & management 58:557-560.

Weltz, M., Nouwakpo, S.K. Rossi, C. Jolley L.W. and Frasier, G. 2014. Salinity mobilization and transport from rangelands: assessment, recommendations, and knowledge gaps. General Technical Report 1. Reno, Nevada. Pp 72.

Western Regional Climate Center (WRCC) 2015. *Cooperative Climatological Data Summaries*. Retrieved from http://wrcc.dri.edu/climatedata/climsum/

Zwikel, S., Lavee, H. and Sarah, P. 2007. Temporal evolution of salts in Mediterranean soils transect under different climatic conditions. CATENA 70:282-295. ISSN: 0341-8162.

The Latest CE-QUAL-W2 Model Developed for Predicting Total Dissolved Gas in Support of the Columbia River System Operations

Zhonglong Zhang, PhD, PE, PH, Research Professor, Department of Civil and Environmental Engineering, Portland State University, Portland, OR 97207, e-mail: zz3@pdx.edu

Abstract

The regression equations included in System Total Dissolved Gas (SYSTDG) model for estimating spillway/gate TDG production have been validated based on extensive TDG field studies conducted for the Columbia and Snake River dams. Currently, SYSTDG is the most complete container of knowledge regarding spillway TDG generation of the Columbia and Snake River dams. In this study, SYSTDG was incorporated into the latest two-dimensional hydrodynamic and water quality CE-QUAL-W2 model for predicting TDG at twelve dams in support of the Columbia River System Operations (CRSO) Environmental Impact Statement. The enhanced model named as CE-QUAL-W2 Version 4.2 (W2V4.2) was tested with a variety of CRSO project datasets and also was compared against SYSTDG calculations. The SYSTDG features included in W2V4.2 function well. W2V4.2 will allow the user to evaluate the impacts of spill operations on the tailwater TDG and may provide insight for efforts to mitigate high TDG levels of such reservoirs. This presentation will give an overview of the newly developed TDG capability in W2V4.2 and its application to the Columbia and Snake River dams.

Introduction

Water temperature and TDG supersaturation are directly impacted by the Columbia River dams. Specifically, temperature can affect timing and survival of adult and juvenile salmon and steelhead migrating through the mainstem Snake and Columbia rivers. The states of Oregon and Washington have identified the Columbia and Snake Rivers as not achieving their temperature standard. TDG refers to the total amount of dissolved gas present in water. High TDG concentrations can cause gas bubble disease and reduce the population of some fish species. In the Columbia River and Snake River system, the most prominent source of TDG supersaturation is often spillway releases or bypass operations, as illustrated in Figure 1. Spillway operations result in atmospheric gases being forced into the water. The TDG concentrations are increased by spills; the turbulent nature of the spill creates air bubbles that are then forced deep into the tailwater where they dissolve and propagate downstream, and TDG supersaturation occurs. The generation of power at each of the Columbia and Snake River dams is a critical component in establishing both voluntary spill for fish passage and involuntary spill due to limited powerhouse capacity (USACE, 2016).

Under the Columbia River System Operations (CRSO) Environmental Impact Statement (EIS) study, the U.S. Army Corps of Engineers (USACE) is in the process of evaluating long-term system operations and configuration of 14 multiple purpose dams and related facilities to better understand water temperature change and TDG saturation levels and assist in their mitigation (USACE, 2016). CE-QUAL-W2 (W2) has been used to predict temperature and TDG released from 14 federal dam and reservoir projects. In this study, the current W2 model was further developed and enhanced with: 1) incorporating TDG production equations from the System

Total Dissolved Gas (called SYSTDG) model into the W2 model to calculate the TDG production in spill flows and tailwaters of reservoirs during spill operations, and 2) adding a spill operation algorithm into the W2 model to assist reservoir operators and decision-makers in managing spill flows set by a TDG target. These two features are unprecedented in the current version of W2 model (Cole and Wells, 2018). The latest version of W2 (W2V4.1) and previous versions are maintained by Portland State University (PSU) and can be freely accessed and downloaded from the PSU website: *http://www.cee.pdx.edu/w2/*.

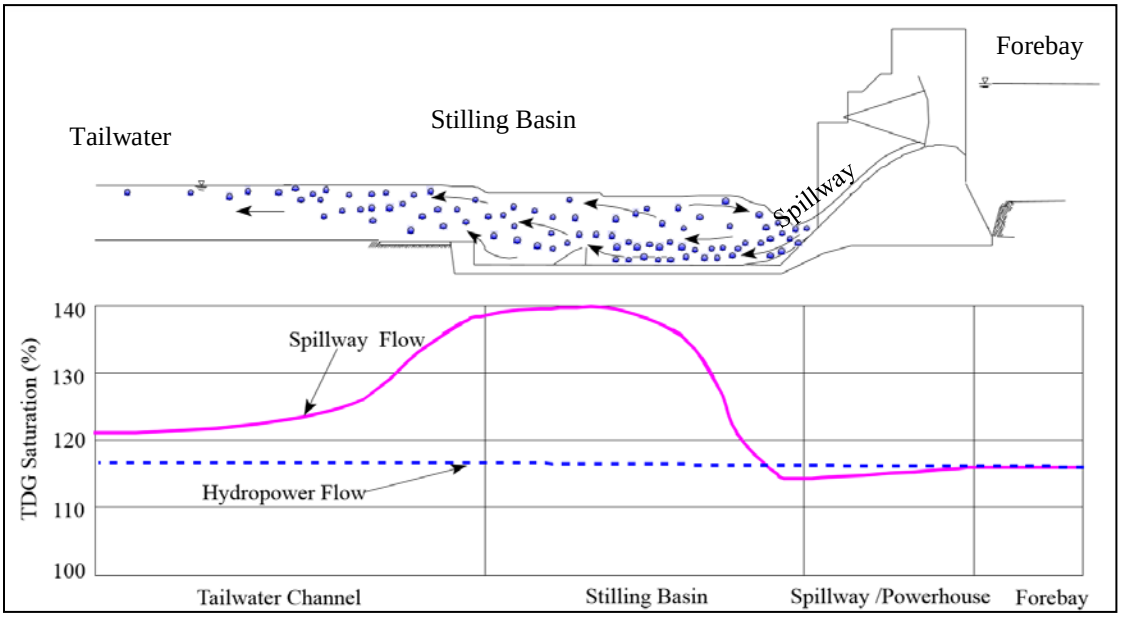

Figure 1. TDG production processes from a spillway (USACE, 2016)

W2 Version 4.2

SYSTDG Model

SYSTDG is an Excel-based spreadsheet model used to compute TDG saturation levels in the Columbia River Basin. Primary use of SYSTDG has been in real-time management to assist in setting daily TDG spill caps, but has occasionally been used in a planning capacity (Scheider and Hamilton, 2015a, 2015b). SYSTDG contains empirical equations for gas generation at each spillway and powerhouse based on outlet flow, tailwater depth, and barometric pressure. In SYSTDG, estimation of TDG production can involve any or all of the following factors:

- Bay-by-bay spillway discharge governed by a spill pattern (table of discharge in each spill bay as a function of total spillway discharge)
- TDG production relations that are specific to a bay (deflectored or non-deflectored bays)
- Downstream stage
- Entrainment of water passing through power house turbine units.

The TDG exchange associated with spillway operation at a dam is a process that couples both the hydrodynamic and mass exchange processes. The hydrodynamics are shaped by the structural characteristics of spillway, stilling basin, and tailrace channel as well as the operating conditions that define the spill pattern, turbine usage, and tailwater stage. The hydrodynamic

conditions are influenced to a much smaller extent by the presence of entrained bubbles. In SYSTDG, downstream TDG is calculated based on two significant physical processes: TDG production through air entrainment and bubble dissolution, and the mixing of spillway flows with lateral powerhouse flows (Figure 1). The production of TDG in the tailrace, represented as a mixed quantity, is governed by the following physically controlled processes:

- Spillway flow
- Powerhouse flow
- Entrainment of powerhouse flow into spillway flow
- Tailwater depth

SYSTDG contains empirical equations for gas generation at each spillway and powerhouse based on outlet flow, depth of the tailwater, and barometric pressure. The following spillway/gate TDG production equations and computation algorithms in SYSTDG are incorporated into W2V4.2.

$$TDG_{sp} = P1 * \left(1 - e^{P3 * Q_{sp}}\right) + bp$$

$$TDG_{sp} = P1 * (twe - twce)^{P2} * \left(1 - e^{P3 * q_s}\right) + P4 + bp$$

$$TDG_{sp} = P1 * (twe - twce)^{P2} * {q_s}^{P3} + P4 + bp$$

$$TDG_{sp} = P1 * (twe - twce) + P2 * {q_s}^{P3} + P4 + bp$$

$$TDG_{sp} = P1 * (1 - e^{P2 * q_s}) + P3 * (Temp_{tw} - P4) + bp$$

Where TDG_{sp} = spillway discharge total gas pressure (mmHg), ΔTGP_{sp} = spillway discharge gas pressure (mmHg), bp = observed barometric pressure (mmHg), twe = observed project tailwater elevation (feet), $twce$ = project specific tailwater channel elevation (feet), twe - $twce$ = tailwater channel depth (feet), $Temp_{tw}$ = tailwater temperature (°C), Q_{sp} = total project spillway discharge (kcfs), q_s = flow weighted specific spill bay discharge (kcfs), *P1* - *P4* = project specific coefficients (unitless).

The unit spillway discharge is a surrogate measure for the velocity, momentum, and exposure time of aerated flow associated with spillway discharge. The higher the unit spillway discharge, the greater the TDG exchange during spillway flows. Flow weighted specific spill bay discharge can be actual measured discharges through each spill bay or computed as a function of the spill pattern:

$$q_s = \frac{\sum_{i=1}^{nb} Q_i^C}{\sum_{i=1}^{nb} Q_i^{(C-1)}}$$

Where Q_i = discharge through spill bay i, nb = the number of project spill bays, C = Project and spill pattern specific constant.

In SYSTDG, the entrainment of powerhouse flows is computed as a simple linear function of spillway flows. Without spillway discharge, there is no mechanism to attract powerhouse flows into the spillway region and no air-entrainment mechanism to drive local TDG supersaturation.

As spillway flows increase relative to powerhouse flows, both bubble production and water entrainment ramp up to a point at which nearly all powerhouse flows are exposed to bubbles entrained at the spillway. Three equations are used to calculate the entrainment of powerhouse flow in SYSTDG.

$$Q_{ent} = E1 * Q_{sp} + E2$$

$$Q_{ent} = min[(Q_{tot} / 60) , 1] * E1 * Q_{sp} + E2$$

$$Q_{ent} = min[(Q_{sp} / 20) , 1] * E1 * Q_{sp} + E2$$

Where Q_{ent} = Total powerhouse flow that is entrained in spillway flow (kcfs), Q_{tot} = total project discharge (power house and spillway) (kcfs), *E1* - *E2* = project specific coefficients (unitless).

Scheider and Hamilton (2015b) provides *P1, P2, P3, P4, C, E1,* and *E2* values for 11 federal dams on the Columbia and Snake River system.

The average tailrace mixing TDG pressures generated from a project are computed from the flow weighted average TDG pressures of the spillway and the powerhouse. TDG pressures of flows released from the powerhouse are assumed equivalent to the TDG pressure in the forebay.

$$TDG_{rel} = \frac{TDG_{sp}(Q_{sp}+Q_{ent})+TDG_{ph}(Q_{ph}-Q_{ent})}{Q_{ph}+Q_{sp}}$$

Where TDG_{rel} = project release TGP after mixing (mmHg), TDG_{sp} = spillway TGP (mmHg), TDG_{ph} = release TGP through the powerhouse turbines (mmHg), Q_{sp} = Total project spill (kcfs), Q_{ph} = Total flow through powerhouse turbines (kcfs).

Spillway Operations Set by TDG Targets

In the Columbia River and Snake River system, the most prominent sources of TDG supersaturation are often spillway releases, which are a prevalent environmental concern during the voluntary spill season that lasts from early April through mid-August. These effects are most pronounced in the tailwaters of reservoirs during spill seasons. There is a highly dynamic relationship between spill releases, downstream zones of TDG supersaturation, and dilutive capacity of powerhouse flows. Projects are required to minimize and manage spill flow, allocate spill flow to specific spill bays, and maximize powerhouse flows in order to meet established limits of TDG saturation level for all surface water.

Knowledge of the effect of spillway operations on tailrace TDG is extremely valuable for forecasting and mitigating TDG supersaturation. Therefore, an option for quantifying how TDG levels change with spillway operations was added in W2V4.2. W2V4.2 can be used to determining if temporal and spatial distribution of spillway release TDG is being met at the right place and time for the spillway operations. This capability allows operators to allocate spill flows to minimize TDG production while meeting powerhouse maximum capacities.

The spillway operation algorithm for allocating spill flows to the powerhouse to meet TDG targets was adopted in part from the water temperature blending algorithms developed by the U.S. Geological Survey (USGS) (Rounds and Buccola, 2015). A constant or an external time-series of TDG targets (TDG_{ta}) can be specified at spillway or tailrace (mixing zone) to represent target TDG gage location. Priority designations can be set for the spill bay to assist in choosing which spill bays are used and in determining which spill bays receive a greater proportion of the flow allocation. In the flow allocation calculation, the TDG target is assumed between TDG_{ph} and TDG_{sp}:

$$TDG_{ph} \le TDG_{ta} \le TDG_{sp}$$

If more than one spill bay exists, then the overall flow to the powerhouse is allocated equally from each spill bay, subject to minimum and maximum flow criteria of the powerhouse. Powerhouse flow patterns correspond with power system requirements, which may vary drastically from the early morning hours through the evening. If more than one powerhouse is included, then the overall flow is allocated to each powerhouse based on their remaining capacities. Priority designations are used to choose the spill bays for corresponding flow allocation. The spill priority list is defined by the user. The numerical dichotomy method was applied to calculate the flow allocation from spill bays to the powerhouse. The algorithm implemented in W2V4.2 is presented in Figure 2.

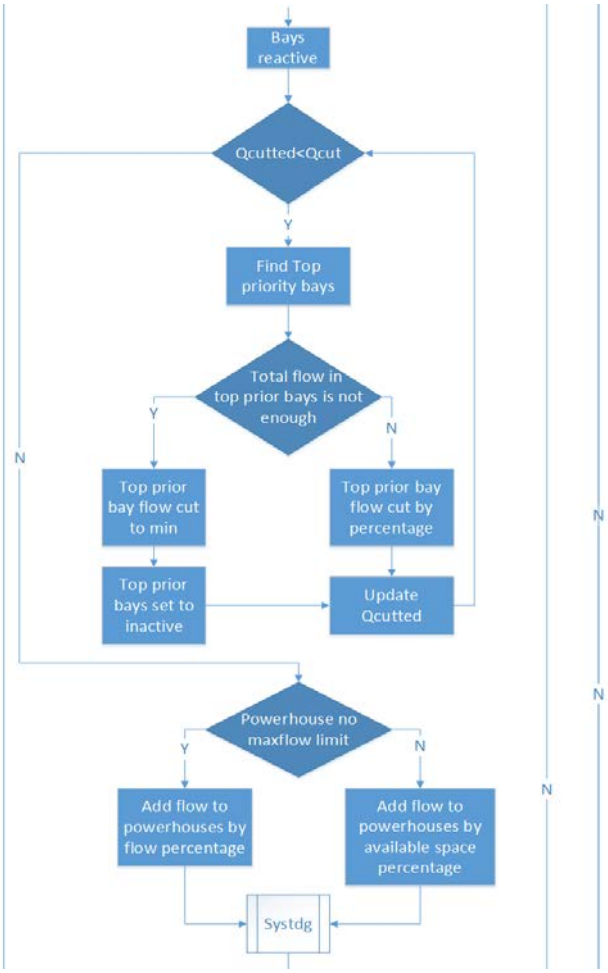

Figure 3. Flowchart of TDG algorithm implemented for the spill flow allocation

Both “Gate” and “Spillway” in W2V4.1 can be used to calculate spillway TDG production. “Gate" has a capability of specifying a time series data of flow rates for individual gates. Therefore the SYSTDG equations and spillway operation algorithms set by TDG targets were implemented through “Gate”. Two TDG target locations were included, one for specified spill flow target, the other one for specified tailrace mixing zone target. TDG concentrations computed with the SYSTDG equations in W2V4.2 are written into withdrawal output files. Withdrawal outflow files contain information with release or withdrawal TDG concentrations in the time series output files. Additional TDG target output file is generated from the W2V4.2 model if a spill flow allocation to meet a TDG target is conducted. This file contains information for outflow release or spillway TDG concentrations and outflows as a time series file.

Validation and Evaluation of W2 Version 4.2

Study Site

The Columbia River flows more than 400 miles through British Columbia before reaching the U.S.-Canada border near Castlegar, British Columbia. It then flows south through Washington before turning west near Wallulla Junction, Washington, forming the Washington-Oregon state border. The headwaters of its largest tributary, the Snake River, are in the Teton Mountains of Wyoming. The Snake River flows through Idaho before forming the Oregon-Idaho state border and discharging to the Columbia River near Pasco, Washington. The Columbia and Snake Rivers are controlled by dams. There are 11 mainstem hydroelectric projects on the Columbia River. The Snake River is also heavily controlled with 19 dams on the mainstem and several impoundments on its tributaries. The CRSO EIS study focuses on 14 multiple purpose and related facilities that are operated as a coordinated system within the interior Columbia River basin in Idaho, Montana, Oregon, and Washington (Figure 2). The W2 model was enhanced to predict temperature and TDG released from individual dams on the Columbia and Snake Rivers.

Figure 3. Study site and federal dams on the Columbia and Snake Rivers

Model Validation and Evaluation

The W2V4.2 models developed for the fourteen dams shown in Figure 3 have been fully calibrated for 5 year (2011-2015) period by the project team. The Bonneville Dam was selected as a demonstration site for this study. The Bonneville Dam is located on Columbia River Mile (RM) 146.1 and is a run-of-river dam. The Dam is 171 feet high and 2,477 feet long. The spillway is 1,070 feet long and contains 18 spill bays each with a 50 feet by 60 feet lift gate. The dam has a navigation lock on the Oregon side of the river and fish ladders on both sides. The first powerhouse opened in 1937 and consists of 10 units with a nameplate capacity of 518 MW, an overload capacity of 574 MW, and a hydraulic capacity of 136,000 cfs. The second powerhouse opened in 1981 and consists of 8 units with a nameplate capacity of 532 MW, an overload capacity of 612 MW, and a hydraulic capacity of 152,000 cfs. Bonneville Dam impounds Lake Bonneville. The reservoir is 48 miles long, from Bonneville Dam to the foot of The Dalles Dam upstream, with a surface area of 29.5 square miles, and a capacity of 537,000 acre-feet. The full forebay elevation is 77 feet, and the maximum forebay elevation is 82.5 feet (WEST, 2012).

The Bonneville W2 model domain extends upstream for 45.9 river miles to the Dalles Dam and has 75 longitudinal segments of varying widths and 56 vertical layers of varying heights. The model includes 2 powerhouse units and 18 spill bays. The fish ladder flow and any flows not accounted for in the spillway and powerhouse were combined into a single miscellaneous flow category.

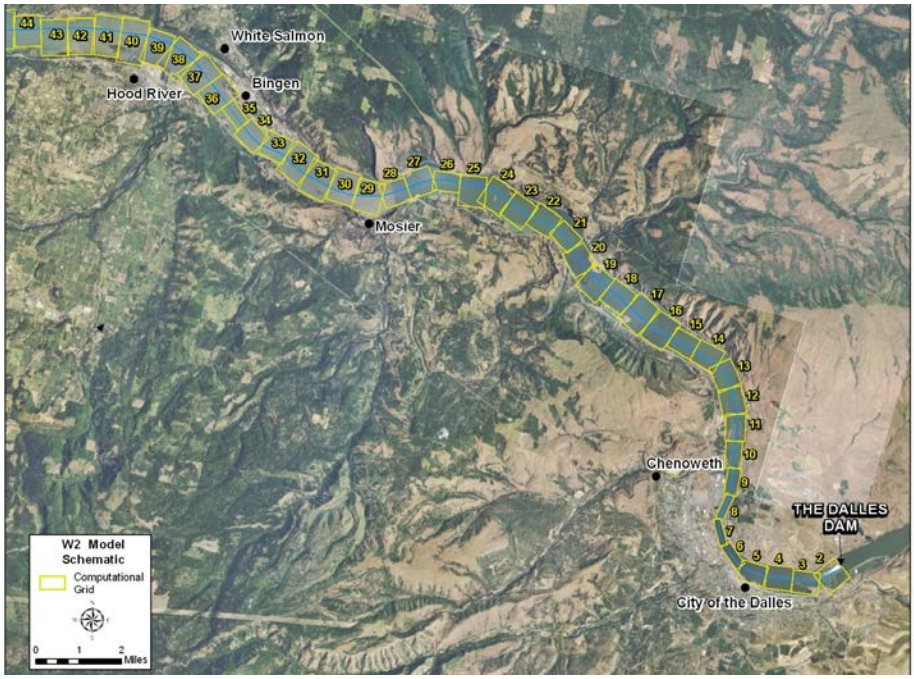

Figure 4. Bonneville Dam W2 model longitudinal segments (WEST, 2012)

Graphical comparison between W2 simulated and observed TDG at the Bonneville Dam tailwater is presented in Figure 5. The statistics of model performance, including mean error (ME), mean absolute error (MAE), and root mean square error (RMSE) were used to assess the predictive capability of the W2 model. The model calibration statistics showing ME of 1.07, MAE of 2.66, and RMSE of 3.50 also reflected an acceptable level of predictive capability of SYSTDG implemented in W2V4.2. The results show that the Bonneville Dam W2 model adequately predicts TDG within the reservoir and outlet releases. The model is able to predict the annual trends and seasonal variations of TDG at the Dam tailwater. The peak TDG concentrations during the spill seasons are well captured by the model.

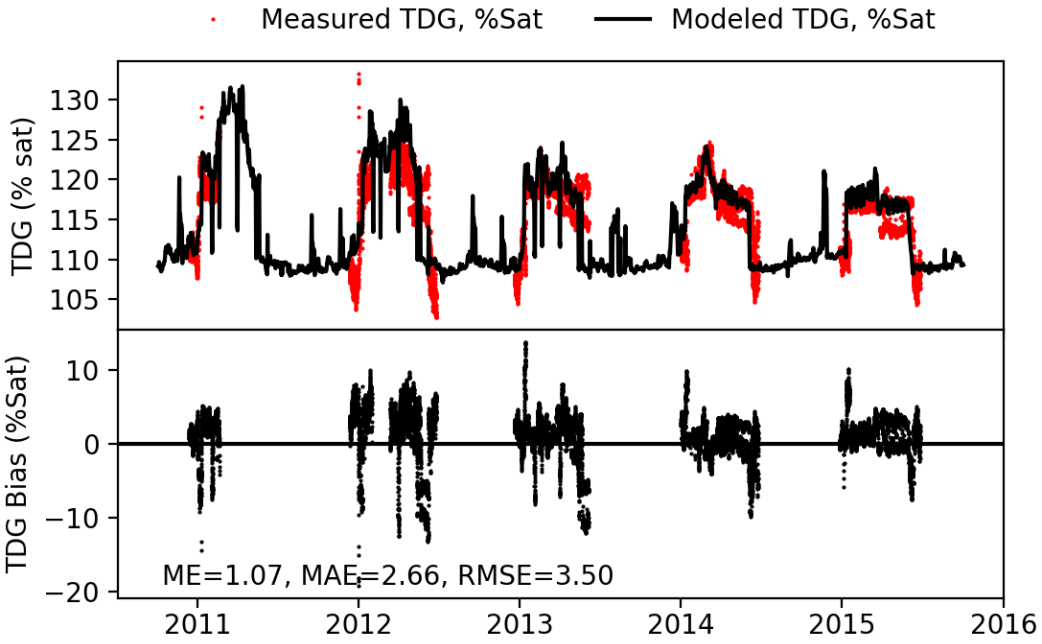

Figure 5. Time series comparison of W2V4.2 computed and observed TDG at Bonneville tailwater

The time series spillway TDG concentrations predicted by the Bonneville Dam W2 model are presented in Figure 5. To demonstrate the spill flow allocation capability implemented in W2V4.2, the seasonal TDG targets at the Dam tailwater set ranging from 115 percent to 125 percent are also included in Figure 6. Spillway TDG concentrations above the TDG targets occurred during the spill seasons. The W2V4.2 model was then applied to allocate spill bay flow into the powerhouse to reduce the saturation of spill TDG and achieve the TDG targets.

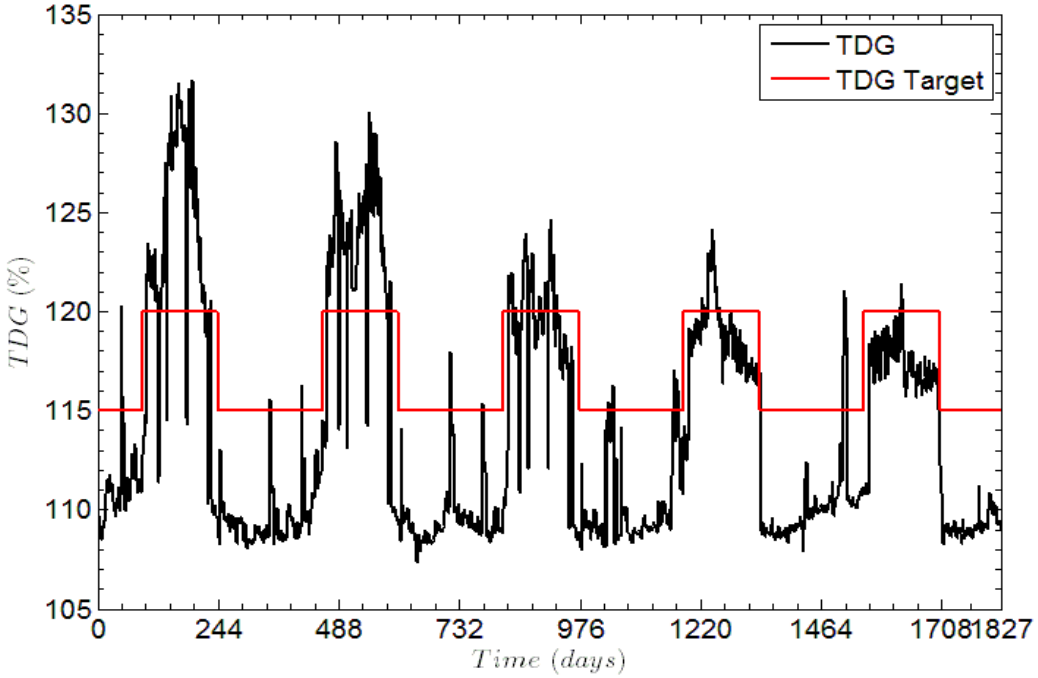

Figure 6. Spillway TDG released from Bonneville Dam for 5 year (2011-2015) with varying TDG standard.

The existing total flow, the power house flow and spillway flows released from the Bonneville Dam are shown in Figure 7(a). The spill volumes were the largest at Bonneville Dam for all four projects on the lower Columbia River. The maximum powerhouse capacity as limited by unit availability for the Bonneville Dam was 212 kcfs.

Figure 7(b) presented the updated spillway and powerhouse flows after an allocation was conducted based on the same priority for all individual spill bays. Under this assumption, a significant amount of spillway flow was allocated into the powerhouse during the spill seasons.

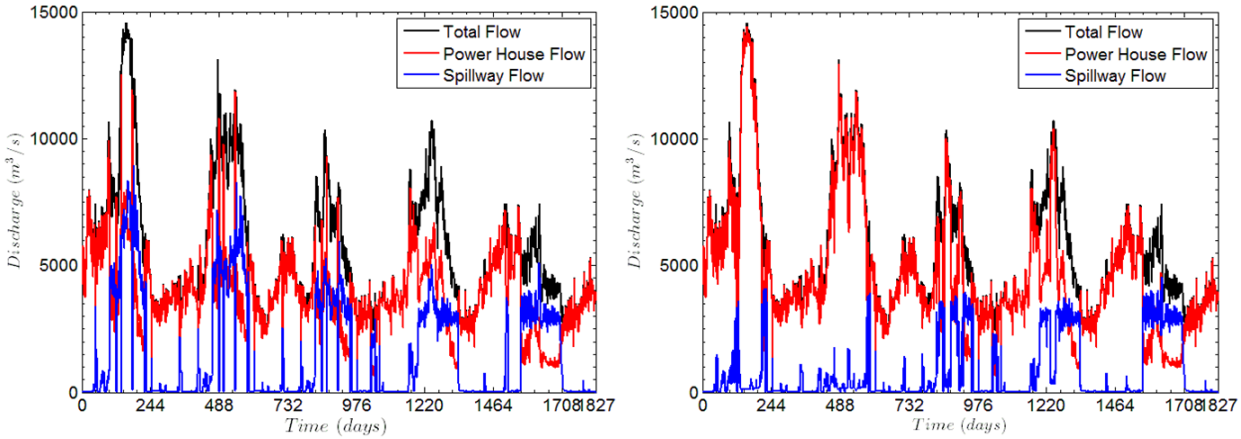

Figure 7. Spillway and powerhouse flows released from Bonneville Dam for (a) before (b) after performing a Spill flow allocation set by the TDG target

Summary

The predictive equations, coefficients, and constraints in SYSTDG were incorporated into W2V4.1 and a new version of W2 model (W2V4.2) was created for predicting TDG in support of the CRSO EIS study. This version was applied to the Columbia and Snake River projects by the CRSO modeling team. The SYSTDG capabilities in W2V4.2 were validated against observed data, the model results from the comparison showed that the W2V4.2 was able to reproduce TDG predictions calculated from SYSTDG. The SYSTDG features included in the W2 model function well.

The algorithm for performing spillway operations set by user-defined TDG targets was also incorporated into W2V4.2. This feature allows the user to conduct optimum spillway operations to allocate flows from spillways to the powerhouse to meet TDG targets. Otherwise, multiple model runs must be performed in an iterative fashion to determine an optimal spillway operations strategy that might best be used to meet TDG targets. However this feature has not been fully tested and verified, needs further testing and validation.

Acknowledgments

This study was funded under the USACE's Columbia River System Operations (CRSO). Kathryn Tackley was the CRSO water quality technical manager. The authors would like to acknowledge the following people for the guidance, advice, testing and assistance: Tammy Threadgill, Dan Turner, Ronald Thomasson, and David Gade of USACE.

References

Columbia River Basin Research. 2000. Columbia River Salmon Passage Model CRiSP 1.6 Theory and Calibration, University of Washington, Seattle, WA.

Cole, T.M. and S.A. Wells. 2018. CE-QUAL-W2: A Two-Dimensional, Laterally Averaged, Hydrodynamic and Water Quality Model, Version 4.1; Portland State University: Portland, OR. *http://www.cee.pdx.edu/w2/*

Colt, J. 1984. Computation of Dissolved Gas Concentrations in Water as Functions of Temperature, Salinity, and Pressure. Report, American Fisheries Society, Bethesda, Maryland. Special Publication 14, ISBN 0-913235-02-4.

Rounds, S.A. and N.L. Buccola. 2015. Improved algorithms in the CE–QUAL–W2 water-quality model for blending dam releases to meet downstream water-temperature targets: U.S. Geological Survey Open-File Report 2015-1027, 40 p., *http://dx.doi.org/10.3133/ofr20151027.*

Schneider, M. and L. Hamilton. 2015a. SYSTDG Developer's Manual. U.S. Army Corps of Engineers, Northwestern Division, Reservoir Control Center.

Schneider, M. and L. Hamilton. 2015b. SYSTDG User's Manual. U.S. Army Corps of Engineers, Northwestern Division, Reservoir Control Center.

U.S. Army Corps of Engineers (USACE), 2016, Update to the Total Dissolved Gas Abatement Plan, Lower Columbia River and Lower Snake River Projects, August 2016. http://www.nwd-wc.usace.army.mil/tmt/wqnew/gas_abatement/2016/USACE_update.pdf

WEST Consultants, Inc. 2012d. Development of a CE-QUAL-W2 Model for Bonneville Dam and Reservoir. Contract W9127N-10-D-0002. U.S. Army Corps of Engineers, Portland District.

Watershed Management

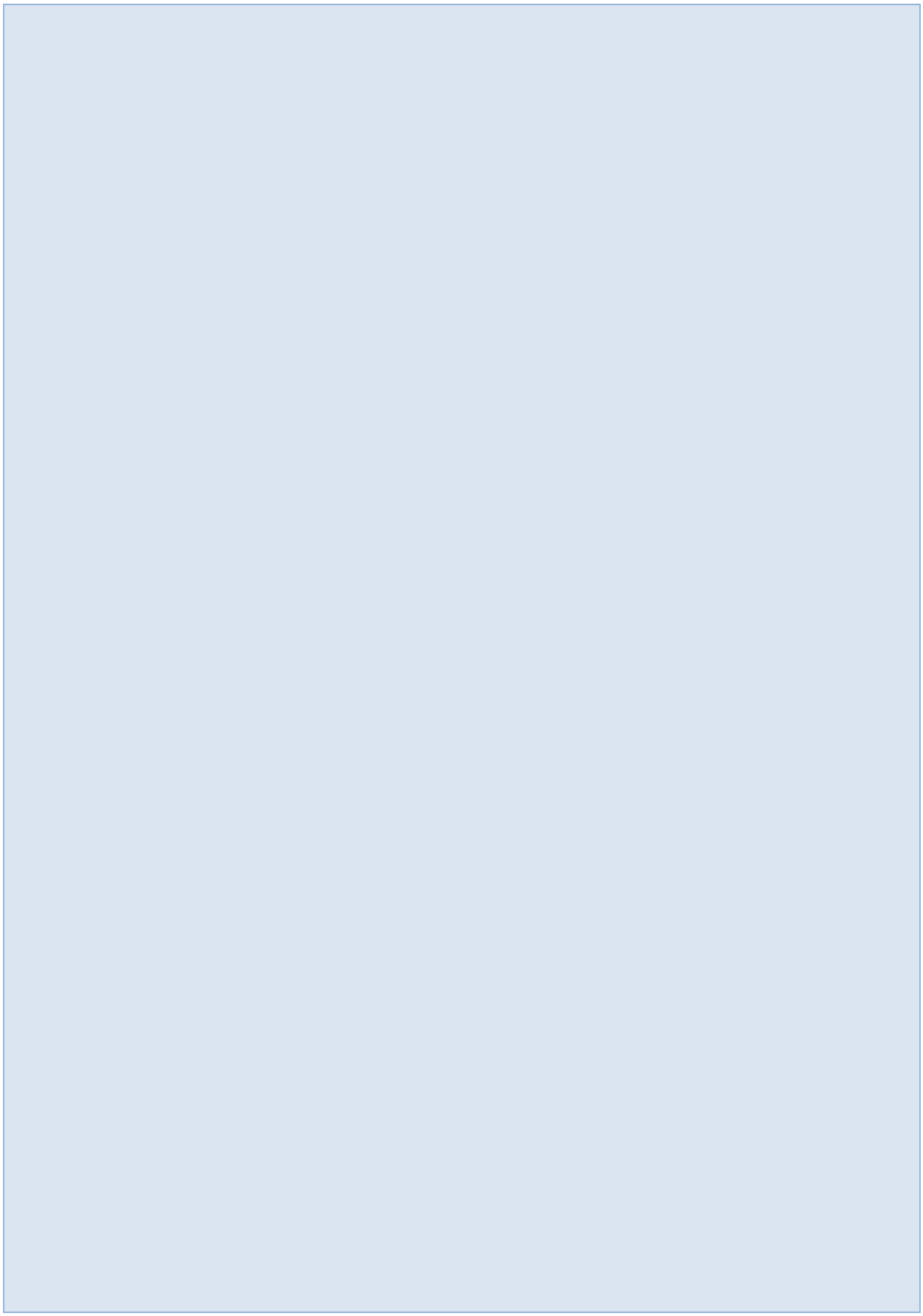

Integrated Hydrologic Modeling of the Salinas River, California, for Sustainable Water Management

Joseph A. Hevesi, Hydrologist, U.S. Geological Survey, Sacramento, CA, jhevesi@usgs.gov
Wesley R. Henson, Hydrologist, U.S. Geological Survey, CA, whenson@usgs.gov
Randall T. Hanson, Hydrologist, U.S. Geological Survey, San Diego, CA, rthanson@usgs.gov
Scott E. Boyce, Hydrologist, U.S. Geological Survey, San Diego, CA, seboyce@usgs.gov

Introduction

Study area and background

The Salinas River drains 4,160 square miles (mi^2) and is the largest river in California's Central Coast (figure 1). It originates in the La Panza Range of central San Luis Obispo County, and flows 170 miles north and northwest through Monterey County to the Monterey Bay National Marine Sanctuary, about 80 miles south of San Francisco. The Salinas River valley is an extensively farmed alluvial basin with mountainous headwater drainages characterized by ephemeral streamflow. The groundwater resources of the basin are used heavily to meet water supply needs, including crop irrigation and municipal water supply. Two 22 mi^2 reservoirs within the Salinas River watershed, Nacimiento and San Antonio, provide flood protection and are operated for a variety of uses that include municipal water supplies, agricultural irrigation, recreation, groundwater recharge, and protection of fish habitat. The Salinas River watershed is currently experiencing insufficient water supplies and stakeholders are facing legal and regulatory restrictions on water use. The historical imbalances between supply and demand have resulted in sinking groundwater levels, seawater intrusion, impaired water supplies, regulatory actions on pumping, adjudication, and requirements for minimum in-stream fish flows. Water imbalances are likely to be further exacerbated by potential future climate change and variability, such as longer and more severe drought periods followed by periods with extreme precipitation events. Finding replacement water supplies and improving watershed management is needed to comply with legal mandates, adapt to future climate variability and changing land use, and improve environmental conditions.

Study objective

The Salinas Valley Integrated Hydrologic Model (SVIHM) was developed to help water managers evaluate and adjust to projected impacts on water supplies and demands in the Salinas Valley watershed caused by changes in land use, population, and climate. The SVIHM provides a tool for predicting how the watershed infrastructure, including reservoir operations, flow diversions, groundwater pumping, irrigation practices, and proposed adaptation strategies, will perform across a range of potential future conditions. The SVIHM includes four modeling components: (1) the Basin Characterization Model (BCM), (2) the Hydrologic Simulation Program – FORTRAN (HSPF), (3) MODFLOW - One Water Hydrologic Model (MF-OWHM), and (4) the Surface Water Operations (SWO) package. The BCM and HSPF components comprise the 4,530 mi^2 Salinas Valley Watershed Model (SVWM). The SVWM domain encompasses the entire Salinas River watershed as well as coastal drainages adjacent to the

Salinas River outflow. The SVWM includes the 2,540 mi² upper Salinas River (USR) and the 1,990 mi² lower Salinas River (LSR) HSPF model domains (figures 1, 2). The USR is connected to the LSR at the location of United States Geological Survey (USGS) streamgage 11150500, Salinas River near Bradley, CA (figure 1). The 840 mi² SVIHM domain includes the areas of productive agricultural and urbanized lands overlying the alluvial valley fill and sediments comprising the aquifers of the Salinas River valley and adjacent coastal basins (figure 1). The MF-OWHM and SWO components of the SHIHM provide a comprehensive and detailed accounting of anthropogenic interactions with the natural hydrologic system, including all processes affecting both groundwater and surface water, allowing for the simulation of managed flows, conjunctive water use, and surface water – groundwater interactions. The SWO component is fully integrated with MF-OWHM and simulates the water budget and reservoir operations for the San Antonio and Nacimiento reservoirs (figure 1). The SWO simulation is used to evaluate how reservoir operations can be managed to better respond to potential changes in land use and climate, climate variability, and in-stream water requirements.

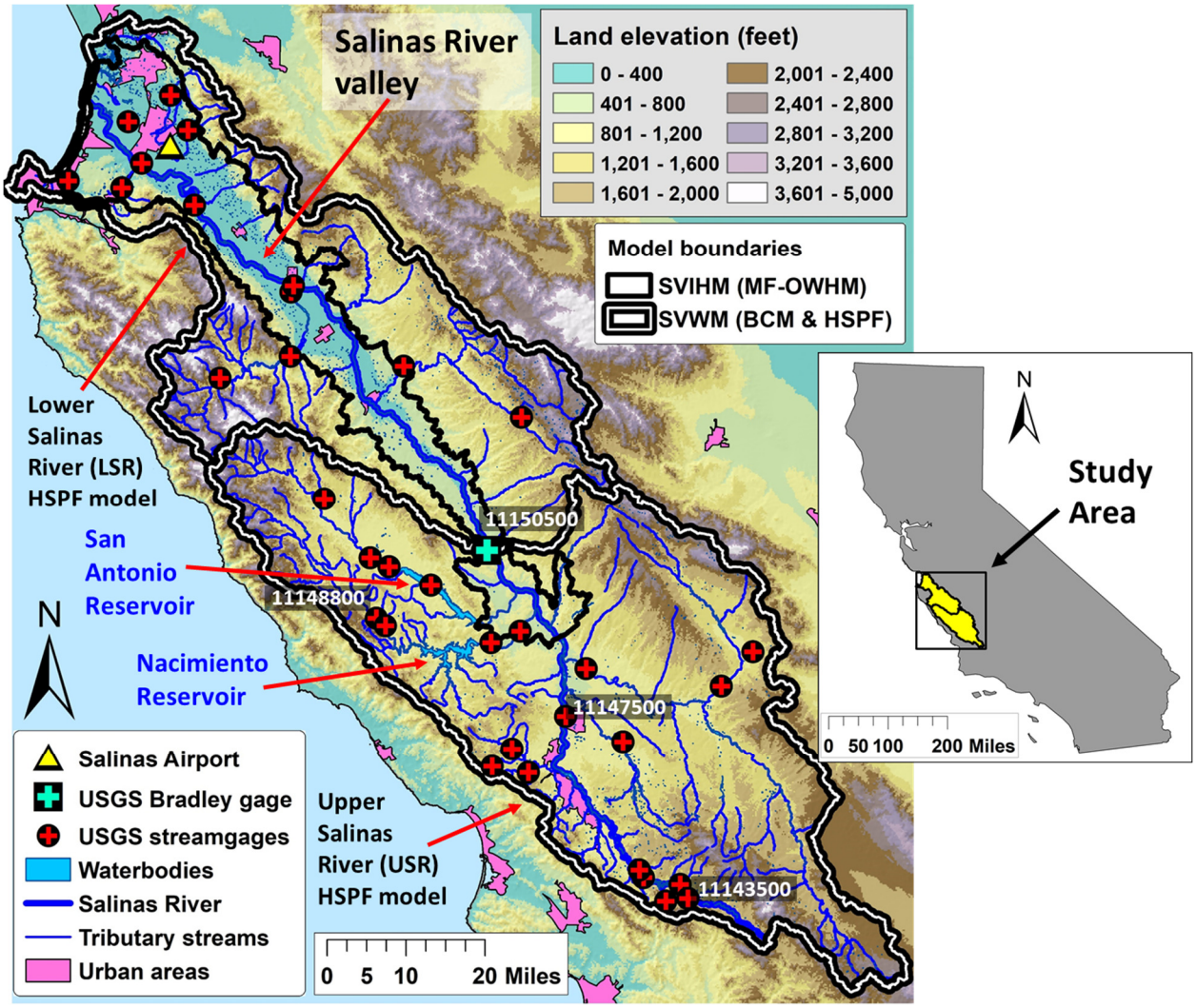

Figure 1. Study area location, boundaries of the various model domains, the Salinas River and its tributary streams, the San Antonio and Nacimiento reservoirs, urban areas, United States Geological Survey (USGS) streamgages, and the Salinas Airport climate station

Model Description

The integrated structure of the SVIHM combines the BCM, HSPF, MF-OWHM, and SWO model components and takes advantage of the different efficiencies and strengths of each component. The BCM and HSPF components simulate the entire Salinas River watershed as well as the coastal basins and smaller drainages adjacent to the mouth of the Salinas River. The HSPF component simulates the surface water inflows from the tributary drainages along the SVIHM boundary (figure 2). Additionally, the HSPF component simulates the water budget for the entire Salinas River basin containing both the SVIHM domain as well as the mountainous terrain of the tributary headwater areas not included in the SVIHM. The BCM component uses preprocessing applications to develop climate datasets consisting of high-resolution, 270-meter (886-foot) gridded maps of daily precipitation and daily maximum and minimum air temperature (Flint et al. 2014; Stern et al. 2016). The gridded daily climate maps are used by the BCM to simulate daily potential evapotranspiration (PET). The gridded daily climate and PET maps are inputs to both the SVWM and SVIHM. The SVIHM uses the MF-OWHM and SWO model components, with MF-OWHM simulating the surface and subsurface hydrology of the main alluvial valley and underlying aquifers of the Salinas River downstream of the reservoirs, and SWO simulating the hydrology and operation of Nacimiento and San Antonio Reservoirs, as well as surface water diversions and deliveries for the Salinas River downstream of the reservoirs. The SWO component uses the MF-OWHM-simulated streamflow gains and losses along the Salinas River network, in conjunction with observed and simulated streamflows on critical tributaries, to simulate optimum reservoir releases for maintaining: (1) required streamflows for fish habitat and migration; (2) deliveries for irrigation; and (3) required Salinas River outflows to the ocean.

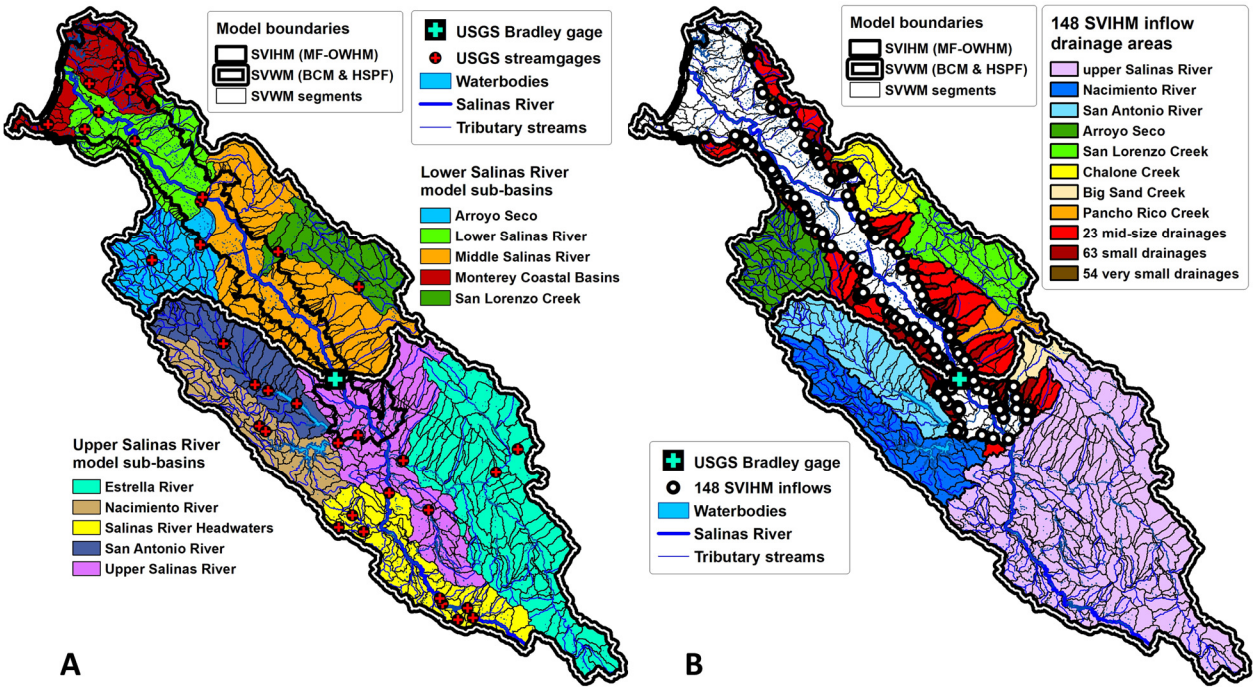

Figure 2. SVWM-HSPF model layout and segmentation: **A**, Major sub-basin areas represented by the SVWM, **B**, 148 inflow pour-points and inflow drainage areas having HSPF-simulated surface water inflows to the SVIHM

The BCM and HSPF components use hourly and daily time steps to run a 71-year historic climate simulation beginning October 1, 1947 and ending September 30, 2018 (water years 1948 to 2018) (figure 3). Water year 1948 is used for model initialization in HSPF simulations. The MF-OWHM component uses a bimonthly time step and the SWO component uses a 5- and 6-day time step for a 51-year simulation beginning October 1, 1967 and ending September 30, 2018 (water years 1968 to 2018). The longer time step and smaller area simulated by the SVIHM allows for faster runtimes and more efficient modeling of groundwater flow, surface water – groundwater interactions, seawater intrusion, and conjunctive water use for the groundwater basins in the alluvial valley and coastal area. The shorter 5- and 6-day time steps used by SWO is needed to simulate reservoir releases that are triggered and controlled by the timing and duration of streamflow conditions. The historical climate simulations are used by the SVWM and SVIHM for model calibration and for establishing baseline results that are compared with simulation results from projected future scenarios. The future scenarios are developed using BCM applications to downscale climate projections from Global Circulation Models (GCMs) for calendar years 2014 through 2100.

Basin Characterization Model (BCM)

The BCM is a distributed precipitation-runoff model that simulates the water balance at monthly and daily time steps using a grid-based discretization that provides a high-resolution mapping of water budget components (Flint and Flint 2014; Flint et al. 2013; Stern et al. 2016). The BCM method includes preprocessing applications for spatially distributing and downscaling historical and future climate conditions, including precipitation and maximum and minimum air temperature. The applications are incorporated into the SVWM and SVIHM preprocessing to develop daily climate inputs consisting of precipitation and maximum and minimum air temperature. The preprocessing creates inputs used by the BCM to simulate daily PET, and the PET grids are in turn used by both the SVWM and SHIHM.

The BCM preprocessing uses the Gradient-Inverse-Distance-Squared (GIDS) method (Nalder and Wein 1998), a 270-meter digital elevation model (DEM) for the Salinas Valley study area, and daily climate records from a network of 155 climate stations to spatially interpolate daily precipitation and maximum and minimum daily air temperature onto the 270-meter DEM grid. The daily climate grids are then adjusted by spatial scaling to better match the monthly precipitation and maximum and minimum air temperature grid-based maps developed by the Parameter-elevation Regression on Independent Slopes Model (PRISM, Daly et al. 2008). Adjusting the daily grids such that monthly precipitation and maximum and minimum air temperature more closely match the PRISM maps provides an improved representation of spatial variability caused by complex climate regimes associated with orography (adiabatic cooling, rain shadows, temperature inversions) and coastal proximity. The daily climate grids, along with DEM-derived parameters that account for topographic shading effects, are used by the BCM to estimate short-wave radiation at hourly time steps, which in turn is used to estimate daily PET (Flint and Flint 2014). The BCM applications are also applied to develop future climate and PET inputs using downscaling methods and simulation results from Global Circulation Models (Stern et al. 2016; Flint and Flint 2012, 2014). The gridded daily climate and PET results are further processed to develop the inputs for HSPF and SVIHM, using area-weighted averaging to remap the 270-meter grid results to the HSPF model segments and the MF-OWHM cells, and calculating hourly inputs for HSPF, 5-day and 6-day inputs for SWO, and bimonthly inputs for MF-OWHM.

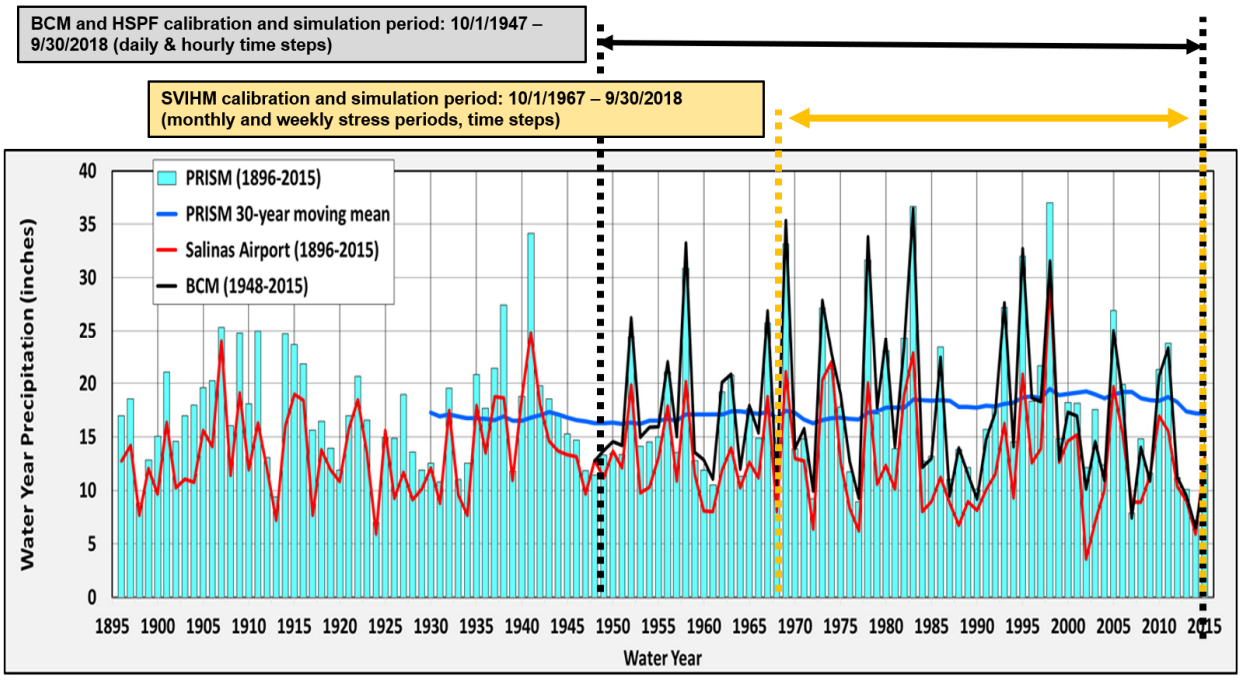

Figure 3. Comparison of long-term annual (water year) precipitation records at Salinas Airport, PRISM estimated annual basin-wide mean precipitation for the SVWM, annual basin-wide mean precipitation for the SVWM estimated using BCM applications, and simulation periods used by the SVWM and SVIHM for calibration and historical-climate applications

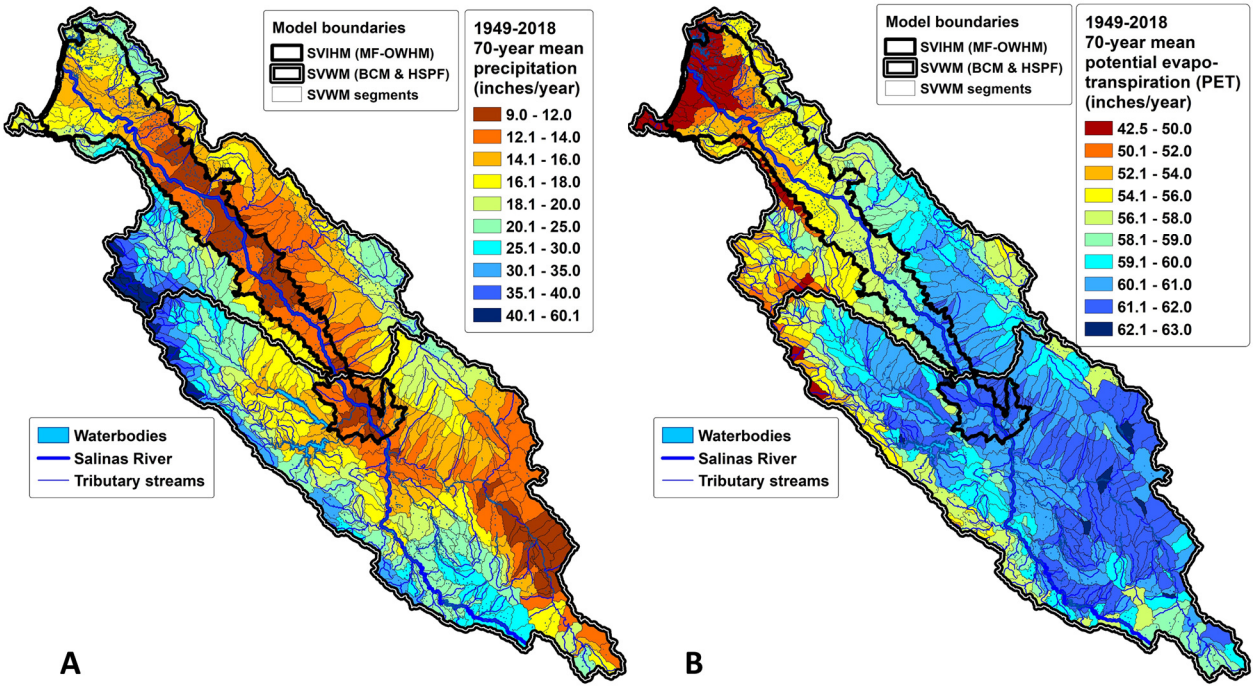

Figure 4. Spatially interpolated climate inputs estimated using BCM applications; shown are long-term 70-year means of daily time series spatially-averaged over HSPF segment areas: **A**, precipitation; **B**, BCM-estimated potential evapotranspiration

The annual (water year) basin-wide mean precipitation estimated for the SVWM using BCM applications indicates high interannual variability, with annual precipitation exceeding 30 inches estimated for 6 water years, and annual precipitation less than 10 inches estimated for 8 water years (figure 3). Estimated annual precipitation using BCM applications is in close agreement with the PRISM-estimated annual basin-wide mean precipitation for water years 1948 to 2015. Annual precipitation recorded at the Salinas Airport climate station (figure 1) indicates interannual variability similar to the estimates by PRISM and BCM applications (figure 3). The 70-year (water years 1949 to 2018) mean precipitation estimated for the SVWM indicates a high degree of spatial variability across the Salinas River study area, ranging from about 60 inches per year (in/yr) along the western boundary to less than 12 in/yr for the central part of the valley and the southeastern part of the SVWM (figure 4A). Precipitation is less variable for the SVIHM domain, ranging from about 8 to 12 in/yr for most locations, with higher values of 16 to 20 in/yr for the coastal basins in the northwest part of the SVWM. Simulated 70-year mean PET ranges from 63 in/yr for segments in the more inland, southeast part of the SVWM to about 42 in/yr for the coastal basins (figure 4B). North- to northeast-facing slopes on the west side of the Salinas valley (particularly in northwestern part of the SVWM) also tend towards lower PET (figure 4B). The basin-wide 70-year mean PET for the SVWM (58.1 in/yr) is more than three times the basin-wide 70-year mean precipitation (18.4 in/yr).

Hydrologic Simulation Program – Fortran (HSPF)

The HSPF model is a lumped-parameter, continuous-simulation watershed model that simulates both water flow and transport processes, including sediment transport (Bicknell et al. 2001; Donigian et al. 1995). Hydrologic processes simulated by HSPF include snow accumulation and melt, pervious and impervious surface storage, surface runoff, pervious land infiltration, soil water storage, percolation, evapotranspiration, interflow, recharge, streamflow, stream losses to evaporation and seepage, and shallow (active) groundwater reservoir storage and discharge (baseflow) contributions to streamflow and riparian evapotranspiration. The HSPF model provides a comprehensive simulation of rainfall-runoff and streamflow processes, allowing for analysis of surface and shallow subsurface water budget components and processes such as soil moisture, evapotranspiration, and recharge for inter-channel areas and components of streamflow (overland runoff, interflow, baseflow, and streamflow seepage) for intra-channel areas.

The HSPF model was discretized into 690 linked model segments, ranging in area from 39.6 to 0.1 mi^2, using topographically defined sub-drainages and the National Hydrography Dataset (NHD) streamlines and sub-drainage boundaries (Simley and Doumbouva. 2012) (figure 2). Each model segment consists of a pervious-land component connected to a stream reach. In urban areas with developed land cover, HSPF segments were further partitioned into pervious and impervious-land areas using the 2011 National Land Cover Data (NLCD) map of percent impervious developed land cover (Wickham et al. 2014). The model segments were linked into a flow routing network of 690 stream reaches representing the NHD streamlines for the Salinas River study area.

The SVWM uses two HSPF sub-models, USR and LSR, connected at the USGS stream gage 11150500 (Salinas River near Bradley, CA), to allow for a greater number of HSPF segments, thereby providing a higher level of spatial resolution to better represent variability in climate and watershed characteristics such as slope, land cover, soil properties, and surficial geology (figure 5). In addition, a high level of segmentation provides a more precise coupling of the

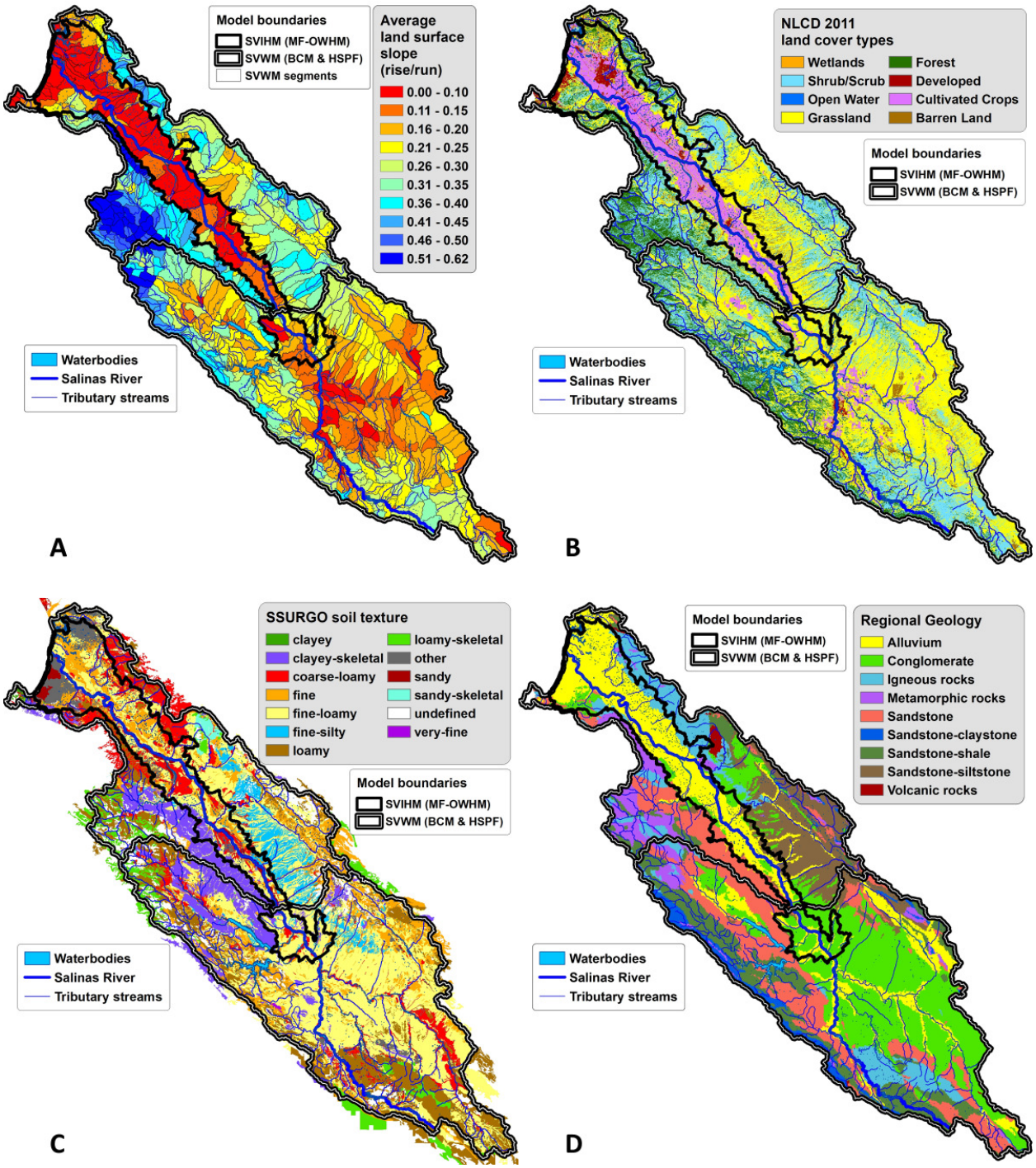

Figure 5. Examples of datasets used to develop input parameters for the HSPF model component; **A**, calculated land-surface slope, area-averaged for model segments; **B**, National Land Cover Dataset (NLCD) 2011 condensed land cover; **C**, Soil Survey Geographic (SSURGO) soil texture (NRCS); **D**, surface geology from Jennings (1997), condensed rock type

HSPF tributary drainages to the SVIHM; a total of 148 tributary drainages were defined using the HSPF segmentation, ranging in size from 1,570 mi^2 for the upper Salinas River to less than 1.6 mi^2 for 54 drainages along the SVIHM boundary (figure 2B). Inflows to the LSR at the Bradley gage are defined by the streamflow record at the Bradley gage or the HSPF simulated streamflow from the USR.

Data used to estimate model parameters for HSPF segments and stream reaches included DEM-derived slope, NLCD 2011 land cover types (Wickham et al. 2014), Soil Survey Geographic (SSURGO) soil properties (Soil Survey Staff, Natural Resources Conservation Service 2017), and the California state-wide geology map from Jennings (1977) (figure 5). Land surface slope, used to estimate parameters controlling runoff and interflow, was calculated using a 30-meter (98 foot) DEM grid and averaged over the areas of HSPF segments. Land cover type was used to estimate parameters affecting interception and retention storage, evapotranspiration, and runoff. NLCD-derived impervious developed land cover and forest canopy cover data were also used to estimate parameters. SSURGO soil texture was used to estimate soil zone water holding capacities and parameters controlling infiltration, percolation, and interflow. Additional SSURGO data used to estimate HSPF parameters included soil hydrologic group, soil runoff potential, and soil maximum available water holding capacity. Surface geology was used to estimate parameters affecting recharge and baseflow.

MODFLOW – One Water Hydrologic Model (MF-OWHM)

The One Water Hydrologic Flow Model (MF-OWHM) (Hanson et al. 2014) is a MODFLOW-2005 based integrated hydrologic flow model (IHM) that includes the Farm-Processes (FMP) and SWO packages. MF-OWHM provides a version of the widely used MODFLOW family of hydrologic simulators, enabling a comprehensive analysis of a broad range of conjunctive-use issues. As the central component of the SVIHM, MF-OWHM provides a fully-coupled and integrated surface water – groundwater model used for simulating the complex hydrologic interactions in the alluvial basins of the Salinas River valley and the adjacent coastal basins. In response to temporally and spatially varying climate and land use changes, MF-OWHM, combined with SWO, simulates groundwater flow and storage changes, crop irrigation, managed water deliveries, managed reservoir releases, seawater intrusion, groundwater pumping, land subsidence in response to groundwater pumping, streamflow, streamflow losses, irrigation return flows, evapotranspiration, runoff, and recharge.

In addition to groundwater, surface-water, and landscape budgets, MF-OWHM can incorporate observations of land subsidence, hydraulic properties, and evapotranspiration. Detailed landscape budgets combined with estimates of actual evapotranspiration facilitate linkage to remotely sensed observations as input or as additional observations for parameter estimation or water-use analysis. Temporally variable water-accounting units (farms) can be linked to land-use models and the specification of both surface-water and groundwater allotments to facilitate sustainability analysis and connectivity to the Groundwater Management Process. An important feature of MF-OWHM is that it allows the simulation of head-dependent flows, flow-dependent flows (flows that originate from other flow processes), and deformation dependent flows that collectively affect conjunctive use of water resources (Hanson et at. 2015). The supply-constrained and demand-driven framework combined with the linkages between packages and processes provides a complete accounting of the water balance.

Surface Water Operations model (SWO)

The SWO component of the SVIHM is a recently developed module of MF-OWHM that allows for the incorporation of complex user-defined surface water flow-augmentation and management practices and is used to simulate reservoir operations for the Nacimiento and San Antonio reservoirs as well as downstream diversions in the Salinas River system. The SWO component is fully integrated with MF-OWHM and simulates outflows and storage changes in the surface water reservoirs, as well as reservoir operations and downstream flow diversions in response to changing water demands. The SWO model component is applied as part of the SVIHM simulation to help reservoir operators better manage and anticipate releases under a variety of climate and land use conditions, in conjunction with management of groundwater pumping for irrigation in the Salinas Valley, mitigation of seawater intrusion in the coastal region, storage requirements for flood control, and minimum flow requirements for fish habitat and migration.

The SWO model is fully integrated with MF-OWHM and uses a flexible rule-based algorithm with user-defined reservoir-release triggers and functions, where the triggers are based on simulated streamflow, downstream water demands, and instream requirements. The SWO model evaluates streamflow gains and losses along the Salinas River network, simulated by the Surface water Flow Routing (SFR, Niswonger and Prudic 2005) package used with MF-OWHM, and makes the appropriate releases to maintain downstream flows for fisheries, provide deliveries for diversions used for irrigation, and maintain sufficient river discharge during low flow conditions. In addition to the simulated stream channel gains and losses, reservoir releases are simulated as a function of observed (recorded) streamflow and HSPF-simulated tributary streamflows, spatially distributed daily precipitation and PET, MF-OWHM simulated downstream water demands for irrigation and municipal uses, simulated reservoir losses due to evaporation, and simulated reservoir storage changes.

Model Calibration and Application

Calibration

Records of daily precipitation, maximum and minimum daily air temperature, and calculated daily PET were used to evaluate results developed by the BCM applications. Records of daily streamflow at 35 USGS streamgages (figure 1) were used to calibrate the HSPF model. Streamflow records, reservoir elevation records, and records of groundwater levels were used to calibrate the MF-OWHM and SWO model components. Calibration of MF-OWHM was done using the Parameter-Estimation (PEST) application (Doherty and Hunt 2010), whereas calibration of the BCM and HSPF models was done with a trial-and-error approach using visual curve fitting of hydrographs and flow-duration curves as well as comparison of goodness-of-fit statistics (Donigian 2002). Comparisons between simulated and observed (recorded) streamflow was done using daily, monthly, and annual (water year) streamflow (figure 6). In general, streamflow in the Salinas Valley is characterized by rapid surface runoff response to precipitation in upland drainages, with ephemeral streamflow in most channels and seasonally negligible to non-existent baseflow in the larger channels of the valley bottoms. To achieve a good calibration for the SVWM, simulated streamflow needed to represent a wide range of flow conditions, from flashy peak flows to very low flows and no-flow conditions. Figure 6 provides

examples of comparisons of simulated and observed streamflow at four streamgages (see figure 1 for gage locations).

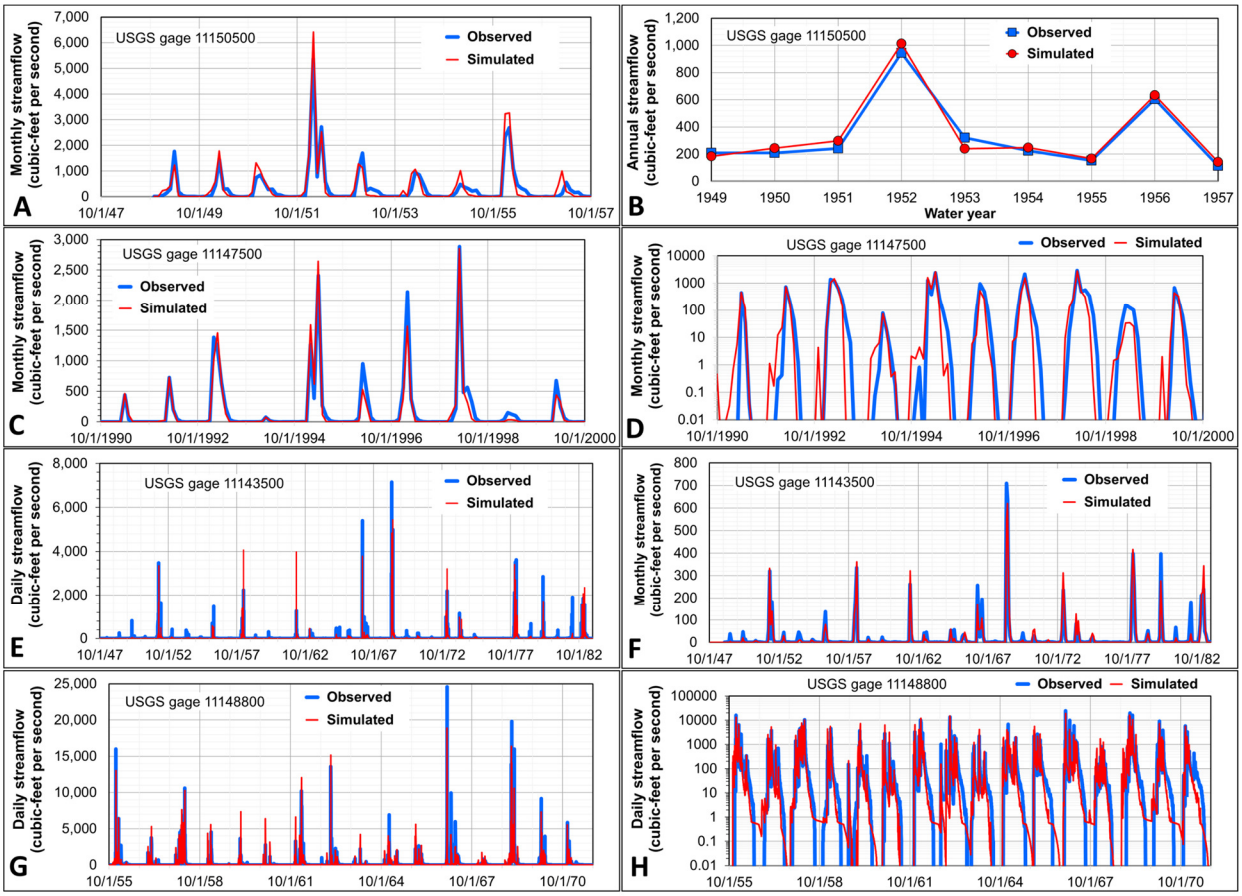

Figure 6. Comparison of HSPF-simulated (red line) and observed (blue line) streamflow at 4 United States Geological Survey (USGS) streamgages: **A,** monthly and **B,** annual (water year) mean streamflow at gage 11150500 (Salinas River near Bradley, CA); **C**, linear-scale and **D,** logarithmic-scale monthly mean streamflow at gage 11147500 (Salinas River at Paso Robles, CA); **E**, daily and **F,** monthly mean streamflow at gage 11143500 (Salinas River near Pozo, CA; **G**, linear-scale and **H**, logarithmic-scale daily mean streamflow at gage 11148800 (Nacimiento River near Bryson, CA)

Preliminary results using the SVWM

The SVWM was used to develop the 148 boundary inflows for the SVIHM (figure 2B) and to simulate the 70-year (October 1, 1948 to September 30, 2018) water budget for the SVWM domain. Preliminary water budget results were used for analyzing hydrologic processes for all upland areas tributary to the SVIHM, and to provide a complete accounting of historic and potential future water budgets for the entire area of the Salinas River watershed. The SVWM simulation results indicate evapotranspiration (ET) is the largest component of the water budget after precipitation, with a 70-year mean basin-wide ET of 13.9 in/yr, compared to the basin-wide mean precipitation of 18.4 in/yr. Simulated ET ranges from 15 to 29 in/yr along the western side of the SVWM to less than 10 in/yr throughout the valley floor and in the southeast part of the Salinas River watershed (figure 7A). The spatial distribution of ET is generally consistent with precipitation (figures 7A, 4A), but is also affected by variations in PET, such as

the high PET in the southern part of the upper Salinas River drainage (figures 7A, 4B), as well soil water storage capacity, percolation rates, land surface slope, and vegetation.

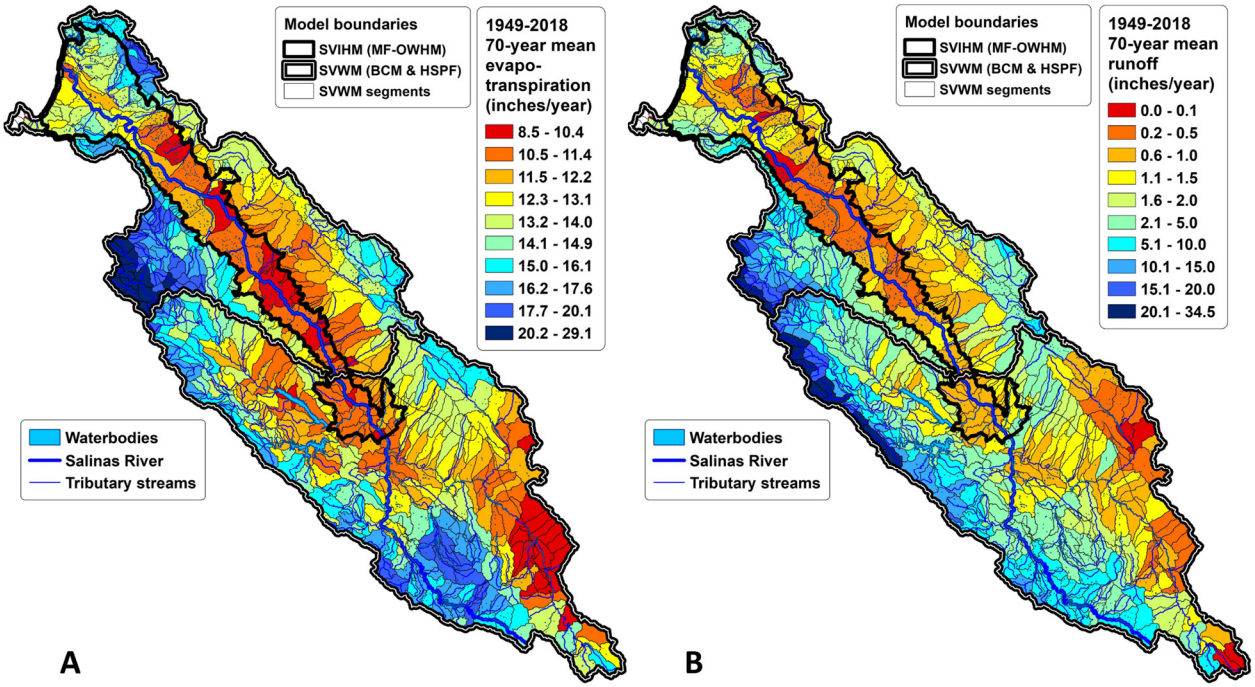

Figure 7. Preliminary results indicating HSPF-simulated 70-year means for model segments; **A,** actual evapotranspiration (ET); **B**, runoff (un-routed)

Preliminary results for simulated runoff include a 70-year basin-wide mean of 4.5 in/yr. Mean runoff (defined as un-routed surface water outflow from individual HSPF segments) of more than 20 in/yr was simulated along the western boundary of the SVWM in response to the high precipitation, low PET, steep terrain, and thin soil cover (figure 7B). Low runoff of 0.2 in/yr and less was simulated for the hotter and drier areas of the SVWM, such as the central valley of the Salinas River and along the southeast part of the SVWM domain. The low runoff simulated for the Salinas River valley does not include irrigation return flows because irrigation is not accounted for by the SVWM (irrigation is simulated in detail by the SVIHM).

Simulated 70-year mean streamflow ranges from a maximum of 606 cubic-feet per second (ft^3/sec) for the Salinas River directly downstream of the Arroyo Seco tributary to less than 0.1 ft^3/sec for most of the small drainages in drier sections of the SVWM and along the SVIHM boundary (figure 8A). The 70-year mean streamflow at the mouth of the Salinas River is 193 ft^3/sec, indicating a high degree of channel losses caused by streambed seepage downstream of the Arroyo Seco tributary. The 70-year mean stream channel losses are as high as 40 ft^3/sec for some stream reaches in the central part of the Salinas Valley. Simulated 70-year mean streamflows for most sections of the Salinas River within the SVIHM domain are between 200 and 500 ft3/sec. The simulated 70-year mean total inflow to the SVIHM is 890 ft3/sec (about 640,000 acre-feet per year), with the highest mean inflow of 270 ft3/sec simulated for the Nacimiento River (figure 8B).

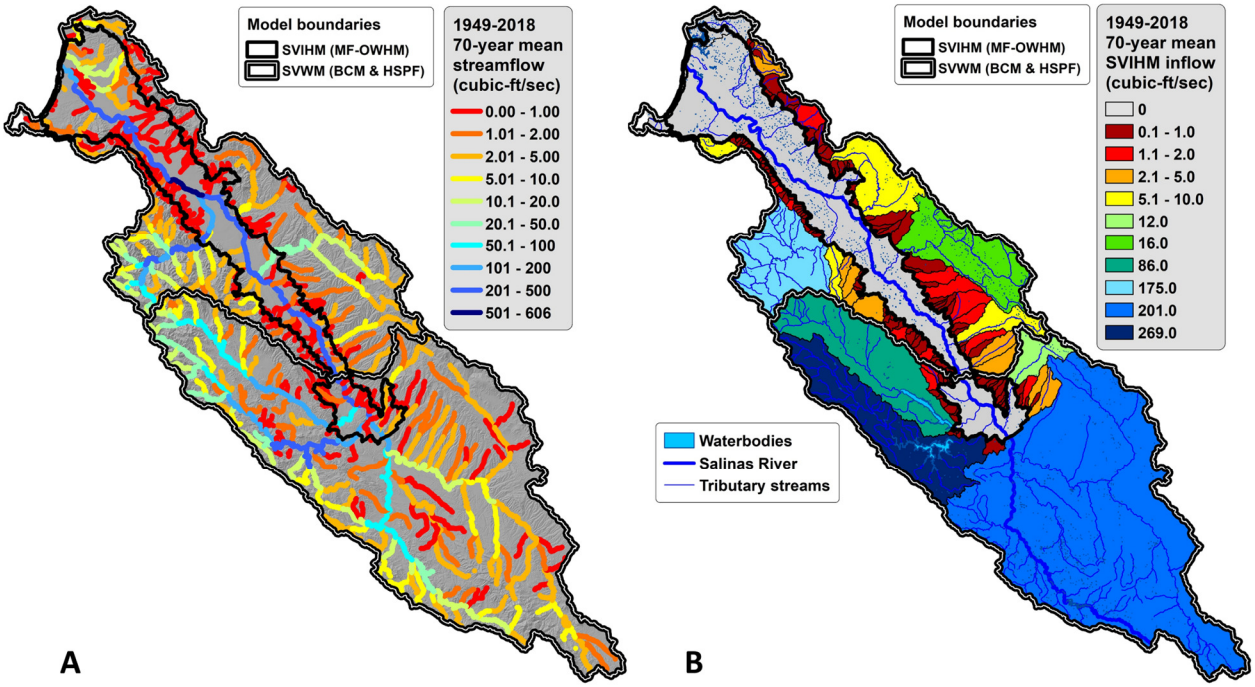

Figure 8. Preliminary results indicating HSPF-simulated 70-year mean streamflow, water years 1949 to 2018, **A**, for the Salinas River and tributaries; **B**, as inflow to the SVIHM from 148 tributary drainages

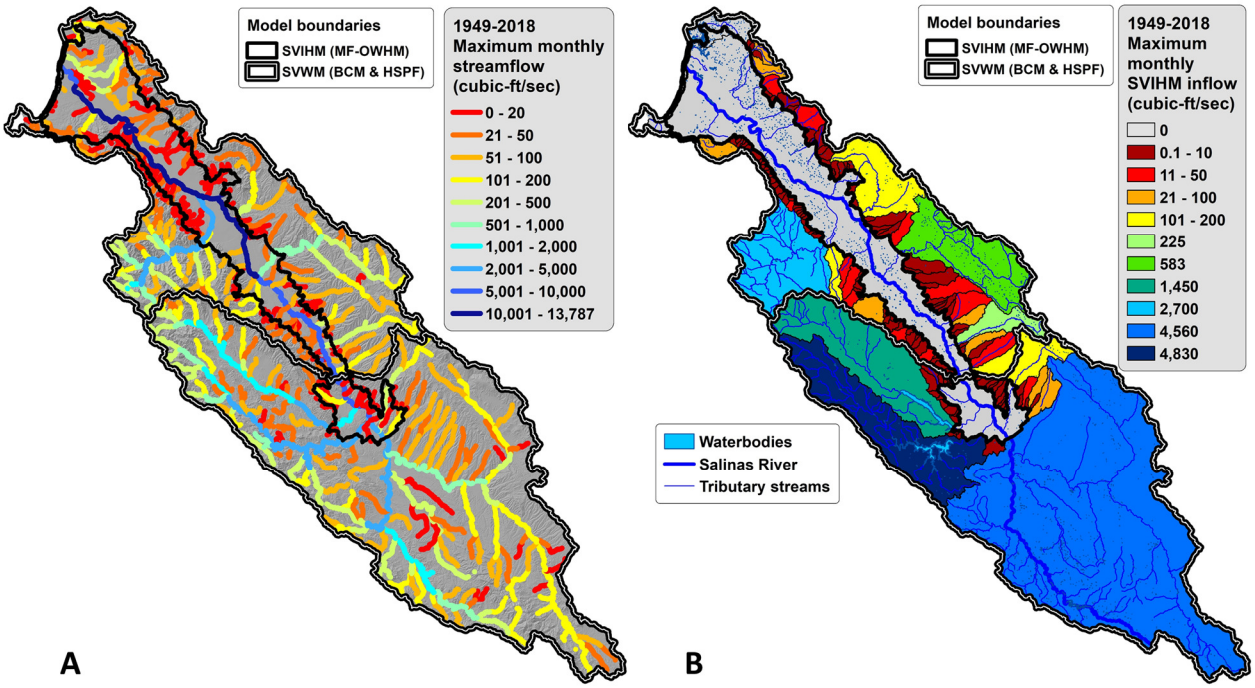

Figure 9. Preliminary results indicating HSPF-simulated maximum monthly streamflow, water years 1949 to 2018, **A**, for the Salinas River and tributaries; **B**, as inflow to the SVIHM from 148 tributary drainages

A maximum monthly streamflow of about 14,000 ft^3/sec was simulated for the Salinas River directly downstream of the Arroyo Seco tributary. In comparison, the maximum monthly streamflow simulated at the mouth of the Salinas River is only about 9,600 ft^3/sec (figure 9A). Simulated maximum monthly streamflow for most of the smaller drainages along the SVIHM boundary and throughout the drier parts of the SVWM is less than 100 ft^3/sec. The highest simulated maximum monthly SVIHM inflows are 4,830 ft^3/sec for the Nacimiento River, 4,560 ft^3/sec for the upper Salinas River, and 2,700 ft^3/sec for Arroyo Seco (figure 9B).

In general, the simulated SVIHM inflows indicate a high degree of temporal variability, with results representative of the observed ephemeral streamflows characteristic of the study area (figure 10). Simulated annual surface water inflow to the SVIHM ranges from about 3,500 ft^3/sec for water year 1969 to about 100 ft^3/sec and less for water years 1976, 1977, 2007, and 2014 (figure 10A). Maximum annual SVIHM inflows were also simulated for the Salinas River (about 1,100 ft^3/sec) and the Arroyo Seco (about 600 ft^3/sec) for water year 1969 (figures 10B, 10C). In contrast, the maximum SVIHM inflow from Chalone Creek, about 58 ft^3/sec, was simulated for water year 1978 (figure 10D). The 5- and 10-year running means for simulated annual streamflows (for all inflows) indicate a general drying trend beginning approximately with water year 1999. The end of the wettest 5-year period, based on a 5-year running mean of simulated annual total inflow to the SVIHM of about 1,600 ft^3/sec, occurs at the end of water year 1998, whereas the end of the wettest 10-year period, based on a 10-year running mean of simulated inflow to the SVIHM of about 1,300 ft^3/sec, occurs at the end of water year 1987. The 10-year running means for most of the simulated inflows indicate the driest period for the SVWM, in terms of SVIHM inflows, was ongoing as water year 2015 ended.

Discussion

Preliminary simulation results using the SVWM indicate a reasonable representation of important characteristics of the Salinas River drainage system, such as a high degree of overland flow contributions to streamflow, the lack of sustained baseflow, the prevalence of losing-stream seepage conditions, particularly over most sections of the central part of the Salinas Valley where the channel bed is coarse and wide, and a high degree of spatial and temporal variability in streamflow. Simulations using the SVWM indicate the dominance of the Nacimiento River drainage in supplying runoff to the Salinas River basin. Compared to the larger drainage area of the upper Salinas River, the Nacimiento drainage area is located closer to the Pacific Ocean moisture source and includes higher-elevation, steeper terrain with higher precipitation and lower PET, all characteristics that are conducive to more runoff generation as compared to other areas of the SVWM, especially the drier, hotter drainages on the east side of the Salinas Valley. The simulated 70-year mean total surface-water inflow to the SVIHM is 890 ft^3/sec, whereas the simulated 70-year mean streamflow at the mouth of the Salinas River is only about 190 ft^3/sec, indicating that most of the streamflow generated in the Salinas River basin is lost to channel seepage. Preliminary results indicate that much of the runoff generated in the basin becomes intra-channel recharge, rather than surface water outflow to the ocean, and this is consistent with independent observations of the surface water system. The lack of sustained baseflow causes streamflow to be highly sensitive to the temporal variability in precipitation, especially during the drier periods, and this increases the importance of developing adequate reservoir management, flow augmentation, and conjunctive water use scenarios for potential future drought periods, potentially warmer future climate, and potentially increased temporal variability in precipitation.

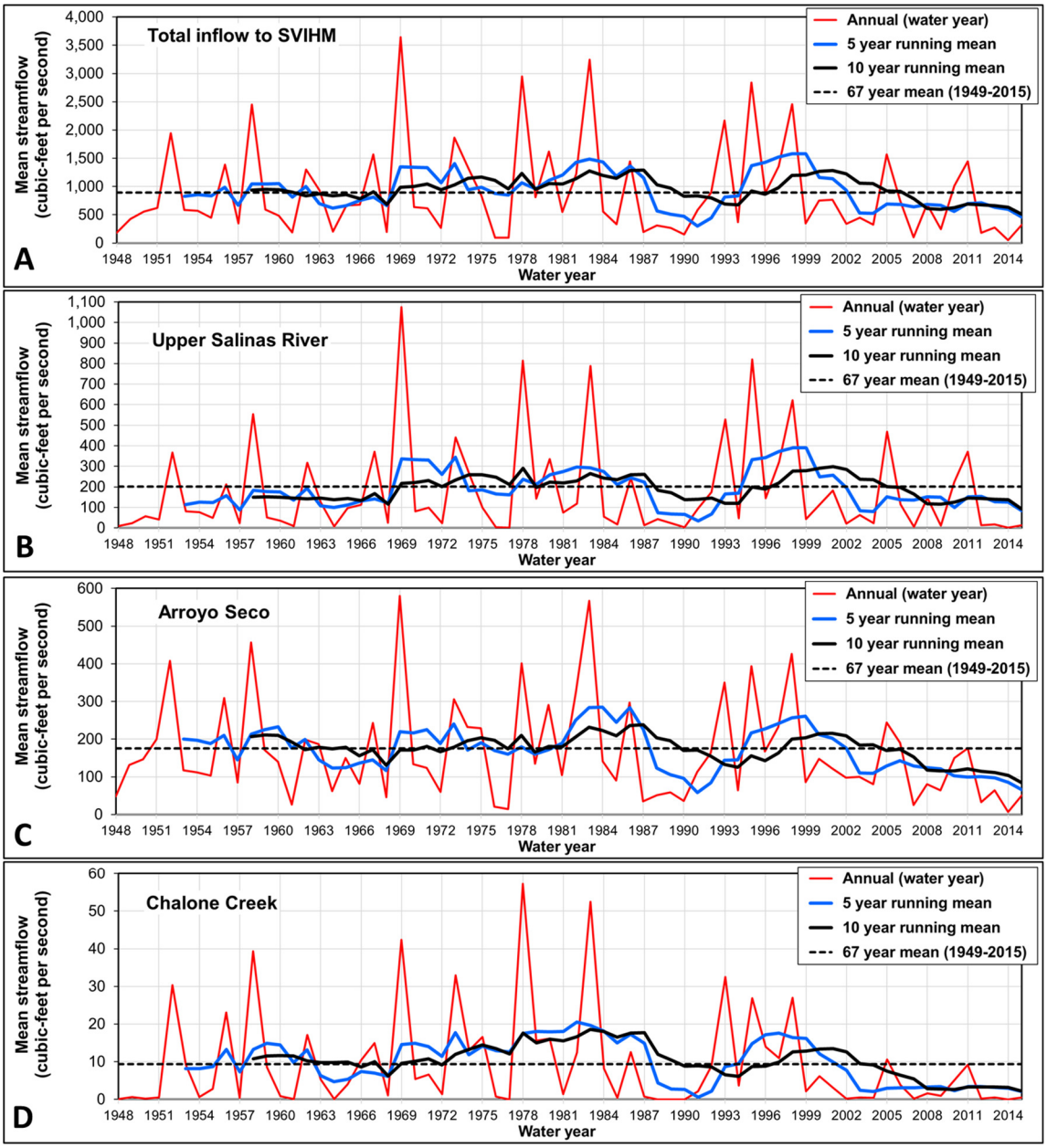

Figure 10. Preliminary results indicating HSPF-simulated annual (water year) and multi-year mean surface water (streamflow) inflows to the SVIHM; **A**, total inflow to the SVIHM; **B**, inflow from the upper Salinas River; **C**, inflow from Arroyo Seco; **D**, inflow from Chalone Creek

References

Bicknell, B.R., Imhoff, J.C., Kittle, J.L., Jr., Donigian, A.S., Jr., Johanson, R.C. 2001. Hydrologic Simulation Program—FORTRAN, User's Manual for Version 12; U.S. EPA Environmental Research Laboratory: Athens, GA, USA, 2001; pp. 1–755.

Daly, C., Halbleib, M., Smith, J., Gibson, W., Doggett, M., Taylor, G. 2008. Physiographically-sensitive mapping of temperature and precipitation across the conterminous United States. International Journal of Climatology, 28, 2031-2064.

Doherty, J.E., and Hunt, R.J. 2010. Approaches to highly parameterized inversion—A guide to using PEST for groundwater-model calibration: U.S. Geological Survey Scientific Investigations Report 2010–5169, 59 p.

Donigian, A.S., Bicknell, B.R., Imhoff, J.C. 1995. Hydrological Simulation Program—FORTRAN (HSPF). In Computer Models of Watershed Hydrology; Singh, V.P., ed.; Water Resources Publications: Highlands Ranch, Colo, USA, 1995; pp. 395–442.

Donigian, A.S. 2002. Watershed model calibration and validation: The HSPF experience. Proc. Water Environ. Fed. 2002, 8, 44–73.

Flint, L.E., and Flint, A.L. 2012. "Downscaling future climate scenarios to fine scales for hydrologic and ecological modeling and analysis", Ecological Processes 2012 1:1.

Flint, L.E. and Flint, A.L. 2014. California Basin Characterization Model: A Dataset of Historical and Future Hydrologic Response to Climate Change, (ver. 1.1, May 2017): U.S. Geological Survey data release, https://doi.org/10.5066/F76T0JPB.

Flint, L.E., Flint, A.L., Thorne, J.H., and Boyton, R. 2013. "Fine-scale hydrologic modeling for regional landscape applications: the California Basin Characterization Model development and performance", Ecological Processes 2013 2:25.

Flint, A.L., Flint, L.E., and Stern, M.A. 2014. "Spatial downscaling and mapping of daily precipitation and air temperature using daily station data and monthly mean maps," Poster presented at 2014 Fall Meeting, AGU, San Francisco, Calif., 15-19 Dec.

Jennings, C.W. 1977. Geologic map of California. California Division of Mines and Geology geologic data: Map number 2, scale 1:750,000.

Hanson, R.T., Boyce, S.E., Schmid, Wolfgang, Hughes, J.D., Mehl, S.M., Leake, S.A., Maddock, Thomas, III, and Niswonger, R.G. 2014. One-Water Hydrologic Flow Model (MODFLOW-OWHM): U.S. Geological Survey Techniques and Methods 6–A51, 120 p., https://dx.doi.org/10.3133/tm6A51.

Hanson, R.T., Flint, L.E., Faunt, C.C., Gibbs, D.R., and Schmid, W. 2015. Hydrologic models and analysis of water availability in Cuyama Valley, California (ver. 1.1, May 2015): U.S. Geological Survey Scientific Investigations Report 2014–5150, 150 p., http://dx.doi.org/10.3133/sir20145150.

Nalder, I.A.; Wein, R.W. 1998. Spatial interpolation of climatic normals: test of a new method in the Canadian boreal forest. Agricultural and Forest Meteorology. 92: 211–225

Niswonger, R.G., and Prudic, D.E. 2005. Documentation of the Streamflow-Routing (SFR2) Package to include unsaturated flow beneath streams—A modification to SFR1: U.S. Geological Survey Techniques and Methods 6-A13, 50 p.

Soil Survey Staff, Natural Resources Conservation Service (NRCS). 2017. United States Department of Agriculture. Soil Survey Geographic (SSURGO) Database for Monterey and San Luis Obispo counties, CA. Available online https://websoilsurvey.nrcs.usda.gov/app/. Accessed 02/10/2017.

Simley, Jeffrey, and Doumbouya, Ariel. 2012. National hydrography dataset—Linear referencing: U.S. Geological Survey Fact Sheet 2012–3068, 2 p.

Stern, M., Flint, L.E., Minear, J., Flint, A.L., and Wright, S. 2016. "Characterizing Changes in Streamflow and Sediment Supply in the Sacramento River Basin, California, Using Hydrological Simulation Program—FORTRAN (HSPF)", Water 2016, 8(10), 432; https://doi.org/10.3390/w8100432

Wickham, J.; Homer, C.; Vogelmann, J.; McKerrow, A.; Mueller, R.; Herold, N.; Coulston, J. 2014. The Multi-Resolution Land Characteristics (MRLC) Consortium — 20 Years of Development and Integration of USA National Land Cover Data. Remote Sens. 2014, 6, 7424-7441.

Military Disturbance Tool in the Automated Geospatial Watershed Assessment (AGWA) Tool for Management of Military Lands

Lainie R. Levick, Principal Research Specialist, University of Arizona, Tucson, Arizona, llevick@email.arizona.edu
Haiyan Wei, Assistant Research Scientist, University of Arizona, Tucson, Arizona, haiyan.wei@ars.usda.gov
I. Shea Burns, Senior Research Specialist, University of Arizona, Tucson, Arizona, shea.burns@ars.usda.gov
D. Philip Guertin, Professor, University of Arizona, Tucson, Arizona, dpg@email.arizona.edu
David C. Goodrich, Research Hydraulic Engineer, USDA-ARS Southwest Watershed Research Center, Tucson, Arizona, dave.goodrich@ars.usda.gov

Abstract

The Military Disturbance Tool is a tool within the Automated Geospatial Watershed Assessment tool (AGWA; https://www.tucson.ars.ag.gov/agwa or www.epa.gov/water-research/automated-geospatial-watershed-assessment-agwa-tool-hydrologic-modeling-and-watershed) used to simulate on-site and downstream effects on runoff and erosion resulting from military training activities. AGWA is a publicly available Geographic Information System (GIS) interface jointly developed by the USDA-Agricultural Research Service, the U.S. Environmental Protection Agency, the University of Arizona, and the University of Wyoming that uses freely available national data layers to parameterize, execute, and visualize output from its watershed-based hydrologic and erosion models (KINEROS2, RHEM, and SWAT) at multiple temporal and spatial scales. The Military Disturbance Tool is an optional tool in AGWA's parameterization step, and includes three general disturbance levels: light, moderate, and heavy. Descriptive and visual examples were developed for each disturbance level to help land managers define these conditions. The tool was developed in cooperation with military installation land managers at the U.S. Army Fort Carson, Colorado, and Fort Bliss, Texas, and is based on published data, previous studies, and a Stryker Brigade training event at the Pinon Canyon Maneuver Site (PCMS), Colorado. It modifies key input parameters for AGWA's embedded hydrologic models based on the disturbance level. Reductions to soil porosity, surface roughness (Manning's n), and canopy cover for each level are applied in KINEROS2, with hydraulic conductivity adjusted according to porosity. For RHEM, reductions are applied to porosity, canopy cover, litter cover, and basal cover which determine friction factor, hydraulic conductivity, and splash and sheet erosion parameters. Curve numbers in SWAT are modified for each disturbance level based on land cover type condition and hydrologic soil group. Currently the tool is implemented only for KINEROS2 but will be available shortly for RHEM. The parameter revisions are in a look-up table that can be modified for a new location if relevant information is available. The spatial capabilities of AGWA allow site-specific analysis of military training disturbances to improve land management and sustainability of training lands. AGWA is best used as a relative change tool unless careful model calibration, supported by high quality observations, is performed. This paper describes the methodology used to develop the disturbance tool and describes an example application at PCMS. The tool was demonstrated through hands-on workshops and site-specific tutorials for Fort Carson, PCMS, and Fort Bliss, under DoD's Environmental Strategic Technology Certification Program (ESTCP; Project RC-201308).

Introduction

The Department of Defense (DoD) manages over 25 million acres of land for realistic military training opportunities and for testing of new technologies. Sustainability of these lands is critical to the military mission; however, training maneuvers can rapidly degrade the land, rendering it unusable. Military training exercises can cause increased soil compaction, reduced vegetation cover, and generally decreased surface roughness from vehicle passes. Jones and Kunze (2004) noted that military vehicle and foot traffic in training areas will typically result in soil compaction, and Donigian (2013) noted a decrease in soil infiltration of 20% per tank pass at Eglin Air Force Base, Florida. Von Guerard (1983) described a study done at Fort Carson, Colorado (Camp, Dresser, and McKee, 1984), to examine the effects of tracked vehicles on soil physical characteristics. Using bulk density measurements to determine changes in soil compaction, they found an 18 percent increase in bulk density due to tracked vehicles. Soil compaction in turn results in changes in porosity for some soil textures. Both of these factors affect the soil hydraulic conductivity, resulting in greater runoff and erosion potential (Braunack, 1986; Thurow et al., 1995). Vegetation and soil disturbance jeopardize the military mission by reducing available training lands, often requiring costly land rehabilitation or recovery (e.g. reseeding), and by increasing flooding and erosion. Determining on-site and off-site runoff and sediment yield is essential to decision-making for rehabilitation choices and cost estimation, as well as to sustain the military mission.

Various studies and models have used data from training events or from experiments using military vehicles to evaluate changes to soil and vegetation properties from military maneuvers for the purpose of determining land condition, carrying capacity, or land rehabilitation costs (e.g., see Donigian, 2013; Guertin and Meyer, 2002; Sullivan and Anderson, 2000). However, due to the wide variability in training activities (i.e. types and numbers of vehicles, duration of the exercise, types of maneuvers, etc.), and in landscapes (i.e. soil types, vegetation communities, topography, and climate) it is difficult to extrapolate results from those studies to other locations or to characterize a training event in terms of direct impacts to soils and vegetation for a particular location.

Since site specific information is difficult to obtain, we developed a simplified scheme to relate training activities to changes in vegetation cover and soil properties. In cooperation with military installation land managers at the U.S. Army Fort Carson, Colorado, and Fort Bliss, Texas, we developed the Military Disturbance Tool (MDT) within the Automated Geospatial Watershed Assessment tool (AGWA; https://www.tucson.ars.ag.gov/agwa) to simulate changes in runoff or erosion from military maneuvers. AGWA is a publicly available Geographic Information System (GIS) interface jointly developed by the USDA-Agricultural Research Service, the U.S. Environmental Protection Agency, the University of Arizona, and the University of Wyoming that uses freely available national data layers to parameterize, execute, and visualize outputs from its embedded watershed-based hydrology and erosion models KINEROS2, RHEM, and SWAT at multiple temporal and spatial scales over a range of environmental conditions. AGWA is an add-in to ESRI ArcGIS 10.x and 9.x (http://www.esri.com/arcgis/about-arcgis). It is a free download from the website www.tucson.ars.ag.gov/agwa as a “package” containing all tables and models required to run AGWA. AGWA is best used as a relative change tool (i.e., pre- versus post-training) unless careful model calibration, supported by high quality observations, is performed. KINEROS2 (KINematic runoff and EROsion model, Smith et al. 1995, Goodrich et al. 2012) is an event-oriented, physically-based model describing the processes of interception, infiltration, surface

runoff, and erosion. RHEM (Rangeland Hydrology and Erosion Model, Hernandez et al. 2017) is the hillslope hydrology and erosion option within KINEROS2, and estimates infiltration and erosion parameters from soils, plant life form, and canopy and ground cover characteristics. SWAT (Soil and Water Assessment Tool version 2000 and version 2005, Arnold and Fohrer 2005) is a basin-scale, continuous-time model that operates on a daily time step and is designed to predict the impact of management on water, sediment, and agricultural chemical yields in ungauged watersheds. AGWA is discussed in more detail in another paper being presented at this conference (Goodrich et al., 2019)

The Military Disturbance Tool relates disturbance of soil and vegetation cover from military maneuvers to changes in soil and vegetation cover properties at three general disturbance levels: light, moderate, and heavy. Model input parameters are modified based on the disturbance level. Changes in soil compaction and soil properties as a function of military traffic were compiled from published data and studies (Affleck, 2005; Althoff et al., 2007; Halvorson et al., 2001; Lindsey et al., 2012; Sullivan and Anderson, 2000; Trumbull et al., 1994; von Guerard et al., 1993; Webb, 2002). Changes in vegetation cover were estimated from satellite imagery and photos, and from consultation with military personnel. Reductions to soil porosity and surface roughness (Manning's n) and canopy cover for each level are applied in KINEROS2, with hydraulic conductivity adjusted according to porosity. In addition, reductions are applied to canopy cover, litter cover, and basal cover for RHEM. Curve numbers in SWAT are modified for each disturbance level based on land cover type condition and hydrologic soil group according to published data (i.e., USDA-NRCS, 2004). The MDT is currently implemented only for KINEROS2 within AGWA but will be available shortly for RHEM. Descriptive and visual examples were developed for each disturbance level to help land managers define these conditions. The tool was demonstrated through hands-on workshops and site-specific tutorials at Fort Carson and Fort Bliss, under DoD's Environmental Strategic Technology Certification Program (ESTCP; Project RC-201308). AGWA and the MDT allow site specific analyses of training disturbances using model input parameters derived from local geospatial data (land cover and soils), and a look-up table that modifies those parameters based on disturbance level. The look-up table provided with the MDT is based on conditions at PCMS, but can be edited for a new location if relevant information is available.

Methods

The levels of disturbance and corresponding modifications to model input parameters are based on reviews of published literature and data, Range and Training Land Assessment (RTLA) data, NRCS soils data, and expert knowledge from installation managers, including natural resources, Integrated Training Area Management (ITAM), and Range Operations personnel, at PCMS. We also conducted an extensive literature search to better understand what occurs during military trainings: types of vehicles (wheeled or tracked), maneuver impact miles (MIMs), types of unit (Stryker Brigade, Armored Brigade, Infantry Brigade, Battalion, etc.), and types of training exercises (Heavy Division/Armored, Armored Division, Heavy Division/Mechanized, Mechanized Infantry Division, etc.). To further support our parameter modifications, Fort Carson staff provided SPOT satellite imagery taken immediately before a large training event in 2015 at PCMS (Stryker Brigade), and imagery and photos taken immediately after that same event. We reviewed these images and photos with Fort Carson staff to confirm the three levels of disturbance and changes to parameters. The managers at Fort Carson and Fort Bliss approved the application of these values in AGWA.

Disturbance Levels

Three levels of disturbance were identified as representative of the most typical types of training effects - light, moderate, and heavy - with the following general descriptions of vehicle use and effects on vegetation and soil:

1. Light: few vehicle passes, mostly foot traffic, short duration, over a small area, little reduction in vegetation cover (ample seed sources remain for natural revegetation), soil stability is good, dry conditions that result in no visible ruts.
2. Moderate: moderate number of wheeled vehicles with some tracked vehicles, multiple vehicle passes, over a moderate area (i.e., approx. less than 50% of a polygon designated as moderate), moderate loss of vegetation cover (some seed sources remain for natural revegetation), soils are disturbed, with some ruts.
3. Heavy: large numbers of heavy wheeled vehicles and tracked vehicles, many vehicle passes, over more than 50% of a polygon designated as heavy, for long duration (i.e., weeks), extreme loss of vegetation cover leaving mostly bare soil (no seed sources remain for natural revegetation), increased soil disturbance with deep and numerous ruts, requires mechanical repair (to smooth ruts and reshape contours), reseeding, and mulch treatment necessary for recovery.

Model Parameter Modifications for each Disturbance Level

Model parameters that are most affected by training activities and that could be represented in KINEROS2, RHEM, and SWAT were identified based on published information and previous studies (Table 1). Reductions to soil porosity, surface roughness (Manning's n), and canopy cover for each level are applied in KINEROS2, with hydraulic conductivity adjusted according to porosity. In RHEM, reductions are applied to porosity, canopy cover, litter cover, and basal cover, which determine friction factor, hydraulic conductivity, and splash and sheet erosion parameters (Table 2). Curve numbers in SWAT are modified for each disturbance level based on land cover type and hydrologic soil group (Table 3). Additional parameter modifications are calculated from these values. Currently, the tool is implemented only for KINEROS2; however, the parameter modifications for SWAT and RHEM are presented here for information purposes.

Table 1. Source and methods for model input parameter modifications due to military training disturbance

Model input parameters	KINEROS2	RHEM
Ks (effective hydraulic conductivity)	Calculated from Rawls et al. (1982)*; Modified values due to training calculated based on porosity change from von Guerard, et al. (1993); expert knowledge	Basal and litter cover (i.e., from RTLA data), and expert knowledge
G (infiltration suction)	Calculated from relationship between Ks and G from AGWA lookup table	Calculated from relationship between Ks and G from AGWA lookup table
Soil Porosity	Based on level of disturbance and resulting soil compaction; von Guerard, et al. (1993); Rawls and Brakensiek (1983); expert knowledge	Based on level of disturbance and resulting soil compaction; von Guerard, et al. (1993); Rawls and Brakensiek (1983); expert knowledge
Surface Roughness	Manning's n, from expert knowledge, based on percent of bare ground	Friction Factor, based on basal and litter cover (Hernandez et al., 2017), expert knowledge
Kss (splash and sheet erosion coefficient)	not a KINEROS2 parameter	Canopy and ground cover, from RTLA 2012 data (IDW interpolation), and expert knowledge
	SWAT	
Curve Number	Curve Numbers from published data in NRCS Urban Hydrology for Small Watersheds (TR-55; USDA-NRCS, 1986) for land cover type, and modified based on vegetation cover condition for level of disturbance	

*Equation to calculate Ks as a function of porosity (Rawls et al., 1982)

$$Ks = a \frac{\theta e^2}{\psi b^2} \frac{\lambda^2}{(\lambda+1)(\lambda+2)}$$

where θe = effective porosity (cm^3/cm^3), λ = pore size distribution, ψb = bubbling pressure (cm), a = a constant

Table 2. Reductions to model parameters for KINEROS2 or RHEM for each disturbance level

Disturbance Level	Reductions to Model Parameters from Undisturbed Condition				
	KINEROS2 and RHEM		RHEM		
	Soil Porosity*	Roughness**	Canopy Cover	Litter Cover	Basal Cover
Undisturbed	0%	0%	0%	0%	0%
Light	-5%	-25%	-15%	-15%	-10%
Moderate	-10%	-40%	-30%	-30%	-20%
Heavy	-20%	-70%	-65%	-65%	-25%

*Soil Porosity is modified according to the degree of soil compaction
**Roughness, or Manning's n, in KINEROS2, is proportional to the amount of bare ground created by training activities. Friction Factor in RHEM is modified based on changes in litter and basal cover.

Table 3. Modifications to Curve Numbers for SWAT based on Land Cover Type and Hydrologic Soil Group for each disturbance level

Disturbance Level	Hydrologic Soil Group	MRLC Cover Type: 71 Grasslands/ Herbaceous	Curve Number	MRLC Cover Type: 52 Scrub/Shrub	Curve Number	MRLC Cover Type: 42 Evergreen Forest	Curve Number
Undisturbed	A	Herbaceous, Good to Fair conditions*	52	Desert Shrub, Fair to Good conditions	52	Pinyon-Juniper, grass story, Fair to Good conditions*	52
	B		67		70		50
	C		78		80		67
	D		87		85		76
Light	A	Herbaceous, Fair conditions	55	Desert Shrub, Fair conditions	55	Pinyon-Juniper, grass story, Fair conditions*	55
	B		71		72		58
	C		81		81		73
	D		89		86		80
Moderate	A	Herbaceous, Fair to Poor conditions*	59	Desert Shrub, Fair to Poor conditions	59	Pinyon-Juniper, grass story, Fair to Poor conditions*	59
	B		76		75		75
	C		84		83		83
	D		91		87		87
Heavy	A	Fallow, crop residue cover, Poor conditions	76	Fallow, crop residue cover, Poor conditions	76	Fallow, crop residue cover, Poor conditions	76
	B		85		85		85
	C		90		90		90
	D		93		93		93

Curve Numbers are based on Chapter 9, Table 9-2, National Engineering Handbook (NEH; USDA-NRCS, 2004)
*Desert Shrub values for HSG A were used where those values were missing from Table 9-2, NEH Part 630 Chapter 9.
Poor condition: <30% ground cover (litter, grass, and brush overstory)
Fair condition: 30 to 70% ground cover
Good condition: >70% ground cover
MRLC: Multi-Resolution Land Cover (www.mrlc.gov)

Hypothetical MDT application example

An example application using the MDT in AGWA with KINEROS2 was created for a PCMS tutorial exercise that looked at three sites in the Taylor Arroyo Watershed that experienced a hypothetical heavy training disturbance. PCMS is located in southeastern Colorado (Figure 1), and is characterized by plains grasslands dissected by deep canyons and arroyos, with some pinon-juniper woodlands in the uplands. The three hypothetical heavily disturbed areas are located in three different types of terrain found in the watershed: a moderately hilly area (disturbance1), a flat grassland area (disturbance2), and a steep shrubland/forested area (disturbance3) (Figure 2). Data used for the simulation were a USGS 10m DEM (https://viewer.nationalmap.gov/advanced-viewer/), NRCS SSURGO soils (http://www.nrcs.usda.gov/wps/portal/nrcs/site/soils/home/), National Land Cover Dataset (NLCD) 2011 land cover data (https://viewer.nationalmap.gov/advanced-viewer/), and a 10-year 1-hour design storm (41.66 mm) from the NOAA Atlas Precipitation Frequency Estimates website (http://hdsc.nws.noaa.gov/hdsc/pfds/pfds_gis.html). A relative change assessment was performed for each site to determine the changes in runoff and sediment yield resulting from the training (i.e. pre-training conditions vs. post-training conditions). Simulation results can be

used to identify the site that experienced the greatest change, and that should be prioritized for recovery and funding.

The steps to run the models in AGWA are: 1) watershed delineation; 2) model selection and watershed discretization (Figure 3); 3) watershed parameterization; 4) precipitation input; 5) model input file creation; 6) model execution; and 7) model results visualization and analysis. The MDT is applied during step 3, watershed parameterization, by providing a feature class containing polygon(s) that indicate the level of disturbance. To perform a relative risk analysis in AGWA, soils and land cover data specific to the area of interest are used to create the pre-disturbance (pre-training) parameterizations for the model. The Military Disturbance Tool is then used to apply the appropriate parameter changes based on the level of disturbance, and the model is run again to create the post-disturbance (post-training) simulation. Differencing the two simulations allows managers to identify specific hillslopes or channel reaches most at risk of increased runoff or sediment yield as a result of the training disturbance (Figure 4). In this example, all three disturbance areas showed an increase in runoff (ft^3) in the channels immediately downstream, and in the watershed planes (hillslopes) directly affected by the training event.

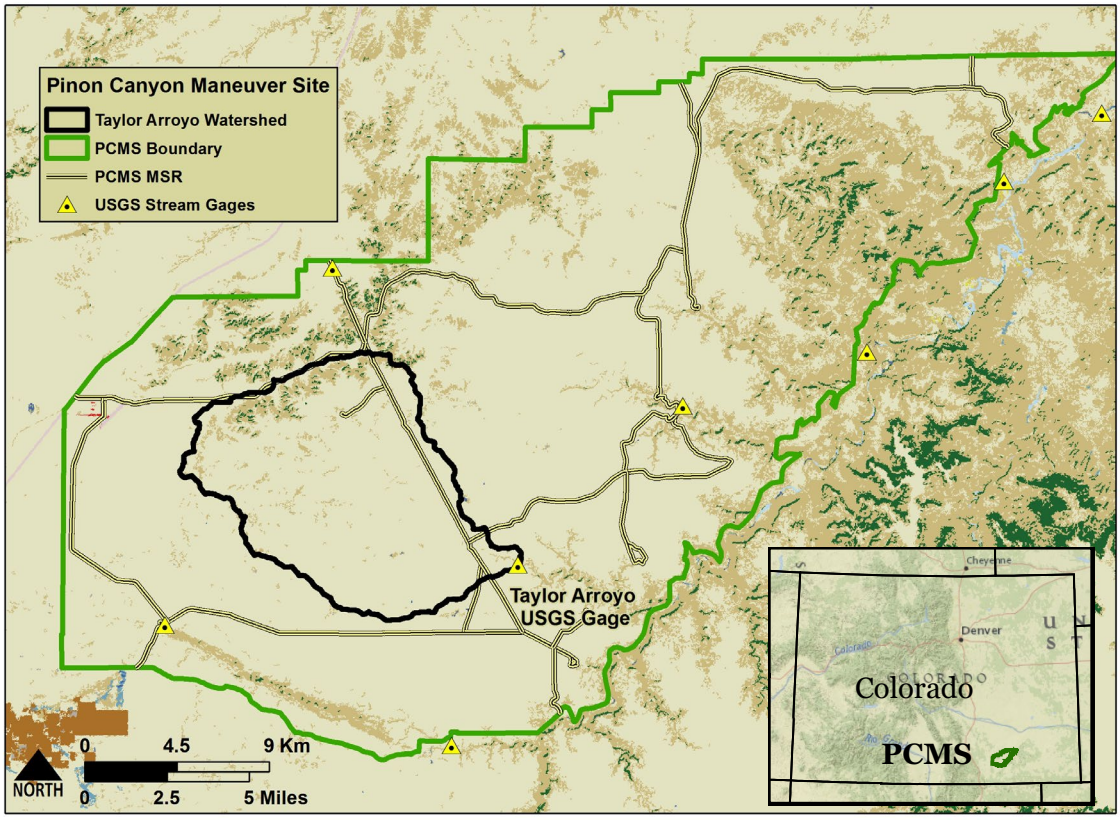

Figure 1. Location map of Pinon Canyon Maneuver Site and Taylor Arroyo Watershed

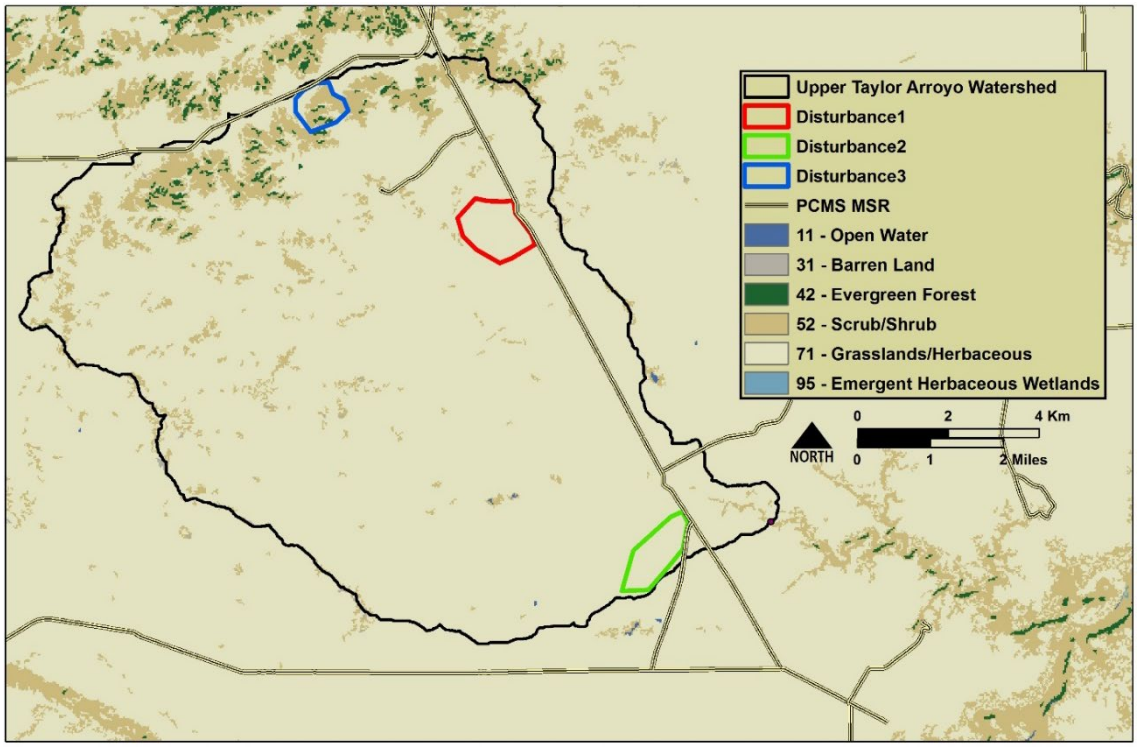

Figure 2. Map of three hypothetical disturbance areas in Taylor Arroyo Watershed, PCMS

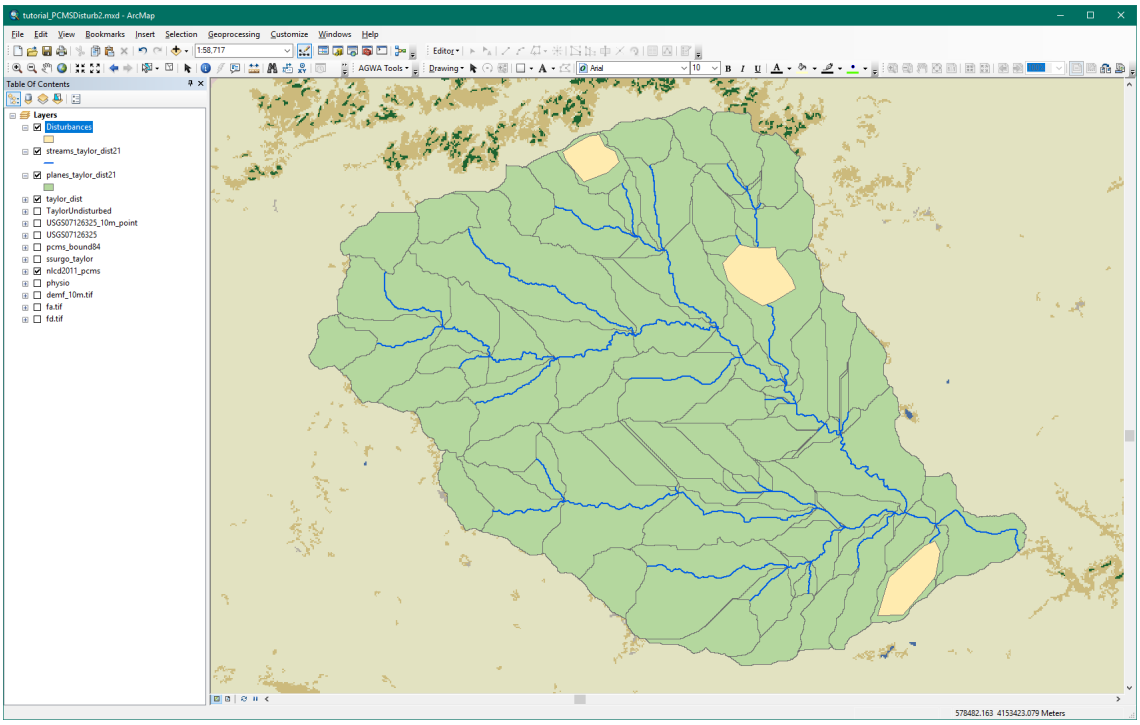

Figure 3. Map of Taylor Arroyo Watershed discretization with three disturbance areas

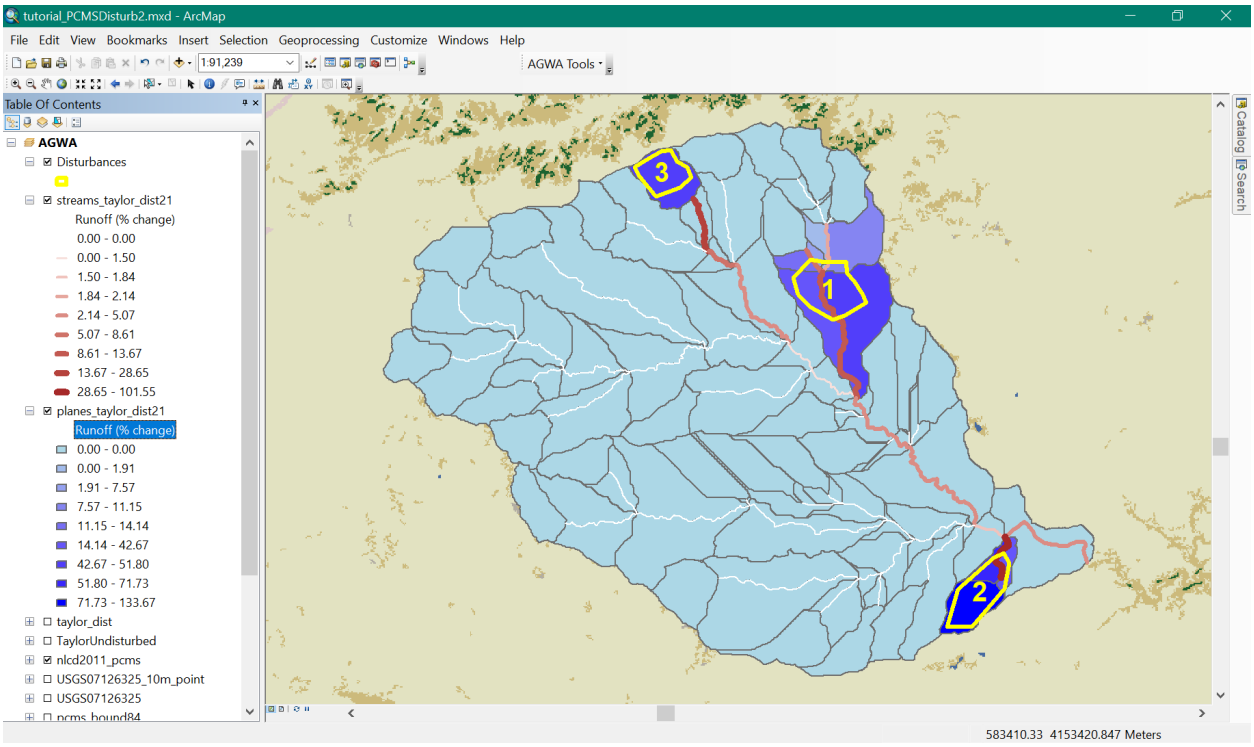

Figure 4. Map of Taylor Arroyo Watershed percent change results for runoff (ft^3) in the channels downstream of the three disturbance areas. Darker colors and thicker lines indicate greater percent change. Note that watershed elements not intersected by disturbance areas did not experience any change in runoff

Figure 5 shows the hydrographs from the pre- and post-training disturbance simulation results for outflow (ft^3/s) at the watershed outlet (Figure 5a), and at the channels directly downstream from each disturbance area (Figures 5 b, c, d). In this hypothetical example, disturbance area 2 (flat, grassland) experienced the greatest increase in outflow following the heavy training event (Figure 5c and Table 4) with up to a 100% increase in peak flow. Little change was observed at the watershed outlet (Figure 5a and Table 4), as expected, since the areas of disturbance represent a small percentage of the overall watershed area and, except for disturbance area 2, are distant from the outlet. Figure 4 shows that the streams further from a disturbance experienced a smaller percent change (lighter, thinner streamline) in runoff than streams closer to the disturbance. This trend is similar for the other model outputs such as peak flow and sediment yield. Infiltration also increases due to the increased flows which result in more wetted area in the channels.

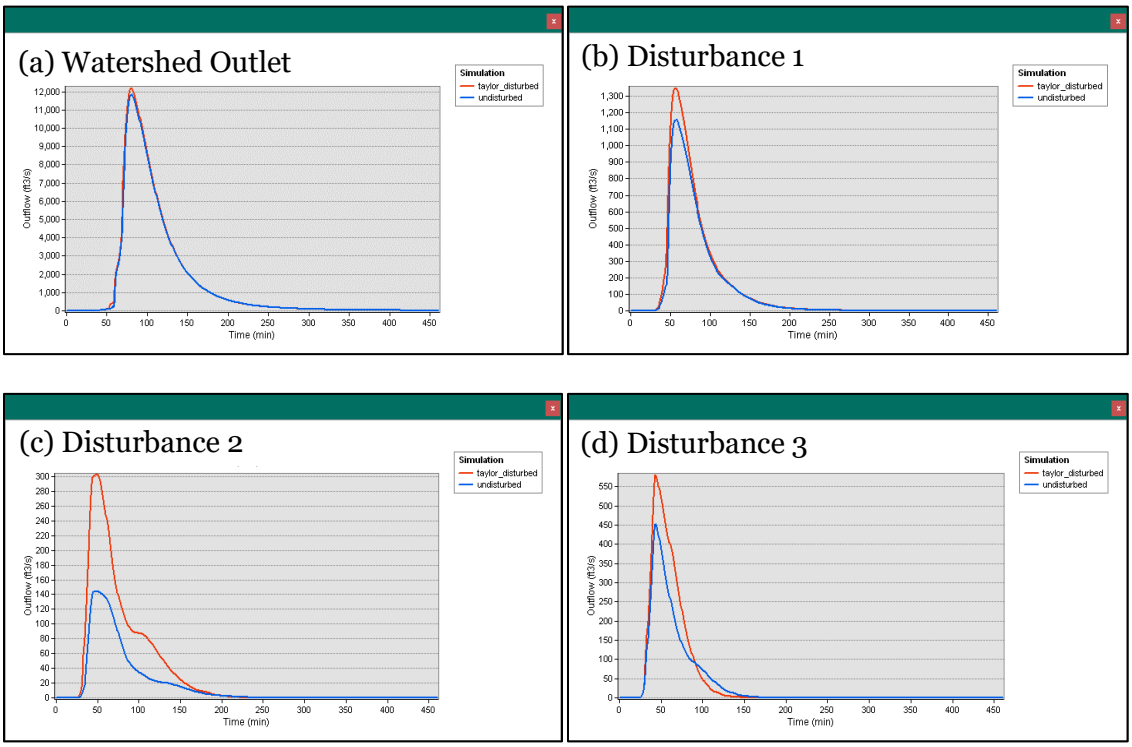

Figure 5. Hydrographs for Taylor Arroyo Watershed comparing pre- and post-disturbance simulation results for peak flow (outflow; ft^3/s) at the watershed outlet and from the three disturbance areas

Table 4. Taylor Arroyo Watershed percent change results for model outputs at the watershed outlet and from the three disturbance areas

OutputType	Watershed Outlet			Disturbance 1		
	Undisturbed	Disturbed	Percent Change (%)	Undisturbed	Disturbed	Percent Change (%)
Infil (acft/mi)	3.13	3.18	1.40	0.698	0.722	3.53
Runoff (in)	0.352	0.362	3.00	0.282	0.320	13.7
Runoff (ft3)	39500000	40600000	3.00	3220000	3660000	13.7
Sed. Yld. (lbs/ac)	1420	1490	4.92	1880	2010	7.12
Peak flow (ft3/s)	11900	12200	2.90	1160	1350	16.5
Peak flow (in/hr)	0.381	0.392	2.90	0.365	0.426	16.5
Sed. (lbs/s)	12900	13600	5.43	1910	2080	8.57

OutputType	Disturbance 2			Disturbance 3		
	Undisturbed	Disturbed	Percent Change (%)	Undisturbed	Disturbed	Percent Change (%)
Infil (acft/mi)	0.232	0.301	30.1	0.259	0.282	9.12
Runoff (in)	0.258	0.520	102	0.501	0.645	28.7
Runoff (ft3)	465000	938000	102	984000	1266088	28.7
Sed. Yld. (lbs/ac)	766	1680	119	5030	8210	63.3
Peak flow (ft3/s)	144	302	109	453	582	28.3
Peak flow (in/hr)	0.288	0.604	109	0.832	1.07	28.3
Sed. (lbs/s)	105	224	113	984	1690	72.2

Conclusions

The spatial capabilities of the MDT in AGWA allow site-specific analyses of military training disturbances to improve land management and sustainability of training lands. The hypothetical example illustrated that watershed response can be strongly affected after a heavy disturbance such as a Stryker Brigade or other large maneuver. Depending on the terrain, runoff, peak flow, or sediment yield can increase by up to 100 percent (Table 4). The MDT can be used to identify which hillslopes or stream reaches are at risk to changes in watershed response due to training events, and can show whether other features such as roads, erosion control dams, training areas, ranges, or facilities may be affected. An editable lookup table allows the tool to be applied at any location where relevant data are available.

AGWA is best used as a relative change tool unless careful model calibration, supported by high quality observations, is performed. The MDT could be improved if land cover and soils data are available before and after a large training event, to refine and validate the parameter changes in the tool.

Acknowledgements

Support for this work was provided by the DoD Environmental Security Technology Certification Program (ESTCP), project RC-201308. Extensive in-kind support was provided by

the USDA Agricultural Research Service, Southwest Watershed Research Center, Tucson, Arizona.

References

Affleck, R.T. 2005. Disturbance measurements from off-road vehicles on seasonal terrain. Final Report, U.S. Army Corps of Engineers, ERDC/CRREL TR-05-12.

Althoff, D.P., Althoff, P.S., Lambrecht, N.D., Gipson, P.S., Pontius, J.S. and Woodford, P.B. 2007. Soil properties and perceived disturbance of grassland subjected to mechanized military training: Evaluation of an index. Land Degradation and Development 18:269-288.

Arnold, J.G. and Fohrer, N. 2005. SWAT2000: Current capabilities and research opportunities in applied watershed modeling. Hydrological Processes 19 (3), 563-572.

Braunack, M.V. 1986. The residual effects of tracked vehicles on soil surface properties. Journal of Terramechanics 23(1):37-50.

Camp, Dresser, and McKee, Inc., 1984, The effects of tracked vehicles traffic on undisturbed soils, Fort Carson Military Reservation: Denver, 44 p.

Donigian, A.S. 2013. A watershed modeling system for Fort Benning, GA using the US EPA BASINS framework. SERDP Project RC-1547 Final Report. Available at https://www.serdp-estcp.org/content/download/18257/202751/file/RC-1547-FR.pdf

Goodrich, D.C., Burns, I.S., Unkrich, C.L., Semmens, D.J., Guertin, D.P., Hernandez, M., Yatheendardas, S., Kennedy, J.R. and Levick L.R. 2012. KINEROS2/AGWA: Model use, calibration, and validation. Transactions of the ASABE 55(4):1561-1574.

Goodrich, D.C., Guertin, D.P., Burns, I.S., Unkrich, C., Levick, L., Korgaonkar, Y., Heilman, P., Hernandez, H., Olimpio, B., Wei, H., Patel, J., Kautz, M. 2019. The AGWA-K2 Suite of Modeling Tools. Proc. 2019 SEDHYD Conf., Reno, Nevada, June 24-28, 2019.

Guertin, P.J. and Meyer, W.D. 2002. Sustainable Army Training Lands/Carrying Capacity: Training Use Distribution Model (TUDM). U.S. Army Corps of Engineers, Engineering Research and Development Center, ERDC/CERL TR-02-13.

Halvorson, J.J., McCool, D.K., King, L.G. and Gatto L.W. 2001. Soil compaction and over-winter changes to tracked-vehicle ruts, Yakima Training Center, Washington. Journal of Terramechanics 38 (2001): 133-151.

Hernandez, M., Nearing, M.A., Al-Hamdan, O., Pierson Jr., F., Armendariz, G., Weltz, M.A., Spaeth, K.E., Williams, C.J., Unkrich, C.L., Nichols, M.H. and Holifield Collins C. 2017. The Rangeland Hydrology and Erosion Model: A dynamic approach for predicting soil loss on rangelands. Water Resources Research. 53: 1-24. doi.org/10.1002/2017WR020651

Jones D, and Kunze, M. 2004. Guide to Sampling Soil Compaction Using Hand-Held Soil Penetrometers. CEMML TPS 04-1, 8p.

Lindsey, M.R., Selim, H.M., Daigle, J., Guillory, C., Elbana, T.A., Bordelon M. and Mouton M. 2012. Soil compaction thresholds for the M1A1 Abrams Tank: Field study at Camp Minden, LA. LSU AgCenter Research Bulletin 891.

Rawls, W.J., Brakensiek, D.L. and Saxton K.E. 1982. Estimation of soil water properties. Transactions of the American Society of Agricultural Engineers 25(5):1316-1320 & 1328.

Rawls, W.J. and Brakensiek, D.L. 1983. A procedure to predict Green and Ampt infiltration parameters. In: Advances in Infiltration – Proceedings of the National Conference Advances in Infiltration. Dec. 12-13, 1983, Chicago, Illinois. American Society of Agricultural Engineers, publisher. p. 102-112.

Smith, R.E., Goodrich, D.C., Woolhiser, D.A. and Unkrich C.L. 1995. KINEROS: a kinematic runoff and erosion model; Chapter 20. In: Singh, V.P. (Ed.), Computer Models of Watershed Hydrology. Water Resources Publications, Highlands Ranch, Colorado, 1130 pp.

Sullivan, P.M. and Anderson A.B. 2000. A methodology for estimating Army training and testing area carrying capacity (ATTACC) vehicle severity factors and local condition factors. U.S. Army Corps of Engineers, ERCD TR-00-2.

Thurow, T.L., Warren, S.D. and Varlson D.H. 1995. Tracked vehicle effects on the hydrological characteristics of Central Texas rangeland. Transactions of the ASAE 36(6):1645-1650.

Trumbull, V.L., Dubois, P.C., Brozka, R.J. and Guyette, R. 1994. Military camping impacts on vegetation and soils of the Ozark Plateau. Journal of Environmental Management 40: 329-330.

USDA-NRCS. 2004. National Engineering Handbook (NEH), Part 630, Hydrology, Chapter 9, Hydrologic Soil-Cover Complexes. Washington, DC.

von Guerard, P., Parker, R.S. and Dash, R.G. 1993. Assessment of Effects of Military Maneuvers on the Streamflow, water quality, and sediment yields at the U.S. Army Pinon Canyon Maneuver Site, Las Animas County, Colorado. USGS Water-Resources Investigations Report 91-4095.

Webb, R.H. 2002. Recovery of severely compacted soils in the Mojave Desert, California, USA, Arid Land Research and Management, 16:3, 291-305.

Sediment Production and Delivery from Unpaved Roads: A Little-Recognized but Significant Sediment Source

Lee H. MacDonald, Senior Research Scientist, NREL and Department of Ecosystem Science and Sustainability, Colorado State University, Fort Collins, Colorado, USA; lee.macdonald@colostate.edu
Gabriel Sosa-Pérez, Instituto Nacional de Investigaciones Forestales, Agrícola y Pecuarias, Chihuahua, Mexico; gsosa@rams.colostate.edu
Carlos Ramos-Scharrón, Department of Geography & the Environment, University of Texas at Austin, Austin, Texas, USA; cramos@austin.utexas.edu

Abstract

Unpaved roads can be a major sediment source, especially in forested areas where the high infiltration rates and nearly continuous ground cover result in very low levels of overland flow and erosion. Yet there is relatively little recognition of the extent to which unpaved roads can adversely affect hillslope erosion, local water quality, aquatic habitat, and increase watershed-scale sediment yields. The objectives of this paper are to: 1) summarize the key processes that control road sediment runoff and erosion; 2) summarize the key processes that affect the delivery of road surface runoff and erosion to streams or other water bodies; 3) show how wildfires can dramatically increase road surface erosion and sediment delivery; and 4) use this understanding to show how road surface erosion and sediment delivery can be minimized.

Road Surface Runoff and Sediment Production

Unpaved roads typically have infiltration rates of only 1-5 mm h^{-1}, resulting in overland flow from nearly all rainstorms as well as snowmelt. In many cases the road surface is almost completely bare, and has large amounts of loose fine sediment generated by vehicle traffic or grading (Figure 1). The combination of surface runoff and readily-available sediment results in annual sediment production rates that typically are around 1 kg per square meter of active road surface per year (4.5 tons ac^{-1} yr^{-1}), with values of around 7 kg m^{-2} (30 tons ac^{-1} yr^{-1}) in highly erodible terrain with summer thunderstorms in the western US (Welsh, 2007) and up to 20 kg m^{-2} (90 tons ac^{-1} yr^{-1}) in sub-tropical high rainfall areas such as Puerto Rico (Ramos-Scharrón and Figueroa-Sánchez, 2017).

The key controls on runoff and sediment production are relatively well known (Fu et al., 2009), but sediment production from unpaved roads is not easily predicted because so many factors are involved. Model predictions are usually based on road segments, where a segment is a hydrologically distinct unit (e.g., the portion of a road between successive waterbars). Two of the most important road segment characteristics for predicting road surface runoff and erosion are road segment area and slope. Road segment area governs the amount of runoff (Q) as indicated by equation 1:

$$Q = (P-I)\,A \qquad \text{(eq. 1)}$$

where P is precipitation and I is infiltration, both in length per unit time, and A is the active road surface area. Road segment slope, in combination with the depth of runoff, governs the amount of energy for detaching and transporting soil particles. Road sediment production and rilling are typically much more sensitive to segment slope than segment area (Figure 2) (Fu *et al.*, 2009).

Figure 1. Unpaved road with drainage rill and a sediment fence to measure sediment production from a road segment on the Pike-San Isabel National Forest in central Colorado, USA.

In addition to road surface area, slope, and rainfall intensity, the supply of readily erodible fine sediment is another major control on road sediment production. The amount of fine sediment is a complex function of the amount and type of traffic, lithology and soil texture, time since grading or road construction, surface cover (including rocks), and antecedent precipitation. A fifth key factor is road design, as this controls whether the road surface runoff is directed into an inside ditch ("insloped"), flows down the road surface (planar or rutted), drains off the downslope side of the road in a dispersed manner ("outsloped"), or flows from the middle off to each side ("crowned") (Weaver *et al.*, 2014). Planar and rutted roads generally have the highest sediment production rates (Fig. 2). Several empirical and physically-based models have been developed to predict road runoff and sediment production at the segment scale, including the semi- empirical SEDMODL2 (NCASI) and READI (Benda et al., 2019), the more physically-

Figure 2. Rills formed on an unpaved road segment in the Sierra Nevada of California due in large part to the steeper slope of the segment and the lack of proper drainage design. This road segment would require relatively frequent grading to remain drivable by normal vehicles at reasonable speeds.

based WEPP:Road (Elliot , 2004), and GRAIP/GRAIP-Lite (Black *et al.* 2012; Cissel *et al.*, 2012). From a practical perspective the amount of road surface erosion and rilling are important also because these determine how often a road needs to be graded, which can be a substantial cost to land managers (Figure 2).

Road Sediment Delivery

For natural resource managers, the most critical question is whether the runoff and sediment from unpaved roads is degrading water quality, increasing peak flows and sediment yields, and/or adversely affecting fish habitat or other aquatic resources. These effects can be expressed both locally, such as in a stream immediately below a road crossing or adjacent to a heavily trafficked unpaved road, and cumulatively at the watershed scale, such as reservoir sedimentation or in a bay or other water body. Any effort to assess these effects requires both an estimation of road surface erosion and how much of the road surface runoff and sediment is being delivered to a stream or other water body ("road-stream connectivity"). Field studies have shown that the percent of road segments or percent of road length connected to streams can range from around 10% to 35% (MacDonald and Coe, 2008). As with road surface erosion, we understand the key factors controlling the delivery of road surface runoff and sediment for a given storm, but accurate predictions are still problematic.

The length of the flow path between a road drain and a stream or water body is generally the most important variable for predicting whether a road segment is connected. Key controls on the length of rills and sediment plumes are the amount of road surface runoff, which depends on rainfall intensity and duration along with road segment area, and the slope, roughness, and infiltration rate along the flow path. Especially in forested areas, the rills and sediment plumes from roads rarely extend for more than 30-50 m (Benda et al., 2019). At the watershed scale road-stream connectivity is heavily influenced by the number of road-stream crossings, which depends on the density and layout of the road network along with the stream channel density. Each of the models mentioned above also attempts to assess road-stream connectivity, although only WEPP:Road and to a lesser extent READI use process-based calculations rather than empirical delivery curves.

Land use activities can greatly increase the amount and delivery of sediment from unpaved roads. Ground-based logging often results in a network of skid trails to access and then yard the trees to landings, and the resulting skid trails effectively behave like unpaved roads and can reach very high densities (Sidle et al., 2004). In areas burned at high and moderate severity, unpaved roads are a major concern because wildfires greatly increase road-stream connectivity as well as road surface erosion (Figure 3) (Sosa-Pérez and MacDonald, 2016). These increases are due to the low post-fire infiltration rates of less than 10 mm hr^{-1} and the loss of surface roughness to slow the runoff and trap sediment. The much larger amounts of post-fire surface runoff and sediment draining onto roads from upslope can greatly increase road surface erosion and the amount of water and sediment that is discharged from road segments onto hillslopes. The result is that road-stream connectivity may approach 100% after high and moderate severity wildfires, regardless of the distance between a road and a stream (Figure 3) (Sosa-Pérez and MacDonald, 2016). Trails for off-highway vehicles often have even higher surface erosion rates than unpaved roads due to the aggressive driving techniques and knobby tires that generate more loose sediment than regular traffic ((Welsh, 2007; Sosa-Pérez and MacDonald, 2017.)

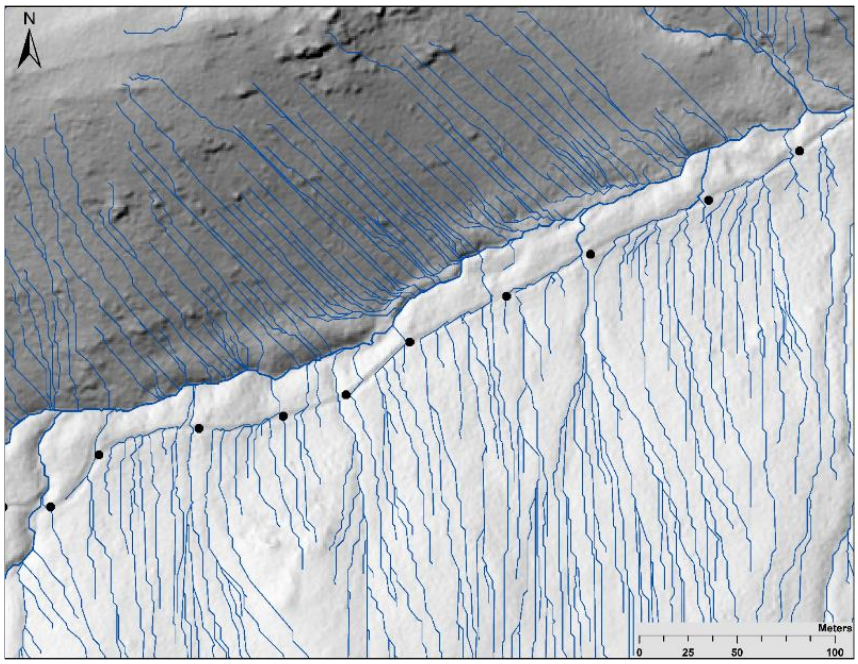

Figure 3. Predicted overland flow lines in a burned area with an unpaved road on the south side of the creek that runs from lower left to upper right, and the opposite hillslope with no road (shown as a darker, shaded hillslope). The flow lines show how the upslope flow lines are intercepted by the road, and the runoff is accumulated and then discharged as concentrated flow, with typically only one drain per segment (black dots show the beginning and end of each road segment as identified by a field survey). In every case the road runoff reaches the stream.

Reducing Road Surface Erosion and Road-stream Connectivity

The techniques for reducing road surface erosion and road-stream connectivity are relatively well understood (Weaver et al., 2014). One of the easiest and most effective techniques is to reduce the spacing between road drains. This first reduces road surface erosion by reducing the volume and velocity of road surface runoff, but a possibly more important effect is that the smaller volumes of runoff and sediment are more likely to infiltrate or be trapped before reaching a stream. Outsloping the road can dramatically reduce road sediment production and delivery as long as the road surface does not become rutted by the passage of vehicles; outsloping is especially difficult to maintain if a road is subject to traffic in wet weather. Rocking the road surface can reduce road sediment production rates by a factor of around 4 to 10 (e.g., Swift, 1984; Coe, 2006), depending on the depth and quality of the rock as well as the type and amount of traffic. However, rocking is usually much more expensive than installing additional drainage dips or waterbars. Land managers are increasingly trying to reduce road sediment impacts by closing or decommissioning roads adjacent to streams, but this can be relatively expensive, especially if replacement roads have to be constructed further upslope or on ridgetops.

Conclusions

Unpaved roads can be a major sediment source with severe downstream impacts. In one study area in Colorado, unpaved roads are probably contributing a similar amount of sediment over time to the stream network as the pulsed sediment input from high severity fires (MacDonald and Larsen, 2009). In the U.S. Virgin Islands, unpaved roads can be the predominant sediment source that threatens the surrounding coral reefs. Although sediment-related impacts from unpaved roads have been the focus of recent regulations and/or BMP guidance in some western states (e.g., California, Oregon, Washington), a much greater awareness is needed by the public, regulators, and resource managers if we are to develop the political will and resources needed to address the persistent and widespread runoff, erosion, and sediment problems posed by unpaved roads.

References

Benda, L., James, C., Miller, D., and Andrus, K., 2019. “Road erosion and delivery index (READI): a model for evaluating unpaved road erosion and stream sediment delivery”, Journal of the American Water Resources Association doi.org/10.11111/1752-1688, 26 pp.

Black, T. A., Cissel, R. M., and Luce, C. H., 2012. The geomorphic road analysis and inventory package (GRAIP) volume 1: data collection method. US Department of Agriculture Forest Service Gen. Tech. Rep. RMRS-GTR-280, Fort Collins, CO. 160 pp.

Cissel, R. M., Black, T. A., Schreuders, K. A., Prasad, A., Luce, C. H., Tarboton, D. G., and Nelson, N. A., 2012. The geomorphic road analysis and inventory package (GRAIP) volume 2: office procedures. US Department of Agriculture Forest Service Gen. Tech. Rep. RMRS-GTR-281, Fort Collins, CO. 160 pp.

Coe, D.B.R., 2006. Sediment production and delivery from forest roads in the Sierra Nevada. M.S. thesis, Colorado State University, Fort Collins, Colorado. 110 pp.

Elliot, W.E., 2004. “WEPP internet interfaces for forest erosion prediction”, Journal of the American Water Resources Association 40(2): 299-309.

Fu, B., Newham, L.T.H., and Ramos-Scharrón, C.E. 2009. ”A review of surface erosion and sediment delivery models for unsealed roads,” Environmental Modelling & Software 25: 1-14.

MacDonald, L.H., and Larsen, I.J., 2009. “Runoff and erosion from wildfires and roads: effects and mitigation”, in Land Restoration to Combat Desertification: Innovative Approaches, Quality Control and Project Evaluation, Bautista, S., Aronson, J., and Vallejo, V.R. (eds.), Fundación Centro de Estudios Ambientes Mediterráneo, Valencia, Spain, pp. 145-167.

MacDonald, L.H., and Coe, D.B.R., 2008. “Road sediment production and delivery: processes and management”, in Proceedings of the First World Landslide Forum, United Nations University, Tokyo, Japan. International Consortium on Landslides, Japan, pp. 385-388.

NCASI. SEDMODL 2.0. http://www.ncasi.org/Programs/Forestry/Resources/SEDMODL-2-0. National Council of Air and Stream Improvement, Cary, North Carolina.

Ramos-Scharrón, C.E., & Figueroa-Sánchez, Y., 2017. “Plot-, farm-, and watershed-scale effects of coffee cultivation in runoff and sediment production in western Puerto Rico”, Journal of Environmental Management 202: 126-136.

Sidle, R.C., Sasaki, S., Otsuki, M., Noguchi, S., and Nik, A.R., 2004. Sediment pathways in a tropical forest: effects of logging roads and skid trails. Hydrological Processes 18: 703-720.

Sosa-Pérez, G., and MacDonald, L.H., 2016. "Wildfire effects on road surface erosion, deposition, and road–stream connectivity," Earth Surface Processes and Landforms 42(5): 735-748.

Sosa-Pérez, G., and MacDonald, L.H., 2017. "Effects of closed roads, traffic, and two road decommissioning treatments on infiltration and sediment production: a comparative study using rainfall simulations", Catena 159: 93-105.

Swift, L.W., 1984. "Gravel and grass surfacing reduces soil loss from mountain roads", Forest Science 30(3): 657-670.

Weaver, W.E., Weppner, E.M., and Hagans, D.K., 2014. Handbook for forest, ranch and rural roads: a guide for planning, designing, constructing, reconstructing, upgrading, maintaining and closing wildland roads. Pacific Watershed Associates, McKinleyville, CA. 342 pp. plus app.

Welsh, M.J., 2008. Sediment production and delivery from forest roads and off-road vehicle trails in the Upper South Platte River Watershed, Colorado. M.S. thesis, Colorado State University, Fort Collins, Colorado. 154 pp. plus app.

The Evaluation of Stormwater Runoff to Recharge Groundwater for use at Fort Irwin, California

Ben Olimpio, Graduate Student, University of Arizona, Tucson, AZ, bolimpio@email.arizona.edu
David Goodrich, Research Hydraulic Engineer, USDA-ARS, Tucson, AZ, Dave.Goodrich@ars.usda.gov
Lainie Levick, Senior Research Specialist, University of Arizona, Tucson, AZ, llevick@email.arizona.edu
Phil Guertin, Professor, University of Arizona, Tucson, AZ, dpg@email.arizona.edu
Mary Nichols, Research Hydraulic Engineer, USDA-ARS, Tucson, AZ, Mary.Nichols@ars.usda.gov
Michelle Cavanaugh, Hydrologic Technician, USDA-ARS, Tucson, AZ, Michelle.Cavanaugh@ars.usda.gov

Extended Abstract

The main source of water at the Fort Irwin National Training Center (NTC) located in the Mojave Desert of California is groundwater. For many years, the pumping of groundwater has led to an imbalance of the Army's Net Zero goals, which means that they are taking out more water than they put in, resulting in aquifer depletion. To address this issue, the NTC wants to capture stormwater from the developed portions of the Fort that will produce more runoff due to constructed impervious areas. To assess and accomplish this goal, the use of modeling technology, in particular the Automated Geospatial Watershed Assessment (AGWA) tool, will be used to demonstrate the potential amount of runoff that could be generated from any given storm. In terms of existing infrastructure, there is a retention basin with a drywell in the bottom to facilitate infiltration into the groundwater located adjacent to the Sleepy Hollow housing development. This can be seen in Figure 1 below. The purpose of this abstract is to address the following: does modeling technology accurately represent the amount of rainfall runoff that goes into the drywell system to recharge groundwater in the local aquifer.

Figure 1. Site location map of Fort Irwin Study area, retention basin, and rain gages.

In order to collect observed data at the ~41-hectare study area, in November of 2017 four Davis weather stations were installed around the housing development to measure rainfall. Figure 1, above, shows the distribution of weather stations around our study area. The weather stations measure temperature, humidity, wind speed, precipitation using a tipping bucket, and barometric pressure. These stations were placed independent of one another to capture the spatial variability of rainfall at this location. In addition to the weather stations, two Solinst Levelogger pressure transducers were installed in the retention basin. The first Levelogger was placed in the drywell to record the depth of water in the pond, and the second Levelogger was placed in a standpipe for added redundancy of data and as a backup in case the first Levelogger experienced any issues in the collection or transmission of observations. Adjacent to the pond, there is a Solinst Barologger that measures barometric pressure at the location. From these measurements, the difference in observed pressures can be converted into a water level in the basin. In addition to the pressure transducers and the weather stations, a weighing rain gage (Keefer et al., 2008) was installed by the USDA ARS. The weighing bucket rain gage measures the weight of water that is collected from each event, and then sends a voltage to a Campbell Scientific data logger that is programmed to convert the voltage into a rainfall measurement, which is then transmitted to our computer for use in the analysis portion of the project. The calibrated weighing rain gage was placed adjacent to the weather station tipping bucket gage to assess whether there are differences between the measurements of the two gage types. Finally, at the outlet of the retention basin, a compound V-notch weir was installed in the existing concrete apron in order to measure any discharge should the pond overflow. By using the water levels that are measured by the pressure transducers, the outflow over the weir can be calculated using the methods described in Piratheepan et al. (2007). A terrestrial laser scan of the detention pond was also completed to estimate stage-volume-surface area relationships.

To perform the modelling analysis, the Automated Geospatial Watershed Assessment (AGWA) tool and the KINEROS2 hydrologic model are used within ESRI ArcMap to estimate the volume of water that discharges into the basin on an event by event basis, and then the results are compared to observed data to validate the accuracy of the model. To date, since installation of the weather station and transducers, there have been two rainfall events which have contributed substantial volumes of water into the basin. The events that occurred on January 9th and March 10th, 2018 had average rainfall totals of 18 mm and 10 mm respectively. For reference, an 18mm storm would compare to a 2-year, 6-hour return period storm for this region. The 10mm storm would compare to a 1-year, 3-hour return period storm. In Figure 2 below, the hyetograph shows the characteristics in terms of duration and rainfall intensity of the January 9th storm at the site of the retention basin. In Figure 3 below, the hyetograph shows the characteristics in terms of duration and rainfall intensity for the March 10th storm.

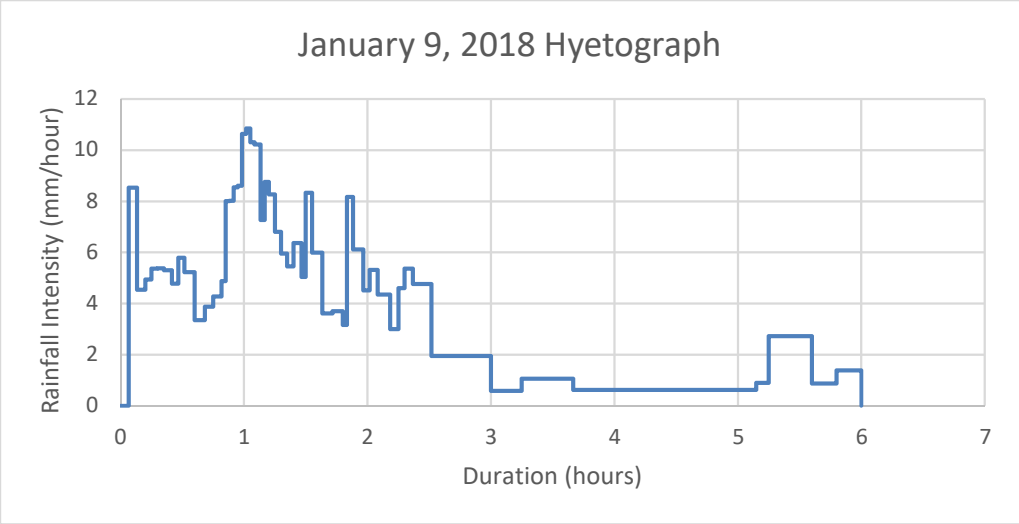

Figure 2. Rainfall hyetograph from the rain gage at the retention basin for the January 9th storm.

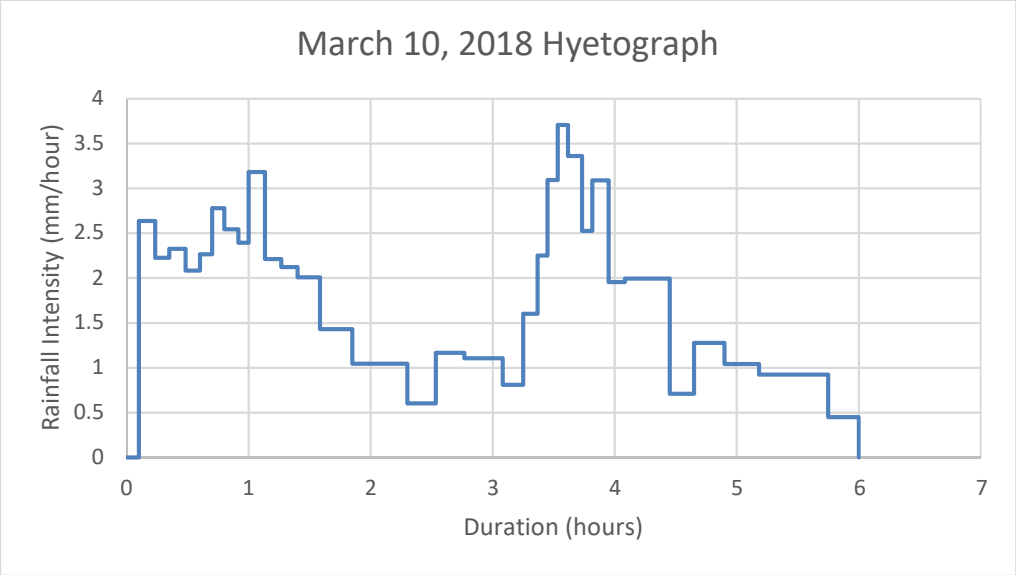

Figure 3. Rainfall hyetograph from the rain gage at the retention basin for the March 10th storm.

As a result of the hyetographs above, the observed stormwater runoff that was stored in the retention basin was 459.4 m^3 for the January 9th event and 96.0 m^3 for the March 10th event. In comparison, the modelled results from AGWA were 471.2 m^3 and 263.5 m^3 which is a difference of 2.50 and 63.57 percent for the two events. The two storms have different percent errors due to the characteristics of each storm. The January 9th storm had a lower percent error, due to the fact that there was only one peak intensity during the event. Having one peak intensity during a storm allows for runoff to be more consistent in terms of accumulated volume over time. For the March 10th storm, the peak intensities that were observed are smaller than the January 9th storm, so the runoff that is generated has a greater potential to infiltrate before it reaches the retention basin. The hypothesized result from this is that more runoff accumulates during the higher intensity storm over time, whereas the lower intensity event causes

fragmented runoff accumulation leading to a smaller volume discharging into the retention basin.

Because the retention basin is a dynamic system, the modelled volumes were adjusted to reflect the impact that infiltration has on the pond. There were three adjustments that were made to the modelled volumes. The first adjustment was taking into account the volume of water that would be infiltrating into the drywell at every time step. This was accounted for by using analyzed drywell infiltration rates from the USDA-ARS Riverside, who performed drywell infiltration pressure head tests on site using a continuous flow of water from a nearby fire hydrant. Since the drywell was not functioning properly, the measured infiltration rate was 0.0001 m/s, which is very low. This value was then converted to m/hour due to the timestep of the infiltration event being selected in hours, and then accumulated over the duration of each event. The second adjustment that was made was for evaporation. Evaporation was calculated by using the Penmen-Monteith equation (Allen et al., 1998). Using the observed water level data that was collected from the pressure transducers, the planar area could be interpolated using GIS software. The calculated evaporation rate from the Penmen-Monteith equation was multiplied by the planar area of the pond to obtain the volume of water that would be lost to evaporation at each timestep. The last adjustment that was made to the final volume of the pond was accounting for how much water would infiltrate at each timestep of the measured event. This was done using a simple differencing of the change in surface area divided by the change in volume at each timestep. From this result, the differencing and division yields an estimated infiltration rate of the areas of the pond that are pervious, and this then is converted into a volume of water lost to infiltration at each timestep. After performing these adjustments to best account for the other factors of the system, the observed results can then be compared to the modelled results in order to determine the validity of the model. When analyzing the adjusted values to the modelled values, the larger storm had a smaller percent difference, which is consistent with previous work that was done in assessing the AGWA tool. The adjusted observed value for the January 9th storm was 470.5 m^3, and this decreased the percent error to 0.15%. For the smaller storm on March 10th, the adjusted observed volume was 99.6 m^3, which only lowered the percent difference to 64.6%. In the case of the larger storm, the percent error decreased by 2.35%, whereas the smaller storm only decreased by 1%. The smaller event had a larger percent difference, showing that the model has a higher sensitivity to rainfall input uncertainties for smaller events. This is also consistent with validation work that has been done on the AGWA tool. To further refine these calculations and obtain better model results, more events would need to occur so that there are more observed data to calibrate and validate the model.

To make up for the absence of observed data in the timeframe since installation of the instrumentation in 2017, there are other data sources used to create design storms. The first source of data came from historical weather data that was observed by nearby stations located at the Bicycle Lake Airfield and in the town of Goldstone, CA. Since there are approximately 70 years and 40 years of data, respectively, the data were evaluated using three different percentiles: the 85th percentile, the 95th percentile, and the 99th percentile. The methodology used to calculate each of these percentiles was under the guidance of the EPA and their standards for design storms used in Low Impact Development scenarios. In addition to these

observed data, the NOAA Atlas 14 Precipitation Frequency Data Server was used to create design storms. The selected return period intervals used are the 2, 5, 10, and 25-year events and the durations selected for each of these return period intervals are 1, 2, 6, and 24 hours. In total, there are an additional 19 design storms that were added to supplement the modelling effort. In addition to the design storms, there are also three different soil parameterizations that were created based on soil samples taken on site. These three soil parameterizations also add to the sample size of selected events in order to gain a better understanding of the sensitivity of each rain event on our study site. In total, with the addition of both the SCS Type II and the NRCS CA-6 rainfall distributions, there are 139 total scenarios to run through the model. In conclusion, based on the results presented above, there would need to be more observed storms with varying depths and durations required to accurately assess recharge capabilities of this drywell system.

Acknowledgements

The research was supported by the EPA-ARS Interagency Agreement DW-012-92465401. Dr. Stephen Kraemer is the EPA Project Officer. Without his expertise, it would be much harder to model various aspects of the project. I would also like to acknowledge Mark Kautz, John Smith, and Chad Radford of the Southwest Watershed Research Center (SWRC) who have graciously helped in both installing and managing some of the data infrastructure, without them, gathering data would not be as efficient as it currently is.

References

Allen, R.G., Pereira, L.S., Raes, D., Smith, M., 1998. Crop Evapotranspiration-Guidelines for Computing Crop Water Requirements-FAO Irrigation and Drainage Paper 56, vol. 300 FAO, Rome (9) D05109.

Keefer, T.O., Unkrich, C.L., Smith, J.R., Goodrich, D.C., Moran, M.S., Simanton, J.R. 2008. An event-based comparison of two types of automated-recording, weighing bucket rain gauges. Water Resources Research, Vol. 44, W05S12.

Piratheepan, H., Winston, N.E.F., and Pathirana, K.P.P. 2007. Discharge measurements in open channels using compound sharp-crested weirs, Engineer, The Institution of Engineers, Sri Lanka, 30(3):31-38.

The Impact of Small Ponds on Streamflow Response and Sediment Yield

D. Phillip Guertin, Professor, University of Arizona, Tucson, AZ, dpg@email.arizona.edu
Jane Patel, GIS Analyst, Tucson Water, Tucson, AZ, jane.patel@tucsonaz.gov
Lainie Levick, Principal Research Specialist, University of Arizona, Tucson, AZ, llevick@email.arizona.edu
Haiyan Wei, Assistant Research Scientist, University of Arizona, Tucson, AZ, haiyan.wei@ars.usda.gov
David C. Goodrich, Research Hydraulic Engineer, USDA Agricultural Research Service, Tucson, AZ, Dave.Goodrich@ars.usda.edu
I. Shea Burns, Senior Research Specialist, University of Arizona, Tucson, AZ, shea.burns@ars.usda.gov
Carl Unkrich, Hydrologist, USDA Agricultural Research Service, Tucson, AZ, carl.unkrich@ars.usda.gov

Abstract

In the western United States the landscape is dotted with small ponds, many of them man-made (farm ponds, stock tanks, sediment basins, erosion control basins, flood control basins, etc.), which capture both streamflow and sediment. In these landscapes it is not uncommon to have over 50% of a watershed area behind storage. Although small ponds can have a significant impact on a watershed's water balance and sediment balance, they are often not included in watershed assessments because they are difficult to locate and characterize. However, new technology, in the form of high resolution imagery and LiDAR-derived products, can facilitate the tasks of locating and characterizing ponds. The Automated Geospatial Watershed Assessment Tool (AGWA) was used to model the runoff and sediment yield. AGWA (see: www.tucson.ars.ag.gov/agwa or https://www.epa.gov/water-research/automated-geospatial-watershed-assessment-agwa-tool-hydrologic-modeling-and-watershed) is a GIS interface jointly developed by the USDA-Agricultural Research Service, the U.S. Environmental Protection Agency, the University of Arizona, and the University of Wyoming to automate the parameterization and execution of a suite of hydrologic and erosion models (RHEM, KINEROS2 and SWAT). A new tool has been developed for AGWA to efficiently identify and characterize small ponds. The use of the tool is illustrated in several case studies that highlight the importance of ponds in determining water and sediment balance in western rangeland watersheds.

Introduction

The abundance of small artificial ponds (farm ponds, stock tanks, sediment basins, erosion control basins, flood control basins, etc.) constitutes a major human alteration of the hydrologic landscape. The total number of such features across the conterminous United States has been estimated to be between 2.6 and the 9 million, with densities in some areas exceeding 5 per km^2 (Renwick et al. 2006). Ponds not only capture water, but also are important sinks for sediment, carbon, and nutrients. In the western United States ponds are commonly used to water livestock. In these landscapes it is not uncommon to have over 50% of a watershed area behind storage. The influence of small ponds on water yield, peak flow and sediment yield is well

documented (Berg et al. 2016, Goff and Gentry 2006, Milne and Young 1989, Nichols et al. 2013, Renwick et al. 2005, Smith et al. 2002). In general, small ponds tend to decrease water yield, peak flows and sediment yield from watersheds. The degree of change is a function of the density and size of ponds within the watershed. Although small ponds can have a significant impact on a watershed's water balance and sediment balance, they are often not included in watershed assessments because they are difficult to locate and characterize. This is especially true in the semi-arid rangelands in the western United States where the ponds are often dry for long periods of time, hence remote sensing methods used in more mesic and humid regions are ineffective because there is no water signature.

The paper will describe the use of the Automated Geospatial Watershed Assessment tool (AGWA; Goodrich et al. 2012) for watershed assessments that include evaluating the impact of ponds. The paper will review an application (Storage Characterization Toolkit) developed within AGWA to quickly identify and characterize ponds using a digital elevation model (Barlow 2017). The paper will review the results from two watershed assessments conducted in Arizona and Colorado that examined the influence of ponds.

AGWA Overview

AGWA (Goodrich et al. 2012) is a Geographic Information System (GIS) based watershed modeling tool. The guiding principles for the development of AGWA were that it: 1) provides simple, direct, transparent, and repeatable parameterization routines through an automated, intuitive interface; 2) is applicable to ungauged watersheds at multiple scales; 3) evaluates the impacts of management and is useful for scenario development; and, 4) uses free and commonly available GIS data layers.

The models currently incorporated in AGWA are KINEROS2 (K2 – KINematic runoff and EROsion model, Smith et al. 1995, Goodrich et al. 2012), RHEM (Rangeland Hydrology and Erosion Model, Hernandez et al. 2017), and SWAT (Soil and Water Assessment Tool version 2000 and version 2005, Arnold and Fohrer 2005). AGWA supports modeling along a continuum of spatial and temporal scales, ranging from hillslopes (~hectares) to large watersheds (>1000 km^2) and from individual storm events (minute time steps) to continuous simulation (daily time steps over multiple years). AGWA supports the parameterization and execution of hydrologic models for watershed modeling efforts by performing the following tasks: watershed delineation; watershed discretization into discrete model elements; watershed parameterization; precipitation definition; simulation creation; simulation execution; and simulation results visualization (). Various data are required to support this functionality, including: a raster-based DEM (digital elevation model); a polygon soil map (NRCS SSURGO, NRCS STATSGO, or FAO soil maps); and a classified, raster-based land cover (NLCD, NALC, and GAP/LANDFIRE datasets are supported via provided look-up tables; however, other datasets may also be used if accompanied with a related look-up table). AGWA does not require observed precipitation or runoff to drive the models when used for relative assessment/differencing between scenarios. For precipitation input, AGWA can use user-defined depths and durations, user-defined hyetographs, or design storms to drive the K2 model, and included weather station-based generated, daily precipitation (U.S. only) to drive the SWAT model.

AGWA is an add-in to ESRI ArcGIS 10.x and 9.x (http://www.esri.com/arcgis/about-arcgis). It is a free download from the website www.tucson.ars.ag.gov/agwa as a "package" containing all tables and models required to run AGWA. AGWA is best used as a relative change tool (i.e., pre-

versus post-change) unless careful model calibration, supported by high quality observations, is performed.

AGWA was designed to support watershed analysis and assessment. AGWA applications include landscape change assessments (Hernandez et al. 2010, Kepner et al. 2008, Levick 2017), rangeland assessments (Goodrich et al. 2011, Weltz et al. 2011), post wildland fire assessments (Goodrich et al. 2012), sustainable urban development (Guertin et al. 2015, Korgaonkar et al. 2018), and flood risk assessment (Yatheendradas et al. 2008, Norman et al. 2010).

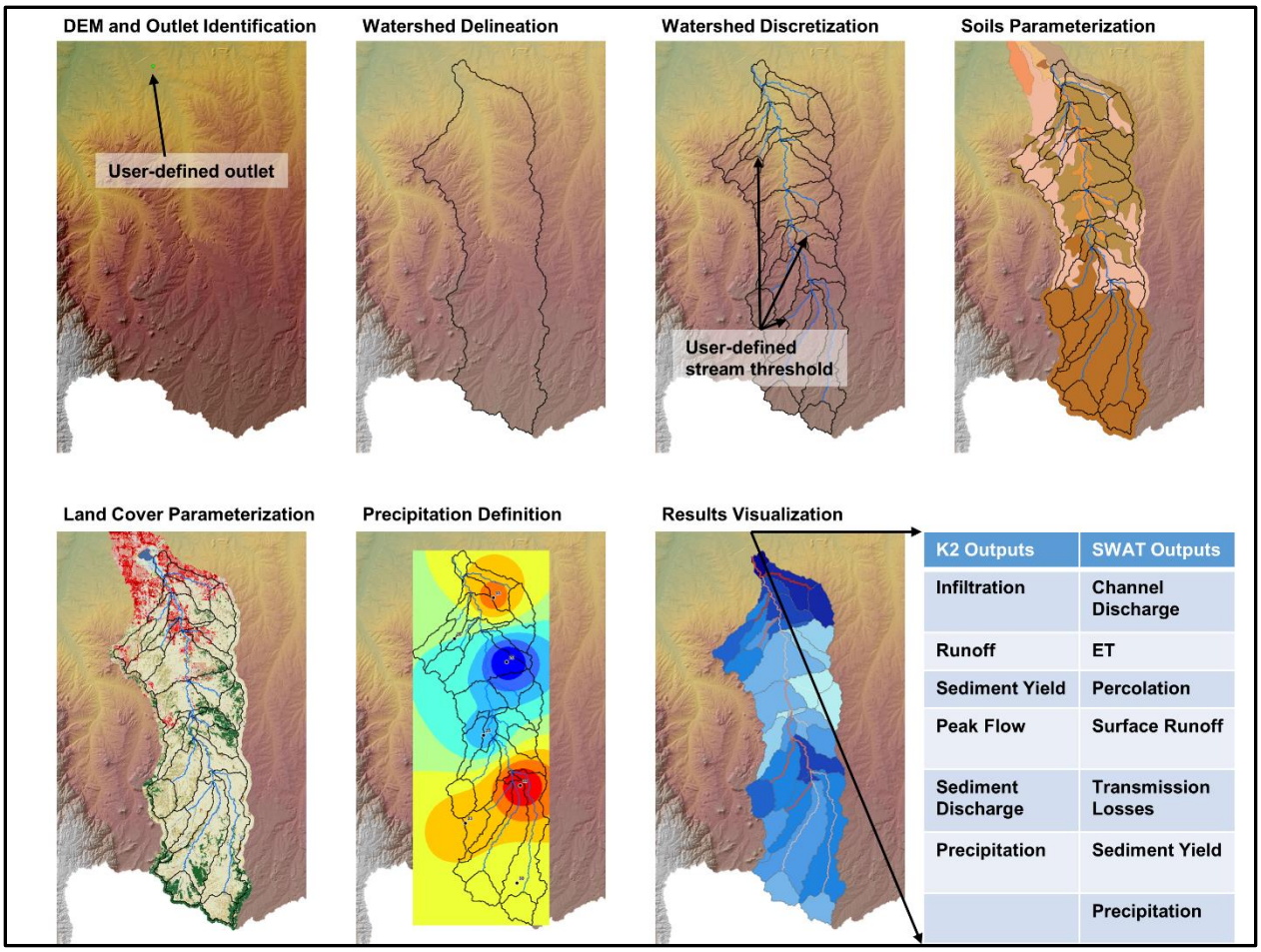

Figure 1. The required steps in AGWA to perform a watershed assessment. A DEM is used to delineate the watershed and subdivide it into model elements (i.e. hillslopes and channels for K2 and subwatersheds and channels for SWAT). The model elements are parameterized based on the DEM, soils, and land cover layers. The precipitation input is then selected from varies sources. After the model is executed, the results are imported and visualized in the GIS.

Storage Characterization Toolkit

Most landscapes will have natural or man-made ponds, lakes or reservoirs. In order to represent a watershed properly for any assessment the ponds, as well as lakes and reservoirs, must be included or the estimates for water and sediment yield will be over-estimated. The Storage Characterization Toolkit (SCT) was developed for AGWA to facilitate and automate the inclusion of pond features into the K2 and SWAT models (Barlow 2017).

The SCT was designed to identify and characterize existing water storage structures as well as to plan for the future installation of water storage structures. The SCT was developed using a Python Toolbox in ESRI ArcMap so that geospatial layers could be organized, used and viewed by the user throughout the process. The SCT has three components:

1. Identify and characterize existing storage,
2. Calculate the discharge from the structure, and
3. Export files for input to K2.

The user must first identify the location of the existing or proposed structure. Existing structures can be identified using high resolution imagery with or without additional information on structure locations. The location of ponds may also be determined using the SCT. Using a digital elevation model (DEM) and the ESRI ArcMap Sink Tool areas of potential ponds can be identified as the low points in the terrain with no drainage. A user set threshold can be used to remove sinks that are too small to be ponds. The software will identify the terrain sinks, but the user must still review identified sinks to confirm they are ponds (Figure 2).

For an existing structure, the dam location (visually identified as a linear feature in the imagery) and the height of the dam at its lowest point must be determined using a digital elevation model (DEM). For a proposed structure the dam locations can be drawn perpendicular to the channel and the dam height determined based on site conditions and objectives.

A protocol was then developed to characterize stage-storage relationships for each water storage feature. Automation of these two steps resulted in the Identify and Characterize Existing Storage tool in the SCT. Automation of this process allows a large number of ponds, across a wide spatial extent, to be identified and characterized in a single batch job.

The tool operates by first comparing a filled and unfilled DEM. The process of filling a DEM removes any sinks or peaks that would prevent flow in an otherwise hydrologically continuous surface (Tarboton et al. 1991). DEM filling is an important first step in watershed modeling to ensure proper stream and watershed delineation and is aimed at artificial sinks (e.g. errors in the DEM), however this process can remove storage features in the landscape which could impact flow (Figure 2).

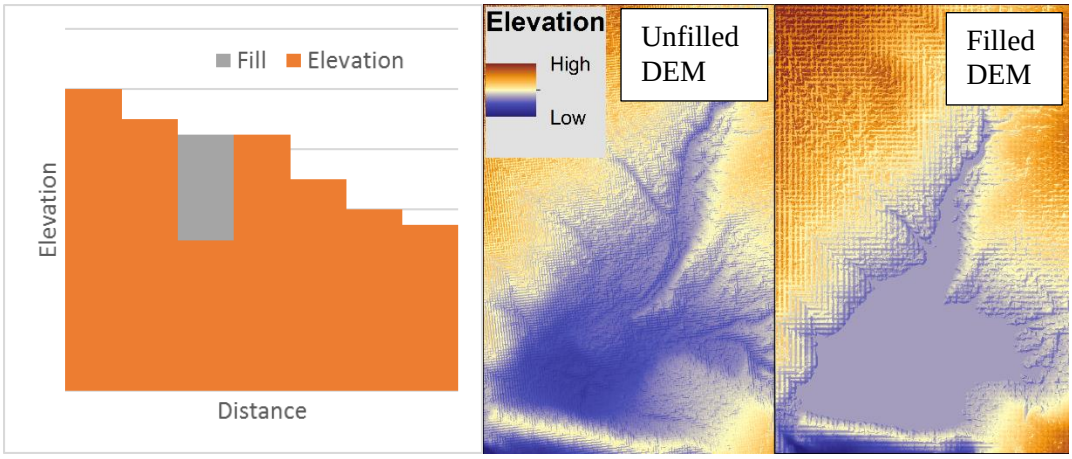

Figure2. Fill Process as it removes sinks in theory (left) and in reality (right).

The cells that are filled are then compared to the unfilled DEM to identify large groups of cells that could be storage sinks. These sinks are then spatially compared to known storage/dam

locations. Sinks closest to known storage/dam locations are associated with those points for identification purposes. At this point a storage feature has been identified and its boundary has been defined.

Next the stage-volume calculations are performed from the features minimum elevation to its maximum elevation. The ESRI ArcMap Cut-Fill tool is used to automate surface area and volume calculations of the unfilled DEM and each stage raster until maximum elevation for each feature is reached (Figure 3). The final product is a stage-volume curve for the pond.

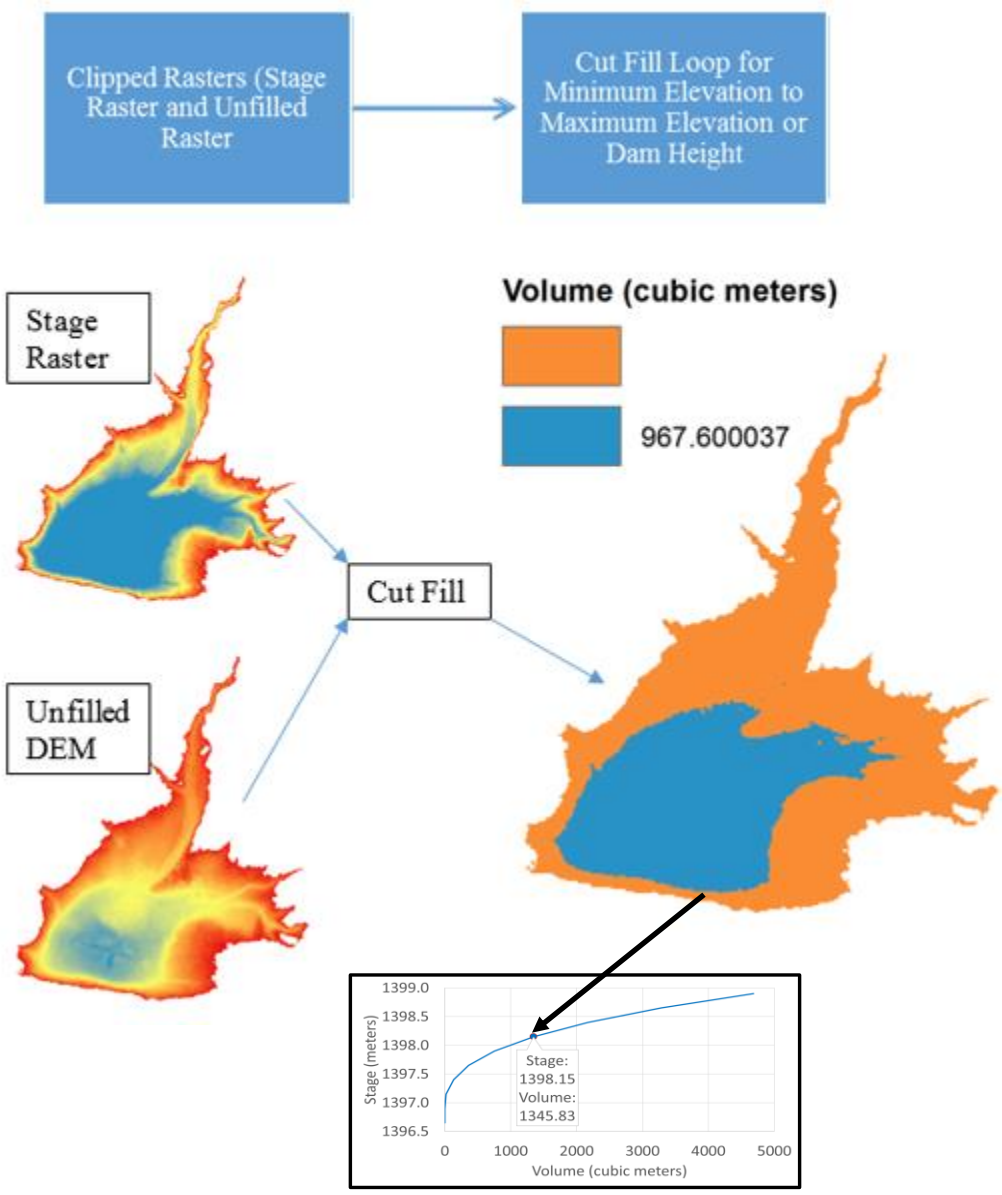

Figure 3. Cut-Fill function is part of a loop that calculates surface area and volume for pond stage from minimum elevation to maximum elevation. The final result is the stage-volume curve for the pond.

For validation, the Storage Characterization Toolbox was used to characterize stage-storage relationships at 0.25 meter increments for Pond 208 on the Walnut Gulch Experimental Watershed (WGEW). For Pond 208, field surveyed stage-storage relationships from February

2016 were compared to modeled relationships derived from LiDAR surveys conducted during September 2015 (M. Nichols, 2016 personal communication). The WGEW LiDAR survey was converted to a bare earth DEM with a cell resolution of 0.5 meters and a vertical accuracy of approximately 0.086 meters (Nagle and Wright 2016).

Percent error was calculated based upon relative stage for each Pond 208 (Table 1). While percent error is much larger in the complex validation than the basic pond, the same pattern is observed where error diminishes as volume increases. Although error exists in the modeling of existing storage, the general shape of the stage-storage relationship was maintained. The complex validation series for pond 208 under predicted volume by at least 20%. While error exists in this validation case studies, the general stage-storage relationship is well captured.

Table 1. Percent Error by Relative Stage for Pond 208.

Relative Stage (m)	Modeled Volume (m3)	Observed Volume (m3)	Percent Error
0.00	0.0	0	0.0
0.25	0.4	2	78.5
0.50	16.9	85	80.2
0.75	133.6	276	51.6
1.00	360.7	608	40.7
1.25	754.3	1130	33.2
1.50	1345.8	1863	27.8
1.75	2169.2	2884	24.8
2.00	3284.8	4233	22.4
2.25	4686.1	5834	19.7

After calculating the basic stage-storage relationship, for each pond the tool allows users to calculate discharge based on known information or size classifications. This is the second part of the SCT known as the Calculate Storage Discharge tool. This step calculates discharge through a culvert and/or spillway as a function of stage and requires information about outlet types and properties.

The basic equations that calculate discharge from stage above the outlet structure are Manning's equation for pipe flow (Equation 1; non-pressurized), the broad-crested weir equation which accounts for discharge at earthen spillways (Equation 2) and the sharp-crested weir equation (Equation 3) (Crowe et al., 2001).

$$Q = \frac{1}{n} A R^{\frac{2}{3}} S_o^{\frac{1}{2}} \quad (1)$$

where: n = Manning's roughness coefficient, A = area of the pipe that is filled with water (m^2), R = hydraulic radius of the wetted pipe (m), and S = slope of the pipe (m/m; default = 0.004).

$$Q = 0.385 L \sqrt{2g} H^{\frac{3}{2}} \quad (2)$$

where: L = length of the weir normal to the direction of water flow (m), g = acceleration due to gravity (9.81 m/s^2), and H = stage of water above the spillway (m).

$$Q = \frac{2}{3} C_d \sqrt{2g} L H^{\frac{3}{2}} \quad (3)$$

where: Cd = coefficient of discharge, g = acceleration due to gravity (9.81 m/s^2), L = length of the weir normal to direction of flow (m), and H = stage of water above the spillway (m).

The final step of the tool prepares the derived input files to be used in a watershed simulation for AGWA/K2. This requires user input for the soil properties of the pond (default is silty clay with hydraulic conductivity of 1.41 mm/hour) then reformats calculated storage-discharge tables and creates a link between the pond shapefile to nodes in the AGWA discretization. K2 models ponds using input files that can contain upstream contributing elements, lateral elements, initial storage, rating tables (volume, discharge and surface area), and saturated hydraulic conductivity. The series of tools in the Storage Characterization toolbox supply K2 with the required pond inputs for AGWA to configure a simulation with storage elements.

Application Examples

Two examples of watershed assessments that utilized the SCT have been completed in Arizona and Colorado. A rangeland assessment was conducted on the Cienega Creek Watershed in southeastern Arizona. In the assessment the impact of a mechanical brush removal treatment on sediment yield from a small watershed was compared to the impact of a stock pond at the outlet of the small watershed. Figure 4 shows that although the mechanical brush removal treatment has a positive impact on sediment yield the sediment storage in the stock pond has far greater impact. The results illustrate that although the mechanical brush removal treatment had other benefits such as increased forage production and decreased soil erosion, the stock pond impact on sediment yield and downstream water quality is very important and must be considered in a watershed analysis and assessment.

The second assessment was conducted on the U.S. Army Pinon Canyon Maneuver Site (PCMS) in Colorado. To mitigate the impact of military training exercises on downstream water quality and to control gullying PCMS has installed Erosion Control Dams (ECDs) across the installation. One watershed on PCMS, Taylor Arroyo (125.6 square kilometers), has 111 ECDs or a pond density of 0.88 ponds per square kilometer (Figure 5). There are over 400 ECDs on PCMS. The SCT was used to identify and characterize the ECDs on Taylor Arroyo and K2 in AGWA was used to evaluate the effectiveness of the ECDs in protecting downstream water quality.

Figures 5 and 6 illustrate the impact of the ECDs on Taylor Arroyo at two locations within the watershed, stream reach #954 in the upper portion of the watershed and the Taylor Arroyo watershed outlet. The figures show the impacts of the dams on peak runoff (Figure 5) and peak sediment yield (Figure 6) from a 10-year return period, one hour, 41.66mm rain event. The ECDs decreased the peak discharge by 66% (from 53.12 m^3/s to 18.20 m^3/s) at stream reach #954 and by 35% (from 77.14 m^3/s to 49.94 m^3/s) at the watershed outlet. The ECDs decreased the peak sediment yield by 88% (from 2217.72 kg/s to 257.06 kg/s) at stream reach #954 and by 57% (from 2914.61 kg/s to 1254.43 kg/s) at the watershed outlet.

The runoff volume for stream reach #954 was 86,576 cubic meters without ponds and 69,358 cubic meters with ponds, a 20% decrease in runoff. The sediment yield for stream reach #954

was 4,031,593 kilograms without ponds and 925,705 kilograms with ponds, a 77% decrease in sediment yield. The runoff volume at the watershed outlet was 381,012 cubic meters without ponds and 286,448 cubic meters with ponds, a 25% decrease in runoff. The sediment yield for stream reach #954 was 14,306,700 kilograms without ponds and 8,271,455 kilograms with points, a 42% decrease in sediment yield. As this single event indicates the high density of ponds in the Taylor Arroyo Watershed caused a substantial decrease in runoff and sediment yield, protecting downstream water quality, and highlighting the importance of including ponds in conducting a watershed assessment.

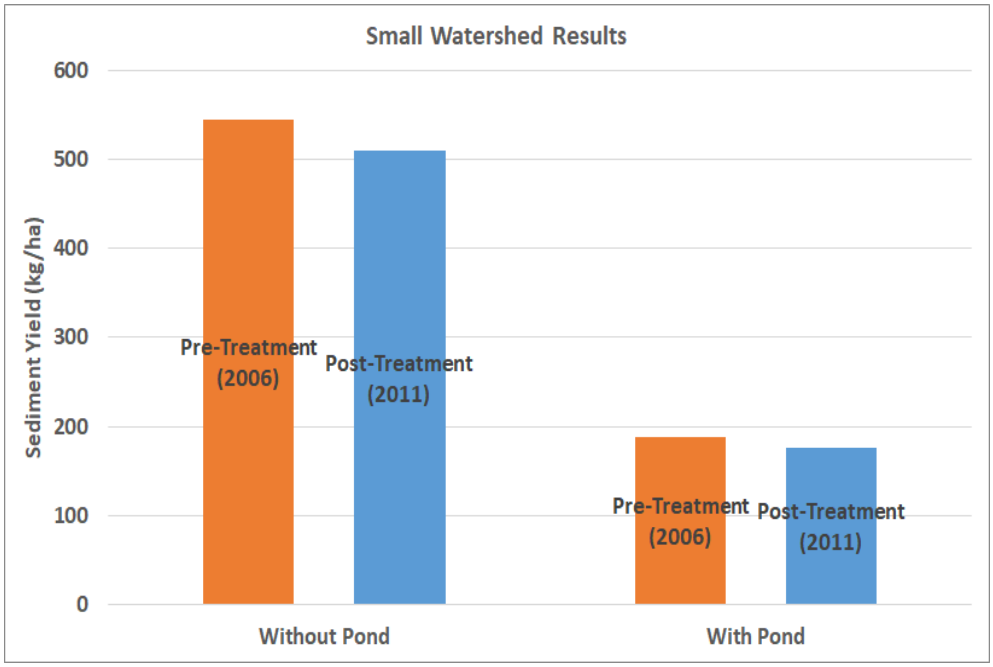

Figure 4. Graph showing the sediment yield pre- and post-treatment and with and without a stock pond for the small watershed on the Cienega Creek Watershed in southeastern Arizona. Mechanical brush removal treatment was performed in the winter of 2010-2011, with an immediate reduction in brush cover observed in 2011, resulting in reductions of sediment yield. Installation of a stock pond reduced sediment in both pre- and post-treatment scenarios, with a greater impact than that of the treatment.

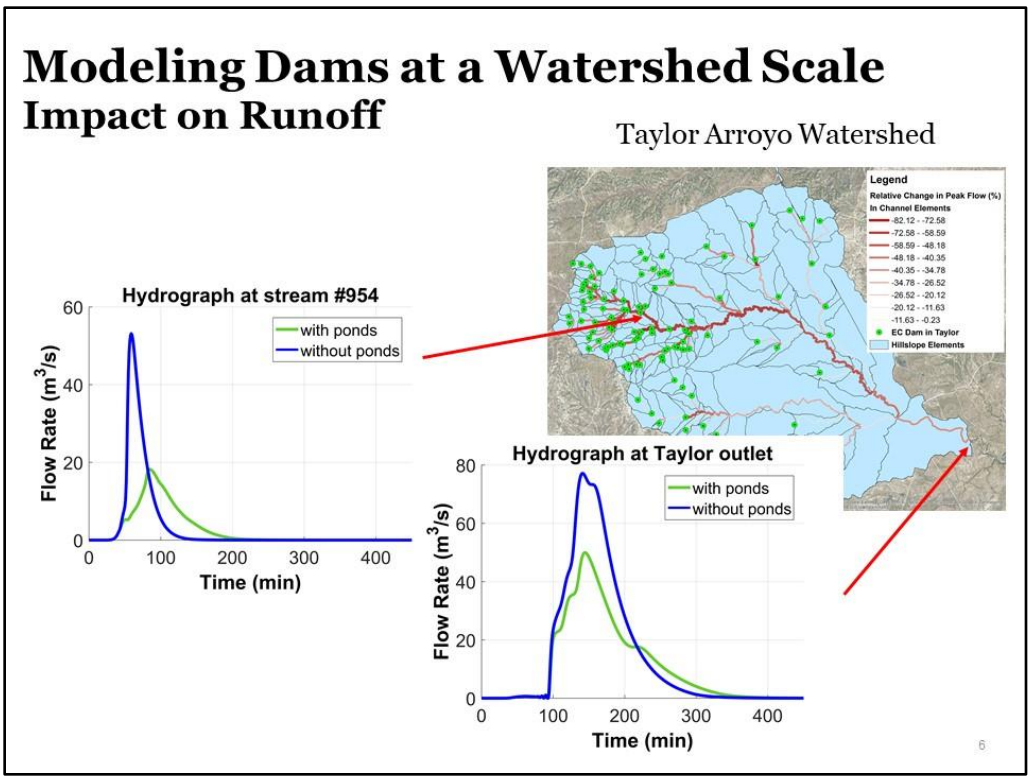

Figure 5. Impact of erosion control dams on hydrology in the Taylor Arroyo Watershed on the U.S. Army Pinon Canyon Maneuver Site, Colorado.

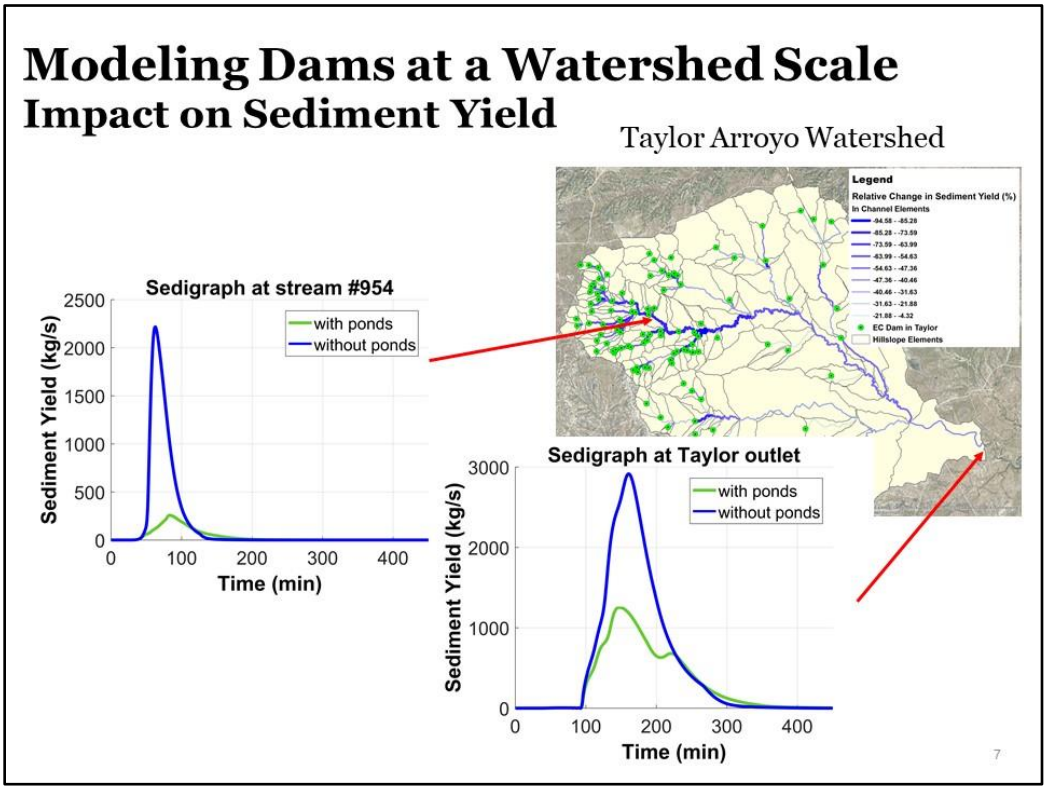

Figure 6. Impact of erosion control dams on sediment yield in the Taylor Arroyo Watershed on the U.S. Army Pinon Canyon Maneuver Site, Colorado.

Conclusions

Ponds can have a significant impact on runoff and sediment yield and it is important to include ponds in any watershed assessment. The SCT provides an effective process for identifying and characterizing ponds for inclusion into hydrologic and erosion models.

Acknowledgements

The research reviewed in this paper were supported by the USDA Agricultural Research Service, the US Environmental Protection Agency and the Department of Defense Environmental Strategic Technology Certification Program (ESTCP; Project RC-201308).

References

Arnold, J.G. and Fohrer, N. 2005. "SWAT2000: current capabilities and research opportunities in applied watershed modeling," Hydrological Processes, 19(3), 563-572.

Barlow, J.E. 2017. Python Tools to Aid and Improve Rapid Hydrologic and Hydraulic Modeling with the Automated Geospatial Watershed Assessment Tool (AGWA). Unpublished M.S. Thesis, University of Arizona.

Berg, M. D., Popescu, S.C., Wilcox, B.P., Angerer, J.P., Rhodes, E.C., McAlister, J., and Fox, W.E. 2016. Small farm ponds: Overlooked features with important impacts on watershed sediment transport. Journal of the American Water Resources Association 52(1): 67-76. DOI: 10.1111/1752-1688.12369

Crowe, C.T., Roberson, J.A., and Elger, D.F. 2001. Engineering Fluid Mechanics, 7th Edition. John Wiley & Sons, Inc.

Hernandez, M., Nearing, M.A., Al-Hamdan, O., Pierson Jr, F., Armendariz, G., Weltz, M.A., Spaeth, K.E., Williams, C.J., Unkrich, C.L., Nichols, M.H., and Holifield Collins, C. 2017. The Rangeland Hydrology and Erosion Model: A dynamic approach for predicting soil loss on rangelands. Water Resources Research. 53: 1-24.

Goodrich, D.C., Burns, I.S., Unkrich, C.L., Semmens, D.J., Guertin D.P., Hernandez, M., Yatheendradas, S., Kennedy, J.R., and Levick, L.R. 2012. "KINEROS2/AGWA: Model use, calibration, and validation," Trans. of the ASABE, 55(4): 1561-1574.

Goodrich, D.C., Guertin; D.P., Burns, I.S., Nearing, M.A., Stone, J.J., Wei, H., Heilman, P., Hernandez, M., Spaeth, K., Pierson, F., Paige, G.B., Miller, S.N., Kepner, W.G., Ruyle, G., McClaran, M.P., Weltz, M.A., and Jolley, L. 2011. AGWA – R: The Automated Geospatial Watershed Assessment Tool for rangelands. Rangelands. Vol. 33, No. 4, pp. 41-47.

Guertin, D.P., Korgaonkar, Y., Burns, I.S., Barlow, J., Unkrich, C.L., Goodrich, and D.C., Kepner, W.G. 2015. Evaluation of green infrastructure designs using the Automated Geospatial Watershed Assessment Tool. American Society of Civil Engineering Watershed Management Conference. Reston, VA, August 5-7, 2015, pp. 229-239.

Goff, K.M. and Gentry, R.W. 2006. The influence of watershed and development characteristics on the cumulative impact of stormwater detention ponds. Water Resources Management 20 (6): 829-860.

Hernandez, M., Kepner, W.G., Goodrich, D.C., and Semmens, D.J. 2010. The Use of Scenario Analysis to Assess Water Ecosystem Services in Response to Future Land Use Change in the Willamette River Basin, Oregon. In: Achieving Environmental Security: Ecosystems Services and Human Welfare, P.H. Liotta and others (Eds.) IOSPress, p. 97-114. doi: 10:3233/978-1-60750-579-2-97.

Kepner, W.G., Hernandez, M., Semmens, D., and Goodrich, D.C. 2008. The Use of Scenario Analysis to Assess Future Landscape Change on Watershed Condition in the Pacific Northwest (USA). In Use of Landscape Sciences for Environmental Security, Springer Publishers, The Netherlands. ISBN 978-1-4020-6588-0, pp. 237-261.

Korgaonkar, Y., Guertin, D.P., Goodrich, D.C., Unkrich, C.L., Kepner, W.G., and Burns, I.A. 2018. Modeling urban hydrology and green infrastructure using the AGWA urban tool and the KINEROS2 model. Frontiers in the Built Environment 4: 58. doi: 10.3389/fbuil.2018.00058

Levick, L. 2017. Automated Geospatial Watershed Assessment (Tool) to aid in sustaining military mission and training. IGI&S News (July): 1-2.

Milne, M.M. and Young, D.W. 1989. The impact of stockwatering ponds (stockponds) on runoff from large Arizona watersheds. Water Resources Bulletin 25(1): 165-174.

Nagle, D. and Wright, C.W., 2016. Algorithms Used in the Airborne Lidar Processing System (ALPS). USGS Open-File Report 2016–1046, 45p

Nichols, M.H. 2016. Personal Communication, USDA Agricultural Research Service, Tucson, Arizona.

Nichols, M.H., Nearing, M.A., Polyakov, V.O., and Stone, J.J. 2013. A sediment budget for a small semiarid watershed in southeastern Arizona, USA. Geomorphology 180-181: 137-145.

Norman, L.M., Huth,,H., Levick, L., Burns, I.S., Guertin, D.P., Lara-Valenciam F., and Semmens, D. 2010. Flood hazard awareness and hydrologic modelling at Ambos Nogales, United States–Mexico border. Journal of Flood Risk Management 3: 151-165.

Renwick, W.H., Smith, S.V. Bartley, J.D., and Buddemeier, R.W. 2005. The Role of impoundments in the sediment budget of the conterminous United States, Geomorphology, 71: 99-111.

Smith, S.V., Renwick, W.H. Bartley J.D., and Buddemeier R.W. 2002. Distribution and significance of small, artificial water bodies across the United States landscape, The Science of the Total Environment 299: 21-36.

Smith, R.E., Goodrich, D.C., Woolhiser, D.A., and Unkrich, C.L. 1995. KINEROS - A kinematic runoff and erosion model. Chap. 20 of Computer Models of Watershed Hydrology, (Ed. by Singh, V. J.). Water Resour. Pub., Highlands Ranch, CO, pp 697-732.

Tarboton, D.G., Bras, R.L., and Rodriguez-Iturbe, I. 1991. On the extraction of channel networks from digital elevation data. Hydrological Processes 5: 81-100.

Weltz, M.A., Jolley, L., Goodrich, D., Boykin, K., Stone, J., Guertin, P., Hernandez, M., Spaeth, K., Pierson, F., Morris, C., and Kepner, B. 2011. Techniques for assessing the environmental outcomes of conservation practices applied to rangeland watersheds. Journal of Soil and Water Conservation 2011 66(5):154A-162A

Yatheendradas, S., Wagener, T., Gupta, H., Unkrich, C.L., Goodrich, D.C., Schaffner, M., and Stewart, A. 2008. Understanding uncertainty in distributed flash flood forecasting for semiarid regions. Water Resources Research, Vol. 44, W05S19

The InFRM Hydrology Assessments for Large River Basins in Texas

Author: Helena Mosser, P.E., Hydraulic Engineer, US Army Corps of Engineers, Fort Worth, Texas, Helena.P.Mosser@usace.army.mil

Abstract

The Interagency Flood Risk Management (InFRM) team is performing Hydrology Assessments for selected large river basins in FEMA Region 6 in order to establish consistent and defendable flow frequency estimates across the basins. The hydrology assessment studies are being performed by a multi-agency scientific team of experts with experience in local and regional hydrology, using a wide range of hydrologic methods. The hydrologic methods employed in these studies includes (1) Statistical Hydrology, (2) Rainfall-Runoff Modeling, including calibration to observed storms, uniformly distributed frequency storms and elliptical shaped frequency storms, (3) Period of record simulations in Riverware, and (4) Reservoir Studies with stochastic inflow analyses in RMC-RFA. The use and comparison of the results from multiple hydrologic methods helps reduce uncertainty in flood risk estimates by ensuring the consideration of all available information that affects the hydrologic processes within the watershed. InFRM hydrology assessments are currently underway for the following river basins in Texas: the Guadalupe, the Trinity and the Neches River Basin. These initial basins were selected based on watersheds where USACE already had sufficiently detailed modeling products available as a starting point for the assessments and where FEMA had future floodplain mapping activities scheduled. The results of the hydrology assessments can be leveraged to support any future floodplain mapping activities within the basin along with any future planning studies authorized by Congress.

Introduction

The InFRM Hydrology Assessments are made up of meteorology and surface water hydrology components. Under meteorology, they study weather patterns and storm events over the State of Texas, and in hydrology, they study how much water will result from a given storm event at a point of interest on a river.

The InFRM Team

Background on the formation of the InFRM team will be given.

Relationship to the National Flood Insurance Program (NFIP)

The NFIP was created in 1968 to help guide development away from flood hazard areas. FEMA's Flood Insurance Rate Maps (FIRMs) are primarily based on the estimated 1% annual chance exceedance (100-yr) floodplain.

a. Definition of the 1% ACE (100-yr) Flood

b. How does one determine if a particular house is in the 100-yr Floodplain?

c. The Problem of Hydrology in relation to the 100-yr Floodplain on FIRMs in Texas.

The Goals of the InFRM Hydrology Assessments

a. Generate a best estimate of the 1% (100-yr) Peak Flows along with other frequencies

b. Calculate & Compare Estimates from Multiple Hydrologic Methods

c. Focus on Larger Rivers

d. Produce Consistent & Defendable Results Across a Basin

Basins in Texas with InFRM Hydrology Assessments Currently Underway

Guadalupe, Trinity, Neches and Colorado Rivers

Hydrologic Methods Used

a. Statistical Hydrology – Bulletin 17C

b. Precipitation Frequency Estimates – NOAA Atlas 14

c. Rainfall Runoff Modeling – Historic Storm Calibrations, Uniform Frequency Storms, Elliptical Frequency Storms

d. Reservoir Simulations - Period of Record Modeling in Riverware, development of regulated / unregulated flows & extension of gage records

e. Reservoir Studies – Pool Elevation Frequency Analysis in RMC-RFA

f. Stochastic Analysis – vary model parameters such as antecedent soil moisture conditions and the development of a weather generator for monte carlo analysis of storm patterns. This is a research and development area.

Unique Components in the InFRM Hydrology Assessments

a. Looking at the Change Over Time in Statistical Estimates
b. Extensive Calibration of Rainfall Runoff Models to Actual Flood Events
c. Incorporating New Methods
d. Elliptical Storms, Stochastic Methods
e. Comparing Results from Multiple Methods
f. Greater Confidence in the Selected Answer
g. Team of Federal Agencies, Scientists & Researchers

Examining How Statistical Results from Bulletin 17C Change over Time

a. Effects of dry periods and wet periods on the statistical answer
b. Change over time plots reveal historic range of frequency estimates

Calibration of the Rainfall Runoff Models

Elliptical Frequency Storms

Extends the depth area reduction beyond the 400 square mile limit of Figure 15 in TP-40. Produces a more realistic runoff volume for larger drainage areas (up to several thousand square miles).

Comparing Results from Multiple Hydrologic Methods

Conclusions - The InFRM Hydrology Assessments:

a. Help Update the Hydrology for Large, Complex River Systems
b. Account for How the100-yr Flood Estimate Changes Over Time
c. Incorporate New Methods and Technology
d. Verify Model Results with Observed Data
e. Reduce the Uncertainty in the 100-yr Flood Estimate by Comparing Results from Multiple Methods

Updating the Curve Number Method for Rainfall Runoff Estimation – Extended Abstract

Richard H. Hawkins, Ph.D., P.E., F. ASCE, F. EWRI, Professor Emeritus, University of Arizona. Tucson AZ 85721, rhawkins@ag.arizona.edu
Tim J. Ward, Ph.D., P.E., F. ASCE, F. EWRI, Dean and Professor, Manhattan College, Riverdale, NY, tim.ward@manhattan.edu
Donald E. Woodward, P.E., F. ASCE, National Hydraulic Engineer, USDA-Natural Resources Conservation Service, Retired, Gaithersburg, MD, dew7718@comcast.net

Introduction and Background

Origins

The well-known Curve Number (CN) method is used to estimate runoff depth, Q, from rainfall depth, P, and is used worldwide in a variety of applications. Since its genesis in the 1950s by the USDA Soil Conservation Service (now Natural Resources Conservation Service or NRCS), it has undergone numerous critical analyses on both practical and theoretical grounds. Originally intended to simply model runoff depth from design rain storms on small agricultural and rangeland watersheds, it has been opportunistically extended to a wide variety of conditions, including urban drainages, green roofs, solar farms, and continental scale river basin runoff.

In brief, the familiar CN method centers on the runoff equation

$$Q = (P-0.2S)^2/(P+0.8S) \qquad \text{for } P>0.2S, \quad Q=0 \text{ otherwise} \qquad (1)$$

where P is the event rainfall depth, Q is the median direct event runoff depth for the given P, and S is a measure of the hydrologic land condition, tied to of the maximum possible difference between P and Q. The CN is related to S by CN = 1000/(10+S) with S in inches. As shown in equation (1), 0.2S serves as an initial abstraction (Ia), or the amount of rainfall required before runoff begins. The S may vary from 0 to ∞, thus CN inversely varies from 100 to 0. CN tables in handbooks give CNs for different soils (Hydrologic Soil Groups or HSGs) and land conditions.

The primary authoritative reference is the NRCS NEH-630 (USDA, 2003). In-house study reviews (Woodward, et al., 2003, 2004) identified issues in the CN method that should be addressed. A state-of-the-practice review was done under the auspices of ASCE in 2009 (Hawkins *et al.,* 2009)

Curve Number Update Task Group

Within the past twenty years, there has been growing awareness of CN limitations and inconsistencies, and for the need to update the method. Accordingly, in late 2015, a joint ASCE-ASABE-NRCS Task Group, comprised of 16 volunteer members and co-chaired by the three authors here, was formed. Quarterly meetings over two years were held to consider needed revisions to review update status. In cooperation with NRCS, and with its support, Task Group delivered its report on October 1, 2017. Referred to as the Update here, it was based on experiences and advances in knowledge and data in watershed hydrology since the 1950s. It is still in agency review: to date (March 2019) changes in technical policy have yet not been endorsed by the NRCS nor incorporated in NEH 630 (USDA, 2003), the agency reference and

guide. The Update covers the four CN-related chapters (8, 9, 10, and 12) in NEH630, and is available on the ASCE-EWRI Collaborate site [https://collaboarate.asce.org/ewristatute] or from the authors. This presentation is intended to inform and solicit feedback from the audience and user community on the Updates and suggested revisions to the CN method.

Important assumptions and limitations in the Update were 1) uses of the CN method extend well beyond the original intended agency in-house applications; 2) data resources, computational abilities, and the quality of practitioners have greatly improved since the 1950s; 3) the work does not consider the many affiliated CN-using technologies of hydrograph generation, timing measures, daily time-step models, or geographic information systems; 4) it is centered on United States experiences; and 5) insofar as possible, strives for lumped model simplicity and consistency with prior offerings

User experiences and data analyses from many sources since the 1950s has led to previously unappreciated findings and insights to rainfall-runoff processes in general. While originally a specific agency methodology, CN procedures are limited by being a subset of general hydrology, all the while complementing general hydrology. While not exhaustive, the major Update points are presented here.

Findings and Recommendations

Runoff Response Behavior

From the rainfall-runoff analysis of several hundred rainfall-runoff data sets, response patterns were found to fall into three distinct groups, not all of which are consistent with the CN runoff equation, *i.e.*, equation (1). The simplest pattern found is a low linear reaction of the form Q=CP, with C values (fraction of P that becomes Q) typically ranging from 0.005 to 0.05. Called the "Complacent" response, it is common even in some extreme rainfall conditions. This response is a version of the oft-used Rational Method.

Starting from low runoff complacent beginnings, there is, at some continuing higher rainfall threshold (P_t, commonly 1.5-3 inches), a much higher incremental response fraction (about 0.6 to 1.0 in/in) that often sharply occurs. Such events, termed "Violent" response, are rarer, but can be quite consequential. Most data sets that have been examined – around 80% - show a "Standard" response, described further below, and which is compatible or compliant with CN procedures.

Following these observations of the different patterns, the Update recommends that the CN method not be applied to watersheds likely to exhibit Complacent or Violent runoff responses. An example is highly forested, base-flow watersheds, with high infiltration capacity that shows little evidence of overland flow. Karst topography with down-channel openings should also be excluded. In the Update, no alternative methods are endorsed for these conditions because they are not CN compliant rainfall runoff watersheds.

Frequency Matching

The original and predominant application of the CN method is the design calculation of event peak runoff from return period rainfall. With this in mind, the event rainfall P and runoff Q are matched by return period (rank-ordered matching). Preserving this in data analysis requires matching the rank-ordered P and rank-ordered Q in to unnatural pairs. Thus, most analyses use

ordered data, as opposed to the natural (Q resulting from P) data. This unusual ordered approach, called "frequency matching", has been both useful and revealing.

Asymptotic Behavior

As evidenced by extensive analyses, data-based CNs –those defined by inverse solution of equation (1) for S and CN on ordered data - are rainfall dependent. When plotted against rainfall P, CNs are high for low rainfalls, but decrease with increasing storm size (depth P), and usually approach a steady state CN, referred to as CN_∞, which is asserted to be equivalent to the NEH 630 handbook reference values. This rainfall-runoff pattern is called "Standard" and is the most common in the situations encountered. The trend of CN to decline with P to a steady state value is called "Asymptotic" and as expressed by the following:

$$CN(P) = CN_\infty + (100 - CN_\infty)\mathbf{exp}(-kP) \quad (2a)$$

where k (1/in) is a measure of the rate of change of CN with P. This is asymptotically consistent with CN method. This relationship is also generated through summed, distributed source-area-weighted area runoffs over an array of rainfall depths.

A subsequent simpler, and preferred, alternative formulation to equation (2a) is:

$$CN(P) = CN_\infty + (100 - CN_\infty)\tau^{P/Pz} \quad (2b)$$

where τ ranges from 0-1 and has a clear geometric representation on the CN:P plot. Pz is the threshold rainfall depth at Q=0, or λS_∞, where λ=Ia/S (here 0.20 or 0.05). The two equations are equivalent with $\tau=\mathbf{exp}(-k\,\lambda S_\infty)$, or $k= -\ln(\tau)/Pz$.

Initial Abstraction ratio

As shown in equation (1), the CN method has used an abstraction ratio (λ) of 0.20. Studies over the past 20 years have shown the value of λ to be more appropriately about 0.05. To apply this in the Update requires revision of the runoff equation (1) to:

$$Q = (P-0.05S_{05})^2/(P+0.95S_{05}) \text{ for } P>0.05S_{05}, Q=0 \text{ otherwise} \quad (3)$$

As inferred by the subscripting, the new S is not the same as the original S in equation (1), and the CN definition must be altered as well. A proposed transfer function in the Update between the long-used S value for λ = 0.20 and the value for λ = 0.05 is:

$$S_{05}=1.42S_{20} \quad (4)$$

Subsequent discussions and analyses by Task Group members have now lead to an alternative formulation of (S values in inches):

$$S_{05}=1.3244(S_{20})^{1.089} \quad (5)$$

This alternative formulation gives conversions very close to results from equation (4) (~1 CN unit) down to about a CN of 71. Equation (5) is now recommended, however.

Distributed-Weighted Runoff

In calculations, the Update recommends the use of distributed weighted runoff from individual CN source area fractions rather than the use an averaged, lumped CNs. That is,

$$Q=\Sigma\alpha[(P-\lambda S_\alpha)^2/(P+(1-\lambda)S_\alpha] \quad \text{for all } \alpha \text{ and for } P>\lambda S_\alpha \text{ , } Q=0 \text{ otherwise} \qquad (6)$$

where α is the fraction of the drainage area represented by the given CN. This enhancement is within the capabilities of most rainfall-runoff modeling software. It should be noted that 1) it calculates runoff Q>0 for every P>minimum I_a, but as a mean for that P, and not a median; 2) it is more important with smaller storm events than with the higher extremes, and; 3) with back-calculating, it generates an asymptotic Standard response and thus is more in line with data-based findings. In short, it is a more realistic portrayal of expected watershed runoff with rainfall.

Secondary Effects

In addition to the direct rainfall effect on runoff Q, deviations, scatter, and variety in runoff due to other watershed and storm variables are expected but are not universally apparent. These include: 1) Land use effects are widely shown, but not for all storms, land uses, and sites. 2) Seasonal effects on CN have been found in some sites with accented moisture effects; 3) Event duration effects on CN are expected, but not widely demonstrated once the rainfall depth effects are excluded; 4) Event intensity distribution (i.e., storm pattern) seems to have inconsistent or minimal effects on CN runoff; 5) Prior rainfall effects, or watershed wetness is seen, but is not universal; and, 6) Effects of watershed slope on back-calculated CN is variable and is not consistent among the studies.

The prior-to-event rainfall criteria endorsed in early versions of the method to adjust for antecedent runoff conditions (ARC) were largely invalid and were discarded. The ARC concept itself was re-expressed as probability bands for ARCI (low runoff condition, 12%), ARCII (median runoff condition, 50%). and ARCIII (high runoff condition, 88%)

Table Curve Numbers

Successful application depends greatly on the choices of appropriate Curve Numbers for the contributing areas. Sensitivity studies show that the calculation (i.e., equation (1)) as more sensitive to variability in CN than to that of the rainfall P. For the user, CN tables for different soils groups and land uses are provided in authoritative guides or by local approving jurisdictions. However, very few of the table entries are documented or based on analysis of field data. Thus, they might be realistically seen as conventions, or agreed-upon values offered in the absence of precise determination. They should be considered estimates based on best judgments of the tables' authors.

Local Calibration

Because of the need for CNs for new/unlisted land uses or unusual watershed conditions, and for authoritative value, determination of CNs from local data sets is strongly encouraged. The original NRCS publications provided no clear instructions but did give an illustration of a median CN selected from annual flood events by graphical means. The Update provides a new procedure for estimating CN values from measured data, as outlined in the following steps. Given event rainfall and runoff values (P, Q), with all $0<Q\leq P$, use these steps in the procedure:

1. Rank order the P and Q separately (smallest to largest values)
2. Match the P:Q pairs based on the same rank-order.
3. Calculate the S (see equations (7) and (8)) and CN for each rank-ordered pair.
4. Plot CN against P with the presumption that the asymptotic standard shape results; if not, this not a CN compliant watershed or data set, i.e., use of the CN method is not recommended.
5. If asymptotic, find by either visual fitting or calculation the stable CN at high P. This is CN_{∞}, taken to be the representative CN for the watershed, comparable to table values.
6. Select a representative CN and P in the P-sensitive drawdown part of the plot.
7. From this (CN,P) pair and CN_{∞}, use equation (2a) or equation (2b) to determine the asymptotic coefficients k and/or τ .

The equations for S under the two Ia/S assumptions (0.20 or 0.05) are:

$$S_{20} = 5(P+2Q-\sqrt{(4Q^2+5PQ)}) \quad (7)$$

$$S_{05} = 20(P+9.5Q-\sqrt{(90.25Q^2+20PQ)}) \quad (8)$$

These two equations are dimensionally homogeneous so that P, Q, and S may be in either inches or mm, for example. However, in both cases, CN=1000/(10+S), with S inches. Optimum data-based values for k and CN_{∞} in asymptotic equation (2a) or (2b) can be determined by iterative methods and root-mean-squared-error (RMSE) criterion, using either CN or the resulting Q as the objective variable. This has been done extensively in the past for the Ia/S cases of both 0.20 and 0.05.

Local calibration of CN on local data is encouraged to deal with new land uses, such as green roofs, solar farms, or porous pavements. As demonstrated by recent wildfire events, Curve Numbers and time recovery parameters for freshly burned watersheds are badly needed. When produced, locally developed tables should be documented and made publically available.

Determining or verifying Curve Numbers by comparing experienced flood peaks or regional studies computed to modeled outputs poses a risk of confusing effects of hydrograph shape, dimensions, and timing measures with the underlying CN.

Output Uncertainly

Comparisons of data-derived CN findings to corresponding table values based on soils and land use usually show nonconformity. Consequently, runoff calculations based on table values are expected to contain uncertainty. Elementary estimates of CN uncertainty provided in the Update can be carried through to modeling calculations, thus providing a measure of scatter in the output. This step, seldom effected in current practice, is recommended, and should fit easily into existing modeling software.

Practice, Research, and Development Suggestions

General

Curve Number technology is still evolving and in need of improvements. Despite its obvious simplifications, development will contribute to an understanding of the general (i.e., non-CN) hydrology into which it conforms. Several issues are presented in the following sections.

Non-CN Compliant watersheds

An important conclusion of the Update was that the CN method/equation does not correspond well to all rainfall-runoff watersheds. It should not be used in Complacent and Violent runoff settings. While the Update gives some suggestions, there is no practice-wide accepted set of alternative approaches. This shortcoming is an area that needs priority attention. An especially problematic case is a forested watershed. Under sufficient environmental conditions, tree-covered lands may display a distinct non-CN hydrologic response pattern (Complacent-Violent). Unfortunately, this is not a mutually exclusive relationship. Some non-forested lands show it as well, and some less-forested sites do not. Means of identifying these cases from land characteristics is needed.

Similarly, in the Violent case the threshold P_t is needed, but not readily defined from site characteristics. The lack of Violent patterns in the data record will continue to hinder progress in better defining its causes. In general, and as suggested previously, there is a need for *a priori* definitions of the three runoff response types based on land and storm attributes.

Asymptotic Relations

The empirical nature of the Asymptotic-Standard procedure suggests unappreciated cause-and-effect connections between the land surfaces and the rainfall. Thus, this should be a productive focus area for further study and development: For examples: 1) What are the reasons/mechanisms for its very occurrence, and, 2) How might the asymptotic coefficients k and τ (equations (2a) and (2b)) and be linked to the land characteristics and general hydrology?

History

The development and professional assimilation of the Curve Number method traces growing hydrologic knowledge and constantly changing user needs, and offers valuable lessons. While most of the original participants have passed, the technical-scientific-cultural-administrative evolution of the method should be documented as a noteworthy part of the history of hydrology. This should include the interfaces with its upland natural resources components.

Discussion

The different recommendations and findings from the Task Group and Update will be presented and discussed at SEDHYD 2019. The Task Group is still active.

Work Group Participants

The major authors and contributors have been, in alphabetical order: Hunter Birckhead, P.E., M.ASCE; James V. Bonta, Ph.D., P.E., F.ASCE; Donald Frevert, Ph.D., P.E., D.WRE (Ret), F.ASCE; Claudia Hoeft, P.E., F.ASCE (USDA NRCS liaison); Richard H. Hawkins, Ph.D., P.E., F.EWRI, F.ASCE (Task Group chair); Rosanna La Plante, P.E., M.ASCE; Michael E. Meadows, Ph.D., P.E., F.ASCE; Julianne Miller, A.M.ASCE; Steven C. McCutcheon, Ph.D., P.E., D.WRE (Ret), F.EWRI, F.ASCE; Glenn Moglen, Ph.D., P.E., F.EWRI, F.ASCE; David Powers, P.E., D.WRE, F.ASCE; John Ramirez-Avila, Ph.D., ING., M.ASCE; E. William Tollner, Ph.D., P.E., M.ASCE, F.ASABE (American Society of Agricultural and Biological Engineers [ASABE] representative); Joseph A. Van Mullem, P.E., M.ASCE; Tim J. Ward, Ph.D., P.E., F.ASCE,

F.EWRI (Task Group co-chair), and Donald E. Woodward , P.E, F.EWRI, ASCE (Task Group co-chair).

The Update was reviewed by a select, three-member external review team composed of Wilbert Thomas, Jr. (Michael Baker International, and USGS retired), Dr. Bill Elliot (U.S.D.A. Forest Service), and Karen Kabbes (Kabbes Engineering). The authors Task Group thank them for their input.

References

Hawkins, R.H., T.W. Ward, T.J., Woodward, D.E. and J.A Van Mullem. 2009. "*Curve Number Hydrology State of the Practice*" American Society of Civil Engineers, Reston Va. 106pp.

USDA, Natural Resource Conservation Service. 2003. NRCS National Engineering Handbook, Part 630, Hydrology. <https://www.nrcs.usda.gov/wps/portal/nrcs/detailfull/national/water/manage/hydrology/?cid=stelprdb1043063> (January 2019)

Woodward, D. E., (Chair), Conaway, G., Plummer, A, Van Mullem, J., Neilsen, R., Goertz, L., Quan, Q. D., Scheer, C, Hjelmfelt, Jr, A.T., Gburek, W., Bonta, J.V., and Hawkins, R. H. 2002. "Report of ARS/NRCS curve number working group." Available from USDA, NRCS, Conservation Engineering Division, Beltsville MD. 38pp.

Woodward, D. E., Hawkins, R. H., Hjelmfelt, Jr, A.T., Quan, Q .D., and Scheer, C. 2003. "ARS/NRCS curve number work group report." Internal report to Conservation Engineering Division NRCS. ca20pp.